STRATOSPHERIC TEMPERATURES : VERTICAL RESOLUTION OF RETRIEVED PROFILES

A thesis
submitted in partial fulfilment
of the requirements for the Degree
of
Doctor of Philosophy in Physics
in the
University of Canterbury
by

Michael J. Uddstrom

University of Canterbury
1980

ERRATA AND COMMENTS

- pp 12,13 equations (2.19),(2.21) and (2.23) replace $K(y)$ by $K_i(y)$
- p16 line 8, section 2.2.1 should read section 2.2.2.
- p17 line 3, should read (exp(-y'))
- p25 after line 8 add (However, see section 4.1.2)
- p25 equation (2.37) replace $\int(\ )$ by $-\int(\ )$
- p33 denominator of equation (2.60) should read $f(\underline{y})$
- p36 line 15, equation (2.75) should read equation (2.73)
- p37 after line 1 add " which, when multiplied by the appropriate pair of inverse matrix quantities, yields
  $(I + K^T S_e^{-1} K S_x)^{-1} K^T = K^T (I + S_e^{-1} K S_x K^T)^{-1}$.
- p37 after equation (2.77) insert: (This equation is usually attributed to Strand, O.N., and Westwater, E.R., (1968) SIAM J., Numer. Anal., 5, 287)
- p37 line 22, first term should read $(\hat{S}K^T S_e^{-1} K-I)$
- p38 add to line 11 the phrase (see matrix inversion lemma, Appendix B).
- p38 equation (2.73) last term should read $-K\bar{\underline{x}}$
- p40 equation (2.82) second line, the K's in parentheses should be lower case.
- p40 between lines 19 and 20 insert "$K = (\underline{k}_1, \ldots, \underline{k}_n)^T$"
- p41 line 2, after the word "introduced" insert (i.e. each channel)
- p51 line 17, after "filter". add "(i.e. ¼,½,¼ filter)"
- p52 equation (2.91) replace S_x by $S_{x_{ij}}$ and delete the sum over i and j.
- p53 line, after "n", add (the reference wavenumber)

p69 equation (2.144) replace the "=" sign on the right hand side by "+"

p71 line 4, Δy_i should read Δy_j

p72 line 20, replace the sentence beginning on this line by: "For any averaging kernel $A_i(z)$ the value c_i for which the spread s_{c_i} about c_i, defined by equation (2.156) is a minimum is given by;

p74 line 28, equation (2.145) should read equation (2.77).

p75 line 16, equation (2.162) should read equation (2.163)

p86 August profiles are included in order to improve the sample size

p231 in equations B7, B8 and B10 replace S_e by S_e^{-1}, in eqations B12, LHS, replace S_e by S_e^{-1}

p232 last sentence should read: "If B.7 is multiplied by $K^T S_e^{-1}$ and B8 is applied, the following result occurs."

p284 The journal reference for RODGERS C.D., 1970 is incorrect, it should read Quart J.R. Met. Soc 96, 654.

p285 before line 1 add the reference RODGERS, C.D. 1976b Retrieval of Atmospheric Temperature and composition from Remote Measurements of Thermal Radiation. Rev. Geophys. Sp Phys, 14, 609.

To Karilyn

Great are the works of the Lord
They are studied by all who
delight in them. (Ps 111; V2, NASB)

ABSTRACT

This work describes the problem of retrieval of temperature profiles from Nimbus 4 Selective Chopper Radiometer (SCR) measurements of emission from the 15μm CO_2 absorption band.

Vertical resolution diagnostics are discussed for : (a) an optimum retrieval estimator which uses a priori statistical information (the maximum likelihood or maximum a posteriori estimator), and (b) a Backus Gilbert estimator which uses essentially no a priori information. Confidence regions are calculated for the optimum retrieval estimator.

At stratospheric heights, and for Nimbus 4 SCR data, the resolving power of the optimum estimator is poorer than that of the satellite observations and is sensitive to the size of the measurement noise, and the choice of first guess profile. The retrieval from the optimum estimator is unstable when detecting vertical wave-like disturbances on temperature profiles.

It is suggested that retrieval estimators using a priori statistical information should not be used when trying to detect vertical wave-like structure in the atmosphere.

ACKNOWLEDGEMENTS

In the preparation of this thesis a number of people have made contributions which have been of assistance.

I am indebted to Dr. G J Fraser, my supervisor, for suggesting this project, and for his support and encouragement during the period in which this research was carried out.

I would also like to thank fellow students and Physics Department staff for their general encouragement and helpful comments. Especially I would thank Mr C W Tomblin for help with the diagram preparation, and Mr L Hunter for the photographic work.

A number of my analysis computer programs used ALGOL procedures from the Burroughs Corporation Large Systems Numerals Numerical Analysis Program Library. The use of these programs is gratefully acknowledged.

It is my pleasure to thank my wife Karilyn for her unending support and encouragement over the duration of this project. She has been a true help-mate who has laboured and sacrificed out of love. Further I thank Karilyn for her substantial assistance with the preparation of the diagrams and proof-reading.

Also, I would like to thank my parents for their real support and encouragement during this project.

Thanks must also go to Mrs H Crawley for her patience in typing this thesis.

Finally I would like to thank the University of Canterbury and the Head of the Physics Department, Professor A G McLellan, for the support of a Teaching Fellowship and for the provision of the facilities required during the course of this project.

TABLE OF CONTENTS

LIST OF FIGURES

TABLE LIST OF TABLES PAGE

CHAPTER 1

INTRODUCTION

In 1959 Kaplan (1959) suggested that the vertical temperature structure of the atmosphere might be determined by utilizing emission from the atmosphere's rotation vibration band of CO_2 centred at 15μm. The subject of this thesis is the analysis of the vertical resolution in temperature profiles retrieved from radiances measured by the Selective Chopper Radiometers mounted on the Nimbus 4 satellite (figure 1).

The motivation for this project was the hope that temperature retrievals from radiance data would have better vertical resolution than the simple observations. These retrievals might then be used to measure any vertical wave-like disturbances found in the radiance observations. Remarks made by Conrath (1972, 1977) and a report by Rodgers (1976a) suggest that retrieved temperature profiles derived with estimators which use statistical a priori information have considerably better resolution than the satellite observations. These authors also suggest that the resolution of this type of estimator is better than that of estimators which use essentially no a priori information. Estimators of the first type (which use a priori statistical data) have been used to study vertical temperature structure by Barnett (1974), Harwood (1975), Hartman (1976), McGregor and Chapman (1978a), Crane (1978), McGregor and Chapman (1978b) and Molnar (1979). However, Barnett (1980) notes "... it is never clear whether medium scale features on the borderline of the vertical resolution are present in the measurements or are artefacts of the retrieval process, or originate from other information used by it, such as atmospheric statistics". This thesis attempts to address some aspects of the questions raised by Barnett in the above quotation.

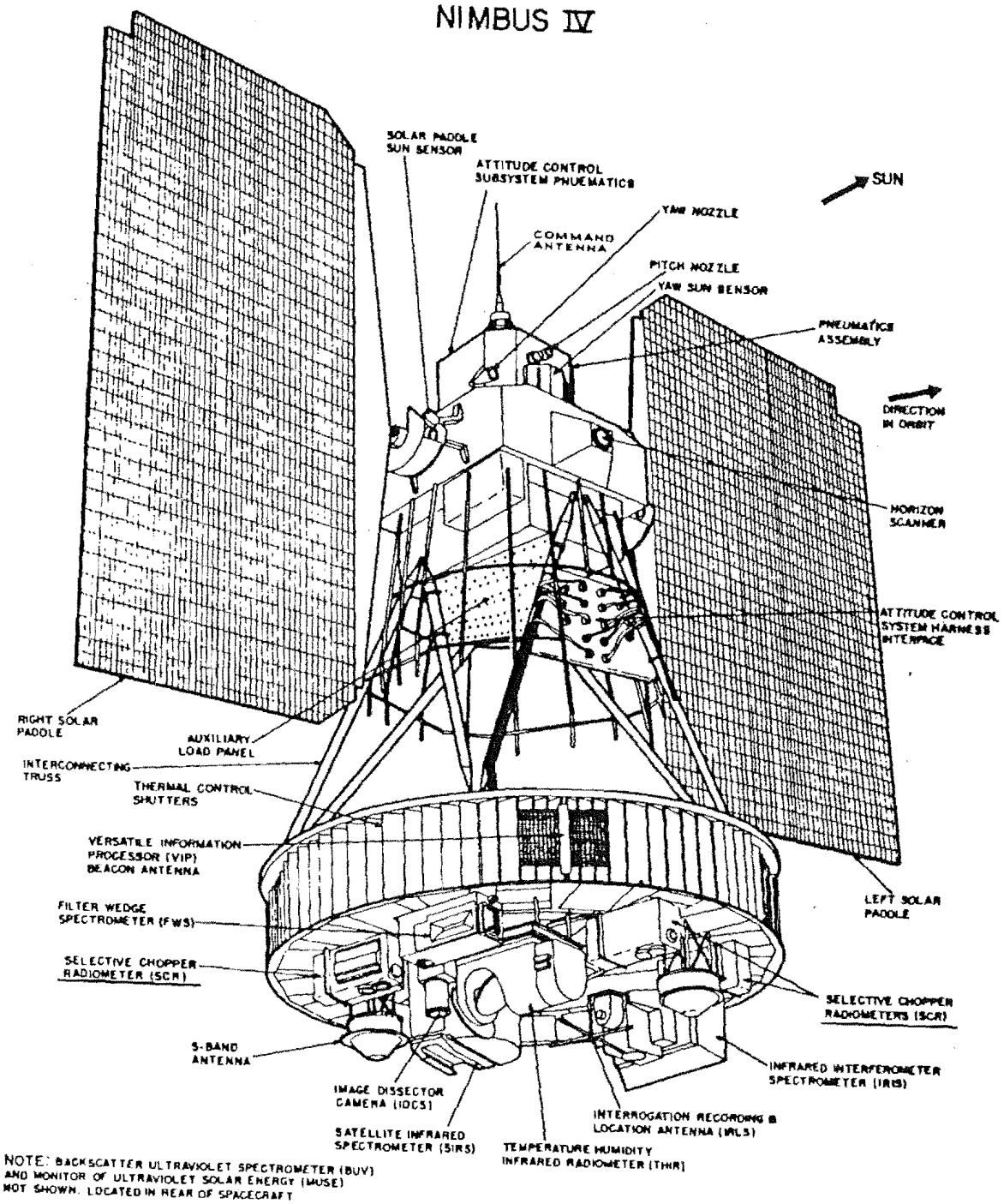

FIGURE 1 : The Nimbus 4 Spacecraft and the Selective Chopper Radiometers (from The Nimbus IV Users Guide)

In Chapter 2 the retrieval problem is discussed and an optimum retrieval estimator, which uses a priori statistical data (of Rodgers (1970)) presented. Intrinsic vertical resolution diagnostics are derived for this estimator, and the theoretical background for determining the retrieval's confidence regions given. The principles of empirical orthogonal function representations of the retrievals are discussed.

Chapter 3 introduces the a priori statistical data, and reports results of calculations which specify the intrinsic vertical resolving power of the optimum estimator; and of the estimator which does not "use" a priori information.

A retrieval simulation study (for the Nimbus 4 SCR data), to substantiate the conclusions of Chapter 3, is presented in Chapter 4. Additionally an overall measure of the information content of the satellite observations is calculated.

Chapter 5 indicates the overall conclusions for this work.

CHAPTER 2

THE RETRIEVAL PROBLEM

The retrieval problem, as it relates to retrieval of atmospheric temperatures from satellite radiance data is a special case of the general physical problem of "inference of some parameter or parameters, given a set of experimental data".

2.1 : INTRODUCTION

Initially it is useful to consider the retrieval or inverse problem in a general way in order that the several aspects of the "solution" process may be outlined. To this end, the problem may be considered as consisting of four contiguous sub problems, as suggested by Jackson (1978). Sabatier (1978) divides the inverse problem into seven sub problems; however, each of the questions raised by that categorisation will be considered in the four part categorisation given here.

(1) The Specification Problem

For any given set of experimental data a mathematical model of the measurement process must be devised. A suitable equation for the general form of this model is :

$$y = f(x) + e \qquad \ldots (2.1)$$

where y is a set of experimental data,

x is a set of unknown parameters,

f is some mathematical operator which maps the parameters x into the observations y, and

e incorporates the effects of all unmodelled parameters.

The operator f maps the model parameter space into the observation (or data) space. If it can be shown that e, the contributions to the

measurements from all parameters (or processes) not explicitly modelled by f affects the measurements in a random way, then e may be considered to be a set of random variables termed the observation (or data) "errors". Under these circumstances equation (2.1) is a suitable model for the measurement process.

This aspect of the problem is termed the "specification" or "construction" problem and involves a definition of the operator f, and a statement indicating the allowed values of the parameters x, together with some statistical statement about the data errors e.

(2) The Direct Problem

It is necessary to provide some method for evaluating the operation of the operator f which maps the parameters x into the data space. This aspect of the retrieval problem is called the direct problem. It is essential that f be accurately known (Sabatier (1978)).

(3) The Mathematical Problem

For any given set of data, y, equation (2.1) must be solved in a mathematical sense in order to determine the unknown parameters x. Formally, this process is specified by the equation :

$$\hat{x} = h(y) \qquad \ldots (2.2)$$

where $\hat{x}$ is the estimate of the unknown parameters x, and it is assumed that

h is some well defined mathematical operator.

h maps the data space into the parameter space and therefore, in some sense, is the inverse of the operator f. There are three possible procedures that may be applied in the problem of determining the inverse operator h.

(i) One method is to look for an exact solution to the inverse problem, whereby an operator h is found such that

$$f(h(y)) = y \qquad \ldots (2.3)$$

for all possible data y, and

$$h(f(x)) = x \qquad \ldots (2.4)$$

for all parameters x; defining the uniqueness of the solution estimate $\hat{x}$ of equation (2.2).

(ii) Another method is to find an optimum estimate for x, say x_{op}. Then x_{op} will be the estimate which minimises some loss function L(x), where L(x) is a function of the operator f, the data, y, the solution estimate x_{op} and the observation errors e. For a definition of the loss function see Deutsch (1965, pg 12). In some areas the term "objective function" is used in place of loss function.

(iii) A final method would be to find a complete set of solutions, $\hat{x}$, given some criterion, for example

$$L(\hat{x}) \leq L_0 \qquad \ldots (2.5)$$

where L_0 is the maximum value of some allowable loss function. The value of L_0 would be set in such a way that $f(\hat{x})$ would be in good agreement with the data.

The estimate of x generated by the operator h, that is, $\hat{x}$, must be consistent with any physical constraints prescribed in the specification of the measurement problem (ie 1, above). Accordingly errors and ambiguities in the estimate $\hat{x}$ due to the operator (or estimator) h must be examined if the problem is to be solved completely.

(4) Test of Solution Estimates

Finally the estimator h must be tested for some known sets of parameters x in order to physically interpret an estimate $\hat{x}$ for some unknown parameter set x. An aspect of this testing might also involve

finding some estimate of the accuracy of the original mathematical model as specified in equation (2.1).

Summary

Schematicaly the inversion problem is portrayed by Figure 2 below:

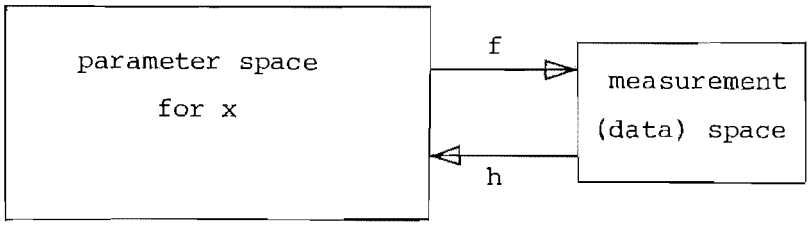

FIGURE 2 : The Retrieval Problem

The problem of inverting the data is reduced to finding a suitable operator h, called an estimator, which satisfies all mathematical and physical constraints associated with the particular inversion problem, and will construct some "best" if not unique estimate $\hat{x}$ of the actual parameter(s) x.

To this end questions directly relevant to the inversion process for satellite radiance data, ie problems 1 through 3 above will be considered in the following sections.

2.2 : THE SPECIFICATION PROBLEM

Henceforth, the term "inverse (or retrieval) problem" will refer to the specific problem of interest in this thesis, that is, the retrieval of atmospheric temperature profiles from satellite radiance measurements of emission from the CO_2 absorption band centred at 15μm in the infra-red. The data set for any particular retrieval is a set of measurements of thermal radiation emitted by the atmosphere and some boundary, for example the Earth's surface or a cloud layer.

The specification problem may be stated as : the problem of modelling the radiative transfer of the thermal radiation in the Earth's atmosphere, together with its measurement by the orbiting satellite.

2.2.1 General Considerations

Consider an idealised atmosphere which is horizontally stratified, is free of scattering agents, and is in local thermodynamic equilibrium. The equation of radiative transfer for this atmosphere is :

$$dI(\nu,\phi) = \{-I(\nu,\phi) + B[\nu,T(u)]\}\, k(\nu,u)\rho(u)\,du \quad \ldots (2.6)$$

where I is the radiance

ϕ is the elevation of the pencil of radiation

u is the geometric path of the pencil of radiation

k is the mass absorption coefficient of the absorber

ρ is the density of the absorbing gas

ν is the spectral frequency

T is the temperature (Kelvin scale) and

B is the Planck Black Body radiance

(see Fritz et al, (1972)). The assumptions imply that

(i) the temperatures are uniform over the horizontal field and

(ii) there are no clouds or other scattering agents in the field.

Using the hydrostatic equation, $dp = -g\rho dz$, the variable "u" can be transformed to pressure (see Figure 3),

$$\rho du = \frac{-q}{g} \sec\theta \, dp \quad \ldots (2.7)$$

where θ is the angle between the path of the beam of radiation and the local vertical,

p is the atmospheric pressure at some altitude,

q is the mass fraction of the absorbing gas, and

g is the acceleration of gravity.

The geometry of the model is given in Figure 3

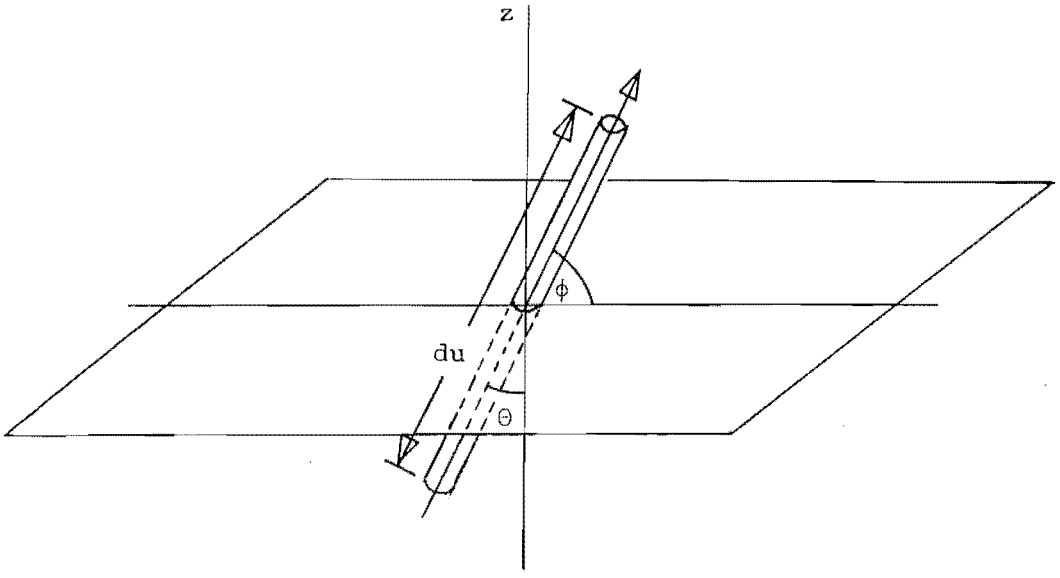

FIGURE 3 : Model Geometry

Substituting equation (2.7) into equation (2.6) yields :

$$dI(\nu,\theta) = \{I(\nu,\theta) - B[\nu,T(p)]\}k(\nu,p)\frac{q(p)}{g}\sec\theta dp \qquad \ldots (2.8)$$

If the surface of the lower boundary is black, the solution to this equation is :

$$I(\nu,\theta) = B[\nu,T(p_o)]\exp\left[-\frac{1}{g}\int_o^{p_0} k(\nu,p')q(p')\sec\theta dp'\right]$$

$$+ \frac{1}{g}\int_o^{p_o} B[\nu,T(p)]\ \exp\left[-\frac{1}{g}\int_o^{p} k(\nu,p')q(p')\sec\theta\ dp'\right]$$

$$x\ k(\nu,p)q(p)\sec\theta\ dp \qquad \ldots (2.9)$$

(Chandrasekhar (1950)). The subscript 0 refers to the lower boundary.

Equation (2.9) indicates that the radiance observed above the atmosphere has two sources :

(i) that arising from the boundary and attenuated by the atmosphere (the first term on the right hand side of equation (2.9)), and

(ii) that arising from the atmosphere itself (and

attenuated by the atmosphere above its source)

Equation (2.9) can be simplified by introducing the defining equation for the fractional transmittance $\tau(\nu,p,\theta)$ between level p and the top of the atmosphere :

$$\tau(\nu,p,\theta) = \exp\left[-\frac{1}{g}\int_0^p k(\nu,p')q(p')\sec\theta\, dp'\right] \qquad \ldots (2.10)$$

On substituting equation (2.10) into equation (2.9) the result is :

$$I(\nu,\theta) = B\left[\nu,T(p_o)\right]\tau(\nu,p_o,\theta) - \int_1^{\tau(\nu,p_o\theta)} B\left[\nu,T(p)\right]d\tau(\nu,p,\theta) \qquad \ldots (2.11)$$

Therefore, if the stated assumptions for equations (2.6) and (2.9), of

(i) a plane parallel stratified atmosphere,

(ii) local thermodynamic equilibrium,

(iii) a black lower boundary, and

(iv) no scattering agents,

are appropriate, then the radiance at the top of the atmosphere depends only upon the temperature variation of the absorber with altitude; given that the atmospheric transmittance is known for the particular absorber (which must be uniformly mixed with altitude), and θ is constant. Assumption (iii) above used in solving equation (2.8) merely implies that the lower boundary is at ground level and has an emissivity equal to unity. This assumption will most probably not be true if the lower boundary is a land surface as opposed to a sea surface, where the assumption is approximately correct (see Houghton and Taylor (1973)).

2.2.2 Instrumental Considerations

The measurement characteristics of the satellite radiometer must be incorporated into the solution of the radiative transfer equation, ie equation (2.11). For then the relationship between the actual radiance from the 15μm absorption band reaching the top of the atmosphere, and the satellite radiometer measurements may be determined.

If the satellite radiometers measure radiation from a narrow cone in the local vertical, secθ varies only slightly over the field of view of each radiometer. Consequently the value of secθ at the centre of the field may be used to represent the entire field. For nadir observations secθ = 1.

The radiance at the top of the atmosphere at a particular spectral wavelength is given by equation (2.11). However, for any realistic instrument, the finite width of the spectral interval being observed requires an appropriate integration over the wavelength response of the instrument. For the Selective Chopper (filter type) Radiometers (henceforth, SCR's) the measured radiance for the i^{th} filter is just :

$$I(\nu_i,0) = \int_0^\infty I(\nu,0) f_i(\nu) d\nu \Big/ \int_0^\infty f_i(\nu) d\nu$$

$$= \Bigg[\int_0^\infty B\left[\nu,T(p_o)\right] \tau(\nu,p_o,0) f_i(\nu) d\nu \; - \int_0^\infty \int_1^{\tau(\nu,p_o,0)} B\left[\nu,T(p)\right] f_i(\nu) d\tau(\nu,p,0) d\nu \Bigg] \Big/ \int_0^\infty f_i(\nu) d\nu \qquad \ldots (2.12)$$

where $f_i(\nu)$ is the frequency dependent part of the optical transmission characterising the response of the i^{th} radiometer channel.

The Nimbus 4 (and5) SCR's are really a cluster of radiometers, each member of the cluster measuring the radiance from the 15μm band over a different wavenumber interval. Each of the radiometers which make up the SCR will be considered to be a "channel" of the SCR. In the work that follows the term channel, when used, should be regarded as being synonymous to the term radiometer.

If the spectral interval over which $f_i(\nu)$ is non zero is small, then the Black Body function $B\left[\nu,T(p)\right]$ varies little and is nearly linear in the interval (Elsasser (1938)). Hence $B\left[\nu,T(p)\right]$ may be factored out of the ν integral for a suitably chosen mean frequency

$\bar{\nu}_i$. Further if the height variable, pressure p is transformed to the variable y where

$$y \equiv - \ln(p) \qquad \ldots (2.13)$$

then equation (2.12) may be written :

$$I(\bar{\nu}_i,0) = B[\bar{\nu}_i,T(p_o)]\,\tau(\bar{\nu}_i,p_o,0) - \int_{\infty}^{-\ln p_o} B[\bar{\nu}_i,T(y)]\frac{d\tau}{dy}(\bar{\nu}_i,y,0)\,dy \qquad \ldots (2.14)$$

where $$\tau(\bar{\nu}_i,p,0) = \frac{\int_0^{\infty}\tau(\nu,p,0)f_i(\nu)\,d\nu}{\int_0^{\infty} f_i(\nu)\,d\nu}, \qquad \ldots (2.15)$$

and $$\frac{d\tau}{dy}(\bar{\nu}_i,y,0) = \frac{\int_0^{\infty}\left(\frac{d\tau}{dy}(\nu,y,0)\right)f_i(\nu)\,d\nu}{\int_0^{\infty} f_i(\nu)\,d\nu} \qquad \ldots (2.16)$$

Generally $$K_i \equiv \frac{d\tau}{dy}(\bar{\nu}_i,y,0) \qquad \ldots (2.17)$$

where K_i is called the "weighting function" for the i^{th} channel of the SCR. The equivalent square bandwidth for the i^{th} channel, $\Delta\bar{\nu}_i$ is defined by the equation

$$\Delta\bar{\nu}_i = \int_0^{\infty} f_i(\nu)\,d\nu \qquad \ldots (2.18)$$

If the radiometer (of the SCR) has an entrance apature $A_i(m^2)$, an angular field of view $\Omega(sr)$, and if all other frequency independent constants combine to form the single constant α_i, then the quantity recorded by the i^{th} radiometer will be $F(\bar{\nu}_i,0)$ where

$$F(\bar{\nu}_i,0) = A_i\Omega_i\alpha_i(\Delta\bar{\nu}_i)\{B[\bar{\nu}_i,T(p_o)]\,\tau(\bar{\nu}_i,p_o,0) - \int_{\infty}^{-\ln p_o} B[\bar{\nu}_i,T(y)]\,K(y)\,dy\} \qquad \ldots (2.19)$$

SEE ERRATA

or equivalently $$F(\bar{\nu}_i,0) = A_i\Omega_i\alpha_i(\Delta\bar{\nu}_i)I(\bar{\nu}_i,0) \qquad \ldots (2.20)$$

if no measurement error is included.

The response of the satellite borne SCR channels will depend upon the radiance from the atmosphere within the field of view. There will of course be noise contamination in the radiometer measurements. From the above details, and for the given assumptions the mathematical equation describing the measurement process is

$$I(\bar{\nu}_i,0) = \frac{F(\bar{\nu}_i,0)}{A_i\Omega_i\alpha_i(\Delta\nu_i)} = B[\bar{\nu}_i,T(p_o)]\tau(\bar{\nu}_i,p_o,0) - \int_{\infty}^{-\ln p_o} B[\bar{\nu}_i,T(y)]K(y)dy \qquad \text{SEE ERRATA}$$

$$\text{where } i = 1,2,\ldots,n \qquad \ldots (2.21)$$

The unit of radiance is the $mW(m)^{-2}(cm^{-1})^{-1}(sr)^{-1}$ which will be abbreviated r.u. The random error contamination in the satellite measurements is specified in the following way

$$I(\bar{\nu}_i,0) = I_T(\bar{\nu}_i,0) + \varepsilon_i \qquad i = 1,2,\ldots,n \qquad \ldots (2.22)$$

where

$I_T(\bar{\nu}_i,0)$ is the "true" radiance in the given frequency window, if the atmosphere obeys the model specification of equation (3.9), and

ε_i is the random measurement error, introduced into the observation (of the model atmosphere) by the measurement process, equation (2.20)

Equation (2.21) may be written, on including equation (2.22), thus

$$I(\bar{\nu}_i,0) = B[\bar{\nu}_i,T(p_o)]\ \tau(\bar{\nu}_i,p_o,0) - \int_{\infty}^{-\ln p_o} B[\bar{\nu}_i,T(y)]K(y)dy + e_i \qquad \text{SEE ERRATA}$$

$$i = 1,2,\ldots,n \qquad \ldots (2.23)$$

where $I(\bar{\nu}_i,0)$ is to be interpreted as a real physical measurement, and

e_i is some (assumed) random "error" which includes the random error introduced by taking the measure-

ment, ε_i, plus the contribution from all unmodelled proscesses(in equation 2.6).

Equation (2.23) is equivalent in form to equation (2.1), apart from an additional constant on the right hand side (of equation (2.23)). All that remains in order to solve the specification problem completely, is to give a description of the error statistics and the domain of $B[\bar{\nu}_i, T(y)]$.

It will be assumed that the "measurement" errors e_i for each radiometer channel are independent random variables with mean values equal to zero and Gaussian statistics. Since the statistics are assumed Gaussian a probability density function (pdf) may be simply written for the errors e_i, $i = 1,2,\ldots,n$ (which will be thought of as forming an $(n \times 1)$ dimensional vector $\underline{e}$). The covariance of $\underline{e}$ is just S_e;

$$S_e = E\{\underline{e}^T\underline{e}\} \qquad \ldots (2.24)$$

and

$$P(\underline{e}) = (2\pi^n |S_e|)^{-\frac{1}{2}} \exp(-\tfrac{1}{2}\underline{e}^T S_e \underline{e}) \qquad \ldots (2.25)$$

where $|S_e|$ is the determinant of S_e and

$P(\underline{e})$ is the probability of $\underline{e}$

As regards the domain of $B[\bar{\nu}_i, T(y)]$, clearly $T(y)$ cannot be negative. Perhaps the domain of $B[\bar{\nu}_i, T(y)]$ could be constrained more tightly by only permitting $T(y)$ to lie within the envelope of largest known deviations from some accepted model atmosphere temperature profile, for example, the US Standard Atmosphere 1976.

2.2.3 Summary Remarks

It is important to note that the step from equation (2.22) to equation (2.23) is not trivial. Equation (2.22) is the radiance that would be measured by a radiometer looking at the model atmosphere described by equation (2.6), whereas equation (2.23) is the radiance measured by a radiometer looking at the real atmosphere. Therefore justification of the assumptions relating to the values of e_i (in equation (2.23)) is important.

Bishof and Bolin (1966) and Georgii and Jost (1969) suggest that CO_2 is uniformly mixed with height to approximately 90 km. Houghton (1969) claims that CO_2 is in local thermodynamic equilibrium up to the same height. Accordingly, in the real atmosphere it will be assumed that up to at least 60 km the absorber CO_2 is uniformly mixed, and is in local thermodynamic equilibrium.

On the problem of the emissivity of the lower boundary, Kornfield and Susskind (1977) quoting from Kondrat'yev (1969), Buettner and Kern (1965), and Hovis (1966) indicate that the land's surface emissivity may differ appreciably from unity. However Houghton and Taylor (1973) indicate that the emissivity of a sea surface lower boundary is, to a good approximation, unity. Konfield and Susskind (1977) have studied the bias that would be introduced by always using a unit emissivity for the lower boundary in the retrieval problem. They find that the temperature bias will be greatest at the surface, but decreases with altitude. Assuming the ground's emissivity is unity over a sea surface is a good approximation, but for retrievals over a land surface unit emissivity will introduce errors at worst as large as $3C^0$ into the retrieved ground and lower atmosphere temperatures (ie those heights for which the corresponding sounder channel's ground transmittences, $\tau(\bar{\nu}_i, p_o, 0)$ are non zero).

Problems arising from not allowing scattering agents (eg clouds) in the model atmosphere of equation (2.6) will result in a measured radiance which is always less than the radiance for the "true" cloudless atmosphere (Barnett et al (1975). The unmodelled "error" due to clouds may be random but will not have a mean of zero. Barnett et al (1975) have suggested a data declouding process. This procedure is designed to detect sudden falls in signal due to clouds, and to interpolate over the low signal regions, thus constructing an envelope curve which is called the "declouded" signal. This procedure has been applied to all radiance data to be used for temperature retrievals.

The problem of scattering agents in the real atmosphere will be greatly reduced through the "declouding" of the satellite measured data. However should cloud problems remain, it is to be expected that these problems will only affect those channels which sound the troposphere and therefore should not introduce large errors into retrieved temperature profiles for the stratosphere.

The questions involved with the instrumental assumptions introduced in Section 2.2.1 will have little effect on the measured radiances. These effects will however be considered in Section 2.3.

Therefore in conclusion, the assumptions involved in equation (2.23) are reasonable. It may be expected that the "errors" introduced into the radiance data by the measuring and declouding processes and arising from unmodelled atmospheric processes will be small for soundings over the sea surface. For soundings over the land surface, an effective emissivity should be included in the ground term (first term on the right hand side of equation (2.23)) of equation (2.23).

2.3 : THE DIRECT PROBLEM

As stated in section 2.1, for the retrieval problem to be solvable a method must be provided for evaluating the operation of the operator f which maps the parameters x into the data space (equation 2.1)). From Section 2.2 the function f of equation (2.1) is identified as the weighting function of equation (2.23).

2.3.1 Theoretical Considerations

The weighting function $K_i(y)$ (of equation (2.23)) is the gradient of the mean transmittance $\tau(\bar{\nu}_i, y, 0)$, hence

$$f = K_i(y) = \frac{d\tau}{dy}(\bar{\nu}_i, y, 0) \qquad \ldots (2.26)$$

where

$$\tau(\bar{\nu}_i, y, 0) = \frac{\int_0^\infty \exp\left[-\frac{1}{g}\int_0^y k(\nu, y')q(y')\sec\theta\, dy'\right] f_i(\nu)\, d\nu}{\int_0^\infty f_i(\nu)\, d\nu} \qquad \ldots (2.27)$$

and $k(\nu,y')$ is the mass absorption coefficient (of the absorbing gas) at frequency ν and pressure $(-p_o \exp(y'))$

For a single collision broadened spectral line of strength s centred at frequency ν_0, the absorption coefficient $k(\nu,p)$ for a path at pressure p is given by the ralation

$$k(\nu,p) = \frac{s\gamma_0 p\pi^{-1}}{(\nu-\nu_0)^2 + \gamma_0^2 p^2} \qquad \ldots (2.28)$$

where γ_0 is the line width at 1 atm pressure (Houghton and Smith (1970)). If the optical characteristics of the radiometer(s), detailed spectral information regarding line position, intensities, widths and shapes for the emmiting gas CO_2 are known, then numerical integration over frequency in equation (2.27) may be performed and $K_i(y)$ found. Unfortunately since there are uncertainties in the widths, positions, intensities, shapes of spectral lines and filter profiles, the calculated weighting functions (using equations (2.26) and (2.27)) are not sufficiently accurate for good temperature retrievals (Barnett et al (1972)). An empirical correction method for the calculated transmissions is needed.

The procedure used to determine the "actual" weighting functions is as follows :

(a) Use the actual satellite radiometer(s) to measure the transmission through a synthetic atmosphere at at varying gas pressures (see Abel (1966) and Barnett et al (1972))

(b) Use equation (2.27) to calculate the theoretical transmissions of the gases of the synthetic atmosphere under the laboratory conditions

(c) From the differences between the results of (a) and (b) above determine an empirical correction factor to be applied to the theoretical calculations.

(d) Apply the correction factor to the theoretical calculations of the radiometer transmission functions under atmospheric conditions.

A good estimate of the function $K_i(y)$ may be determined.

The absorption coefficient $k(\nu,p)$ varies rapidly with frequency therefore different frequencies possess weighting functions peaking at different altitudes. If a set of n frequency intervals is chosen such that the corresponding weighting functions each peak at different heights, then remote sensing over a range of altitudes is possible. Radiation from the wings of the absorption band will originate near the lower boundary (since $k(\nu,p)$is small at these frequencies) whereas radiation from the centre of the absorption band will originate near the top of the atmosphere ($k(\nu,p)$ is large at these frequencies).

2.3.2 : Principles of Selective Absorption

The infra-red emission from the ν_2 band of CO_2 at 15μm contains many lines with widths varying from 0.1 cm^{-1} to 0.001 cm^{-1} for the range of atmospheric pressures involved. The resolution of conventional satellite radiometers is such that they are unable to resolve details of the structure near the line centres (ie the spectral regions where the absorption is high) corresponding to soundings of high altitudes. In order to construct a radiometer which would have sufficient resolution to measure the structure of the line centres Smith and Pidgeon (1964) suggested that a cell of CO_2 (at some pressure) be used to filter the incoming radiation. This enables radiation to be selected from regions where the absorption coefficient has a given value in the vicinity of many lines in the band (see Peckham et al (1967)). This type of radiometer has high spectral resolution (of the order of 0.1 cm^{-1}) and reasonably good energy grasp since radiation is collected from many lines.

Peckham et al (1967) shows that for heights below approximately 30 km, a single selective absorbing cell of CO_2 is appropriate as a

filter. Between 30 km and 50 km, selective chopping between two such cells is required. To exclude radiation not near the frequency of interest, interference filters are used. A number of spectral channels can be obtained by constructing a set of separate filter radiometers.

Additional details on selective absorption, the selective chopper radiometer, choice of spectral intervals, the interference filters, optical system and calibration technique for the Nimbus 4 SCR are given in Abel et al (1970), Abel et al (1972) and Houghton and Smith (1970).

2.3.3 : The Nimbus 4 Weighting Functions

The Oxford University Selective Chopper Radiometer on board Nimbus 4 consists of six independent filter radiometers. The lower four channels utilize absorbing paths of CO_2 in order that these channels will not be sensitive to radiation originating near the centres of the absorption lines. The upper two channels are obtained by optically chopping the incoming radiation between two cells; one containing CO_2, the other being empty (channel A) or containing CO_2 at low pressure (channel B).

The satellite weighting function curves used for this work are those given by Barnett et al (1972) and are illustrated in Figure 4. In the calculations of these curves Barnett et al (1972) assumed :

(i) that the humidity is everywhere 70% in the troposphere, and

(ii) that the ozone amount is fixed.

In the absence of analytic functions for the weighting function curves of Figure 4, the function values were digitized from a suitable photographic reproduction of the curves. Following this, analytic equations for the weighting function curves were generated from the digitized data by a non linear gradient expansion least squares function fitting program. The precision of the generated equations is equal to the error in the digitization, that is, ± 0.001 units on the abcissa scale of Figure 4.

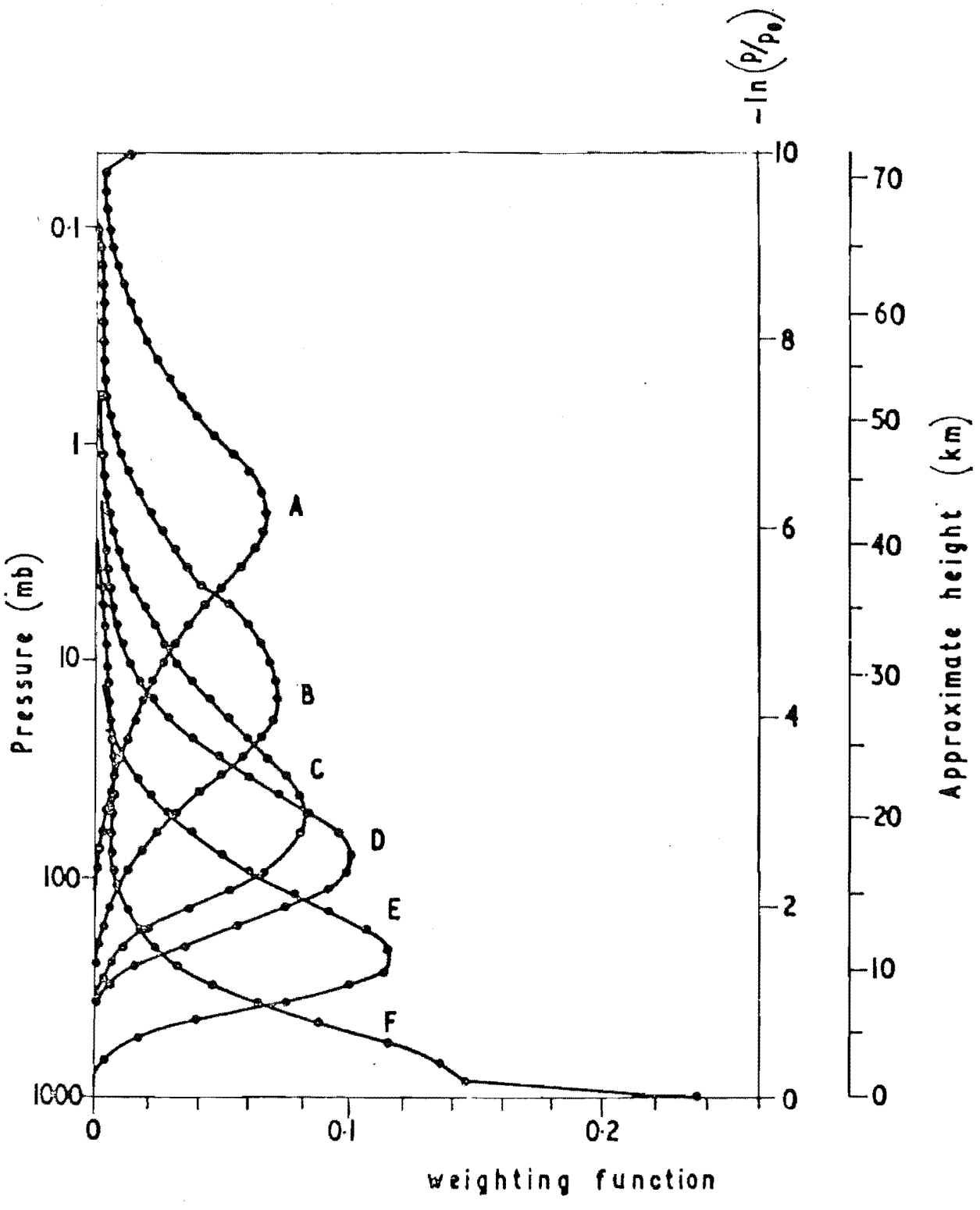

FIGURE 4 : The Nimbus 4 SCR Weighting Functions
(from Barnett et al (1972))

TABLE 1 : Nimbus 4 SCR Channel Details

Channel Designation	Number of Absorbing Cells	CO_2 cell Path Length (cm)	CO_2 cell Pressure (atm)	Filter Centre (cm^{-1})	Equivalent Square Bandwidth After Selective Absorption or Selective Chopping (cm^{-1})	Noise Equivalent Temperature ΔT_N For 1s Measurement (Note 1) (K)	Integration Time Required For $\Delta T_N \sim 1K$
A	2	1 1	0 0.05	668	1.35	7.1	50
B	2	1 1	0.05 0.20	668	1.3	3.5	12
C	1	7	0.03	668	3.9	1.5	2.3
D	1	7	0.20	673	3.2	0.71	0.5
E	1	7	0.60	695	3.2	0.38	0.15
F	1	7	1.0	728	5	0.52	0.27

NOTE 1 : Defined so that the r.m.s noise at the output is equivalent to the change in signal from a black body near 250K if its temperature changed by $\Delta T_N K$

The analytic fitting equations are presented in Appendix A. Details of the Nimbus 4 SCR channels are given in Table 1 (from Abel et al (1970).

2.4 : THE MATHEMATICAL PROBLEM

For a given set of declouded radiance observations, equation (2.23) must be solved in the "mathematical sense" so that the operator h of equation (2.2) can be found and the unknown function $B[\bar{\nu}_i, T(y)]$ determined.

Equation (2.23) is non linear and cannot be solved analytically. The equation must be linearized. In Section 2.4.1 consideration is given to the problems of linearizing (and discretizing) equation (2.23).

As noted in Section 2.1(3) there are three approaches available when solving the inversion problem, equation (2.23). However, it can be shown that in all problems involving overlapping weighting functions the "exact" method of equation (2.4) is highly sensitive to observation noise owing to the ill-conditioned nature of equation (2.23). In fact, the "exact" solution's sensitivity to data noise is unacceptably large (Rodgers (1976b)). For completeness, the nature of the ill-conditioning of equations like equation (2.23) is considered in Section 2.4.2. Rodgers (1976b) states :

> "there is clearly no logical reason for us to try to find an exact solution. We can only reasonably require that the solution be within the experimental error of the measurements."

To determine the form of operator h in equation (2.2), for use in inverting equation (2.23), it is necessary to consider a number of intrinsic problems which arise owing to the nature of the satellite weighting functions and measurement errors (in equation (2.23)). There will be an infinite manifold of solutions which satisfy equation (2.23). No unique solution may be found for $B[\bar{\nu}_i, T(y)]$ for the following reasons:

(i) There is noise in the radiometer measurements and therefore a non uniqueness in the original observations.

(ii) The problem is ill-conditioned since there are components of the atmospheric temperature profile which make no contribution to the quantities measured by the radiometers.

(iii) The weighting functions overlap, thus implying a lack of vertical independence for the set of observations.

(Reasons (ii) and (iii) above are not entirely independent since the two effects are interconnected). Four problems must be considered in determining an "inversion operator" for equation (2.23):

(i) the inversion of the integral equation of radiature transfer (equation (2.23)).

(ii) as (i) above is an ill-conditioned problem, no mathematically unique solution (as indicated above) can be found. A meteorologically "best" or most likely solution must be found.

(iii) the confidence regions for the estimated "best" solution must be determined, and finally

(iv) the resolving power of the estimator must be established.

These aspects of the inversion problem will be considered in Sections 2.4.3 through 2.4.7. Finally, a convenient and concise method for representing the retrieved temperature profiles will be considered in Section 2.4.8.

2.4.1 Linearization of the Specification Equation

Consider the specification equation (that is, equation (2.23)).

$$I(\bar{\nu}_i,0) = B[\bar{\nu}_i,T(p_o)]\ \tau(\bar{\nu}_i,p_o,0) - \int_{\infty}^{-\ln p_o} B[\bar{\nu}_i,T(y)]\frac{d\tau}{dy}(\bar{\nu}_i,y,0)dy + e_i \qquad i = 1,2,\ldots,n \qquad \ldots (2.23)$$

If the $\bar{\nu}_i$, $i = 1,2,\ldots,n$ for each channel of the radiometer are not too dissimilar in magnitude then equation (2.23) may be linearized by selecting a suitable mean wavenumber $\bar{\nu}$ of the $\bar{\nu}_i$. The resulting effects due to this method of linearization of equation (2.23) can be considered by expanding the black body function in a Taylor series about the mean frequency $\bar{\nu}$, thus :

$$B[\bar{\nu}_i,T(y)] = B[\bar{\nu},\ T(y)] + \frac{dB}{d\nu}[\bar{\nu},\ T(y)]\ (\bar{\nu}_i - \bar{\nu}) + \ldots (2.29)$$

On substituting this equation into equation (2.23)

$$I(\bar{\nu}_i,0) = B[\bar{\nu}_i,T(p_o)]\ \tau(\bar{\nu}_i,p_o,0) - \left\{\int_{\infty}^{-\ln p_o} B[\bar{\nu},T(y)]\ \frac{d\tau}{dy}\,dy + \int_{\infty}^{-\ln p_o}(\bar{\nu}_i - \bar{\nu})\frac{dB}{d\nu}[\bar{\nu},T(y)]\ \frac{d\tau}{dy}\,dy\right\} + e_i \qquad \ldots (2.30)$$

when neglecting all terms of order $(\bar{\nu}_i-\bar{\nu})^2$ and higher.

The third term on the right hand side of equation (2.30) may be regarded as a radiance "correction" term. Let $T(y) = \bar{T}(y)$ in this term (where $\bar{T}(y)$ is some mean atmospheric temperature profile), the equation (2.30) may be written :

$$I(\bar{\nu}_i,0) = B[\bar{\nu}_i,\ T(p_o)]\tau(\bar{\nu}_i,p_o,0) - \left\{\int_{\infty}^{-\ln p_o} B[\bar{\nu},T(y)]\ \frac{d\tau}{dy}\,dy + (\bar{\nu}_i - \bar{\nu})\int_{\infty}^{-\ln p_o}\frac{dB}{d\nu}[\bar{\nu},\bar{T}(y)]\frac{d\tau}{dy}\,dy\right\} + e_i$$

$$i = 1,2,\ldots,n \qquad \ldots (2.31)$$

Since all quantities in the correction term

$$(\bar{\nu}_i-\bar{\nu})\int_{\infty}^{-\ln p_o}\frac{dB}{d\nu}[\bar{\nu},\bar{T}(y)]\ \frac{d\tau}{dy}\,dy \qquad \ldots (2.32)$$

are constants, it may be regarded as a channel ($\bar{\nu}_i$) dependent term which can be evaluated for each channel for a given function $\bar{T}(y)$. Rodgers (1970) indicates that this term (equation (2.32)) may be neglected for the SCR instruments. Therefore on linearization about the $\bar{\nu}$,

$$B[\bar{\nu}_i, T(y)] = B[\bar{\nu}, T(y)] \quad \ldots (2.33)$$

For succinctness let

$$B[T(y)] \equiv B[\bar{\nu}, T(y)] \quad \ldots (2.34)$$

and the linearized form of equation (2.23) has

$$I(\bar{\nu}_i, 0) = B[\bar{\nu}_i, T(p_o)]\, \tau(\bar{\nu}_i, p_o, 0) - \int_{\infty}^{-\ln p_o} B[T(y)]\, K_i(y)\, dy + e_i \quad \ldots (2.35)$$

Alternatively, equation (2.23) could be linearized by taking the Taylor expanison of $B[\bar{\nu}_i, T(y)]$ about some mean profile $\bar{T}(y)$. Neglecting all non-linear terms:

$$I(\bar{\nu}_i, 0) = B[\bar{\nu}_i, T(p_o)]\, \tau(\bar{\nu}_i, p_o, 0) - \left\{ \int_{\infty}^{-\ln p_o} (T-\bar{T})(y)\, \frac{dB}{dT}[\bar{\nu}_i, \bar{T}(y)] \cdot \frac{d\tau}{dy}(\nu, y, 0)\, dy + \int_{\infty}^{-\ln p_o} B[\bar{\nu}_i, \bar{T}]\, \frac{d\tau}{dy}(\bar{\nu}_i, y, 0)\, dy \right\} + e_i \quad \ldots (2.36)$$

and if

$$\bar{I}(\bar{\nu}_i, 0) \equiv \int_{\infty}^{-\ln p_o} B[\bar{\nu}_i, \bar{T}]\, \frac{d\tau}{dy}(\bar{\nu}_i, y, 0)\, dy \quad \ldots (2.37)$$

then

$$I(\bar{\nu}_i, 0) - \bar{I}(\bar{\nu}_i, 0) = B[\bar{\nu}_i, T(p_o)]\, \tau(\bar{\nu}_i, p_o, 0) -$$

$$\int_{\infty}^{-\ln p_o} (T-\bar{T})(y)\frac{dB}{dT}[\bar{\nu}_i,\bar{T}(y)]\ K_i(y) + e_i$$

$$i = 1,2,\ldots,n \qquad \ldots (2.38)$$

where equation (2.38) is an alternative linearized form of equation (2.23), and the "weighting" functions are temperature dependent.

The first term on the right hand side of equation (2.35) is a constant for each channel and given ground temperature $T(p_o)$. This term does not contribute to the problem of inverting equation (2.35) in order to determine $B[T(y)]$. Formally it may be neglected in what follows since the term is incorporated as a "correction" term on the declouded measured radiances $I(\bar{\nu}_i,0)$, $i = 1,2,\ldots n$. Therefore, let

$$I(\bar{\nu}_i,0) = -\int_{\infty}^{-\ln p_o} B[T(y)]\,K_i(y)\,dy + e_i$$

$$i = 1,2,\ldots,n \qquad \ldots (2.39)$$

The retrieval problem (equation (2.39) is more easily solved using the algebra of matrices rather than the algebra of Hilbert space. Accordingly, equation (2.39) is expressed in a discrete form through discretization of the continuous functions $B[T(y)]$ and $K_i(y)$, and replacement of the integral by a suitably weighted matrix multiplication. Using matrix algebra, equation (2.39) may be written

$$\underline{y} = K\underline{x} + \underline{e} \qquad \ldots (2.40)$$

where

$\underline{y}$ is an (nxl) dimensional vector of the n measured radiances $(I(\bar{\nu}_i,0))$ for an observation, (NB, not the scalar height variable, y of equation (2.39))

$\underline{x}$ is the (pxl) dimensional vector of the unknown profile $B[T(y)]$, to be estimated,

K is an (nxp) dimensional matrix and

$\underline{e}$ is the (nxl) dimensional vector of measurement errors.

The elements of the matrix K are just

$$K_{ij} = hK_i(jh) \qquad \ldots (2.41)$$

where

h is the tabulation interval in the vertical

i refers to the i^{th} weighting function, and

j refers to the j^{th} level of discretization (jh is the altitude (interms of $-\ln(p/p_o)$), at level j).

The equation to be inverted by the inversion procedure is just equation (2.40) above.

Finally, it is convenient to define the true radiance $\underline{y}'$ that would be measured by a perfect SCR looking at the model atmosphere of equation (2.6):

$$\underline{y}' = K\underline{x} \qquad \ldots (2.42)$$

Equation (2.40) above is just a discrete, linearized form of equation (2.1).

2.4.2 Nature of Ill-Conditioning in Specification Equation

It has been stated that equation (2.40) is ill-conditioned (since this equation is just the linearized and discretized form of equation (2.23)) with the result that no unique solution for $\underline{x}$ may be found, given a set of radiance data $\underline{y}$. This non-uniqueness may be demonstrated by the following argument (which follows Jackson (1978)).

Given equation (2.40), assume that there exists an estimate $\hat{\underline{x}}$ (of $\underline{x}$) defined by some linear operation H (the estimator) on $\underline{y}$, thus

$$\hat{\underline{x}} = H\underline{y} \qquad \ldots (2.43)$$

The estimator's residuals are:

$$\hat{\underline{x}} - \underline{x} = HK\underline{x} - \underline{x} + H\underline{e}$$

or

$$\hat{\underline{x}} - \underline{x} = (HK - I)\underline{x} + H\underline{e} \qquad \ldots (2.44)$$

since $\underline{y} = \underline{y}' + \underline{e}$ as defined by equations (2.42) and (2.40). Further, assume that the "errors" in the estimate are random with zero mean and therefore are unbiased. The first term on the right hand side of equation (2.44) is zero. Equivalently, $\hat{\underline{x}}$ is the "exact" solution of the inverse problem since $\hat{\underline{x}}$ is unique and the residuals, $\underline{r}$:

$$\underline{r} = \underline{y} - K\hat{\underline{x}} \qquad \ldots (2.45)$$

must be equal to the random "measurement" errors $\underline{e}$

Hence :

$$HK\underline{x} = \underline{x}, \qquad \ldots (2.46)$$

so that equation (2.44) may be written

$$\hat{\underline{x}} - \underline{x} = H\underline{e} \qquad \ldots (2.47)$$

The probability density function (henceforth pdf) for the data errors maps directly onto the pdf for the estimation errors.

The pdf of a vector of random variables can be described in terms of a vector of means and a covariance matrix. If the vector of measurement errors $\underline{e}$ has zero mean (as assumed) and covariance matrix S_e, then the covariance matrix for the estimation errors is just :

$$\mathrm{cov}(\hat{\underline{x}} - \underline{x}) = E\{(\hat{\underline{x}} - \underline{x})(\hat{\underline{x}} - \underline{x})^T\} \qquad \ldots (2.48)$$

where $E\{\cdot\}$ is the expectation of $\{\cdot\}$. Then

$$\mathrm{cov}(\hat{\underline{x}} - \underline{x}) = E\{H\,\underline{e}\,\underline{e}^T H^T\}$$

$$= H\,S_e H^T$$

since $S_e = E\{\underline{e}\,\underline{e}^T\}$.

So if,

$$S_{\hat{x}} \equiv \text{cov}\ (\hat{\underline{x}} - \underline{x}) \qquad \ldots (2.49)$$

then $$S_{\hat{x}} = H\, S_e H^T \qquad \ldots (2.50)$$

$S_{\hat{x}}$ is the covariance matrix for the estimator errors.

If the data errors are Gaussian the pdf for the data errors is :

$$p(\underline{e}) = (2\pi^n |S_e|)^{-\frac{1}{2}} \exp(-\tfrac{1}{2}\underline{e}^T S_e^{-1} \underline{e}) \qquad \ldots (2.51)$$

where $|S_e|$ is the determinant of the matrix S_e and n is the dimension of the vector $\underline{y}$ (and $\underline{e}$).

The solution for $\underline{x}$ determined from equation (2.43) may be "checked" by calculating the residuals, $\underline{r}$, (of equation (2.45)) and substituting these for $\underline{e}$ in equation (2.51). However, since the solution vector $\hat{\underline{x}}$ (and therefore the estimator H) only enters equation (2.51) via the relation :

$$L(\hat{\underline{x}}) = \underline{r}^T S_e^{-1} \underline{r} \qquad \ldots (2.52)$$

the value of the loss function $L(\hat{\underline{x}})$ is a measure of the accuracy of the estimated solution $\hat{\underline{x}}$.

In order to procede further with the analysis, the form of the operator H must be given. For the stated conditions on the estimator and observation errors, the Gauss Markov theorem (Beck and Arnold (1977) may be applied to give the form for the minimum variance unbiased estimator H :

$$H = (K^T S_e^{-1} K)^{-1} K^T S_e^{-1} \qquad \ldots (2.53)$$

and

$$\hat{\underline{x}} = (K^T S_e^{-1} K)^{-1} K^T S_e^{-1} \underline{y} \qquad \ldots (2.54)$$

The matrix $(K^T S_e^{-1} K)$ cannot be singular. Define

$$N \equiv (K^T S_e^{-1} K) \qquad \ldots (2.55)$$

where N is called the normal matrix.

In order to understand the uniqueness or non-uniqueness of the estimated solution profile $\underline{\hat{x}}$, the condition of matrix N must be considered. If the matrix N is singular, or nearly singular then the 'singularity' can be investigated by examining the eigenvalues of matrix N. If some or all of the eigenvalues of N vanish, then N is a singular matrix. If this is so, it will be shown that no unique solution $\underline{\hat{x}}$ for the inverse problem can be found. To demonstrate this point consider an eigenvector $\underline{l}_i$ of matrix N associated with eigenvalue λ_i^2. Then :

$$N\underline{l}_i = \lambda_i^2 \underline{l}_i \qquad \ldots (2.56)$$

(i.e. N must be non-negative definite). Further, consider a "perturbation" on the solution vector $\underline{\hat{x}}$ such that

$$\underline{x}' = \underline{\hat{x}} + \Delta \underline{l}_i \qquad \ldots (2.57)$$

where $\underline{x}'$ is the pertubed solution profile,

$\underline{\hat{x}}$ is the "exact" solution and

Δ is some arbitrary scalar,

then

$$L(\underline{x}') = \underline{r}^T S_e^{-1} \underline{r} \qquad \ldots (2.58)$$

$$= [K(\underline{\hat{x}} - \underline{x})]^T S_e^{-1} K(\underline{\hat{x}} - \underline{x}) + [K\Delta \underline{l}_i]^T S_e^{-1} K\Delta \underline{l}_i$$

$$= L(\underline{\hat{x}}) + \Delta^2 \underline{l}_i^T K^T S_e^{-1} K \underline{l}_i$$

$$= L(\underline{\hat{x}}) + \Delta^2 \underline{l}_i^T N \underline{l}_i$$

$$= L(\underline{\hat{x}}) + \Delta^2 \lambda_i^2 \underline{l}_i^T \underline{l}_i$$

$$\therefore \quad L(\underline{x}') = L(\underline{\hat{x}}) + \Delta^2 \lambda_i^2 \qquad \ldots (2.59)$$

(since the eigenvectors of N are orthonormal).

Consequently if λ^2 is small, the loss function $L(\underline{x}')$ is rather insensitive to the size of the perturbation. However, should $\lambda_i^2 = 0$ then any vector $\Delta \underline{l}_i$ (Δ a real number) may be added to the "exact" solution $\hat{\underline{x}}$ without changing the value of the loss function $L(\underline{x}')$. Under these circumstances the estimated solution vector is not unique since any solution vector, chosen under the conditions of equation (2.57) is "correct" in the mathematical sense (i.e. $L(\underline{x}')$ does not change).

It is evident from this simple argument, that should the normal matrix be singular or nearly singular, that is the inversion problem is at best poorly conditioned, then for any given data set ($\underline{y}$) no unique solution for the vector $\underline{x}$ of equation (2.40) can be found. Consequently for a given set of declouded radiance data the problem of inverting equation (2.40) cannot be solved.

Equation (2.40) can only be solved if it is "transformed" to a well-conditioned form. This transformation process is called regularization. Regularization implies that a priori (or virtual) data (information) must be "included" so that the inversion problem will be well-conditioned and therefore solvable. Since a priori data is added to equation (2.40) only a "best" or most likely solution for $\underline{x}$, consistant with both sets of data may be found. Also, it may be expected that the resultant estimator H will be a biased estimator since the a priori data may not have zero mean values.

In the case of the equation of radiative transfer (equation 2.23) and hence equation (2.40)) as applied to the SCR radiometers of Nimbus 4, the inversion problem is poorly conditioned since the weighting functions overlap. A priori data must be used in order to determine good retrievals of temperature profiles through inversion of equation (2.23). The method that will be used here is due to Rodgers (1970,1971,1976b) but the development follows that of Beck and Arnold (1977).

The approach to the inversion problem here, is that of section 2.1(3(ii)).

2.4.3 The Maximum A Posteriori Estimator

From Section 2.4.2 above it is evident that there are components in the atmospheric temperature profile which may not contribute to the quantities measured by the SCR radiometers. For example (from equation (2.40)), any function orthogonal to the weighting functions may be added to the temperature profile without altering the measured SCR radiances. These components are unmeasureable and must be estimated from the additional a priori data.

Maximum a Posteriori (henceforth MAP) estimation utilizes prior information regarding the atmospheric temperature structure in addition to the information contained in the satellite measurements and the statistics of the data errors.

The equation to be inverted, equation (2.40), is a linear equation, and in order to retain the linear nature of the inversion problem (i.e. determine a linear estimator), the a priori information must also be expressed in a linear form. A suitable form for the a priori data is the value of a known linear function of the temperature profile together with an error covariance matrix for this function. Accordingly there are two sets of input data for the inversion problem:

(i) The set of declouded satellite radiance measurements and,

(ii) the set of a priori data, consisting of a vector $\bar{\underline{x}}$ a mean profile for atmospheric temperature and the associated atmospheric temperature covariance matrix.

The data sets are independent with the first being small and relatively noise free, and the second being large but "noisey". To sum-

marize, the inversion (retrieval) procedure requires that these two independent data sets be combined in such a way that the inversion problem is well-conditioned and the estimated retrieval for the unknown vector $\underline{x}$, (the estiamte) is meteorologically the "best" or most likely consistant with all available data. To this end, a Bayesian approach will be used (although, this is not the only approach that will produce the MAP estimator, for example, see Rodgers (1976b), and Deutsch (1965)).

For MAP estimation, the estimated atmospheric temperature profile (simply, the profile vector) is the vector that maximises the conditional probability density function (henceforth cpdf) $f(\underline{y}|\underline{x})$. This cpdf is related to $f(\underline{x}|\underline{y})$ and that for the random atmospheric temperature vector $f(\underline{x})$ by Bayes' Theorem. Thus

$$f(\underline{x}|\underline{y}) = \frac{f(\underline{y}|\underline{x})\ f(\underline{x})}{f(\underline{y})} \qquad \ldots (2.60)$$

where

$f(\underline{x}|\underline{y})$ is the cpdf of $\underline{x}$ given $\underline{y}$,

$f(\underline{y}|\underline{x})$ is the cpdf of $\underline{y}$ given $\underline{x}$,

$f(\underline{x})$ is the pdf of the atmospheric temperature profiles, and

$f(\underline{y})$ is the pdf of the satellite measurements

If the elements e_i of vector $\underline{e}$ ($i = 1,2,\ldots,n$) in equation (2.40) are additive, with zero mean and are normally distributed with known covariance, then the cpdf $f(\underline{y}|\underline{x})$ is a Gaussian mutlivariate pdf and may be written :

$$f(\underline{y}|\underline{x}) = (2\pi^n|S_e|)^{-\frac{1}{2}} \exp\left[-\tfrac{1}{2}(\underline{y}-\underline{y}')^T S_e^{-1}(\underline{y}-\underline{y}')\right] \qquad \ldots (2.61)$$

where

n is the number of satellite measurements for each observation and

S_e is the covariance matrix of the "measurement" errors $\underline{e}$

Assume that the temperature profile to be retrieved i.e. $\underline{x}$ (by the inversion procedure) is a random variable with known mean value $\bar{\underline{x}}$ and covariance matrix S_x, and that its pdf is Gaussian.

The values of $\bar{\underline{x}}$ and S_x are obtained from suitable seasonal and latitudinal balloonsonde and rocketsonde data as will be described in Section 2.4.5. Rodgers (1970) reports that examination of the available data indicates that the statistics for the whole Earth and all seasons are by no means Gaussian. However, the temperatures for smaller regions in space and time do behave in a Gaussian way, to a good approximation. The pdf for a temperature profile $\underline{x}$ may be expressed thus :

$$f(\underline{x}) = (2\pi^p |S_x|)^{-\frac{1}{2}} \exp\left[-\tfrac{1}{2}(\underline{x}-\bar{\underline{x}})^T S_x^{-1} (\underline{x}-\bar{\underline{x}})\right] \quad \ldots (2.62)$$

where

S_x is the covariance matrix of a sample of atmospheric temperature profiles,

$\bar{\underline{x}}$ is the mean profile for the sample

$\underline{x}$ is any given profile, and

p is the dimension of the profile vector.

The pdf $f(y)$ need not be known since $f(\underline{x}|\underline{y})$ may be maximized by maximizing the numerator of equation (2.60).

Take natural logorithms of both sides of equation (2.60) :

$$\ln[f(\underline{x}|\underline{y})] = \ln[f(\underline{y}|\underline{x})\ f(\underline{x})] - \ln[f(y)] \quad \ldots (2.63)$$

The maximum of equation (2.63) with respect to the vector $\underline{x}$ may be found by finding the maximum of

$$\ln[f(\underline{x}|\underline{y})] = \ln[f(\underline{y}|\underline{x})\ f(\underline{x})] \quad \ldots (2.64)$$

The term $\ln[f(y)]$ is a constant in the maximization since it is not dependent upon the vector $\underline{x}$. Substituting equations (2.61) and (2.62)

into equation (2.64) :

$$\ln[f(\underline{x}|\underline{y})] = -\tfrac{1}{2}[(n+p)\ln 2\pi + \ln|S_e| + \ln|S_x| + S] \qquad \ldots (2.65)$$

where

$$S = (\underline{y}-\underline{y}')^T S_e^{-1}(\underline{y}-\underline{y}') + (\underline{x}-\bar{\underline{x}})^T S_x^{-1}(\underline{x}-\bar{\underline{x}}) \qquad \ldots (2.66)$$

and is the MAP equivalent of the loss function of equation (2.58). The loss function S is minimized with respect to $\underline{x}$, since this is equivalent to maximizing $\ln[f(\underline{x}|\underline{y})]$ in equation (2.63).

Substitute equation (2.42) into equation (2.66) thus :

$$S = \underline{y}^T S_e^{-1}\underline{y} - \underline{x}^T K^T S_e^{-1}\underline{y} - \underline{y}^T S_e K\underline{x} + \underline{x}^T K^T S_e^{-1} K\underline{x}$$

$$+ \underline{x}^T S_x^{-1}\underline{x} - \bar{\underline{x}}^T S_x^{-1}\underline{x} - \underline{x}^T S_x^{-1}\bar{\underline{x}} + \bar{\underline{x}}^T S_x^{-1}\bar{\underline{x}} \qquad \ldots (2.67)$$

The principle of MAP estimation asserts that an estimate of the elements of vector $\underline{x}$ will be obtained on minimizing equation (2.67) with respect to $\underline{x}$, that is by finding $\nabla_{\underline{x}} S = 0$ and then finding the resultant value for $\underline{x}$ which is $\hat{\underline{x}}$, the MAP estiamte of $\underline{x}$. Accordingly :

$$\nabla_{\underline{x}} S|_{\hat{\underline{x}}} = \nabla_{\underline{x}} \underline{y}^T S_e^{-1}\underline{y}|_{\hat{\underline{x}}} - \nabla_{\underline{x}} \underline{x}^T K^T S_e^{-1}\underline{y}|_{\hat{\underline{x}}} - \nabla_{\underline{x}} \underline{y}^T S_e K\underline{x}|_{\hat{\underline{x}}}$$

$$+ \nabla_{\underline{x}} \underline{x}^T K^T S_e^{-1} K\underline{x}|_{\hat{\underline{x}}} + \nabla_{\underline{x}} \underline{x}^T S_x^{-1}\underline{x}|_{\hat{\underline{x}}} - \nabla_{\underline{x}} \bar{\underline{x}}^T S_x^{-1}\underline{x}|_{\hat{\underline{x}}}$$

$$- \nabla_{\underline{x}} \underline{x}^T S_x^{-1}\bar{\underline{x}}|_{\hat{\underline{x}}} + \nabla_{\underline{x}} \bar{\underline{x}}^T S_x^{-1}\bar{\underline{x}}|_{\hat{\underline{x}}}$$

$$= 2[-K^T S_e^{-1}\underline{y} + K^T S_e^{-1} K\hat{\underline{x}} - S_x^{-1}\bar{\underline{x}} + S_x^{-1}\hat{\underline{x}}]$$

$$= 0 \qquad \ldots (2.68)$$

Since $$\nabla_{\underline{x}} (K\underline{x})^T S_e^{-1} K\underline{x} = 2K^T S_e^{-1} K\underline{x} \qquad \ldots (2.69)$$

and $$\nabla_{\underline{x}} S_x^{-1} = S_x^{-1}, \qquad \ldots (2.70)$$

if S_x^{-1} is not a function of the vector $\underline{x}$. Solving for $\hat{\underline{x}}$ in equation (2.68) results in

$$\hat{\underline{x}} = \hat{S}\left[K^T S_e^{-1} \underline{y} + S_x^{-1} \bar{\underline{x}} \right] \quad \ldots (2.71)$$

where

$$\hat{S}^{-1} = K^T S_e^{-1} K + S_x^{-1} \quad \ldots (2.72)$$

By adding and subtracting $2K^T S_e^{-1} K\bar{\underline{x}}$ in equation (2.71) the following expression for $\hat{\underline{x}}$ is obtained,

$$\hat{\underline{x}} = \bar{\underline{x}} + \hat{S}\, K^T\, S_e^{-1}\, (\underline{y} - K\bar{\underline{x}}) \quad \ldots (2.73)$$

where $\hat{\underline{x}}$ is, as stated, the MAP estimate of the unknown vector $\underline{x}$.

In Section 2.4.2 it was stated that regularization of the inverse problem in general introduces a bias into the estimator H (of equation (2.43)) used to determine the unknown profile, since the vector of means for the a priori data is not the null vector. However, the MAP estimator of equation (2.73) is not a biased estimator. In order to indicate why this is so, rearrange equation (2.75) above,

$$\hat{\underline{x}} - \bar{\underline{x}} = \hat{S} K^T S_e^{-1} (\underline{y} - \bar{\underline{y}}) \quad \ldots (2.74)$$

where $$\bar{\underline{y}} = K\bar{\underline{x}} \quad \ldots (2.75)$$

Consequently, the MAP estimator estimates the most likely perturbation of the profile vector $\underline{x}$ on the mean temperature profile $\bar{\underline{x}}$. The MAP estimator of equation (2.74) is an unbiased estimator. The covariance matrix for the estimate is just the covariance matrix of the estimator, as will be shown later in this section.

Equation (2.73) for the MAP estimate of $\underline{x}$ may be rearranged into a computationally more manageable expression via the matrix identity :

$$K^T(I + S_e^{-1} K S_x K^T) = K^T + K^T S_e^{-1} K S_x K^T$$

SEE ERRATA

$$= (I + K^T S_e^{-1} K S_x) K^T \qquad \ldots (2.76)$$

whence equation (2.73) may be written

$$\hat{\underline{x}} = \bar{\underline{x}} + S_x K^T (K S_x K^T + S_e)^{-1} (\underline{y} - K\bar{\underline{x}}) \qquad \ldots (2.77)$$

This is the equation that should be used for any computations since it only requires the inversion of an (nxn) dimensional matrix rather than a (pxp) dimensional matrix (and $n<<p$).

Comparison of equations (2.73) and (2.72) with equations (2.53) and (2.55) illustrates how the addition of the a priori data has conditioned the inverse problem, that is, the normal matrix of equation (2.55). The matrix of equation (2.72) is called the augmented normal matrix. When this matrix is well conditioned a solution $\hat{\underline{x}}$ for $\underline{x}$ will exist and it can be interpreted as the most probable temperature profile consistent with the satellite data $\underline{y}$ and S_e, and the a priori data $\bar{\underline{x}}$ and S_x.

The covariance matrix for the MAP estimator is just the covariance of $(\hat{\underline{x}} - \underline{x})$, where $\hat{\underline{x}}$ is the MAP estimate of the true atmospheric temperature profile $\underline{x}$. Hence

$$\hat{\underline{x}} - \underline{x} = \hat{S} K^T S_e^{-1} (K\underline{x} + \underline{e}) - \underline{x} + \hat{S} S_x^{-1} \bar{\underline{x}}$$

$$= (\hat{S} K^T S_e^{-1} K - I)\underline{x} + \hat{S} S_x^{-1} \bar{\underline{x}} + \hat{S} K^T S_e^{-1} \underline{e} \qquad \ldots (2.78)$$

since $\underline{y} = K\underline{x} + \underline{e}$ (equation (2.40) and

$$\mathrm{cov}(\hat{\underline{x}} - \underline{x}) = E\{(\hat{\underline{x}} - \underline{x})^T (\hat{\underline{x}} - \underline{x})\}$$

$$= (\hat{S} K^T S_e^{-1} - I) S_x (\hat{S} K^T S_e^{-1} K - I)^T$$

$$+ (\hat{S} K^T S_e^{-1}) S_e (S_e^{-1} K \hat{S})$$

$$= \hat{S} K^T S_e^{-1} K S_x K^T S_e^{-1} K \hat{S} - \hat{S} K^T S_e^{-1} K S_x$$

$$- S_x K^T S_e^{-1} K\hat{S} + S_x + \hat{S}K^T S_e^{-1} K\hat{S}$$

$$= - S_x K^T S_e^{-1} K\hat{S} + S_x$$

$$= - S_x K^T S_e^{-1} K \hat{S} + S_x \hat{S}^{-1}\hat{S}$$

$$= S_x [- K^T S_e^{-1} K + \hat{S}^{-1}] \hat{S}$$

$$= S_x [- K^T S_e^{-1} K + K^T S_e^{-1} K + S_x^{-1}] \hat{S}$$

$$= \hat{S} \qquad \ldots (2.79)$$

The covariance of $\hat{\underline{x}} - \underline{x}$ is just

$$\text{cov}(\hat{\underline{x}} - \underline{x}) = \hat{S} = (K^T S_e^{-1} K + S_x^{-1})^{-1} \qquad \ldots (2.80)$$

that is, the inverse of the augmented normal matrix. By applying the matrix identity of equation(2.76), equation (2.80) may be written in a computationally simpler form

$$\hat{S} = S_x - S_x K^T (K S_x K^T + S_e)^{-1} K S_x \qquad \ldots (2.81)$$

To summarize, the MAP estimator equations necessary to determine the best estimate of the unknown profile vector $\underline{x}$ in equation (2.40) are:

$$\hat{\underline{x}} = \bar{\underline{x}} + \hat{S}K^T S_e^{-1} (\underline{y} - k\bar{\underline{x}}) \qquad \ldots (2.73)$$

with

$$\text{cov}(\hat{\underline{x}} - \underline{x}) = \hat{S} = [K^T S_e^{-1} K + S_x^{-1}]^{-1} \qquad \ldots (2.72)$$

or alternatively

$$\hat{\underline{x}} = \bar{\underline{x}} + S_x K^T (K S_x K^T + S_e)^{-1} (\underline{y} - K\bar{\underline{x}}) \qquad \ldots (2.77)$$

with

$$\text{cov}(\hat{\underline{x}} - \underline{x}) = \hat{S} = S_x - S_x K^T (K S_x K^T + S_e)^{-1} K S_x \qquad \ldots (2.81)$$

When $\bar{\underline{x}}$ is the mean profile of the sample of profiles used to deter-

mine S_x, the MAP estimate $\hat{\underline{x}}$ is an unbiased estimate of the unknown vector, $\underline{x}$.

Some Comments on Equations (2.72) and (2.73)

The a priori covariance matrix is responsible for regularizing the inversion problem, so that a "stable" estimate of the vector $\underline{x}$ of equation (2.40) may be found. Consequently, establishing the matrix S_x is an important aspect of the retrieval problem since :

(i) S_x should regularize the equation so that equation (2.72) is well conditioned and

(ii) S_x must be a defensable statement about the temperature variations of the atmosphere. The matrix S_x must be constructed from the best available data set.

The problems involved in determining the a priori data S_x and $\bar{\underline{x}}$, are correctly an aspect of the mathematical problem and so will be considered in Section 2.4.5.

Equations (2.72) and (2.73) may be derived without appealing to Bayes' Theorem, as previously stated. Simply consider the combination of two independent data sets (in this case, satellite and a priori data), and minimize the appropriate loss (or objective) function. This approach is followed by Rodgers (1976b), Jackson (1978) and Deutsch (1965).

The MAP estimator is an optimum estimator since it is a minimum variance estimator. When $\bar{\underline{x}}$ is the mean of the sample of profiles used to determine S_x, the MAP estimator for determining $(\hat{\underline{x}} - \bar{\underline{x}})$ is an unbiased estimator.

Finally, it should be noted that in the literature the MAP estimator is also called a maximum likelihood estimator (e.g. Rodgers (1970, 1971) and Jackson (1978)). The term maximum a posteriori estimator as suggested by the Beck and Arnold (1977) is used here.

The Latin term a posteriori conveys the idea of reasoning from effects to causes, or inductively. The retrieved profile is only the most likely in the sense that it is based upon the a priori data.

2.4.4 The Sequential Form of the Maximum a Posteriori Estimator

The sequential MAP estimator given in this section enables the retrieved profile vector to be continually updated as new observation measurements are added, or become available. Further, the sequential estimator will effect computational advantages and simplifications.

It is a good approximation in the case of the Nimbus 4 SCR, to assume that the satellite radiance observations are independent in time and that the observation errors are independent. With these assumptions a sequential MAP estimator may be derived. Let

$$\underline{\hat{x}} \rightarrow \underline{\hat{x}}_{i+1}; \quad \underline{\bar{x}} \rightarrow \underline{\hat{x}}_i, \quad y_i \rightarrow y_{i+1}$$

$$S_{e_{ii}} \rightarrow \sigma^2_{i+1}; \quad K_i \rightarrow K_{i+1} = (K_{i+1\,1}, K_{i+1\,2}, \cdots K_{i+1\,p})$$

$$\hat{S} \rightarrow \hat{S}_{i+1}; \quad S_x \rightarrow \hat{S}_i; \quad i = 0,1,\ldots,n \qquad \ldots (2.82)$$

where

$\underline{y}^T = (y_1\ y_2 \cdots y_n)$,

σ^2_{i+1} is the variance of y_{i+1},

i refers to the i^{th} iteration,

$\rightarrow$ indicates the new meaning of certain vector and matrix quantities, and

$i=0$ corresponds to the a priori data

The equations for the MAP estimator, equations (2.72) and (2.73)

may be written in a form which in effect may be iterated at each step as new data is introduced. Before writing down the form of the sequential estimators it is necessary to note two matrix identities (proofs are given in Appendix B), which are required in the following manipulations :

$$\text{(i) if } \hat{S}_{i+1} = \left[\underline{k}_{i+1}^T (\sigma_{i+1}^2)^{-1} \underline{k}_{i+1} + \hat{S}_i^{-1}\right]^{-1}$$

$$\text{then } \hat{S}_{i+1} = \hat{S}_i - \hat{S}_i \underline{k}_{i+1}^T (\underline{k}_{i+1} \hat{S}_i \underline{k}_{i+1}^T + \sigma_{i+1}^2)^{-1} \underline{k}_{i+1} \hat{S}_i \quad \ldots (2.83)$$

called the matrix inversion lemma, and

$$\text{(ii) } \hat{S}_{i+1} \underline{k}_{i+1}^T (\sigma_{i+1}^2)^{-1} = \hat{S}_i \underline{k}_{i+1}^T (\underline{k}_{i+1} \hat{S}_i \underline{k}_{i+1}^T + \sigma_{i+1}^2)^{-1} \quad \ldots (2.84)$$

Substitute equations (2.82) into equation (2.73) :

$$\hat{\underline{x}}_{i+1} = \hat{\underline{x}}_i + \hat{S}_{i+1} \underline{k}_{i+1}^T (\sigma_{i+1}^2)^{-1} (y_{i+1} - \underline{k}_{i+1} \hat{\underline{x}}_i) \quad \ldots (2.85)$$

On substituting the matrix identity, equation (2.84) into equation (2.85) :

$$\hat{\underline{x}}_{i+1} = \hat{\underline{x}}_i + \hat{S}_i \underline{k}_{i+1}^T (y_{i+1} - \underline{k}_{i+1} \hat{\underline{x}}_i) \Big/ (\underline{k}_{i+1} \hat{S}_i \underline{k}_{i+1}^T + \sigma_{i+1}^2) \quad \ldots (2.86)$$

Similarly, the sequential (or iterative) form of equation (2.72) may be deduced. Substitute equations (2.82) into equation (2.72) :

$$\hat{S}_{i+1} = \left[\underline{k}_{i+1}^T (\sigma_{i+1}^2)^{-1} \underline{k}_{i+1} + \hat{S}_i^{-1}\right]^{-1} \quad \ldots (2.87)$$

On substituting the matrix inversion lemma, equation (2.83) into equation (2.87) :

$$\hat{S}_{i+1} = \hat{S}_i - \hat{S}_i \underline{k}_{i+1}^T \underline{k}_{i+1} \hat{S}_i \Big/ (\underline{k}_{i+1} \hat{S}_i \underline{k}_{i+1}^T + \sigma_{i+1}^2) \quad \ldots (2.88)$$

In summary, the sequential forms of equations (2.73) and (2.72) are, respectively;

$$\hat{\underline{x}}_{i+1} = \hat{\underline{x}}_i + \hat{S}_i \underline{k}_{i+1}^T (y_{i+1} - \underline{k}_{i+1} \hat{\underline{x}}_i) \Big/ (\underline{k}_{i+1} \hat{S}_i \underline{k}_{i+1}^T + \sigma_{i+1}^2) \quad \ldots (2.86)$$

and

$$\hat{S}_{i+1} = \hat{S}_i - \hat{S}_i \underline{k}_{i+1}^T \underline{k}_{i+1} \hat{S}_i \Big/ (\underline{k}_{i+1} \hat{S}_i \underline{k}_{i+1}^T + \sigma_{i+1}^2) \quad \ldots (2.88)$$

where $i = 0,1,2,\ldots,n$,

$\hat{\underline{x}}_o = \bar{\underline{x}}$, and

$\hat{S}_o = S_x$

Alternatively, these equations could be determined directly through substitution of equation (2.82) into equations (2.77) and (2.81) respectively, since the matrix inversion lemma has already been applied in the derivation of those results.

A rigorous development for these equations is given by Deutsch (1965). However it is easy to understand equation (2.82), and those that follow by letting the dimension of the observation vector $\underline{y}$ become one. There will be n such observation vectors, and each succeeding solution can be considered as a refinement on the solution derived using the previous observation.

Equations (2.86) and (2.88) have computational advantages over equations (2.73) and (2.72) since the largest matrix to be inverted for the sequential estimator is of dimension (1x1), rather than (pxp), as in equation (2.73). Further, the sequential (or iterative) solution procedure is helpful for demonstrating effects on the solution through addition of the satellite observations to the MAP estimator. Owing to these advantages, equations (2.86) and (2.88) will be used for all retrieval calculations.

2.4.5 The a Priori Covariance Matrices

From the preceding discussion in Sections 2.4.2 and 2.4.3 the

importance of the "quality" of the a priori covariance matrix S_x has been established. Should the a priori covariance matrix not portray the variance and covariance of the atmospheric region (latitude and season) in which the retrieval is being performed, then it is clear that :

(i) The solution (estimate) will be biased, since the MAP estimator finds the profile which is most probable, given the observations and the a priori data.

(ii) The inversion problem may still be poorly conditioned; hence the retrieved profile will be unstable to measurement noise.

It is important to determine suitably "correct" atmospheric mean temperature profiles and covariance matrices.

2.4.5.1 The a Priori Data

The data set used in the construction of the mean profiles and their covariance matrices is the United States of America Department of Commerce magnetic tape file : "Tape Deck 5850 : Rocketsonde Observations". This magnetic tape file contains all available high altitude meteorological data for the years 1969 to 1972 inclusive, arising from the following two sources :

(i) Meteorological rocket observations, and

(ii) Conjunctive balloonsonde observation.

A balloonsonde (or rawinsonde) observation is considered to be conjunctive if the balloon is released within four hours before, or two hours after the rocket launch time.

Unfortunately a major problem in the use of rocketsonde (also called radiosonde) data is the incidence of measurement errors, which increase with height, above 100 mb. (Finger and McInturff (1969) and Ezemenari (1976). These measurement "errors" include both random

and systematic components. The random errors will accordingly be regarded as having zero mean. The systematic errors arise since at some altitudes the temperature sensing device may not actually measure the temperature of the atmosphere. This problem is further compounded when different measurement techniques are used. These problems arise since the majority of temperature data is measured using a 0.010 inch (or 10 mil) bead thermistor. The temperature of the ambient low density air of the upper atmosphere as measured by the thermistor will differ from the true atmospheric temperature since the heat exchange between the thermistor and the air is poor and a function of the method by which the thermistor is mounted.

There are two important mounting systems :

(i) For the Arcasonde-1A instrument the thermistor is mounted on a mylar flat plate, part of which is coated with a silver film, whereas

(ii) for the Datasonde instrument the thermistor is mounted on a loop of silverized mylar (this is referred to as the "loop mount").

The differences, and weaknesses, in using temperature data from these two measuring systems must be considered when establishing a data set to determine atmospheric temperature statistics.

The major weakness involved in the use of a bead thermistor is its susceptability to radiation and aerodynamic heating effects (see Leviton(1969) and Ezemenari (1972)). There are several sources for these affects :

(i) radiative errors from both solar and infra-red energy exchanges with the environment both above and below the sonde,

(ii) aerodynamic (frictional) heating of the thermistor, a function of the payload fall velocity and sensor geometry,

(iii) convection,

(iv) conduction of heat from the payload body,

(v) electrical heating of the thermistor by the current passing through it (Joule heating), and

(vi) time lag effects due to the low efficiency of the heat exchange between the thermistor and the ambient air.

When the thermistor is exposed at high altitude it responds to a complex heat transfer environment in a way that defies theoretical description. However, estimates of corrections for some of these effects are deduced by modelling the heat transfer processes (see for example, Ballard (1967)).

In order to determine the best estimate of the true atmospheric temperature of the region through which the thermistor sensor is passing it is important to apply the best available correction estimates for each of the effects (i) to (vi) above.

Correction Techniques

The National Aeronautics and Space Administration in the Federal Meteorological Handbook (henceforth FMH) No 10 : Meteorological Rocket Observations (1975), give correction equations for Arcasonde-1A and Datasonde derived temperature profiles, for altitudes to 70 km. These equations incorporate corrections for aerodynamic heating, ohmic heating, time lag effects, radio-frequency and long wave emission, and, in the case of the Datasonde measurements, short wave radiation effects. The correction equations are given by the following expressions :

$$T_{atm}(z) = T_t(z) - A(z)V^2 + B(z)\frac{dT_t}{dt} - C(z) + D(z)T_t^4 \quad \ldots (2.89)$$

and

$$T_{atm}(z) = T_t(z) - K_1(z)V^2 + K_2(z)\frac{dT_t}{dt} - K_4(z) + K_3(z)T_t^4 \quad \ldots (2.90)$$

where

$T_{atm}(z)$ is the corrected atmospheric temperature at height z,

$T_t(z)$ is the measured thermistor temperature at height z,

V is the ventilation velocity of the sensor system,

$\frac{dT_t}{dt}$ is the rate of change of temperature as time increases during the payloads fall,

A,B,C,D, are height dependent coefficients derived from the heat transfer equations for the Arcasonde-1A measurement configuration, and

K_1,K_2,K_3,K_4, are height dependent coefficients derived from the heat transfer equation for the Datasonde measurement configuration.

The correction equations are based on work performed by Henry (1967) for the Arcasonde-1A equation, and by Krumins and Lyons (1972) for the Datasonde equations. Plots of the height dependent coefficients A,B,C,D,K_1,K_2,K_3 and K_4 are given in figures 5 to 8. On examining these graphs it is clear that the correction coefficients become large at altitudes higher than approximately 60 km.

Ezemenari (1972) has also conducted a study on correction terms for the Arcasonde-1A instrument. He finds that realistic temperature profiles may be deduced for altitudes up to the 60 km region. Above this altitude he suggests that problems due to high ventilation speeds (causing aerodynamic heating and time lag effects) may cause a degradation in the quality of the derived corrected temperatures. For the Datasonde device with its Starute decelerator and loop mounted thermistor, these problems are not so important at the same altitudes. (Ezemenari (1972)).

Under these circumstances it is important to consider the size of errors in the corrected temperature profiles. The FMH No 10 does

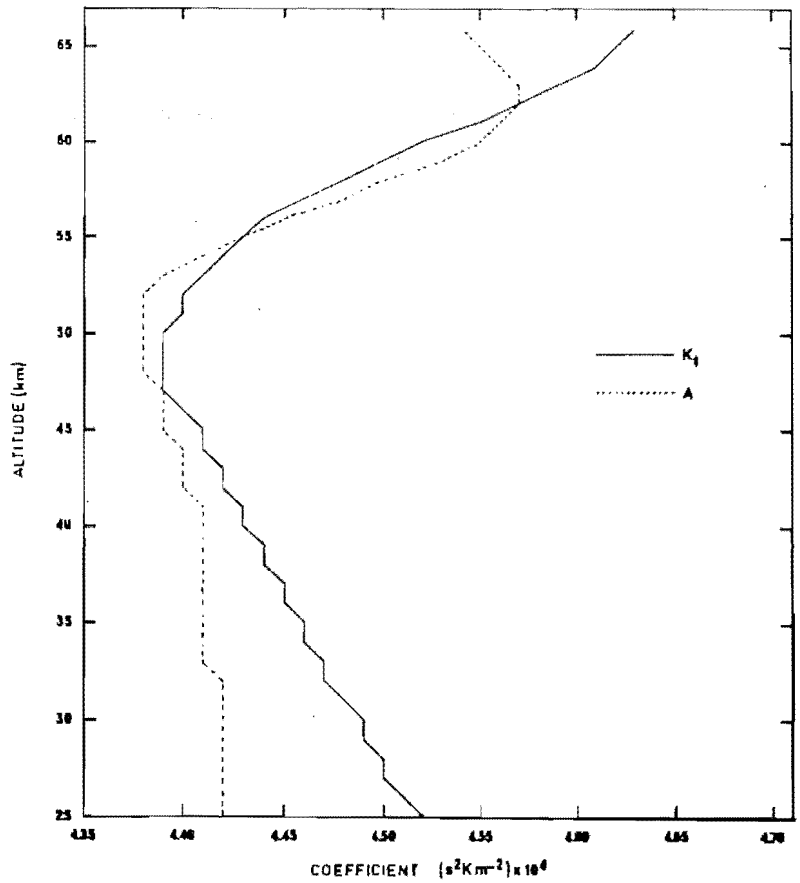

FIGURE 5 : Rocketsonde Temperature Correction Coefficients K_1 and A

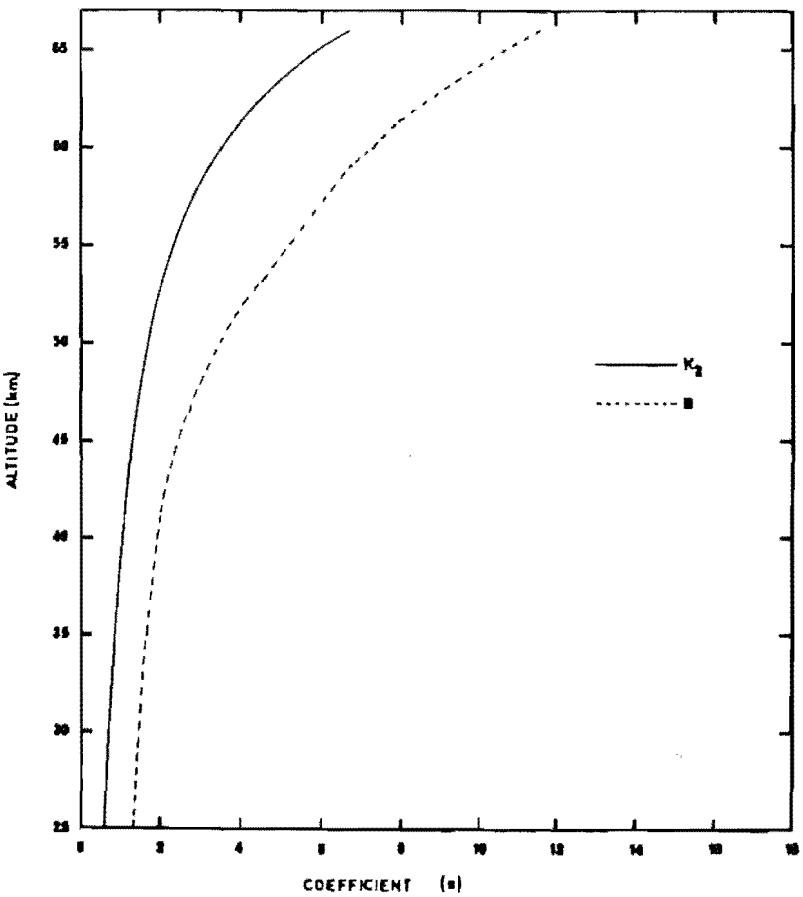

FIGURE 6 : Rocketsonde Temperature Correction Coefficients K_2 and B

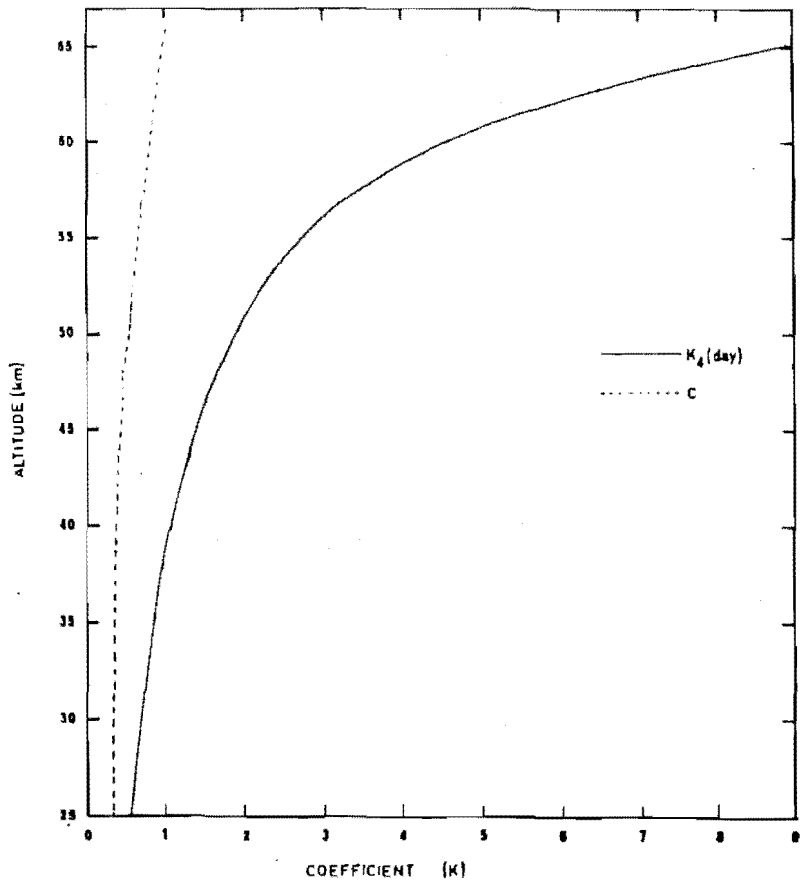

FIGURE 7 : Rocketsonde Temperature Correction Coefficients K_4 (day values) and C

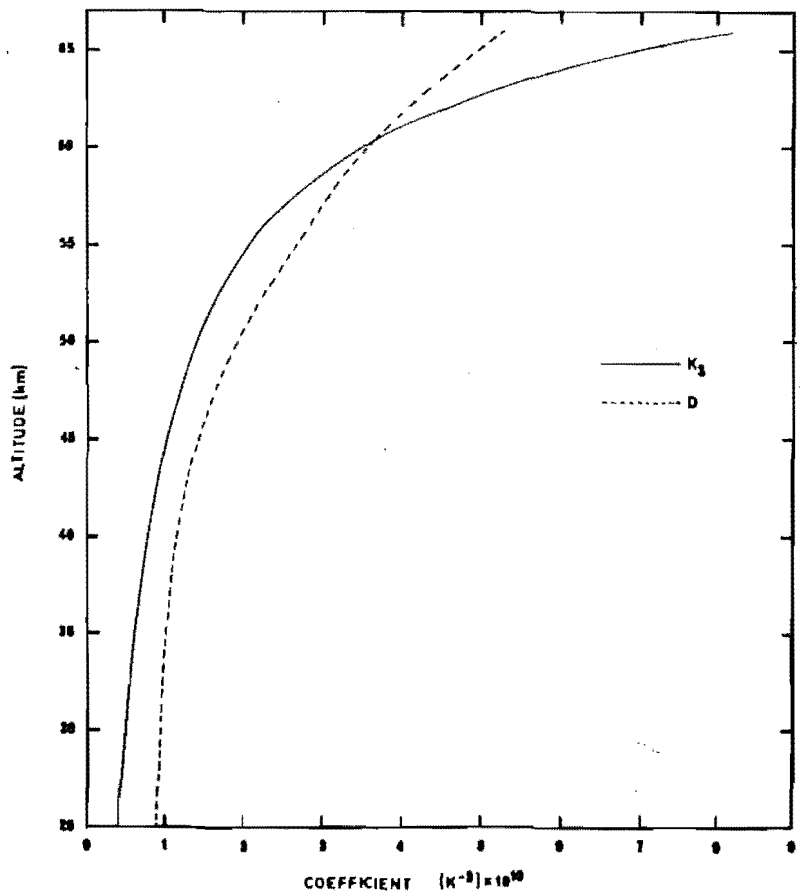

FIGURE 8 : Rocketsonde Temperature Correction Coefficients K_3 and D

not give an estimate of the possible errors in the correction procedures of equations (2.89) and (2.90). However, an upper limit on the size of these errors may be suggested using Ezemenari's (1972) paper. For his correction scheme, he suggests that the errors in the corrected profiles may be as high as ±2.9 K at 50 km and ±5.5 K at 60 km. However, Ezemenari's correction procedure is a set of computed "standard" correction curves to be applied to any uncorrected Arcasonde-1A measured profile. These standard curves cannot take into account the effects due to differing ventilation velocities (at high altitudes) as do the FMH No 10 corrections. It is the corrections which arise from the high ventilation velocities that produce the largest correction terms and accordingly may contribute the largest errors to the derived temperature profile. Hopefully it is safe to assume that the errors in the corrected temperatures of equations (2.89) and (2.90) for a particular profile will be smaller than those estimated by Ezemenari (1972) with his correction scheme.

Given the above doubts about rocketsonde derived temperature profiles above approximately 60 km it was decided that a top limit of approximately 60 km altitude should be applied to all data input to the covariance matrix calculations. This altitude was chosen for three reasons :

(i) Above this altitude the correction terms, especially for solar radiation and aerodynamic heating become very large and correspondingly the errors in the estimated correction terms must increase.

(ii) temperature measurements are obtained at altitudes above the stratopause so that if necessary, temperatures in the mesosphere may be estimated by using an appropriate lapse rate, and

(iii) rocketsonde flights involving Arcasonde-1A and Datasonde payloads do not in general produce data

at altitudes much greater than 60 km

Rocketsonde and Ballonsonde Data Compatability

There is one remaining problem to be considered in constructing a complete (ground to 60 km) temperature profile (for input to the covariance matrix calculation). This is the problem of "joining" the rocketsonde profiles to the conjuncture rawinsonde profiles.

It is generally concluded that for altitudes below 25 km the measured thermistor temperatures are accurate to less than $\pm 1C^0$ (see Ezemenari (1972) and Ballard and Rubio (1968)). No correction need be applied to rocketsonde temperatures below 25 km. In order to determine a suitable scheme for joining the balloonsonde profile to the rocketsonde profile, the following two problems are considered :

(i) The balloonsonde and rocketsonde observations at overlapping altitudes are not measuring the temperature of the same piece of atmosphere since:
   (a) the balloonsonde-rocketsonde time difference may be as large as four hours
   (b) the balloonsonde and rocketsonde will in general measure the temperature of different "pieces" of the atmosphere (even if the time difference is zero), unless the atmosphere is at rest (static).

(ii) The "temperature" sensors on board the balloonsondes and rocketsondes may not measure the same parameter of the atmosphere. For example, the balloonsonde temperature sensor may be measuring the temperature of the wake of the balloon (which may be heated by radiation, conduction and convection from the hot sunlit surface of the balloon).

Finger and McInturff (1969) have studied results from a large number of conjunctive balloonsondes and rocketsondes. It is their conclu-

sion that below 25 km altitude and for daytime soundings, the two sounding techniques are in good agreement. Therefore it will be assumed that below 25 km altitude the rocketsondes and balloonsondes would measure the same temperature for the same "piece" of atmosphere.

Given the above information it was decided that an appropriate way to join the rocketsonde profile to the balloonsonde profile was to simply concatenate the two profiles. In regions of overlap the rocketsonde profile is regarded as being the most accurate, since :

(i) at these altitudes no temperature corrections need be applied to the measured temperatures,

(ii) the balloonsonde is approaching its upper limit for obtaining accurate data (Godson (1969)), and

(iii) the balloonsonde rocketsonde time difference will be smallest (in general) at the lowest altitude before the rocketsonde data drops out.

Discontinuities arising from the concatenation process are smoothed using a suitable filter.

Effects of Daily Temperature Variations on the Data Set

Finally, consideration must be given to the problem of introducing a bias into the temperature profile sample by including profiles which may be systematically different. For example, profiles from night flights for which the solar correction term is no longer important. If the daily temperature variation were large, then temperature profiles observed at different local times may introduce a bias into the calculated covariance matrix.

Finger and McInturff (1968) have determined the daily temperature range between 25 km and 36 km altitude by using means of 12 hour temperature differences obtained from successive balloonsonde observations over North America. They find that during summer at 10 mb and 45 N, the daily variation of temperature is of the order

of $\pm 0.5C^0$, and in winter, of the order $\pm 0.3C^0$. Ezemenari (1976) on analysing a series of September Arcasonde-1A flights from Fort Churchill ($58^0 44'N$) finds that the daily variation of temperature over the altitude range 25 km to 60 km ranges from $\pm 1.4C^0$ to $\pm 4.2C^0$ (with 95% confidence).

From the above findings it may be concluded that no serious bias will be introduced into the calculated mean profiles and covariance matrices by constructing them from a data set of temperature observations clustered near local noon. The satellite radiance observations also occur at local noon since the Nimbus 4 satellite is in a sun synchronous orbit.

Summary

A method for determing consistent and accurate (in the sense of small systematic error) temperature profiles from ground level to approximately 60 km has been outlined. It may be expected that a representative sample mean profile and covariance matrix can be determined from a suitably chosen sample of balloonsonde-rocketsonde derived atmospheric temperature profiles.

2.4.5.2 The Covariance Calculation

The covariance matrices are calculated using equation (2.91) below :

$$S_x = \sum_{ij}^{p} \frac{1}{M} \sum_{m=1}^{M} (b_{im} - \bar{b}_i)(b_{jm} - \bar{b}_j) \qquad \ldots (2.91)$$

where

M is the sample size,

p is the number of levels of discretization,

$$b_{im} = \frac{c_1 n^3}{\exp\left(\frac{c_2 n}{T_{im}}\right) - 1} \qquad \ldots (2.92)$$

is the black body radiance for the temperature T_{im} at level i, profile m of the sample and wavenumber n,

c_1 and c_2 are constants,

$$\bar{b}_i = \frac{1}{M} \sum_{m=1}^{M} b_{im} \quad \ldots (2.93)$$

is the mean black body radiance at level i and wavenumber n for the given sample, and

S_x is the resultant covariance matrix

By choosing a suitable sample of atmospheric temperature profiles for a given season and latitude zone, an appropriate covariance matrix may be calculated. Hopefully this matrix is representative of the temperature variances and covariances of the atmosphere for that season and latitude zone.

Practical Considerations

Table 2 below indicates the total number of observations available on the Tape Deck 5850 (the magnetic tape file). The profiles have been sorted into six latitudinal zones.

TABLE 2 : Rocketsonde-Balloonsonde Temperature Profiles on Tape Deck 5850

Latitude Zone	80^0-50^0 N	50^0-30^0 N	30^0-0^0 N	0^0-30^0 S	30^0-50^0 S	50^0-80^0 S
Number of Profiles	1296	2737	2447	570	40	0

These figures will of course contain a number of unacceptable profiles which may not be used in the covariance calculations. A map of the Meteorological Rocket Network stations, their latitudes and longitudes and the details on the number of profiles available for each station and year are given in Appendix C.

The covariance data sample is divided into 12 "seasons" as indicated in Table 3 below :

TABLE 3 : Seasonal Division of Data

"Season"	Months
1	12,1,2
2	1,2,3
3	2,3,4
4	3,4,5
5	4,5,6
6	5,6,7
7	6,7,8
8	7,8,9
9	8,9,10
10	9,10,11
11	10,11,12
12	11,12,1

Using the above data sample for some season and latitudinal zone, a covariance matrix and mean atmospheric temperature profile are calculated.

The computer program written to calculate the covariance matrix processes the raw data in the following way :

(i) A pair of rocketsonde and balloonsonde profiles are read from a data file. These profiles are accepted as input to the covariance calculating procedure if the following criteria are met :

(a) the rocketsonde is either an Arcasonde-1A or Datasonde instrument,

(b) the rocketsonde flight occurred between 0900 and 1600 hours local time

(c) the rocketsonde reached an altitude of $-\ln(p_1/p_o)$ equal to 8.0 (approximately 60 km), where p_1 is the atmospheric pressure at the highest recorded data point and p_o is the ground pressure.

(d) there are less than five questionable data layers in the profile,

(e) there is no data gap larger than 2.5 km,

(f) the rocketsonde and balloonsonde profiles overlap,

(g) all necessary data (for use in correction procedures) is present. However, should there be an absence of fall velocity data above height $-\ln(p/p_0) = 7.1$, the fall velocities are modelled using equation (2.94) below.

$$V(-\ln(p/p_o)) = -39.5(\text{data max} - (-\ln(p/p_o)) + V(\text{data max}) \quad \ldots (2.94)$$

where $V(-\ln(p/p_o))$ is the estimated fall velocity at altitude $-\ln(p/p_o)$ and data max is the highest altitude for which fall velocity data is given. Equation (2.94) was derived from a small sample of Arcasonde-1A and Datasonde fall velocity curves. In practice, this program option is not often used.

(ii) All data is interpolated to standard levels, for which $-\ln(p/p_o) = 0, 0.1, 0.2, \ldots, 8.0$, by linearly interpolating between nearest neighbour levels. This is adequate since the number of standard levels is in general approximately equal to the number of observation levels

(iii) If the World Data Centre A have applied corrections to the thermistor measured temperatures, then the correction procedure is reversed.

(iv) The rocketsonde temperature profile is corrected using either equation (2.89) or (2.90).

(v) The rocketsonde and balloonsonde profiles are joined together.

(vi) The complete temperature profile above the tropopause is twice smoothed by a quarter half, quarter filter.

(vii) The final profile is saved for input to the covariance procedure.

The above steps (i) through (vii) are repeated until all profiles in the sample have been processed. When this is completed the sample mean profile and standard deviations for each level of discretization are determined. These values are used to filter out gross errors in the sample by checking that all profiles lie within three standard deviations of the mean profile. When profiles are rejected the sample size is adjusted accordingly. Finally, the covariance matrix and mean profile of the final sample are calculated using equations (2.91) and (2.93).

2.4.6 Confidence Regions of the Maximum a Posteriori Estimated Retrieval

Uncertainty in the solution profile, $\hat{\underline{x}}$

$$\hat{\underline{x}} = \bar{\underline{x}} + \hat{S}K^T S_e^{-1}(\underline{y}-K\bar{\underline{x}}) \qquad \ldots (2.73)$$

is a consequence of uncertainty in the satellite measurements, overlap of the weighting functions and noise in the a priori data. In Section 2.4.3 it was shown that if the statistics for the satellite and a priori measurements are Gaussian then the retrieval covariance of the MAP estimator $\hat{\underline{x}}$ is the covariance matrix $\hat{S}$ (that is, the inverted augmented normal matrix).

$$\hat{S} = [\, K^T S_e^{-1} K + S_x^{-1} \,]^{-1} \qquad \ldots (2.72)$$

In order to appreciate the implications of this equation it is necessary to interpret it in terms of possible deviations from the true value of the unknown profile. The confidence regions of the solution estimate must be established.

The principal diagonal of the solution covariance matrix $\hat{S}$, contains the variances of the individual components of the estiamted profile $\underline{\hat{x}}$. Since $\hat{S}$ in general will have no zero entries, the temperatures at all levels are correlated to some degree. Jackson (1976) has shown that even in the case of an overdetermined inversion problem and univariate observation errors, the solution confidence regions have magnitudes of approximately $\pm p^{\frac{1}{2}}\sigma_i$ where p is the dimension of the solution vector and σ_i is the corresponding standard deviation for element i of the solution vector. The standard deviation of a level (i e. the square root of the appropriate diagonal term of the covariance matrix) is not a good estimate of the size of the confidence regions for the MAP estimated solution profile. This result is understandable since in using the variance as a measure of the confidence regions not all available information is being considered, and the size of the confidence regions will probably be underestimated. A transformation is needed which will allow the error estimate (or at the very least, an estimate of the errors) to be expressed as a sum of individual components such that the components are independent of each other. The solution to this problem is outlined in this section.

Since Gaussian statistics have been assumed throughout, the pdf for the estimated profile vector $\underline{\hat{x}}$ may be written thus :

$$f(\underline{\hat{x}}) = (2\pi^p|\hat{S}|)^{-\frac{1}{2}}\exp\left[-\tfrac{1}{2}(\underline{\hat{x}} - \underline{x})^T\hat{S}^{-1}(\underline{\hat{x}} - \underline{x})\right] \quad \ldots \quad (2.95)$$

where, as before

p is the dimension of the solution profile vector,

$|\hat{S}|$ is the determinant of $\hat{S}$,

$\underline{\hat{x}}$ is the MAP estimated solution profile,

$\underline{x}$ is the true atmospheric temperature profile and

$\hat{S}$ is the covariance matrix of the MAP estimator

Under these assumptions it is possible to determine approximate confidence regions for the estimated profile $\underline{\hat{x}}$.

Consider the objective function of equation (2.95). Let the objective function have some value r^2, since, by definition it is a quadratic form ($\hat{S}^{-1}$ is symetric) and therefore a non negative scalar, thus

$$r^2 = (\underline{\hat{x}} - \underline{x})^T \hat{S}^{-1} (\underline{\hat{x}} - \underline{x}) \quad \ldots (2.96)$$

$\hat{S}$ is a positive definite matrix with non vanishing, positive eigenvalues. Equation (2.96) is also the general equation for the surface of an hyperellipsoid centred at $\underline{\hat{x}}$. If ℓ^2 is some specific value of the quadratic form (equation (2.96)) then for $r^2 < \ell^2$, equation (2.96) represents the interior of the hyperellipsoid. When $r^2 = \ell^2$, equation (2.96) represents the hypersurfaces of constant probability density (from equation (2.95)). If the orientation of the hyperellipse and the lengths of it's principal axes in some independent, physically understandable co-ordinate system can be determined for a value of ℓ^2, then the confidence regions for $\underline{\hat{x}}$ will be known. The value of ℓ will simply specify the confidence in the estimated confidence regions.

The orientation and lengths of the principal axes of the hyperellipse will be determined by finding the eigenvectors and eigenvalues of the matrix $\hat{S}^{-1}$, i.e. by transforming the problem to the principal axes co-ordinate system. The principal axes of the hyperellipse are those vectors which extend from the origin of the hyperellipse to points on the surface of the ellipsoid such that the vectors are normal to the hyperellipse at those points. The lengths of these axes

are just the inverse square roots of the corresponding eigenvalues (for details, see Franklin (1968)).

Let

$$\Sigma \equiv \hat{S}^{-1} \qquad \ldots (2.97)$$

Σ is a real symmetric matrix by definition. There is a theorem (Thompson (1969)) which states that for every real symmetric matrix A there exists an orthogonal matrix B such that B^TAB is a diagonal matrix Λ, whose diagonal elements are eigenvalues of A. Therefore there exists an orthogonal matrix L such that

$$L^T \Sigma L = \Lambda \qquad \ldots (2.98)$$

where Λ is a diagonal matrix ($\Lambda = \text{diag}[\lambda_1\lambda_2\ldots\lambda_p]$), and its components are the eigenvalues of Σ. The λ_i may be ordered so that $\lambda_i \leq \lambda_j$ for $i<j$. The matrix L is orthogonal by the theorem and if chosen to be orthonormal, then

$$L^TL = I \qquad \ldots (2.99)$$

or

$$L^T = L^{-1} \qquad \ldots (2.100)$$

(where L is sometimes called the orthonormal modal matrix). The matrix Σ of equation (2.98) can be written in the form :

$$\Sigma = L\Lambda L^T \qquad \ldots (2.101)$$

therefore

$$\Sigma L = L\Lambda \qquad \ldots (2.102)$$

and

$$L = \begin{pmatrix} l_{11} & l_{12} & \cdots & l_{1p} \\ l_{21} & l_{22} & \cdots & l_{2p} \\ & & & \\ & & & \\ l_{p1} & l_{p2} & \cdots & l_{pp} \end{pmatrix} = [\underline{l}_1\ \underline{l}_2\ \underline{l}_3 \cdots \underline{l}_p] \qquad \ldots (2.103)$$

The $\underline{l}_i$, $i = 1,2,\ldots,p$ are the eigenvectors of matrix Σ. Therefore

from this equation and equation (2.99)

$$\underline{l}_i^T \underline{l}_i = 1 \quad \text{for } i=1,2,\ldots p \qquad \ldots (2.104)$$

Hence equations (2.102) and (2.104) imply :

$$\Sigma \underline{l}_i = \lambda_i \underline{l}_i \qquad i=1,2,\ldots p \qquad \ldots (2.105)$$

The matrix $\hat{S}$ need not be inverted in order to determine the eigenvectors and eigenvalues of Σ. From the theorem given above there exists an orthogonal (which may be chosen orthonormal) matrix B such that $B^T \hat{S} B$ is a diagonal matrix Λ' whose diagonal elements are the eigenvalues of $\hat{S}$. Hence

$$B^T \hat{S} B = \Lambda' \qquad \ldots (2.106)$$

therefore $$\hat{S} B = B\Lambda' \qquad \ldots (2.107)$$

since $$BB^T = I. \qquad \ldots (2.108)$$

Consequently $$(B^T \hat{S} B)^{-1} = \Lambda'^{-1} \qquad \ldots (2.109)$$

implies that $$B^{-1} \hat{S}^{-1} (B^T)^{-1} = \Lambda'^{-1} \qquad \ldots (2.110)$$

but $$(B^T)^{-1} = B \qquad \ldots (2.111)$$

therefore $$B^T \hat{S}^{-1} B = \Lambda'^{-1} \qquad \ldots (2.112)$$

The eigenvectors of $\hat{S}^{-1}$ are just the eigenvectors of $\hat{S}$, however the eigenvalues of $\hat{S}^{-1}$ are reciprocals of the eigenvalues of the matrix $\hat{S}$.

Following Beck and Arnold (1977), and Deutsch (1965) define a new co-ordinate vector $\underline{g}$, such that

$$\underline{g} \equiv L^T (\hat{\underline{x}} - \underline{x}) \qquad \ldots (2.113)$$

thus $$g_i = \underline{l}_i^T (\hat{\underline{x}} - \underline{x})$$

On substituting equation (2.101) into equation (2.96) :

$$r^2 = (\hat{\underline{x}} - \underline{x})^T L \Lambda L^T (\hat{\underline{x}} - \underline{x}) \qquad \ldots (2.114)$$

Substituting the new co-ordinates $\underline{g}$ into this equation gives :

$$r^2 = \underline{g}^T \Lambda \underline{g}$$

$$= \sum_{i=1}^{p} \lambda_i g_i^2 \qquad \ldots (2.115)$$

The vector $\underline{g}$ can be thought of as the projection of the error vector $(\hat{\underline{x}} - \underline{x})$ onto the orthonormal set of vectors $\underline{l}_i$, i=1,2,...,p. This forms a good co-ordinate system since if all the eigenvalues of Σ are distinct then the eigenvectors $\underline{l}_i$ form a complete basis set (Franklin (1968)).

Finally, let

$$z_i^2 = \lambda_i g_i^2 \qquad \ldots (2.116)$$

It follows from equation (2.115) and (2.116) that equation (2.96) may be written in the new co-ordinate system, thus :

$$r^2 = \underline{z}^T \underline{z}$$

$$= z_1^2 + z_2^2 + \ldots + z_p^2 \qquad \ldots (2.117)$$

where the z_i are independent since the g_i are independent (owing to the orthonormality of the $\underline{l}_i$). For the given assumptions the error estimate can be expressed as a sum of individual components which are independent of each other (i.e. equation (2.117)). That is, the problem has been rewritten in the principal axes co-ordinate system of matrix Σ.

The probability that the vector $\underline{z}$ (and therefore $\hat{\underline{x}} - \underline{x}$) lies inside the hyperellipsoid where $\ell^2 \geq r^2$ (ℓ some fixed confidence value) can be found using equation (2.117) and equation (2.95). The probability that the solution elements $\hat{x}_1, \hat{x}_2, \ldots, \hat{x}_p$ lie simultaneously in the range $\hat{x}_1, \hat{x}_1 + d\hat{x}_1$; $\hat{x}_2, \hat{x}_2 + d\hat{x}_2$; ....; $\hat{x}_p, \hat{x}_p + d\hat{x}_p$ is given by the expression (from equation (2.95))

$$(2\pi^p\ |\hat{S}|)^{-\frac{1}{2}}\exp\ [-\tfrac{1}{2}(\hat{\underline{x}}\ -\ \underline{x})^T\hat{S}^{-1}(\hat{\underline{x}}\ -\ \underline{x})\ ]\ d\hat{x}_1 d\hat{x}_2 \ldots d\hat{x}_p$$

... (2.118)

for Gaussian error statistics. The probability that $\ell^2 \geq r^2$ i.e. $P(r^2 \leq \ell^2)$ is :

$$P(r^2 \leq \ell^2) = \iint \ldots \int (2\pi^p|\hat{S}|)^{-\frac{1}{2}}\exp\ [-\tfrac{1}{2}(\hat{\underline{x}}\ -\ \underline{x})^T\hat{S}^{-1}(\hat{\underline{x}}\ -\ \underline{x})\ ]$$

$$\cdot\, d\hat{x}_1 d\hat{x}_2 \ldots d\hat{x}_p$$

... (2.119)

Using the transformation of equation (2.113), this equation can be rewritten, thus

$$P(r^2 \leq \ell^2) = \iint \ldots \int (2\pi^p|\hat{S}|)^{-\frac{1}{2}}\exp\ -\tfrac{1}{2}(\underline{g}^T L^T \hat{S}^{-1} L\underline{g})\, dg_1 dg_2 \ldots dg_p$$

... (2.120)

since $\underline{x}$ is not a variable. Upon substituting equations (2.115) and (2.116) into (2.120) :

$$P(r^2 \leq \ell^2) = \iint \ldots \int (2\pi^p|\hat{S}|)^{-\frac{1}{2}}\exp\left[\frac{-r^2}{2}\right]\frac{1}{\lambda_1^{\frac{1}{2}}}\, dz_1 \frac{1}{\lambda_2^{\frac{1}{2}}} dz_2 \ldots \frac{1}{\lambda_p^{\frac{1}{2}}}\, dz_p$$

... (2.121)

But $\underline{L}$ is a similarity transformation so the determinant of the matrix is not changed under the transformation, i.e.

$$|\hat{S}^{-1}| = |\Sigma| = |\Lambda| = \lambda_1 \cdot \lambda_2 \cdot \ldots, \lambda_p \qquad \ldots (2.122)$$

Equation (2.121) can be simplified on considering equation (2.122),

$$P(r^2 \leq \ell^2) = \iint \ldots \int (2\pi)^{-\frac{p}{2}} \exp\left[\frac{-r^2}{2}\right] dz_1 dz_2 \ldots dz_p \qquad \ldots (2.123)$$

where the z_i are independent, and the integration is performed over the interior of the hyperellipse defined by equation (2.117). The

volume element $dz_1 dz_2 \ldots dz_p$ of the p dimensional ellipse $r^2 = \underline{z}^T \underline{z}$ can be described by the following expression (Beck and Arnold (1977)).

$$dz_1 dz_2 \ldots dz_p = dV = \frac{p\pi^{p/2} r^{p-1} dr}{\Gamma\left(\frac{p}{2} + 1\right)} \qquad \ldots (2.124)$$

where $\Gamma(\cdot)$ is the gamma function. Equation (2.123) may be written on substituting equation (2.124) ;

$$P(r^2 \leq \ell^2) = \frac{p2^{-\frac{p}{2}}}{\Gamma(\frac{p}{2}+1)} \int_0^{\ell} \exp\left(\frac{-r^2}{2}\right) r^{p-1} dr \qquad \ldots (2.125)$$

This equation gives the probability that the error vector $\underline{z}$ lies within an error ellipsoid corresponding to $r^2 \leq \ell^2$. The integral is easily evaluated since the general form for the chi-square distribution is

$$F_{\chi^2}(y) = \frac{1}{2^{\frac{\nu}{2}} \Gamma\left(\frac{\nu}{2}\right)} \int_0^{y} u^{\left(\frac{\nu}{2}\right)-1} \exp\left(\frac{-u}{2}\right) du, \qquad \ldots (2.126)$$

for ν degrees of freedom. Letting $r^2 = u$, $p = \nu$ and $y = 1$ in equation (2.125) the equation is transformed to a form which is the integral of the chi-square pdf, with p degrees of freedom ($p >> 1$). Therefore

$$P(r^2 \leq \ell^2) = pF_{\chi^2}(\ell) \qquad \ldots (2.127)$$

and the value of ℓ is chosen so that the desired level of confidence in the solution estimates error envelope may be achieved. If $\ell_{1-\alpha}$ is the ℓ value associated with the $100(1-\alpha)\%$ confidence region, then

$$\ell_{1-\alpha}(p) = [\chi^2(p)]^{\frac{1}{2}} \qquad \ldots (2.128)$$

where

$\chi^2(p)$ is the chi square value for p degrees of freedom and $100(1-\alpha)\%$ confidence.

The 100(1-α)% confidence region of $\hat{\underline{x}}$ is the interior of the hyper-ellipsoid

$$(\hat{\underline{x}} - \underline{x})^T \hat{S}^{-1} (\hat{\underline{x}} - \underline{x}) = \ell^2_{1-\alpha}(p) \qquad \ldots (2.129)$$

All that remains, is to find estimates of the values of the confidence regions at each level of discretization. The confidence regions, in the principal axes co-ordinate system can be determined without difficulty. The extreme "lengths" of these axes are expressed in terms of the set of co-ordinates $g_1, g_2, \ldots g_p$ of equation (2.113), since the g_i, i=1,2,...,p are just the projections of the profile vector "errors" $(\hat{\underline{x}} - \underline{x})$ onto the principal axes (the $\underline{l}_i$, i = 1,2,...,p) of the hyperellipsoid of equation (2.96). From equation (2.117)

$$\begin{aligned} r^2 &= \underline{z}^T \underline{z} \\ &= z_1^2 + z_2^2 + \ldots + z_p^2 \\ &= \lambda_1 g_1^2 + \lambda_2 g_2^2 + \ldots + \lambda_p g_p^2 \end{aligned} \qquad \ldots (2.130)$$

using equation (2.116). Therefore, with confidence 100(1-α)%, the maximum "lengths" (or co-ordinate values) for the principal axes (of $\hat{S}$) are given by the set of equations (from equations (2.129) and (2.130)) :

$$g_1 = \pm \ell_{1-\alpha}(p) \lambda_1^{-\frac{1}{2}} \quad , \quad g_2 = 0 \quad , \quad g_3 = 0, \ \ldots\ldots\ldots\ldots \ g_p = 0$$

$$g_1 = 0, \quad g_2 = \pm \ell_{1-\alpha}(p) \lambda_2^{-\frac{1}{2}}, \quad g_3 = 0, \ \ldots\ldots\ldots\ldots \ g_p = 0$$

$$g_1 = 0, \qquad g_2 = 0, \quad g_3 = 0, \ \ldots\ldots\ldots\ldots \ g_p = \pm \ell_{1-\alpha}(p) \lambda_p^{-\frac{1}{2}}$$

$$\ldots (2.131)$$

since the g_i (and therefore the z_i) are independent. Alternatively

equation (2.131) can be understood as follows. The lengths of the principal axes of the hyperellipsoid (equation (2.129)) are given by the reciprocals of the square roots of the eigenvalues of $\hat{S}^{-1}$. Therefore the projections of the estimate errors $(\underline{\hat{x}} - \underline{x})$ onto the principal axes with $100(1-\alpha)\%$ confidence (i.e. $r^2 = \ell^2_{(1-\alpha)}(p)$) are just

$$g_i = \pm \ell_{1-\alpha}(p) \lambda_i^{-\frac{1}{2}} , \quad i = 1,2,\ldots,p \qquad \ldots (2.132)$$

In order to determine the confidence regions of $\underline{\hat{x}}$ as specified by $\hat{S}$, all that need be determined is the relationship between the g_i $(i = 1,2,\ldots,p)$ values in the principal co-ordinate system $(l_i, i=1,2,\ldots,p)$ and the orthonormal basis vectors of the profile estimate $\underline{\hat{x}}$.

Equation (2.131) may be rewritten, thus :

$$G = \pm \ell_{1-\alpha}(p) \; \mathrm{diag}\left[\lambda_1^{-\frac{1}{2}} \; \lambda_2^{-\frac{1}{2}} \ldots\ldots \lambda_p^{-\frac{1}{2}} \right] \qquad \ldots (2.133)$$

equation (2.113) specifies :

$$G = L^T X' \qquad \ldots (2.134)$$

where

$$X' = \left[\underline{X}'_1 \; \underline{X}'_2 \ldots\ldots \underline{X}'_p \right] \qquad \ldots (2.135)$$

and the $\underline{X}'_i$ are the co-ordinates of $(\underline{\hat{x}} - \underline{x})$ for the i^{th} axis of the hyperellipsoid. Therefore

$$L^T X' = \pm \ell_{1-\alpha}(p) \mathrm{diag}\left[\lambda_1^{-\frac{1}{2}} \; \lambda_2^{-\frac{1}{2}} \ldots \lambda_p^{-\frac{1}{2}} \right] \qquad \ldots (2.136)$$

from equations (2.133) and (2.134). Hence,

$$X' = \pm \ell_{1-\alpha}(p) L \, \mathrm{diag}\left[\lambda_1^{-\frac{1}{2}} \; \lambda_2^{-\frac{1}{2}} \ldots\ldots \lambda_p^{-\frac{1}{2}} \right] \qquad \ldots (2.137)$$

Therefore

$$X' = \pm \ell_{1-\alpha}(p) \begin{pmatrix} l_{11}\lambda_1^{-\frac{1}{2}} & l_{12}\lambda_2^{-\frac{1}{2}} & \cdots\cdots\cdots & l_{1p}\lambda_p^{-\frac{1}{2}} \\ l_{21}\lambda_1^{-\frac{1}{2}} & l_{22}\lambda_2^{-\frac{1}{2}} & \cdots\cdots\cdots & l_{2p}\lambda_p^{-\frac{1}{2}} \\ & & & \\ & & & \\ & & & \\ l_{p1}\lambda_1^{-\frac{1}{2}} & l_{p2}\lambda_2^{-\frac{1}{2}} & \cdots\cdots\cdots & l_{pp}\lambda_p^{-\frac{1}{2}} \end{pmatrix} \quad \ldots (2.138)$$

and the columns of the right hand side of equation (2.138) (multiplied by $\pm \ell_{1-\alpha}(p)$) are the co-ordinates of $(\underline{\hat{x}} - \underline{x})$ for any particular axis of $\hat{S}^{-1}$.

In order to find an estimate of the confidence regions at each level j of discretization (j = 1,2,...,p) it is necessary to find the projections of X'_{ji} , i = 1,....,p onto the p dimensional orthonormal solution profile basis vectors $\underline{b}_j$ where $b_i = 0$ when $i \neq j$ and $b_i = 1$ when i = j. The estimate of the magnitude of the 100(1-α)% confidence region at the j^{th} level of discretization will just be the largest projection of the $\underline{X}'_i$(i = 1,2,...,p) onto the basis vector $\underline{b}_j$. This will be a "good" estimate of the magnitudes of the confidence regions of the solution $\underline{\hat{x}}$, if either :

(i) the orientation of the hyperellipsoid principal axes are not very dissimilar from those of the basis vector $\underline{b}_i$ (in this case all other axes will have small projectors on the basis vectors $\underline{b}_i$ (i = 1,...,p)

or (ii) the hyperellipsoid is approximately spheroidal, in which case the orientation of the principal axes of the "hyperellipse" may be chosen to lie along the set of basis vectors $\underline{b}_j$ (j = 1,2,...,p)

If the inversion problem is poorly-conditioned, the covariance matrix $\hat{S}$ will be nearly singular. If $\hat{S}$ is singular (or nearly so), then given the argument of Section 2.4.2 it would be expected that no unique (or best) solution estimate could be defined. This indicates that the confidence regions for such a "solution" are infinitely large. The expression in equation (2.121) demonstrates the effects of a singularity in $\hat{S}$. This integral can be separated into p integrals multiplied together (since the z_i are independent). Whence, even if only one of the eigenvalues of $\hat{S}$ is zero, the probability that $r^2 \leqslant \ell^2$ (i.e. that any vector $\underline{z}$ lies in the "hyperellipsoid" of equation (2.129)) will be one. Accordingly, it is then not possible to find a "best" estimate $\underline{\hat{x}}$ for $\underline{x}$, since the confidence region for any $\underline{\hat{x}}$ are infinite, as expected from the discussion of Section 2.4.2.

A situation may arise whereby, although the inversion problem may not be ill-conditioned (or poorly conditioned) it may also not be "well"-conditioned. This situation exists when the condition number

$$\frac{\lambda_1}{\lambda_p} << 1 \qquad \ldots (2.139)$$

where

λ_p is the largest eigenvalue of $\hat{S}^{-1}$ and

λ_1 is the smallest eigenvalue

If this is the case, then effectively the hyperellipsoid is "elongated" along a number of its axes (i.e. those with small eigenvalues relative to λ_p)

It would seem that for the temperature retrieval problem the equations will probably never be very "well-conditioned" since in the atmosphere there are high correlations between temperatures at different altitudes. The elements of one row of the a priori covariance matrix S_x may be similar to a multiple of the corresponding elements

of some other row or rows of S_x. Therefore $\hat{S}$ will not be well conditioned since the matrix will be "nearly" singular.

In summary, it is evident from the foregoing discussion that it is not sufficient to just find a "best" estimate $\underline{\hat{x}}$ of the unknown temperature vector $\underline{x}$. The confidence regions, and therefore the extremal solutions of section 2.1(3(iii)) should also be found so that effects due to the "condition" of the inversion problem equations can be investigated.

2.4.7 Intrinsic Resolving Power of the MAP Estimator

In the case where there is no a priori data, and therefore no inversion of equation (2.40) in a MAP sense, an estimate of the vertical resolution in the satellite data may still be given. Backus and Gilbert (1967,1968,1970) have developed a theory which will give some understanding of the vertical resolution under these circumstances. The aim of the theory is to form a set of averages from the data, using a linear operation of the form

$$\underline{x}_a - \underline{\bar{x}} = G_a(\underline{y} - \underline{\bar{y}}) \qquad \ldots (2.140)$$

where $\underline{y}$ is the vector of direct satellite measurements,

$\underline{\bar{x}}$ is some mean state of the atmosphere, which would produce satellite observations $\underline{\bar{y}}$,

G_a is some linear operator, and

$\underline{x}_a$ is the "averaged" solution

Since $\underline{y}$ contains information about the correct solution (from equation (2.40)), equation (2.140) provides an "averaged" version of the correct unknown profile $\underline{x}$, thus

$$\underline{x}_a - \underline{\bar{x}} = R(\underline{x} - \underline{\bar{x}}) + \underline{e}_a \qquad \ldots (2.141)$$

where $e_a = G_a e$ is the random "error" in the estimate $\underline{x}_a - \underline{\bar{x}}$, and the matrix R (which depends on G_a and the weighting functions) provides

a "window" through which the "correct" solution is viewed, with error $\underline{e}_a$, and is therefore an estimate of the intrinsic resolving power of the estimator. It is a result of the Backus and Gilbert (henceforth BG) theory that some balance (or tradeoff) must be sought between the "size" of the window and the size of the random error $\underline{e}_a$. That is, as the window size is decreased, the random error $\underline{e}_a$ increases (e.g. see Conrath (1972)).

The purpose of this section is to determine the intrinsic vertical resolving power of a MAP estimator by deducing for the MAP estimator the form of the window function R of equation (2.141) above. Relevant estimator diagnostic properties of the BG theory will be reviewed (following Conrath (1972)) and applied to the MAP estimator of equation (2.77).

Estimator Diagnostic Properties of the Backus and Gilbert Theory

Consider equation (2.77) :

$$\hat{\underline{x}} - \bar{\underline{x}} = S_x K^T (K S_x K^T + S_e)^{-1} (\underline{y} - \bar{\underline{y}}) \qquad \ldots (2.77)$$

where

$$\bar{\underline{y}} = K\bar{\underline{x}} \qquad \ldots (2.142)$$

and all other variables have the same meaning as before. The matrices S_x, K and S_e are constant for a given MAP estimator (i.e. a priori matrix S_x and satellite measurement noise matrix S_e). If these quantities are not altered, equation (2.77) may be written :

$$\hat{\underline{x}} - \underline{x} = G(\underline{y} - \bar{\underline{y}}) \qquad \ldots (2.143)$$

where

$$G = S_x K^T (K S_x K^T = S_e)^{-1} \qquad \ldots (2.144)$$

and G is a matrix linear operator (dimension pxn) used to determine the MAP estimate of $\underline{x} - \bar{\underline{x}}$, that is $\hat{\underline{x}} - \bar{\underline{x}}$.

Let

$$\Delta\underline{x} \equiv \hat{\underline{x}} - \bar{\underline{x}} \qquad \ldots (2.145)$$

and

$$\Delta\underline{y} \equiv \underline{y} - \bar{\underline{y}} \qquad \ldots (2.146)$$

From equation (2.143) on substituting equations (2.145) and (2.146)

$$\Delta\hat{\underline{x}} = G\Delta\underline{y} \qquad \ldots (2.147)$$

Consider the linearized form of the radiative transfer equation (equation (2.35)). Neglecting the ground and noise terms in this equation, and writing it in terms of continuous functions for $\underline{x}$ and K, then :

$$y_j = \int_{z=0}^{z=z_t} x(z)K_j(z)\,dz \qquad \ldots (2.148)$$

where y_j is the radiance for the j^{th} channel,

$x(z)$ is the "actual" or "true" temperature profile, a function of height z,

$K_j(z)$ is the satellite weighting function for the j^{th} channel, and

z_t is the effective top of the atmosphere.

This equation may also be written in matrix component form :

$$y_j = \sum_{i=1}^{p} K_{ji}x_i \qquad \ldots (2.149)$$

where the vector components have the same meaning as in equations (2.40) and (2.41). On combining equations (2.149) and (2.142)

$$y_j - \bar{y}_j = \sum_{i=1}^{p} K_{ji}(x_i - \bar{x}_i)$$

or

$$\Delta y_j = \sum_{i=1}^{p} K_{ji}\Delta x_i \qquad \ldots (2.150)$$

where i refers to the level of discretization

$\Delta x_i \equiv x_i - \bar{x}_i$, and

j refers to the j^{th} channel of the SCR

In terms of perturbations Δy_i and $\Delta x(z)$, (now considered a continuous function) equation (2.148) may be written

$$\Delta y_j = \int_{z=0}^{z_t} \Delta x(z) K_j(z) dz \qquad \ldots (2.151)$$

Finally, consider equation (2.147) in component form. For a particular level of discretization i,

$$\Delta \hat{x}_i = \sum_{j=1}^{n} G_{ij} \Delta y_j \qquad \ldots (2.152)$$

On substituting equation (2.151) into equation (2.152),

$$\Delta \hat{x}_i = \int_{z=0}^{z_t} \sum_{j=1}^{n} G_{ij} K_j(z) \Delta x(z) dz \qquad \ldots (2.153)$$

or

$$\Delta \hat{x}_i = \int_{z=0}^{z_t} A_i(z) \Delta x(z) dz \qquad \ldots (2.154)$$

where

$$A_i(z) = \sum_{j=1}^{n} G_{ij} K_j(z) \qquad \ldots (2.155)$$

and i,j and z are the same quantities as defined above, except that z in equation (2.155) is discretized by the tabulation interval (z=ih)

From equation (2.154) it can be seen that the estimate of the perturbation from the mean profile $\Delta \hat{x}$ at level i, calculated with the MAP estimator is just the weighted average of the true pertur-

bation $\Delta x(z)$. The weighting is simply determined by the "averaging kernel" $A_i(z)$. The vector $A_i(z)$ provides a window through which the correct solution profile $(\underline{x} - \bar{\underline{x}})$ is viewed, as stated in the introduction to this section. Accordingly, the intrinsic vertical resolution of an estimated profile at some height (level of discretization) i is determined by the behaviour of the averaging kernel $A_i(z)$ relevant to height z_i (i.e. level i).

In the ideal case $A_i(z)$ is a Dirac Delta function, but since equation (2.155) only has a finite number of terms there will be some spread in $A_i(z)$ about the level i. A measure of this spread is given by Backus and Gilbert (1970).

$$s_i = 12 \int_{z=0}^{z_t} (z_i - z)^2 A_i^2(z)\,dz \qquad \ldots (2.156)$$

where s_i is the Backus and Gilbert measure for the spread of the averaging kernel $A_i(z)$ and

z_i refers to the height at discretization level i

The normalising factor 12 has been chosen such that when $A_i(z)$ is a rectangular function of width ℓ centred on z_i and satisfying the equation

$$\int_{z=0}^{z_t} A_i(z)\,dz = 1 \qquad \ldots (2.157)$$

then $s_i = \ell$. For any averaging kernel $A_i(z)$ the function to be integrated in the calculation of s_i is a quadratic polynomial in z with a minimum at $z=c_i$;

$$c_i = \int_{z=0}^{z_t} z A_i^2(z)\,dz \Bigg/ \int_{z=0}^{z_t} A_i^2(z)\,dz \qquad \ldots (2.158)$$

where c_i by definition is called the "centre" of the averaging kernel $A_i(z)$. The "spread" of $A_i(z)$ about the "centre" of $A_i(z)$ may also be specified. This value is called the "resolving length" of $A_i(z)$,

written w_i, and

$$w_i = s_{c_i}$$

$$= 12 \int_{z=0}^{z_t} [c_i - z]^2 A_i^2(z)\, dz \qquad \ldots (2.159)$$

The "length" of the interval around c_i that contains the heavily weighted values of Δx is the resolving length of the estimator near c_i. It can also be shown (by substitution) that the spread of the averaging kernel $A_i(z)$ may be expressed in terms of the centre and resolving length of $A_i(z)$.

$$s_i = w_i + 12\,[z_i - c_i]^2 \int_{z=0}^{z_t} A_i^2(z)\,dz \qquad \ldots (2.160)$$

The spread of $A_i(z)$ can be large either because the resolving length of $A_i(z)$ is large or because the centre of $A_i(z)$ is not near level i (that is, height z_i).

The BG theory can also be used to determine the size of the errors in the estimated solution vector $(\underline{\hat{x}} - \underline{\bar{x}})$ due to the measurement errors in the satellite SCR data (i.e. the propogation errors). Consider equation (2.147) :

$$\Delta\underline{\hat{x}} = G\Delta\underline{y} \qquad \ldots (2.147)$$

If the errors in Δy are given by the measurement covariance matrix S_e, then the variance $\sigma^2_{\Delta\underline{\hat{x}}}(z_i)$ in the MAP estimated perturbation profile, due to this measurement error is just

$$\sigma^2_{\Delta\underline{\hat{x}}}(z_i) = \sum_{jk=1}^{n} G_{ij} S_{e_{jk}} G^T_{ik} \qquad \ldots (2.161)$$

If each of the σ_{e_i} of S_e, $i = 1,2,\ldots,n$ is the same magnitude, say σ_e^2, then

$$S_e = \sigma_e^2 \, I \qquad \ldots (2.162)$$

and

$$\frac{\sigma_{\Delta\hat{\underline{x}}}(z_i)}{\sigma_e} = \left[\sum_{j=1}^{n} G_{ij} G_{ij}^T \right]^{\frac{1}{2}} \qquad \ldots (2.163)$$

defines a noise amplification factor for the retrieval estimator.

To summarize, if the averaging kernel $A_i(z)$ resembles a Dirac delta function, centred near z_i, then the estimated temperature $\Delta\hat{x}_i$ at level i (corresponding to height z_i) is an estimate of the true temperature Δx_i with intrinsic resolving power s_i. The error in the estimate $\Delta\hat{x}_i$ due to the measurement error in the satellite observations is given by equation (2.161). This value is not an estimate of the confidence region of $\Delta\hat{\underline{x}}$ at level i; only the full error analysis of Section 2.4.6 can give an estimate of the confidence regions for the MAP estimated retrieval profile $\Delta\hat{\underline{x}}$.

Data Information Content

If the averaging kernel, $A_i(z)$, (equation (2.155)) has large weight at altitudes not near level i (i.e. height z_i), the MAP estimated solution $\Delta\hat{x}_i$ for that level is constructed from the temperature information at levels not near the height z_i. The averaging kernel "window" is shifted from the height z_i. Alternatively, it could be said that the estimator is unable to retrieve a "correct" estimate of the temperature for level z_i since it does not "contain" the "intrinsic information" necessary for a retrieval at the height. This lack of intrinsic information is due to the shape of the weighting functions K, the atmospheric covariance matrix S_x, and the satellite measurement noise matrix S_e. A qualitative measure of the ability of the MAP estimator (of equation (2.145)) to retrieve temperature profiles, given a series of satellite weighting functions,

their covariance matrix S_e, and a set of a priori data, can be determined by examining :

(i) the calculated values for the centres of the averaging kernels $A_i(z)$, for a suitably chosen set of heights (ranging from i = 1 to i = p) and

(ii) examining the spread and resolving length characteristics of the averaging kernels at the same set of heights.

If the centre of the averaging kernel $A_i(z)$, for some height z_i is not close to the height z_i, then the MAP estimator cannot correctly retrieve the atmospheric temperature at this height. If the resolving lengths of a set of averaging kernels $A_i(z)$, where the z_i are appropriate to the heights of the peaks of the weighting functions are larger than the resolving lengths of the corresponding satellite weighting functions, and the error amplification term (of equation (2.162)) is greater than one; the MAP estimator actually reduces the resolving power of the satellite data. Under these circumstances an inversion of the satellite data should not be performed since vertical resolution in the data is lost.

Final Comments

Jackson (1978) performed an interesting analysis on the resolving power of data using BG theory. He considers a perturbation on an a priori vector $\underline{\bar{x}}$. When the estimated solution vector (of equation (2.141)) perturbation term is small, and the elements may be treated as random variables which have mean zero and some covariance matrix C_x, ie a priori data, then the solution can be treated as a vector of random variables with mean zero and covariance matrix:

$$\mathrm{cov}\left[(\underline{x}_a - \underline{\bar{x}}) - (\underline{x} - \underline{\bar{x}}) \right] = (R-I)C_x(R-I)^T + G_a C_e G_a^T \quad \ldots (2.164)$$

where

$\text{cov}\ [\ (\underline{x}_a - \bar{\underline{x}}) - (\underline{x} - \bar{\underline{x}})\ ]$ is the covariance of the estimate,

C_e is the measurement covariance matrix,

$\underline{x}$ is the true profile vector,

$\bar{\underline{x}}$ is the mean profile vector and

$\underline{x}_a$ is the "averaged" solution profile vector.

Equation (2.164) can be used to optimize the tradeoff between resolving errors (the first term on the right hand side of equation (2.164)) and data errors (the second term on the right hand side). If G_a is chosen so as to minimize the variance of the total averaging errors (given in equation (2.164)), then the operator G_a is just the MAP estimator since $R = G_a K$. The optimum "averaged" solution $\underline{x}_a - \bar{\underline{x}}$, obtained from BG theory on including a priori data is just the solution estimator that would be found if MAP theory were used. It follows that the solution covariance matrices will also be identical.

Jackson (1978) has demonstrated that under the given assumptions, (and on including a priori data), an optimum estimator may be found using the BG theory. This retrieval estimator minimizes the total variance of the solution covariance matrix, and is therefore optimum in that it "finds" the optimum tradeoff between vertical resolution and random error in the temperature profile estimates. Without using a pirori data, it is not possible to define this optimum tradeoff (see for example Conrath (1972)). Accordingly inclusion of a priori data :

(i) makes the problem solvable, in the sense that the variance of the solution profile is not to large, and

(ii) enables the BG theory to be used to define an optimum tradeoff between vertical resolution and error magnification. This estimator is the MAP estimator.

2.4.8 An Empirical Orthogonal Function Representation of the Retrievals

One problem remains, how the represent the estimated solution vector $\underline{\hat{x}}$ in a concise and physically meaningful way?

If the p eigenvalues of a given a priori atmospheric temperature covariance matrix S_x (dimension pxp) are all distinct then S_x has p linearly independent eigenvectors. Moreover, these eigenvectors $\underline{1}_i$ i=1,2,...,p belonging to eigenvalues λ_i, i=1,2,...,p are unique apart from a non zero scalar multiplier (Franklin (1968)). This set of eigenvectors is also called a set of empirical orthogonal functions (henceforth EOF's). Since the series of EOF's form a complete basis set they may be used as a basis set for the representation of any p dimensional vector $\underline{\hat{x}}$. The profile $\underline{\hat{x}}$ can be represented by a set of projection coefficients. However, a more logical approach is to specify the mean profile $\underline{\bar{x}}$ for the set of profiles making up the a priori sample used to calculate S_x, and to construct the difference profile $\underline{\hat{x}} - \underline{\bar{x}}$. In this case, the form of the profile $\underline{\hat{x}}$ need not be constructed, only the detailed differences $\underline{\hat{x}} - \underline{\bar{x}}$. If the number of EOF's needed to "correctly" represent the vector $\underline{\hat{x}} - \underline{\bar{x}}$ is much smaller than p then this is a concise representation of the solution profile $\underline{\hat{x}}$.

EOF Analysis Details

Consider the pxp dimensional a priori atmospheric temperature covariance matrix S_x. This matrix is constructed from a sample of atmospheric temperature profiles for a particular latitude zone and season. The sample's mean temperature profile $\underline{\bar{x}}$ is constructed using equation (2.93), an unbiased estimator for $\underline{\bar{x}}$ (Deutsch (1965)). If the set of profiles making up the sample is truely representative of atmospheric temperature variations (i.e. contains"all" information about atmospheric temperature variations) then S_x will describe well the variance and covariance of the atmospheric temperatures. The

total atmospheric temperature variance is just the trace of S_x since the diagonal components of S_x are the variances of the temperatures at each level.

Transforming S_x to its principal axes co-ordinate system

$$L^T S_x L = \Lambda \qquad \ldots (2.165)$$

where

L is an orthonormal matrix, and

$\Lambda = \text{diag}[\lambda_1 \lambda_2 \ldots . \lambda_p]$ is a diagonal matrix of the eigenvalues of S_x,

$$L^T L = I \qquad \ldots (2(166)$$

therefore

and
$$L^T = L^{-1}$$
$$L = [\underline{l}_1 \; \underline{l}_2 \; \underline{l}_3 \ldots . \underline{l}_p] \qquad \ldots (2.167)$$

If the $\underline{l}_i$, i=1,2,...,p are distinct then the eigenvectors form a complete basis set, as noted in the introduction to this section. The eigenvalues and their eigenvectors can be ordered such that $\lambda_i \leqslant \lambda_j$ if $i > j$.

Since L is a similarity transformation

$$\text{tr}(S_x) = \text{tr}(\Lambda) \qquad \ldots (2.168)$$

where tr(·) is the trace of (·). The total variance of the atmospheric temperatures is just the sum of the eigenvalues of S_x. Each eigenvector $\underline{l}_i$, i=1,2,...,p explains a certain amount of the temperature variance of the atmosphere (about the mean state $\underline{\bar{x}}$). The actual amount explained (by each eigenvector) is just :

$$100 \left(\frac{\lambda_i}{\text{tr}(\Lambda)} \right) \% \qquad i = 1,2,\ldots,p \qquad \ldots (2.169)$$

Owing to the nature of the matrix S_x discussed in Section 2.4.6 it is to be expected that a large percentage of the total atmospheric temperature variance can be explained by a small number (compared

with p) of eigenvectors (EOF's) $\underline{l}_i$ of S_x, i=1,2,...,n. The vector $\hat{\underline{x}} - \bar{\underline{x}}$ can therefore be constructed, "correctly", using only a subset of the EOF's of matrix S_x.

The vector $\hat{\underline{x}} - \underline{x}$ may be written

$$\hat{\underline{x}} - \bar{\underline{x}} = \sum_{i=1}^{n} c_i \underline{l}_i + \text{residual}(n) \qquad \ldots (2.170)$$

where the c_i, i=1,2,...,n are a set of projection coefficients and the vector residual(n), is a function of n. If a reason for truncating the set of EOF's at $\underline{l}_n$ can be established then it is possible to represent some estimated retrieval profile $\hat{\underline{x}}$ by a set of n projection coefficients c_i, plus the mean profile vector $\bar{\underline{x}}$. This new concise representation of $\hat{\underline{x}}$ is a "good" representation if $n << p$ and some criterion for using only the first n EOF's in reconstructing the vector $\hat{\underline{x}} - \bar{\underline{x}}$ can be established.

Truncation Criteria

Rinne and Jarvenoja (1979) have examined four suggested methods for finding the value of n above. These may be stated as follows :

(a) Eigenvectors corresponding to eigenvalues much larger than others should be retained, (Beale et al (1967)).

(b) From a log (eigenvalue) versus eigenvalue ordinal number graph called a LEV diagram. For this criterion the EOF series is truncated at the point where the LEV graph can be started by approximating it with a straight line. (Craddock and Flood (1969), Craddock and Flintoff (1970), Farmer (1971)).

(c) If the measurement noise in the profiles of the sample set is known, say α% then only (100-α)% of the total variance represents real atmospheric variance that can be measured. If α can be estimated, then a suitable truncation value for n can

be determined.

(d) Rinne and Jarvenoja suggest that an optimum truncation is when the expansion has "included" as much noise as real information still remains "unexplained".

These truncation methods have been examined by Rinne and Jarvenoja as they apply to the problem of specifying 500 mb height fields over the northern hemisphere. They have tested truncation criteria (a) to (d) above and find :

(i) method(a) is unsatisfactory, and

(ii) For large samples (for covariance matrix) criterion (c) requires fewer EOF's than do criteria (b) and (d)

Their interpretation of conclusion (ii) above is that method (c) considers the significance of a single profile (input to the covariance matrix) whereas criteria (b) and (d) concentrate on the efficiency of the EOF expansion and on the explanation of the true information. The LEV diagram technique of method (b) would seem to have little theoretical justification, except that, quoting Craddock and Flood (1969), "in meteorology, noise eigenvalues are in geometrical progression".

The problem of the variance of 500 mb height fields is physically different to the problem of the variance of vertical atmospheric temperature fields however the truncation criteria tested by Rinne and Jarvenoja should still be applicable. The principles involved are quite general (within meteorology) and no factor would seem to limit their applicability to only the analysis of truncated EOF series for 500 mb height field specifications. For the case of representation of atmospheric temperature profiles, truncation methods (b) and (c) will be used to determine suitable EOF series. Method (d) cannot be applied as the data set of profiles is too small to construct a matrix S_x which may be said to contain "all real temperature

information". The values of n determined from (b) can be expected to be larger than or approximately equal to that for the optimum method (d) (Rinne and Jarvenoja (1979)). No real atmospheric variance should be left out of an EOF expansion whose truncation point is determined by method (b).

A retrieved temperature profile should be able to be represented by a small set of EOF's. The EOF's are physically meaningful since they describe the variance structure of the atmosphere, and noise in the a priori data due to random measurement noise will be removed from the retrievals.

CHAPTER 3

INTRINSIC VERTICAL RESOLVING POWER

3.1 : INTRODUCTION

The purpose of this chapter is the examination of the intrinsic vertical resolution characteristics of MAP estimated temperature profiles retrieved from Nimbus 4 SCR data.

The temperature profile estimate derived with a MAP estimator is from equation (2.147);

$$\underline{\hat{x}} = \underline{\bar{x}} + G(\underline{y} - \underline{\bar{y}}) \qquad \ldots (3.1)$$

where $\underline{\hat{x}}$ is the retrieved temperature profile estimate, given a set of satellite observations $\underline{y}$, an a priori first guess profile $\underline{\bar{x}}$ and the estimator matrix G. In the following analyses it is assumed that vertical temperature structure of interest is not present in the a priori profile $\underline{\bar{x}}$. Rather, this temperature structure is determined by the second term on the right hand side of equation (3.1). Accordingly the intrinsic vertical resolution in the retrieved temperature profile $\underline{\hat{x}}$ is determined by the MAP estimator matrix of coefficients G. This matrix incorporates the height distribution and shape of the satellite weighting functions (or kernels). In order to specify the intrinsic vertical resolution in the retrieved profiles the Backus Gilbert resolution characteristics of MAP estimator matrices G are determined, as are the characteristics of the satellite weighting functions and Backus Gilbert defined linear combinations of the weighting functions.

From the discussion of Chapter 2 it is evident that the retrieval problem may not be well posed. The "conditioning" effect of the satellite "measurement" noise variance is therefore investigated

by considering the sensitivity of the MAP estimator Backus Gilbert resolution characteristics to changing satellite measurement noise variances.

The vertical resolving powers of six sets of MAP estimators are investigated. These estimators would be used to retrieve temperature profiles from Nimbus 4 SCR data at all latitudes between approximately 80^0S and 80^0N during two seasons which approximate summer and winter conditions in either hemisphere. The sets of estimators are divided into three latitude zones in order to account for the differences in atmospheric temperature structure with changing latitude. The zones are defined thus : equatorial (0^0 - 30^0), mid-latitudes (30^0 - 50^0) and high latitudes (50^0 - 80^0).

In the following results 1 scale height (sh) is assumed to be 7.5 km.

Finally, from case studies of these six sets of MAP estimators, and the resolution of Backus Gilbert retrieval estimators, general criteria relating the intrinsic vertical resolution of a set of satellite weighting functions to the vertical resolution of deduced retrieved temperature profiles are given.

3.2 : THE A PRIORI DATA SETS

The a priori data set for input to the MAP estimator calculation (equation (2.77)) is a suitable mean temperature profile and its covariance matrix, as discussed in Sections 2.4.3 and 2.4.5. This data set is sometimes referred to as the set of virtual observations, or more simply, the virtual observations (Rodgers (1976b)).

3.2.1 Virtual Observations

The mean profiles and covariance matrices are calculated from sets of suitable conjunctive rocketsonde-balloonsonde temperature profile observations for different latitude zones and"seasons". These

observations, which in the main are north-western hemisphere observations, are separated into three latitudinal zones : 0^0 to 30^0N, 30^0N to 50^0N and 50^0N to 80^0N, and two "seasons" : "summer" and "winter". The term seasons is used here to specify certain periods in the year (table 3), as opposed to a strict definition of the seasons. In the following, this meaning should be taken and the quotation marks will be deleted.

A measure of the accuracy of the mean profile estimate for each sample of profiles is determined by regarding the sample as an ensemble of non stationary "time series" of temperature as a function of height. A measure of the variance of the mean profile temperature error at some height z is just (by Bendat and Piersol (1966)) :

$$\mathrm{Var}\left[\hat{\bar{T}}(z)\right] = \frac{\sigma^2(z)}{M} \qquad \ldots (3.2)$$

where $\mathrm{Var}\left[\hat{\bar{T}}(z)\right]$ is the variance of the estimate of the mean temperature $\bar{T}$ at height z. The quantity $\sigma^2(z)$ is the associated variance of the temperature at height z and M is the sample size. The magnitude of the quantity $\mathrm{Var}[\cdot]$ will be used as an indication of the adequacy or inadequacy of a particular sample of profiles used to represent the nature of temperature fluctuations in the atmosphere.

The following subsections document the specifications of the latitudinal and seasonal a priori data sets.

The Equatorial "Summer" A Priori Data Set

The term "summer" is used here only in the sense that it refers to an a priori data set constructed from a sample of temperature profiles for months May, June and July from equatorial (0^0 - 30^0N) observation stations. The sample contains 203 profiles from years 1969 through 1972 , weighted toward the June temperature structure. The estimated mean profile and the calculated covariance matrix are reproduced in appendix D.

The largest mean profile variance occurs at mesospheric heights

where the variance is of the order of $30(r.u)^2$ corresponding from equation (3.2) to a mean temperature profile variance of the order of $0.15K^2$. Since the error is less than 1K the sample size is considered adequate.

On considering the structure of the covariance matrix (appendix D) it is observed that temperatures in the middle and upper stratosphere and the lower mesosphere correlate negatively with temperatures in the region of the tropopause. Near the stratopause there is also a negative correlation with temperatures in the troposphere. Both these correlations are relatively weak, as are the corresponding positive correlations with temperatures in the troposphere. Temperatures in the lower stratosphere and in the tropopause region correlate nagatively with temperatures in the troposphere.

The tropopause region is centred on 2.3 sh altitude (≈17 km) and the stratopause lies in the region of 6.8 sh altitude (≈51 km).

The Equatorial "Winter" A Priori Data Set

The term "winter" is used here only in the sense that it refers to an a priori data set constructed from a sample of temperature profiles for months December, January and February from equatorial observations stations. The sample consists of 155 profiles from years 1969 through 1972. The calculated mean temperature profile and covariance matrix are to be found in appendix E.

The heights for which the variance in the mean profile estimate is largest occur in the mesosphere, where the atmospheric temperature variance is of the order of $45(r.u)^2$ indicating a mean profile variance of approximately $0.3K^2$, and at ground level where the mean profile variance is of the order of $0.6K^2$. The sample size is considered adequate.

Examination of the covariance matrix indicates that temperatures in the lower mesosphere have a weak negative correlation with temperatures at the stratopause and tropopause. Temperatures in

the stratopause region have a weak positive correlation with temperatures at the tropopause and a stronger negative correlation with temperatures in the troposphere and lower stratosphere. At heights below the stratospause and above the tropopause there is a strong negative correlation with temperatures in the region of the tropopause. This negative correlation is strongest for heights in the lower stratosphere. There is also a weak negative correlation between the temperatures in the middle stratosphere and those in the lower troposphere. However, at all other heights below the stratopause and above the tropopause, temperatures are strongly positively correlated with those in the troposphere. In the region of the tropopause the temperatures have strong negative correlations with those in the lower troposphere.

The stratopause is in the region of 6.7 sh altitude (≈50 km) the tropopause occurs in the region of 2.5 sh altitude (≈19 km).

The Mid Latitude Summer a priori Data Set

A sample of 139 May, June, July and August temperature profiles were used to calculate the covariance matrix and mean temperature profile for this zone and season. Four summer seasons observations are included in the sample . The calculated mean profile and corresponding covariance matrix are recorded in appendix F.

The largest variance in the estimates of the mean temperature profile occurs near ground level where the atmospheric temperature variance is of the order of 55 $(r.u)^2$. The corresponding error in the mean profile estimate is therefore approximately $0.4K^2$. The atmospheric temperature variance in the lower mesosphere and stratopause region is of the order of $45(r.u)^2$ corresponding to a mean profile estimate variance of the order of $0.3K^2$. The sample size is considered adequate.

The correlations between the temperatures at different levels may be indicated on considering the covariance matrix in appendix F.

At heights above the middle of the stratosphere, extending into the lower mesosphere there is a negative correlation with the temperatures in the troposphere. Additionally at heights in the lower mesosphere, below the stratopause region and above the middle stratosphere there is a weak negative correlation with temperatures near the tropopause. In the lower stratosphere the temperatures have a strong positive correlation with temperatures in the troposphere and a weak negative correlation with temperatures in the region of the tropopause. Temperatures at tropopause heights correlate negatively with those in the troposphere.

The stratopause lies in the region of 6.7 sh altitude (≃50 km) and the tropopause in the region of 2.2 sh altitude (≃17 km).

The Mid-Latitude Winter a priori Data Set

The covariance matrix and mean temperature profile were constructed from a sample of 142 northern mid-latitude (30^0N - 50^0N) rocketsonde-balloonsonde temperature profiles. The sample profiles span four years, 1969 through 1972, for months December, January and February. Accordingly data from five winters are included in the sample. The covariance matrix and the calculated mean profile are listed in appendix G.

On examination of the covariance matrix it is found that the largest atmospheric temperature variances, 170 $(r.u)^2$, occur at heights near the stratopause. The corresponding variance in the mean profile estimate at these heights is of the order of $1.2K^2$. At other heights below the stratopause, the variance is much smaller, being of the order of $0.3K^2$. Accordingly it is expected that the sample size is adequate, if not completely satisfactory.

Further examination of the covariance matrix indicates that there is a strong negative correlation between temperatures in the lower mesosphere and those in the upper stratosphere and stratopause region. There is also a weak negative correlation with temperatures

in the troposphere. Temperatures at heights near the stratopause correlate negatively with temperatures in the stratosphere and troposphere, but have a positive correlation with temperatures at the tropopause. Both these correlations are weak. Temperatures in the middle and upper stratosphere correlate negatively with temperatures in the lower stratosphere and the upper troposphere, but positively with temperatures in the lower troposphere. Finally at heights in the lower stratosphere and in the vicinity of the tropopause, the temperatures correlate negatively with temperatures in the troposphere.

The stratopause occurs in the region of 6.9 sh altitude (≃51 km) and the tropopause in the region of 2.5 sh altitude (≃19 km).

The High Latitude Summer a priori Data Set

Ninety six profiles satisfied the selection criteria of the covariance calculation program, for high latitude stations (50^0N to 80^0N) and months May, June, July and August in years 1969 through 1972. The covariance matrix and sample mean profile can be found in appendix H.

The largest variances in atmospheric temperatures occur near ground level and in the upper stratosphere. The respective values are approximately 100 $(r.u)^2$ and $50(r.u)^2$. Using equation (3.2) these values indicate that the variances in the mean profile estimate at these heights are of the order of $1K^2$ and $0.5K^2$ respectively. Consequently the sample size is considered to be adequate although smaller than would be desired since errors in the mean profile estimate are of the order of 1K.

On consideration of the calculated covariance matrix it is apparent that temperatures in the region of the upper stratosphere, the stratopause and the lower mesosphere have a positive correlation with temperatures in regions at and above the tropopause, but a strong negative correlation with temperatures in the troposphere. At hei-

ghts in the middle stratosphere near 4 sh altitude (≈30 km) the temperatures correlate positively with all other levels. However, in the lower stratosphere and in the region of the tropopause the temperatures have a strong negative correlation with temperatures in the troposphere.

The stratopause is in the region of 6.9 sh altitude (≈52 km), the tropopause in the region of 1.7 sh altitude (≈13 km).

The High Latitude Winter a priori Data Set

From the TD5850 file of rocketsonde and balloonsonde temperature profiles for this latitudinal zone and season (months December, January and February), only 102 temperature profiles satisfied the selection criteria of the covariance calculation program (see Section 2.4.5). The sample incorporates data from five winter seasons for the years 1969 through 1972. The covariance matrix and sample mean profile are reproduced in appendix I.

The largest values of the temperature variance of the atmosphere occur at heights near 6 sh altitude. This variance is of the order of 210 $(r.u)^2$, corresponding to a variance in the mean profile estimate at these heights, of approximately $2K^2$. At other heights in the stratosphere and troposphere the atmospheric temperature variance is much smaller resulting in a mean profile estimate error of the order of $0.5K^2$. From this result it is apparent that the sample size for this zone is probably smaller than is desirable.

Consideration of the structure of the covariance matrix indicates that for temperatures at heights above 7.5 sh altitude, in the region of the stratopause, there is a weak negative correlation with temperatures in the stratosphere and at the tropopause. Additionally there is a weak positive correlation with temperatures in the troposphere. For heights below approximately 7.0sh altitude and above 2 sh altitdue there is a weak negative correlation with temperatures in the lower stratosphere, tropopause region and troposphere. Near 2 sh

altitude, in the isothermal region of the stratosphere there is a weak positive correlation with temperatures near ground level and in the lower troposphere. However at lower altitudes, but above 1.3 sh altitude, there is again a negative correlation with temperatures in the troposphere.

The "tropopause" is in the region of 1.3 sh altitude, (≃10 km) and the lower stratosphere is approximately isothermal. The stratopause is not well defined, but would appear to lie in the region of 7.5 to 8.0 sh altitude (≃58 km).

Comparisons between a priori Data Sets

The main characteristics of the different a priori data sets are displayed in table 4 below. Several observations may be made from the data in the table :

(a) For each latitudinal zone the average variance of the lowest four levels of the atmosphere (i.e. 0 to 0.3 sh altitude) is smaller in summer than in winter. The recorded value for the high latitudes winter ground level variance is probably underestimated since a large number of the sample's profiles did not have ground level temperatures reported. In these cases the ground level temperatures were inferred from previous observations.

(b) For the equatorial and mid-latitude data sets there is an approximate change of 20% in the temperature variances at tropopause heights, between the summer and winter data. However at high latitudes the difference in the variances of the tropospheric temperatures is much larger. The summer variance being larger than the winter variance.

TABLE 4 : CHARACTERISTICS OF THE A PRIORI DATA SETS

Latitudinal Zone	Season (Months)	Sample Size	Near Ground Level Temperature Variance $(r.u.)^2$ Δ	Tropopause Temperature Variance $(r.u.)^2$	Stratopause Temperature Variance $(r.u.)^2$	Largest Variance of Mean Temperature estmate K^2	Mean Profile Tropopause Height (sh)	Temperature of Tropopause ^0C	Mean Profile Stratopause Height (sh)	Temperature at Stratopause ^0C
EQUATORIAL (0^0-30^0N)	Summer (5,6,7)	203	~12	~10	~24	~0.15	2.3	-72.4	6.8	-5.5
	Winter (12,1,2)	155	~40	~8	~38	~0.3	2.4	-75.9	6.7	-4.1
MID-LATITUDES (30^0N-50^0N)	Summer (5,6,7,8)	139	~53	~8	~45	~0.3	2.2	-62.5	6.8	-3.2
	Winter (12,1,2)	145	~130	~10	~160	~1	2.5	-64.3	6.8	-7
HIGH-LATITUDES (50^0N-80^0N)	Summer (5,6,7,8)	96	~130	~19	~45	~1	1.7	-51	6.9	2
	Winter (12,1,2)	102	~140*	~10	~190	~2	~1.3	-54	~7.5	-21

Δ The near ground level temperature variance is the arithmetic average of the variances of the four lowest "levels" of the atmosphere. The abbreviation r.u. is short for radiance unit i.e. 1 $mWm^{-2}(cm^{-1})^{-1}st^{-1}$

* see text

(c) The variances of temperatures at the stratopause are much larger in winter than summer, for each of the latitude zones. The variances for each season also increase with increasing latitude. Additionally, on consideration of the covariance matrices of appendices D to I it is evident that the region of the stratopause is much wider in winter than in summer.

(d) The sample sizes are probably adequate for all but the high latitude data sets

(e) The temperature of the winter tropopause at high latitudes is much warmer than the mid latitudes tropopause, which in turn is warmer than the equatorial tropopause.

(f) At high latitudes the tropopause occurs at a lower altitude than either the mid-latitude or equatorial tropopauses. The height of the high latitudes winter tropopause is ill defined since the lower stratosphere is essentially isothermal, and is at a temperature close to that of the tropopause.

(g) For equatorial latitudes the summer stratopause is slightly cooler than the winter stratopause, however, for mid and high latitudes the reverse situation occurs. The temperature difference is large for the high latitude results. The winter stratopause becomes cooler with increasing latitude, whereas the summer stratopause becomes warmer with increasing latitude.

The broad features of the structures of the covariance matrices for the three latitudinal zones and two seasons may also be compared.

Firstly, consider the summer covariance matrices. The temper-

atures at upper stratospheric and lower mesospheric heights, for the mid and high latitude matrices, tend to have a negative correlation with tropospheric temperatures the correlation being stronger for the high latitudes case. Whereas, for the equatorial matrix temperatures at all heights above the middle of the stratosphere have a weak positive correlation with temperatures in the troposphere and a negative correlation with temperatures at the tropopause. For the mid and high latitude matrices at mid and lower stratospheric heights, there is a strong positive correlation with tropospheric temperatures. However, in this height range the equatorial matrix has a strong negative correlation with tropospheric temperatures. At tropopause heights the temperatures have a negative correlation with tropospheric temperatures, in each latitudinal zone.

Secondly, consider the winter covariance matrices for the three latitude zones. For the equatorial and mid latitudes matrices, temperatures in the mesosphere have a weak negative correlation with temperatures in the region of the stratopause. The equatorial matrix also has a negative correlation with temperatures at the tropopause whereas the mid-latitudes matrix has a positive correlation with temperatures in the troposphere. In each of the matrices, temperatures at the stratopause tend to correlate nagatively with temperatures in the troposphere and positively with temperatures at the tropopause. The mid and high latitudes matrices also have negative correlations between temperatures at the stratopause and those in the stratosphere. At mid and upper stratospheric heights the temperatures of the equatorial and mid-latitudes matrices correlate negatively with temperatures at the tropopause. At the same heights the mid latitude matrix temperatures also correlate negatively with temperatures in the lower stratosphere and middle troposphere. Also at these heights the temperatures of the high latitude matrix correlate negatively with temperatures in the lower stratosphere, tropopause region and tropo-

sphere. For low stratospheric heights the equatorial matrix retains the negative correlation with temperatures at the tropopause, whereas the mid and high latitudes matrices have strong negative correlations with temperatures in the troposphere. In the region of the tropopause the temperatures correlate negatively with temperatures in the troposphere in each latitude zone.

One feature of the covariance structure is present during both seasons in all three latitudinal zones, this is the negative correlation between tropopause and tropospheric temperatures.

During both seasons the equatorial matrices tend to have a negative correlation between temperatures in the stratosphere and those in the region of the tropopause. Similar comparisons cannot be made for the mid-latitudes seasons. At high latitudes, during both seasons, the temperatures in the stratosphere correlate negatively with temperatures in the troposphere. The overall structure of the correlations between different levels for the summer and winter matrices at high latitudes is not dissimilar, whereas they are quite dissimilar for the other two latitude zones considered.

3.2.3 Additional a priori "Information"

Additional a priori information may be used to modify the covariance matrices determined above.

The calculated covariance matrices include a component for the variance of the ground level temperature as well as components for the covariances between ground level temperatures and the temperatures at all other levels. If the ground temperature is known a priori, from some other measurement, then the associated covariance matrix is modified by this knowledge. The modification is given by Peckham (1974), and in terms of the atmospheric covariance matrix S_x, is expressed by the relation

$$S'_{x_{ij}} = S_{x_{ij}} - S_{x_{oi}} S_{x_{oj}} \Big/ S_{x_{oo}} \qquad \ldots (3.3)$$

where $S'_{x_{ij}}$ is an element of the modified (ground corrected) covariance matrix, (i,j=1,2,...,p). The suffix o refers to the ground values. The matrix S_x shall be termed the "original" a priori covarinace matrix in the following sections. The column and row of the ground corrected covariance matrix S'_x referring to ground level are transformed to zero vectors by equation (3.3).

A further "piece" of a priori information may be used to modify the original (or ground corrected) a priori covariance matrices. This piece of information puts a constraint on the allowed sizes of the covariances between temperatures at different levels in the atmosphere.

As mentioned in the preceeding sections, it is apparent that in each of the a priori (original) covariance matrices, there are heights where strong correlations exist between levels in the atmosphere widely separated in altitude. These correlations may have an adverse effect upon the intrinsic vertical resolution and stability of the derived MAP estimators, as will be shown in the following sections of this chapter. When this situation arises, the strong covariances between levels in the atmosphere widely separated in height may be removed by applying a gaussian "filter" to the original or ground corrected covariance matrices. The filter has the following form :

$$S'_{x_{ij}} = S_{x_{ij}} \exp\left(-\tfrac{1}{2}\left(\frac{i-j}{w}\right)^2\right) \qquad \ldots (3.4)$$

where $S'_{x_{ij}}$ is an element of the modified constrained matrix, (i,j=1,2,...,p), w is a parameter which shall be called the filter width, and $S_{x_{ij}}$ is an element of the original or ground corrected covariance matrix.

Alternatively this filter could be interpreted as a modification of the expectation operator used in the calculation of the original a priori covariance matrices. The defining equation for the $(i,j)^{th}$ element of the original matrix is equation (2.91), reproduced below :

$$S_{x_{ij}} = \frac{1}{M} \sum_{m=1}^{M} (b_{im} - \bar{b}_i)(b_{jm} - \bar{b}_j) \qquad \ldots (3.5)$$

where all quantities are as defined in equation (2.91). Application of the "filter" of equation (3.4) results in the equation :

$$S'_{x_{ij}} = \frac{1}{M} \exp\left[-\tfrac{1}{2}\left(\frac{i-j}{w}\right)^2\right] \sum_{m=1}^{M} (b_{im} - \bar{b}_i)(b_{jm} - \bar{b}_j) \qquad \ldots (3.6)$$

The "filter" modifies the form of the probability density function of the assumed random variable $(b_{km} - \bar{b}_k)$ for which k is an integer and $1 \leqslant k \leqslant p$. In the calculation of the original a priori covariance matrices, the density function is just the inverse of the sample size. The modified, constrained matrix is calculated using a density function dependent upon the sample size M, the height separation (i-j) and the parameter w. When (i-j) is large the density function value is small, and the corresponding covariance is smaller than that of the original matrix. Physically, the modified density function for the covariance calculation reduces the effect of any large correlations between temperatures at levels widely separated in height, that are present in the original samples of temperature profiles. The degree to which these correlations are removed is dependent upon the choice of the filter width parameter w. For a filter width of the order of 20 (i.e. 2 sh) the size of covariances close to the principal diagonal are not changed significantly, but large covariances far from the diagonal are reduced considerably.

3.2.3 Extrapolation of the Virtual Observations

The covariance matrices and sample mean temperature profiles calculated from the samples of rocketsonde-balloonsonde profiles extend from ground level to 8 sh altitude (approximately 60 km), in intervals of 0.1 sh. The satellite kernel for channel A of the Nimbus 4 SCR has non zero weighting at heights up to approximately 10 sh (≈75 km). The mean profiles and covariance matrices are "extrapolated" from 8 sh to 10.2 sh altitude.

The mean temperature profiles are simply extended by assuming the temperature profile has a constant lapse rate in the mesosphere. A lapse rate of -19 K/sh (which is much less than the dry adiabatic lapse rate) has been chosen. This figure being calculated from "US Standard Atmosphere 1976", atmospheric temperature-pressure tables. The equation for the extrapolation is :

$$T(z) = \frac{dT}{d(-\ln(p/p_o))} (z-8.0) + T(z_o=8.0) \quad \ldots (3.7)$$

where

$T(z)$ is the temperature at height z, for 8.1 sh $\leqslant z \leqslant$ 10.2sh,

$T(z_o=8.0)$ is the value of the mean profile temperature at 8 sh altitude, and

$\frac{dT}{d(-\ln(p/p_o))}$ is the lapse rate

The covariance matrices are extrapolated by assuming that the covariance matrix has only non zero entries on the principal diagonal at heights greater than 8.0 sh. The variances at each level are calculated for a given atmospheric temperature variance about the mean temperature profile. The value for the temperature variance is chosen such that the variance above 8.0 sh altitude is not larger than the variance at 8 sh. The variance is further assumed to be constant in the extrapolation height range. In practice, the assumed values

for the temperature variances are rather less than the range of highest and lowest mean monthly temperature variances of the US Standard Atmosphere 1976. This is expected since these are extremes for any location between the equator and the pole.

This method of extrapolating the covariance matrices does not introduce large errors into any MAP estimated temperature profiles since the channel A kernel weighting at heights above 8 sh altitude is not large. This point will be considered again in the final comments of Section 3.5.

3.3 : BACKUS GILBERT RETRIEVAL CHARACTERISTICS FOR THE NIMBUS 4 SCR KERNELS

The theory of Backus and Gilbert, discussed in Section 2.4.7 was originally proposed so that some useful information could be deduced from non well-posed problems. Conrath (1972) applied the theory to the atmospheric remote sensing problem. However, as Jackson (1978) has pointed out, the Backus and Gilbert technique is only of value when determining small perturbations on an a priori model. By definition, the observations do not contain enough information to form a complete solution, other than when the solution lies close to a zero vector (which of course is a priori data). In Section 2.4.7, only the diagnostic properties of the Backus Gilbert (henceforth,BG) technique, as applied to the MAP estimator, were considered. The theory can however be applied so that it may be used to determine the G matrix of equation (2.147), (see introduction of Section 2.4.7):

$$\Delta\hat{\underline{x}} = G\Delta y \qquad \ldots (2.147)$$

As stated above, the BG inversion technique uses only the information available in the satellite measurements. The satellite measurement kernels (weighting functions) are combined linearly, such that at some height the resultant "averaging kernel" is interpreted as repre-

senting the mean temperature over a layer of the atmosphere. The width of the layer is defined by the width (i.e. the spread) of the averaging kernel.

Since the BG inversion estimator is formed from the satellite information alone, the corresponding averaging kernels may be used to define the intrinsic information content and vertical resolution of the satellite measurements, that is, of the satellite weighting functions.

3.3.1 The Backus Gilbert Retrieval Estimator

Outlined in the following paragraphs is the derivation of the BG inversion (retrieval) estimator, the equivalent of the G matrix of equation (2.147).

Consider a row vector $\underline{g}_i$ of the G matrix, referring to some height z_i. For the choice of a particular $\underline{g}_i$, there will be an associated error variance $\sigma^2_{\Delta\hat{\underline{x}}}(z_i)$ given by equations (2.161) or (2.163). As Conrath (1972) states; "Ideally one would like to be able to choose the vector $\underline{g}_i$ such that both the error variance, $\sigma_{\Delta\hat{\underline{x}}}(z_i)$ and the spread s_i (equation (2.156)) are minimized. This cannot be done". Instead, a linear combination of the spread and noise variance is minimized. Consequently, there is a tradeoff between vertical resolution and noise.

The averaging kernel formed on choosing a particular vector $\underline{g}_i$ is given by equation (2.155), that is :

$$A_i(z) = \sum_{j=1}^{n} g_{i_j} K_j(z) \qquad \ldots (3.7)$$

The spread of the averaging kernel is found, using equation (2.156). Hence :

$$s_i = 12 \int_0^{z_t} (z_i - z)^2 \sum_{j\,l}^{n} g_{i_j} K_j(z) g_{i_l} K_l(z) dz \qquad \ldots (3.8)$$

or $$s_i = \sum_{j}^{n} \sum_{l} g_{i_j} g_{i_l} S_{jl}(z_i) \qquad \ldots (3.9)$$

where

$$S_{jl}(z_i) = 12 \int_0^{z_t} (z_i - z)^2 K_j(z) K_l(z) dz \qquad \ldots (3.10)$$

Following Conrath (1972), the following matrix a linear combination of the averaging kernel spread and the satellite measurement noise variance S_e is defined :

$$W_{jl}(z_i, q) = qS_{jl}(z_i) + (1-q) r S_{e_{jl}} \qquad \ldots (3.11)$$

where the constant r is included to make the physical dimensions of the two terms on the right hand side of equation (3.11) identical. The parameter q is varied between 0 and 1 and is used to tradeoff the vertical resolution against the noise. The problem of finding a suitable vector $\underline{g}_i$ is reduced to finding the vector which has the smallest spread s_i when the matrix $W(z_i, q)$ is substituted in place of matrix $S_{jl}(z_i)$ in equation (3.9). The minimization problem requires the spread s_i of equation (3.9) to be minimized subject to the constraint that the averaging kernel is unimodular, as required by the BG theory. The solution $\underline{g}_i = 0$ is excluded. If

$$u_i = \int_0^{z_t} K_i(z) dz \quad , \quad i = 1, 2, \ldots, n \qquad \ldots (3.12)$$

then from equation (3.9), the expression to be minimized is :

$$Q = \underline{g}_i W(z_i, q) \underline{g}_i^T \qquad \ldots (3.13)$$

subject to the constraint

$$\underline{g}_i \underline{u}^T = 1 \qquad \ldots (3.14)$$

Hence, to find the solution vector $\underline{g}_i$ the equation to be solved is:

$$\frac{\partial}{\partial \underline{g}_i} \left[q(\underline{g}_i S \underline{g}_i^T) + (1-q)(\underline{g}_i S_e \underline{g}_i^T) + \lambda \underline{g}_i \underline{u}^T \right] = 0 \qquad \ldots (3.15)$$

where λ is an undetermined multiplier. The solution is given by Conrath (1972) and Rodgers (1976b) :

$$\underline{g}_i(q) = \frac{W(z_i,q)^{-1} \underline{u}^T}{\underline{u}\, W(z_i,q)^{-1} \underline{u}^T} \qquad \ldots (3.16)$$

The vector $\underline{g}_i$ is a function of the tradeoff parameter q.

The BG measures of spread, centre and resolving length of a minimum spread linear combination of the satellite weighting functions; the BG averaging kernel, may be used to provide a means of establishing the information content and resolution of the satellite observations.

In the following subsections the calculated BG averaging kernels are used to determine the intrinsic resolution of the Nimbus 4 SCR satellite measurements.

3.3.2 Resolution Characteristics of Nimbus 4 SCR Data

To specify the vertical resolution of the individual channel observations, the BG measures of spread, centre and resolving length are calculated for the Nimbus 4 SCR weighting functions (that is, the satellite kernels). The value of z_i used in equation (2.156) is chosen to be the height of the peak of the particular weighting function. The results of these calculations are given in table 5 below. These values shall be used as bench marks in examining the vertical resolving power of all retrieval estimators.

TABLE 5 : NIMBUS 4 SCR WEIGHTING FUNCTION CHARACTERISTICS

CHANNEL	z_i (sh) (±.1 sh)	CENTRE (sh)	RESOLVING LENGTH (sh)	SPREAD (sh)
A	6.1	6.15	2.05	2.06
B	4.2	4.38	1.88	1.97
C	2.9	3.19	1.83	2.12
D	2.5	2.68	1.41	1.54
E	1.5	1.69	1.27	1.44
F	0.0	0.42	1.32	2.56

BG averaging kernel tradeoff curves were calculated using the assumptions that the satellite measurement errors are uncorrelated and of equal magnitude for all six channels. A noise amplification factor α, at some height z_i is defined thus :

$$\alpha(z_i) \equiv \frac{\sigma_{\Delta\hat{\underline{x}}}(z_i)}{\sigma_e} = (\underline{g}_i \, \underline{g}_i^T)^{\frac{1}{2}} \qquad \ldots (3.17)$$

where $S_e = \sigma_e^2 I$. Equation (3.17) is equivalent to equation (2.163). The quantity α is a dimensionless number when the input satellite measurement noise σ_e , and the output noise $\sigma_{\Delta\hat{\underline{x}}}(z_i)$ are expressed in radiance units.

Tradeoff curves of spread against noise amplification α, for a set of representative heights are plotted in figure 9. The heights chosen are : (a) in the troposphere (1.5 sh altitude), (b) near the tropopause (2.5 sh altitude), (c) in the stratosphere (4.5 sh altitude), and (d) and (e), near the stratopause (5.5 sh and 6.0 sh altitude). The gross features of the tradeoff curves are the same for all heights, with the spread increasing as the noise amplification factor α decreases, that is, as the value of q (equation (3.11)) is decreased from a value of one, to zero. For q=0 the value of α is

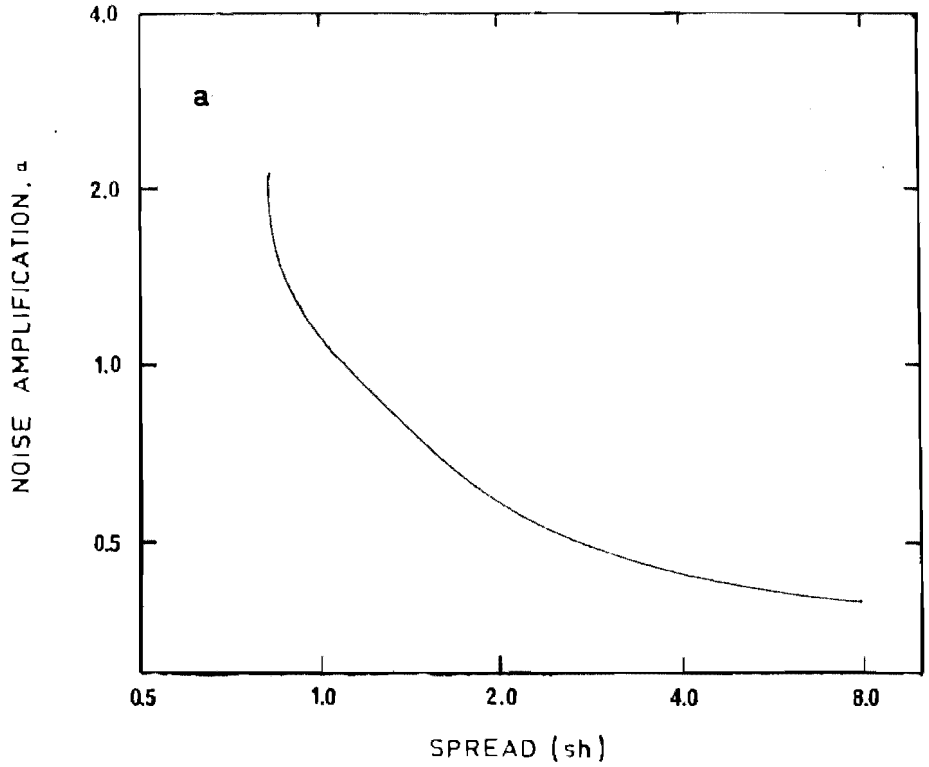

FIGURE 9 (a) : Backus Gilbert Tradeoff Curve for height 1.5 sh

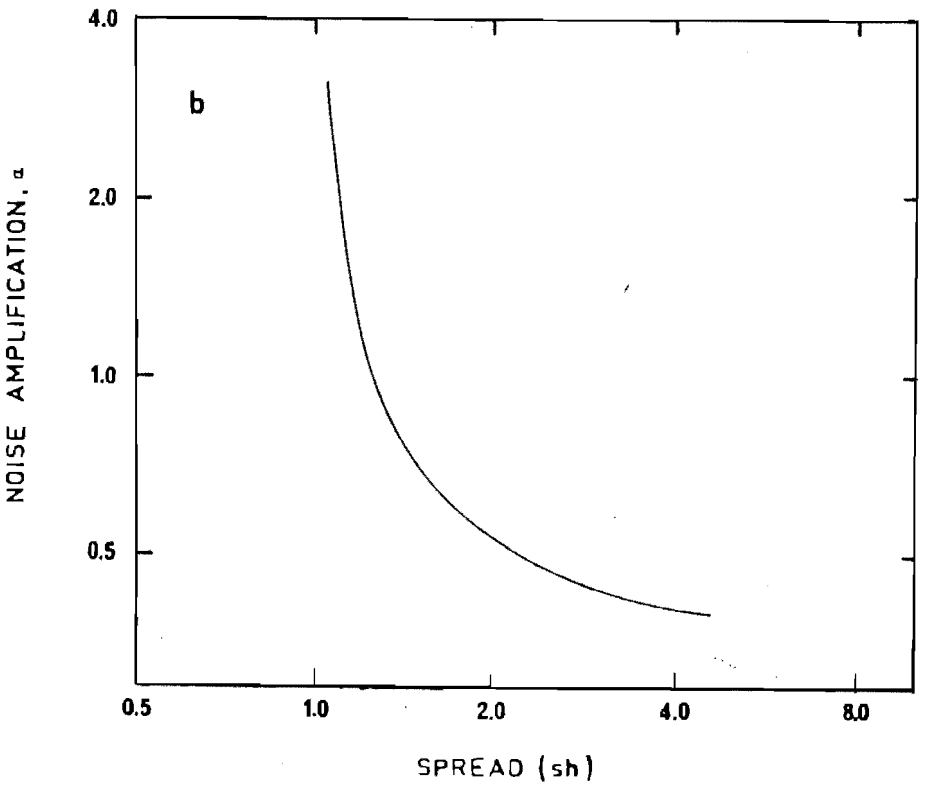

FIGURE 9 (b) : Backus Gilbert Tradeoff Curve for height 2.5 sh

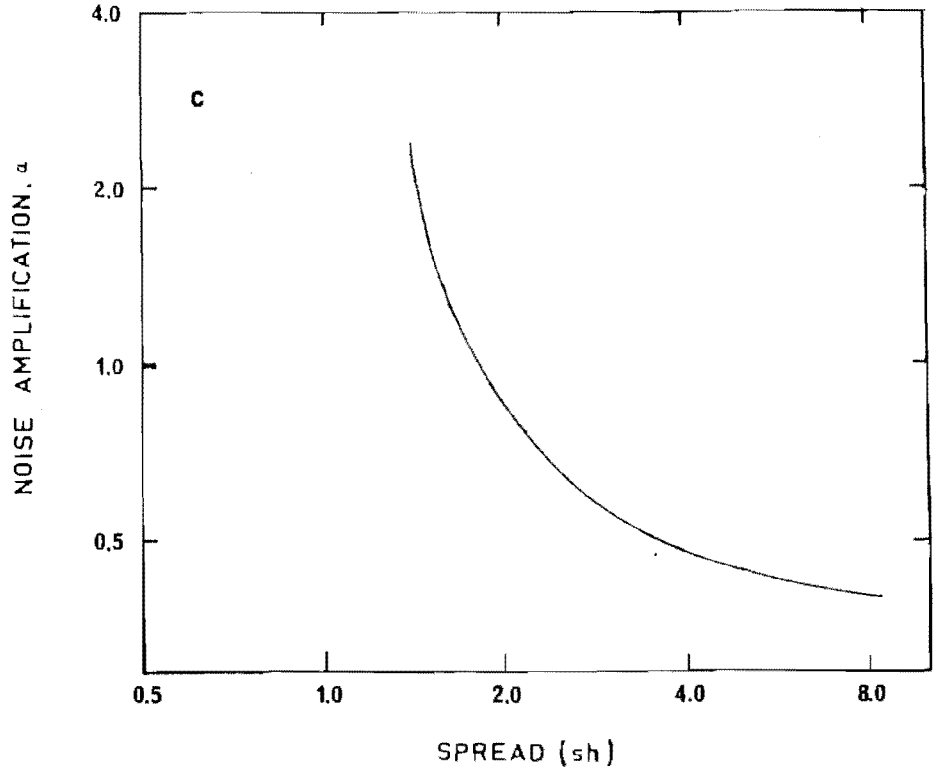

FIGURE 9 (c) : Backus Gilbert Tradeoff Curve for Height 4.5 sh

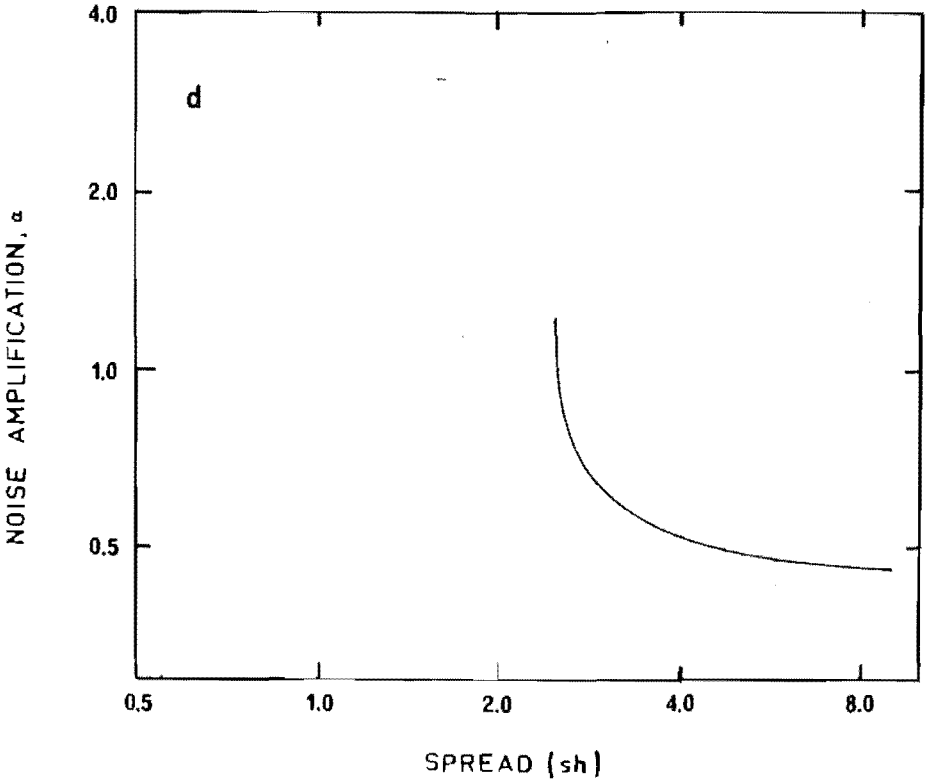

FIGURE 9 (d) : Backus Gilbert Tradeoff Curve for Height 5.5 sh

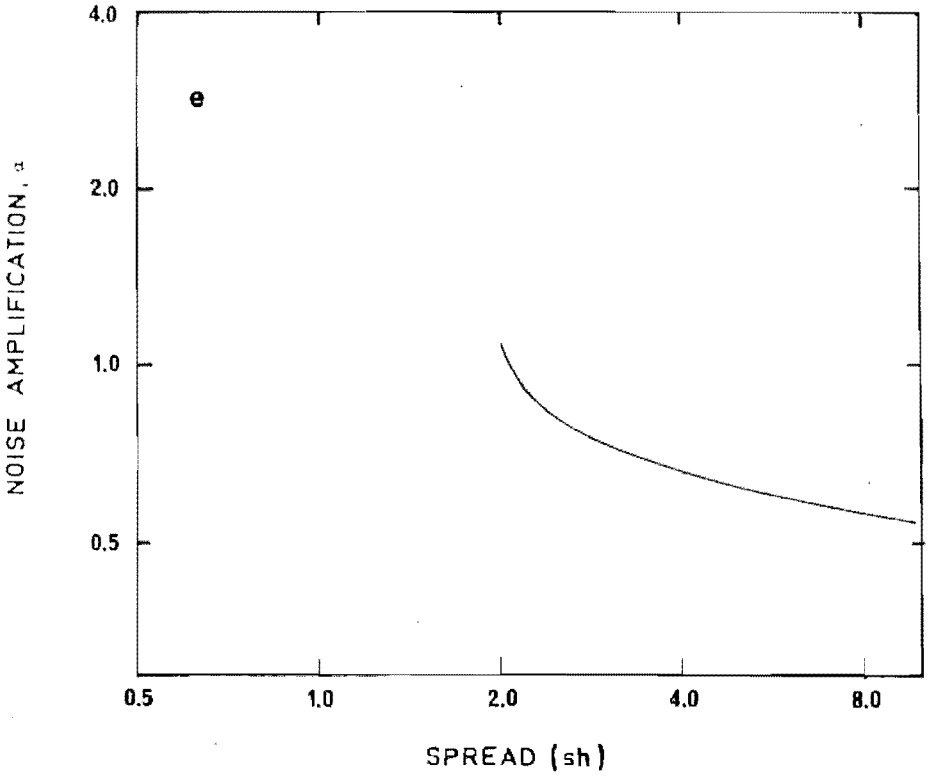

FIGURE 9 (e) : Backus Gilbert Tradeoff Curve for Height 6.0 sh

independent of height, it depends instead upon the number of satellite weighting functions.

The minimum spread (q=1) maximum noise averaging kernels for the same heights as in figure 9, are presented in figure 10. For each of these curves the resultant temperature error $\sigma_{\Delta\underline{\hat{x}}}(z_i)$ would not be larger than $\pm 1C^0$ for realistic satellite measurement noise levels (smoothed data series), since the value of α at heights below 5 sh altitude is in the range 3-4, and above 5 sh altitude is in the range 1-2. In figure 11 the BG averaging kernels at 3.5 sh altitude and for q values of 0, 0.2, 0.4, 0.6, 0.8, and 1.0 are given. The resultant effect through changing the value of q in the BG retrieval estimator calculation is clearly evident in this figure.

The altitude - spread characteristics of the BG averaging kernels at three values of q, are given in figure 12. The crosses on this figure are the spread characteristics of the individual satellite weighting functions, from table 5. The general trend in this figure is towards increasing spread of the averaging kernels with height. For q larger than approximately 0.2 the resolution of the BG estimator averaging kernels is better than that of the satellite kernels. Also from this figure it is evident that at some heights the BG averaging kernels have spread characteristics up to 40% better than those of the corresponding satellite kernels. At high altitudes, near 6 sh (≈45 km), the spread of the BG averaging kernel is similar to the spread of the corresponding satellite kernel (channel A). For all values of q the spread at 5.5 sh altitude is rather poorer than that at any other height below 6.5 sh altitude, similarly, at 1 sh altitude the averaging kernel spread is as much as 50% larger than that at 1.5 sh or 0.5 sh altitude. The best vertical resolutions obtainable from a linear combination of Nimbus 4 SCR weighting functions near 1 sh and 5.5 sh altitude is rather poorer than that obtainable at levels nearby.

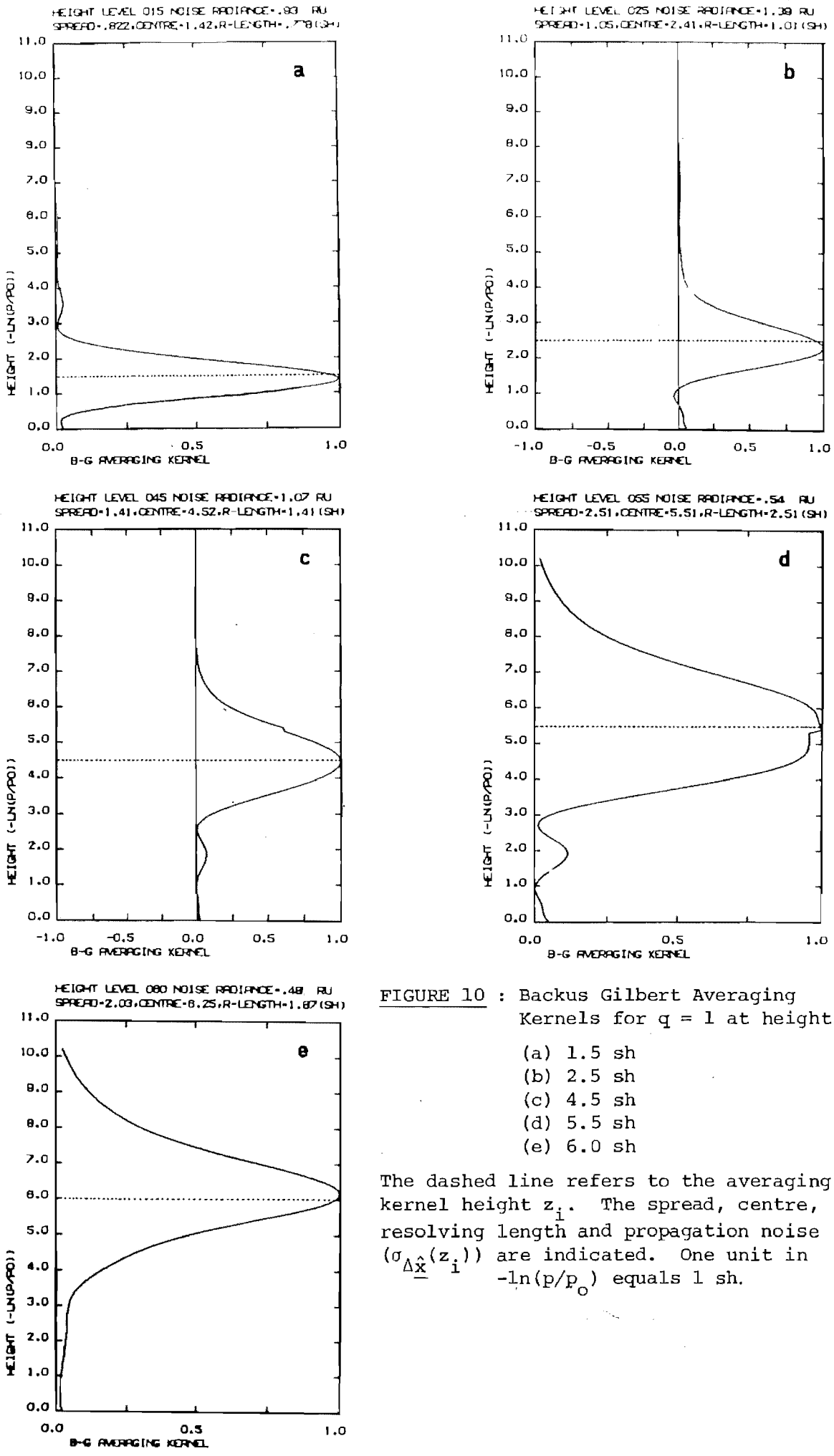

FIGURE 10 : Backus Gilbert Averaging Kernels for q = 1 at heights :

(a) 1.5 sh
(b) 2.5 sh
(c) 4.5 sh
(d) 5.5 sh
(e) 6.0 sh

The dashed line refers to the averaging kernel height z_i. The spread, centre, resolving length and propagation noise ($\sigma_{\Delta\hat{\underline{x}}}(z_i)$) are indicated. One unit in $-\ln(p/p_o)$ equals 1 sh.

FIGURE 11 : Backus Gilbert Averaging Kernels for z_i = 3.5 sh altitude and,

(a) q = 0
(b) q = 0.2
(c) q = 0.4
(d) q = 0.6
(e) q = 0.8
(f) q = 1.0

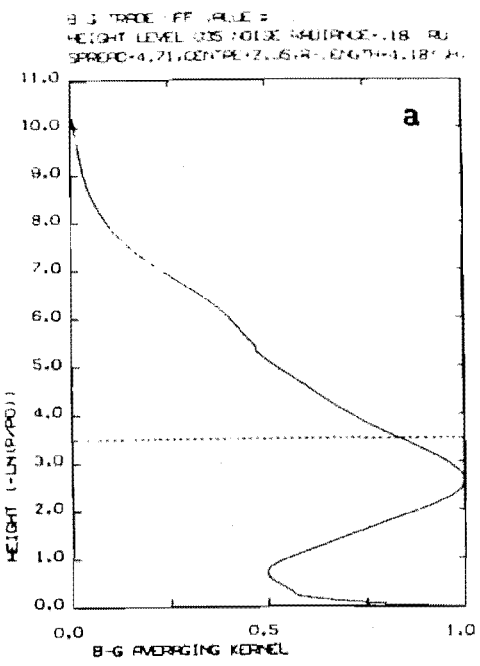
B-G TRADE OFF VALUE =
HEIGHT LEVEL 035 NOISE RADIANCE=.18 RU
SPREAD=4.71,CENTRE=2.65,R-LENGTH=4.18(SH)
a
HEIGHT (-LN(P/P0))
B-G AVERAGING KERNEL

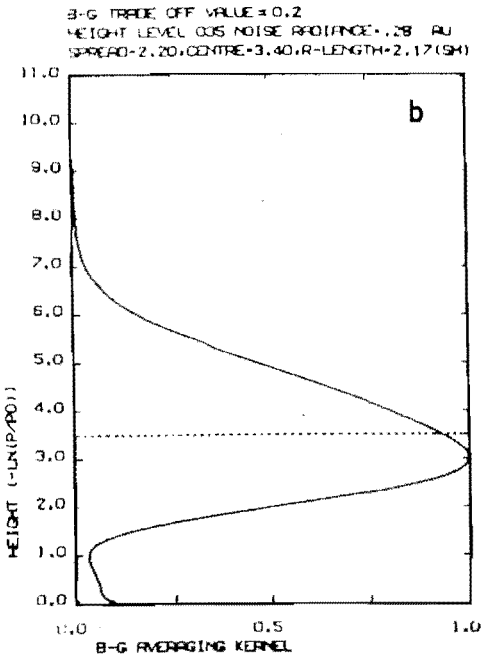
B-G TRADE OFF VALUE=0.2
HEIGHT LEVEL 035 NOISE RADIANCE=.28 RU
SPREAD=2.20,CENTRE=3.40,R-LENGTH=2.17(SH)
b
HEIGHT (-LN(P/P0))
B-G AVERAGING KERNEL

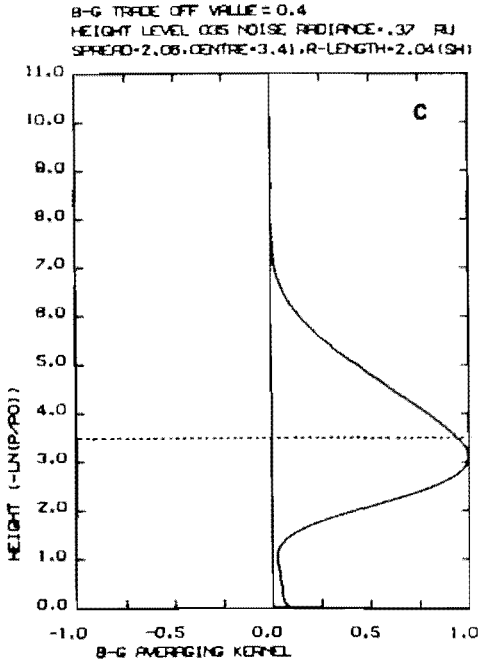
B-G TRADE OFF VALUE=0.4
HEIGHT LEVEL 035 NOISE RADIANCE=.37 RU
SPREAD=2.08,CENTRE=3.41,R-LENGTH=2.04(SH)
c
HEIGHT (-LN(P/P0))
B-G AVERAGING KERNEL

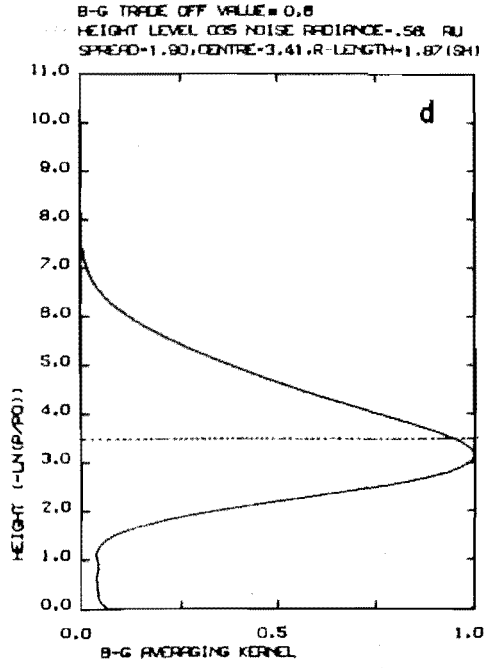
B-G TRADE OFF VALUE=0.6
HEIGHT LEVEL 035 NOISE RADIANCE=.58 RU
SPREAD=1.90,CENTRE=3.41,R-LENGTH=1.87(SH)
d
HEIGHT (-LN(P/P0))
B-G AVERAGING KERNEL

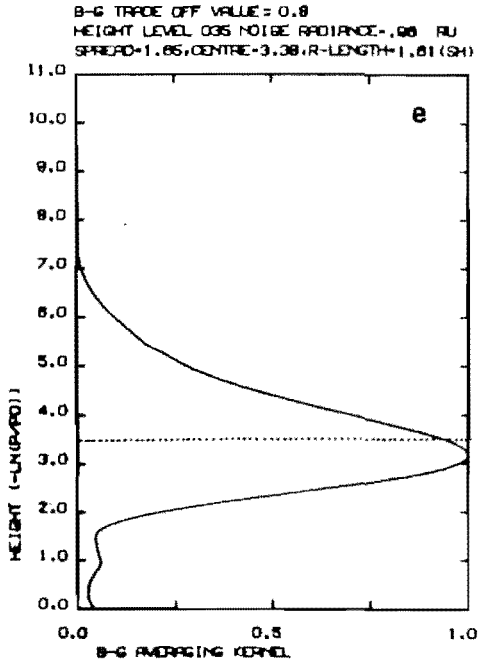
B-G TRADE OFF VALUE=0.8
HEIGHT LEVEL 035 NOISE RADIANCE=.98 RU
SPREAD=1.65,CENTRE=3.38,R-LENGTH=1.61(SH)
e
HEIGHT (-LN(P/P0))
B-G AVERAGING KERNEL

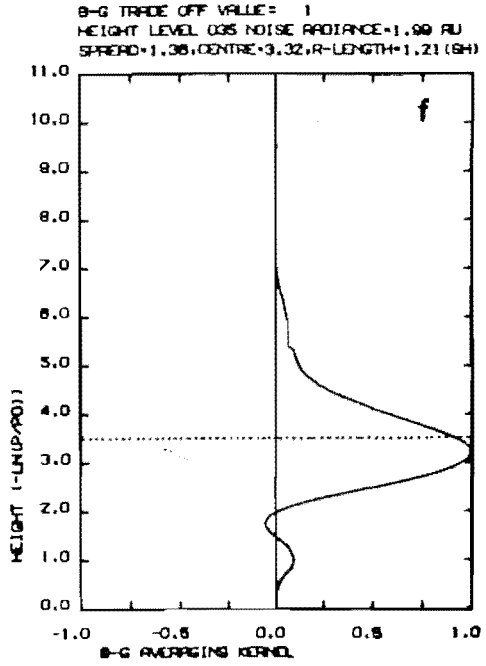
B-G TRADE OFF VALUE= 1
HEIGHT LEVEL 035 NOISE RADIANCE=1.99 RU
SPREAD=1.36,CENTRE=3.32,R-LENGTH=1.21(SH)
f
HEIGHT (-LN(P/P0))
B-G AVERAGING KERNEL

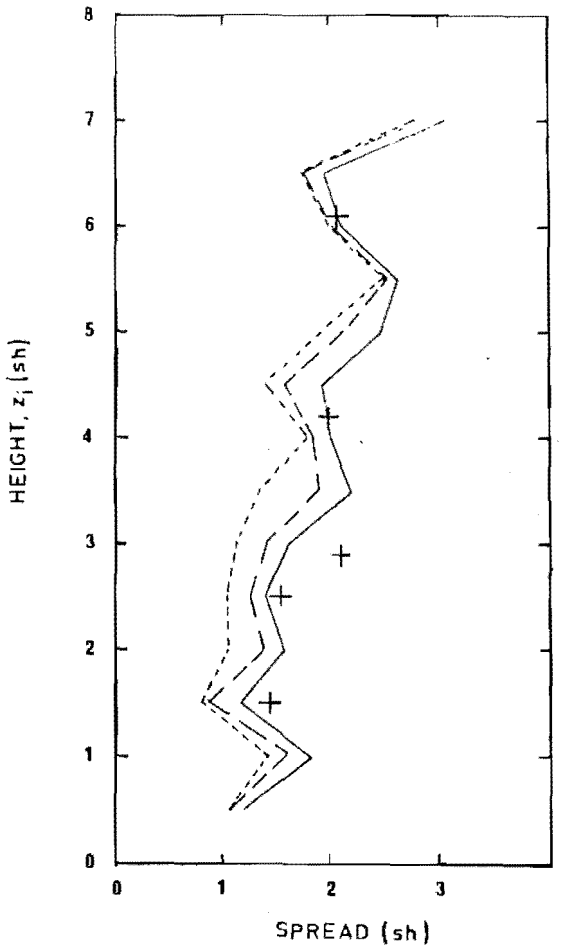

FIGURE 12 : Height, z_i, - Spread Curve for

——— q = 0.2
– – – – q = 0.6
…… q = 1.0

+ indicates SCR Weighting Function Characteristics

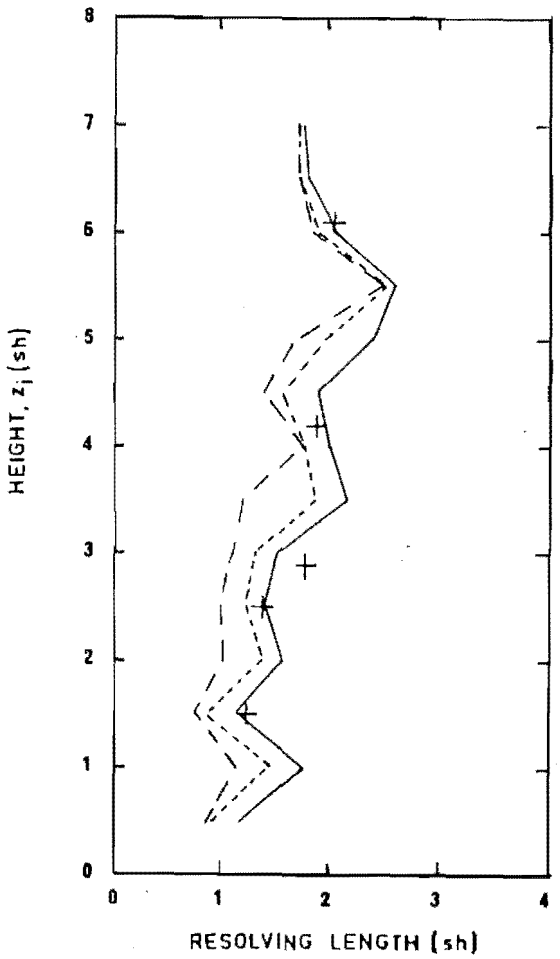

FIGURE 13 : Height, z_i,- Resolving Length Curve for :

——— q = 0.2
…… q = 0.6
– – – – q = 1.0

+ indicates SCR Weighting Function Characteristics

The reason the spread measure at 5.5 sh altitude is large and insensitive to changes in the value of the tradeoff parameter q may be appreciated on considering the equations for the BG formulation. The BG estimator averaging kernel at 5.5 sh altitude is essentially determined by a linear combination of channels A and B weighting functions since the weighting functions of channels C, D, E and F do not have significant "weight" at this height. The weighting functions for channels A and B both have spreads of the order of 2 sh. Therefore since the BG averaging kernel must be unimodular, and the weighting functions are normalised, it is not unexpected that the BG averaging kernel at this height should have a spread greater than 2 sh. A similar situation occurs for the averaging kernels at 1 sh altitude.

The spread of averaging kernels at heights greater than 6.5 sh altitude becomes large.

Resolving lengths of the BG averaging kernels for three values of q are plotted in figure 13. The crosses again refer to the corresponding satellite weighting function parameters. As in the case of the spread characteristics, when q is greater than approximately 0.2 the resolving lengths of the BG averaging kernels are better than those of the corresponding satellite weighting functions. At altitudes below 6.5 sh, comments stated with regard to the spread characteristics of the averaging kernels also apply to the resolving length characteristics. However, at altitudes above 6.5 sh, while the spread characteristic is poor the resolving length characteristic remains constant at a value of approximately 1.75 sh. The cause for this difference is evident on examination of figure 14, a plot of the averaging kernel centre heights against their heights (z_i). In this figure it is evident that the limiting height of the centre of the BG averaging kernels is approximately 6.5 sh. Accordingly, it may be stated that Nimbus 4 SCR weighting functions "contain" information on the atmos-

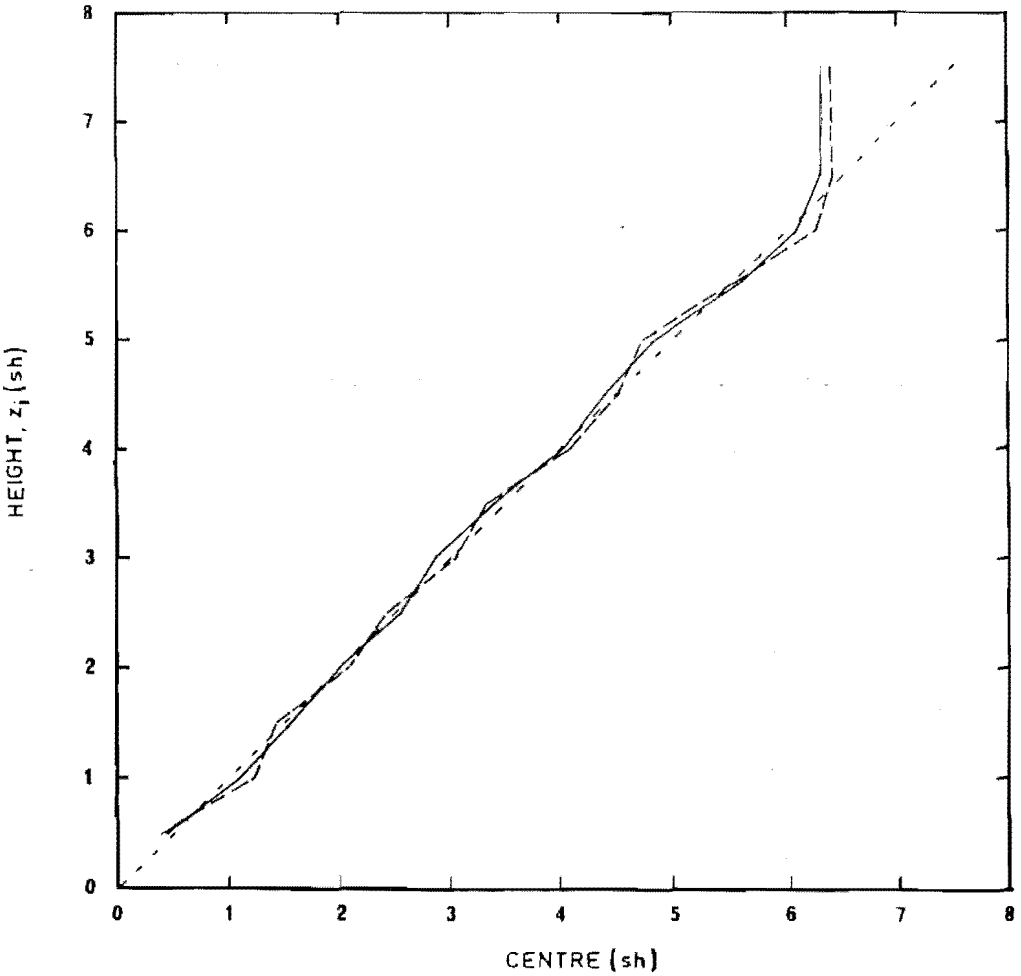

FIGURE 14 : Averaging Kernel Height, z_i, - Centre Height Curves for

——— q = 0.2
----- q = 1.0

pheric temperature structure for heights up to approximately 6.5 sh altitude. Since the spread is a measure of the width of an averaging kernel about the averaging kernel height, and the resolving length is a measure of the spread of the averaging kernel about its centre height, the spread characteristic must be degraded at heights above 6.5 sh, whereas the resolving length characteristic may not be degraded (equation (2.160).

The best resolution (i.e. when q=1) that may be obtained from a linear combination of the Nimbus 4 SCR weighting functions in the altitude range 0.5 sh to 3.5 sh, is approximately 1 sh, with a corresponding temperature error of the order of $\pm 1C^0$ when realistic satellite noise variances are assumed. Above 3.5 sh altitude the resolution is in the range 1.5 - 2 sh, except in the immediate region of 5.5 sh altitude where the resolution is closer to 2.5 sh. The resultant temperature error for this height range is also approximately $\pm 1C^0$. These values specify the intrinsic vertical resolving power of a linear combination of the set of Nimbus 4 SCR weighting functions.

Summary

From the foregoing discussion some observations on the intrinsic vertical resolution of a set of satellite weighting functions may be made. At heights where more than two weighting functions overlap (in altitude) with not insignificant "weight", the resolution of the corresponding BG averaging kernel will be considerably improved upon that of the individual satellite weighting functions. Associated with this high resolution will be a large error magnification factor α (therefore, higher noise $\sigma_{\Delta\hat{\underline{x}}}(z_i)$) since a number of satellite weighting functions are contributing in a significant way to the resulting BG averaging kernel. At heights between the peaks of two weighting functions and for which other weighting functions do not overlap in a significant way, the resolution of the BG averaging kernel will be poorer than the resolution of either or both

these satellite weighting functions. Similarly, near the peak height of a satellite weighting function which is not overlapped (at that height) significantly by another weighting function the BG averaging kernel resolution will be similar to that of the satellite weighting function. Temperature information cannot be deduced for heights much above the peak height of the top satellite weighting function.

Accordingly, if BG estimators are to be used to improve the vertical resolution of the measured radiances the measurement noise should be small and the satellite weighting functions should overlap significantly at the heights of interest.

3.4 : INTRINSIC VERTICAL RESOLVING POWER OF THE MAP ESTIMATORS

The techniques for determining the intrinsic vertical resolution in temperature profiles retrieved from satellite radiance data have been discussed in Sections 2.4.7 and 3.1. Accordingly the BG measures of spread, centre and resolving length will be used to specify resolution characteristics of an estimator's averaging kernels. The true intrinsic vertical resolution in a retrieved temperature profile is best expressed by the BG measure of spread of the corresponding estimator's averaging kernels. The spread of an averaging kernel specifies the resolution in the profile at the averaging kernel height, whereas the resolving length of the averaging kernel only specifies the spread about it's centre height. If the centre height is not the same as the averaging kernel height then the resolving length of the averaging kernel will not be a good measure of the intrinsic resolution in the retrieved profile (i.e. the resolving power of the estimator).

In this section, resolution characteristics of six sets of MAP estimators are considered. The estimators are constructed with the a priori data sets calculated and discussed in Section 3.2. It

is to be hoped that the resolution characteristics of these estimators are representative for MAP estimators used to deduce temperature profiles from Nimbus 4 SCR radiance data at latitudes between the equator and poles, during summer and winter seasons.

In Section 2.4.2 the ill-conditioned, or, non well-posed nature of the retrieval problem was discussed. Evidently the satellite measurement noise matrix S_e may tend to condition, or regularize the problem. Therefore in determining the vertical resolution of the MAP estimators it is important to consider the sensitivity of the estimator resolution to differing values of the assumed measurement noise. This sensitivity is investigated by considering the relationship between the amplification of the measurement noise through the MAP estimator (the noise propagation error) and the spreads of the corresponding estimator averaging kernels.

The effects of applying additional a priori information to the retrieval problem may also be determined in part by specifying the effect this additional "information" has upon the vertical resolution of the resulting MAP estimators. To this end the effect of prior knowledge of the ground level temperatures will be considered. The a priori covariance matrices (Section 3.2.1) indicate that between some levels, widely separated in height, the temperatures are strongly correlated during some seasons. The resulting effect upon the resolving power of the MAP estimators may be considered by applying the filter of equation (3.4) to the original a priori matrices, and consideration of the changes in the BG measures of the resulting estimator averaging kernels.

Accordingly, in considering the intrinsic vertical resolution of the MAP estimators it will important to consider :

(a) the sensitivity of the estimator resolution to the assumed value of the satellite measurement noise, and

(b) the effects of additional a priori "information" that may be used in a retrieval.

In the following subsections 3.4.1 to 3.4.4, resolution characteristics are examined for a set of MAP retrieval estimators for summer and winter seasons in three latitudinal zones. In the analysis of the resolution of the MAP estimators for each of these latitude zones and seasons, results from five different MAP estimators are considered. These estimators are constructed using; the original a priori covariance matrix (the only estimators which give meteorologically most probable retrievals), the ground corrected a priori matrix, the filtered (filterwidth w=20) a priori matrix, the ground corrected and filtered (w=20) matrix and finally the ground corrected and filtered (w=10) matrix. In each analysis it is assumed that the measurement noise statistics of each satellite channel are identical. The channels are assumed to be independent. For Nimbus 4 SCR data the channel independence assumption is appropriate. The assumption that the noise levels are identical, is not appropriate. However, the assumption of identical noise variances is useful in specifying the noise amplification and BG averaging kernel measures of MAP estimators, since relative noise conditioning effects will not affect the specification. Further, the MAP estimator results may be compared with those of the BG retrieval estimator.

3.4.1 Noise Amplification

Curves relating noise amplification to averaging kernel spread have been calculated for all five estimators for the three latitude zones and two seasons. The values of the noise amplification factor α (equation (3.17)) were derived for estimates of the satellite r.m.s. measurement noise lying in the range 0.045 to 3.16 ru. Upon examination of the results of these calculations it is evident that essentially two types of noise amplification-spread curves occur.

Their attributes may be stated thus :

Type 1 : on increasing the value of the estimate of the satellite measurement noise the spread of the corresponding averaging kernel increases monotonically and the amplification factor α decreases monotonically

Type 2 : where, upon increasing the size of the satellite measurement noise estimate used in the calculation the spread of the corresponding averaging kernel does not necessarily increase. The amplification factor α does however decrease monotonically with increasing values of the measurement noise.

The type 2 curves may be subdivided into two further catagories which shall be referred to as the strong and weak, type 2 noise amplification-spread curves. In the strong case, the value of the noise amplification factor α and the spread are strongly dependent upon the size of the measurement noise estimate. In the weak case the value of α is not strongly dependent upon the size of the measurement noise estimate. Additionally there is a range of noise estimates for which the spread of the corresponding averaging kernel decreases slowly with increasing levels of measurement noise.

Examples of these two types of curves are presented in figure 15. Figure 15(a) is the 1.5 sh altitude curve of the equatorial summer estimator derived with the filtered (w=20) a priori covariance matrix. This curve is representative of the type 1 noise amplification-spread curves where the estimator averaging kernel spread is insensitive to the size of the measurement noise estimate over a certain range of noise values. In this same range the value of α may change significantly. As the level of measurement noise is increased beyond this range the spread of the averaging kernel increases rapidly as the value of α falls slowly. The overall trend of a strong type 2 curve is represented by figure 15(b), the 5.5 sh altit-

FIGURE 15 : Noise Amplification-Spread Curves for MAP Estimators :

(a) Equatorial Summer Estimator (w=20), 1.5 sh altitude
(b) Mid-Latitudes Summer Estimator (w=20), 5.5 sh altitude
(c) High Latitudes Summer Estimator (w=20), 1.5 sh altitude
(d) High Latitudes Winter Estimator (w=20), 5.5 sh altitude

r.m.s. measurement noise values are : · 0.045 ru; + 0.1 ru;
x 0.32 ru; ⊠ 0.71 ru; ○ 1.0 ru; □ 2 ru.

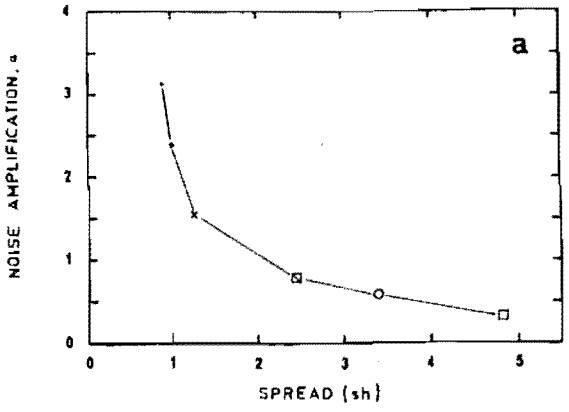
a
NOISE AMPLIFICATION, a
SPREAD (sh)

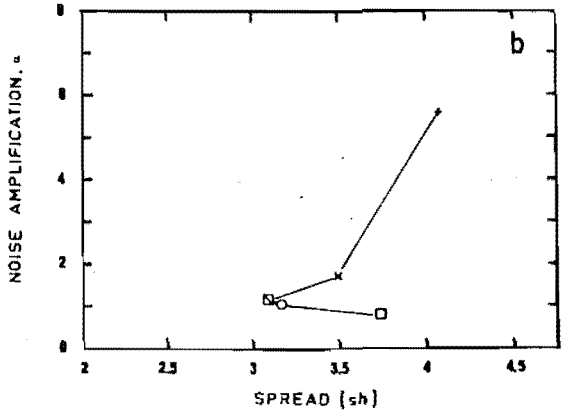
b
NOISE AMPLIFICATION, a
SPREAD (sh)

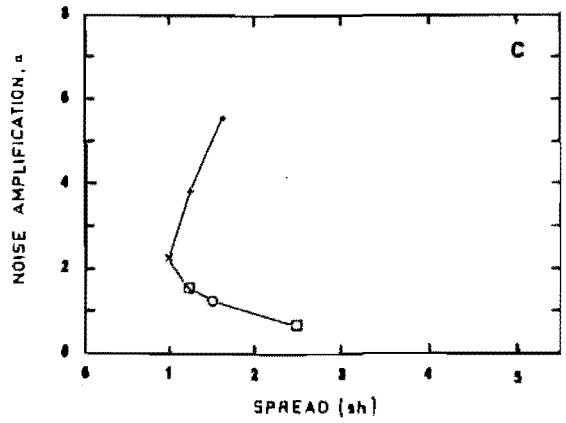
c
NOISE AMPLIFICATION, a
SPREAD (sh)

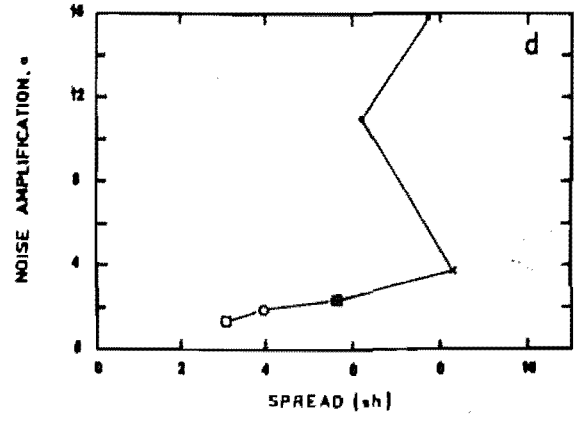
d
NOISE AMPLIFICATION, a
SPREAD (sh)

ude averaging kernel of the mid-latitude summer estimator constructed with the filtered (w=20) a priori covariance matrix. An important feature of this type of curve is its indication of the sensitivity of the estimator averaging kernel spread (i.e. resolution), to the size of the satellite r.m.s. measurement noise estimate. In general, for these curves the spread of the corresponding averaging kernel decreases significantly as the size of the satellite noise estimate is increased to a certain level but increases again as the noise estimate is increased still further. It is also found that the minimum spread for these curves is rather larger than that for either the type 1 or weak type 2 curves.

It is evident from the whole set of calculations that the weak type 2 curve is the most common form for the noise amplification-spread curves. For most heights and for most all of the estimators the spread of the corresponding averaging kernels is not minimum when the satellite measurement noise is smallest (i.e. 0.045 r.u). An example of the weak form of the type 2 curve is given in figure 15(c); the curve for the 1.5 sh altitude averaging kernel of the high latitudes summer estimator constructed with the filtered (w=20) a priori covariance matrix. The shape of the strong type 2 noise amplification-spread curves may be quite complex as is evident in figure 15(d), the curve for the 5.5 sh averaging kernel of the high latitude winter estimator constructed with the filtered (w=20) covariance matrix.

The results of figure 15 are, as stated, for estimators constructed with filtered (w=20) a priori covariance matrices. These curves are representative of results obtained with the other four estimators. Differences in detail do occur, with those of estimators constructed with the original and ground corrected matrices being more sensitive to the size of the measurement noise estimate while those constructed with the ground corrected and filtered, matrices,

are less sensitive to the size of the measurement noise estimate. This observation is general for all three latitudinal zones and two seasons considered here. It is also apparent that filtering the a priori covariance matrices used in the calculations of the estimators reduces the range of the noise magnification values of the estimator. These effects are illustrated in figure 16, an example of the overall differences which result for estimators constructed with different sets of additional a priori "information". In this figure it is also evident that for this set of estimators, the "best"(noise dependent) resolution at 1.5 sh altitude is reduced by filtering or ground correcting the a priori matrix. This is not a general result for all heights, as will be illustrated in the discussion on the spread (Section 3.4.4) of the estimator averaging kernels.

The overall height sensitivity of the noise amplification factor α for estimators constructed with different values of satellite measurement noise is illustrated in figure 17. When the measurement noise estimate is small the noise amplification factor α is large and strongly height dependent. At larger values of the measurement noise the size of α is much smaller and less height dependent. In general terms the results of figure 17 are representative of those for each of the estimators, for each latitudinal zone during both summer and winter seasons. Further, when the estimate of the satellite measurement noise is small the corresponding values of the noise amplification factor α increase with increasing latitude.

In each of the latitude zones, during both summer and winter seasons, three height regions may be discerned in the noise amplification-spread characteristics of the estimators. For the equatorial, mid-latitudes, and high latitudes summer estimators, at heights below approximately 4.5 sh altitude the noise amplification-spread curves are essentially type 1 or weak type 2 curves. In the height region above 4.5 sh and below 6 sh altitude each of the noise amplifi-

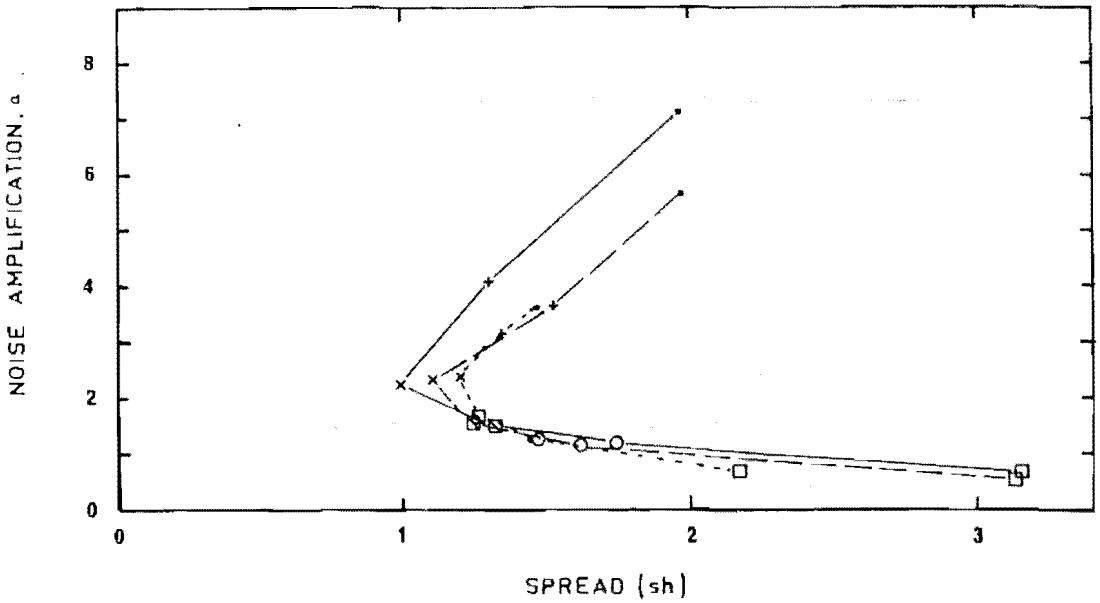

FIGURE 16 : Noise amplification-spread curves for High Latitudes summer estimators at 1.5 sh altitude : ——— original, – – – – ground corrected, ------- ground corrected and filtered (w=20). Noise values as for Figure 15.

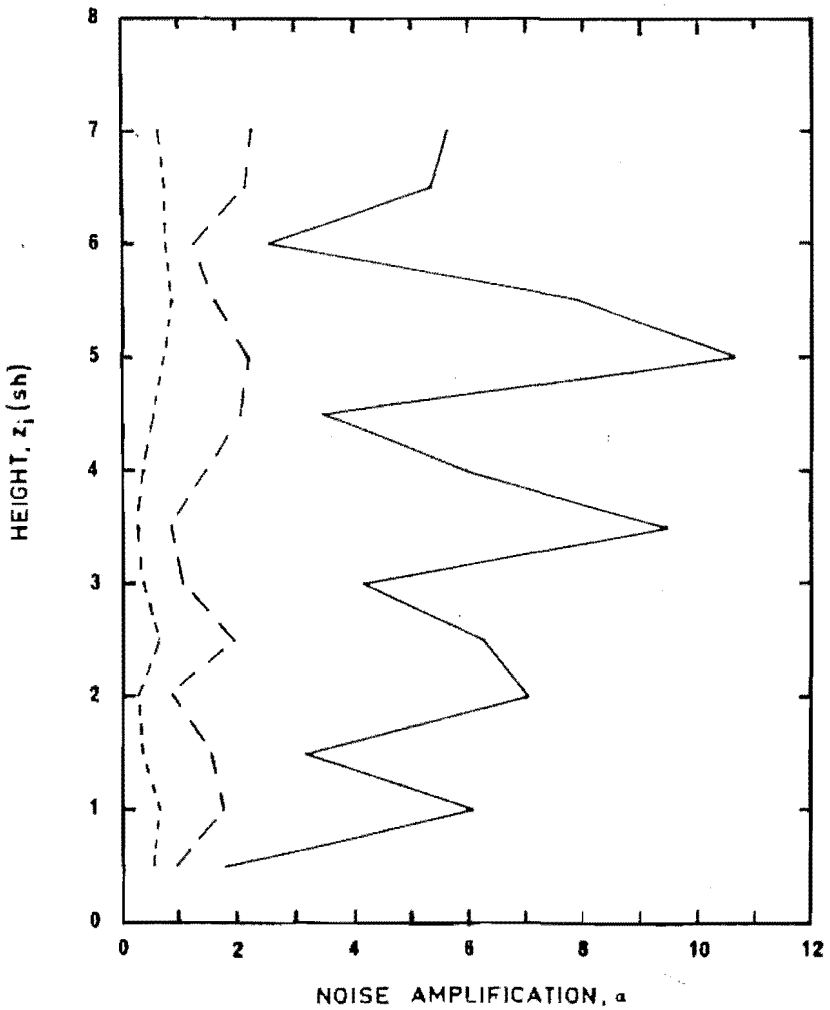

FIGURE 17 : Height, z_i, - Noise Amplification Curves for the Equatorial Summer Estimator (w=20) and r.m.s. measurement noise values : ——— σ_e=0.045ru, – – – σ_e=0.32ru, ----- σ_e=2.0 ru

cation-spread curves is of the strong type 2 form. The third region is evident in the results for heights near 6 sh altitude where the noise amplification-spread curves are again of the type 1 or weak type 2 form. For the high latitudes winter estimators the type 1 region extends only to approximately 3 sh altitude and the strong type 2 region extends from 3 sh altitude to approximately 6 sh altitude. The return to a type 1 region only occurs for altitudes near 6.5 sh altitude. In general, in the second height (z_i) region (4.5 sh < z_i < 6 sh altitude) the winter estimators are more sensitive than the summer estimators to the size of the measurement noise estimate, both in terms of the largest magnitude of the amplifications factor α, and the size of the spread of the averaging kernels. This effect is particularly noticable on considering the differences between the high latitudes summer and winter estimators.

Discussion

It is apparent from the results given above that, at some heights in the atmosphere the intrinsic resolving power of the retrieval estimators is poor, and quite sensitive to the assumed value of the estimate for the satellite r.m.s measurement noise σ_e. This is particularly evident at heights for which the noise amplification-spread characteristics are of the strong type 2 form. The noise sensitivity of the spread characteristics of the estimators at these heights may be appreciated on consideration of the corresponding estimator averaging kernels.

Representative of this condition are the 5.5 sh altitude averaging kernels of the equatorial winter estimator constructed with the filtered (w=20) a priori covariance matrix and four estimates of the satellite measurement noise ranging from 0.1 ru to 2 ru, illustrated in figure 18. The noise amplification-spread curve of these averaging kernels is given in figure 19. The discontinuity in gradient, present in some of these curves near 5.4 sh altitude arises

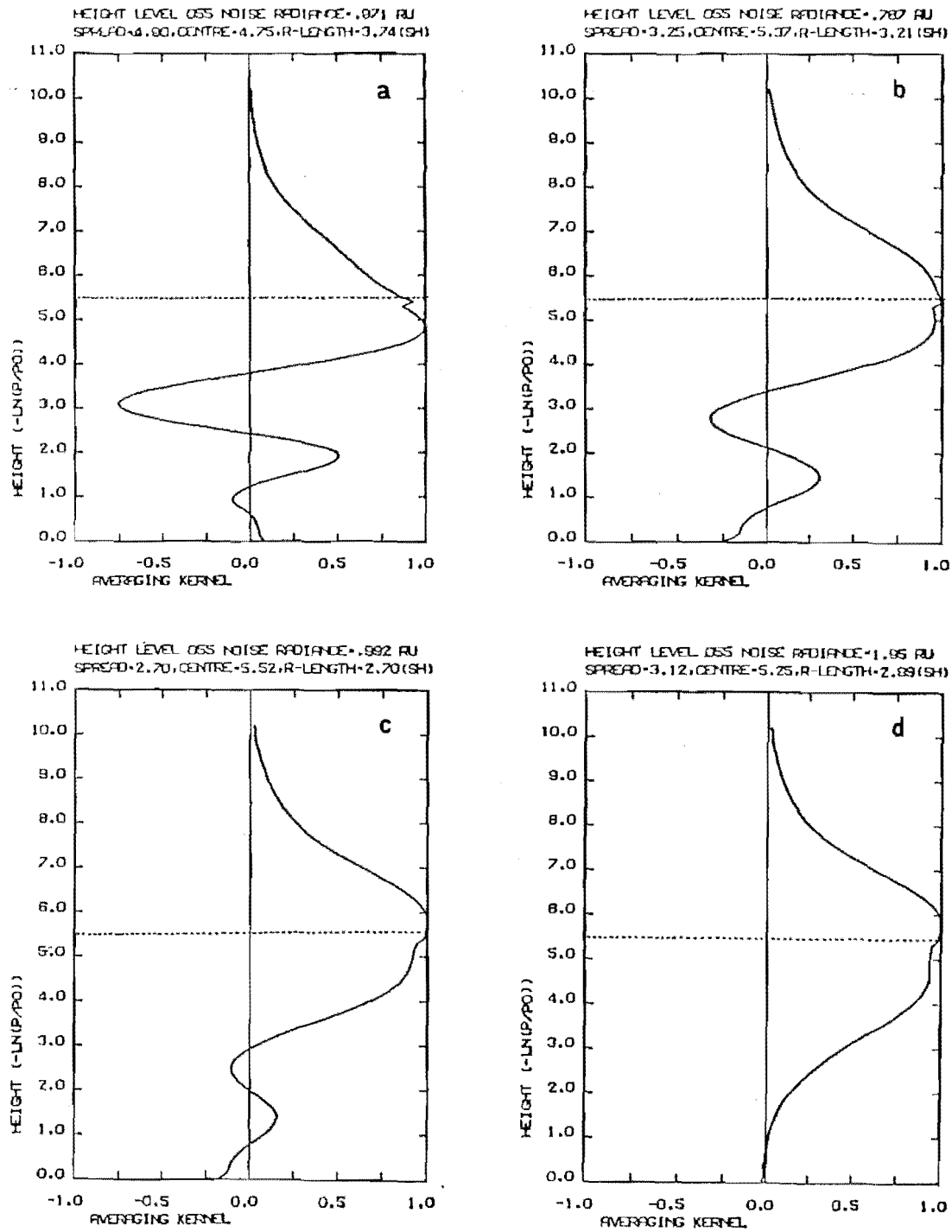

FIGURE 18 : Averaging Kernels of the Equatorial Winter estimator (w=20) at z_i = 5.5 sh and r.m.s. measurement noise values :

(a) σ_e = 0.1 ru (b) σ_e = 0.32 ru

(c) σ_e = 0.71 ru (d) σ_e = 2 ru

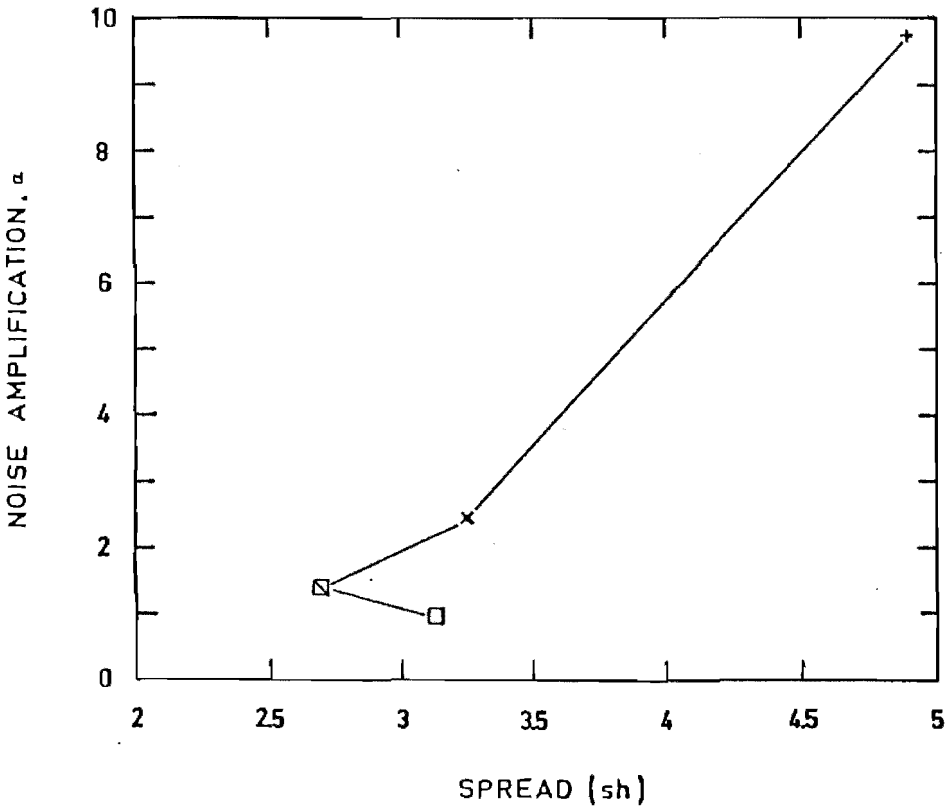

FIGURE 19 : Noise amplification-spread curve for averaging kernels of Figure 18. Noise value symbols as for Figure 15.

owing to inaccuracies in the equations used to fit the shape of the channel B weighting function of figure 4 (see Section 4.2). This discontinuity will not affect, significantly, the results of this study. The evolution of the shape of the averaging kernel with the increasing size of the satellite noise σ_e is clearly evident in figure 18. When the noise estimate is 0.1 ru the main peak of the averaging kernel is centred near 5 sh altitude, but a strong negative side lobe at approximately 3 sh altitude and a weaker positive side lobe near 2 sh altitude are present. On increasing the value of the measurement noise the peak height of the main averaging kernel peak moves closer to 5.5 sh altitude, the width of this peak broadens and the "strength" of the side lobes is reduced. When σ_e=2 ru the main peak is very broad and there are essentially no side lobes.

The following simple argument is suggested as the mechanism through which results like those of figure 18 (and figure 19) arise, whereby for some estimator at some height the spread of the corresponding averaging kernel is very sensitive to the size of the satellite measurement noise estimate. Consider the equation for the MAP estimator :

$$\hat{\underline{x}} - \bar{\underline{x}} = S_x K^T (K S_x K^T + S_e)^{-1} (\underline{y} - \bar{\underline{y}}) \qquad \ldots (2.77)$$

First, an argument will be given which instead indicates conditions under which the results of figure 18 could not arise.

If the a priori covariance matrix S_x were essentially diagonal in that the off diagonal elements were small, then the (pxn) matrix product $S_x K^T$ for any particular row (i.e. height), assuming the weighting functions do not overlap significantly, would only have an element of significant size for the weighting function corresponding closest to that height. If the height in question lies between the peaks of two such satellite weighting functions then the row of the matrix $S_x K^T$ corresponding to this height will have elements of sig-

nigicant size for contributions from both these weighting functions. Under these conditions the matrix $(KS_xK^T + S_e)^{-1}$ will be approximately diagonal since the matrix KS_xK^T will be nearly diagonal. Accordingly the (pxn) matrix $S_xK^T(KS_xK^T + S_e)^{-1}$, the G matrix of equation (3.1), at each height will only have large elements for satellite weighting functions which peak near that height. Therefore large side lobes in the averaging kernels at heights not near the averaging kernel height, will not occur.

Now, if at some height the a priori covariance matrix S_x has strong off diagonal elements corresponding to strong correlations between temperatures at levels separated in height then it is possible that the averaging kernel associated with this height may have strong side lobes at heights not near the averaging kernel height. For, under these conditions the row of the (pxn) matrix S_xK^T which refers to this height may have large elements for satellite weighting functions whose peaks do not lie close to the height in question. In this situation the matrix KS_xK^T may have off diagonal elements which are not insignificant and if the measurement noise σ_e is small then the resulting averaging kernel will have strong side lobes. However, if the value of the measurement noise σ_e is increased such that the matrix $(KS_xK^T + S_e)^{-1}$ is more nearly diagonal then the strength of the side lobes will be reduced. At the same time this may also result in the main peak of the averaging kernel increasing in width if other satellite weighting functions have peaks which lie close to the averaging kernel height.

In detail, the temperature covariance matrices for the atmosphere are considerably more complex than allowed in the above argument, however, the suggested effects are observed in the estimator averaging kernels whose noise amplification-spread curves are of the strong type 2 form. It may be expected that for a MAP estimator constructed with a realistic a priori covariance matrix, which will

indeed contain correlations between levels well separated in height, that at heights which lie between the peaks of the satellite weighting functions the averaging kernel peak width may be larger than either of the spreads of these weighting functions. If this is not the case, strong side lobes will probably be present in the averaging kernel. Consequently the corresponding measure of the averaging kernel spread will be sensitive to the size of the measurement noise estimate. Which ever is the case, the averaging kernel spread will be large. These effects are clearly demonstrated in figure 18. Accordingly in cases where the noise amplification-spread curves are of the strong type 2 form the satellite noise σ_e could be interpreted as a smoothing parameter since it may be "used" to "smooth" out the side lobes in the averaging kernels.

It might be expected from the discussion above that filtering of the covariance matrix used on the construction of the estimator would improve the spread characteristics of the corresponding averaging kernels since the size of the temperature correlations between different levels in the atmosphere is reduced. This is generally true as illustrated in figure 20, which should be compared with figure 18. Figure 20 contains the 5.5 sh altitude averaging kernels of the equatorial winter estimator constructed with the original a priori matrix at satellite measurement noise levels of 0.32 r.u. and 2 r.u. respectively.

From the above discussion the presence of three, possibly four, different height regions in the noise amplification-spread characteristics is not unexpected. In the height region 1.5 sh altitude to approximately 4.5 sh altitude the Nimbus 4 SCR weighting functions overlap significantly at most heights, accordingly type 1 or weak type 2 noise amplification-spread curves are expected. In the height region 4.5 sh to 5.5 sh altitude only two weighting functions overlap significantly, and neither of them peak in this altitude range

FIGURE 20 : 5.5 sh Altitude Averaging Kernels for the Equatorial Winter Estimator, with Measurement Noise Values

(a) σ_e = 0.32ru, and
(b) σ_e = 2.0ru

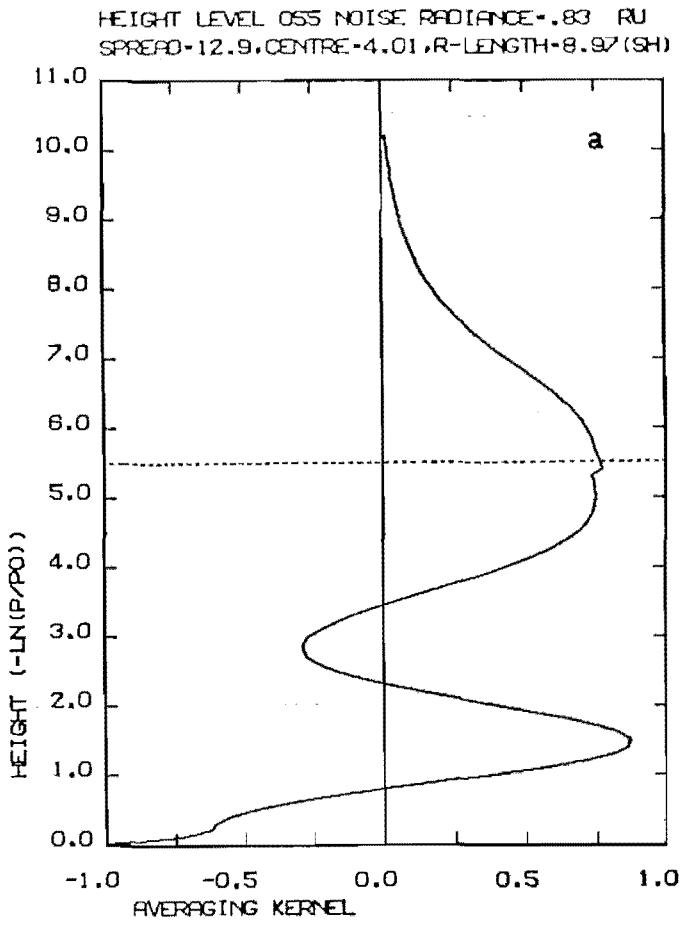
HEIGHT LEVEL 055 NOISE RADIANCE=.83 RU
SPREAD=12.9,CENTRE=4.01,R-LENGTH=8.97(SH)
a
HEIGHT (-LN(P/PO))
AVERAGING KERNEL
11.0
10.0
9.0
8.0
7.0
6.0
5.0
4.0
3.0
2.0
1.0
0.0
-1.0
-0.5
0.0
0.5
1.0

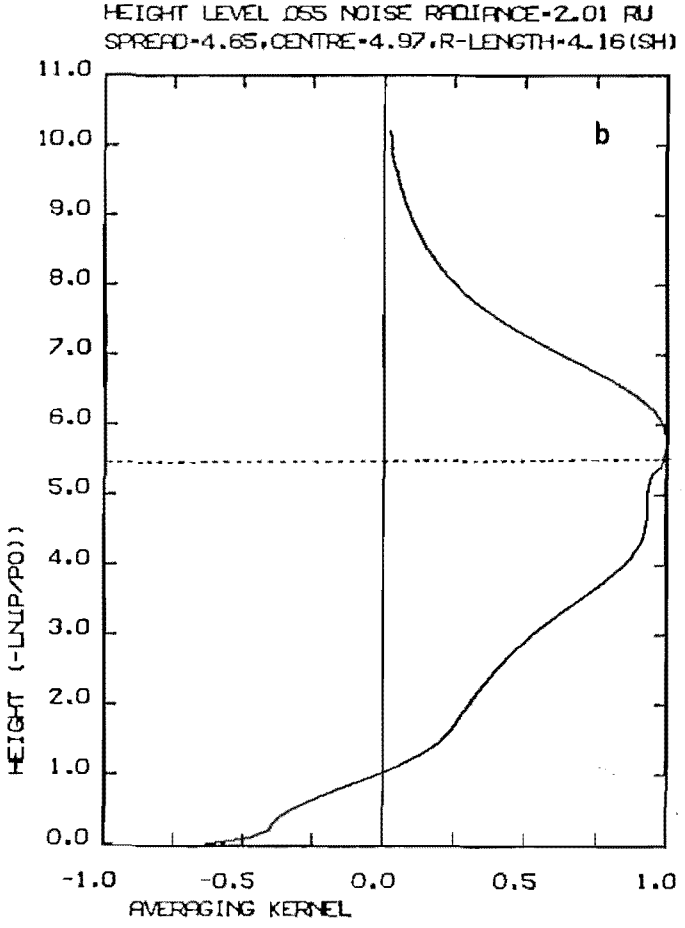
HEIGHT LEVEL 055 NOISE RADIANCE=2.01 RU
SPREAD=4.65,CENTRE=4.97,R-LENGTH=4.16(SH)
b
HEIGHT (-LN(P/PO))
AVERAGING KERNEL
11.0
10.0
9.0
8.0
7.0
6.0
5.0
4.0
3.0
2.0
1.0
0.0
-1.0
-0.5
0.0
0.5
1.0

thus resulting in noise amplification-spread curves of the strong type 2 form. A similar strong type 2 noise amplification-spread situation occurs near 1 sh altitude where, essentially, only channel E and F weighting functions overlap significantly. Near 6 sh altitude the estimator averaging kernels will be constructed in the main, through contributions from the channel A weighting function. The spread characteristic of the averaging kernel will be less sensitive to the satellite noise estimate and is consequently a type 1 or weak type 2 region.

At heights which lie between the peaks of the satellite weighting functions the noise amplification factor α will be larger owing to the "difficulty" of constructing a peaked averaging kernel function by taking the differences between the weighting functions. This point is evident in figure 17.

3.4.2 The Averaging Kernel Centre Height

The centre height of an averaging kernel, equation (2.158), is essentially the "average" height of the averaging kernel "weight". When the centre height of a particular averaging kernel deviates significantly from its averaging kernel height (z_i), the implied conclusion is that the estimator's information for a retrieval at this height is deduced from temperatures at heights not near the averaging kernel height. This is equivalent to saying that at this height the estimator does not have the intrinsic vertical information necessary to make a "good" retrieval of the temperature. Accordingly examination of the centre heights of a set of averaging kernels of an estimator will indicate heights where the retrieval estimators lack intrinsic information.

The centre heights of averaging kernels of all five estimators for the three latitudinal zones and two seasons have been calculated. The allowed range of the size of the satellite r.m.s measurement noise

estimates was 0.045 r.u. to 3.16 r.u. In figure 21 (a through f) some of the results of these calculations are given. It is evident from this figure that for all three latitude zones and during both seasons the centres of all averaging kernels for heights near 5 sh altitude deviate significantly from the corresponding averaging kernel heights. It is also apparent that within a latitude zone the deviations are largest for the winter estimators. The maximum height of the centre of any estimator averaging kernel is approximately 6.5 sh.

For each latitude zone and during both summer and winter seasons, in the height range 1.5 sh to 4.5 sh altitude the centre heights for each set of estimators for a particular measurement noise estimate are in general very similar. Above 4.5 sh altitude in the equatorial zone during both summer and winter seasons, the centre heights of the different estimator averaging kernels do differ considerably. Below 1.5 sh altitude the results for the mid-latitude winter and high latitude summer estimators show some variation in averaging kernel centre heights. In this region, when the centre heights of averaging kernels of the estimator constructed with the original a priori covariance matrix deviate significantly from the averaging kernel heights, ground correction of the a priori matrix used in the construction of the estimator tends to improve the correspondence between centre and averaging kernel heights. For all three latitude zones and both seasons, excepting the high latitudes winter estimators, the centre heights of the estimators constructed with the filtered, or ground corrected and filtered, a priori matrices lie closest (generally) to the corresponding averaging kernel heights.

In the summer results, three main height regions may be identified. In the height range 0.5 sh altitude to approximately 4.5 sh altitude, the centre heights are generally close to the averaging kernel heights. Above 4.5 sh and below 6.0 sh altitude the centre

FIGURE 21 : Height (z_i) - Centre Height Curves for :

(a) Equatorial summer estimators, σ_e = 0.1 ru
(b) Equatorial winter estimators, σ_e = 0.71 ru
(c) Mid-Latitudes summer estimators, σ_e = 0.71 ru
(d) Mid-Latitudes winter estimators, σ_e = 0.71 ru
(e) High Latitudes summer estimators, σ_e = 0.32 ru
(f) High Latitudes winter estimators, σ_e = 0.32 ru

The estimators are identified by :

——— original
– – – – – ground corrected
- - - - - - - - filtered (w=20)
O O ground corrected and filtered (w=20)
□ □ ground corrected and filtered (w=10)

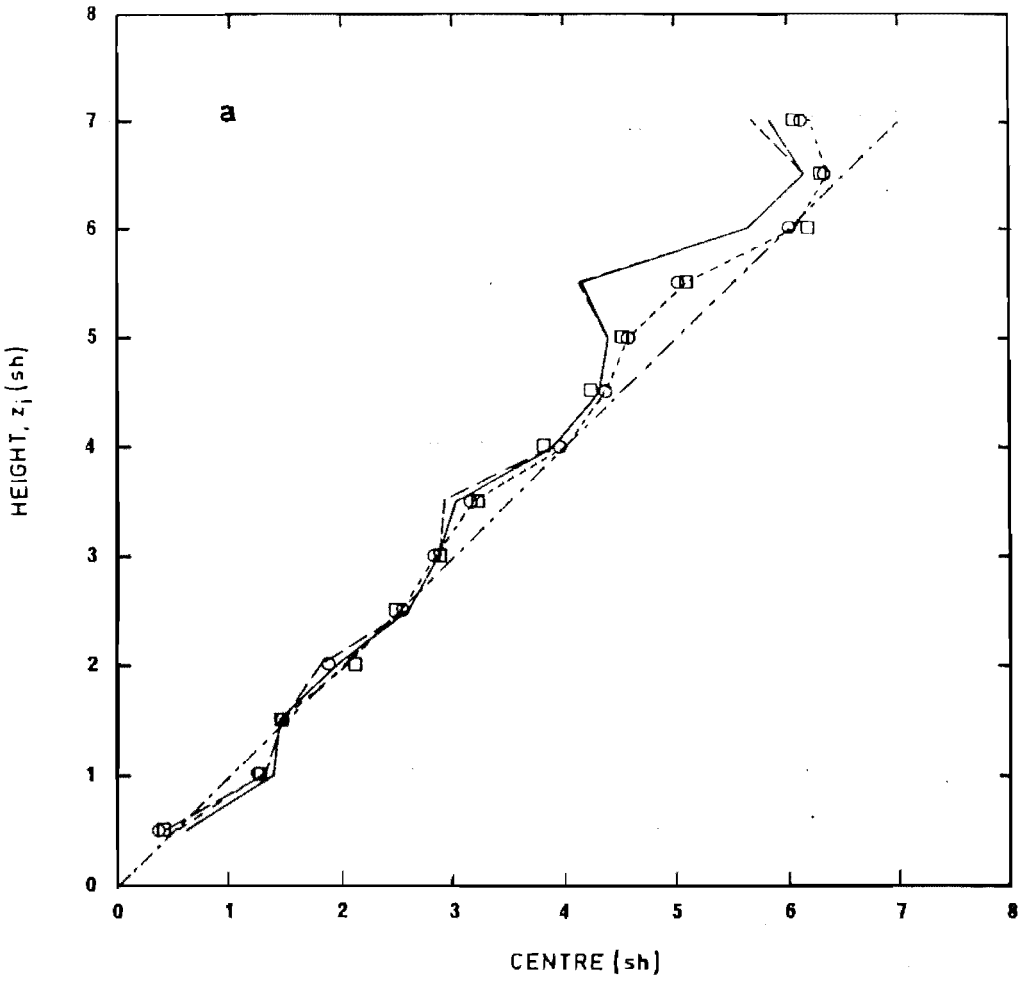
a
HEIGHT, z_i (sh)
CENTRE (sh)
0
1
2
3
4
5
6
7
8

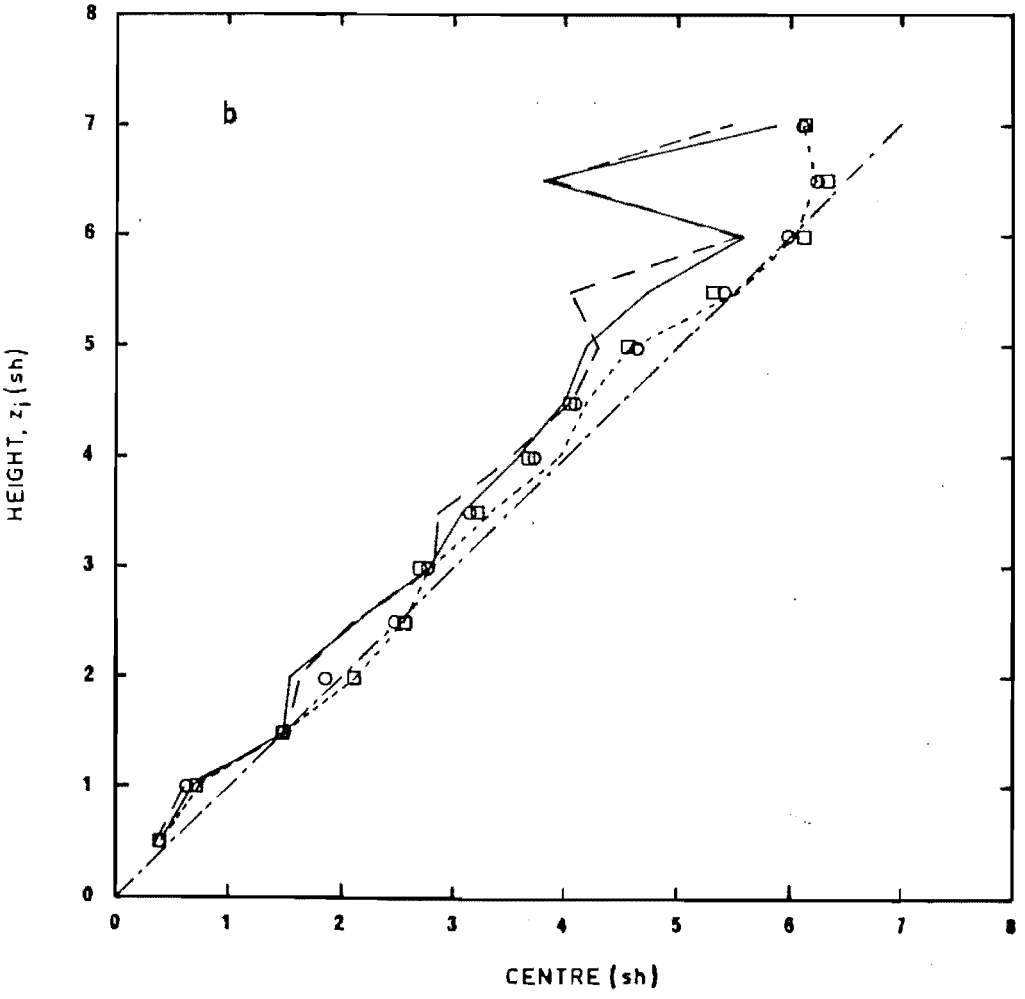
b
HEIGHT, z_i (sh)
CENTRE (sh)
0
1
2
3
4
5
6
7
8

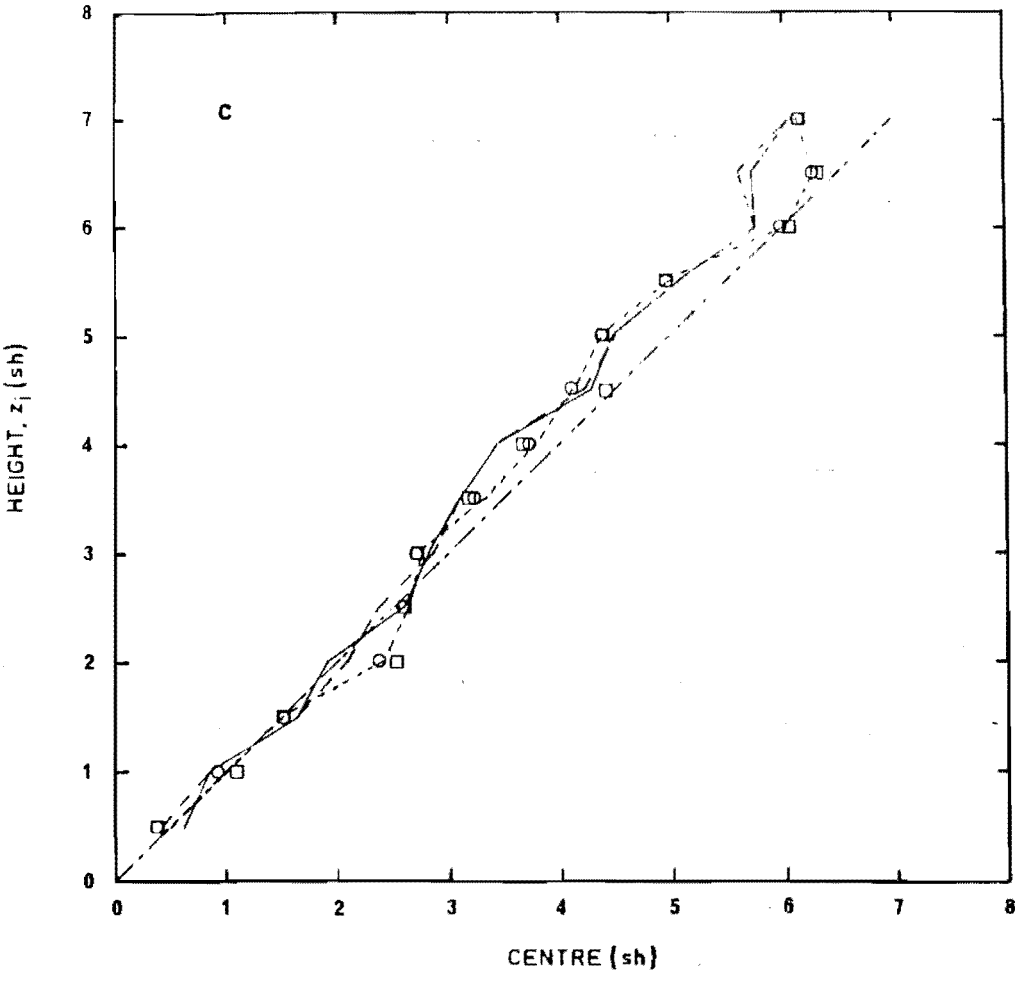
c
HEIGHT, z_i (sh)
CENTRE (sh)
0
1
2
3
4
5
6
7
8

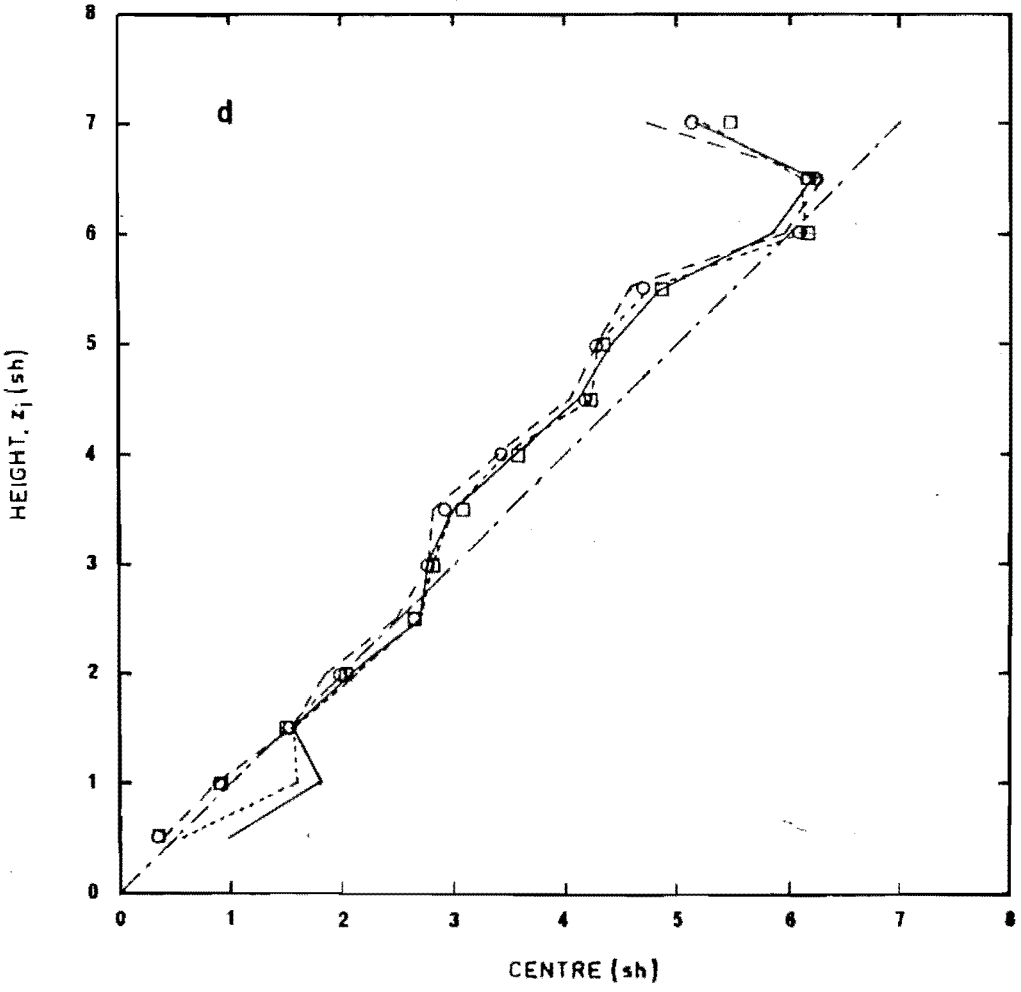
d
HEIGHT, z_i (sh)
CENTRE (sh)
0
1
2
3
4
5
6
7
8

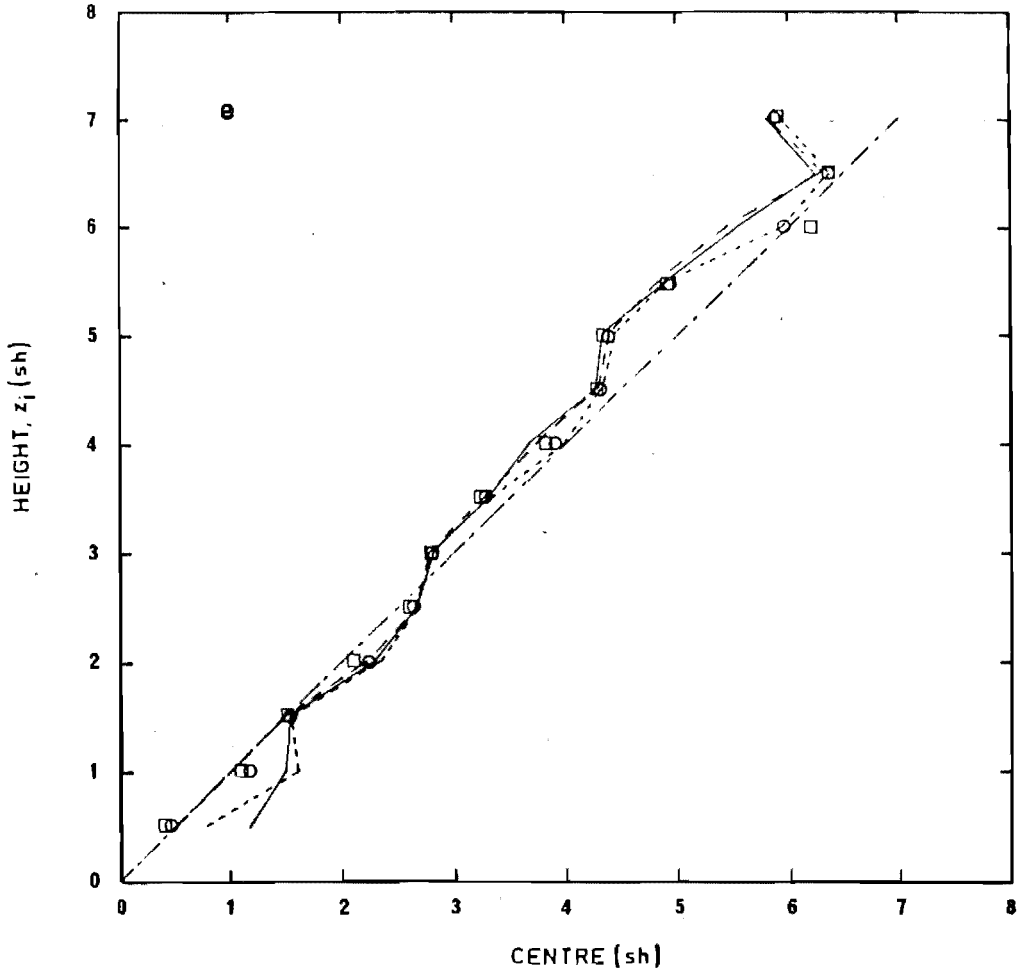
e
HEIGHT, z_i (sh)
CENTRE (sh)
0
1
2
3
4
5
6
7
8

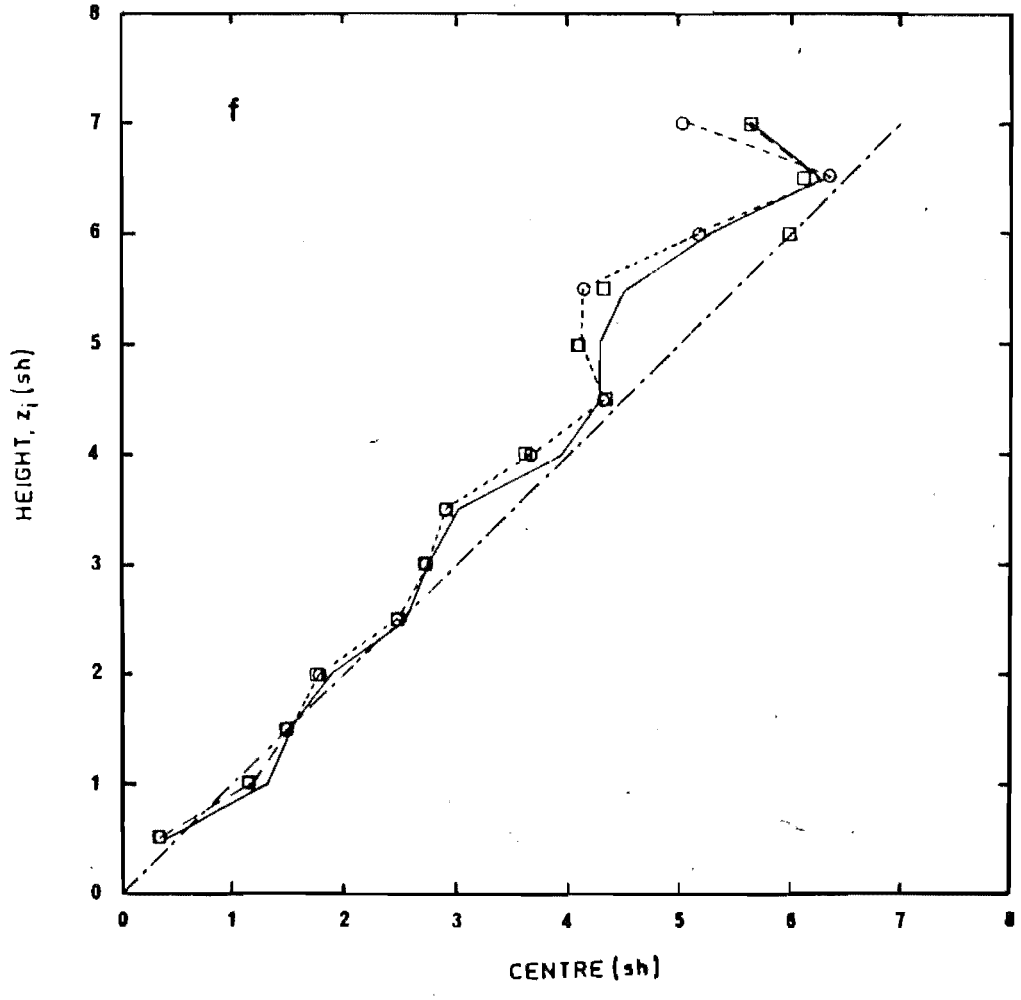
f
HEIGHT, z_i (sh)
CENTRE (sh)
0
1
2
3
4
5
6
7
8

heights tend to deviate more significantly from the averaging kernel heights. Near 6 sh altitude the centre heights of the estimator averaging kernels are close to the averaging kernel heights. Additionally for the equatorial and high latitudes estimators the centre heights of averaging kernels at 1 sh altitude may deviate significantly from 1 sh, as already mentioned.

In the winter results similar trends may be identified, but they tend to be obscured by the differences between the estimators.

The centre heights of the estimator averaging kernels are dependent upon the size of the satellite measurement noise estimate. Representative of these effects are the results of figures 22(a) and 22(b) for an equatorial summer estimator and an high latitudes winter estimator respectively. In figure 22(a) it is evident that for some heights near 5.5 sh altitude increasing the magnitude of the measurement noise estimate causes the centre heights to move closer to the averaging kernel heights. At other heights the reverse occurs, an example of which are the 1.5 sh altitude averaging kernels. In the case of figure 22(b), at heights above 5 sh altitude and below 6.5 sh altitude, an increase in the size of the noise estimate improves, considerably, the correspondence between the centre and averaging kernel heights.

From the full set of results (not given) it is apparent that estimators constructed with the original a priori covariance matrices are usually more sensitive to changes in the size of the measurement noise estimate while those constructed with ground corrected and filtered matrices are usually less sensitive to the same changes.

Discussion

From the preceding results it is evident that in each latitudinal zone, during summer and winter seasons, there are heights below 6 sh altitude for which the MAP retrieval estimators lack the intrinsic information necessary for a good temperature retrieval.

FIGURE 22 : Height (z_i) - Centre Height Curves for :

(a) Equatorial summer estimator (ground corrected, w=20),

(b) High Latitudes winter estimator (w=20).

Measurement noise values are :

——— σ_e = 0.045 ru

- - - - - σ_e = 0.71 ru

. . . . . σ_e = 2.0 ru

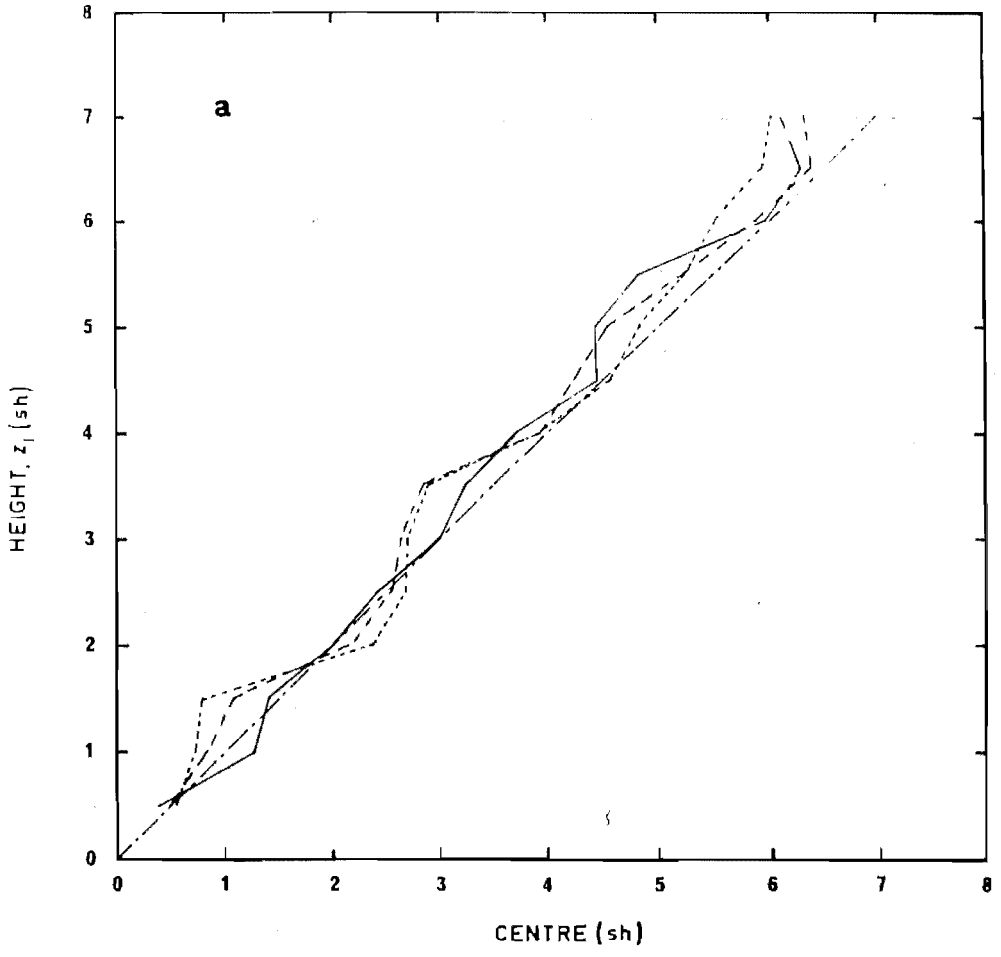
a
HEIGHT, z_i (sh)
CENTRE (sh)
0
1
2
3
4
5
6
7
8

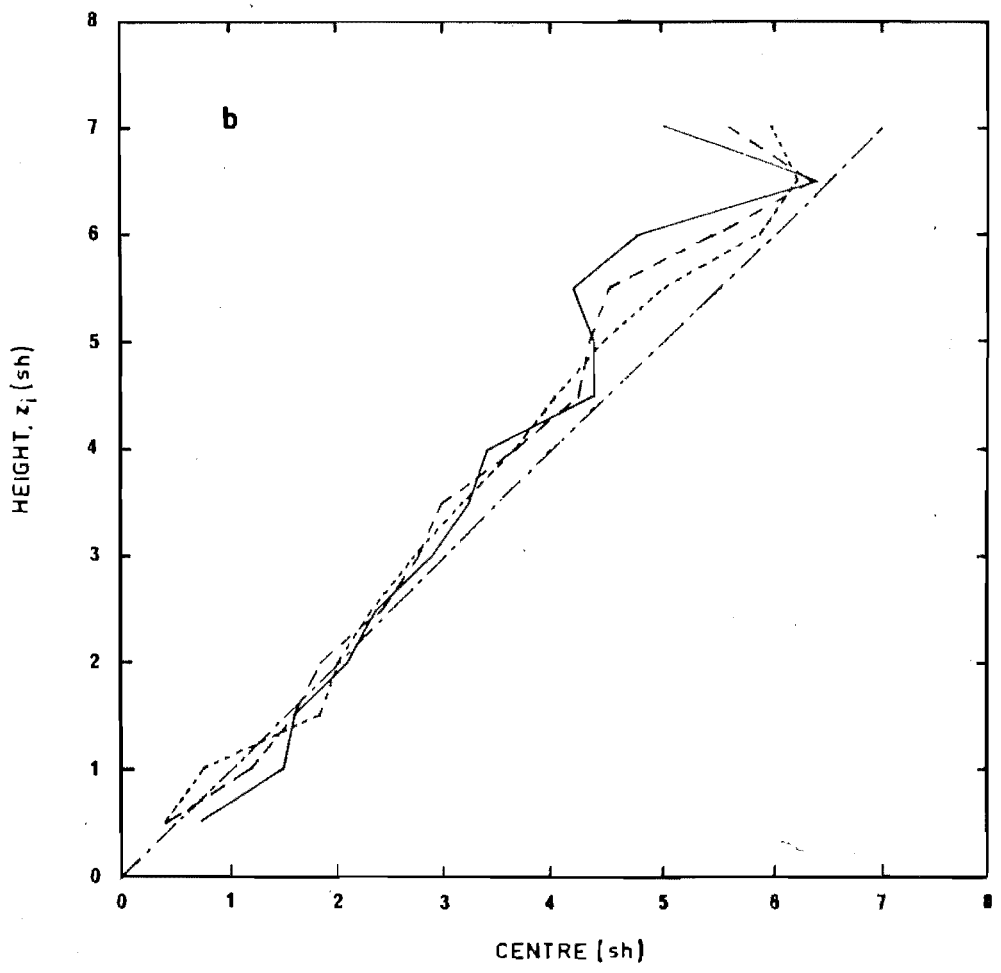
b
HEIGHT, z_i (sh)
CENTRE (sh)
0
1
2
3
4
5
6
7
8

It is also evident that at these heights the averaging kernel centre heights are sensitive to the size of the satellite measurement noise estimate. These height regions correspond to those heights for which the noise amplification-spread curves of the estimators are of the strong type 2 form. Evidently the centre height of an estimator averaging kernel is sensitive to the presence of side lobes in the averaging kernel. This result is expected, given the equation of the centre height, equation (2.158), the shape of the averaging kernels at these heights (see for examples figures 18 and 20) and the discussion of Section 3.4.1. The averaging kernel side lobes arise owing to the nature of the correlations in the atmospheric temperatures at different levels and the height distribution of the satellite weighting function peaks.

In regions where the centre heights of the averaging kernels are insensitive to a wide range of measurement noise estimates and the centre and averaging kernel heights correspond well, the noise amplification-spread curves are of the type 1 or weak type 2 forms, and the satellite weighting functions overlap significantly.

The maximum height for which temperature retrievals may be made with the given sets of a priori data, the Nimbus 4 SCR weighting functions and the calculated MAP estimators, is 6.5 sh altitude.

3.4.3 The Spread

The spread of the estimator averaging kernels as a function of the size of the satellite r.m.s measurement noise estimate σ_e has already been discussed in Section 3.4.1. In this section, the overall estimator intrinsic resolution (i.e. resolving power) as a function of altitude will be considered.

Calculations on an altitude grid of 0.5 sh intervals from 0.5 sh to 7.0 sh altitude have been chosen to represent the height dependent resolution of the estimators. The ground level results

FIGURE 23 : Height (z_i) - Spread Curves for

(a) Equatorial summer estimators, σ_e = 0.045 ru
(b) Equatorial winter estimators, σ_e = 0.1 ru
(c) Mid-Latitudes summer estimators, σ_e = 0.1 ru
(d) Mid-Latitudes winter estimators, σ_e = 0.32 ru
(e) High Latitudes summer estimators, σ_e = 0.045 ru
(f) High Latitudes winter estimators, σ_e = 0.1 ru

The estimators are identified by :

——— original
– – – – ground corrected
------- filtered (w=20)
O O ground corrected and filtered (w=20)
□ □ ground corrected and filtered (w=10)

The + symbols indicate the weighting function spread characteristics.

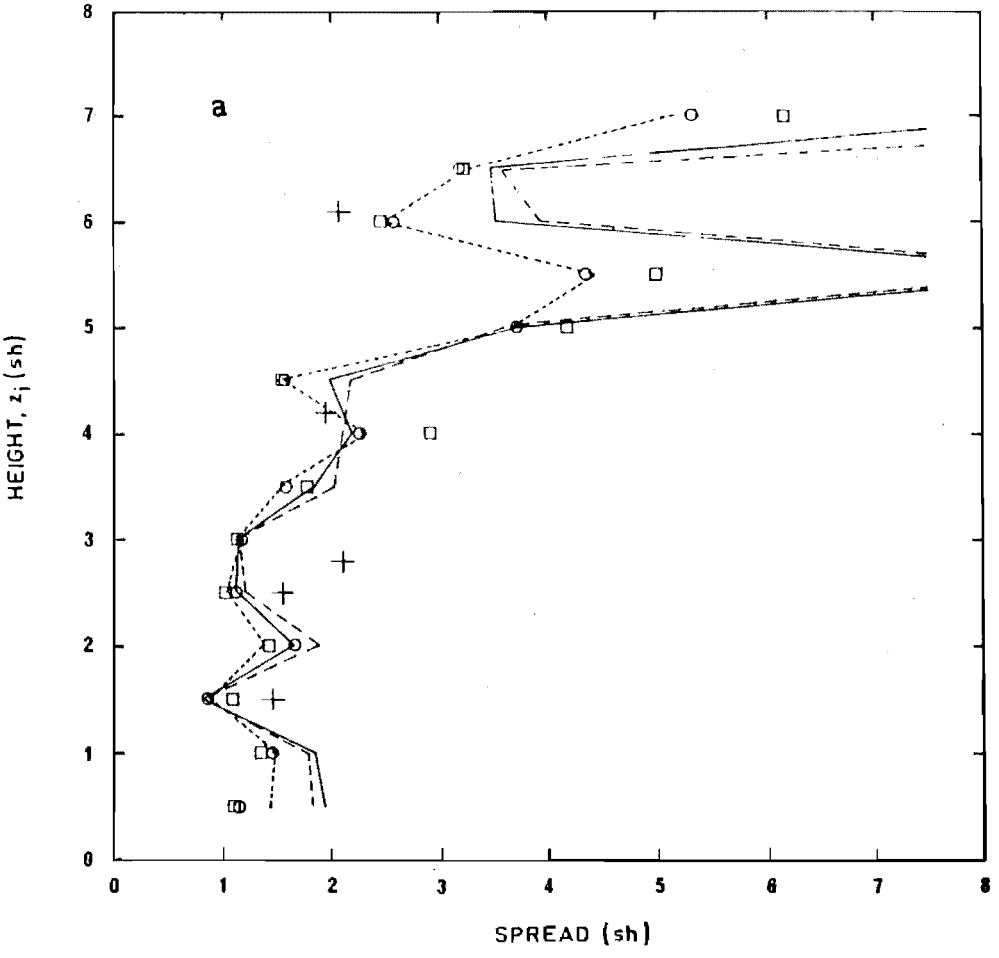
a
HEIGHT, z_i (sh)
SPREAD (sh)
0
1
2
3
4
5
6
7
8

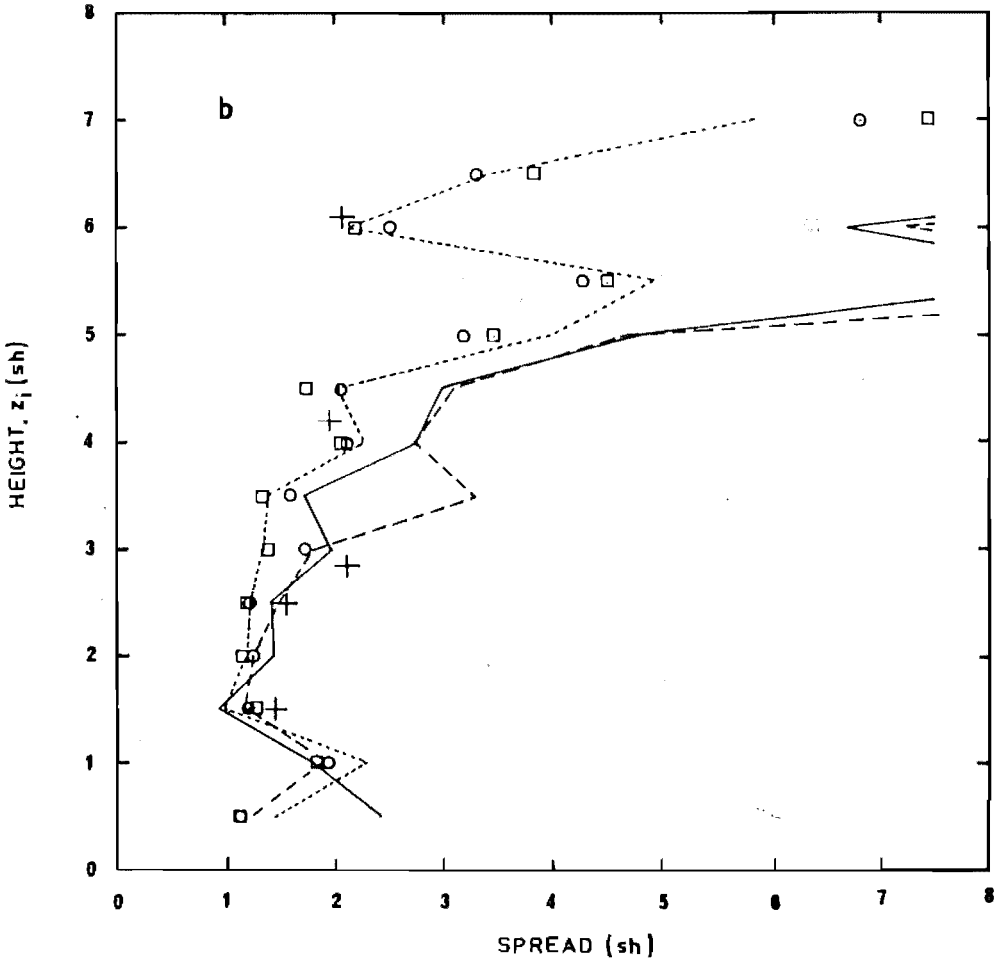
b
HEIGHT, z_i (sh)
SPREAD (sh)
0
1
2
3
4
5
6
7
8

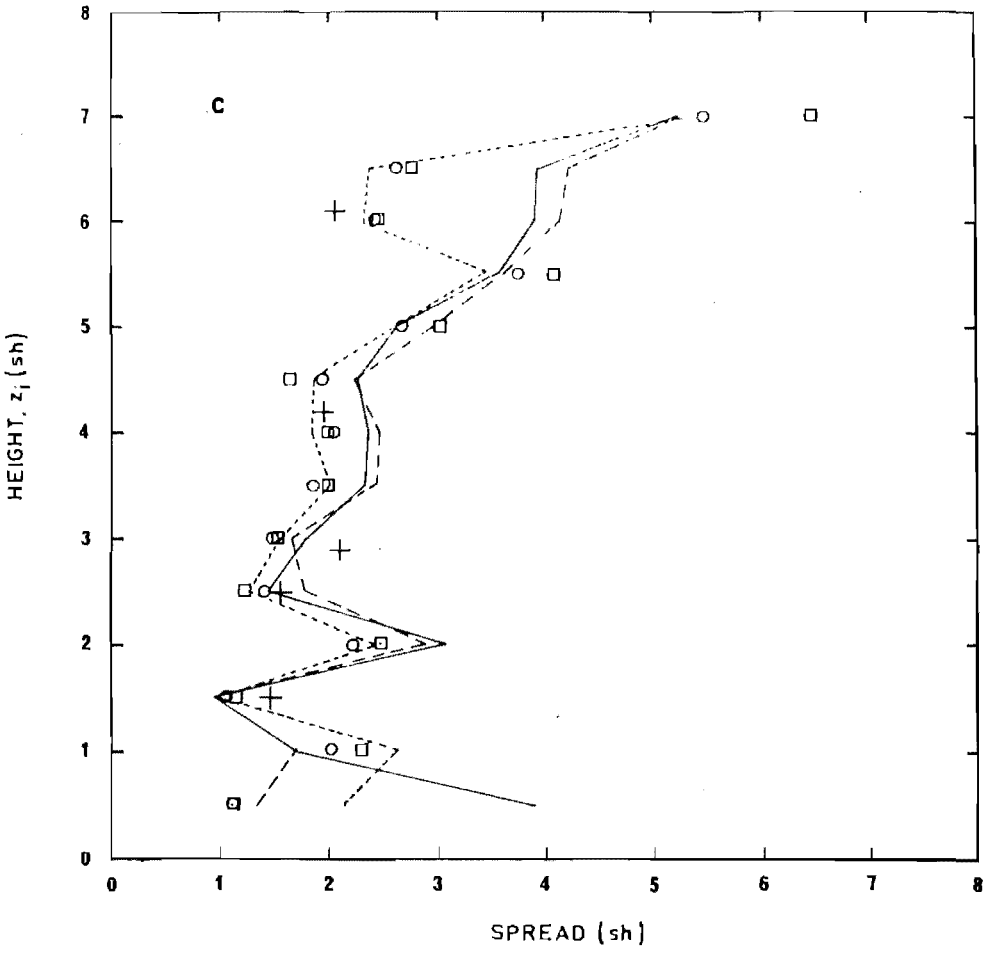
c
HEIGHT, z_i (sh)
SPREAD (sh)
0
1
2
3
4
5
6
7
8

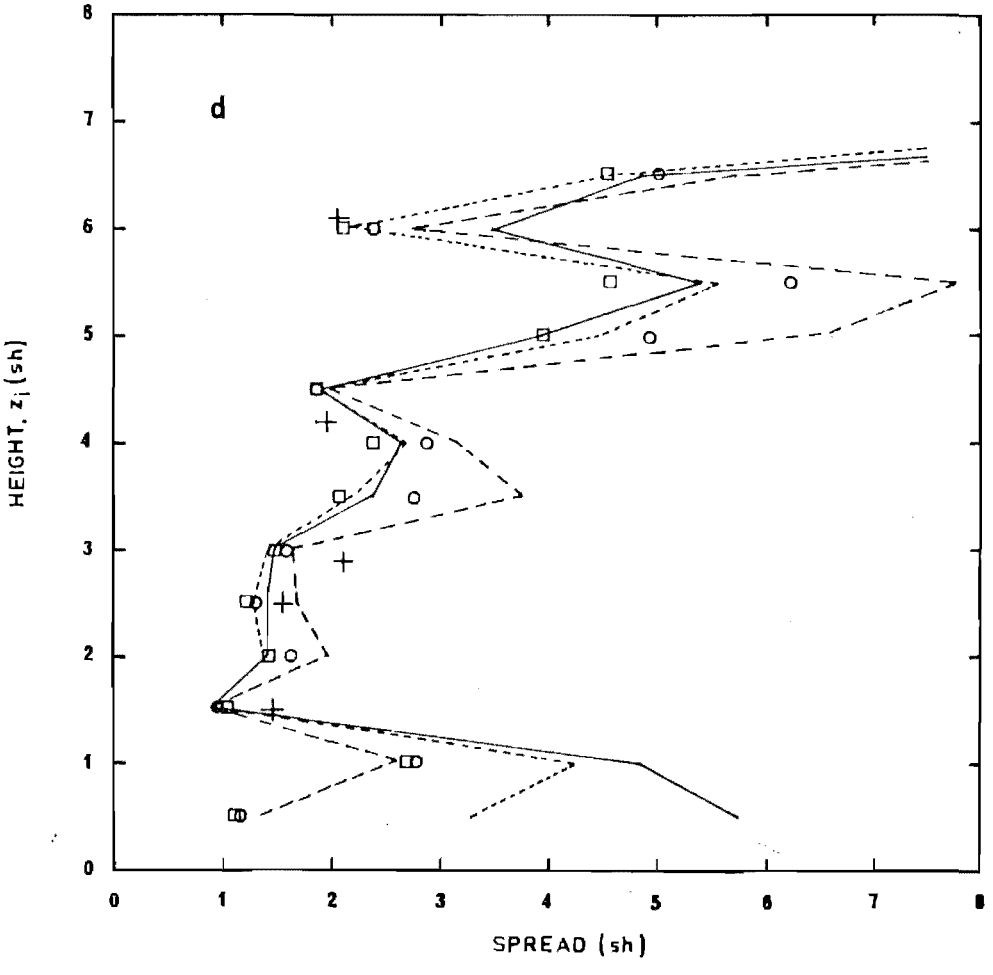
d
HEIGHT, z_i (sh)
SPREAD (sh)
0
1
2
3
4
5
6
7
8

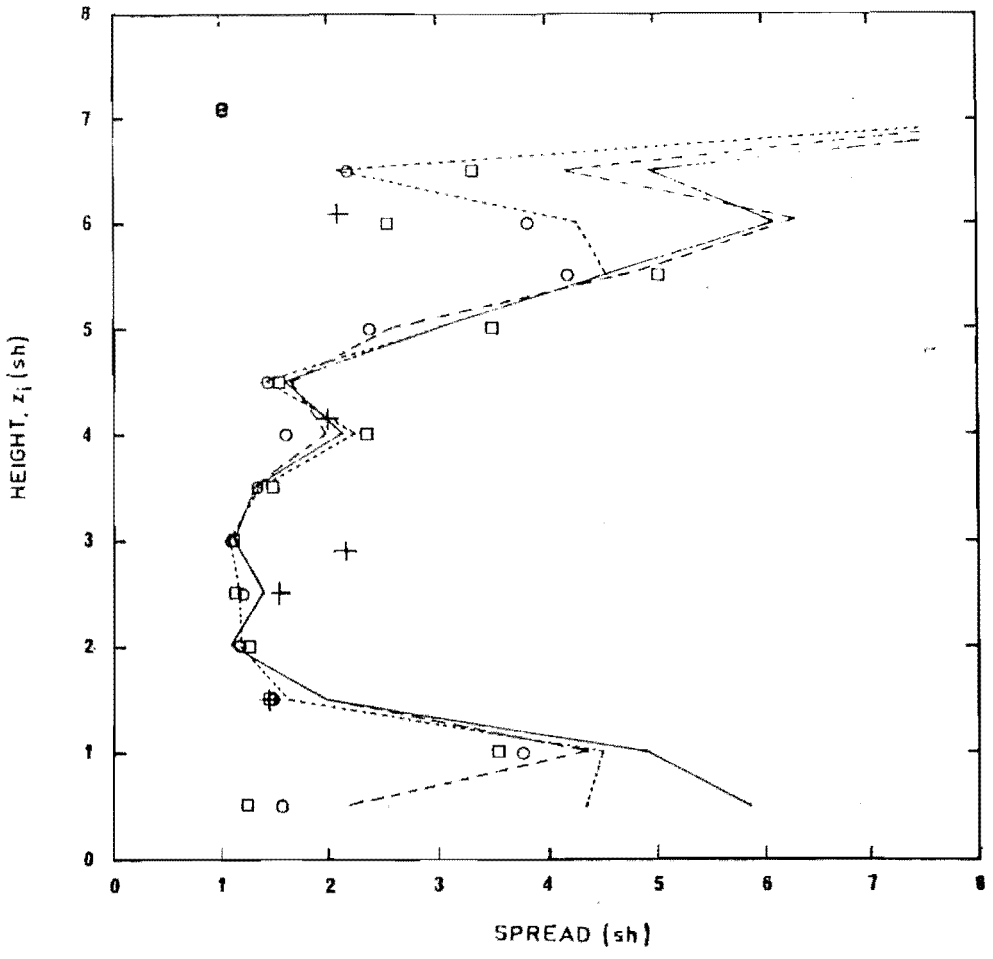
e
HEIGHT, z_i (sh)
SPREAD (sh)
0
1
2
3
4
5
6
7
8

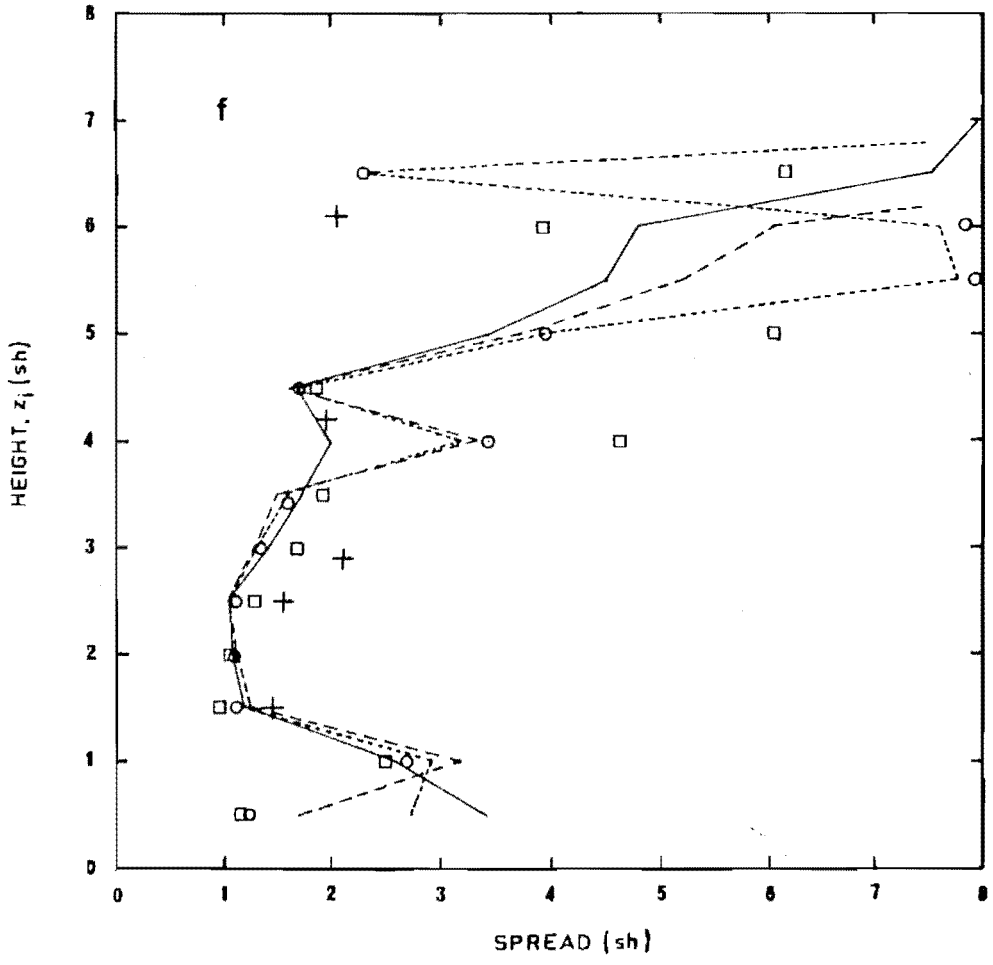
f
HEIGHT, z_i (sh)
SPREAD (sh)
0
1
2
3
4
5
6
7
8

are not included since the spread for all estimators near ground level is large and strongly dependent upon the size of the satellite noise estimate. Resolution of the ground level temperature is poor, even assuming that the radiances have been completely declouded.

The spread characteristics of the estimator averaging kernels for all three latitudinal zones for summer and winter conditions were calculated and noise amplification-spread curves determined. In figure 23 (a through f) the height-spread curves of the estimators are plotted using satellite noise value estimates which below 5 sh altitude result in approximately minimum spread in the averaging kernel noise amplification-spread curves. The spread characteristics of the channel A, B, C, D and E satellite weighting functions at their peak heights are also indicated in these figures. Different levels of the measurement noise do affect the size of the spread values of the estimator averaging kernels as detailed in Section 3.4.1. The results of figure 23 do not indicate the minimum spread values of the averaging kernels at all heights. This point is illustrated in fig-24, the spread-height curves of the high latitudes estimator constructed with the filtered (W=20) a priori covariance matrix and three different values for the measurement noise estimate. It is evident from this figure and the discussion of Section 3.4.1 that a large value for the measurement noise estimate improves the resolution of the estimator in height regions for which the noise amplification-spread curves are of the strong type 2 form. However, in regions where the noise amplification-spread curves are of the type 1 or weak type 2 form the resolution is decreased by assuming a larger value for the measurement noise. For this reason detailed differences in the spread-height curves for different seasons and latitude zones cannot be simply compared.

From the results of figure 23 it is evident that at heights below 4.0 sh altitude and corresponding to the peak heights of chan-

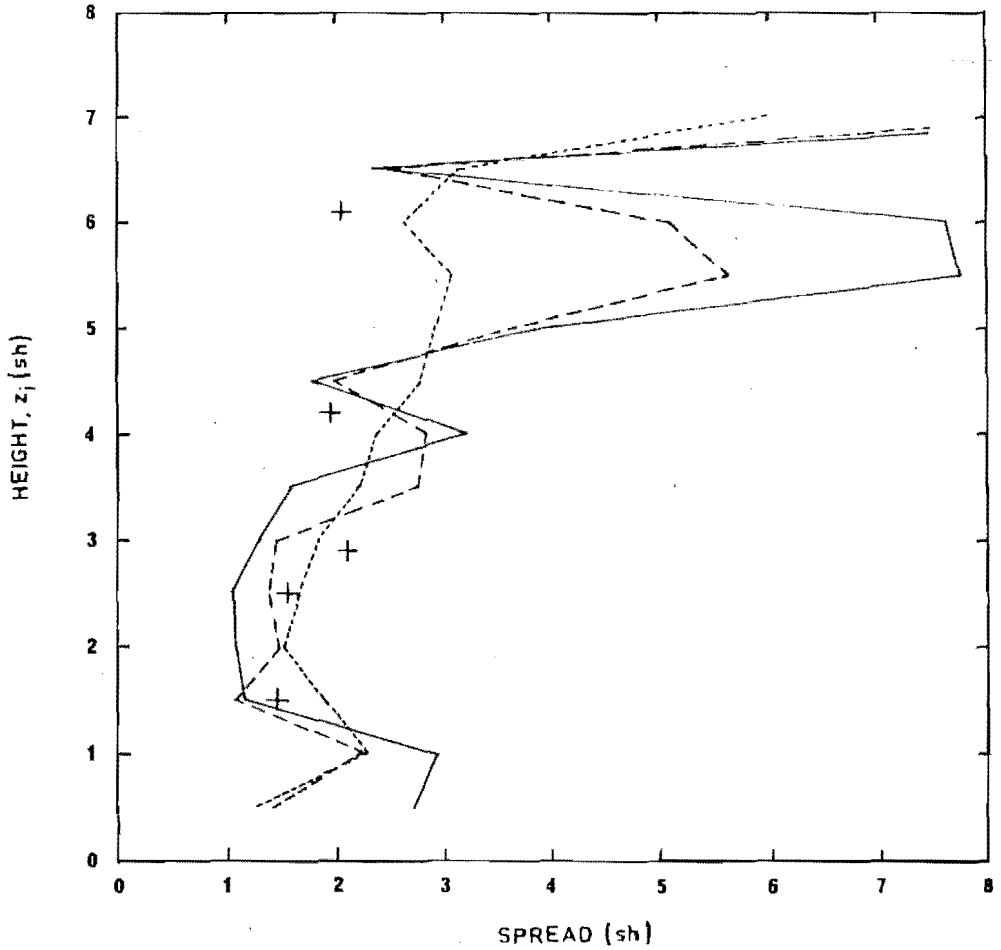

FIGURE 24 : Height (z_i) - spread curves for the High Latitudes winter estimators (w=20) and r.m.s. measurement noise values : ——— σ_e = 0.045 r.u., – – – – σ_e = 0.71 r.u., ------- σ_e = 2.0 r.u.

The + symbols indicate the weighting function spread characteristics

nels C D and E, the resolution of the MAP estimators is generally better than that of the satellite weighting functions. Above 4.0 sh altitude the resolution at 4.5 sh altitude is usually better than the resolution of the channel B weighting function. Between 4.5 sh and 6 sh altitude the resolution of all the estimators is very poor. Near 6 sh altitude, the peak height of the channel A weighting function, the resolution of the MAP estimators is in all cases no better than the resolution of the channel A weighting function. In general, the estimator resolution at these heights is rather poorer than that of channel A. Also, from figure 23 it is apparent that for the mid and high latitudes estimators the resolution near 1 sh altitude is rather poor.

The major differences between the spreads of the estimators for a particular latitude zone and season (in figure 23) may be compared. In the height range 1 sh to approximately 5 sh altitude the resolutions of the different estimators are similar. Above 5 sh altitude however, there is some variation between the estimator resolution characteristics. Generally, estimators constructed with the filtered a priori covariance matrices tend to have rather better resolution than those constructed from unfiltered covariance matrices. Below 1.5 sh altitude the spreads of averaging kernels of estimators constructed with the ground corrected and or filtered covariance matrices are generally much improved upon those for the estimators constructed with the original a priori matrix. The amount of this improvement is dependent upon the temperature correlations in the a priori covariance matrices. However it is apparent that knowledge of the ground temperature generally improves the resolution of the resultant estimator at heights near ground level.

Discussion

It is evident from the preceding results that the intrinsic resolving power of MAP estimators used to retrieve temperature pro-

files from Nimbus 4 SCR radiance data is not a constant function or even a smooth function of height. Instead the resolution in the retrieved temperature profiles is strongly dependent upon height and there are some heights for which the MAP estimators have essentially no resolving power. At heights below 4.5 sh altitude and near the peak of a satellite weighting function, the intrinsic resolution of the estimators is generally better than that of the satellite observations.

On consideration of the results of figure 23 and the discussion of Section 3.4.1 it is evident that the resolving power of the estimators is poor at those heights for which the noise amplification-spread curves are of the strong type 2 form. That is, those heights for which the resolving power of the estimators is strongly dependent upon the size of the satellite measurement noise estimate. For small satellite noise values the spread measures at these heights are poor owing to the strength of the side lobes in the estimator averaging kernels associated with these heights (see for example figures 18 and 20). Accordingly a poor result for the measure of the spread of an estimator averaging kernel, when the satellite measurement noise is small, indicates that a portion of the information for a retrieval at this height is determined by the temperature structure at other levels not near the averaging kernel height. This understanding of the spread measure of some averaging kernels explains the meaning of the condition noted in Section 3.4.2 which indicated that at some heights the estimators lack the intrinsic vertical information necessary for a good temperature retrieval.

The poor resolution of the MAP estimators at some heights is simply a result of the height distribution of the set of Nimbus 4 SCR weighting functions together with the temperature correlation structure of the a priori covariance matrices.

3.4.4 The Resolving Length

The resolving length characteristics of the sets of retrieval estimators for the three latitudinal zones and two seasons were calculated for the same height grid and satellite noise statistics as in the above section on estimator averaging kernel spread. Representative examples of these calculations are given in figures 25 (a and b); some results for the equatorial summer estimators and the high latitudes winter estimators respectively. The resolving length characteristics of the satellite weighting functions are also plotted on these curves. The sensitivity of the estimator resolving lengths to the size of the satellite noise estimates is indicated in figure 26, the results for an high latitudes winter estimator.

For each of the estimators, the resolving lengths of the averaging kernels at heights near 5.5 sh altitude are poor and quite sensitive to the size of the satellite noise as illustrated in figures 25 and 26. The resolving length characteristics, figure 25, are plotted for estimators using a satellite r.m.s noise estimate which results in near minimum spread in the corresponding averaging kernels at heights below approximately 4.5 sh. It is found that under these conditions for each latitude zone and season the resolving lengths of the estimators are similar except above 5 sh and below 1 sh altitude. They are also "smoother" functions of height than the corresponding spread characteristics. In general, this "smoothness" is increased by increasing the value of the measurement noise estimate. There are height regions where dissimilarities between the results for the five estimators result. Below 1 sh altitude, ground correction of the a priori covariance matrix improves the resolving length measure of the estimator considerably. Above 5 sh altitude filtering of the a priori matrix improves the estimator resolution.

FIGURE 25 : Height (z_i) - Resolving Length Curves for

(a) Equatorial summer estimators, σ_e = 0.045 ru

(b) High Latitudes winter estimators, σ_e = 0.1 ru

Symbols as for Figure 23.

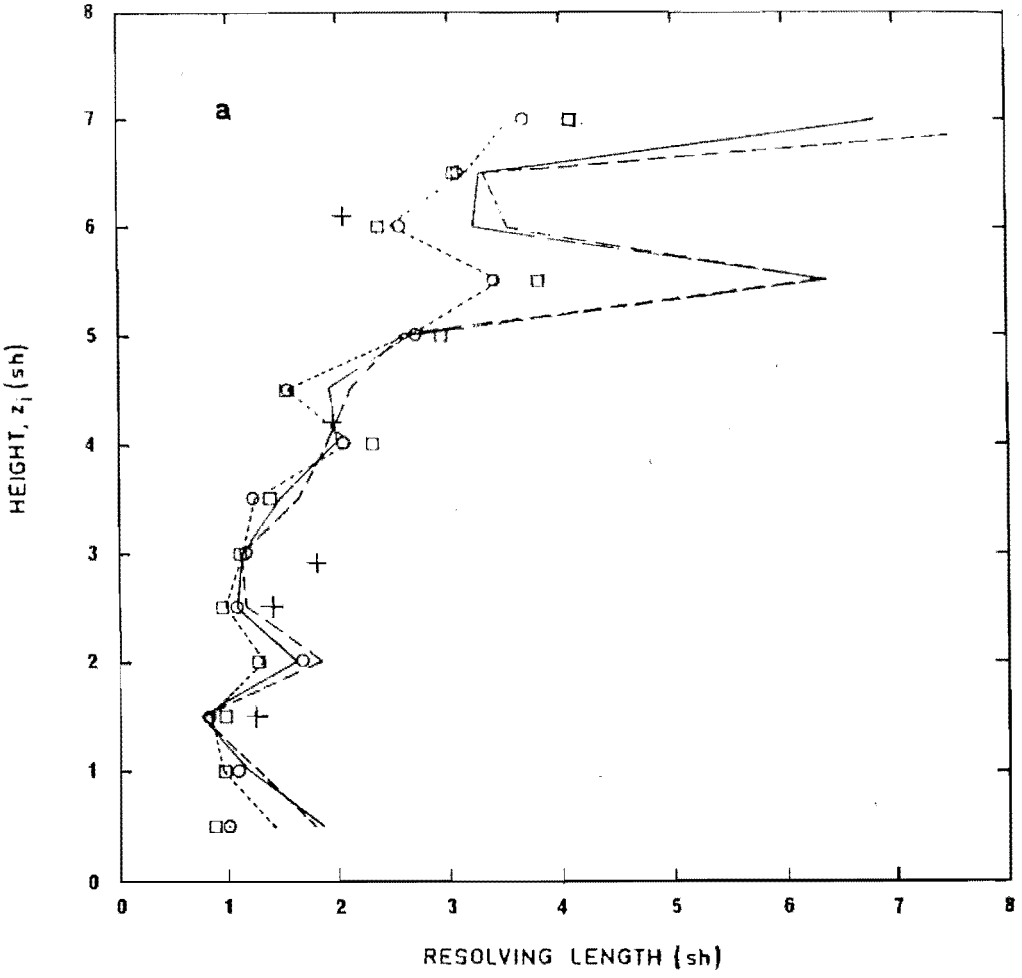
a
HEIGHT, z_i (sh)
RESOLVING LENGTH (sh)
0
1
2
3
4
5
6
7
8

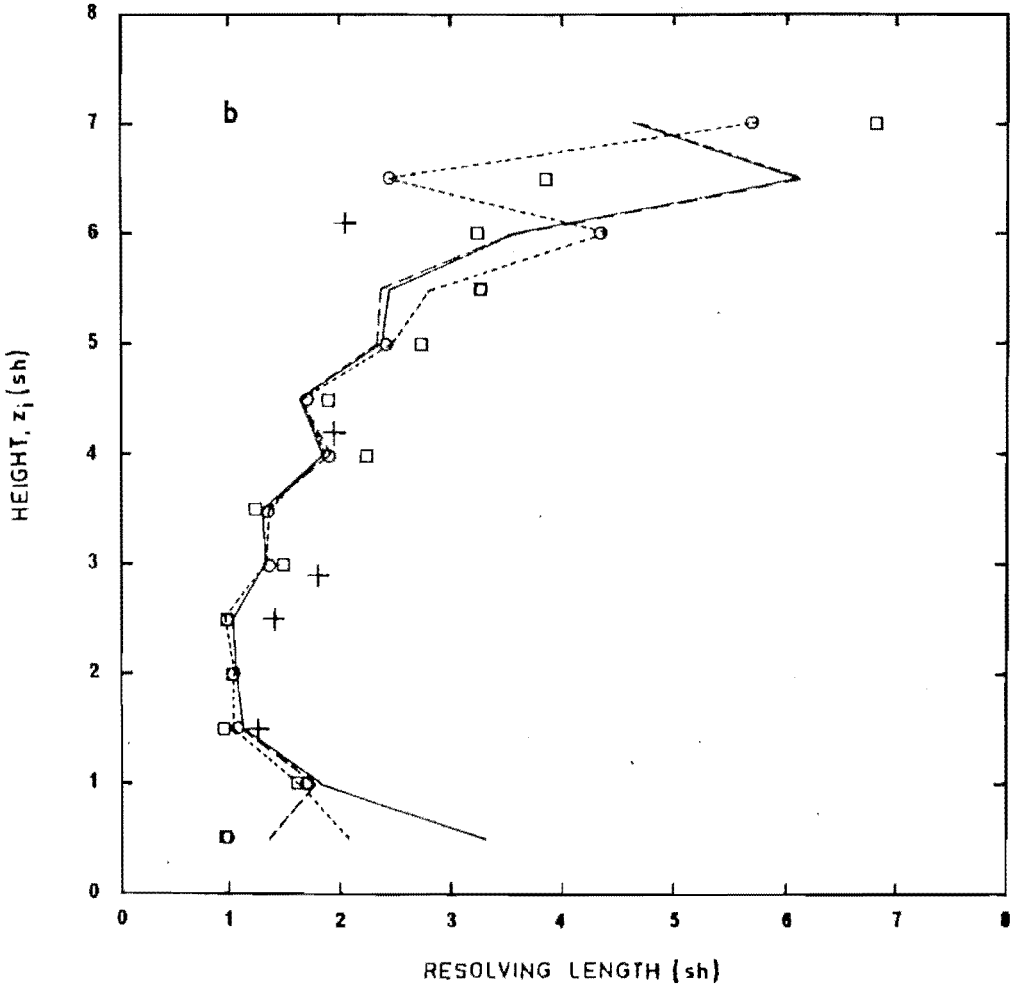
b
HEIGHT, z_i (sh)
RESOLVING LENGTH (sh)
0
1
2
3
4
5
6
7
8

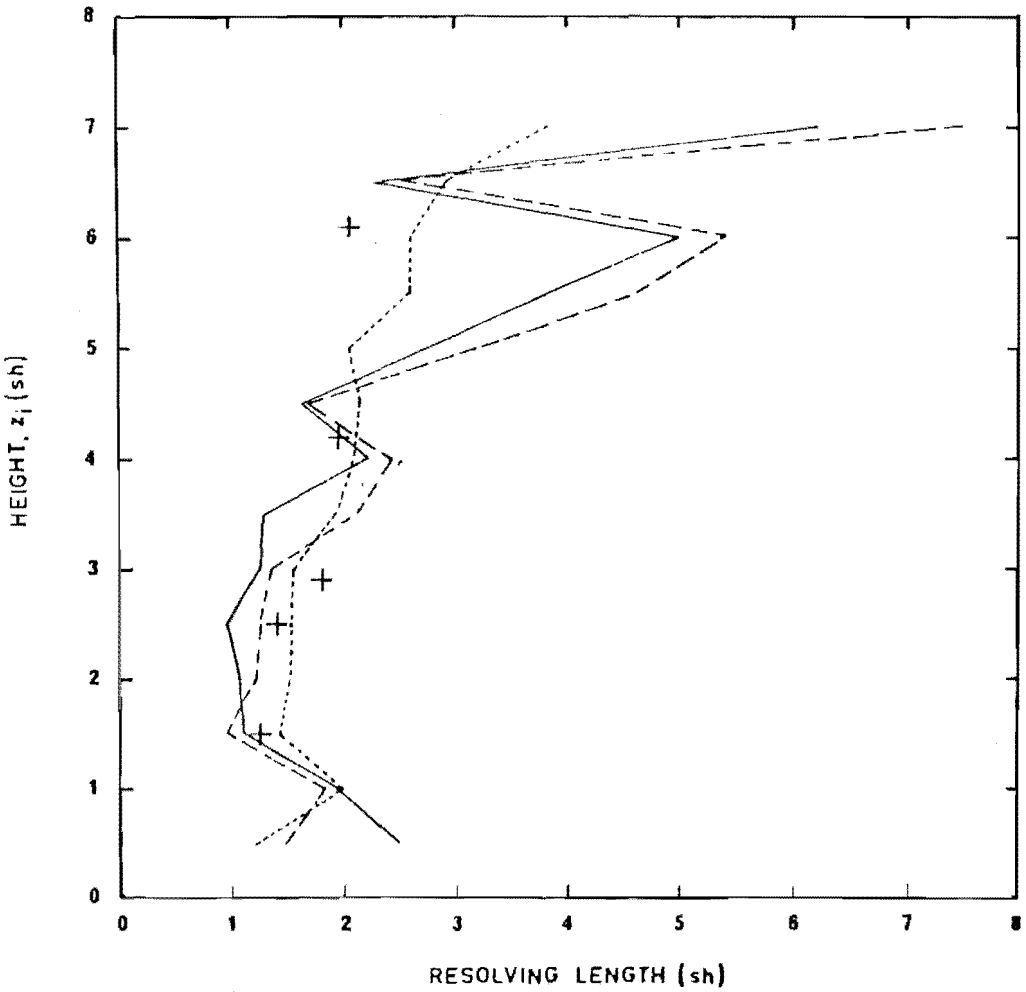

FIGURE 26 : Height (z_i) - resolving length curves for High Latitudes winter estimators (W=20), and r.m.s measurement noise values : ——— σ_e = 0.045 ru, ----- σ_e = 0.32 ru, ... σ_e = 2.0 ru, + symbol indicates satellite weighting function characteristics

Discussion

The resolving lengths of the estimator averaging kernels are a "measure" of the size of detail that will be "seen" by the MAP estimator combination of satellite and a priori data sets and are measures of the spread of the averaging kernels about their centres. As such it is not a good measure of the resolution, or resolving power of the estimator owing to the sometimes large deviations of the centre heights from the averaging kernel heights. For example, see figure 21. The above interpretation of the estimator resolving length is not appropriate if the corresponding averaging kernel has more than one "major" peak, as for example in figure 18. By definition the measure of the resolving length is large, but this in itself does not define a limit to the size of the structure the estimator will "see". Instead, the result indicates a lack of intrinsic information in the measurements at this height. Therefore, in interpreting the resolving length (as well as the spread) results the noise amplification-spread curves, the centre heights and the averaging kernels should be examined. These results indicate that at heights below 4.5 sh altitude and corresponding to the peak heights of the satellite weighting function, the estimator resolving lengths are of the order of or better than those of the satellite measurements. At channel A heights, near 6 sh altitude, the satellite measurement has a better resolving length value than any of the corresponding estimator averaging kernels.

The resolving lengths at all heights are functions of the size of the satellite measurement noise estimates, an the additional information (if any) applied to the a priori covariance matrices.

3.5 : FINAL COMMENTS

Since the problem of retrieving temperature profiles from satellite radiance data is ill-posed, it cannot be solved without the

use of some form of additional, a priori, information. The a priori information (data) says something about the height structure of atmosperhic temperatures.

The results for two fundamentally different retrieval methods have been considered in the preceding sections of this chapter. The first, the BG retrieval method, utilizes both the information in the satellite measurements and some a priori first guess temperature profile. The BG method does require a priori data if a complete solution is to be found. Without the a priori data the BG method can in principal say nothing about the atmospheric temperature structure (see Section 3.3). However, if temperature perturbations on some mean or first guess profile are required, the BG estimator determines these estimates by forming a linear combination of the satellite measurements. The resulting estimates are average values of the temperature perturbations over well defined layers in height.

In the second method, MAP estimation, the satellite data and error statistics are combined with a set of a priori data and the most likely temperature profile (given the two sets of data) is calculated. In this case, the a priori data are a first guess profile, (which is in this work, a mean profile for some latitude zone and season) and a temperature covariance matrix which says something about the expected temperature structure of the atmosphere. The estimated retrieval profile is the meteorologically most probable temperature profile which could give rise to the given satellite observations.

The task of the preceding sections has been to specify the intrinsic vertical resolving power of these two fundamentally different retrieval methods. To this end the BG parameters of the averaging kernels of both estimation procedures have been examined, the latter under widely differing a priori conditions. Equation (2.154) defines the relationship between the intrinsic resolving power of

an estimator at some height and the shape of the averaging kernel for that height. If the retrieved perturbation of the temperature at some height z_i is $(\underline{\hat{x}} - \underline{\bar{x}})_i$ then this perturbation is just the weighted average of the true temperature perturbation $(\underline{x} - \underline{\bar{x}})$ where the weighting function is the estimator averaging kernel for that height. The averaging kernel is therefore a "window" through which the true temperature profile is viewed. If the spread of the averaging kernel is small, the retrieved temperature at height z_i is determined by the true temperatures at heights near z_i and the resolving power of the estimator at that height is high. However, if the averaging kernel is broad or has more than one peak it is evident that the temperature retrieved for height z_i will depend upon the structure of the true temperature profile and first guess profile $(\underline{x} - \underline{\bar{x}})$ at heights not near z_i.

It is in the shape of the averaging kernels of the BG and MAP retrieval estimators that the importance of their fundamental differences is most apparent, and accordingly their fundamentally different resolving powers.

For the BG retrieval estimator, the averaging kernels are constructed by forming a linear combination of the set of satellite weighting functions by trading off the spread of the averaging kernel against the noise in the associated retrieved temperature. Therefore, for a high resolution estimate the noise, $\sigma_{\Delta\underline{\hat{x}}}(z_i)$, in the retrieved estimate at height z_i is large while for low resolution the temperature error is small. The key feature of the BG averaging kernels is that they are essentially single peaked functions for which the centre heights lie close to the averaging kernel heights if the noise trade-off parameter q is not equal to zero.

For the MAP estimators it is apparent that there are two fundamentally different types of averaging kernels. Those which are essentially single peaked functions, as with the BG estimator averaging

kernels, and those which have multiple peaks, unlike the BG estimator averaging kernels. In terms of resolving power characteristics, as discussed here (see Section 3.1) this result indicates there are fundamental and significant differences between the two estimator types.

Over the height range of the set of satellite weighting functions there are height regions in which the information content of the satellite measurements is poor, relative to adjacent nearby heights. For the BG estimator the spread of the averaging kernels at these heights is somewhat larger than at the nearby heights and the centre may deviate a little from the averaging kernel height. The information poor regions correspond to those heights for which there are no nearby satellite weighting function peaks, and the overlap of the satellite weighting functions is less than at adjacent information richer heights. However, for the MAP estimator averaging kernels at these same measurement information poor heights the kernels are in general multi-peaked functions of height. The MAP estimator determines the meteorologically most probable temperature for the height, given the satellite observations and the prior information on the nature of the temperature structure of the atmosphere, that is, the covariance matrix. It happens therefore, that at heights where satellite information is lacking, the retrieved temperature's estimate is essentially determined by the a priori data. At any latitude and during any season (see Section 3.2) there are correlations between the temperatures at different levels in the atmosphere. Consequently the shape of the estimator averaging kernel for these heights is strongly determined by these temperature correlations. That is, the MAP estimator makes use of these correlations to estimate the temperatures in the satellite information poor regions thus resulting in multiple peaked averaging kernels. The intrinsic resolving power of the MAP estimator at these heights is accordingly poor, and a retrieval is strongly influenced by the covariance matrix. The intrinsic ver-

tical resolution of MAP estimated temperature profile retrievals at heights where the satellite weighting functions lack intrinsic information will also be strongly dependent upon the shape of the true temperature profile difference vector $(\underline{x} - \bar{\underline{x}})$ at other, sometimes distant heights. In these height regions the MAP estimator makes a temperature retrieval based on the assumption that the correlations between the temperatures at different levels, as defined by the a priori covariance matrix, are real causal connections. The resolution is therefore poor owing to the bias introduced by the a priori data. At these same heights the resolution is also strongly affected by small changes in the satellite measurement noise statistics, indicating that effects due to near ill-conditioning of the MAP estimator equations are present and important. The BG retrieval method, while not retrieving the meteorologically most probable temperature profile, does not suffer from similar problems. In general the BG retrieval method's resolving power, in the sense understood here (i.e. Section 3.1), is better than that of the MAP estimators.

The conclusions of the analyses in Section 3.3 on the retrieval of temperature profiles from Nimbus 4 SCR data using BG estimators may be summarized as follows :

(a) Temperature retrievals may be made for heights from ground level to 6.5 sh altitude.

(b) At heights near the peaks of channels B, C, D, and E, when the tradeoff parameter q is greater than 0.2, the resolution of the estimator is better (by up to 40%) than that of the satellite measurements. At heights near the peak of channel A the resolving power of the estimators is similar to that of the satellite measurement.

(c) When the tradeoff parameter $q = 1$, the estimator intrinsic resolving power is of the order of 1 sh

in the troposphere, tropopause and lower stratoshpere. At greater heights it is of the order of 1.5 to 2 sh, except near 5.5 sh altitude where the resolution is only 2.5 sh. The corresponding temperature errors in the retrieved profiles due to satellite measurement noise values in the range 0.2 r.u to 1.7 r.u are of the order of $\pm 1 - 2C^0$.

The conclusions for the analyses of Section 3.4 on the intrinsic resolving power of temperature profiles retrieved from Nimbus 4 SCR data in three latitude zones during the summer and winter seasons using MAP estimators, are summarized below.

(a) The maximum height for which retrievals may be made is 6.5 sh altitude.

(b) At heights near 1 sh and 5.5 sh altitude the resolution of the estimators is poor. The retrieved temperatures at these heights are determined by the temperature correlation structure of the a priori covariance matrices and the resolution is sensitive to the size of the satellite measurement noise estimate.

(c) At heights below 4.5 sh altitude, corresponding to the peak heights of channels B, C, D and E, the maximum estimator resolution is if not better than that of the satellite observations, comparable to them. The maximum resolution is similar for both summer and winter seasons, for each latitudinal zone. At heights near the peak of channel A the estimator resolution is generally poorer than that of the satellite measurements.

(d) When the spread of the estimator averaging kernels is minimum, corresponding to maximum estimator resolving power, the noise amplification factor α is greater than one at all heights apart from those near 5.5 sh and 1 sh altitude. The contribution to the profile estimate's confidence regions due to the satellite measurement noise, when the estimator has maximum resolution, is at most $\pm 2C^0$.

(e) Knowledge of the ground level temperature may "improve" the resolution of the estimator at heights below 1.5 sh altitude but may also result in a degradation of the estimator resolution at greater altitudes.

(f) Filtering of the a priori covariance matrices improves the "resolving power" of the estimator at those heights for which the satellite data lacks intrinsic information (i.e. near 1 sh and 5.5 sh altitude) by reducing the strength of averaging kernel side lobes.

(g) Ground correction and filtering of the a priori covariance matrices generally results in an overall improvement in estimator resolving power at heights below 1.5 sh altitude and above 4.5 sh altitude.

(h) Simple extrapolations of the a priori covariance matrices for heights above 8.0 sh altitude will not seriously affect the resolution of the MAP estimators since the maximum height for which realistic retrievals can be made is 6.5 sh altitude.

CHAPTER 4

SIMULATION RESULTS

INTRODUCTION

The intrinsic vertical resolving power of MAP estimators for use in retrieving temperature profiles from Nimbus 4 SCR data has been discussed in Chapter 3. In the present chapter, section 4.1, these deductions are tested through consideration of a series of simulated retrievals. Section 4.2 gives results of calculations for an empirical orthogonal function representation of the retrieved profiles. In section 4.3 the 95% confidence regions of the a priori mean profiles and MAP estimators are calculated together with an estimate of the overall information content in the satellite measurements.

4.1 : SOME TEMPERATURE RETRIEVALS

In Chapter 3 the intrinsic vertical resolving powers of six sets of MAP retrieval estimators were considered. A prediction of these analyses was that the vertical resolution in a retrieved profile at heights greater than approximately 4 - 4.5 sh (≃30 km) is in general poorer than that of the satellite measurements. In this section this deduction is tested through consideration of results for simulated retrievals.

4.1.1 Simulation of Satellite Radiances

When the atmosphere is assumed to have some temperature structure $T(y)$, $(y = -\ln(p/p_o))$ in the field of view of the satellite the measured radiances for a cloudless atmosphere may be simulated using equation (2.23) :

$$I(\bar{\nu}_i,0) = B\left[\bar{\nu}_i,T(p_o)\right]\tau(\bar{\nu}_i,p_o,0) - \int_{\infty}^{-\ln p/p_o} B\left[\bar{\nu}_i,T(y)\right]\frac{d\tau}{dy}(\bar{\nu}_i,y,0)dy$$

$$+ e_i \qquad i = 1,2,\ldots,6 \qquad \ldots(2.23)$$

In this simulation study the values of e_i ($i = 1,2,\ldots,6$) are calculated by a random noise generator, the $\bar{\nu}_i$ are those of table 1 and the integration is performed for 103 quadrature points between heights 0 sh and 10.2 sh (~76 km) altitude using Weddles Rule.

The r.m.s. values for the measurement noise e_i are chosen according to the averaging processes that would be applied to the raw satellite data. Barnett et al (1972) suggest that for a single observation "frame" the possible random errors in the radiances (due to measurement) from all known sources are those given in table 6 below :

TABLE 6 : Possible Errors in Radiances (r.m.s.)

Channel	A	B	C	D	E	F
Noise (r.u.)	2.5	1.3	0.6	0.3	0.5	0.2

The errors include contributions arising from problems with the electronics, calibrations and noise. Systematic error components may account for perhaps another 3 r.u., but are neglected in the present study.

It will be assumed that the random noise in the data can be reduced sufficiently through somoothing and averaging for features of interest to be seen. The rms noise values used in this simulation study could be obtained from the original data by averaging samples of N observation frames for channels A, B, C, D and E, and N/2 observations for channel F.

Values of the transmission term $\tau(\bar{\nu}_i,p_o,0)$, $i = 1,2,\ldots,6$ were not available to the author. It was found that the values for the

integrals of the published weighting functions A, B, C and D (figure 4) were equal within numerical error, whereas the integrals for channels E and F were smaller. It was assumed that the differences between the integrals arose from a non zero constant of integration $\tau(\bar{\nu}_i, p_o, 0)$ for these channels. Accordingly values of $\tau(\bar{\nu}_i, p_o, 0)$ for channels E and F were derived, being 0.05 and 0.14 respectively. The values of $\tau(\bar{\nu}_i, p_o, 0)$ for channels A, B, C and D are assumed zero.

Kornfield and Susskind (1977) suggest $\tau(725, p_o, 0)$ has a value of 0.141 (for the Vertical Temperature Profile Radiometer instrument) for an "average" April 40^0N atmosphere. This value corresponds well with that derived above for the Nimbus 4 SCR 728 cm^{-1} channel.

The satellite weighting functions of figure 4 are normalised to unit area.

4.1.2 Linearization Aspects

In Section 2.4.1 it was indicated that the radiative transfer equation (equation (2.23)) must be linearized when deriving the inversion equations. It is found that the radiance "correction term" of equation (2.32) is important and must be incorporated if non linear effects owing to the choice of $\bar{\nu}$, the mean (or reference) wavenumber, are not to be important. If this term is not incorporated, calculations of radiance using the non linearized and linearized forms of equation (2.23) may result in differences as large as ±3-4 r.u. When the correction term is included the error is not larger than ±0.02 r.u.

4.1.3 Resolution Characteristics

Theoretical aspects of the intrinsic resolution of MAP estimated retrievals have been considered in Chapter 3. The discussion of the results given there indicated that the actual resolution in the retrieved profiles should be strongly dependent upon the shape of the difference profile vector $\underline{x} - \bar{\underline{x}}$. ($\underline{x}$ is the profile to be retrieved

and $\bar{\underline{x}}$ is the first guess profile). A further important result of Chapter 3 was the finding that the values used for the measurement noise statistics are important in determining the intrinsic resolving power of the MAP estimators at some heights. The intrinsic resolving power of an estimator is not necessarily greatest when the measurement noise is least. This point is important when calculating estimators to be used to determine vertical structure in retrieved profiles.

If the structure to be investigated in a retrieval causes changes in the observed radiances which are much less than the random noise in the observations then the raw data must be suitably smoothed. However the resulting (decreased) noise statistics may, on insertion in the MAP estimator equations produce an estimator which has effectively poorer intrinsic vertical resolution than an estimator constructed with larger noise variance estimates. Generally, increases in the spread of estimator averaging kernels as the noise is decreased are due to increases in the strength of averaging kernel sidelobes, (Sections 3.4.3 and 3.4.4) even though the width of the main peak of the averaging kernel may decrease. Hence as the noise in the radiances is decreased through data smoothing the resulting vertical resolution in a retrieved profile becomes more dependent upon the first guess profile. It may also become more difficult to find a "solution" which satisfies equation (4.1), the residual criterion :

$$\left| \underline{y}_{\underline{x}_i} - \underline{y}_{\hat{\underline{x}}_i} \right| \leq e_i \quad i = 1,2,\ldots,6 \qquad \ldots (4.1)$$

where $\underline{y}_{\underline{x}_i}$ is the i^{th} component of the radiance observations and $\underline{y}_{\hat{\underline{x}}_i}$ is the equivalent component for the retrieved profile. That the retrieval should satisfy the residual criterion is a necessary requirement for a "correct" retrieval estimate of the unknown profile $\underline{x}$. If after performing a MAP retrieval the residual criterion is not satisfied, then the retrieval procedure is iterated until convergence occurs. Unfortunately if this is the case, the retrieved estimate

of the unknown profile will be biased since after the first iteration the first guess profile is not the mean profile for which the a priori covariance matrix is calculated. (see Section 2.4.3)

In order to examine the importance of these aspects of the estimator averaging kernels, resolution characteristics of estimators used to retrieve temperature profiles from equatorial "summer" and high latitudes winter observations will be considered here in detail. These cases correspond to situations in which the atmospheric temperature structure has respectively the least and greatest variance at any particular height. Results for averaged data using five different sized data samples are considered. The measurement noise variances for each channel in these averaged data are given in table 7.

TABLE 7 : Observational Noise Variance Statistics

DATA SERIES	CHANNEL NOISE VARIANCES $(r.u.)^2$					
	A	B	C	D	E	F
1	3.0	0.85	0.18	0.05	0.12	0.02
2	1.5	0.43	0.09	0.02	0.06	0.02
3	0.60	0.16	0.04	0.008	0.024	0.008
4	0.15	0.04	0.009	0.002	0.006	0.002
5	0.07	0.02	0.004	0.001	0.003	0.001

In the following work the noise statistics assumed in any particular MAP estimator will be referenced by the data series number used in table 7.

The BG height-spread curves for MAP estimators constructed with these noise statistics in both latitude zones and seasons are given in figures 27(a) and 27(b). These results are for estimators constructed with the original a priori covariance matrices and are therefore the optimum MAP estimators. Results for estimators constructed with filtered (w=20) a priori matrices are also given for data series 2 noise statistics in order to indicate the response of the MAP estim-

FIGURE 27 : Height (z_i) - Spread Curves for :

(a) Equatorial summer estimators

(b) High Latitudes winter estimators

and r.m.s. measurement noise values :

——— data series 1

—·—·— data series 2

o o data series 3

------- data series 4

——·—— data series 5

□ □ filtered estimator (w=20) and data series 2 noise values

\+ refers to weighting function characteristics

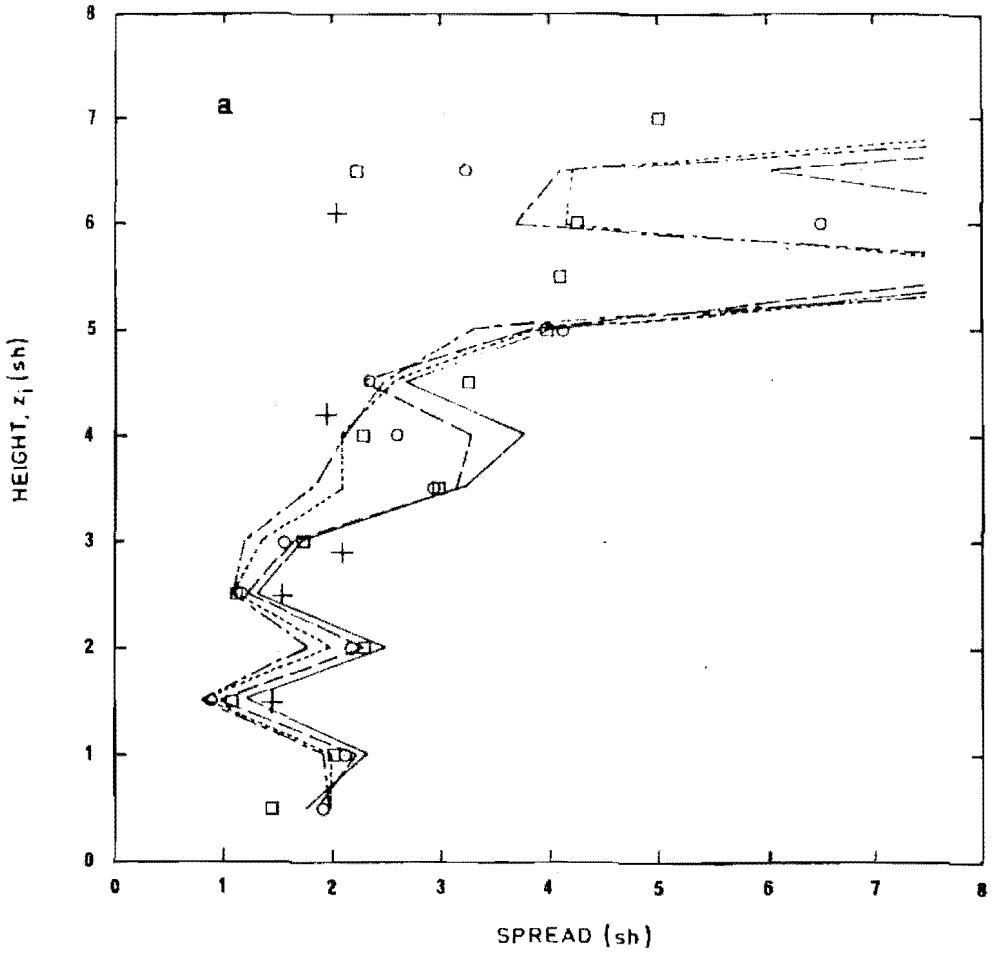
a
HEIGHT, z_i (sh)
SPREAD (sh)
0
1
2
3
4
5
6
7
8

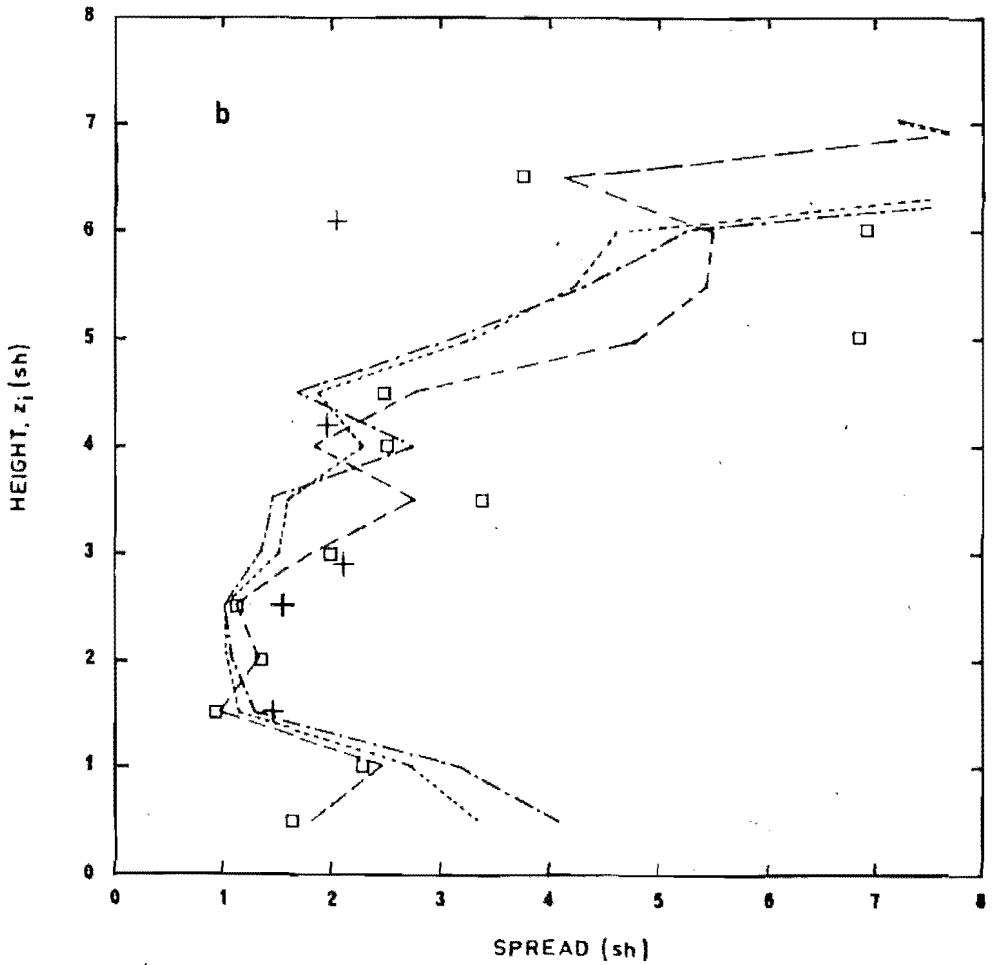
b
HEIGHT, z_i (sh)
SPREAD (sh)
0
1
2
3
4
5
6
7
8

ators to filtering of the a priori covariance matrices. These are not optimum estimators.

It would seem that the noise differential between channels has had a conditioning effect upon the equations so that at most heights, decreasing the noise in the measurements improves the resolution of the estimators. However, there are exceptions as expected from the results of Chapter 3. For the case of the Equatorial summer estimators the intrinsic resolution at 5.5 sh altitude is better for data series 2 noise statistics than for data series 5 values, whereas at 6.5 sh altitude the resolution when using data series 3 values is better than that for data series 5 values. In the high latitudes winter case similar results arise, see for example, the spread characteristics at 0.5 sh and 6.5 sh altitude. In each case these curves indicate that the intrinsic resolving power of the MAP estimators at heights greater than approximately 4 sh (≃30 km) is poorer than that of the satellite weighting functions.

The averaging kernels for those estimators which use noise statistics corresponding to the values given for data series 2 and 5 can be found in appendix J.

On comparing the averaging kernels of estimators using different noise statistics (appendix J); within either latitude zone and season, it is evident that in general for heights where the satellite weighting functions do not overlap significantly, decreasing the noise variances decreases the widths of the main peaks in the averaging kernels. Accompanying this decrease is an increase in the strength (magnitude) of the side lobes in the averaging kernels and perhaps an increase in the spread characteristic for the curves.

The centre-height, and measurement noise propagation error ($\sigma_{\Delta\hat{\underline{x}}}(z_i)$) curves are given in figures 28(a) and 28(b). The noise values are given in radiance units at the reference wavenumber $\bar{\nu}$ (690 cm^{-1}). For temperatures involved here (approximately 200 K to

FIGURE 28 : Height (z_i) - Centre Height Curves and Height (z_i) - r.m.s. propagation noise values for estimators of Figure 27. Symbols as for Figure 27.

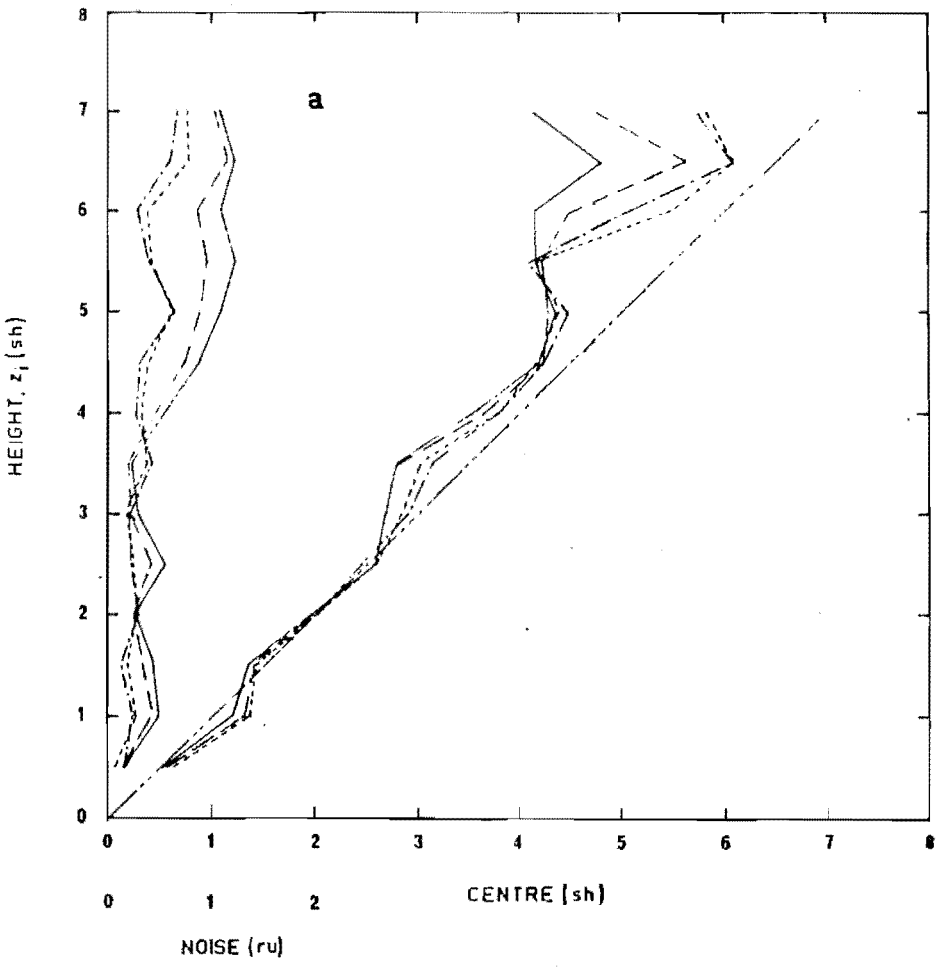
a
HEIGHT, z_i (sh)
CENTRE (sh)
NOISE (ru)

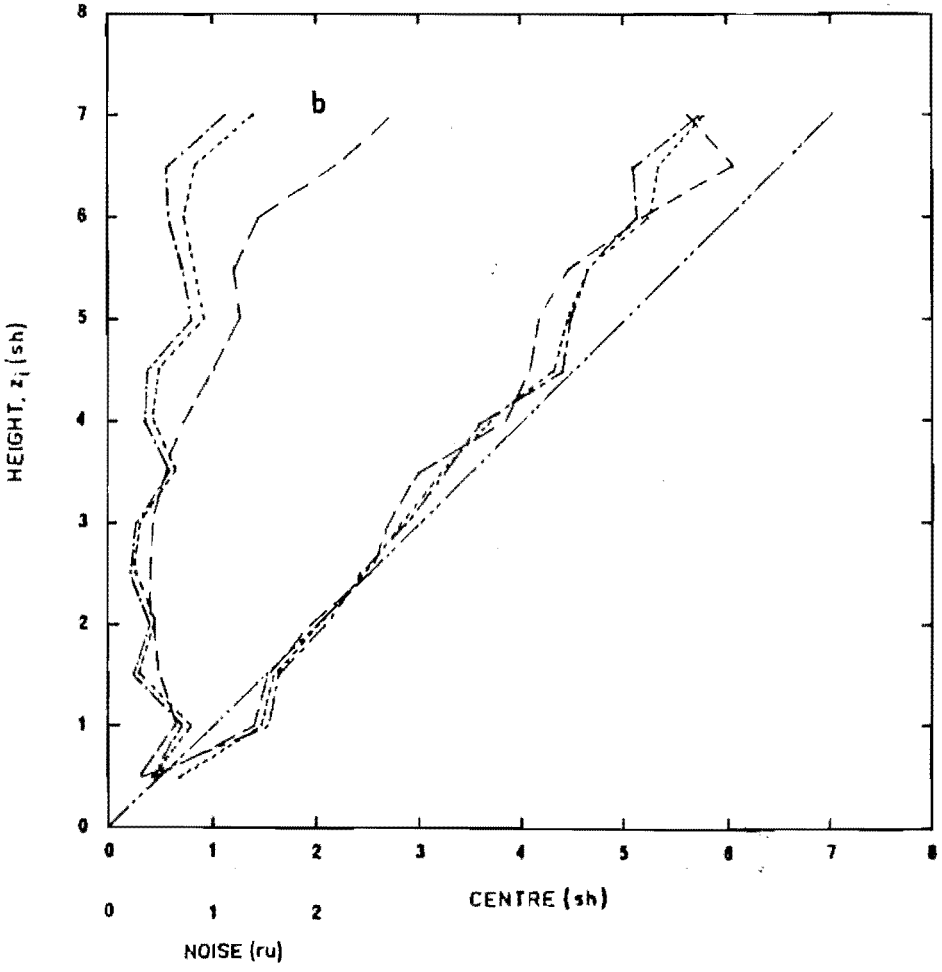
b
HEIGHT, z_i (sh)
CENTRE (sh)
NOISE (ru)

280 K), 1 r.u. corresponds to approximately $1C^0$.

The centre-height curves and the relationships between the curves for different measurement noise values are similar to those found in Chapter 3. However, the noise differential between channels has improved results at high altitudes. A decrease in the measurement noise is at most heights associated with a decrease in the size of the error in the retrieved profile due to noise propagation, but not by the same factor since the error magnification increases as the noise is reduced.

Figures 27(a) and 27(b) indicate that the "best" intrinsic resolving power for the MAP estimators occurs at heights near the peaks of the satellite weighting functions, as also noted in Chapter 3.

4.1.4 Retrieval Results

The actual resolving power of an estimator can, to some degree, be determined through numerical experimentation. Essentially the resolving power is determined by the estimator's ability to retrieve a perturbation of some vertical dimension in the atmospheric temperature structure being sounded by the satellite. When the vertical dimension is such that the perturbation cannot be resolved, a measure of the resolving power of the estimator is obtained.

A series of experiments have been carried out in order to determine the importance for a retrieval of the MAP estimator averaging kernel side lobes (artefacts) discussed in Chapter 3 and Section 4.1.3 above. These experiments will assess the significance of the averaging kernel centre and spread measures in specifying the resolving power of an estimator.

Corrected, concaternated, smoothed rocketsonde-balloonsonde temperature profiles $T(z)$ (where $z \equiv y = -\ln(p/p_o)$) for each latitude zone and season were chosen at random from an independent sample of profiles not used in the determination of the a priori covariance

matrices. Assuming the atmosphere has the temperature structure defined by these profiles clear column radiances were calculated using equation (2.23). In order to specify the retrieval of a determinable structure of known vertical dimension in the true profiles, the profiles were perturbed by a wave of the form :

$$T'(z) = A \exp(\alpha z) \sin\left(\frac{2\pi}{\lambda_z} z + \phi\right) \qquad \ldots (4.2)$$

where λ_z is the "wavelength" of the vertical structure, z is the height (sh), ϕ the initial phase, A some initial amplitude and α is a factor which determines the wave's growth or decay with height. Satellite radiances for the new profiles $\bar{T}(z) + T'(z)$ are calculated.

Simulation experiments were conducted in order to determine whether a structure of wavelength λ(sh) and amplitude A exp (αz) could or could not be resolved in the retrieved profiles.

Equation (2.154) states that the retrieved temperature at some height z_i is

$$(\hat{\underline{x}} - \bar{\underline{x}})_i = \int_{z=0}^{z_t} A_i(z)(x - \bar{x})(z)dz \qquad \ldots (4.3)$$

therefore

$$(\widehat{\underline{x} + \underline{x}'} - \bar{\underline{x}})_i = \int_{z=0}^{z_t} A_i(z)((x + x') - \bar{x})(z)dz \qquad \ldots (4.4)$$

$$= \int_{z=0}^{z_t} A_i(z)(x - \bar{x})(z)dz$$

$$+ \int_{z=0}^{z_t} A_i(z)x'(z)dz \qquad \ldots (4.5)$$

where x'(z) is the applied perturbation T'(z) (equation (4.2)).

Substituting equation (4.3) into equation (4.5) and rearranging :

$$(\widehat{\underline{x} + \underline{x}'} - \underline{\bar{x}})_i - (\underline{\hat{x}} - \underline{\bar{x}})_i = \int_{z=0}^{z_t} A_i(z)x'(z)dz \qquad \ldots (4.6)$$

The MAP estimator is a linear estimator, hence

$$\widehat{\underline{x} + \underline{x}'} = \underline{\hat{x}} + \underline{\hat{x}}' \qquad \ldots (4.7)$$

Substitution of equation (4.7) into equation (4.6) gives

$$\underline{\hat{x}}'_i = \int_{z=0}^{z_t} A_i(z)x'(z)dz \qquad \ldots (4.8)$$

and

$$\underline{\hat{x}}' = (\widehat{\underline{x} + \underline{x}'} - \underline{\bar{x}}) - (\underline{\hat{x}} - \underline{\bar{x}}) \qquad \ldots (4.9)$$

Accordingly, examination of the perturbation estimate $\underline{\hat{x}}'$ (equations (4.9) and (4.8)) is useful in determining the significance, in terms of vertical resolution, of the side lobes in the estimator averaging kernels, when retrieving a wave-like pertubation on some temperature profile.

In reality the equals sign of equation (4.8) should be replaced by an approximately equals sign since the retrieval residuals will not in general be identical for the perturbed and unperturbed profile retrievals. This is so since perturbing the profile to be retrieved could equally well be considered as a change in the first guess profile.

In the following work both the effects due to the averaging kernels and the residual convergence criterion will be examined.

The profiles used for these experiments are given in table 8 below:

TABLE 8 : Profiles Used in Simulation Study

Latitudinal Zone	Launch Site	Latitude	Season	Date	Time (GMT)
Equatorial	Antigua	17^0 09'N	Summer	14/7/71	1350
	C. Kennedy	28^0 27'N	Summer	7/6/72	1354
	Ft. Sherman	9^0 20'N	Winter	16/1/70	1725
	Barking Sands	22^0 02'N	Winter	28/12/71	2242
Mid-Latitudes	Pt. Mugu	34^0 08'N	Summer	2/6/71	1859
	Wallops Is.	37^0 50'N	Summer	24/7/72	1914
	Pt. Mugu	34^0 08'N	Winter	4/12/70	1715
	Wallops Is.	37^0 50'N	Winter	21/1/70	2058
High-Latitudes	Ft. Churchill	58^0 44'N	Summer	9/6/71	1514
	Ft. Greely	64^0 00'N	Summer	8/6/70	1900
	Ft. Churchill	58^0 44'N	Winter	4/1/70	1803
	Primrose Lk.	54^0 45'N	Winter	10/1/72	1655

Detailed results for only two of these experiments are given here since they indicate the important consequences of estimator averaging kernel side lobe structure and incorporate effects which arise from differences between the true and first guess profiles.

The equatorial summer atmospheric temperature structure does not change significantly in time (see table 4 and appendix D), therefore temperature profiles for this latitudinal zone and season can be expected to lie close to the sample mean profile (the first guess profile). The difference vector $(\underline{x} - \bar{\underline{x}})$ will have small elements for most heights. In terms of the difference vector structure, the opposite extreme is represented by the high latitudes winter atmosphere which experiences large temperature fluctuations about the mean profile (see table 4 and appendix I). For a high latitudes retrieval it may be expected that the profile $\underline{x}$ may not lie close to the sample mean profile. The vector $(\underline{x} - \bar{\underline{x}})$ may have large elements at some heights. Results for the summer Antigua (14/7/71, 1350 GMT) and winter Ft Churchill (4/1/70, 1803 GMT) simulated retrievals will be considered here in detail.

The sequential MAP estimator of Section 2.4.4 is used to per-

form all retrievals. After the satellite measurements have been added the residuals $|y_{\underline{x}_i} - y_{\underline{\hat{x}}_i}|$ are calculated. If they are not less than or equal to the assumed r.m.s. measurement noise values, the retrieval procedure is iterated. The solution of the preceding iteration becomes the first guess profile for the next iteration. This will result in a biased estimate (see Section 2.4.3), however if the residuals are not less than the r.m.s. noise values then a solution has not been found (see Section 2.1). All that can be done in the absence of more precise a priori statistics is to iterate the procedure until the residual criterion (equation (4.1)) is satisfied. In most of the examples tested it was found that the channel F residual was difficult to reduce below its r.m.s. noise value owing to this channel's sensitivity to temperature changes at and near ground level. In practice the iteration is stopped and a solution is assumed found when the residual criterion is satisfied for channels A, B, C, D and E, or after five iterations.

To dectect a perturbation in a temperature profile retrieval the r.m.s. values of the measurement noise must be less than the magnitude of the perturbation in the measured satellite radiances. The following estimators will in general use noise values which correspond to those for data series 5 unless otherwise stated. So that an estimate of the best possible resolving power of the estimators can be deduced, the radiances used in the simulated retrievals will be noise free. Later this assumption will be shown to be justifiable on the grounds that the noise statistics used in determining the MAP estimators are rather smaller than the perturbations in the radiance measurements due to the perturbation on the simulation profile.

It is predicted a priori from the BG spread-height curves figures 27 and 23(a) and (f) that the resolution in the retrievals is best at altitudes corresponding to heights near the peaks of the satellite weighting functions. (The side lobe structure is least

and the averaging kernels are narrowest.) The resolution of the satellite observations is best if the "height" of the observation is regarded as the centre height rather than the peak height. The resolving length of the weighting function is then equal to the spread of the observation. To compare the resolution in the retrieved profiles with that in the radiance observations and hence compare the resolving power of the measurements with that of the MAP estimators the retrieved perturbation temperatures at heights corresponding to the weighting function centre heights will be compared with those deduced from the brightness temperatures (the black body equivalent temperatures for the radiances).

Four different perturbations (equation (4.2)) have been applied to the rocketsonde-balloonsonde temperature profiles. The essential vertical features of these perturbations are specified as :

(a) a perturbation which is essentially an evanescent wave over the height range of interest, with an exponentially growing amplitude.

(b) a perturbation with vertical wavelength λ_z equal to 6 sh (≃45 km).

(c) a perturbation with vertical wavelength λ_z equal to 4 sh (≃30 km) and

(d) a perturbation with vertical wavelength λ_z equal to 3 sh (≃23 km).

The vertical dimension of these perturbations to be resolved by the estimator is half the wavelength λ_z, for cases (b) through (d). A perturbation of the first kind, type (a), indicates the type of biases introduced into the retrieved temperature structure by the retrieval procedure.

4.1.4.1 An Equatorial Summer Retrieval

The profile to be retrieved $\underline{x}$, and the first guess $\bar{\underline{x}}$, are illustrated in figure 29(a), while the difference profile $\underline{x} - \bar{\underline{x}}$ is

FIGURE 29 : Equatorial summer simulation profiles.

(a) ——— profile to be retrieved, $\underline{x}$

------- first guess profile, $\underline{\bar{x}}$

(b) difference vector $(\underline{x} - \underline{\bar{x}})$

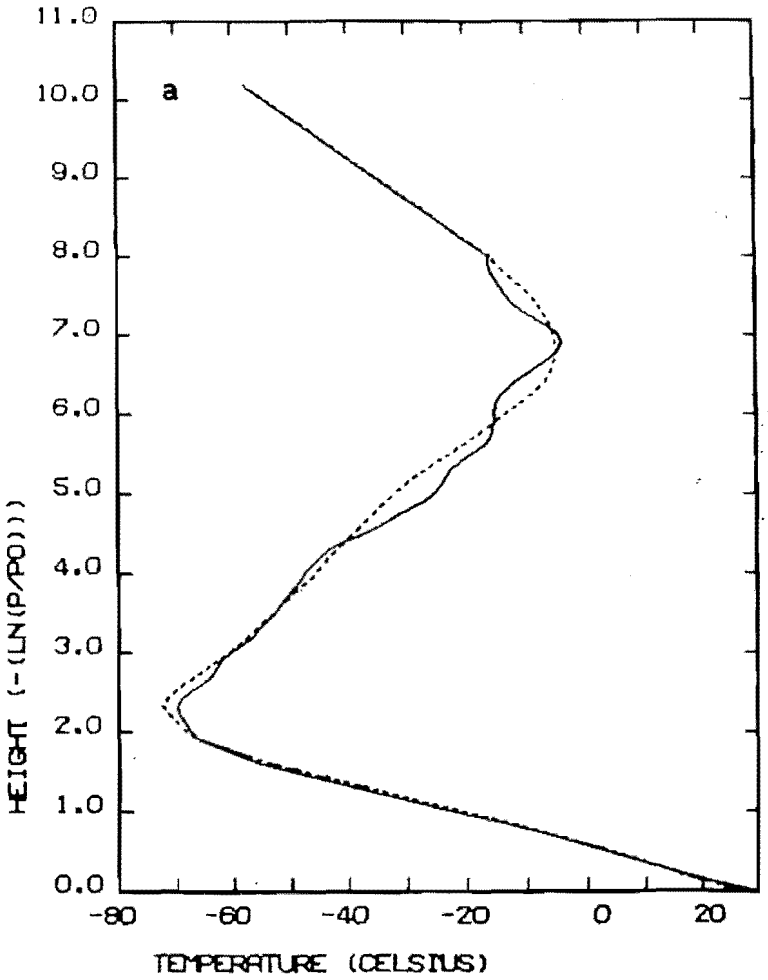
a
11.0
10.0
9.0
8.0
7.0
6.0
5.0
4.0
3.0
2.0
1.0
0.0
HEIGHT (-(LN(P/PO)))
-80
-60
-40
-20
0
20
TEMPERATURE (CELSIUS)

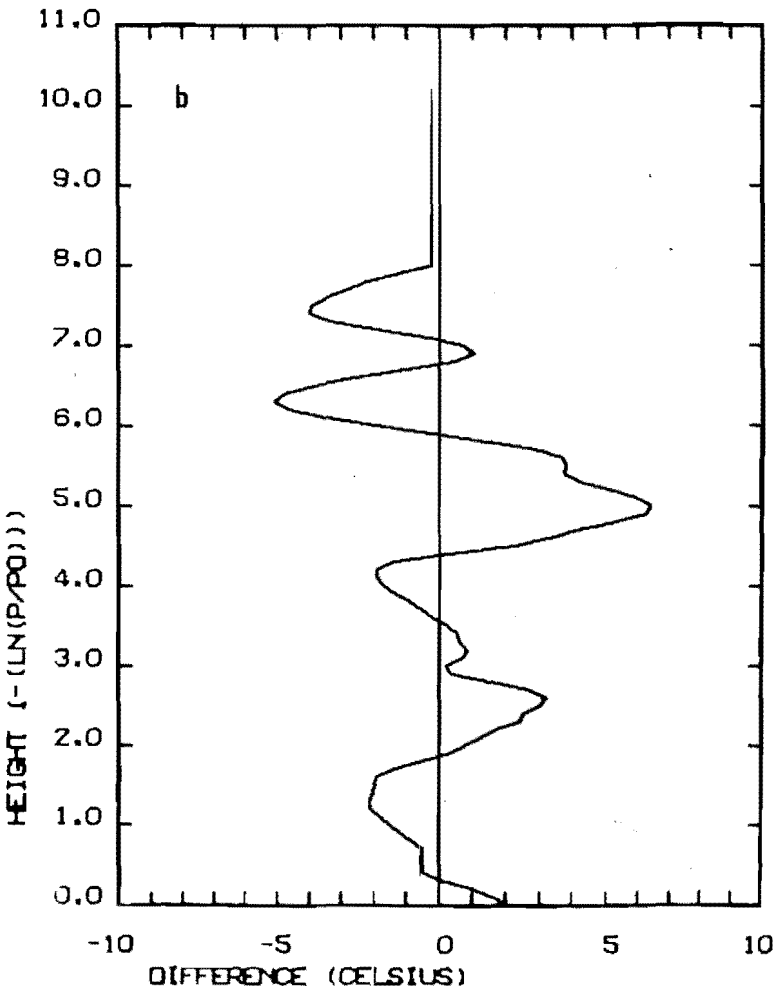
b
11.0
10.0
9.0
8.0
7.0
6.0
5.0
4.0
3.0
2.0
1.0
0.0
HEIGHT (-(LN(P/PO)))
-10
-5
0
5
10
DIFFERENCE (CELSIUS)

figure 29(b). At no height does the difference profile have an element larger than $\pm 7C^0$.

The Evanescent Wave

A perturbation having the form of equation (4.2) with $A = 0.5C^0$, $\alpha = 0.29$, $\lambda_z = 100$ sh ($\simeq$700 km) and $\phi = \pi/2$ was applied to the simulation profile (figure 29(a)). This perturbation would approximate (to 10 sh altitude) the vertical structure of a Lamb wave, where the value of α is $(\gamma - 1)/\gamma$. (Madden (1979)).

The clear column (noise free) radiances for the perturbed and unperturbed profiles are given in table 9.

TABLE 9 : Clear Column Radiances for Perturbed Profile where $A = 0.5C^0$, $\alpha = 0.29$, $\lambda_z = 100$ sh, $\phi = \pi/2$

Channel	A	B	C	D	E	F
Unperturbed profile (r.u.)	81.64	62.11	47.06	41.61	51.47	99.98
Perturbed profile (r.u.)	85.38	64.24	48.39	42.68	52.25	100.40
Difference (r.u.)	3.74	2.13	1.33	1.07	0.78	0.42

The r.m.s noise values used in the MAP retrieval estimator are those for data series 5 data, that is 0.26, 0.14, 0.06, 0.03,0.06 and 0.03 r.u. for channels A through F respectively. These values are much less than the perturbation differences. The estimator is appropriate to perform the retrieval and random noise in the simulated radiances (with variances e_i^2, i = 1,2,...,6) would not significantly alter the results.

The residuals for the unperturbed and perturbed retrievals are given in figure 30. The retrieval for the perturbed profile is essentially convergent in three iterations. The unperturbed profile is not convergent after five iterations. The retrieval for the unperturbed profile (3 iterations) is given in figure 31(a) while the error vector $(\underline{x} - \hat{\underline{x}})$ is figure 31(b). Below 4.0 sh altitude the retrieval error is not more than $\pm 2C^0$, above this height the maximum

FIGURE 30 : Residuals for unperutrbed retrieval ——— ;
and for perturbed (λ_z = 100 sh) retrieval --------.
The size of the r.m.s. measurement error for
each channel is indicated on the right hand
side of the diagrams.

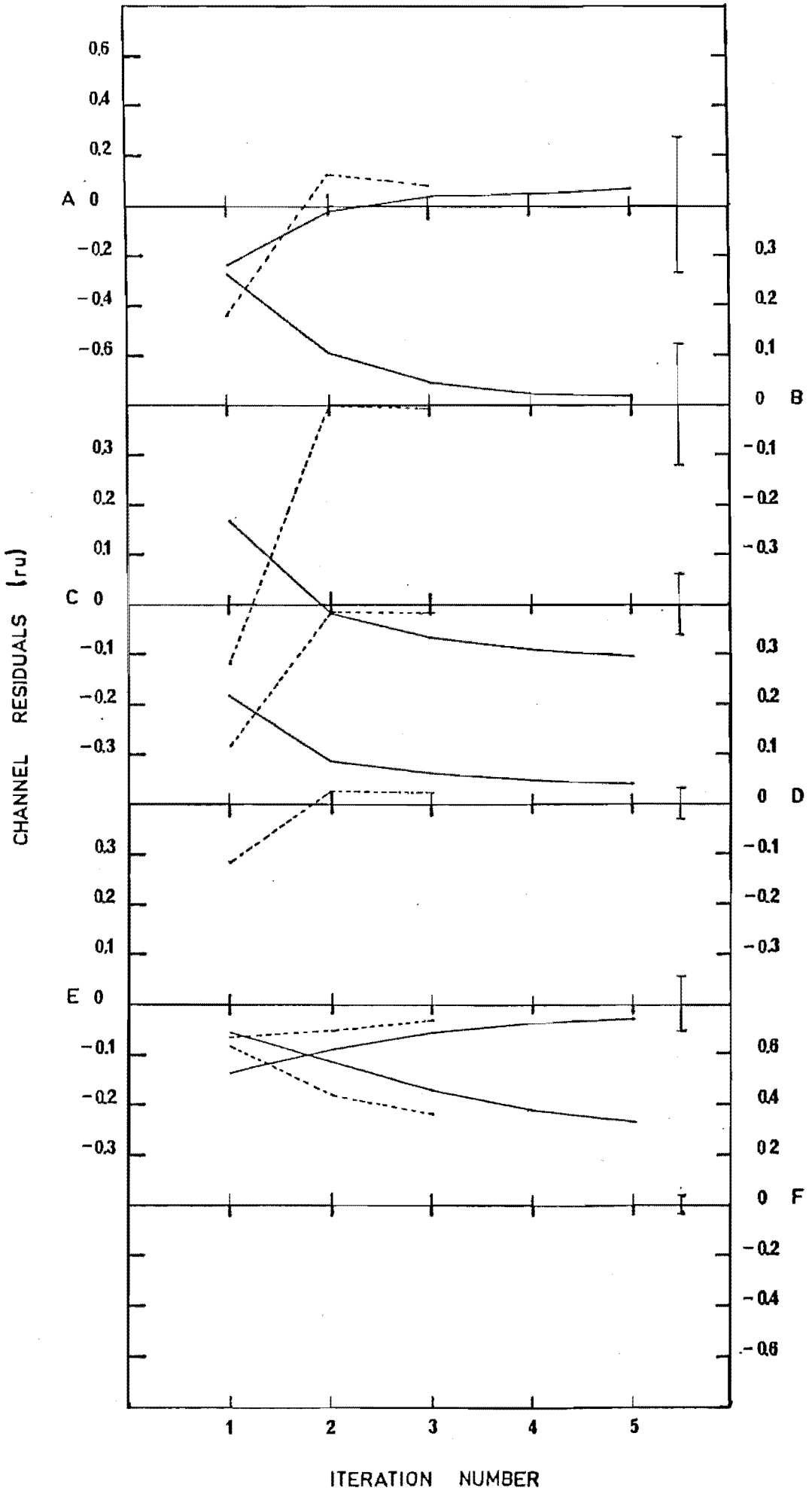
CHANNEL RESIDUALS (ru)
A
B
C
D
E
F
0.6
0.4
0.2
0
-0.2
-0.4
-0.6
0.3
0.2
0.1
0
-0.1
-0.2
-0.3
0.6
0.4
0.2
0
-0.2
-0.4
-0.6
1
2
3
4
5
ITERATION NUMBER

FIGURE 31 : Retrieval of unperturbed profile at 3 iterations.

(a) the retrieved profile ------- $\underline{\hat{x}}$,
and the true profile ——— $\underline{x}$

(b) the error vector $\underline{x} - \underline{\hat{x}}$

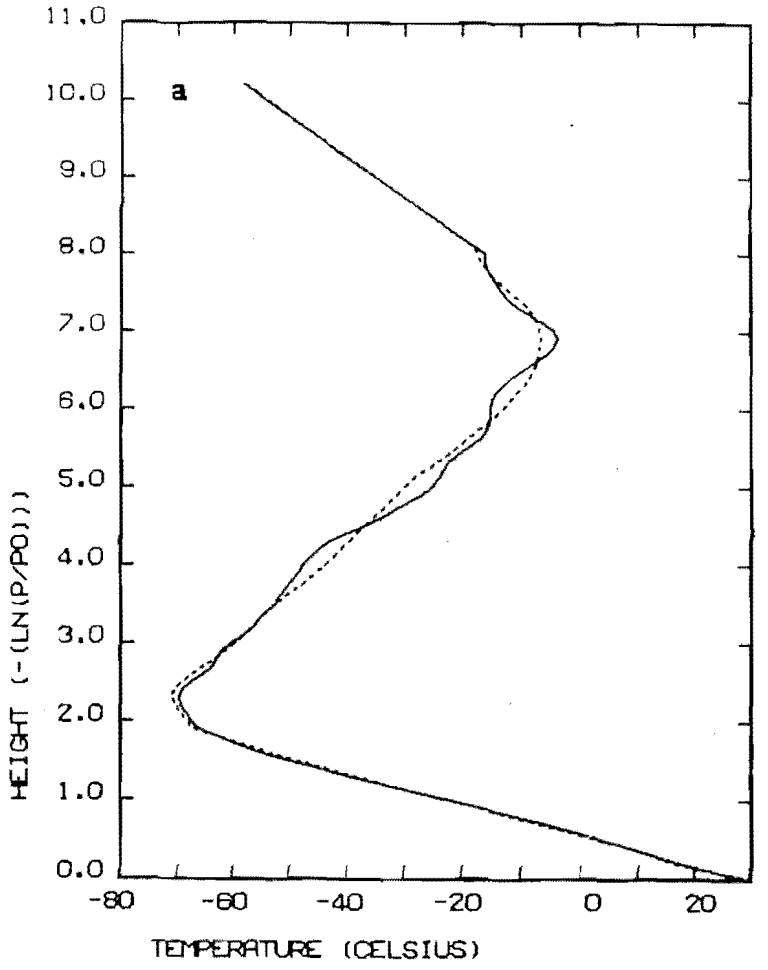
a
11.0
10.0
9.0
8.0
7.0
6.0
5.0
4.0
3.0
2.0
1.0
0.0
HEIGHT (-(LN(P/PO)))
-80
-60
-40
-20
0
20
TEMPERATURE (CELSIUS)

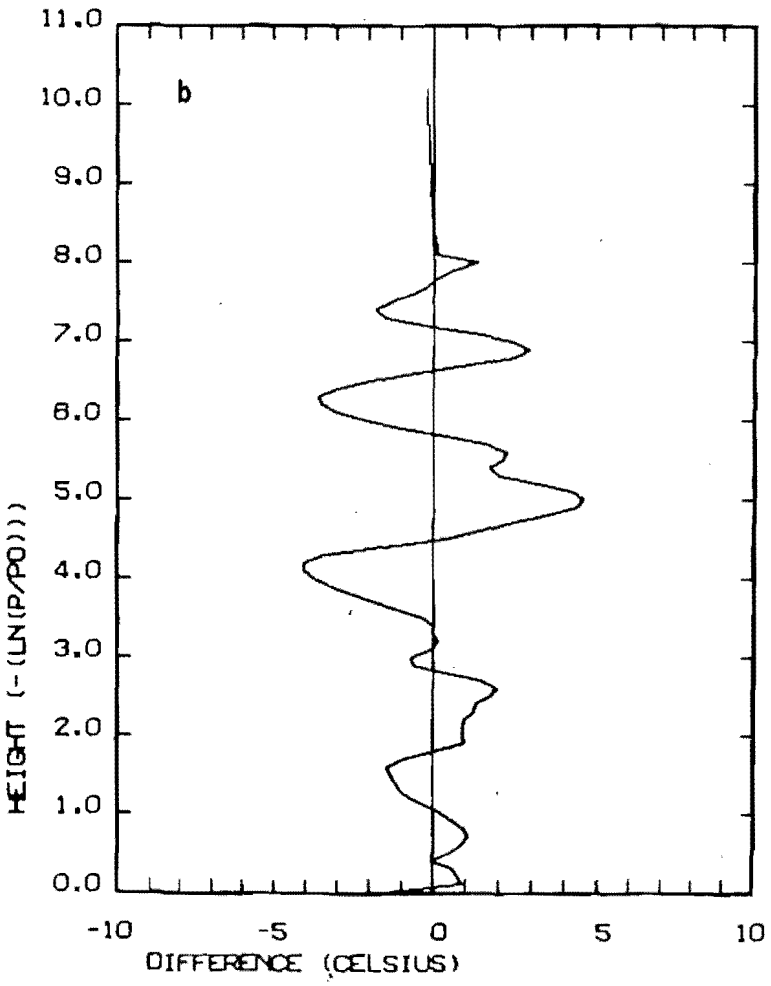
b
11.0
10.0
9.0
8.0
7.0
6.0
5.0
4.0
3.0
2.0
1.0
0.0
HEIGHT (-(LN(P/PO)))
-10
-5
0
5
10
DIFFERENCE (CELSIUS)

error is approximately $\pm 4C^0$. The error vector $(\underline{x}_p - \underline{\hat{x}}_p)$ for the perturbed (P) retrieval is figure 32. The form of the applied perturbation and its retrieved estimate are given in figure 33.

The magnitude of the retrieved perturbation at heights corresponding to the centre heights of the weighting functions (table 5) and the implied perturbation deduced from the brightness temperatures T^*, are given in table 10.

TABLE 10 : Resolution Results for Perturbation Wave with $A = 0.5C^0$, $\alpha = 0.29$, $\lambda_z = 100$ sh, $\phi = \pi/2$

Height (sh)	Perturbation Temperature T' (C^0)	T' estimate from T* values (C^0)	T' estimate from retrieval (C^0)
6.2	2.79	3.0 ± 0.2	3.5 ± 0.4
4.4	1.72	1.94±0.13	1.8 ± 0.3
3.2	1.24	1.42±0.06	0.5 ± 0.3
2.7	1.08	1.22±0.03	0.7 ± 0.2
1.7	0.81	0.78±0.06	0.3 ± 0.2
0.4	0.56	0.39±0.03	0.49±0.05

The noise values for the inversion estimates are those in figure 28, the propagated measurement noise. From the table it is evident that the brightness temperatures (satellite observations) are better able to detect the perturbation in terms of absolute magnitude and relative magnitude between heights, when compared with results from the retrieval estimator. Additionally the noise is smaller by as much as an order of magnitude.

Equation (4.8) indicates that deviations between the perturbation x_i' at height z_i, and the estimate of the perturbation $\hat{x}_i'$ are due to artefacts introduced by the retrieval estimator and the inability of the estimator to "find" completely convergent solutions (i.e. "correct" retrievals). The results of figure 33 and table 10

FIGURE 32 : Error Vector for Perturbed Retrieval, $\underline{x}_p - \hat{\underline{x}}_p$

FIGURE 33 : Results for "Evanescent" Perturbation (λ_z = 100 sh)

$\underline{x}'_p$ ------- ; retrieved perturbation $\hat{\underline{x}}'_p$ ——— .

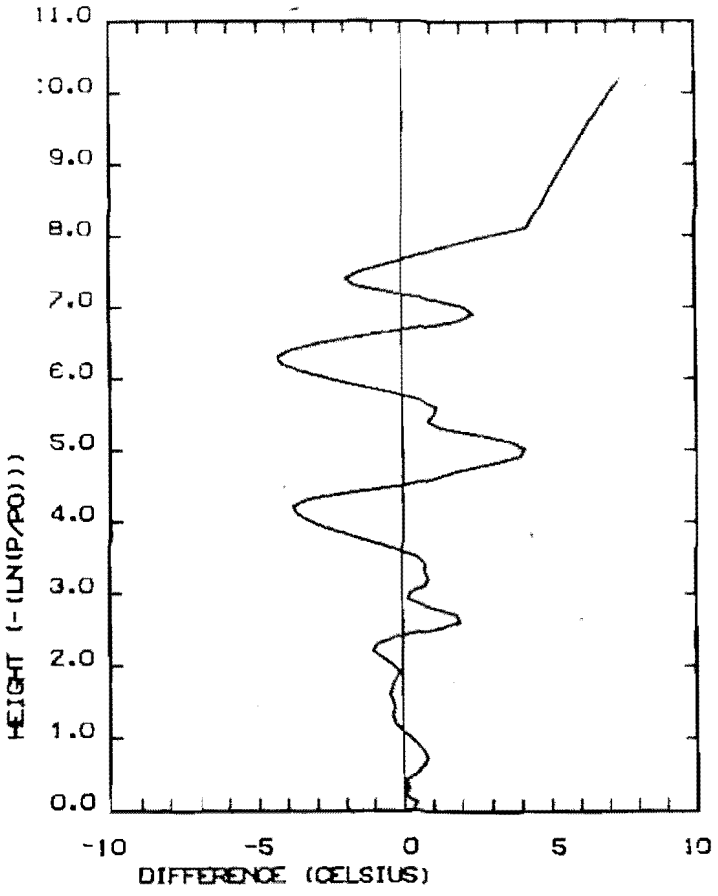
11.0
10.0
9.0
8.0
7.0
6.0
5.0
4.0
3.0
2.0
1.0
0.0
HEIGHT (-(LN(P/PO)))
-10
-5
0
5
10
DIFFERENCE (CELSIUS)

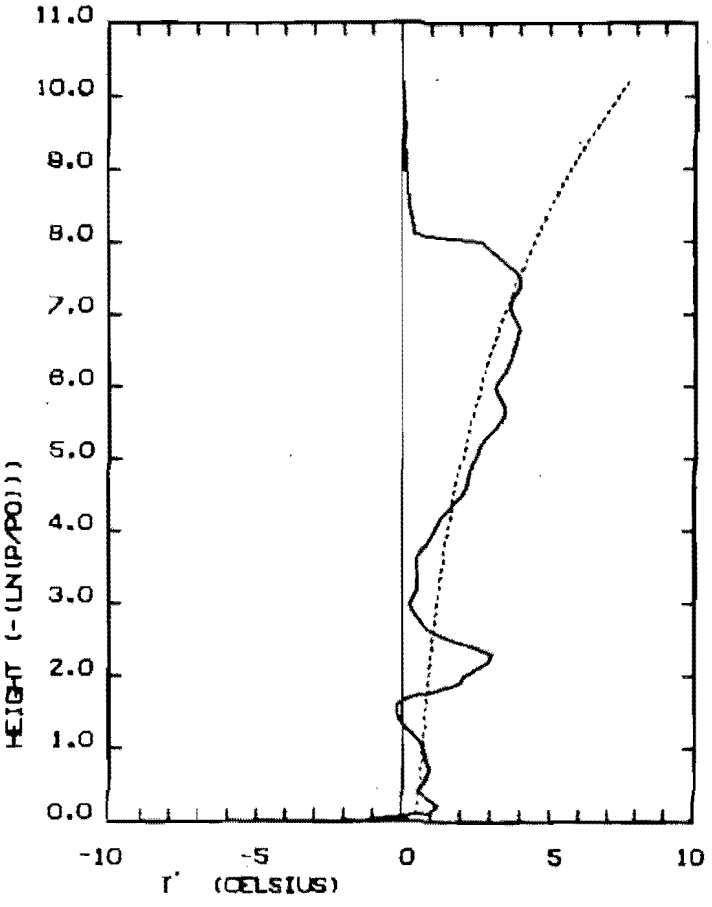
11.0
10.0
9.0
8.0
7.0
6.0
5.0
4.0
3.0
2.0
1.0
0.0
HEIGHT (-(LN(P/PO)))
-10
-5
0
5
10
T' (CELSIUS)

imply that the averaging kernel side lobes make an important contribution to the retrieved temperatures and that non convergence in the residuals at the first iteration introduces a bias into the retrieved profile. This point can be seen by superimposing the perturbation onto the relevant averaging kernels of appendix J, as suggested by equation (4.8). While the observation "averaging" kernels, that is, the satellite weighting functions, have wider main peaks than the estimator averaging kernels, they do not have side lobes. The "retrieved" temperature perturbations (from brightness temperatures) are not biased by including strong contributions from temperatures at other levels not near the centre heights of the averaging kernels.

The 6 sh Wavelength Perturbation

Results for estimates of two different λ_z = 6 sh perturbations are given in figures 34(a) and 34(b). The parameters used in the perturbation equation (4.2) were A = $2C^0$, α = 0.1, λ_z = 6 sh, ϕ = 0 and $\phi = \pi/2$. In both cases the differences between the perturbed and unperturbed radiances are rather larger than the r.m.s. measurement noise values so that an estimator using data series 5 noise values should be adequate.

When ϕ = 0 the retrieval residuals converge(essentially) in three iterations, while for the $\phi = \pi/2$ case the retrieval residuals converge to values outside the r.m.s. measurement noise values for both channels C, D and E (figure (35).

The curves in figures 34(a) and 34(b) clearly indicate that the ability of the retrieval estimator to retrieve a perturbation is very dependent upon the phase-height relationship of the perturbation. This result would be expected if a retrieval estimate at some height were dependent upon the temperature structure at other non nearby levels. This result is anticipated through equation (4.8) given the shape of the MAP estimator averaging kernels (appendix J). The averaging kernel side lobes interfere with the perturbation causing

FIGURE 34 : Retrievals of λ_z = 6 sh perturbations after 3 iterations,

(a) $\phi = 0$,

(b) $\phi = \pi/2$.

Original perturbations $\underline{x}'$ indicated by ------- .

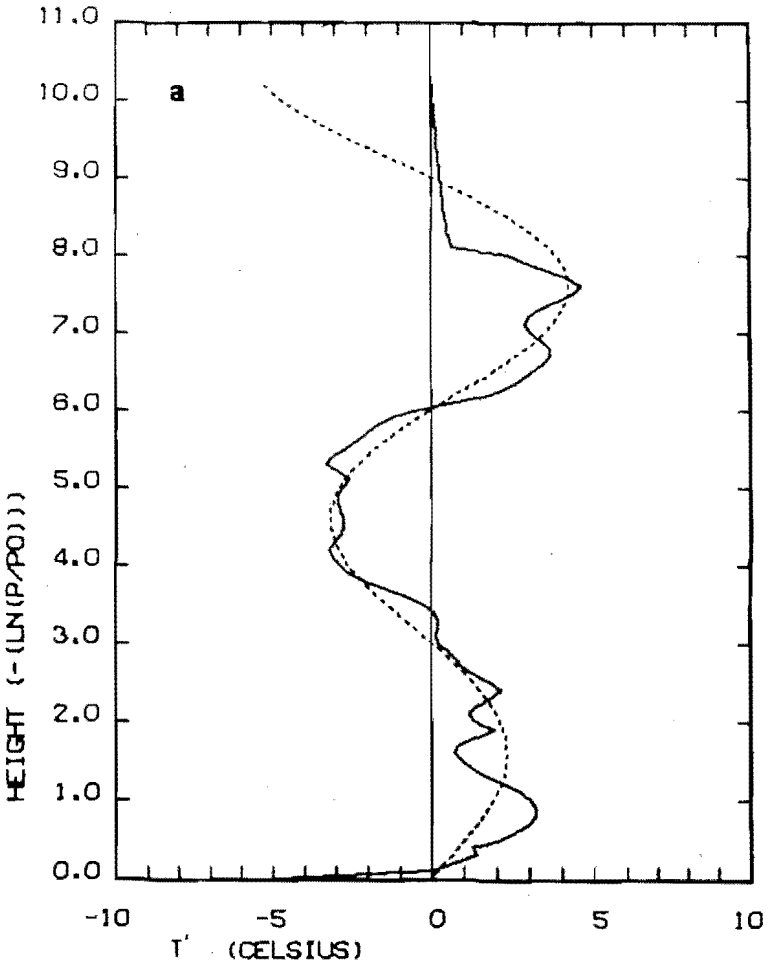
a
11.0
10.0
9.0
8.0
7.0
6.0
5.0
4.0
3.0
2.0
1.0
0.0
HEIGHT (-(LN(P/PO)))
-10
-5
0
5
10
T' (CELSIUS)

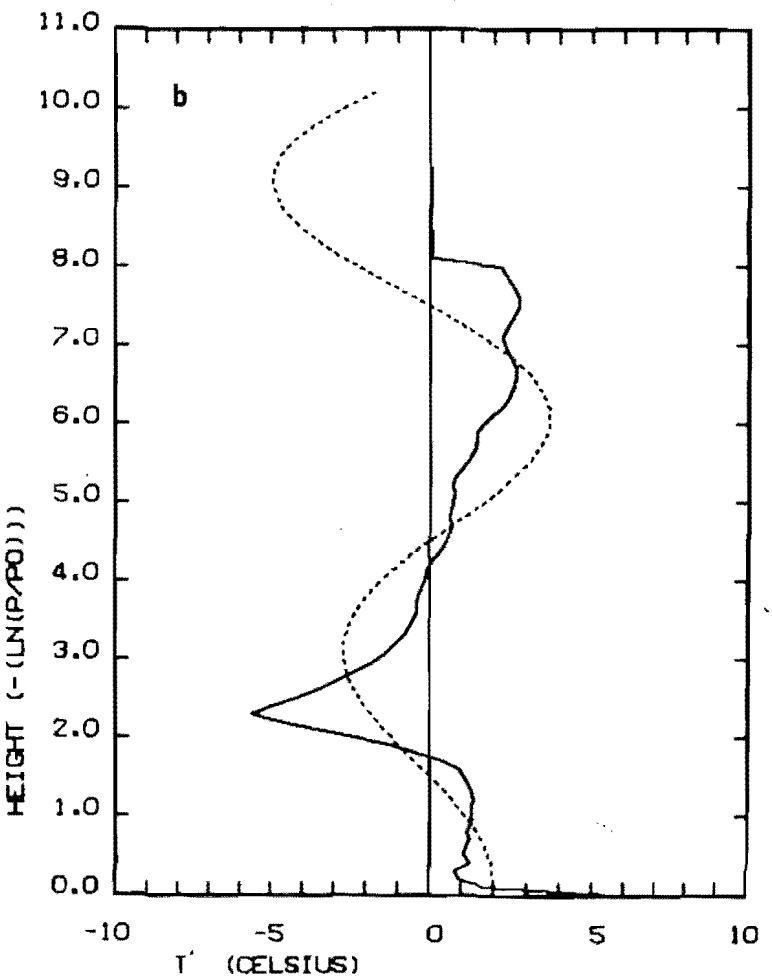
b
11.0
10.0
9.0
8.0
7.0
6.0
5.0
4.0
3.0
2.0
1.0
0.0
HEIGHT (-(LN(P/PO)))
-10
-5
0
5
10
T' (CELSIUS)

FIGURE 35 : Residuals for perturbed retrievals with λ_z = 6 sh :

——— $\phi = 0$,

------ $\phi = \pi/2$

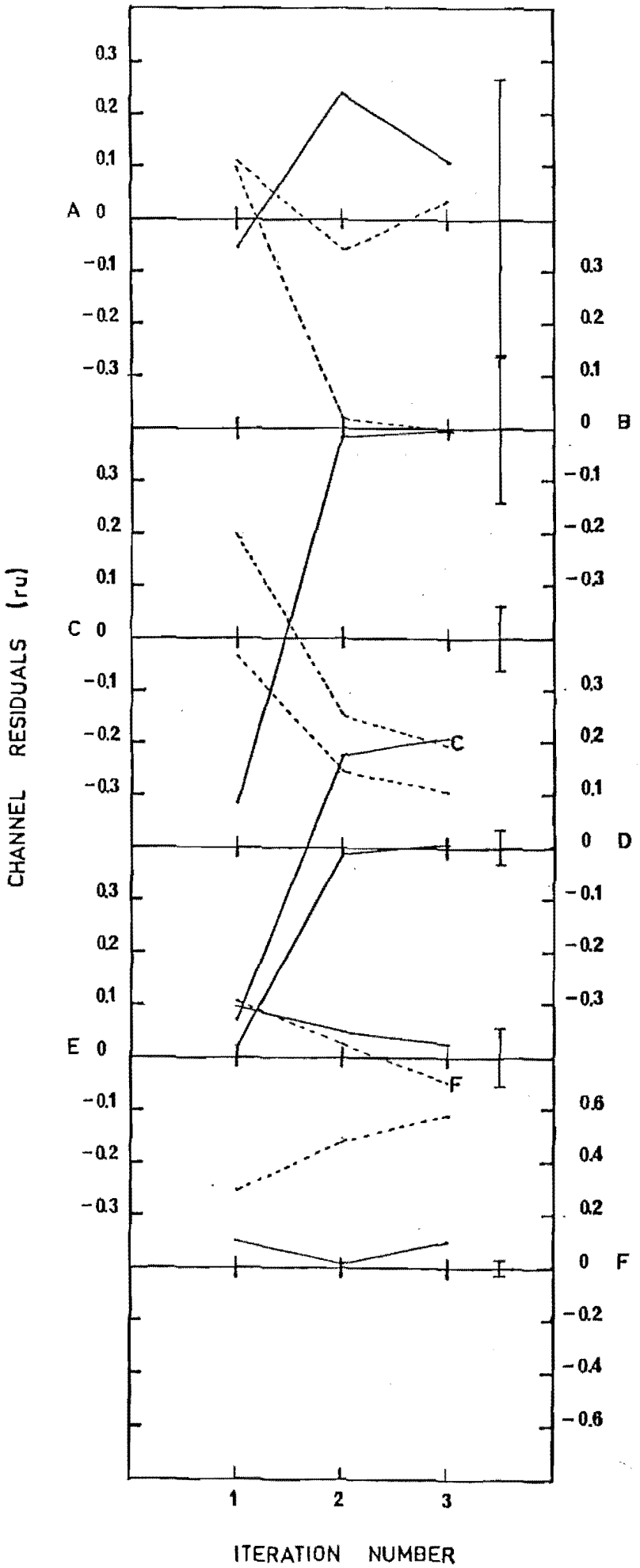
CHANNEL RESIDUALS (ru)
A
B
C
D
E
F
0.3
0.2
0.1
0
-0.1
-0.2
-0.3
0.6
0.4
-0.4
-0.6
1
2
3
ITERATION NUMBER

amplification or attenuation of the true perturbation in the retrieved profile.

The 4 sh Wavelength Perturbation

Two differing perturbations were applied to the simulation temperature profile. The corresponding parameters for equation (4.2) were A = $2C^0$, α = 0.1, λ_z = 4 sh, ϕ = 0 and ϕ = $\pi/2$. The resulting perturbation retrievals are given in figures 36(a) and 36(b); the residuals are figure 37.

The retrieved solution residuals are approximately convergent when ϕ = $\pi/2$ but do not converge to values within the r.m.s. measurement noise regions for channels C and D when ϕ = 0.

Comparing the results in figures 36(a) and 36(b), it is evident that the perturbation is not well retrieved, the faithfulness of the retrieved perturbation being sensitive to the phase height relationship of the true perturbation. Careful comparison of the results in figures 36(a) and 36(b) shows that at heights greater than approximately 3.5 sh, the phase height relationships of both retrieved perturbations are nearly identical, even though the true perturbations are shifted relative to each other by 1 sh (7.5 km). The estimator averaging kernel side lobes are important in determining the phase height relationship and magnitude of the retrieved perturbation.

Estimates of the perturbation magnitude may be obtained from the brightness temperatures. Tables 11 and 12 below, list the results.

The magnitudes of the temperature perturbations at the weighting function centre heights are rather less than the true values, however these estimates are better able to consistently detect the relative magnitudes of the perturbations between different heights. This is particularly evident in the results of table 12. The brightness temperature results are not particularly dependent upon the phase of the perturbation for a perturbation with λ_z = 4 sh. The

FIGURE 36 : Retrievals of λ_z = 4 sh perturbations after 5 iterations,

(a) $\phi = 0$
(b) $\phi = \pi/2$

Original perturbations $\underline{x}'$ ------ .

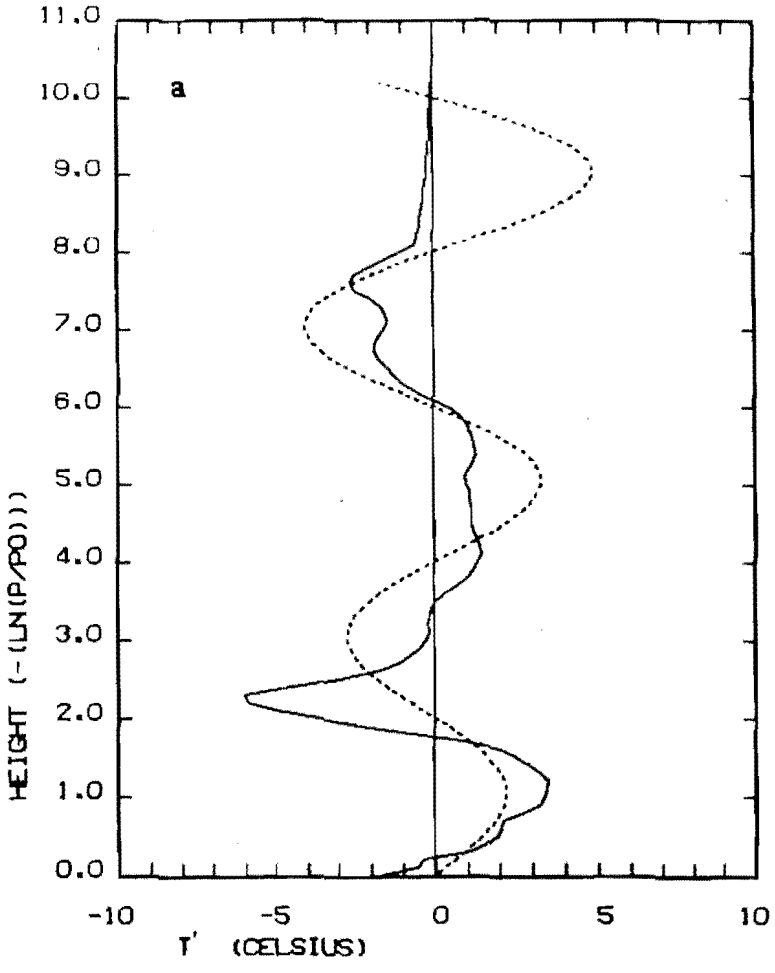
a
11.0
10.0
9.0
8.0
7.0
6.0
5.0
4.0
3.0
2.0
1.0
0.0
HEIGHT (-(LN(P/PO)))
-10
-5
0
5
10
T' (CELSIUS)

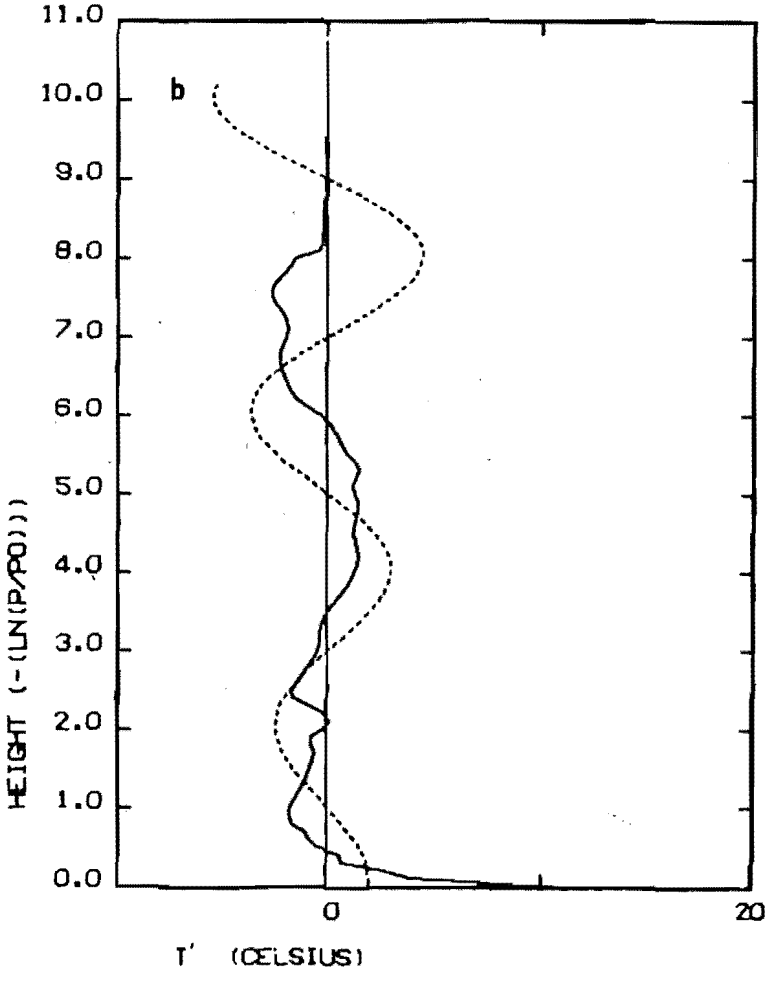
b
11.0
10.0
9.0
8.0
7.0
6.0
5.0
4.0
3.0
2.0
1.0
0.0
HEIGHT (-(LN(P/PO)))
0
20
T' (CELSIUS)

FIGURE 37 : Residuals for perturbed retrievals with λ_z = 4 sh :

——— $\phi = 0$

------- $\phi = \pi/2$

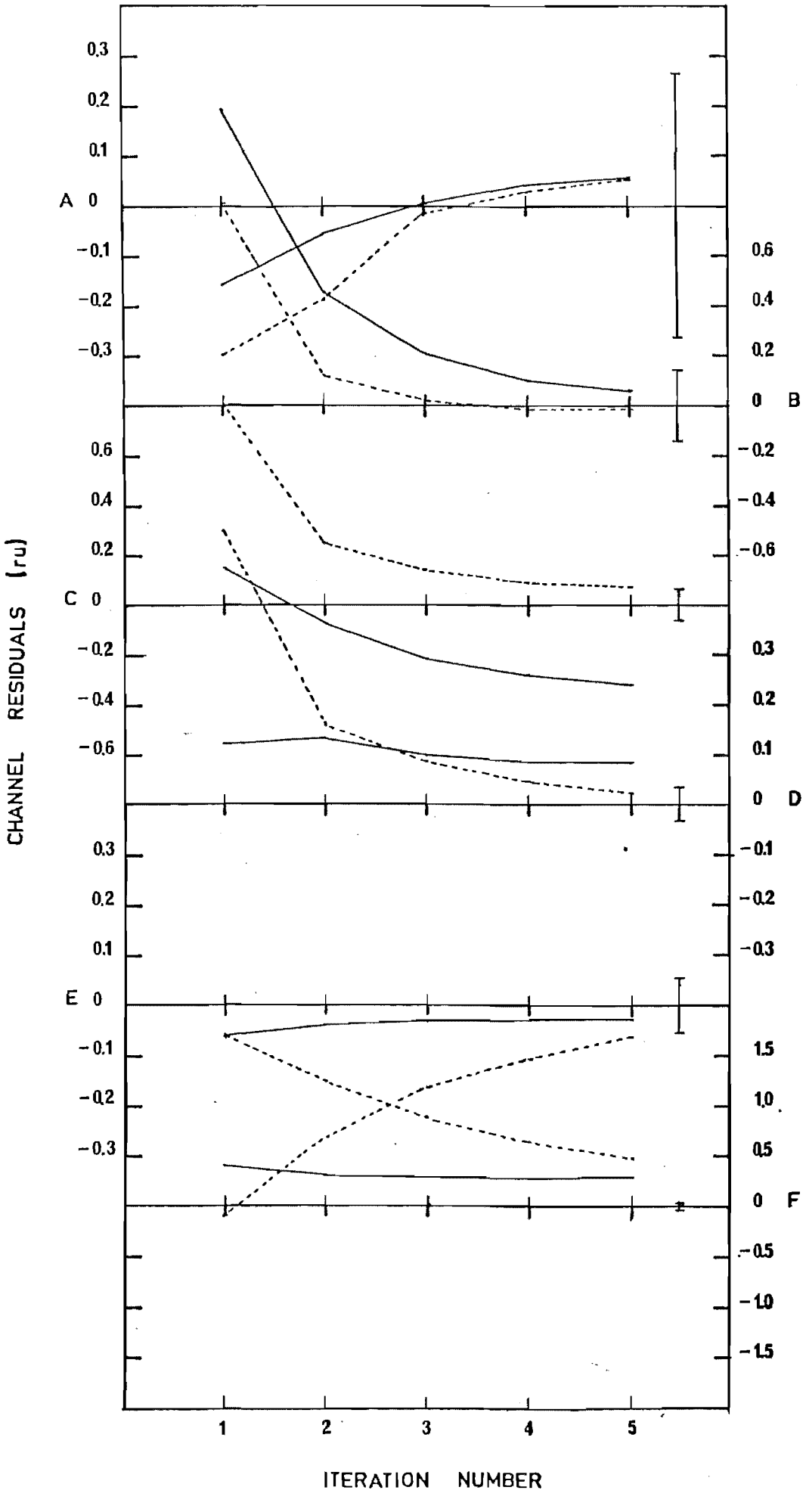
CHANNEL RESIDUALS (ru)
A
B
C
D
E
F
0.3
0.2
0.1
0
-0.1
-0.2
-0.3
0.6
0.4
0.2
0
-0.2
-0.4
-0.6
1.5
1.0
0.5
-0.5
-1.0
-1.5
1
2
3
4
5
ITERATION NUMBER

TABLE 11 : Resolution Results for Perturbation Wave with $A = 2C^0$, $\alpha = 0.1$, $\lambda_z = 4$ sh, $\phi = 0$

Height (sh)	Perturbation Temperature T' (C^0)	T' estimate from T* values (C^0)	T' estimate from retrieval (C^0)
6.2	-1.15	-0.3 ±0.2	-0.6 ± 0.3
4.4	1.83	0.52±0.14	1.2 ± 0.3
3.2	-2.62	-0.53±0.06	-0.2 ± 0.3
2.7	-2.33	-0.85±0.03	-1.1 ± 0.3
1.7	1.08	0.58±0.06	0.9 ± 0.2
0.4	1.22	0.84±0.03	1.60 ± 0.05

TABLE 12 : Resolution Results for Perturbation Wave with $A = 2C$, $\alpha = 0.1$, $\lambda_z = 4$ sh, $\phi = \pi/2$

Height (sh)	Perturbation Temperature T' (C^0)	T' estimate from T* values (C^0)	T' estimate from retrieval (C^0)
6.2	-3.54	-0.6 ±0.2	-1.4 ± 0.3
4.4	2.51	0.41±0.14	1.3 ± 0.3
3.2	0.85	0.26±0.06	-0.4 ± 0.3
2.7	-1.19	-0.36±0.03	-1.2 ± 0.2
1.7	-2.11	-0.67±0.06	-0.7 ± 0.2
0.4	1.54	1.25±0.03	0.61 ± 0.05

degree of attenuation in the brightness temperature results is of course different for each channel since the spread characteristics for each channel are different, ranging from 1.27 sh for channel E to 2.05 sh for channel A (see table 6). The random noise in the perturbation estimates are smaller for the brightness temperature derived results at channel C, D, E and F heights. This may not be so at channel A and B heights. Further smoothing of the data would directly decrease the noise in the brightness temperature derived perturbation estimates. The noise in the retrieval estimates would not be

reduced by the same factor owing to the increasing propagation noise magnifications with decreasing measurement noise.

From tables 11 and 12, and figure 36 it is evident that the resolving power of the MAP estimator is rather dependent upon the side lobe structure of the averaging kernels since, for a wave like perturbation there is a correlation between perturbation temperatures at different levels.

In the sense that the relative magnitude of the perturbation at different heights should be retrievable it is evident from the above results that the resolution of the satellite observations is better than that of the retrieval estimator, since

(a) the random noise in the T* estimate is generally smaller, and

(b) the T* estimates of the magnitude of the perturbations are essentially independent of the phase-height relationship of the perturbation since the satellite kernels do not have side lobes.

Similar calculations were performed for perturbation waves of the form of equation (4.2) having parameters $A = 0.5C^0$, $\alpha = 0.29$, $\lambda_z = 4$ sh, $\phi = 0$ and $\phi = \pi/2$. Again it was found that the brightness temperatures were better able to detect the presence of the perturbation and specify its relative magnitude with height. The MAP estimates of the perturbation were unable to detect the change of phase between the two perturbations at heights above 3 sh altitude (channel C).

The 3 sh Wavelength Perturbation

Finally calculations were performed for a perturbation (equation 4.2)) with parameters $A = 2C^0$, $\alpha = 0.1$, $\lambda_z = 3$ sh, $\phi = 0$ and $\phi = \pi/2$. It was found that neither the brightness temperatures nor the retrieval estimate of the perturbation could detect adequately, independent of the initial phase, the presence of this wave above

FIGURE 38 : Retrievals of λ_z = 3 sh perturbations after 3 iterations,

(a) $\phi = 0$

(b) $\phi = \pi/2$

Original perturbations $\underline{x}'$ -------.

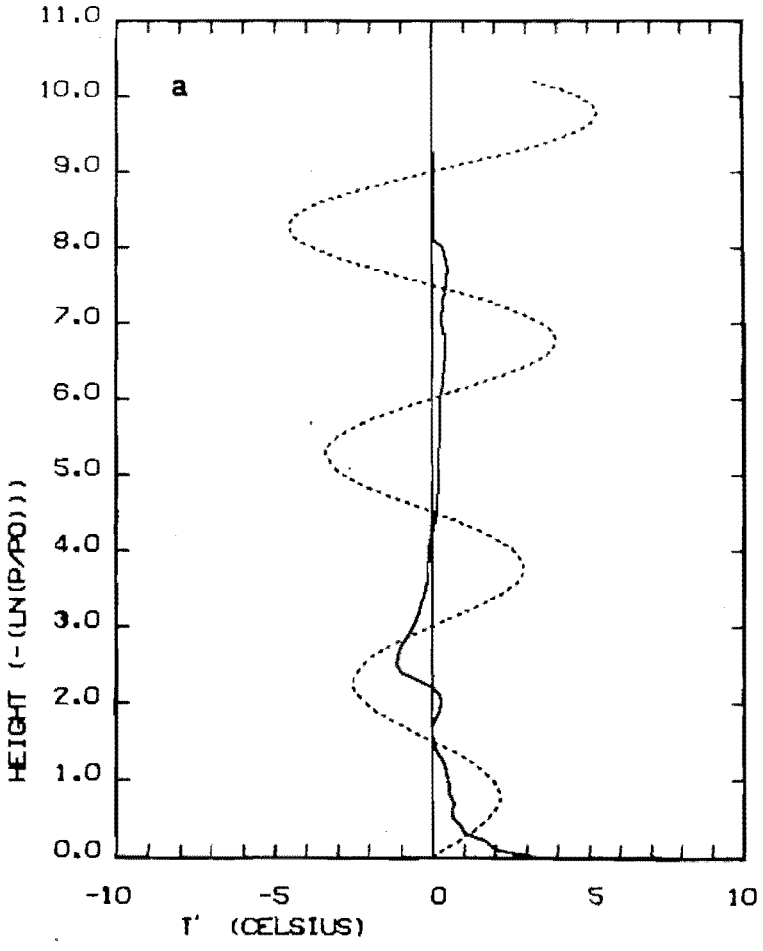
a
11.0
10.0
9.0
8.0
7.0
6.0
5.0
4.0
3.0
2.0
1.0
0.0
HEIGHT (-(LN(P/PO)))
-10
-5
0
5
10
T' (CELSIUS)

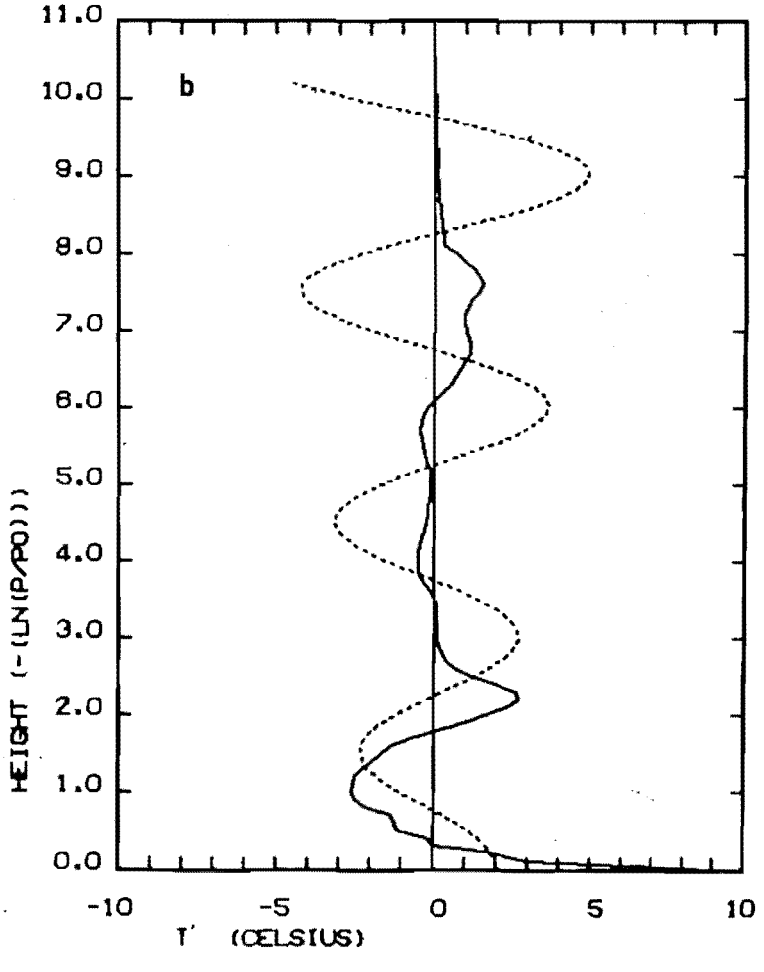
b
11.0
10.0
9.0
8.0
7.0
6.0
5.0
4.0
3.0
2.0
1.0
0.0
HEIGHT (-(LN(P/PO)))
-10
-5
0
5
10
T' (CELSIUS)

3 sh altitude. The MAP estimator retrievals are given in figures 38(a) and 38(b).

4.1.4.2 An High-Latitudes Retrieval

Similar calculations to those above are presented here for the Ft. Churchill (4/1/70, 1803 GMT) simulated temperature profile retrieval.

The first guess profile $\underline{\bar{x}}$ and the unperturbed profile to be retrieved $\underline{x}$ are illustrated in figure 39(a). The difference vector $(\underline{x} - \underline{\bar{x}})$ is figure 39(b). The extrapolation at heights above 8.0 sh is probably not appropriate, however this is not important in the retrieval problem (Nimbus 4 SCR data) since the maximum height for which a realistic retrieval can be made is approximately 6.5 sh altitude (≃50 km). The first guess profile and the unknown profile to be retrieved need only be similar at altitudes above 8 sh since the weighting for channel A at these heights is small.

In any retrieval the maximum number of iterations allowed is five, since in practice it is found that if the retrieval residuals do not converge in five iterations they have in general converged to values which lie outside the residual criteria of equation (4.1). Unless stated otherwise estimator measurement noise levels as for data series 5 will be assumed.

The residual characteristics for the retrieval of the unperturbed profile are given in figure 40. Channel D does not converge, the channel B residual would converge in six iterations. The retrieved profile (after 5 iterations) is given in figure 41(a). The error vector $(\underline{x} - \underline{\hat{x}})$ is figure 41(b).

The Evanescent Wave Retrieval

As with the equatorial summer case a wave perturbation (equation (4.2)) with $A = 0.5C^0$, $\alpha = 0.29$, $\lambda_z = 100$ sh and $\phi = \pi/2$ was applied to the given profile $\underline{x}$ and a retrieval performed.

The residual characteristics for this retrieval are given in

FIGURE 39 : High Latitudes winter simulation profiles :

(a) ——— profile to be retrieved, $\underline{x}$

------ first guess profile, $\underline{\bar{x}}$

(b) difference vector $(\underline{x} - \underline{\bar{x}})$

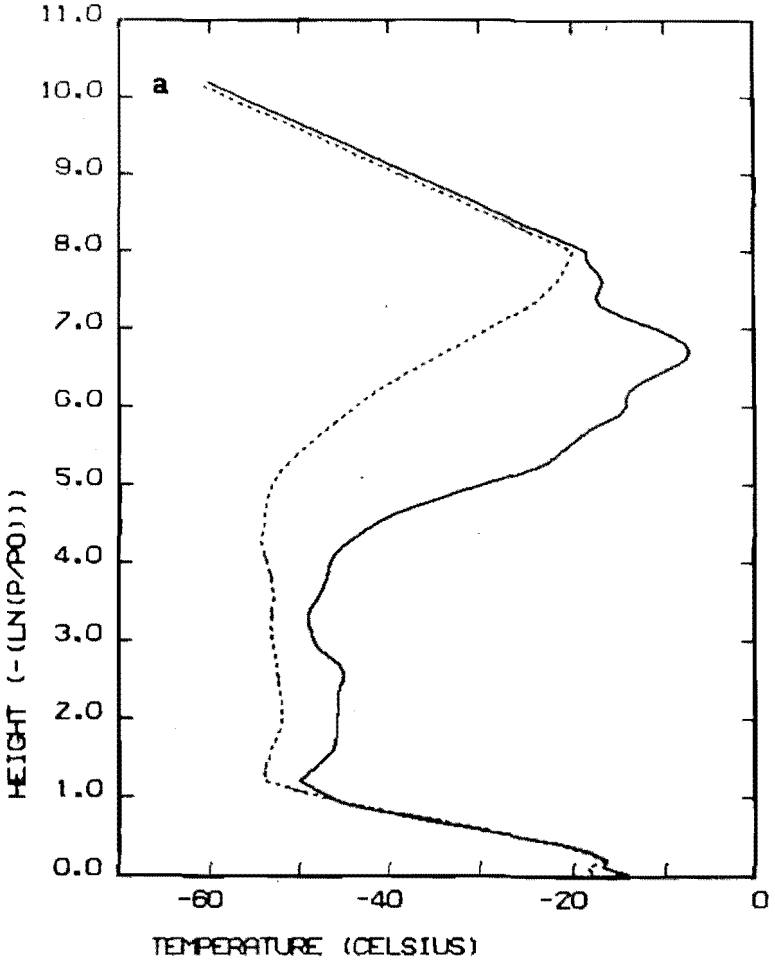
a
11.0
10.0
9.0
8.0
7.0
6.0
5.0
4.0
3.0
2.0
1.0
0.0
HEIGHT (-(LN(P/PO)))
-60
-40
-20
0
TEMPERATURE (CELSIUS)

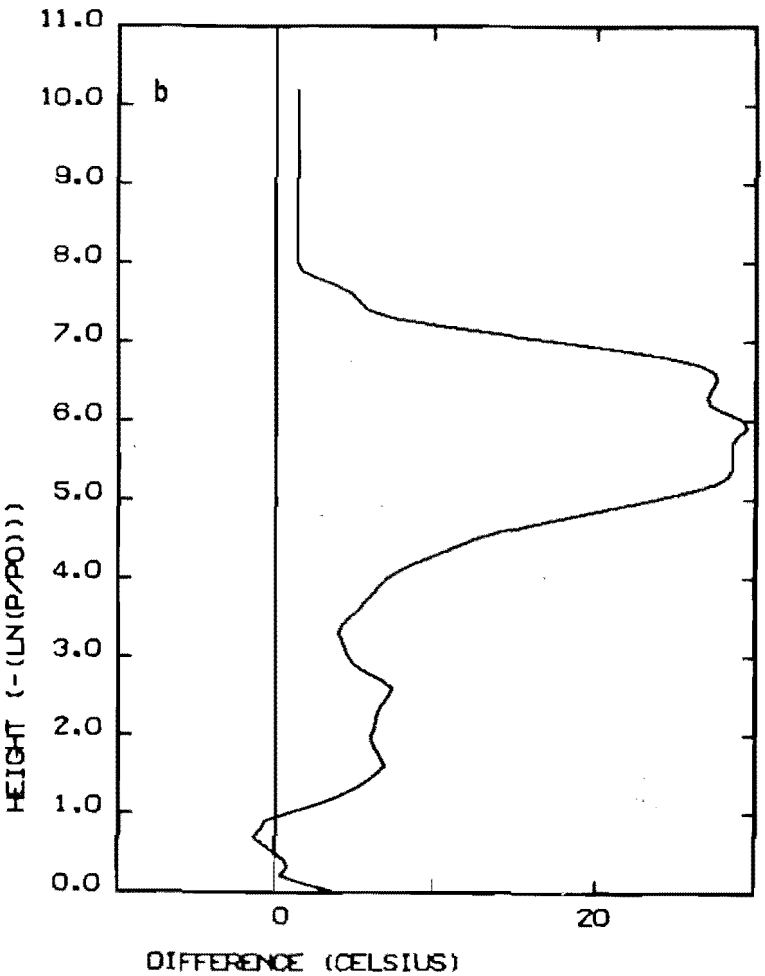
b
11.0
10.0
9.0
8.0
7.0
6.0
5.0
4.0
3.0
2.0
1.0
0.0
HEIGHT (-(LN(P/PO)))
0
20
DIFFERENCE (CELSIUS)

FIGURE 40 : Residuals for unperturbed retrieval ——— .
The size of assumed measurement error in each channel is given on the right hand side of the diagrams.

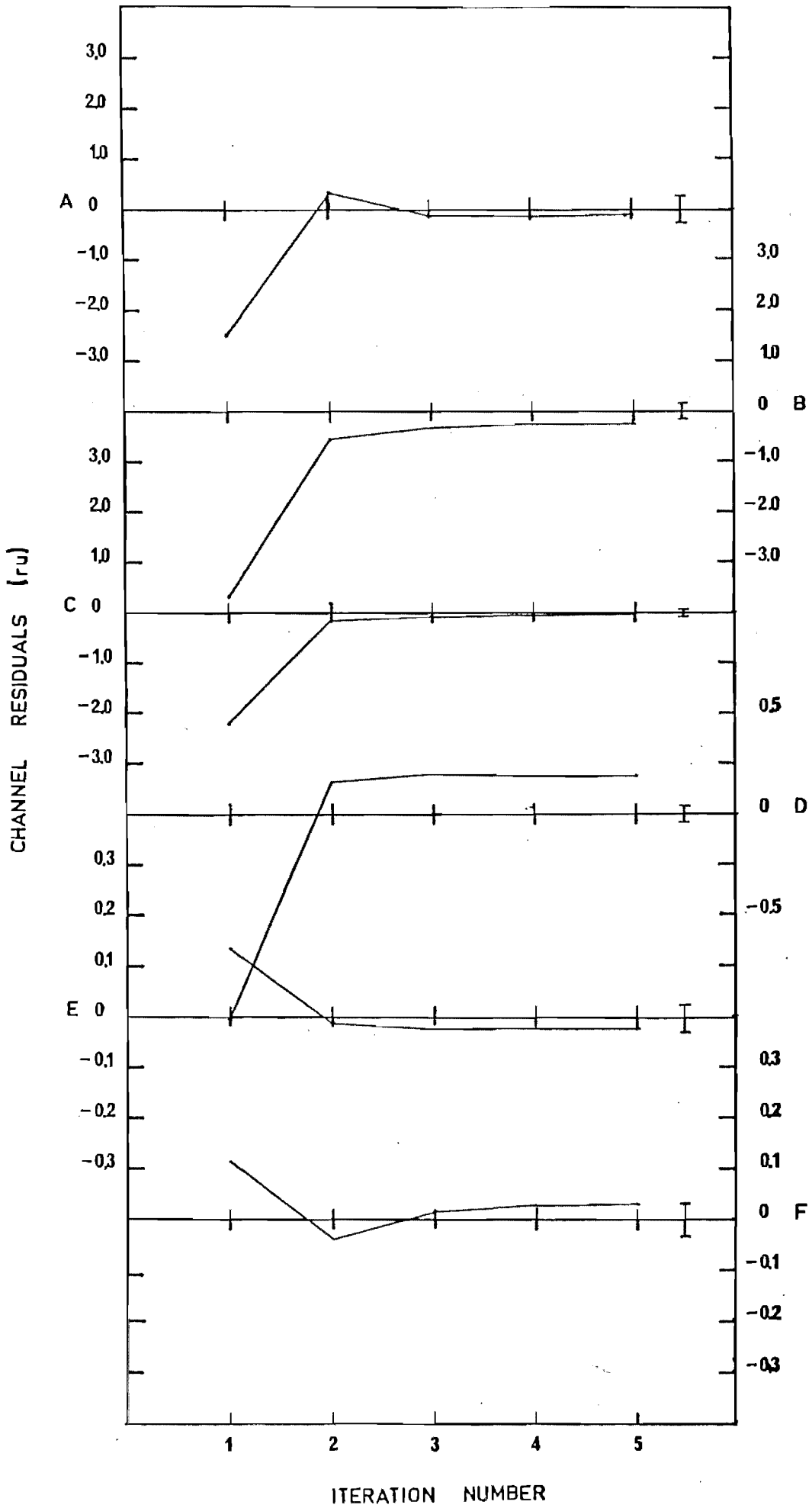
CHANNEL RESIDUALS (ru)
A
B
C
D
E
F
3,0
2,0
1,0
0
-1,0
-2,0
-3,0
0,5
-0,5
0,3
0,2
0,1
-0,1
-0,2
-0,3
1
2
3
4
5
ITERATION NUMBER

FIGURE 41 : Retrieval of unperturbed profile at 5 iterations :

(a) the retrieved profile $\underline{\hat{x}}$ - - - - - - , and
the true profile $\underline{x}$ ——— ;

(b) the error vector $\underline{x} - \underline{\hat{x}}$

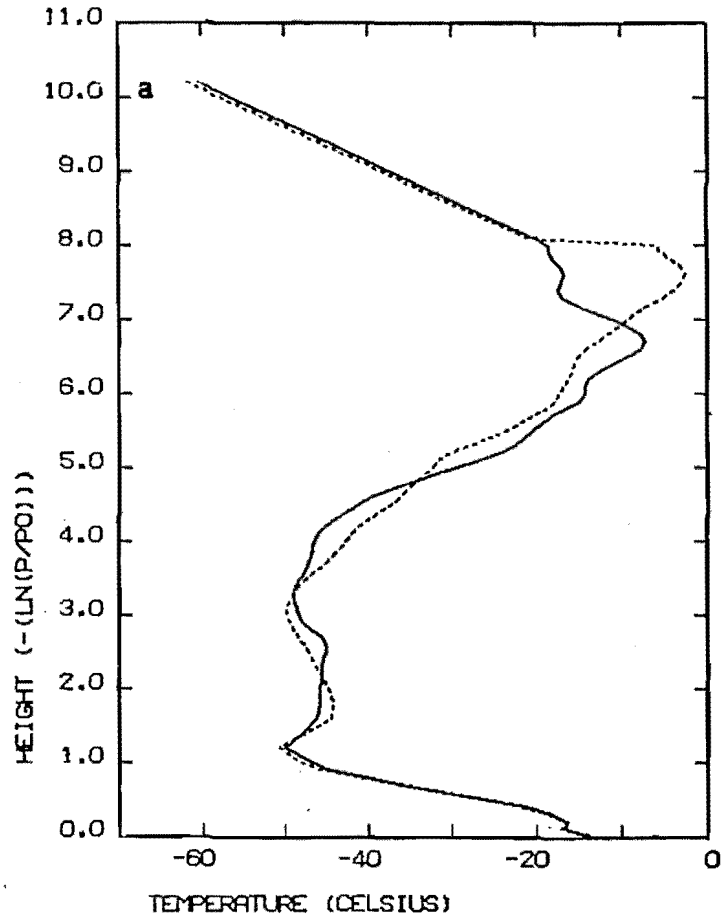
a
11.0
10.0
9.0
8.0
7.0
6.0
5.0
4.0
3.0
2.0
1.0
0.0
HEIGHT (-(LN(P/PO)))
-60
-40
-20
0
TEMPERATURE (CELSIUS)

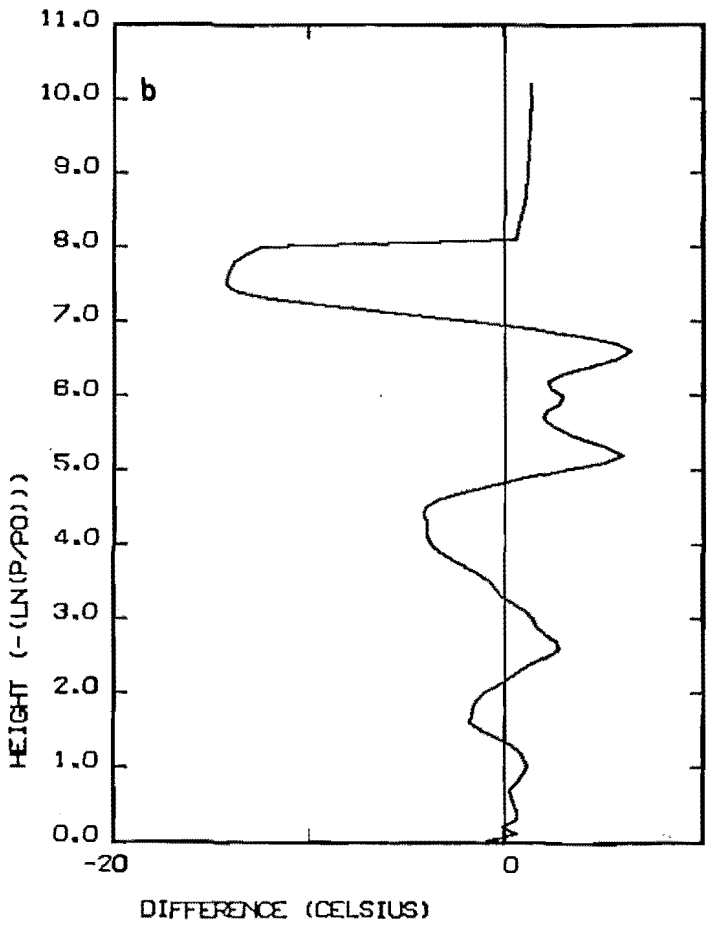
b
11.0
10.0
9.0
8.0
7.0
6.0
5.0
4.0
3.0
2.0
1.0
0.0
HEIGHT (-(LN(P/PO)))
-20
0
DIFFERENCE (CELSIUS)

figure 42. The retreived profile residuals on iterating do not converge to give a "correct" retrieval. Only radiances for channel A are convergent, while radiances for channels B, C, D and E converge to values outside those regions defined by equation (4.1).

The perturbation retrieval is given in figure 43. It is evident that the strong side lobe structure in the estimator averaging kernels and the non convergence of the retrieval residuals are responsible for generating artefacts in the retrieved perturbation. A comparison of the values for the perturbation at the satellite centre heights, deduced from both the brightness temperatures and the MAP retrieval, are given in table 13.

TABLE 13 : Resolution Results for Perturbation Wave with $A = 0.5C$, $\alpha = 0.29$, $\lambda_z = 100$ sh, $\phi = \pi/2$

Height (sh)	Perturbation Temperature T' (C^0)	T' estimate from T* values (C^0)	T' estimate from retrieval (C^0)
6.2	2.79	3.0 ± 0.2	2.8±0.5
4.4	1.72	1.92 ± 0.14	2.5±0.4
3.2	1.24	1.40 ± 0.06	-0.2±0.3
2.7	1.08	1.21 ± 0.03	0.6±0.3
1.7	0.81	0.85 ± 0.06	1.7±0.3
0.4	0.56	0.64 ± 0.03	0.2±0.4

At heights for which the MAP estimator has best intrinsic resolution the retrieval does not well represent the true perturbation, while the brightness temperatures as would be expected in this situation "retrieve" the form of the perturbation well.

The 4 sh Wavelength Perturbation

Perturbations (equation (4.2)) with parameters $A = 2C^0$, $\alpha = 0.1$, $\lambda_z = 4$ sh, $\phi = 0$ and $\phi = \pi/2$ were added to the Ft. Churchill profile and retrievals performed. The residual characteristics are

FIGURE 42 : Residuals for perturbed (λ_z = 100 sh) retrieval ———— . The size of the assumed measurement error in each channel is given on the right hand side of the diagrams.

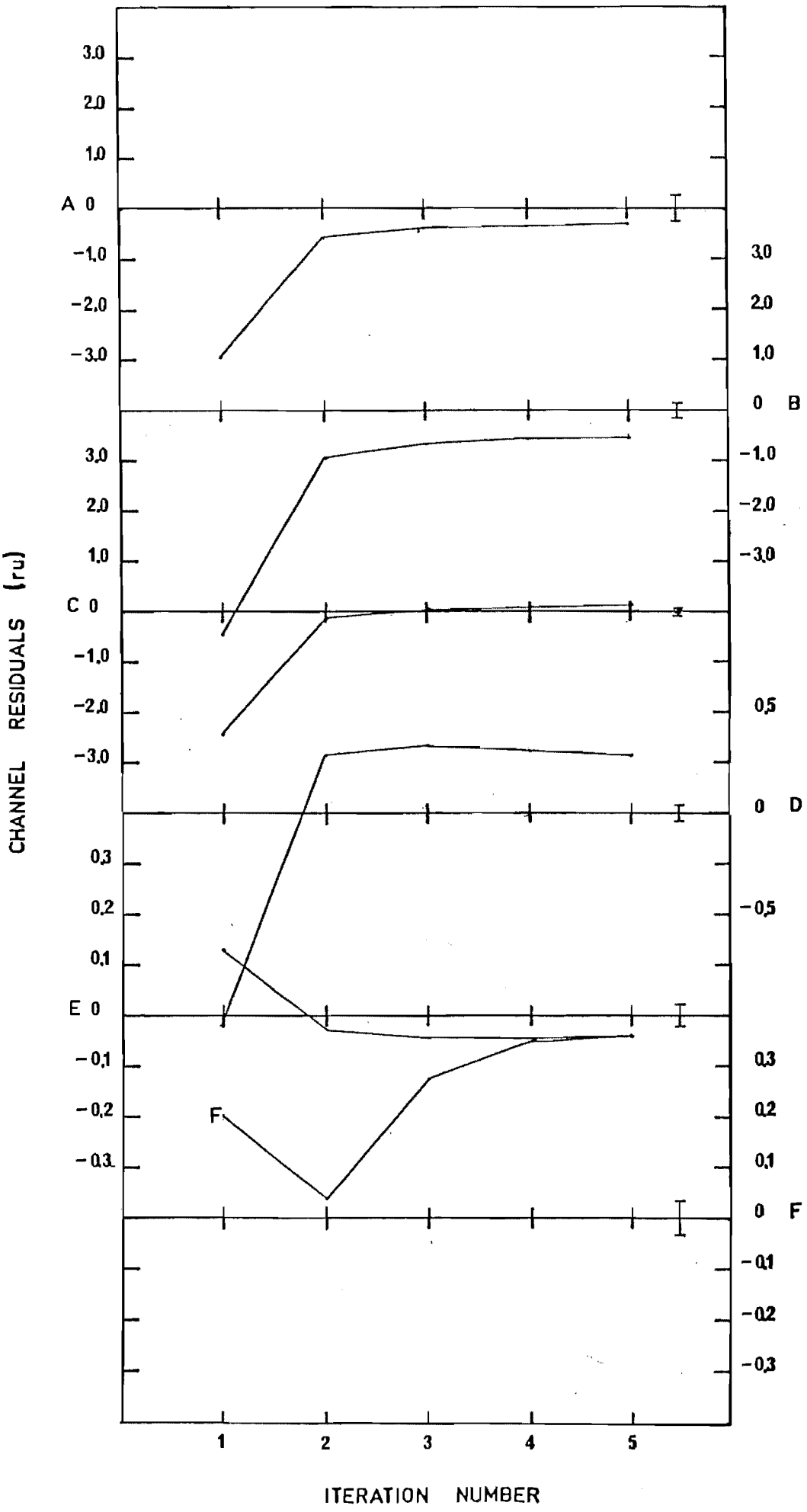
CHANNEL RESIDUALS (ru)
A
B
C
D
E
F
3.0
2.0
1.0
0
-1.0
-2.0
-3.0
0.5
-0.5
0.3
0.2
0.1
-0.1
-0.2
-0.3
1
2
3
4
5
ITERATION NUMBER

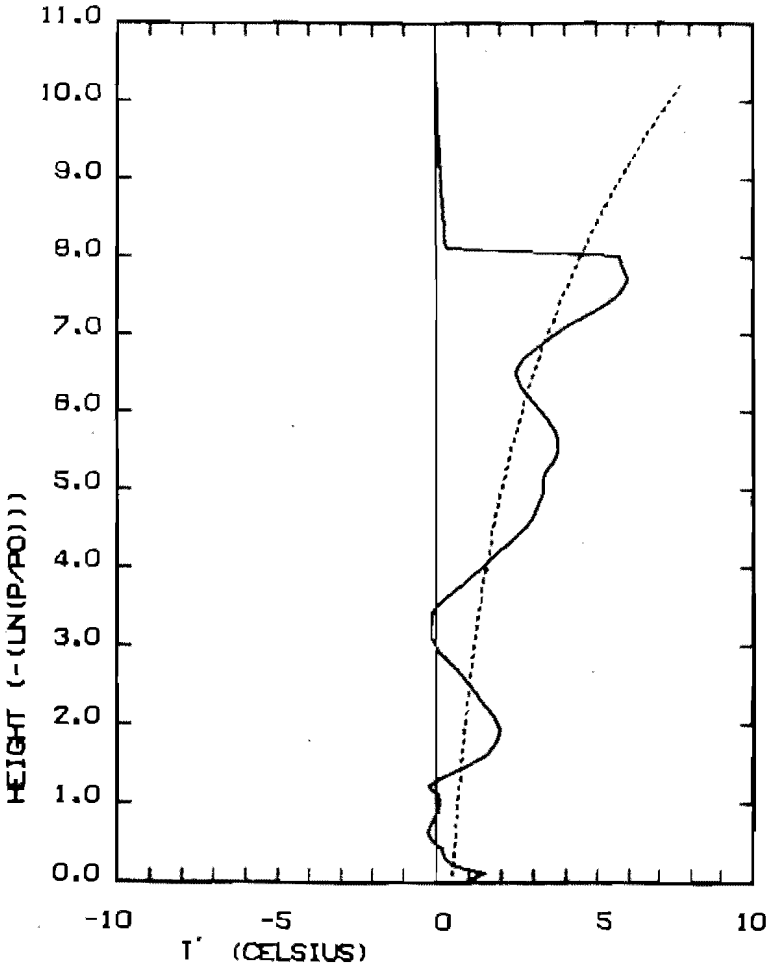

FIGURE 43 : Results for "Evanescent" Perturbation (λ_z=100sh), $\underline{x}'$------- ; Retrieved Perturbation $\underline{\hat{x}}'$ ——— .

given in figure 44. In neither case does complete convergence occur. In particular, when $\phi = 0$ the retrieval residuals converge to values which lie outside the residual criterion (equation (4.1)) for channels A, B, C, D and E. In a practical sense it can be said that convergence occurs for the $\phi = \pi/2$ perturbation retrieval.

The perturbation retrievals are given in figures 45(a) and 45 (b). When $\phi = 0$ the perturbation retrieval is particularly bad, whilst when $\phi = \pi/2$ the wave is well retrieved to heights near 3.5 sh. In the latter case ($\phi = \pi/2$) it would seem that at heights above 5.5 sh altitude the estimator describes the temperature at lower levels, as expected from the centre height curves of figure 28.

Using measurement noise values as for data series 2, results in convergence in three iterations for the $\phi = 0$ perturbation. The resulting perturbation retrieval is given in figure 46. Comparison of figure 46 with figure 45(a) indicates the perturbation is retrieved marginally better by the high noise estimator, as anticipated from figure 27. Tables 14 and 15 give the magnitudes of the perturbations at the weighting function centre heights as deduced from the brightness temperatures and the retrievals. Results for retrievals with estimators using data series 2 and data series 5 noise values are given.

TABLE 14 : Resolution Results for Perturbation Wave with $A = 2C^0$, $\alpha = 0.1$, $\lambda_z = 4$ sh, $\phi = 0$

Height (sh)	Perturbation Temperature T' (C^0)	T' estimate From T* values (C^0)	T' estimate from retrieval (C^0)	
			Data Series 2	Data Series 5
6.2	-1.15	-0.3 ± 0.2	2.0±1.4	3.7±0.5
4.4	1.83	0.44 ± 0.14	-0.8±0.9	-2.2±0.4
3.2	-2.62	-0.64 ± 0.06	0.4±0.4	2.1±0.3
2.7	-2.33	-0.93 ± 0.03	-1.5±0.4	-0.3±0.3
1.7	1.08	0.40 ± 0.06	-0.4±0.5	-1.2±0.3
0.4	1.22	0.85 ± 0.03	3.4±0.3	3.0±0.3

FIGURE 44 : Residuals for perturbed (λ_z = 4 sh) retrieval :

——— $\phi = 0$, ------ $\phi = \pi/2$

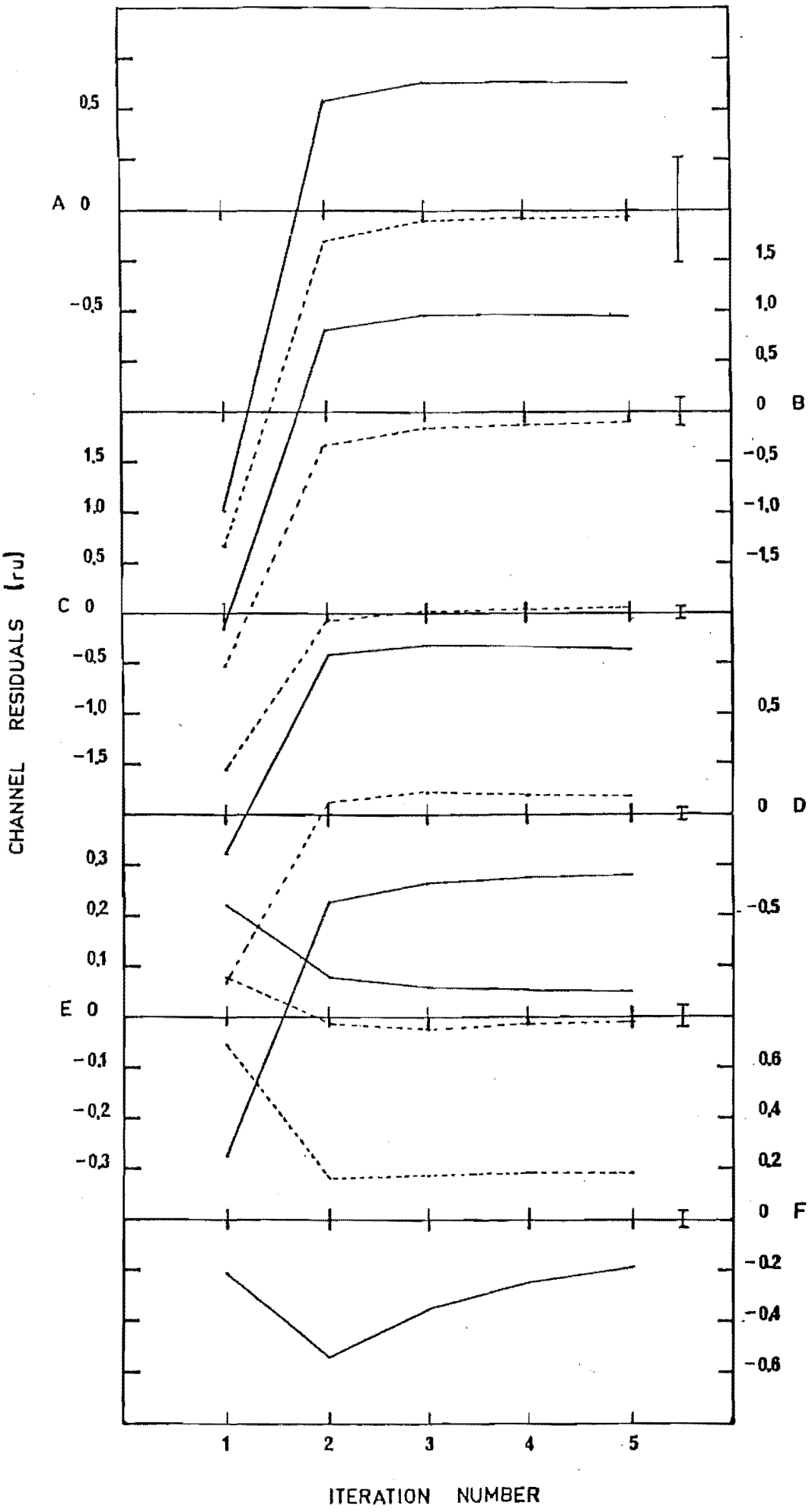
CHANNEL RESIDUALS (ru)
A
B
C
D
E
F
0.5
0
-0.5
1.5
1.0
0.5
0
-0.5
-1.0
-1.5
0.3
0.2
0.1
-0.1
-0.2
-0.3
0.6
0.4
0.2
-0.4
-0.6
1
2
3
4
5
ITERATION NUMBER

FIGURE 45 : Retrievals of $\lambda_z = 4$ sh perturbations after 5 iterations,

(a) $\phi = 0$

(b) $\phi = \pi/2$

Original perturbations $\underline{x}'$ ------- .

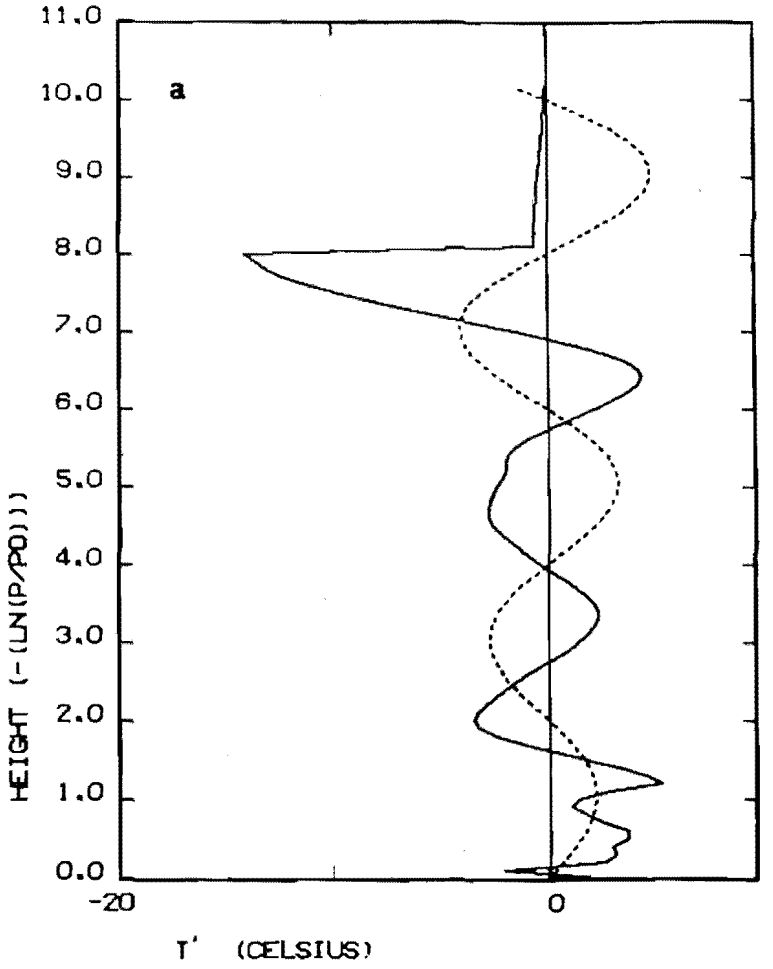
a
11.0
10.0
9.0
8.0
7.0
6.0
5.0
4.0
3.0
2.0
1.0
0.0
HEIGHT (-(LN(P/PO)))
-20
0
T' (CELSIUS)

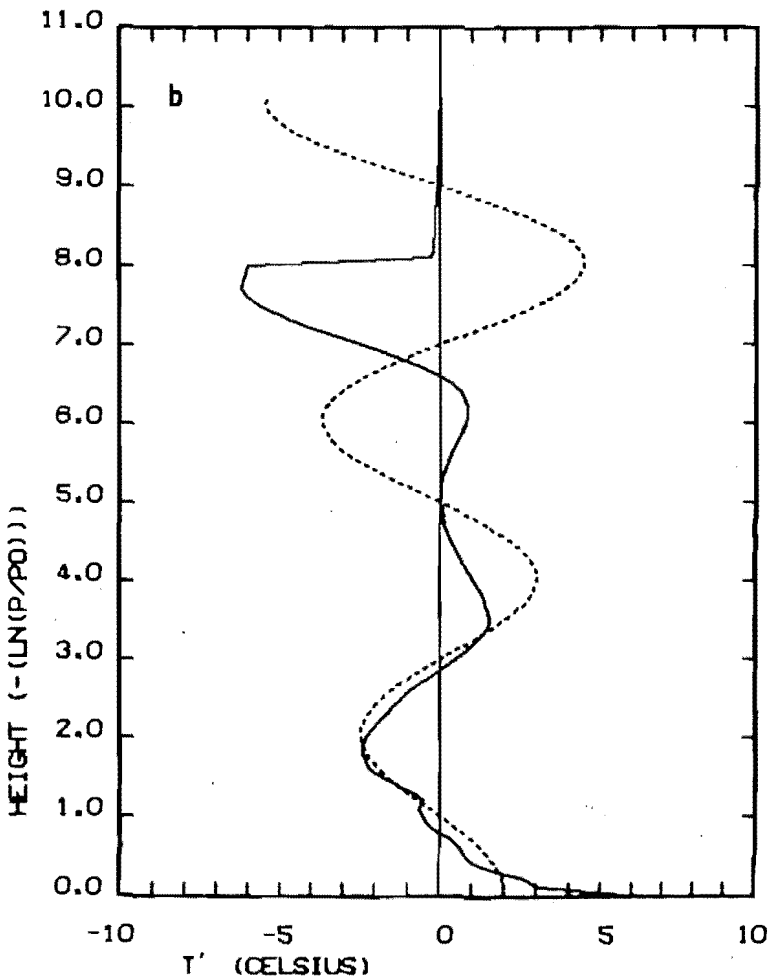
b
11.0
10.0
9.0
8.0
7.0
6.0
5.0
4.0
3.0
2.0
1.0
0.0
HEIGHT (-(LN(P/PO)))
-10
-5
0
5
10
T' (CELSIUS)

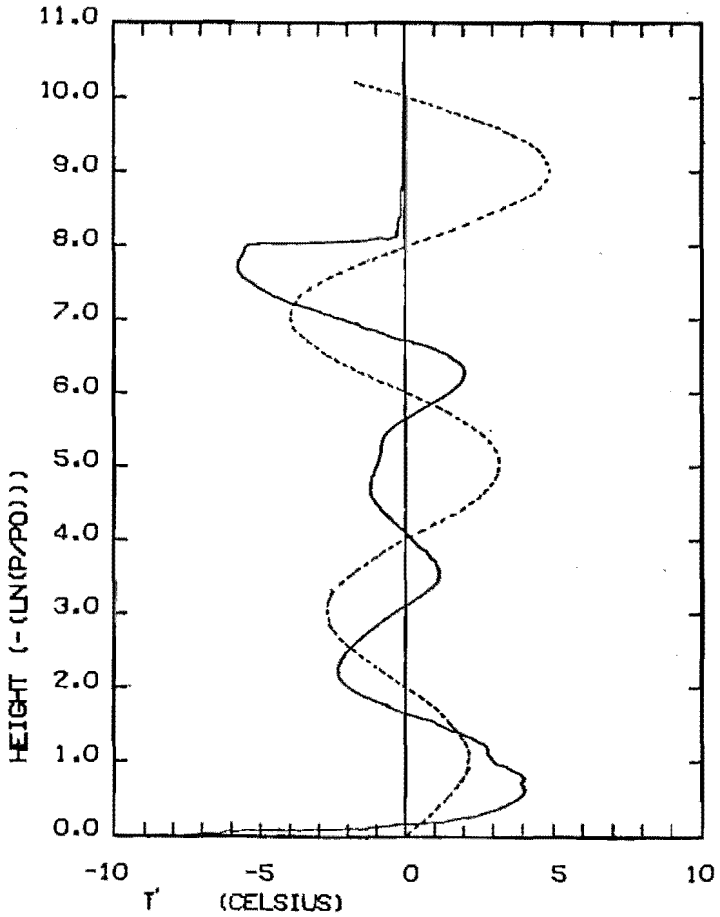

FIGURE 46 : Retrieval of λ_z = 4 sh (ϕ = 0) perturbation with an estimator using data series 2 noise statistics.

TABLE 15 : Resolution Results for Perturbation Wave with $A = 2C^0$, $\alpha = 0.1$, $\lambda_z = 4$ sh, $\phi = \pi/2$

Height (sh)	Perturbation Temperature T' (C^0)	T'estimate from T* values (C^0)	T' estimate from Retrieval (C^0)	
			Data Series 2	Data Series 5
6.2	-3.54	-0.7 ±0.2	0.2±1.4	0.6±0.5
4.4	2.51	0.39±0.14	1.3±0.9	0.5±0.3
3.2	0.85	0.13±0.06	0.6±0.4	1.0±0.3
2.7	-1.19	-0.50±0.03	-1.0±0.4	-0.5±0.3
1.7	-2.11	-0.92±0.06	-2.0±0.5	-2.2±0.2
0.4	1.54	1.18±0.03	0.9±0.3	0.9±0.4

It is evident that the brightness temperatures are able to consistently detect the sign and relative magnitude of the perturbation best. This is particularly evident for the $\phi = 0$ case, but also for the $\phi = \pi/2$ case. The MAP estimators are unable to retrieve the form of the perturbation (independent of phase) even at heights where the intrinsic resolution is best.

Comparison of the results for the retrievals from the two MAP estimators, (tables 14 and 15) implies that when $\phi = \pi/2$ and for noise free radiances, at heights above channel C the high noise estimator is better able to detect the perturbation than the low noise estimator. For the $\phi = 0$ perturbation similar small improvements occur, although the estimator is still unable to retrieve the perturbation. Unfortunately the noise in the retrieval estimate due to propogation of the measurement noise is rather larger for the data series 2 estimator than for the data series 5 estimator. But more importantly, when random noise with variances as for data series 2 is added to the radiance data, changes in the radiances due to the perturbation are submerged inside the noise.

The 3 sh Wavelength Perturbation

Calculations have been performed for perturbations of the form

of equation (4.2) and with parameters $A = 2C^0$, $\alpha = 0.1$, $\lambda_z = 3.0$ sh, $\phi = 0$ and $\phi = \pi/2$. The resulting retrievals for these calculations are given in figures 47(a) and 47(b). When $\phi = 0$ the retrieval is approximately convergent in three iterations (only the channel C residual does not satisfy equation (4.1)) whereas for the $\phi = \pi/2$ case only the channel E residual satisfies equation (4.1). This result would be expected, given figure 47(b).

Comparison of figures 47(a) and 47(b) indicates the estimator's sensitivity to the phase-height relationship of the perturbation. A strong spurious perturbation is excited in the retrieval by altering the initial phase by $\pi/2$. (When $\phi = \pi/2$ the brightness temperatures are able to correctly detect the sign of the perturbation.) On comparing the results of figure 47(b) with those of figure 45(a) it is apparent that the retrieved perturbation of figure 45(a) is almost a mirror image of the retrieved perturbation of figure 47(b). Assuming equation (4.8) is valid the source of this result is evident. The estimator averaging kernels (appendix J) have strong side lobes near 3 sh altitude. The true perturbation T' of figure 45(a) has a negative "peak" at 3 sh altitude whereas in figure 47(b) the true perturbation T' has a positive "peak" at this height. The estimator averaging kernel side lobes, in this case, control the shape of the retrieved perturbation since they are narrow and interfere constructively with the perturbation. Consideration of the 7.5 sh averaging kernel indicates the source of the strong perturbation amplification (of temperatures at lower levels) near 7.5 sh altitude in figures 45(a) and 47(b). An estimator constructed with higher noise values, for example, data series 1, does not excite such large spurious perturbations on the retrieved profile, neither can it "see" the perturbation, see figure 48.

These results indicate that estimators which have averaging kernels with strong side lobe structure may be sensitive to some per-

FIGURE 47 : Retrievals of $\lambda_z = 3$ sh perturbations after 3 iterations

(a) $\phi = 0$

(b) $\phi = \pi/2$

Original perturbation --------.

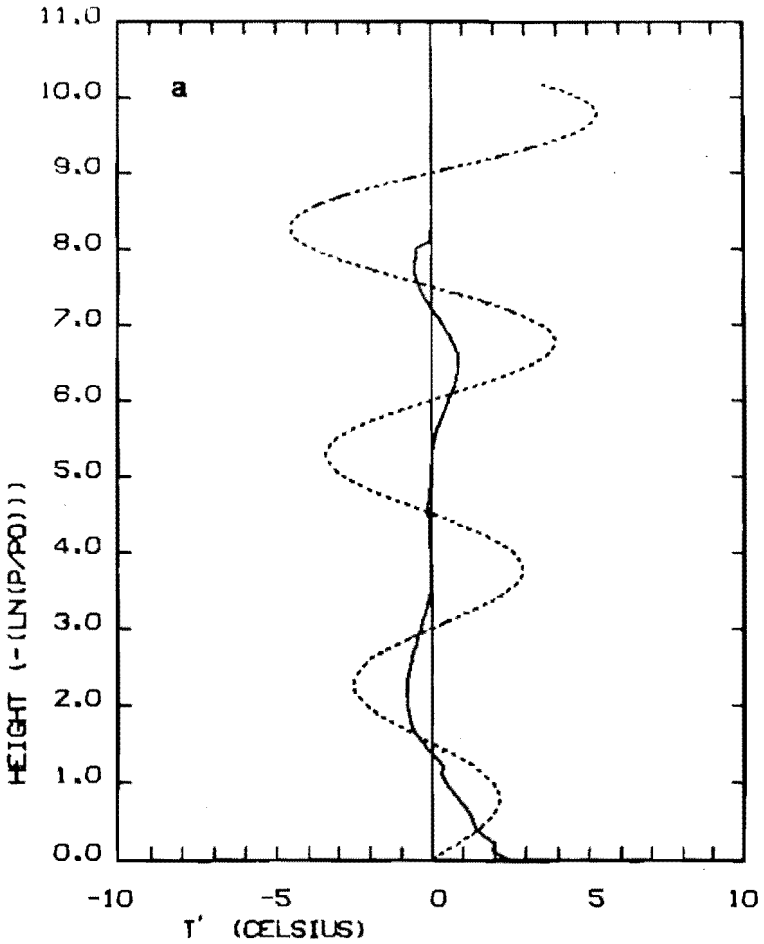
a
11.0
10.0
9.0
8.0
7.0
6.0
5.0
4.0
3.0
2.0
1.0
0.0
HEIGHT (-(LN(P/PO)))
-10
-5
0
5
10
T' (CELSIUS)

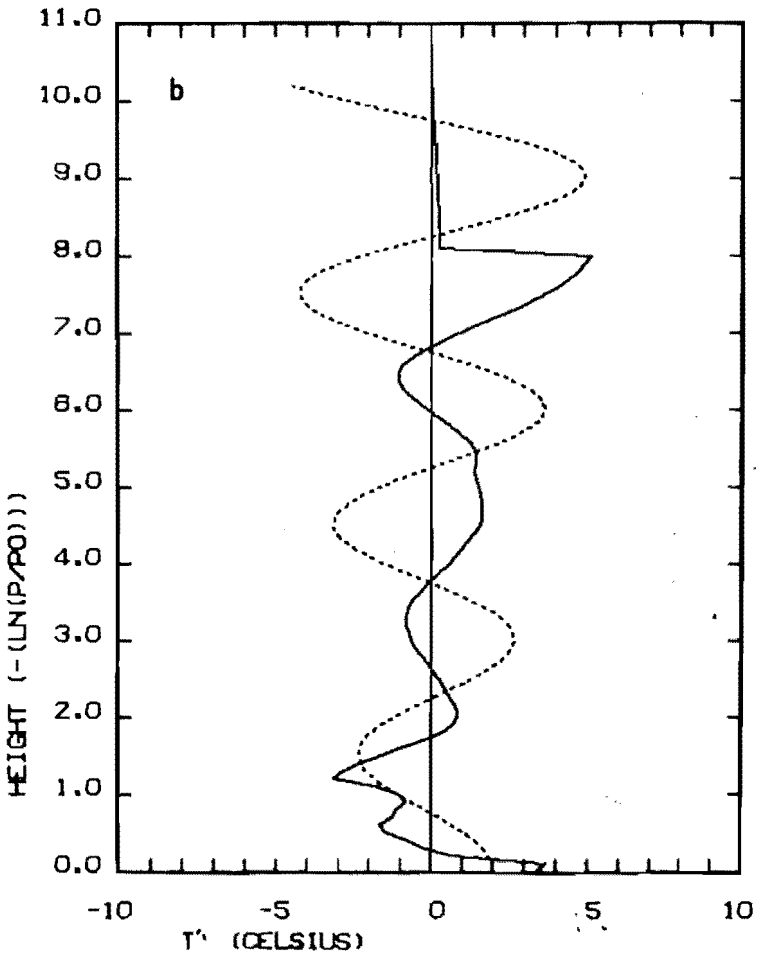
b
11.0
10.0
9.0
8.0
7.0
6.0
5.0
4.0
3.0
2.0
1.0
0.0
HEIGHT (-(LN(P/PO)))
-10
-5
0
5
10
T' (CELSIUS)

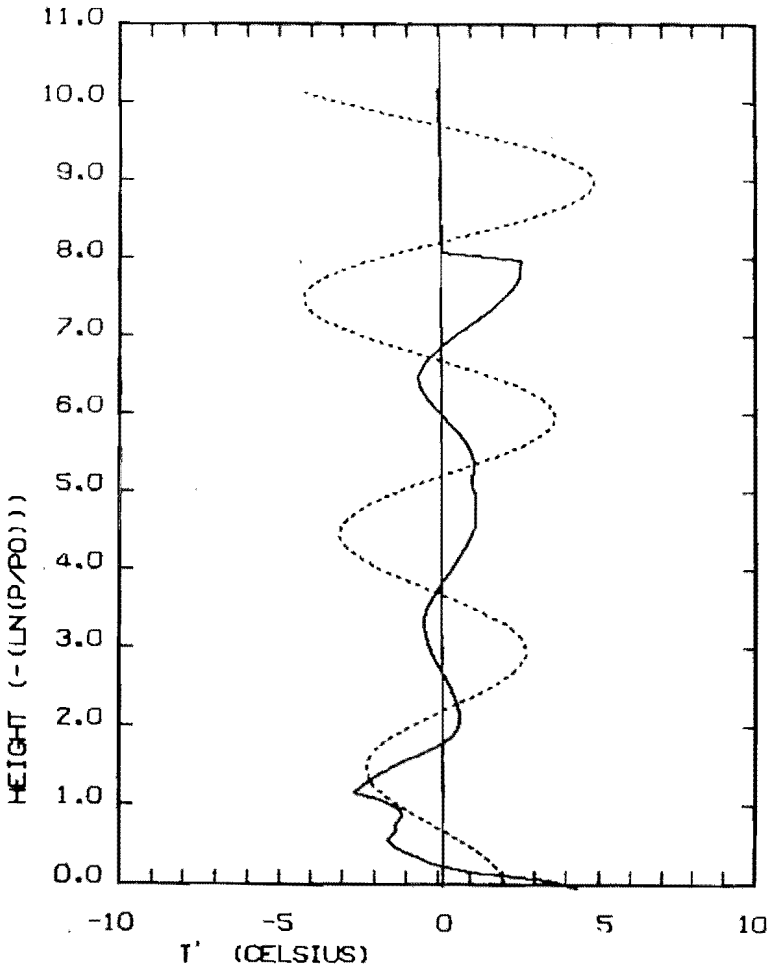

FIGURE 48 : Retrieval of λ_z = 3 sh ($\phi = \pi/2$) perturbation with estimator using data series 1 noise statistics

turbations in the observed radiances, and so produce spurious results. In turn this indicates that the averaging kernels of the estimators do say something about the vertical resolving power of the estimators.

4.1.5 Summary

From the preceding results a number of conclusions may be drawn.

When using smoothed data series with small random noise values the residuals of the resultant (iterated) MAP estimated retrievals do not in general satisfy the requirement for a "correct" solution, that is

$$\left| y_{\underline{x}_i} - y_{\hat{\underline{x}}_i} \right| \leq e_i \qquad i = 1,2,\ldots,6$$

If larger noise values are assumed then convergence generally occurs within a few iterations, typically less than three. Unfortunately if these measurement noise values are used, wave-like features of interest at heights above 4 sh (≈30 km) are submerged within the noise and will probably not be detected.

All MAP estimators introduce biases or artefacts into the retrieved temperatures. The source of these artefacts is the presence of side lobes in the estimator averaging kernels. The side lobes arise due to the apparent statistical correlations between different levels in the atmosphere, sometimes widely spaced in height, present in the a priori covariance matrices. The strength of these side lobes and the "widths" of the main peaks of the averaging kernels are sensitive to the assumed random measurement noise values, as described in Chapter 3.

The estimator averaging kernels and their measures of spread and centre height are meaningful descriptors of the vertical resolving power of an estimator. However, the spread of a multipeaked averaging kernel cannot be regarded as the smallest structure the estim-

ator can resolve. The averaging kernels describe the regions within the atmosphere that are used to determine the retrieved temperature at some specified height .

From a study on the retrieval of various simulated perturbations it is found that the "shape" of the initial perturbation $\underline{x}'$ or (T') as a function of height is important in determining the "shape" of the perturbation that the MAP estimators will retrieve. A consequence of this result is the indication that any temperature retrieval $(\underline{\hat{x}} - \underline{\bar{x}})$ will be sensitive to the shape of the difference vector $(\underline{x} - \underline{\bar{x}})$ that is, the choice of first guess profile.

In all cases studied it was found that the satellite brightness temperatures were better able to consistently detect wave-like perturbations on simulated profiles than could the MAP estimated temperature retrievals. These results would substantiate the conclusions of Chapter 3.

Finally, a comment on the use of the a priori information of Section 3.2.2. An aim of this simulation study has been to demonstrate the usefulness of the BG diagnostics (Section 2.4.6) in determining the vertical resolving power of a MAP estimator. This point has been shown, as noted above. The estimators used in this study were constructed from the original a priori matrices since these retrievals are optimum as demonstrated in Section 2.4.3. Using additional information such as ground correction or filtering would improve the results at some levels since side lobe structure in the estimator averaging kernels is decreased. However, the retrieval is no longer optimum or meteorologically most probable. Even so, the satellite observations are still better able to consistently detect perturbations in the temperature profiles. The MAP estimators show instability when retrieving wave-like perturbations on temperature profiles. This instability is a apparently a fundamental property of the MAP estimator, and is probably not greatly altered by the addition of further a priori

"information".

4.2 : EMPIRICAL ORTHOGONAL FUNCTION REPRESENTATIONS

The empirical orthogonal functions (eigenvectors) and eigenvalues of each of the six a priori covariance matrices have been calculated. In this section these results are presented and discussed, with special emphasis on the equatorial summer and high latitudes winter EOF (empirical orthogonal function) series.

4.2.1 EOF's of the a priori Covariance Matrices

The a priori covariance matrices are extrapolated from 8.1 sh to 10.2 sh altitude by providing variance values for these levels, as discussed in Section 3.2.3. All covariances are zero. The EOF's which contain information about these heights are therefore identical to the profile basis vectors, where if $\underline{b}_i$ is the i^{th} basis vector, then an element b_j of $\underline{b}_i$ equals one iff j=i, otherwise it equals zero. The eignevalues are just the corresponding variances. In the following results these EOF's shall be excluded from the discussion since they are only of value in constructing the profiles at levels above 8.0 sh altitude.

The five EOF's having the largest eigenvalues for each latitudinal zone and for both summer and winter seasons, are reproduced in figures 49 through 54. The associated eigenvalues of these EOF's are given on table 16.

The curves in figures 49 to 54 for the first EOF of the mid-latitudes and high latitudes winter matrices are similar peaked functions, indicating that for these seasons the largest contributions to the temperature variance occur near the stratopause. The first EOF of the high latitudes and mid-latitudes summer matrices are similar in shape as are the first EOF's of the equatorial summer and winter matrices. None of the other EOF's of figures 49 to 54 show such

FIGURE 49 : EOF's (eigenvectors) of the Equatorial"summer" covariance matrix

(a) 1st EOF

(b) ——— 2nd EOF

\- - - - - - 3rd EOF

(c) ——— 4th EOF

\- - - - - - - - 5th EOF

FIGURE 50 : EOF's (eigenvectors) of the Equatorial"winter" covariance matrix. Function numbering as for Figure 49.

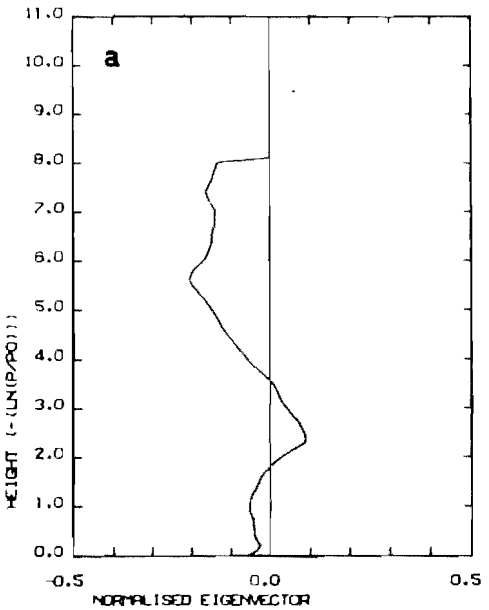

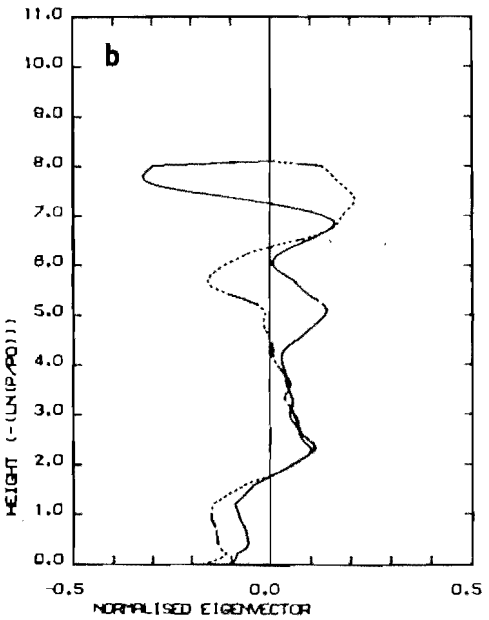

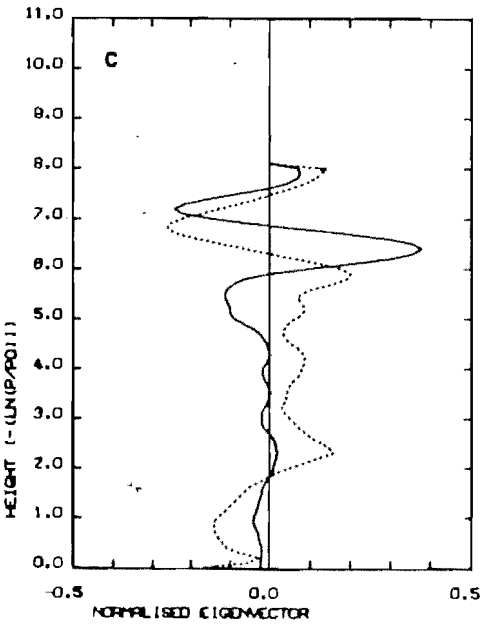

FIGURE 49

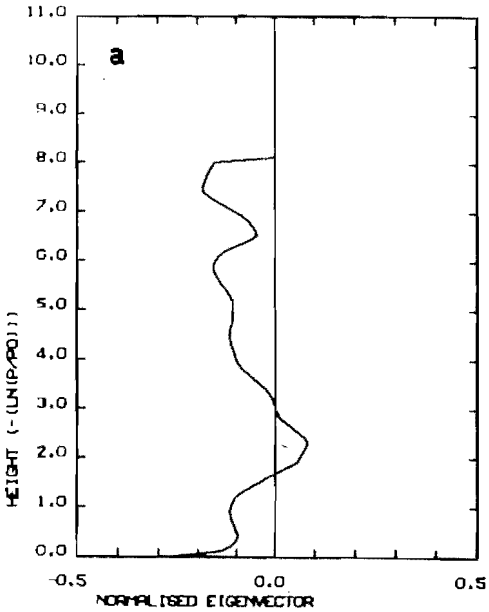

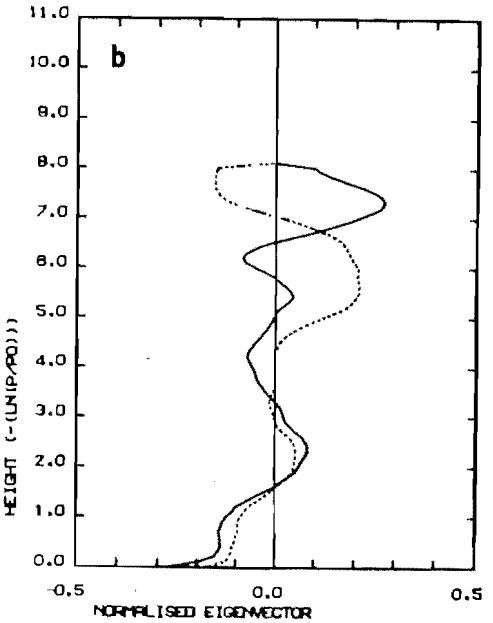

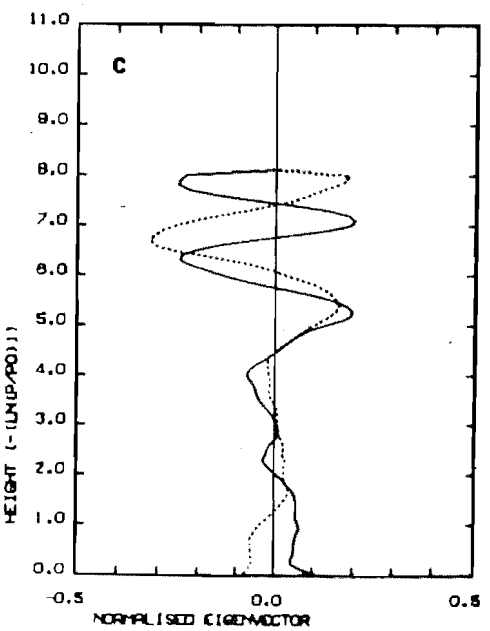

FIGURE 50

FIGURE 51 : EOF's (eigenvectors) of the Mid-Latitudes summer covariance matrix. Function numbering as for Figure 49.

FIGURE 52 : EOF's (eigenvectors) of the Mid-Latitudes winter covariance matrix. Function numbering as for Figure 49.

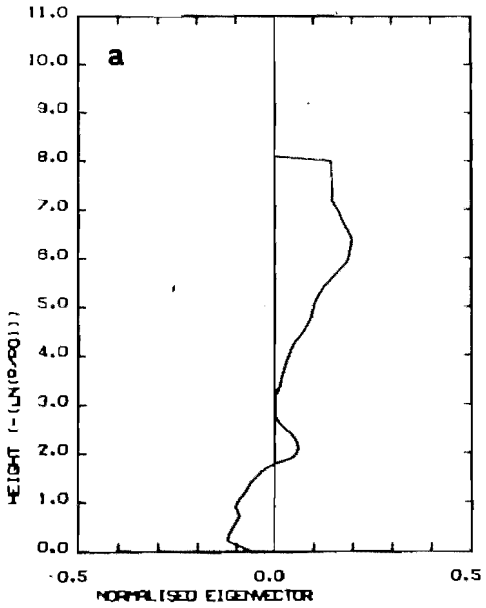

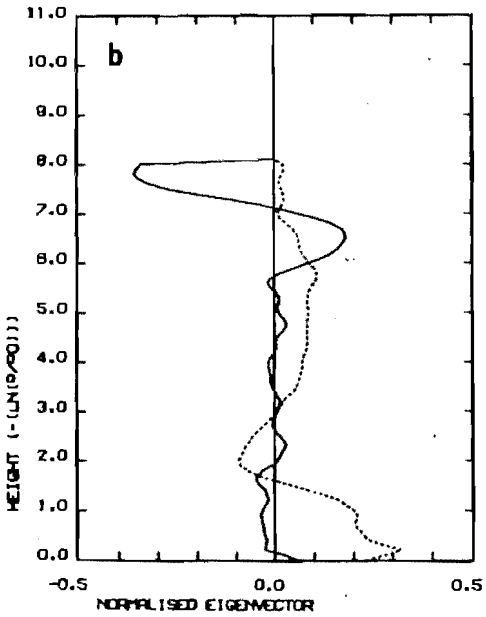

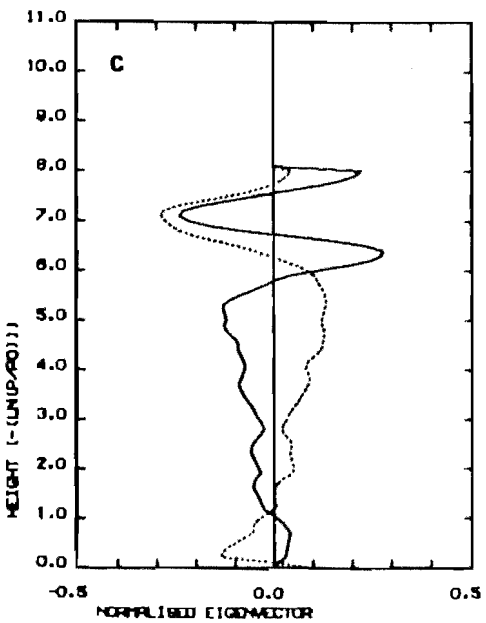

FIGURE 51

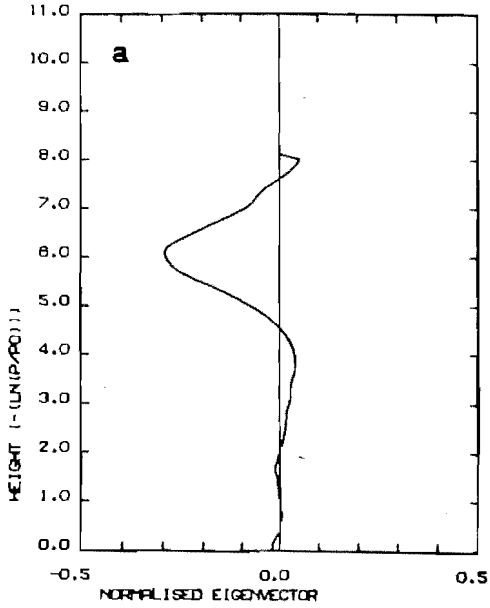

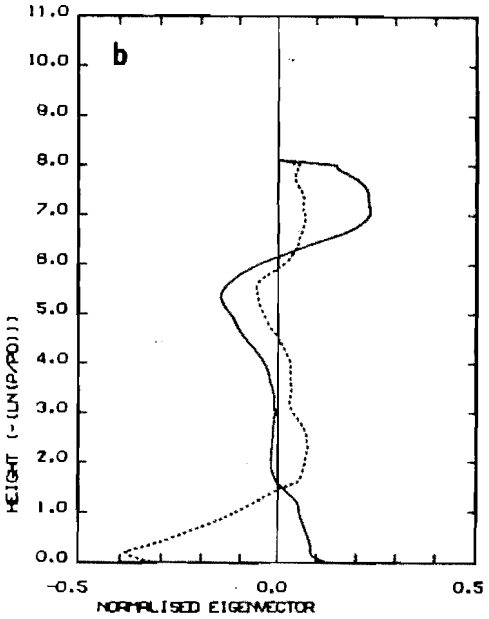

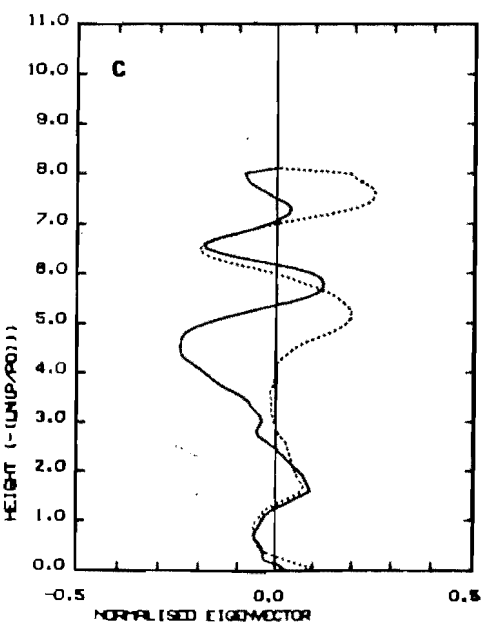

FIGURE 52

FIGURE 53 : EOF's (eigenvectors) of the High Latitudes summer covariance matrix. Function numbering as for Figure 49.

FIGURE 54 : EOF's (eigenvectors) of the High Latitudes winter covariance matrix. Function numbering as for Figure 49.

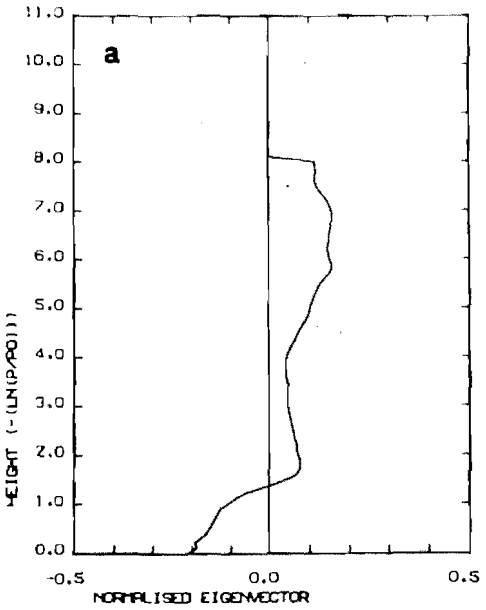

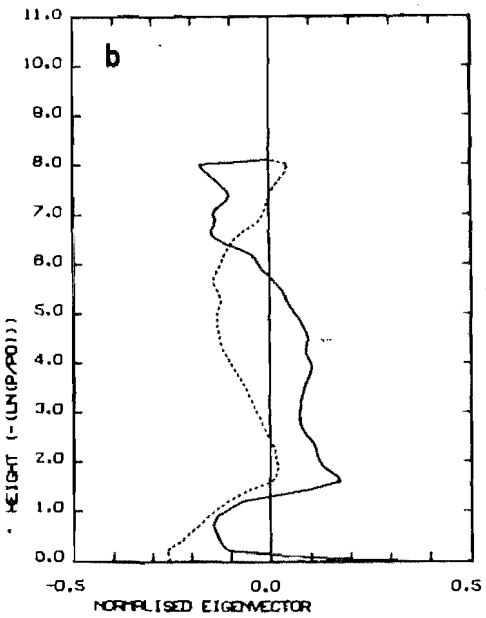

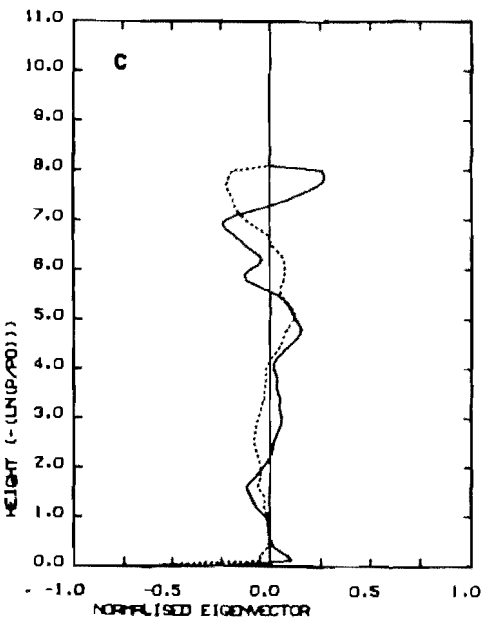

FIGURE 53

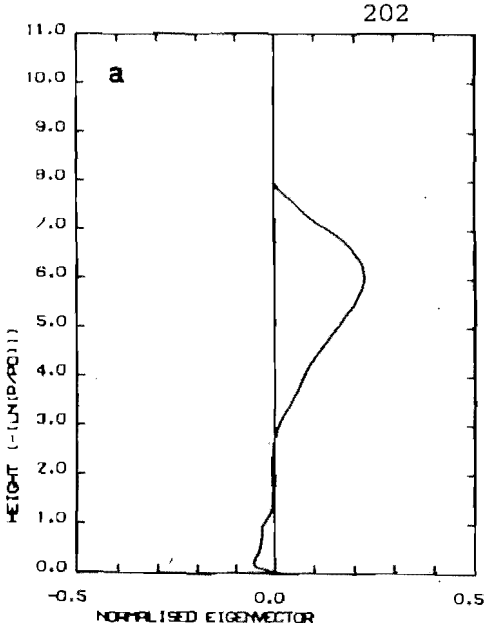

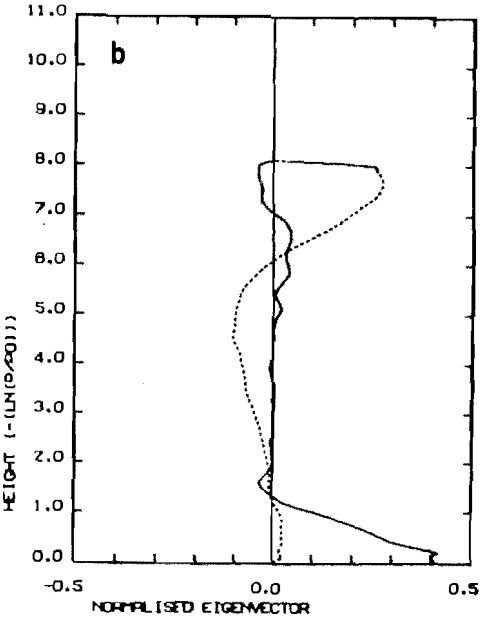

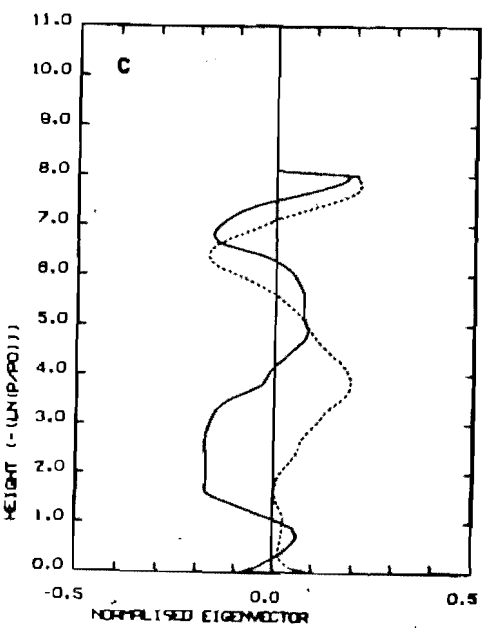

FIGURE 54

TABLE 16 : Eigenvalues of the Five Most Significant EOF's in Each Latitude Zone and Season

EOF Ordinal Number	EIGENVALUES $(r.u.)^2$ Equatorial Summer	Equatorial Winter	Mid-Lats Summer	Mid-Lats Winter	High-Lats Summer	High-Lats Winter
1	382.5	530.5	877.9	1841.4	1398.8	4089.2
2	128.1	391.7	364.8	838.6	703.8	1708.0
3	124.9	224.0	145.9	627.1	179.8	558.4
4	96.2	173.5	80.8	282.1	116.0	273.3
5	67.2	108.5	72.1	156.9	61.7	201.1

similarities between latitudinal zones and seasons. The amounts of temperature variance explained by these EOF's (equation 2.169) are given in table 17.

TABLE 17 : Temperature Variance Explained by the First Five EOF's

EOF Ordinal Number	Equatorial Summer	Equatorial Winter	Mid-Lats Summer	Mid-Lats Winter	High Lats Summer	High Lats Winter
1	35.79	29.47	48.16	42.55	50.70	55.16
2	11.98	21.76	20.01	19.38	25.50	23.04
3	11.69	12.44	8.00	14.49	6.52	7.53
4	9.00	9.64	4.43	6.52	4.20	3.69
5	6.29	6.03	3.96	3.63	2.24	2.71
Cumulative Total (%)	74.75	79.34	84.56	86.57	89.16	92.13

In all six cases a small number of EOF's explain a large percentage of the temperature variance in the a priori covariance matrices. The condition number (equation 2.139) for each of these matrices is of the order of 10^{-10}.

Details of the equatorial summer and high latitudes winter EOF series are presented in the following paragraphs. These series are given in detail in order to be consistent with the results presented in Section 4.1. They also represent extremes in terms of the cumulative variance explained with respect to the number of EOF's

included (table 17). Table 18 lists the variances and cumulative totals for the first 15 EOF's.

TABLE 18 : Temperature Variances Explained by the First 15 EOF's of the Equatorial Summer and High Latitudes Winter Covariance Matrices.

EOF Ordinal Number	Equatorial Summer Variance Explained (%)	Equatorial Summer Cumulative (%)	High Latitudes Winter Variance Explained (%)	High Latitudes Winter Cumulative (%)
1	35.79	35.79	55.16	55.16
2	11.98	47.77	23.04	78.20
3	11.69	59.46	7.53	85.73
4	9.00	68.46	3.69	89.42
5	6.29	74.75	2.71	92.13
6	4.02	78.77	2.23	94.36
7	3.28	82.05	1.61	95.97
8	2.89	84.94	0.87	96.84
9	2.48	87.42	0.70	97.54
10	1.85	89.27	0.54	98.08
11	1.69	90.96	0.45	98.53
12	1.22	92.18	0.31	98.84
13	1.02	93.20	0.22	99.06
14	0.94	94.14	0.18	99.24
15	0.84	94.98	0.15	99.39

When compared with the high latitudes EOF series results, rather more equatorial summer EOF's are needed to explain the same amount of variance.

A LEV diagram for the first 60 equatorial summer EOF's is given in figure 55. A similar diagram for the first 40 high latitudes winter EOF's is figure 56. In the case of figure 56 it is evident that the Craddock and Flood criterion (see Section 2.4.8) for truncation of the EOF series gives a truncation point at 12 -14 EOF's. This implies that the other 67 or so EOF's explain random noise in the a priori matrix, not true temperature variance. These 12 - 14 EOF's explain 98.84% - 99.24% of the original variance. In the case of figure 55, the equatorial summer results, there is no point which satisfies the above criterion, since at no point can the curve of ln (eigenvalue) against ordinal number be approximated by a straight line.

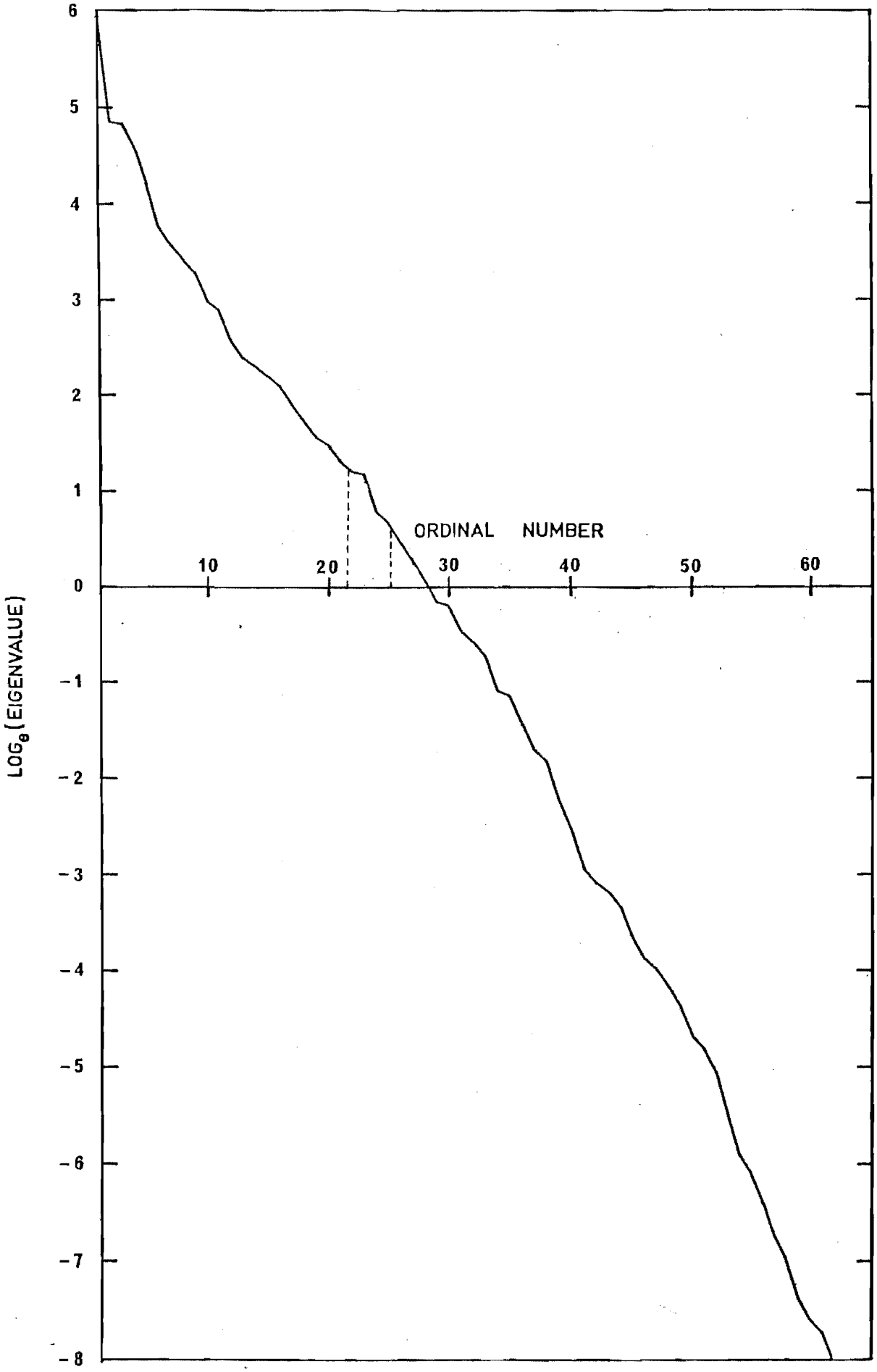

FIGURE 55 : LEV diagram for first 60 Equatorial summer EOF's

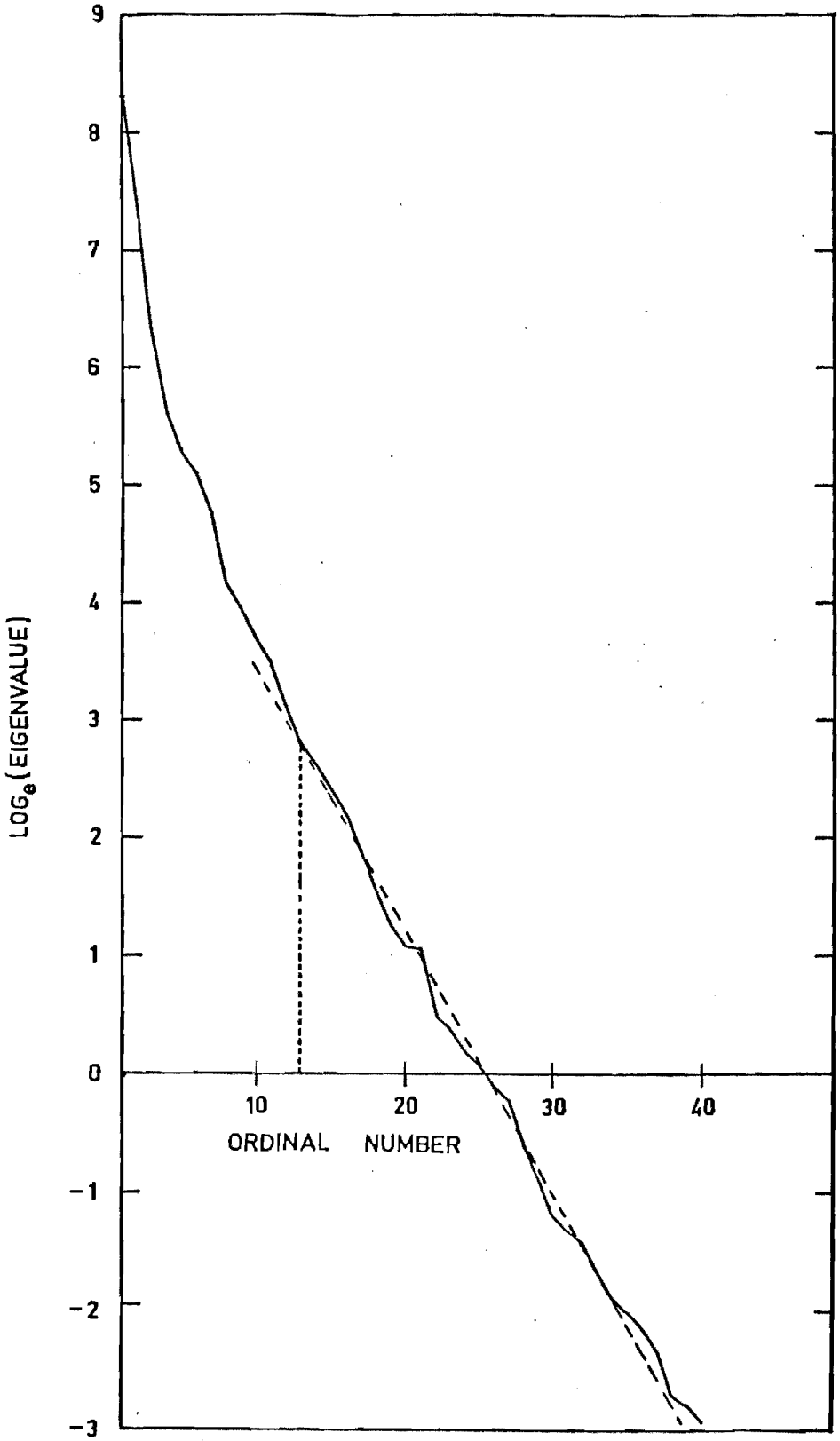

FIGURE 56 : LEV diagram for first 40 High Latitudes winter EOF's

A point of inflexion is evident in figure 55. If this point is taken as defining the truncation point then approximately 21 - 25 EOF's are required to explain the real temperature variance described by the covariance matrix. These EOF's cumulatively explain 98.16% - 99.16% of the variance of the a priori covariance matrix.

An alternative truncation criterion, labelled (c) in Section 2.4.8, may be applied. Ezemenari (1972) suggests that the random noise in the rocket measurements (used to construct the a priori covariance matrices), from all known sources, is of the order of ±1.3% since the standard known resistors used for inflight calibration of the thermistor resistance have tolerances of the order of ±1% (Ballard (1967(b)). If it is assumed that 1.3% of the variance in the covariance matrices arises from this source, then this implies a truncation point for the equatorial summer series, of 22 - 23 EOF's, and for the high latitudes winter series of 11 - 12 EOF's. These numbers are similar, but smaller in both cases, to those indicated by the LEV diagram technique.

Whatever the precise truncation point, these results indicate that a large number of the covariance matrix EOF's explain random noise, not true temperature variance information. The noise EOF's are all characterised by having a similar shape; highly oscillatory with small vertical dimension.

4.2.2 Examples of EOF Representations

To evaluate the "accuracy" of the truncation points determined above, the retrievals of Section 4.1 were represented using truncated sets of EOF's and equation (2.170).

The Equatorial Summer Case

Three different basis sets were used to reconstruct the retrieved equatorial summer profiles of Section 4.1.4. The basis sets contained 22, 23 and 28 EOF's of the equatorial summer covariance

matrix (i.e. n = 22,23 and 28 in equation (2.170)), explaining 98.47%, 98.78% and 99.53% respectively of the total variance.

If in equation (2.170) a vector $\underline{x}_T$ is defined such that

$$\underline{\hat{x}}_T - \underline{\bar{x}} = \sum_{i=1}^{n} c_i \underline{l}_i \qquad \ldots (4.10)$$

then

$$\underline{\hat{x}} - \underline{\hat{x}}_T = \text{residual}(n) \qquad \ldots (4.11)$$

For the three basis sets above, and for a particular retrieval, the vectors residual(n), are plotted in figures 57(a), (b) and (c). These curves are representative of the results obtained for the three basis sets. Using 22 EOF's the residual error is of the order of $\pm 0.5C^0$; with 28 EOF's the error is not larger than $\pm 0.3C^0$. The structure in the residual curves is much smaller than can be physically present in the retrieved profiles since the resolution in the retrieval is at best only 1 sh. The magnitude of the truncation errors is smaller than or approximately equal to the magnitude of the errors in the retrieval due to measurement noise propogation. Accordingly a representation using 22 - 28 EOF's should be able to represent the known information in some retrieved profile in this latitudinal zone and season.

An additional experiment was performed in which the basis set of EOF's used to represent the profile were those of the high latitudes winter matrix. It was found that this basis set which included 99.7% of the total variance was unable to reconstruct the tropopause accurately.

The High Latitudes Winter Case

The LEV diagram and rocket measurement noise exclusion techniques suggest that 11 - 13 EOF's are required to reconstruct a temperature profile for this latitudinal zone and season. Truncation residual vectors for a representative retrieval and for basis sets con-

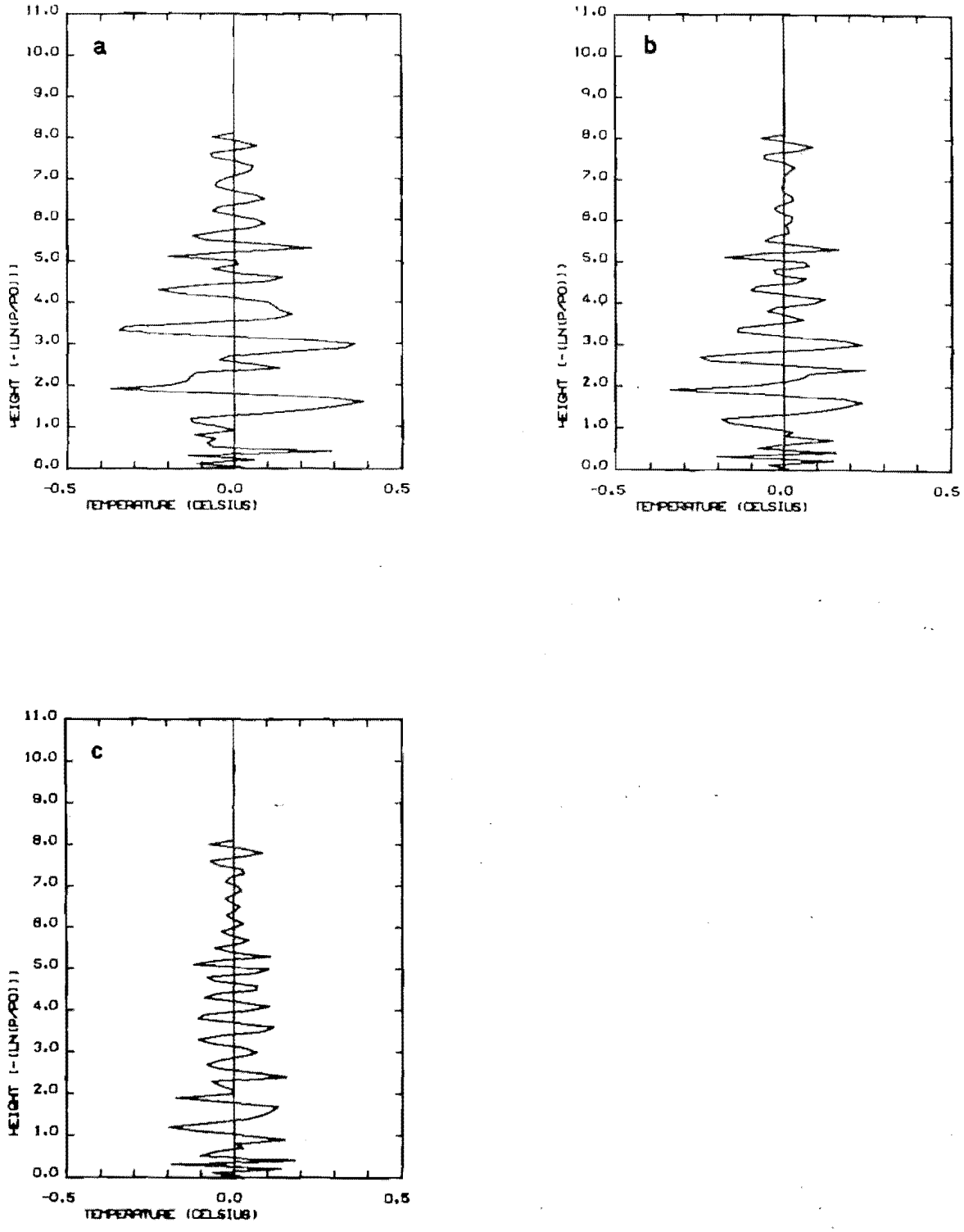

FIGURE 57 : Truncation errors for an EOF representation of an Equatorial summer retrieval using

(a) 22 EOF's

(b) 23 EOF's

(c) 28 EOF's

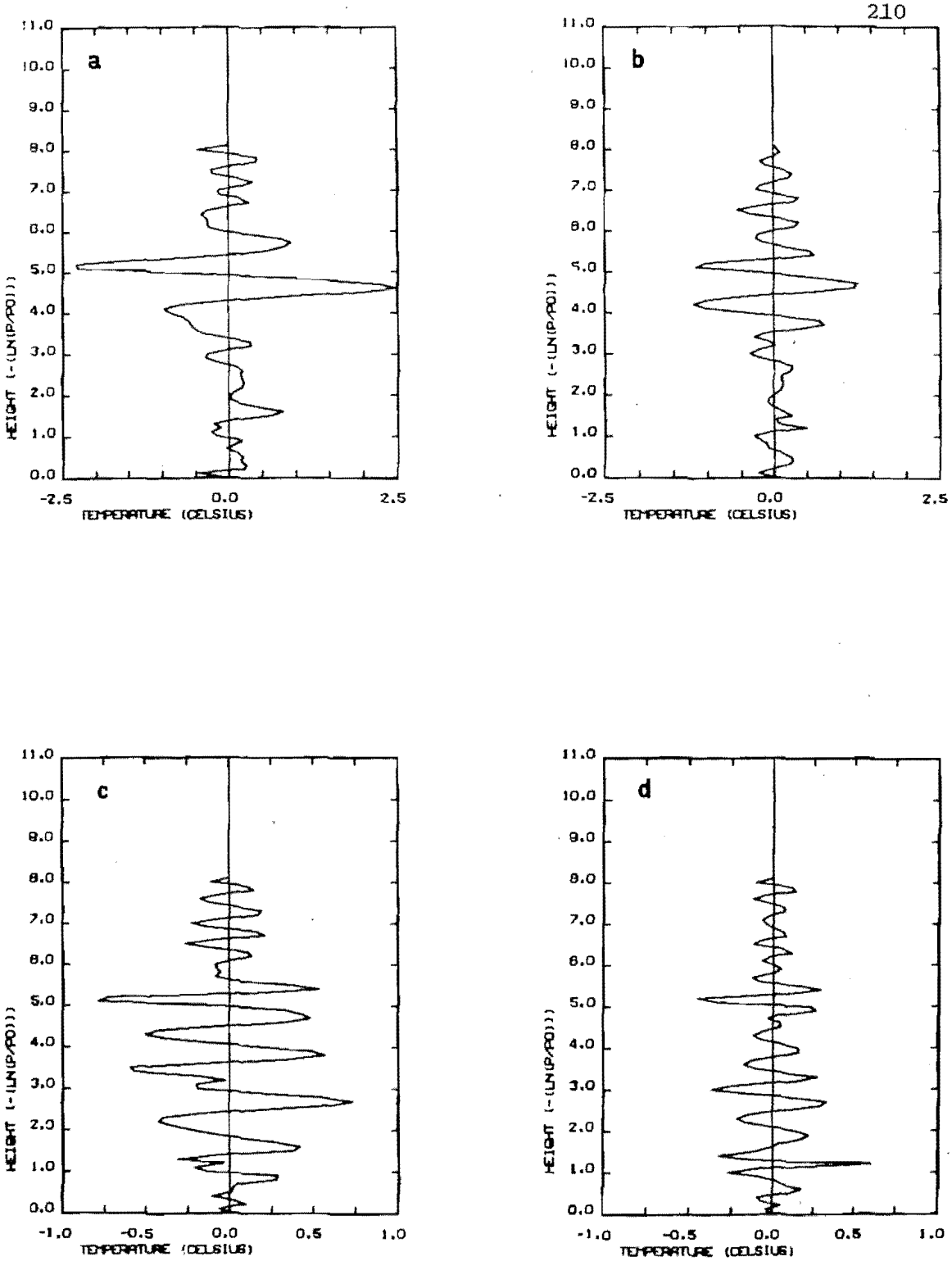

FIGURE 58 : Truncation Errors for an EOF representation of an High Latitudes retrieval using

(a) 13 EOF's
(b) 18 EOF's
(c) 23 EOF's
(d) 28 EOF's

sisting of 13, 18, 23 and 28 EOF's are presented in figure 58(a), (b), (c) and (d). These basis sets incorporate 99.07%, 99.70%, 99.90% and 99.97% of the temperature variance in the a priori covariance matrix. In figure 58(a), the largest truncation error occurs near 5 sh altitude and has a magnitude of approximately $\pm 2C^0$ and is caused through the vector $(\hat{\underline{x}} - \underline{x})$ having large elements at these heights. This error is of the order of the noise in the retrieval due to noise in the radiance measurements (at this height). The vertical structure in the residual is however smaller than the resolution in the retrieval. When the number of EOF's used in the reconstruction is increased to 23 the residual elements are smaller than $\pm 1C^0$ and the vertical structure has dimension less than approximately 0.5 sh. With the use of 28 EOF's the average value of the residual elements is approximately $\pm 0.25^0$C.

A basis set of 28 EOF's of the equatorial summer covariance matrix (representing 99.53% or the total variance) was also used to represent the same profile as above. The average size of the residual above 0.5 sh altitude was $\pm 0.5C^0$. Below this height the error was as large as $\pm 3C^0$. This set of EOF's was unable to reconstruct the temperature inversion structure in the retrieval at heights near ground level.

4.3.3 Discussion and Summary

It is apparent from the foregoing results that a large number of the a priori covariance matrix EOF's (eigenvectors) explain only random noise, not true temperature variance. The number of EOF's required to explain some amount of temperature variance would seem to be a function of both latitude zone and season. The lower latitudes requiring more EOF's to explain the atmospheric temperature variance. Taking into account the "shape" of the EOF's for the latitude zones and seasons it would seem that the overall temperature variance in the atmosphere at lower latitudes is not so "confined" in height as it is in high latitudes, hence more EOF's are required.

Both the LEV diagram and measurement noise exlcusion methods

deduce similar truncation points for the EOF series, although in all cases studied (six) the measurement noise method tended to reduce the number of EOF's required for an adequate basis set by one or two, over that derived with the LEV diagram method. This result is similar to that found by Rinne and Jarvenoja (1979). The resultant residual vectors may have elements as large as ±1 or $2C^0$, but at most heights the error is much smaller. The vertical structure in the residual is smaller than the resolution in the retrievals, therefore minor smoothing of the retrieved profiles would most probably remove these errors.

The LEV diagram technique is able to specify a realistic truncation point for the EOF series.

The truncated EOF series basis sets should probably only be used for representing retrievals in the latitude zones and seasons for which they were calculated since the variance structure between latitude zones is quite different.

Using an EOF series basis set, a retrieved profile (with dimension 81) may be specified with between approximately 11 and 28 projection coefficients depending upon the latitude zone and season in which the retrieval is performed.

4.3 : THE COVARIANCE ANALYSIS

The theoretical background for determining approximate confidence regions of a retrieved profile given the estimator covariance matrix, has been presented in Section 2.4.6.

In this section confidence regions of the equatorial "summer" and high latitudes winter estimators are presented. The results are representative of two atmospheric temperature variance extremes, as discussed in Section 4.1.4. The 95% confidence regions have been calculated assuming a retrieval at 103 discretization points, from ground level to 10.2 sh altitude (approximately 75 km). The value, 11.32,

of $\ell_{1-\alpha}(p)$, p=103 in equation (2.129) is from the chi-squared tables of the CRC Handbook of Tables for Probability and Statistics.

4.3.1 The Equatorial Summer Estimators

Confidence regions for estimators using measurement noise values appropriate to data series 2, 4 and 5 data have been calculated in addition to the confidence regions of the a priori first guess profile. Plots of these confidence regions together with curves for the square root of the variance at each level, are given in figures 59 and 60. It is evident in each of these figures that the curves for the square roots of the diagonal components of the covariance matrices do not well represent the magnitude of the confidence regions of the a priori and solution profiles. In general they do however follow the trends in the confidence regions. As suggested in Section 2.4.6 the correct confidence regions have magnitudes of the order of $\pm p^{\frac{1}{2}}\sigma_i$ where i = 1,2,...,p, and σ_i is the standard deviation at level i.

The a priori profile confidence regions, figure 59, indicate the effects of large covariances and variances in the a priori covariance matrix near the tropopause and in the region of the stratopause. The confidence regions above 8 sh altitude (≈60 km) are determined by the extrapolation of the a priori matrix since as the covariance matrix is diagonal at these altitudes the corresponding eigenvectors have the form of the profile basis vectors.

Figures 60(a), (b) and (c) are graphs of the confidence regions of MAP retrieval estimators for differing r.m.s. measurement noise levels in the satellite observations. At all heights above approximately 2 sh the confidence regions of the estimator using data series 4 noise values are significantly smaller than those for the estimator using data series 2 noise values. However a similar reduction in the size of the confidence regions does not occur for estimators using noise levels as for data series 4 and 5 data. Instead, the confidence reg-

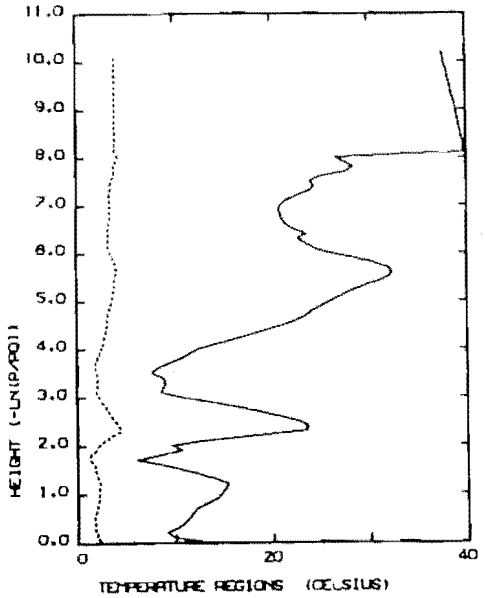

FIGURE 59 : Confidence regions (————) and square root of variance (--------) curves for the Equatorial Summer first guess (mean) temperature profile

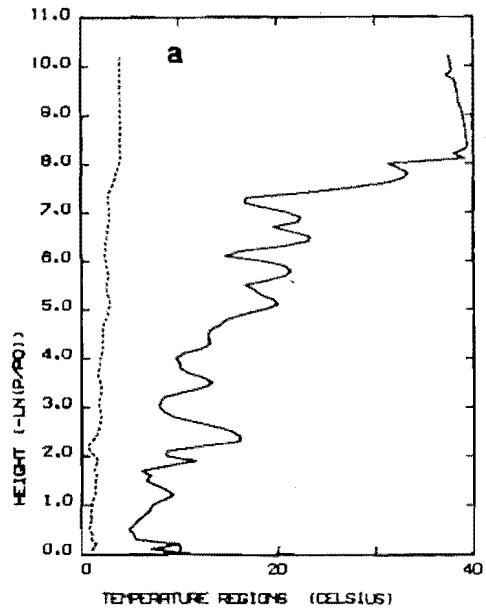

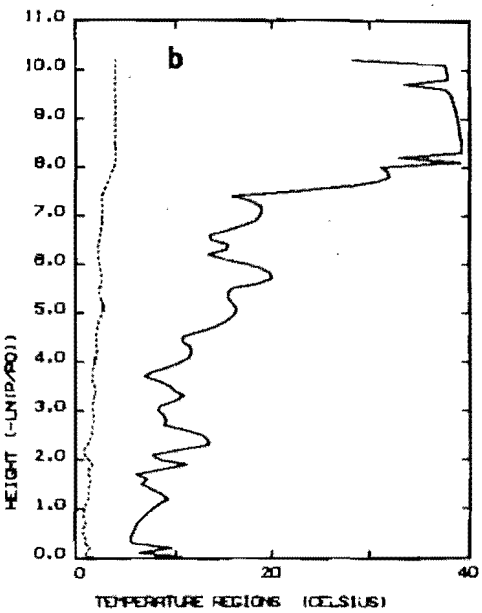

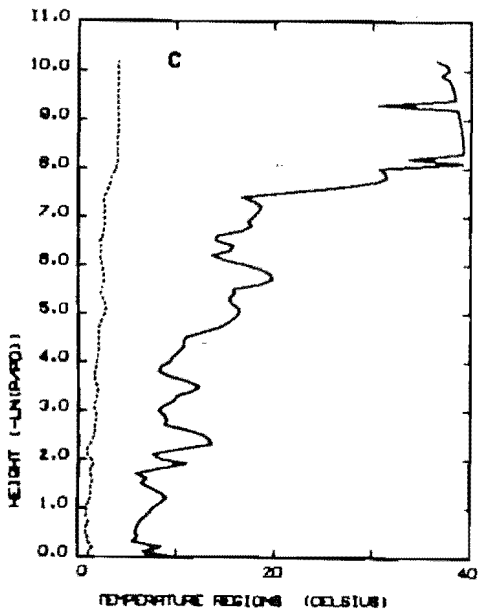

FIGURE 60 : Confidence regions (————) and square root of variance (--------) curves for Equatorial Summer MAP retrieval estimators using measurement noise values as for

(a) data series 2
(b) data series 4
(c) data series 5

ions of the data series 5 estimator are marginally larger at some heights than those for the data series 4 estimator. This suggests that the size of the confidence regions is not a simple function of the noise in the measurements.

For each of the figures 60(a), (b) and (c), addition of the satellite information does not effectively reduce the size of the confidence regions at heights above 8 sh (when compared with the a priori regions). This is not unexpected since the satellite measurements do not contain significant information about the temperatures at these heights. The size of the confidence regions when compared with those of the a priori profile at heights below approximately 7 sh, are improved by the measurements as expected. Below 7 sh altitude the magnitudes of the estimator confidence regions is of the order of $\pm 10C^0$.

An overall measure of the change in the size of the confidence regions owing to the addition of the satellite measurements can be given by considering the sizes of the confidence region hyper-rectangle volumes of the a priori and retrieval estimator covariance matrices. These values are given in table 19 below

TABLE 19 : Confidence Region Volumes for the Equatorial Summer Estimators

Noise Values as for Data Series	Confidence Region Volume $(r.u.)^{103}$
a priori	2.928×10^{134}
2	2.525×10^{125}
4	5.253×10^{121}
5	8.587×10^{121}

If the information content of the satellite measurements is regarded as the amount by which the confidence regions of the first guess a priori profile are reduced by the impact of the measurements then it is apparent from the results of figures 59 and 60, and table

19, that an estimator using the smallest measurement noise values may not have the smallest confidence regions. This implies that reducing the noise in the radiance data series, beyond a certain point, may result in a degraded retrieval owing to the fact that less information is apparently "contained" in these measurements when used in a MAP retrieval estimator. This suggests that the noise statistics may be important in determining the results of a MAP estimator retrieval, independent of how small the noise in the data may actually be.

4.3.2 The High Latitudes Winter Estimators

The approximate confidence regions for the winter high latitudes a priori first guess profile and for various retrieval estimators are given in figures 61 and 62.

From figure 61, the a priori results, the temperatures at heights near 6 sh altitude (≃45 km) show large variations over this season, as do the temperatures near ground level. Although the square roots of the variances of the temperatures do in general indicate the correct shapes of the confidence regions, the magnitudes are underestimated by a factor of approximately $p^{\frac{1}{2}}$. Consideration of figures 62(a), (b) and (c), the results for estimators using data measurement noise values as for data series 2, 4 and 5, clearly shows the height regions for which the satellite measurements contain little information. Above 8 sh altitude there is little information in the satellite measurements as expected. Additionally from these figures it is apparent that the confidence regions for the retrievals at altitudes near 5 sh (≃38 km) are little different in magnitude to those for the a priori profile. There is little information in the satellite measurements at these heights, a fact also deduced from consideration of the BG centre heights of the estimator averaging kernels.

Comparison of the results for the retrieval estimators using

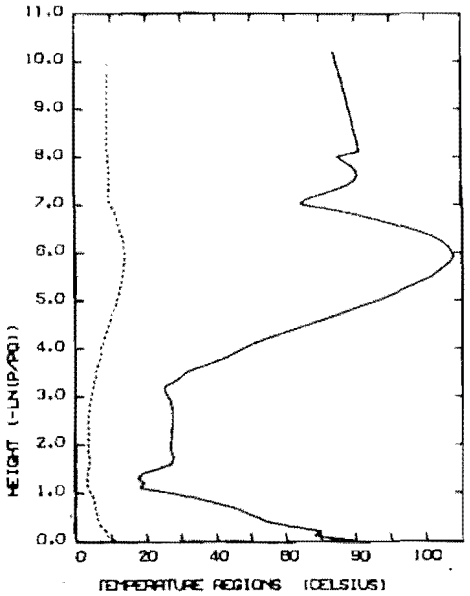

FIGURE 61 : Confidence regions (————) and square root of variance (--------) curves for the High Latitudes Winter first guess (mean) temperature profile

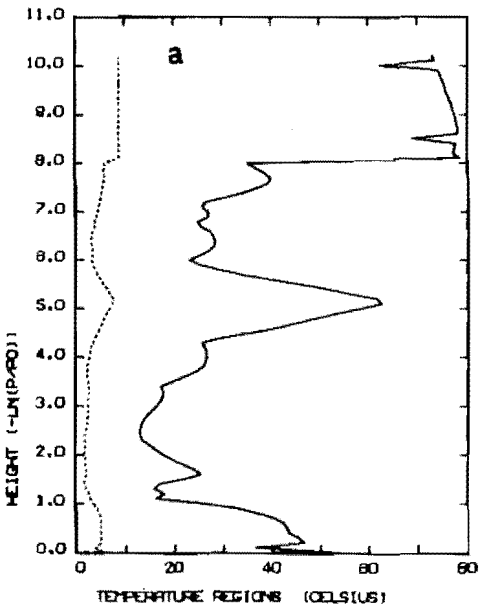

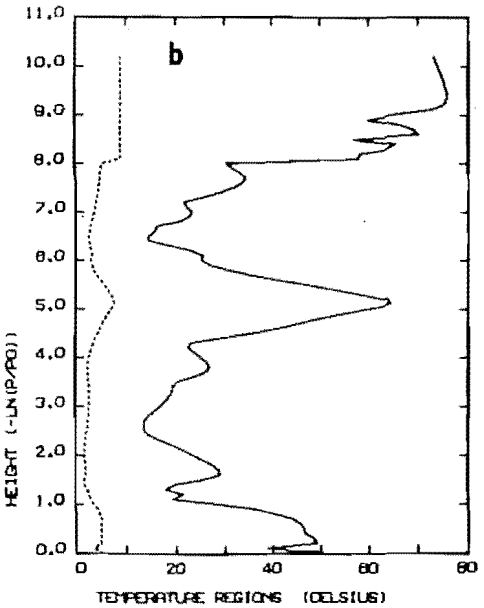

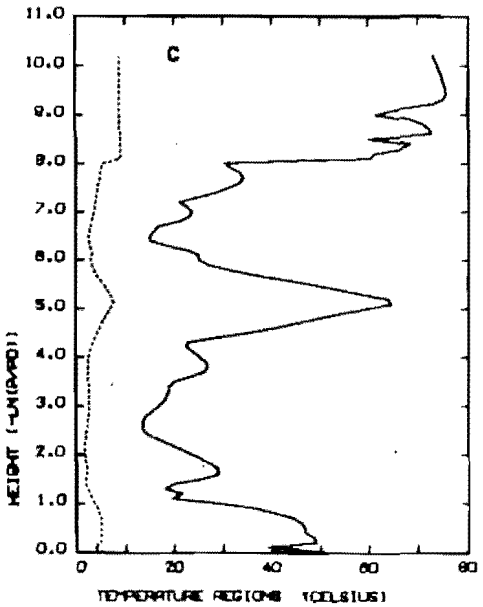

FIGURE 62 : Confidence regions (————) and square root of variance (--------) curves for High Latitudes winter MAP retrieval estimators using measurement noise values as for

(a) data series 2
(b) data series 4
(c) data series 5

data series 2 and 4 noise statistics indicates that the confidence regions for the data series 4 estimator are smaller above 6 sh altitude than those for the data series 2 estimator. The reverse occurs for altitudes below 2 sh. Similar results are apparent on comparing the curves for the data series 5 estimator with those for the data series 2 estimator. The confidence regions for the data series 4 and 5 estimators are almost identical except above 8 sh altitude where the data series 4 estimator has smaller confidence regions.

The volumes of the confidence region hyper-rectangles are given in table 20.

TABLE 20 : Confidence Region Volumes for the High Latitudes Winter Estimators

Noise Values as for Data Series	Confidence Region Volumes $(r.u.)^{103}$
a priori	2.942×10^{184}
2	1.966×10^{158}
4	6.647×10^{156}
5	1.081×10^{157}

The decrease in the confidence region volumes is not a simple function of the noise in the satellite data. As noted from the results in Section 4.2.1 it would appear that it is not necessarily true that decreasing the noise beyond a certain point improves the apparent information "content" in the MAP estimated retrieved temperature profiles. These results suggest that the assumed values for the measurement noise statistics are important parameters in determining the "quality" of an estimated retrieved profile.

The 95% confidence regions for these estimators are of the order of $\pm 20C^0$ from 1 sh to approximately 7 sh altitude, excluding the regions close to 5 sh altitude. The sizes of the confidence reg-

ions near ground level and 5 sh altitude are somewhat larger.

4.3.3 Discussion and Summary

The confidence regions of the retrievals are indicative of the overall performance of the estimators. Two factors contribute in determining the confidence regions of the solution profiles. There is a noise contribution from measurement noise propagation through the estimator and also from the a priori data. The contribution arising from the measurement noise propagation is not larger than approximately $\pm 2C^0$ and has been discussed in Chapter 3 and in Section 4.1. This contribution will not be considered further here. The "noise' which produces the large confidence regions shown in figures 60(a), (b) and (c) and figures 62(a), (b) and (c) arises mainly from the second source, "noise" in the a priori data. It is this noise which will be discussed here.

In the absence of the satellite measurements of the temperature structure, the best estimate of the temperature profile of the atmosphere at some time, for a given set of a priori data, is given by the mean profile for the data. The confidence regions for that estimate are determined by the mean profile's covariance matrix. On taking measurements of the atmospheric temperature structure the estimate for the unknown temperature profile is improved and the size of the confidence regions is reduced. If the information content of the measurements and retrieval process is to be specified, then the amount by which the confidence regions of the a priori profile are reduced by making the measurements might be considered as an indication of the information content of the observation. Peckham (1974) suggests that the volume of the a priori and estimator error hyper-ellipsoids can be used to specify the information content of the satellite observations. Using information theory (see Beck and Arnold (1977) page 476), the information I in a set of measurements is defined as

$$I = \int p(\underline{\hat{x}}) \ln p(\underline{\hat{x}}) dx - \int p(\underline{x}) \ln(p(\underline{x})) dx \qquad \ldots (4.12)$$

where $p(\underline{x})$ is the probability density function of the random variable $\underline{x}$. Here the function is assumed to be Gaussian, therefore $p(\underline{x})$ and $p(\underline{\hat{x}})$ are determined by the covariance matrices of the a priori and estimator distributions. Under these assumptions equation(4.12) may be written (by Beck and Arnold (1977) and Peckham (1974))

$$I = \tfrac{1}{2}\{\ln|S_x| - \ln|\hat{S}_x|\} \qquad \ldots (4.13)$$

where $|S_x|$ is the determinant of the a priori covariance matrix and $|\hat{S}_x|$ is the determinant of the solution covariance matrix. These values are related to the respective hyperellipsoid volumes by multiplicative constants. Equation (4.13) gives a precise information theory meaning to the information content of the satellite measurements. This expression is used by Peckham (1974).

The condition number (equation (2.139)) for each of the a priori matrices is of the order of 10^{-10}. Accordingly the estimator equations are not well conditioned, although they are not singular. The matrices S_x and $\hat{S}_x$ are not well conditioned. A large number of the eigenvalues of these matrices are small in magnitude when compared to the largest eigenvalues. As noted in Sections 2.4.8 and 4.2, these small eigenvalues are associated with noise eigenvectors and correspond to noise in the measurements used to construct the a priori statistics. Since

$$|S_x| = \prod_{i=1}^{p} \lambda_i \qquad \ldots (4.14)$$

where the λ_i are the eigenvalues of S_x, it is apparent that the value of $|S_x|$ is essentially determined by the random noise in the a priori measurements. Therefore equation (4.13) which takes the difference

of the natural logarithm (or perhaps $\log_2$ if the answer is required in bits) of the error ellipsoid volumes will probably not be a good measure of the information content of the observations since it is sensitive to random noise in the covariance matrices.

A physically meaningful parameter which will be used here to define the information content of the satellite measurement, incorporating any effects introduced by the retrieval estimator, is the difference between the confidence region volumes of the a priori and estimator covariance matrices. This result should be physically meaningful since the confidence regions are determined by the eigenvectors which explain most of the real temperature variance in the covariance matrices. In order to specify the information "content" of the measurements in different estimators, information content I' will be defined as

$$I' = \ln[\text{Volume of a priori confidence regions}] - \ln[\text{Volume of estimator confidence regions}] \quad \ldots (4.15)$$

Table 21 lists the results for the estimators discussed in Sections 4.3.1 and 4.3.2

TABLE 21 : Information Content I' for Retrieval Estimators

Noise Values as for Data Series	Equatorial Summer	High Latitudes Winter
2	20.87	60.27
4	29.35	63.65
5	28.86	63.17

The differences between equatorial summer and high latitudes winter values of I' relate to the fact that the a priori confidence regions are different and have different relative magnitudes at heights corresponding to the peaks of the satellite weighting functions.

In table 21, within a particular season the "apparent" information content of the observations is dependent upon the size of the measurement noise statistics. The information content increases as the measurement noise levels are decreased from those of data series 2 to those of data series 4, but decreases (marginally) as the noise levels are reduced still further to those of data series 5. Similar results are found to occur if the confidence region volumes are calculated for a retrieval to only 8 sh altitude (i.e. does not include the extrpolated region). The differences in table 21 are not a result of effects from altitudes above 8 sh. These results suggest that the values assumed for the measurement noise statistics are important in determining the "quality" of the profile retrieved with the MAP estimator, and in maximising the "information content" of the satellite observations. This type of sensitivity of the MAP estimator to the measurement noise statistics is also apparent in the results from the BG analysis of the estimator averaging kernels given in Chapter 3.

The square roots of the variances of the covariance matrices of the estimators are not good measures of the confidence regions, since they underestimate the sizes of the confidence regions. This is not unexpected since not all available information is used in these calculations. Further, it is evident from a careful comparison of the confidence regions and the values for the square roots of variances in figures 60(a), (b) and (c) and figures 62(a), (b) and (c) that in some cases, at some heights (e.g. figure 62(c)), the square root of variance curves do not follow the shape of the confidence region curves. The square root of the estimator variances may not be a good indicator to specify the effect of the measurement noise on the estimator (this method is used by Rodgers (1970)).

Finally, it is evident from the magnitudes of the confidence regions of the estimators that the quality of the first guess profile is the most important factor in determining the actual error in the

retrieved profile. The retrieved profile should lie close to the first guess profile, otherwise the errors in the retrieval may be large.

CHAPTER 5

CONCLUSIONS

Linear retrieval estimators form linear combinations of the satellite observations in some way. The form of the linear combination determines the intrinsic resolving power of the estimator. In the present work two fundamentally different types of estimator have been considered in connection with retrieval of vertical wave-like perturbations in temperature structure sounded by the Nimbus 4 SCR instrument. The first type of estimator uses essentially no a priori data in making a retrieval and accordingly defines the resolving power of the satellite observations. This is the Backus Gilbert estimator. The second type is an optimum estimator which uses a priori statistical data. The MAP estimator is a minimum variance estimator which retrieves the meteorologically most probable temperature profile. Backus Gilbert theory also indicates that the MAP estimator has the best vertical resolution versus noise of linear estimators using a priori data (with certain assumptions).

It is found that the intrinsic resolving power of the Backus Gilbert estimator is a function of the overlap of the satellite weighting functions. In regions where the weighting functions overlap significantly the intrinsic vertical resolution of the estimator is much better than that of the single channel observations. At heights where the weighting functions do not overlap significantly the intrinsic resolution is similar to that of the single channel observations. For Nimbus 4 SCR data the best resolution obtainable at channel A heights ($\simeq$45 km) is essentially the same as the radiance observations.

The Backus Gilbert resolving power diagnostics of averaging kernel spread and centre height have been applied to the MAP estimator averaging kernels. These diagnostics do not take account of all

available information since the observations are not used (as noted also by Newman (1979)) therefore only the intrinsic resolving power of the estimator can be specified with the diagnostics. A simulation study has shown that the diagnostics are useful descriptors of the actual resolving power of the MAP estimators when wave-like perturbations are to be retrieved. However, when the averaging kernels are multipeaked functions the spread cannot be interpreted as the smallest structure the estimator can "see". Instead, a correct interpretation is that the original satellite observations lack the intrinsic information necessary to make a good retrieval at these heights. The retrieval is determined from the temperature correlation structure of the a priori covariance matrix, and the shape of the first guess profile. At heights where the MAP estimator averaging kernels are multipeaked functions the temperature retrievals are unstable to vertical wave-like perturbations on the temperature profiles sounded by the satellite. This instability also results in a poor retrieval for the unknown profile since the radiance residuals do not converge to values less than or equal to the satellite r.m.s. measurement noise estimates.

The Backus Gilbert MAP estimator diagnostics also indicate that the resolution of the estimators is quite sensitive to values assumed for the measurement noise statistics. As the noise in the measurements is decreased the side lobe structure in the estimator averaging kernels increases, increasing the instability of the estimator to vertical temperature perturbations. This noise sensitivity of the estimator is probably a result of the non well-conditioned nature of the estimator equations. The noise statistics help to regularize the estimator equations.

The Backus Gilbert diagnostics for the optimum (MAP) retrieval estimator indicate that the estimator's resolving power is poorer than that of the satellite single channel observations at stratospheric

heights. The simulation study proved this prediction since the satellite brightness temperatures were better able to consistently detect wave-like perturbations in the atmospheric temperature profiles than the MAP estimators. This result occurs owing to the instability introduced into the MAP estimator by the a priori information at heights where the satellite observations lack information. The MAP estimator's retrieval of temperatures at some heights is strongly affected by the temperatures at other non nearby heights.

A confidence region analysis substantiates the Backus Gilbert diagnostic results for the MAP estimators. It is evident from these results that there are heights for which the satellite measurements cannot reduce the size of the confidence regions of the a priori profile. These heights correspond with those indicated by the centre height curves of the MAP estimators. The confidence region volumes suggest a new a priori noise independent method for determining the information content of the satellite observations. Information content results using this method indicate that the apparent "information content" of the satellite observations is measurement noise dependent. The minimum measurement noise values (used here) do not seem to result in maximum information in the MAP estimator. This result indicates that the measurement noise does not behave simply as a noise parameter but is important in determining the performance of the MAP retrieval estimator. The result is in agreement with that suggested by the Backus Gilbert diagnostics, and also by the simulation study.

Retrieved profiles may be represented by a small set of empirical orthogonal functions of the a priori covariance matrices without loss of physical information.

It is an overall conclusion of this work that for Nimbus 4 SCR data, at heights above approximately 25 km, the resolving power of the MAP estimators is poorer than that of the original radiance observations, and would be poorer than that of the Backus Gilbert

estimator. This result is contrary to that predicted by Conrath (1972) and reported by Rodgers (1976(a)).

It is suggested that if vertical wave-like perturbations are to be retrieved from radiance data then a method which uses a priori statistics should probably not be used, since the theoretically optimum estimator of this type produces poor a priori statistics dependent results. The Backus Gilbert diagnostics for the Backus Gilbert retrieval estimator suggest that this would be a "good" estimator for use in retrieving vertical wave structure from the satellite radiance data, since the estimator averaging kernels are essentially single peaked functions. Additionally, the intrinsic resolving power of this estimator is better than that of the satellite observations.

APPENDIX A

NIMBUS 4 SCR WEIGHTING FUNCTIONS

The satellite SCR weighting functions are represented by the equations given below.

The height variable, z, is expressed as :

$$z = \ln(p/p_o)$$

where p and p_o are as already defined.

Channel A

$$y(z) = \exp-\left[a_1 + a_2 (z-a_6) + a_3(z-a_6)^2 + a_4(z-a_6)^3 + a_5(z-a_6)^4 \right] + a_7 \exp-\left[a_8(z-a_9)^2 \right]$$

Channel B

Two separate functions are required for a suitably accurate fit to the discretized data points :

(i) for $z \leqslant 5.4$

$$y(z) = \exp-\left[a_1 + a_2(z-a_6) + a_3(z-a_6)^2 \right] \times (a_4 z + a_5 z^2)$$

(ii) For $z \geqslant 5.4$

$$y(z) = a_7 \exp-\left[a_8(z-a_9)^2 \right]$$

Channel C

$$Y(z) = \exp-\left[a_1 + a_2(z-a_6) + a_3(z-a_6)^2 + a_4(z-a_6)^3 + a_5(z-a_6)^4 \right] \times (a_7 + a_8 z + a_9^2)$$

Channel D

$$y(z) = \exp-\left[a_1 + a_2(z-a_6) + a_3(z-a_6)^2 + a_4(z-a_6)^3 + a_5(z-a_6)^4 \right] \times (a_7 + a_8 z + a_9 z^2).$$

Channel E

$$y(z) = \exp-\left[a_1 + a_2(z-a_6) + a_3(z-a_6)^2 + a_4(z-a_6)^3 + a_5(z-a_6)^4 \right] \times (a_7 + a_8 z + a_9 z^2)$$

Channel F

Two separate functions are required for a suitably accurate fit to the discretized data points :

(i) For $z \geq 0.17$

$$y(z) = \exp-\left[a_1 + a_2(z-a_6) + a_3(z-a_6)^2 + a_4(z-a_6)^3 + a_5(z-a_6)^4 \right] + a_7 \exp-\left[a_8(z-a_9)^2 \right]$$

(ii) For $Z \leq 0.17$

$$y(z) = -0.6429\, z + 0.2363.$$

The coefficients a_i, $i = 1,2,\ldots,6$ are given in table A.1 below

TABLE A.1 : Weighting Function Equation Coefficients

	Channel A	Channel B	Channel C	Channel D	Channel E	Channel F
a_1	2.977567	4.130931	1.825558	3.014476	2.540197	1.919749
a_2	0.030070	0.081956	0.135437	-0.253694	0.504519	0.139179
a_3	0.612385	0.425562	0.665981	1.066743	1.340218	1.551304
a_4	-0.203292	1.193764	-0.215337	-0.266736	-0.755421	-0.590243
a_5	0.027237	-0.023867	0.028406	0.022430	0.159017	0.061235
a_6	6.396557	4.159521	2.569883	2.055876	1.376097	0.200756
a_7	0.029149	48.052378	-0.588145	-1.165643	-0.335004	0.003193
a_8	0.427481	0.035406	0.316914	1.429447	1.342166	4.100470
a_9	5.133507	-8.592527	-0.502054	-0.026566	-0.021751	3.350990

APPENDIX B

MATIRX INVERSION LEMMA

Let A be p x m and B be m x p matrices. I_m is the m x m identity matrix, and I_p the p x p identity matrix

Then

$$- A(I_m + BA) = - (I_p + AB)A \qquad \ldots (B.1)$$

$$\therefore \quad - A(I_m + BA)(I_m + BA)^{-1} = - (I_p + AB)A(I_m + BA)^{-1} \qquad \ldots (B.2)$$

$$- AB = - (I_p + AB)A(I_m + BA)^{-1}B \qquad \ldots (B.3)$$

and $$I_p = I_p + AB - AB \qquad \ldots (B.4)$$

$$\therefore \quad I_p = (I_p + AB) - (I_p + AB)A(I_m + BA)^{-1} B \qquad \ldots (B.5)$$

Premultiplying equation (B.5) by $(I_p + AB)^{-1}$ gives

$$(I_p + AB)^{-1} = I_p - A(I_m + BA)^{-1} B \qquad \ldots (B.6)$$

If $\hat{S}$ is defined to be

$$\hat{S} \equiv (K^T S_e K + S_x^{-1})^{-1}$$

$$= (S_x K^T S_e K + I_p)^{-1} S_x \qquad \ldots (B.7)$$

and if $\hat{S}$ is chosen to be $(I_p + AB)^{-1} S_x$ then from equations (B.6) and (B.7)

$$A = S_x K^T S_e \qquad \ldots (B.8)$$

and $B = K$

the following equation arises

$$\hat{S} = [I - S_x K^T S_e (I + K S_x K^T S_e)^{-1} K] S_x \qquad \ldots (B.10)$$

therefore

$$\hat{S} = S_x - S_x K^T (K S_x K^T + S_e)^{-1} K S_x \quad \ldots (B.11)$$

This equation is the matrix inversion lemma

By a suitable matrix multiplication equation (B.1) may be rewritten thus :

$$(I_p + AB)^{-1} A = A(I_m + BA)^{-1}$$

If the substitutions of equations (B.7), (B.8), and (B.9) are applied, the following result occurs :

$$\hat{S} K^T S_e = S_x K^T (K S_x K^T + S_e)^{-1} \quad \ldots (B.12)$$

APPENDIX C

HIGH ALTITUDE METEOROLOGICAL DATA

The raw data used in the calculation of the estimator a priori observations is contained in the US Department of Commerce, Environmental Data Service magnetic tape file "Tape Deck 5850 : Rocketsonde Observations". The data included observations for years 1969 through 1972. Figure C.1 is a map of the possible locations of reporting points (as of 1970) for data in the file. However, only observations for those stations listed in table C.1 are present in the file.

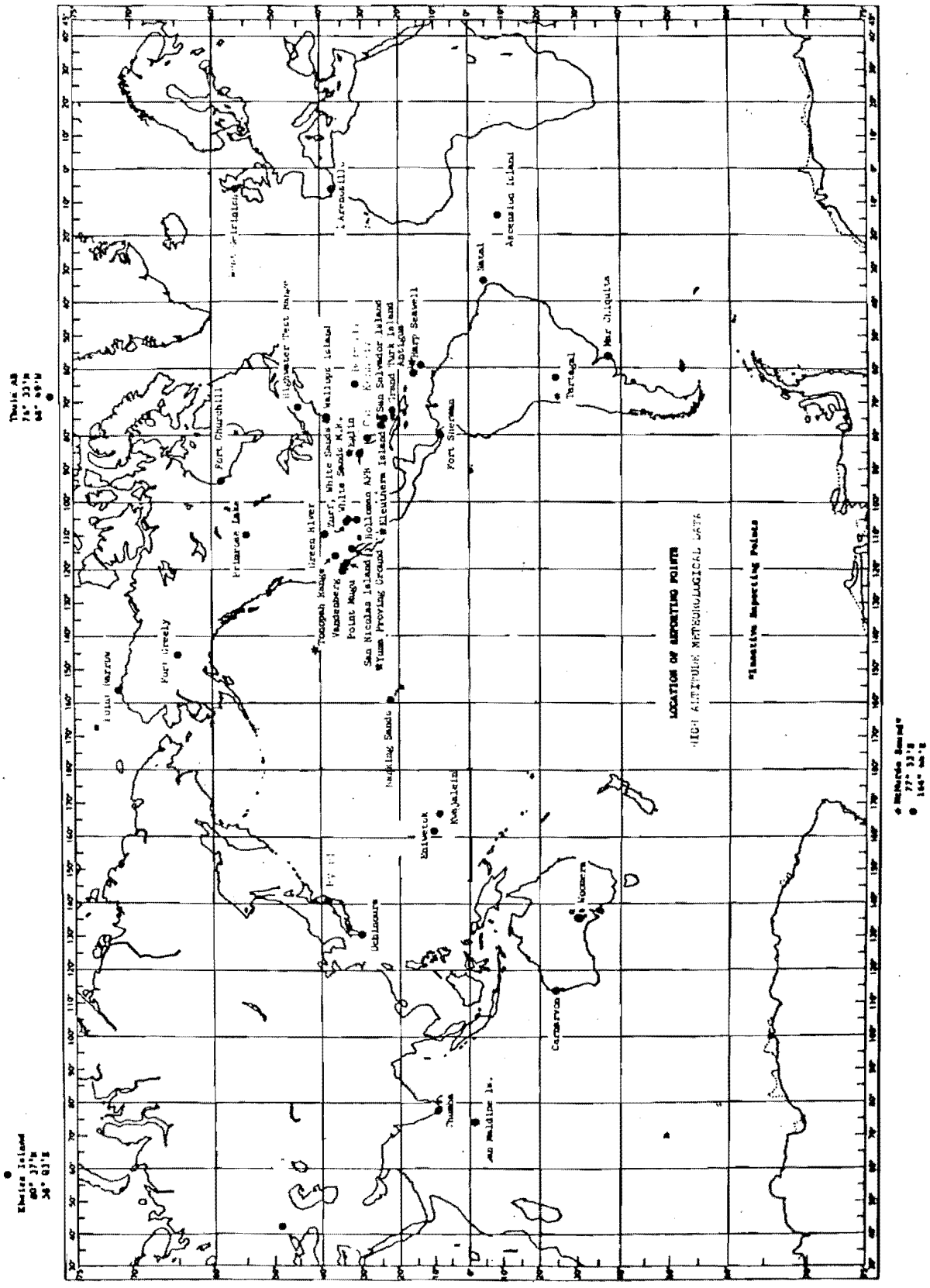

FIGURE C.1 : Map of the locations of reporting points for High Altitude Meteorological Data (in 1970) (From the World Data Centre A, Data Report : High Altitude Meteorological Data, January 1970)

TABLE C.1 : Rocketsonde-Balloonsonde Profile Data For Tape Deck 5850

Station Code	Station Name	Latitude	Longitude	Number of Profiles 1969	1970	1971	1972	Total
78861	Antigua, AAFB	17°09'N	61°47'W	78	96	59	56	289
08384	Arenosillo, Spain	37°06'N	6°44'W	13	30	23	23	89
61902	Ascension Is	7°59'S	14°25'W	140	150	154	126	570
91162	Barking Sands	22°02'N	159°47'W	179	182	227	114	702
74794	Cape Kennedy	28°27'N	80°32'W	210	100	163	173	646
72913	Ft. Churchill	58°44'N	93°49'W	130	116	56	147	449
70266	Ft. Greely	64°00'N	145°44'W	87	158	42	52	339
78783 78801	Ft. Sherman	9°20'N	79°59'W	84	104	88	123	399
72477	Green River	38°56'N	110°04'W	3	1	19	9	32
78016	Kindley AFB	32°21'N	64°39'W		1			1
91366	Kwajalein, MI	8°44'N	167°44'E	55	130	168	81	434
87689	Mar Chiquita	37°45'S	57°25'W	13	4	10	13	40
82599	Natal	5°55'N	35°10'W	3	16	5	12	36
70192	Poker Flats	65°06'N	147°30'W				38	38
74124	Primrose Lake	54°45'N	110°03'W	86	70	86	62	304
72391	Pt Mugu	34°07'N	119°07'W	222	204	221	150	797
72291	San Nicolas Is.	33°14'N	110°25'W	1	1			2
04202	Thule	76°33'N	68°49'W	81	29	57	37	204
72402	Wallops Is.	37°50'N	75°29'W	190	191	154	141	706
72269	White Sands Missile Range	32°23'N	106°29'W	341	236	231	262	1070

APPENDIX D

EQUATORIAL "SUMMER" A PRIORI DATA

The statistics were consturcted from 203 May, June and July profiles, for years 1969 through 1972. The mean profile is given below

TABLE D.1 : The Mean Profile* (^{0}C)

-16.46	-15.63	-14.28	-12.77	-11.30	- 9.98	- 8.84	- 7.87
- 7.08	- 6.44	- 5.94	- 5.62	- 5.54	- 5.67	- 6.02	- 6.60
- 7.49	- 8.74	-10.32	-12.12	-13.97	-15.76	-17.53	-19.35
-21.25	-23.21	-25.20	-27.18	-29.07	-30.79	-32.34	-33.79
-35.20	-36.57	-37.93	-39.32	-40.69	-42.00	-43.29	-44.63
-46.01	-47.50	-48.79	-50.20	-51.66	-53.12	-54.57	-56.04
-57.57	-59.13	-60.76	-62.55	-64.51	-66.61	-68.69	-70.50
-71.76	-72.38	-71.22	-69.78	-68.34	-66.62	-62.53	-58.43
-54.07	-48.80	-43.52	-38.21	-32.88	-27.44	-22.01	-16.70
-11.78	- 6.87	- 2.26	2.35	6.97	10.93	14.59	19.74
25.73							

*Listed from 8 sh altitude to ground level in steps of 0.1 sh.

The original a priori covarinace matrix is given in Table D.2. The indices indicate the height in sh (i.e. $-\ln(p/p_o)$).

TABLE D.2 : The Equatorial "summer" a priori covariance matrix

	8	7.9	7.8	7.7	7.6	7.5	7.4	7.3	7.2	7.1	7	6.9	6.8	6.7	6.6	6.5	6.4	6.3	6.2	6.1
8	31.10																			
7.9	29.17	28.61																		
7.8	25.58	26.70	27.20																	
7.7	21.43	23.64	26.07	26.99																
7.6	17.76	20.27	23.49	25.78	26.28															
7.5	14.56	16.78	19.78	22.54	24.53	24.95														
7.4	11.45	13.03	15.24	17.78	20.66	23.09	23.82													
7.3	8.518	9.377	10.68	12.69	15.75	19.31	22.21	23.27												
7.2	6.162	6.484	7.052	8.437	11.12	14.83	18.79	21.96	23.20											
7.1	4.464	4.527	4.638	5.437	7.521	10.80	14.82	18.92	22.09	23.33										
7	3.212	3.253	3.188	3.596	5.198	7.989	11.56	15.54	19.41	22.37	23.60									
6.9	2.525	2.690	2.681	2.962	4.310	6.723	9.696	12.91	16.29	19.72	22.66	24.06								
6.8	2.655	2.972	3.121	3.406	4.561	6.577	8.841	10.98	13.22	16.10	19.68	22.97	24.29							
6.7	3.418	3.823	4.099	4.378	5.254	6.739	8.220	9.291	10.35	12.29	15.61	19.67	22.86	23.78						
6.6	4.313	4.734	5.084	5.342	5.893	6.776	7.510	7.750	7.957	9.103	11.75	15.56	19.44	22.15	22.83					
6.5	4.890	5.311	5.729	5.999	6.283	6.627	6.760	6.463	6.187	6.804	8.188	11.70	15.18	18.58	21.08	21.71				
6.4	5.146	5.546	6.003	6.309	6.447	6.442	6.178	5.544	4.965	5.192	6.436	8.417	11.01	14.18	17.52	20.11	20.98			
6.3	5.525	5.862	6.271	6.566	6.653	6.508	6.049	5.190	4.382	4.216	4.876	6.034	7.756	10.28	13.52	16.97	19.72	20.72		
6.2	6.267	6.559	6.825	6.972	6.946	6.713	6.169	5.215	4.225	3.802	4.011	4.584	5.603	7.363	9.960	13.23	16.67	19.39	20.33	
6.1	7.267	7.455	7.487	7.313	7.038	6.684	6.129	5.268	4.356	3.797	3.650	3.750	4.163	5.156	6.939	9.545	12.99	16.25	19.07	20.27
6	8.059	8.148	7.916	7.424	6.975	6.628	6.210	5.623	4.943	4.343	3.871	3.535	3.448	3.824	4.910	6.830	9.520	12.86	16.48	19.66
5.9	8.250	8.232	7.863	7.340	7.042	6.981	6.897	6.585	6.053	5.389	4.663	4.028	3.653	3.697	4.392	5.840	7.928	10.65	14.06	17.97
5.8	7.677	7.596	7.292	7.032	7.117	7.495	7.816	7.707	7.164	6.424	5.628	4.945	4.524	4.485	5.074	6.311	7.923	9.935	12.61	16.14
5.7	6.652	6.588	6.479	6.543	6.947	7.678	8.360	8.429	7.900	7.230	6.592	6.055	5.704	5.656	6.215	7.332	8.591	9.998	11.87	14.50
5.6	5.783	5.765	5.838	6.117	6.666	7.578	8.497	8.742	8.360	7.928	7.553	7.184	6.879	6.782	7.233	8.176	9.145	10.09	11.65	13.95
5.5	5.354	5.325	5.451	5.802	6.404	7.401	8.450	8.849	8.666	8.464	8.264	7.958	7.627	7.436	7.720	8.462	9.233	9.895	10.56	11.54
5.4	5.189	5.075	5.119	5.425	6.027	7.080	8.229	8.777	8.757	8.658	8.479	8.144	7.780	7.550	7.729	8.309	8.936	9.449	9.858	10.44
5.3	5.031	4.830	4.727	4.898	5.463	6.580	7.853	8.547	8.612	8.490	8.272	7.958	7.674	7.530	7.680	8.071	8.465	8.827	9.174	9.657
5.2	4.736	4.491	4.224	4.230	4.801	6.063	7.521	8.370	8.454	8.216	7.955	7.757	7.625	7.541	7.572	7.684	7.795	8.030	8.446	9.067
5.1	4.294	4.026	3.606	3.500	4.185	5.679	7.349	8.363	8.469	8.104	7.796	7.716	7.678	7.517	7.316	7.156	7.084	7.270	7.771	8.563
5	3.903	3.632	3.121	2.951	3.716	5.326	7.070	8.164	8.328	7.955	7.675	7.700	7.722	7.494	7.143	6.839	6.682	6.833	7.331	8.166
4.9	3.709	3.537	3.007	2.761	3.410	4.864	6.446	7.481	7.729	7.506	7.369	7.497	7.595	7.435	7.121	6.800	6.578	6.644	7.078	7.881
4.8	3.629	3.698	3.232	2.929	3.362	4.522	5.829	6.718	7.032	7.017	7.030	7.179	7.308	7.289	7.140	6.889	6.602	6.524	6.843	7.587
4.7	3.936	3.878	3.579	3.314	3.609	4.541	5.603	6.306	6.598	6.697	6.765	6.847	6.958	7.086	7.159	7.046	6.715	6.433	6.529	7.135
4.6	3.934	3.986	3.843	3.652	3.877	4.638	5.486	5.989	6.177	6.264	6.301	6.307	6.395	6.633	6.912	6.969	6.640	6.195	6.044	6.490
4.5	4.165	4.209	4.095	3.910	4.030	4.579	5.176	5.465	5.515	5.517	5.489	5.443	5.513	5.817	6.250	6.450	6.165	5.664	5.442	5.816
4.4	4.620	4.576	4.384	4.130	4.109	4.423	4.747	4.811	4.709	4.590	4.473	4.382	4.441	4.802	5.359	5.673	5.468	5.060	4.928	5.311
4.3	4.882	4.747	4.446	4.097	3.964	4.118	4.261	4.178	3.961	3.727	3.525	3.398	3.443	3.822	4.447	4.856	4.779	4.547	4.576	4.987
4.2	4.690	4.498	4.105	3.674	3.488	3.605	3.731	3.648	3.415	3.142	2.912	2.774	2.765	3.031	3.568	4.001	4.058	4.013	4.203	4.651
4.1	4.136	3.952	3.544	3.090	2.910	3.080	3.301	3.308	3.129	2.900	2.723	2.607	2.505	2.529	2.810	3.142	3.268	3.346	3.633	4.122
4	3.436	3.333	3.013	2.611	2.461	2.676	2.975	3.057	2.928	2.772	2.705	2.665	2.508	2.298	2.281	2.432	2.522	2.614	2.905	3.409
3.9	2.738	2.736	2.539	2.207	2.058	2.240	2.529	2.634	2.545	2.472	2.545	2.641	2.514	2.181	1.941	1.886	1.845	1.854	2.083	2.560
3.8	1.972	2.030	1.921	1.648	1.502	1.643	1.894	2.005	1.970	1.994	2.204	2.439	2.394	2.032	1.645	1.388	1.167	1.044	1.178	1.576
3.7	1.070	1.148	1.112	.9450	.8720	1.020	1.241	1.338	1.340	1.446	1.754	2.080	2.115	1.787	1.339	.9488	.5905	.3494	.3606	.6075
3.6	.1257	.2142	.2831	.2830	.3090	.4409	.6017	.6711	.7045	.8691	1.204	1.530	1.597	1.343	.9507	.5718	.2105	-.075	-.194	-.139
3.5	-.883	-.765	-.572	-.407	-.313	-.226	-.112	-.014	.1127	.3529	.6650	.8924	.9049	.7126	.4396	.1777	-.073	-.311	-.505	-.609
3.4	-1.84	-1.70	-1.44	-1.20	-1.08	-.996	-.854	-.652	-.371	-.007	.3176	.4541	.3752	.1815	-.028	-.223	-.405	-.581	-.763	-.921
3.3	-2.29	-2.18	-1.98	-1.79	-1.68	-1.57	-1.36	-1.03	-.605	-.133	.2216	.3197	.1748	-.066	-.316	-.589	-.864	-1.08	-1.23	-1.33
3.2	-2.21	-2.18	-2.10	-2.01	-1.92	-1.76	-1.50	-1.07	-.557	-.077	.2132	.2362	.0396	-.236	-.541	-.929	-1.37	-1.72	-1.91	-1.95
3.1	-2.04	-2.10	-2.12	-2.10	-2.04	-1.91	-1.62	-1.15	-.622	-.193	-.041	-.165	-.450	-.746	-1.04	-1.40	-1.86	-2.30	-2.56	-2.61
3	-2.11	-2.22	-2.33	-2.36	-2.35	-2.28	-2.05	-1.59	-1.05	-.655	-.590	-.843	-1.25	-1.60	-1.86	-2.12	-2.44	-2.81	-3.09	-3.19
2.9	-2.51	-2.68	-2.85	-2.93	-2.96	-2.92	-2.69	-2.23	-1.65	-1.23	-1.15	-1.42	-1.88	-2.29	-2.59	-2.83	-3.06	-3.36	-3.61	-3.71
2.8	-3.14	-3.37	-3.61	-3.74	-3.75	-3.66	-3.40	-2.92	-2.34	-1.89	-1.71	-1.85	-2.20	-2.60	-2.96	-3.29	-3.60	-3.92	-4.13	-4.15
2.7	-3.61	-3.89	-4.20	-4.37	-4.38	-4.27	-4.02	-3.63	-3.17	-2.77	-2.48	-2.40	-2.55	-2.83	-3.17	-3.57	-3.97	-4.31	-4.42	-4.32
2.6	-3.76	-4.06	-4.39	-4.59	-4.62	-4.51	-4.30	-4.05	-3.83	-3.59	-3.32	-3.11	-3.06	-3.16	-3.41	-3.80	-4.21	-4.51	-4.53	-4.37
2.5	-3.88	-4.17	-4.48	-4.66	-4.68	-4.53	-4.26	-4.08	-4.04	-4.02	-3.88	-3.66	-3.50	-3.45	-3.62	-4.00	-4.41	-4.69	-4.70	-4.60
2.4	-4.11	-4.39	-4.68	-4.84	-4.85	-4.63	-4.26	-3.99	-3.99	-4.08	-4.03	-3.85	-3.64	-3.54	-3.69	-4.07	-4.48	-4.76	-4.80	-4.76
2.3	-4.14	-4.47	-4.81	-5.01	-5.03	-4.80	-4.36	-4.00	-3.92	-3.99	-3.97	-3.82	-3.62	-3.49	-3.58	-3.89	-4.26	-4.52	-4.59	-4.58
2.2	-3.57	-3.79	-4.02	-4.15	-4.13	-3.86	-3.39	-2.98	-2.80	-2.75	-2.65	-2.47	-2.32	-2.28	-2.43	-2.73	-3.08	-3.36	-3.51	-3.58
2.1	-2.71	-2.84	-2.97	-3.04	-2.99	-2.73	-2.33	-1.99	-1.81	-1.72	-1.57	-1.41	-1.31	-1.33	-1.48	-1.75	-2.06	-2.33	-2.50	-2.62
2	-1.81	-1.83	-1.87	-1.88	-1.78	-1.54	-1.21	-.946	-.784	-.644	-.465	-.314	-.275	-.350	-.513	-.745	-1.01	-1.27	-1.47	-1.64
1.9	-.992	-.921	-.861	-.820	-.722	-.539	-.335	-.171	.021	.1861	.4187	.5654	.5638	.4503	.2862	.0850	-.160	-.420	-.656	-.861
1.8	-.506	-.428	-.296	-.155	-.038	.0373	.0434	-.002	.0056	.1365	.3349	.5060	.5866	.5654	.4716	.3261	.1577	.0011	-.156	-.304
1.7	.0674	.1637	.2803	.3258	.3504	.3916	.4626	.1721	.0085	.0454	.1969	.3843	.5454	.6192	.6004	.5174	.4412	.4138	.3652	.2958
1.6	.5463	.6528	.7767	.8269	.8395	.8213	.7773	.4776	.2030	-.074	.0327	.2276	.4484	.5985	.6515	.6413	.6651	.7646	.8194	.8202
1.5	.8593	.9348	1.069	1.146	1.220	1.283	.7823	.2557	-.090	-.075	.0316	.1987	.4234	.5788	.6732	.7424	.8496	1.015	1.120	1.165
1.4	1.209	1.248	1.422	1.634	1.642	1.339	.7061	.2205	-.072	-.069	.0299	.1987	.3940	.5515	.6904	.8462	1.042	1.276	1.457	1.531
1.3	1.743	1.744	1.844	1.961	1.870	1.473	.8517	.2621	-.098	.0188	.1220	.2554	.4206	.5641	.7417	.9003	1.287	1.609	1.859	2.042
1.2	2.271	2.248	2.279	2.295	2.100	1.612	.9272	.3146	.0572	.1054	.2098	.3242	.4611	.5817	.7790	.9696	1.471	1.871	2.210	2.488
1.1	1.982	1.996	2.055	2.095	1.967	1.592	1.033	.5297	.3474	.4499	.6116	.7674	.8899	.9373	1.038	1.262	1.546	1.867	2.177	2.481
1	1.627	1.674	1.761	1.836	1.796	1.560	1.158	.7959	.7084	.8728	1.098	1.303	1.411	1.376	1.371	1.493	1.674	1.900	2.166	2.495
0.9	1.280	1.382	1.522	1.640	1.663	1.514	1.197	.8979	.8665	1.100	1.390	1.622	1.709	1.612	1.523	1.578	1.714	1.901	2.139	2.447
0.8	.6472	.8054	1.068	1.331	1.467	1.377	1.080	.7818	.7409	.9743	1.280	1.520	1.597	1.481	1.373	1.455	1.690	1.969	2.181	2.342
0.7	.0598	.2539	.6189	1.020	1.266	1.237	.9604	.6555	.5976	.8390	1.182	1.459	1.567	1.473	1.368	1.452	1.724	2.024	2.158	2.148
0.6	.1931	.3186	.6003	.9361	1.129	1.047	.7361	.4317	.3835	.6227	.9739	1.272	1.401	1.347	1.305	1.442	1.731	2.018	2.125	2.082
0.5	.3556	.4056	.5959	.8605	.9957	.8615	.5133	.1987	.1474	.3774	.7364	1.062	1.224	1.220	1.251	1.448	1.754	2.026	2.100	2.015
0.4	.5478	.5053	.5870	.7684	.8342	.6359	.2446	-.078	-.119	.1222	.5042	.8646	1.070	1.135	1.253	1.506	1.808	2.036	2.051	1.913
0.3	1.420	1.192	1.035	1.032	.9637	.6500	.1486	-.309	-.528	-.519	-.409	-.226	.0084	.2320	.5175	.9410	1.418	1.764	1.833	1.767
0.2	2.894	2.454	1.992	1.734	1.476	.9904	.2894	-.458	-1.06	-1.51	-1.88	-2.00	-1.74	-1.28	-.750	-.120	.5568	1.052	1.224	1.297
0.1	2.706	2.306	1.902	1.715	1.526	1.047	.3172	-.332	-.673	-.864	-1.12	-1.26	-1.08	-.712	-.230	.3797	1.021	1.448	1.530	1.550
0	2.604	2.256	1.877	1.690	1.522	1.112	.6547	.6807	1.319	2.046	2.319	2.107	1.656	1.269	1.299	1.843	2.614	3.197	3.320	3.140

	6	5.9	5.8	5.7	5.6	5.5	5.4	5.3	5.2	5.1	5	4.9	4.8	4.7	4.6	4.5	4.4	4.3	4.2	4.1
8																				
7.9																				
7.8																				
7.7																				
7.6																				
7.5																				
7.4																				
7.3																				
7.2																				
7.1																				
7																				
6.9																				
6.8																				
6.7																				
6.6																				
6.5																				
6.4																				
6.3																				
6.2																				
6.1																				
6	21.56																			
5.9	21.71	24.10																		
5.8	20.36	24.26	26.39																	
5.7	18.14	22.37	25.93	27.38																
5.6	15.66	19.40	23.33	26.12	26.65															
5.5	13.45	16.41	19.82	22.62	24.58	24.40														
5.4	11.77	13.98	16.53	18.92	20.93	22.29	22.39													
5.3	10.68	12.29	14.08	15.68	17.28	19.15	20.87	21.31												
5.2	10.05	11.32	12.54	13.50	14.47	16.00	18.07	19.78	19.99											
5.1	9.632	10.75	11.60	12.08	12.51	13.40	14.96	16.90	18.42	18.66										
5	9.269	10.29	10.91	11.11	11.20	11.56	12.39	13.86	15.77	17.28	17.43									
4.9	8.932	9.827	10.30	10.39	10.30	10.27	10.52	11.41	13.02	14.84	16.00	15.86								
4.8	8.576	9.384	9.786	9.838	9.638	9.350	9.276	9.796	10.97	12.42	13.72	14.42	14.10							
4.7	8.094	8.952	9.417	9.490	9.239	8.837	8.633	8.963	9.751	10.63	11.45	12.20	12.68	12.50						
4.6	7.444	8.432	9.036	9.183	8.957	8.535	8.254	8.408	8.865	9.242	9.471	9.828	10.55	11.35	11.46					
4.5	6.755	7.805	8.487	8.669	8.503	8.071	7.703	7.689	7.910	7.990	7.844	7.839	8.445	9.585	10.52	10.59				
4.4	6.175	7.132	7.743	7.918	7.745	7.307	6.890	6.796	6.938	6.945	6.695	6.531	6.913	7.860	8.954	9.741	9.836			
4.3	5.710	6.457	6.916	7.041	6.880	6.445	6.004	5.898	6.073	6.158	5.988	5.821	5.996	6.543	7.351	8.313	9.074	9.154		
4.2	5.257	5.834	6.201	6.333	6.196	5.738	5.237	5.084	5.269	5.434	5.383	5.272	5.304	5.512	5.960	6.749	7.699	8.382	8.369	
4.1	4.716	5.277	5.650	5.818	5.686	5.205	4.638	4.381	4.466	4.607	4.625	4.576	4.553	4.588	4.822	5.384	6.192	7.019	7.507	7.291
4	4.060	4.700	5.121	5.259	5.114	4.677	4.136	3.802	3.748	3.797	3.833	3.846	3.827	3.816	3.965	4.357	4.919	5.559	6.138	6.393
3.9	3.234	3.907	4.308	4.389	4.248	3.928	3.528	3.213	3.079	3.045	3.070	3.135	3.171	3.175	3.279	3.544	3.893	4.285	4.728	5.154
3.8	2.174	2.771	3.095	3.113	2.983	2.790	2.563	2.376	2.262	2.193	2.201	2.308	2.419	2.459	2.516	2.667	2.865	3.093	3.396	3.802
3.7	1.031	1.477	1.708	1.681	1.551	1.436	1.369	1.349	1.340	1.307	1.313	1.427	1.564	1.605	1.599	1.648	1.755	1.917	2.161	2.511
3.6	.0867	.3984	.5946	.5838	.4681	.3899	.4119	.5020	.5798	.5880	.5855	.6606	.7539	.7473	.6831	.6707	.7387	.8960	1.134	1.445
3.5	-.532	-.281	-.038	.0378	-.016	-.062	-.033	.0457	.1097	.1021	.0640	.0777	.1056	.0564	-.030	-.059	-.008	.1316	.3353	.5914
3.4	-.927	-.723	-.467	-.346	-.343	-.337	-.284	-.203	-.134	-.143	-.209	-.247	-.263	-.324	-.409	-.457	-.446	-.370	-.243	-.065
3.3	-1.33	-1.17	-.989	-.941	-.957	-.888	-.713	-.491	-.293	-.219	-.278	-.358	-.393	-.421	-.480	-.562	-.626	-.626	-.564	-.439
3.2	-1.88	-1.70	-1.58	-1.63	-1.72	-1.61	-1.29	-.880	-.508	-.298	-.309	-.423	-.479	-.458	-.447	-.512	-.614	-.659	-.626	-.525
3.1	-2.51	-2.31	-2.19	-2.30	-2.46	-2.35	-1.95	-1.44	-.953	-.612	-.537	-.650	-.745	-.717	-.622	-.569	-.586	-.602	-.575	-.494
3	-3.12	-2.96	-2.88	-3.05	-3.25	-3.15	-2.73	-2.20	-1.66	-1.24	-1.08	-1.15	-1.26	-1.26	-1.10	-.871	-.713	-.637	-.585	-.494
2.9	-3.67	-3.57	-3.56	-3.79	-4.02	-3.93	-3.52	-2.98	-2.42	-1.98	-1.78	-1.78	-1.86	-1.85	-1.63	-1.26	-.936	-.753	-.632	-.470
2.8	-4.08	-4.00	-4.04	-4.30	-4.57	-4.54	-4.19	-3.66	-3.08	-2.64	-2.41	-2.35	-2.35	-2.31	-2.03	-1.57	-1.14	-.852	-.630	-.375
2.7	-4.22	-4.20	-4.28	-4.58	-4.94	-5.02	-4.75	-4.23	-3.64	-3.19	-2.96	-2.84	-2.77	-2.64	-2.33	-1.84	-1.35	-.970	-.634	-.296
2.6	-4.31	-4.38	-4.53	-4.90	-5.36	-5.54	-5.27	-4.68	-4.04	-3.64	-3.44	-3.30	-3.13	-2.93	-2.58	-2.08	-1.60	-1.16	-.734	-.308
2.5	-4.62	-4.72	-4.86	-5.25	-5.80	-6.03	-5.57	-4.90	-4.18	-3.81	-3.71	-3.61	-3.42	-3.16	-2.78	-2.30	-1.85	-1.42	-.935	-.416
2.4	-4.81	-4.87	-4.94	-5.31	-5.92	-6.17	-5.71	-4.79	-3.97	-3.60	-3.57	-3.57	-3.44	-3.21	-2.85	-2.41	-2.01	-1.61	-1.09	-.513
2.3	-4.67	-4.72	-4.73	-5.09	-5.72	-5.96	-5.40	-4.32	-3.35	-2.92	-2.98	-3.14	-3.15	-3.02	-2.73	-2.35	-1.98	-1.59	-1.08	-.515
2.2	-3.67	-3.69	-3.66	-3.90	-4.35	-4.47	-3.96	-3.07	-2.30	-1.95	-2.00	-2.17	-2.26	-2.23	-2.06	-1.82	-1.60	-1.34	-.944	-.461
2.1	-2.75	-2.79	-2.77	-2.94	-3.22	-3.22	-2.76	-2.07	-1.50	-1.26	-1.30	-1.43	-1.53	-1.54	-1.44	-1.29	-1.16	-1.00	-.730	-.357
2	-1.79	-1.84	-1.84	-1.93	-2.04	-1.92	-1.53	-1.04	-.679	-.542	-.568	-.657	-.761	-.825	-.799	-.744	-.719	-.650	-.507	-.266
1.9	-1.02	-1.08	-1.09	-1.11	-1.05	-.834	-.522	-.266	-.144	-.121	-.117	-.125	-.197	-.280	-.312	-.351	-.420	-.450	-.392	-.235
1.8	-.360	-.288	-.163	-.049	.0754	.1901	.2329	.2128	.1846	.1774	.2084	.2364	.1893	.1098	.0532	-.027	-.135	-.204	-.201	-.127
1.7	.3421	.5357	.7855	1.048	1.259	1.254	.9863	.6533	.4635	.4376	.5110	.5868	.5707	.4972	.4162	.2951	.1537	.0498	-.006	-.028
1.6	.9513	1.249	1.615	2.015	2.298	2.170	1.611	.9936	.6609	.6195	.7304	.8521	.8756	.8232	.7325	.5829	.4190	.2941	.1966	.0900
1.5	1.334	1.671	2.083	2.542	2.863	2.691	1.995	1.209	.7441	.6507	.7824	.9508	1.019	.9960	.9011	.7233	.5432	.4263	.3426	.2280
1.4	1.751	2.127	2.579	3.095	3.454	3.233	2.390	1.422	.8131	.6607	.8154	1.039	1.163	1.176	1.077	.8683	.6701	.5621	.4947	.3738
1.3	2.346	2.793	3.312	3.890	4.251	3.923	2.897	1.736	.9694	.7260	.8531	1.118	1.299	1.372	1.301	1.085	.8726	.7645	.7091	.5824
1.2	2.870	3.370	3.935	4.563	4.930	4.508	3.314	1.974	1.061	.7397	.8718	1.161	1.397	1.527	1.486	1.263	1.031	.9172	.8724	.7430
1.1	2.898	3.401	3.940	4.543	4.917	4.551	3.432	2.138	1.237	.9311	1.087	1.387	1.610	1.708	1.624	1.341	1.022	.8200	.7275	.5947
1	2.956	3.475	3.992	4.559	4.925	4.615	3.591	2.367	1.494	1.205	1.379	1.682	1.886	1.945	1.812	1.462	1.045	.7430	.5939	.4563
0.9	2.876	3.353	3.850	4.425	4.850	4.594	3.645	2.450	1.564	1.268	1.459	1.775	1.963	1.984	1.906	1.402	.9225	.5672	.3963	.2680
0.8	2.578	2.929	3.429	4.054	4.660	4.214	3.294	2.142	1.283	1.001	1.203	1.534	1.750	1.738	1.543	1.155	.7320	.4416	.2975	.1619
0.7	2.207	2.471	3.001	3.581	4.108	3.804	3.035	1.913	1.021	.6787	.8535	1.199	1.419	1.423	1.223	.8471	.4641	.2278	.1211	.0179
0.6	2.125	2.381	2.887	3.562	4.028	3.842	2.990	1.925	1.164	.9380	1.127	1.404	1.521	1.448	1.210	.8380	.4704	.2465	.1503	.0562
0.5	2.035	2.286	2.777	3.456	3.965	3.812	2.970	1.967	1.341	1.231	1.428	1.622	1.632	1.470	1.196	.8333	.4832	.2730	.1896	.1072
0.4	1.921	2.191	2.681	3.362	3.917	3.811	2.992	2.048	1.537	1.512	1.599	1.810	1.716	1.472	1.166	.8085	.4668	.2645	.2006	.1333
0.3	1.918	2.375	2.975	3.566	3.875	3.569	2.688	1.724	1.158	1.040	1.122	1.208	1.186	1.046	.8867	.7527	.6348	.5660	.5752	.5663
0.2	1.649	2.328	3.046	3.480	3.424	2.861	1.932	.9071	.1318	-.259	-.367	-.260	-.063	.0725	.2287	.5016	.7820	.9511	1.102	1.153
0.1	1.909	2.587	3.285	3.776	3.872	3.409	2.420	1.247	.3521	-.081	-.130	.0994	.3956	.5430	.5837	.6556	.7649	.8455	.9063	.8794
0	3.065	3.273	3.772	4.476	4.975	4.706	3.555	2.099	1.045	.6022	.7007	1.135	1.488	1.451	1.070	.6442	.4082	.3466	.2937	.0970

	4	3.9	3.8	3.7	3.6	3.5	3.4	3.3	3.2	3.1	3	2.9	2.8	2.7	2.6	2.5	2.4	2.3	2.2	2.1
8																				
7.9																				
7.8																				
7.7																				
7.6																				
7.5																				
7.4																				
7.3																				
7.2																				
7.1																				
7																				
6.9																				
6.8																				
6.7																				
6.6																				
6.5																				
6.4																				
6.3																				
6.2																				
6.1																				
6																				
5.9																				
5.8																				
5.7																				
5.6																				
5.5																				
5.4																				
5.3																				
5.2																				
5.1																				
5																				
4.9																				
4.8																				
4.7																				
4.6																				
4.5																				
4.4																				
4.3																				
4.2																				
4.1																				
4	6.149																			
3.9	5.402	5.229																		
3.8	4.241	4.466	4.199																	
3.7	2.945	3.319	3.454	3.273																
3.6	1.810	2.169	2.493	2.791	2.953															
3.5	.8845	1.189	1.557	2.102	2.776	3.216														
3.4	.1689	.4523	.8363	1.442	2.306	3.142	3.525													
3.3	-.236	.0525	.4595	1.050	1.861	2.736	3.351	3.483												
3.2	-.344	-.065	.3411	.9030	1.606	2.318	2.868	3.166	3.162											
3.1	-.338	-.094	.2729	.7930	1.414	1.966	2.341	2.625	2.873	2.993										
3	-.329	-.096	.2258	.6874	1.250	1.720	1.980	2.182	2.512	2.958	3.364									
2.9	-.237	.0298	.3272	.7292	1.244	1.682	1.895	2.028	2.321	2.866	3.579	4.207								
2.8	-.067	.2471	.5506	.9201	1.395	1.798	1.972	2.056	2.285	2.776	3.557	4.476	5.154							
2.7	.0605	.4139	.7518	1.128	1.568	1.908	2.022	2.072	2.266	2.690	3.411	4.392	5.350	5.952						
2.6	.1079	.5137	.9068	1.316	1.733	2.008	2.073	2.113	2.306	2.710	3.372	4.282	5.290	6.190	6.881					
2.5	.0921	.5781	1.042	1.503	1.936	2.207	2.277	2.330	2.534	2.938	3.571	4.400	5.326	6.303	7.345	8.312				
2.4	.0596	.6056	1.122	1.630	2.107	2.431	2.554	2.627	2.825	3.217	3.827	4.604	5.444	6.360	7.515	8.837	9.791			
2.3	.0539	.6112	1.147	1.683	2.210	2.598	2.762	2.821	2.981	3.345	3.933	4.696	5.517	6.380	7.465	8.808	9.940	10.51		
2.2	.0499	.5419	.9949	1.428	1.837	2.129	2.248	2.287	2.410	2.694	3.140	3.713	4.339	4.995	5.823	6.908	7.900	8.433	7.003	
2.1	.0391	.4384	.8032	1.135	1.423	1.607	1.659	1.667	1.758	1.973	2.299	2.710	3.186	3.653	4.257	5.047	5.776	6.175	5.305	4.226
2	.0313	.3316	.6055	.8320	.9974	1.069	1.052	1.027	1.083	1.228	1.428	1.671	1.953	2.268	2.646	3.132	3.583	3.835	3.541	3.099
1.9	-.007	.2277	.4251	.5632	.6285	.6108	.5352	.4773	.4964	.5723	.6605	.7588	.8922	1.052	1.219	1.419	1.603	1.706	1.901	2.017
1.8	-.012	.0921	.1743	.2363	.2723	.2631	.2105	.1642	.1542	.1507	.1274	.0938	.0867	.1231	.1723	.2155	.2496	.2610	.5856	.8644
1.7	-.052	-.100	-.144	-.156	-.139	-.129	-.153	-.184	-.225	-.315	-.462	-.644	-.809	-.914	-1.00	-1.15	-1.29	-1.39	-.923	-.455
1.6	-.095	-.258	-.419	-.496	-.497	-.474	-.472	-.489	-.554	-.715	-.963	-1.27	-1.57	-1.79	-1.99	-2.29	-2.60	-2.79	-2.22	-1.60
1.5	.0284	-.232	-.460	-.602	-.672	-.708	-.732	-.753	-.827	-1.01	-1.29	-1.64	-1.99	-2.24	-2.47	-2.83	-3.22	-3.49	-2.84	-2.11
1.4	.1297	-.201	-.501	-.715	-.866	-.970	-1.02	-1.05	-1.13	-1.34	-1.65	-2.05	-2.46	-2.74	-2.99	-3.41	-3.91	-4.25	-3.51	-2.68
1.3	.2879	-.126	-.513	-.812	-1.05	-1.21	-1.30	-1.34	-1.44	-1.67	-2.04	-2.51	-2.98	-3.29	-3.56	-4.04	-4.63	-5.05	-4.22	-3.26
1.2	.4043	-.085	-.549	-.919	-1.22	-1.45	-1.57	-1.63	-1.74	-2.00	-2.41	-2.94	-3.47	-3.83	-4.13	-4.67	-5.34	-5.84	-4.92	-3.83
1.1	.2733	-.196	-.647	-1.02	-1.33	-1.56	-1.69	-1.76	-1.88	-2.14	-2.55	-3.08	-3.61	-4.01	-4.38	-4.99	-5.70	-6.20	-5.18	-4.00
1	.1567	-.287	-.725	-1.10	-1.43	-1.68	-1.82	-1.89	-2.02	-2.29	-2.69	-3.20	-3.74	-4.18	-4.62	-5.31	-6.04	-6.54	-5.41	-4.14
0.9	-.006	-.427	-.853	-1.22	-1.54	-1.78	-1.91	-1.99	-2.12	-2.39	-2.78	-3.27	-3.80	-4.26	-4.77	-5.53	-6.29	-6.79	-5.59	-4.26
0.8	-.112	-.522	-.943	-1.29	-1.55	-1.70	-1.77	-1.84	-1.98	-2.24	-2.58	-3.00	-3.44	-3.86	-4.37	-5.13	-5.87	-6.33	-5.22	-3.98
0.7	-.201	-.560	-.964	-1.31	-1.53	-1.62	-1.64	-1.72	-1.89	-2.14	-2.44	-2.78	-3.14	-3.49	-3.98	-4.71	-5.41	-5.84	-4.79	-3.65
0.6	-.147	-.484	-.869	-1.19	-1.38	-1.45	-1.49	-1.60	-1.79	-2.04	-2.33	-2.67	-3.04	-3.38	-3.85	-4.55	-5.25	-5.63	-4.64	-3.56
0.5	-.078	-.393	-.759	-1.05	-1.20	-1.25	-1.32	-1.46	-1.67	-1.92	-2.20	-2.55	-2.92	-3.25	-3.68	-4.35	-5.04	-5.37	-4.45	-3.44
0.4	.0160	-.253	-.595	-.868	-.997	-1.05	-1.15	-1.34	-1.57	-1.81	-2.09	-2.43	-2.80	-3.12	-3.49	-4.12	-4.77	-5.06	-4.20	-3.28
0.3	.4015	.0775	-.265	-.495	-.588	-.639	-.765	-.969	-1.18	-1.39	-1.63	-1.92	-2.22	-2.45	-2.69	-3.16	-3.73	-4.06	-3.43	-2.72
0.2	.9327	.5163	.1672	-.003	-.042	-.078	-.234	-.464	-.658	-.811	-.961	-1.13	-1.30	-1.37	-1.41	-1.68	-2.14	-2.60	-2.32	-1.91
0.1	.6183	.2026	-.163	-.426	-.590	-.661	-.732	-.857	-1.03	-1.24	-1.47	-1.69	-1.91	-2.02	-2.12	-2.51	-3.07	-3.50	-3.02	-2.42
0	-.308	-.849	-1.47	-2.10	-2.57	-2.72	-2.65	-2.60	-2.73	-3.00	-3.32	-3.75	-4.23	-4.60	-5.09	-6.05	-7.13	-7.54	-6.26	-4.79

	2	1.9	1.8	1.7	1.6	1.5	1.4	1.3	1.2	1.1	1	0.9	0.8	0.7	0.6	0.5	0.4	0.3	0.2	0.1	0
8																					
7.9																					
7.8																					
7.7																					
7.6																					
7.5																					
7.4																					
7.3																					
7.2																					
7.1																					
7																					
6.9																					
6.8																					
6.7																					
6.6																					
6.5																					
6.4																					
6.3																					
6.2																					
6.1																					
6																					
5.9																					
5.8																					
5.7																					
5.6																					
5.5																					
5.4																					
5.3																					
5.2																					
5.1																					
5																					
4.9																					
4.8																					
4.7																					
4.6																					
4.5																					
4.4																					
4.3																					
4.2																					
4.1																					
4																					
3.9																					
3.8																					
3.7																					
3.6																					
3.5																					
3.4																					
3.3																					
3.2																					
3.1																					
3																					
2.9																					
2.8																					
2.7																					
2.6																					
2.5																					
2.4																					
2.3																					
2.2																					
2.1																					
2	2.633																				
1.9	2.130	2.166																			
1.8	1.150	1.377	1.157																		
1.7	.0297	.4756	.8831	1.311																	
1.6	-.952	-.327	.6171	1.646	2.505																
1.5	-1.35	-.621	.4552	1.634	2.649	2.986															
1.4	-1.80	-.949	.2673	1.606	2.784	3.335	3.921														
1.3	-2.25	-1.28	.0683	1.555	2.887	3.640	4.452	5.257													
1.2	-2.70	-1.60	-.139	1.480	2.949	3.886	4.905	5.964	6.917												
1.1	-2.77	-1.59	-.143	1.467	2.922	3.850	4.861	5.905	6.879	7.093											
1	-2.82	-1.56	-.130	1.456	2.881	3.793	4.786	5.805	6.789	7.279	7.772										
0.9	-2.87	-1.55	-.148	1.417	2.814	3.699	4.663	5.639	6.615	7.296	7.992	8.415									
0.8	-2.69	-1.48	-.148	1.328	2.642	3.441	4.305	5.172	6.029	6.585	7.154	7.638	7.550								
0.7	-2.46	-1.33	-.074	1.291	2.498	3.202	3.960	4.726	5.460	5.882	6.321	6.851	7.410	7.984							
0.6	-2.43	-1.36	-.095	1.292	2.516	3.182	3.900	4.617	5.309	5.674	6.042	6.461	6.765	7.079	6.680						
0.5	-2.38	-1.37	-.106	1.298	2.535	3.159	3.831	4.494	5.136	5.437	5.730	6.027	6.059	6.092	6.232	6.363					
0.4	-2.31	-1.36	-.092	1.318	2.554	3.131	3.754	4.361	4.947	5.179	5.392	5.558	5.277	5.054	5.753	6.486	7.262				
0.3	-1.97	-1.22	-.057	1.239	2.404	2.998	3.636	4.244	4.801	4.823	4.811	4.753	4.384	4.042	4.710	5.417	6.157	6.572			
0.2	-1.46	-.982	-.033	1.029	2.037	2.664	3.334	3.969	4.519	4.253	3.921	3.585	3.208	2.850	3.206	3.597	3.994	6.697	10.60		
0.1	-1.78	-1.11	-.015	1.165	2.276	2.989	3.757	4.516	5.159	4.970	4.741	4.467	4.074	3.767	3.927	4.103	4.323	6.370	9.278	9.409	
0	-3.25	-1.79	-.343	1.247	2.695	3.597	4.575	5.570	6.476	6.577	6.653	6.737	6.561	6.379	6.219	6.036	5.851	5.478	4.792	7.814	19.91

APPENDIX E

EQUATORIAL "WINTER" A PRIORI DATA

The statistics were constructed from 155 December, January, February profiles, for years 1969 through 1972. The mean profile is given below :

TABLE E.1 : The Mean Profile* (^{0}C)

-12.89	-12.27	-11.26	-10.15	- 9.11	- 8.20	- 7.42	- 6.69
- 5.97	- 5.37	- 4.96	- 4.65	- 4.32	- 4.06	- 4.12	- 4.68
- 5.74	- 7.16	- 8.85	-10.90	-13.27	-15.82	-18.36	-20.82
-23.15	-25.33	-27.35	-29.25	-31.08	-32.90	-34.74	-36.58
-38.31	-39.84	-41.23	-42.57	-43.89	-45.20	-46.53	-47.91
-49.31	-50.71	-52.16	-53.72	-55.31	-56.81	-58.22	-59.69
-61.30	-63.00	-64.85	-66.96	-69.32	-71.75	-73.86	-75.33
-75.88	-75.11	-72.59	-70.01	-67.43	-64.78	-61.27	-57.75
-53.92	-49.15	-44.37	-39.51	-34.57	-29.29	-24.03	-18.80
-13.74	- 8.69	- 4.01	0.70	5.40	9.17	12.55	17.33
21.76							

*Listed from 8 sh altitude to ground level in steps of 0.1 sh

The original a priori covariance matrix is given in table E.2. The indices indicate the height in sh, (i.e. $-\ln(p/p_o)$)

TABLE E.2 : The Equatorial "winter" a priori covariance matrix

	8	7.9	7.8	7.7	7.6	7.5	7.4	7.3	7.2	7.1	7	6.9	6.8	6.7	6.6	6.5	6.4	6.3	6.2	6.1
8	46.65																			
7.9	45.91	46.35																		
7.8	42.79	44.64	45.27																	
7.7	37.62	40.24	43.06	44.07																
7.6	32.36	35.08	39.14	43.04	45.56															
7.5	27.64	30.16	34.57	40.05	45.33	48.22														
7.4	22.66	24.87	29.08	34.87	41.36	46.72	48.55													
7.3	17.15	18.97	22.63	27.92	34.32	40.80	45.54	46.40												
7.2	11.66	13.10	16.10	20.52	26.06	32.31	38.38	42.36	42.26											
7.1	6.639	7.790	10.18	13.64	17.99	23.23	29.14	34.56	37.70	37.34										
7	2.205	3.171	5.095	7.676	10.82	14.84	19.90	25.41	30.28	33.49	34.01									
6.9	-1.29	-.371	1.304	3.264	5.404	8.217	12.15	16.98	22.16	27.27	31.25	32.55								
6.8	-3.66	-2.70	-1.07	.5376	1.864	3.514	6.412	10.05	14.83	20.45	26.26	30.84	33.03							
6.7	-5.54	-4.62	-3.08	-1.76	-1.12	-.489	1.153	4.174	8.557	14.20	20.62	26.90	32.07	34.65						
6.6	-7.28	-6.55	-5.28	-4.31	-4.18	-4.27	-3.37	-.873	3.250	8.695	14.89	21.28	27.65	33.03	35.19					
6.5	-7.85	-7.28	-6.32	-5.66	-5.82	-6.29	-5.95	-4.00	-.385	4.355	9.561	15.02	21.12	27.72	32.89	34.41				
6.4	-6.45	-5.90	-5.09	-4.60	-4.80	-5.37	-5.44	-4.25	-1.65	1.796	5.475	9.534	14.68	21.04	27.39	31.95	33.68			
6.3	-4.14	-3.51	-2.68	-2.16	-2.19	-2.58	-2.87	-2.47	-1.09	.8245	2.893	5.562	9.604	15.10	21.24	27.19	32.35	35.20		
6.2	-2.26	-1.56	-.705	-.148	.0855	.0540	-.158	-.200	.2207	.9273	1.861	3.612	6.784	11.33	16.61	22.32	28.64	34.36	37.07	
6.1	-.797	-.090	.6236	.9898	1.288	1.590	1.683	1.638	1.680	1.847	2.392	3.849	6.495	10.15	14.23	18.68	24.30	30.78	36.07	38.50
6	1.066	1.697	2.115	2.073	2.168	2.574	2.877	2.946	2.997	3.189	3.806	5.189	7.410	10.22	13.08	16.16	20.57	26.45	32.59	37.63
5.9	3.356	3.865	3.956	3.475	3.257	3.563	3.857	3.926	4.074	4.469	5.161	6.260	7.864	9.831	11.69	13.78	17.26	22.36	28.08	34.11
5.8	4.834	5.207	5.035	4.265	3.828	4.027	4.317	4.475	4.820	5.435	6.086	6.710	7.567	8.739	9.851	11.34	14.32	18.70	23.84	29.66
5.7	4.907	5.118	4.750	3.873	3.391	3.574	3.961	4.381	5.097	6.055	6.788	7.082	7.360	7.938	8.554	9.689	12.41	16.40	20.90	25.98
5.6	4.283	4.363	3.876	3.011	2.619	2.888	3.400	4.046	5.081	6.416	7.416	7.662	7.610	7.779	8.041	8.896	11.37	15.07	19.03	23.31
5.5	3.527	3.671	3.171	2.385	2.165	2.636	3.302	4.008	5.034	6.414	7.528	7.772	7.511	7.392	7.419	8.077	10.36	13.87	17.46	21.00
5.4	2.724	2.774	2.308	1.655	1.700	2.498	3.390	4.085	4.863	5.928	6.836	6.971	6.568	6.299	6.297	7.002	9.301	12.78	16.16	19.12
5.3	1.356	1.362	.9137	.4411	.8382	2.033	3.181	3.866	4.378	5.083	5.759	5.842	5.410	5.081	5.146	6.052	8.555	12.17	15.50	18.08
5.2	.2815	.2348	-.167	-.401	.3392	1.824	3.084	3.633	3.811	4.168	4.759	4.985	4.729	4.447	4.505	5.459	8.070	11.80	15.11	17.38
5.1	.6018	.5866	.3314	.3290	1.212	2.655	3.708	3.889	3.596	3.577	4.038	4.507	4.654	4.598	4.556	5.238	7.609	11.17	14.26	16.13
5	2.261	2.347	2.260	2.327	3.016	4.058	4.649	4.354	3.595	3.234	3.606	4.325	4.937	5.153	4.912	5.098	6.937	10.00	12.65	14.13
4.9	4.228	4.377	4.367	4.326	4.611	5.118	5.232	4.540	3.477	2.955	3.311	4.181	5.046	5.340	4.832	4.573	5.937	8.489	10.95	11.81
4.8	5.637	5.798	5.836	5.734	5.740	5.882	5.708	4.816	3.645	3.068	3.315	4.032	4.766	4.890	4.158	3.719	4.928	7.219	9.068	9.917
4.7	6.259	6.455	6.631	6.710	6.794	6.883	6.617	5.668	4.467	3.774	3.701	3.958	4.279	4.137	3.319	2.954	4.296	6.606	8.269	9.021
4.6	6.232	6.513	6.923	7.346	7.756	7.971	7.655	6.619	5.334	4.469	4.063	3.870	3.797	3.469	2.689	2.498	4.031	6.501	8.250	8.921
4.5	5.904	6.289	6.908	7.647	8.318	8.597	8.153	6.958	5.572	4.638	4.131	3.767	3.529	3.167	2.489	2.440	4.073	6.606	8.402	9.064
4.4	5.583	6.153	6.901	7.748	8.437	8.607	7.981	6.636	5.214	4.342	3.923	3.616	3.435	3.189	2.670	2.720	4.330	6.789	8.555	9.195
4.3	5.758	6.266	7.020	7.795	8.330	8.291	7.464	5.988	4.533	3.717	3.413	3.255	3.237	3.165	2.811	2.939	4.490	6.824	8.561	9.212
4.2	6.001	6.496	7.161	7.772	8.098	7.838	6.833	5.261	3.780	3.006	2.848	2.917	3.094	3.125	2.819	2.955	4.422	6.665	8.404	9.141
4.1	6.317	6.758	7.288	7.699	7.799	7.330	6.223	4.687	3.291	2.606	2.620	2.938	3.280	3.303	2.915	2.989	4.381	6.530	8.273	9.125
4	6.570	6.933	7.344	7.615	7.550	6.943	5.858	4.526	3.328	2.711	2.754	3.129	3.477	3.423	2.955	2.979	4.280	6.314	8.026	8.943
3.9	6.366	6.671	7.021	7.250	7.132	6.504	5.545	4.486	3.522	2.936	2.847	3.049	3.248	3.122	2.672	2.685	3.842	5.706	7.342	8.232
3.8	5.440	5.733	6.067	6.261	6.111	5.524	4.717	3.888	3.152	2.685	2.558	2.648	2.763	2.644	2.268	2.257	3.218	4.877	6.393	7.162
3.7	4.172	4.497	4.851	5.008	4.818	4.280	3.582	2.888	2.350	2.101	2.120	2.282	2.435	2.357	2.027	1.964	2.739	4.199	5.552	6.139
3.6	3.186	3.521	3.905	4.091	3.933	3.439	2.768	2.120	1.708	1.620	1.744	1.926	2.036	1.933	1.644	1.592	2.254	3.515	4.649	5.036
3.5	2.666	2.928	3.274	3.508	3.436	2.999	2.327	1.665	1.251	1.124	1.133	1.140	1.067	.8882	.6882	.7282	1.312	2.349	3.235	3.448
3.4	2.363	2.515	2.781	3.023	3.035	2.719	2.158	1.544	1.060	.7146	.4132	.1293	-.141	-.379	-.511	-.431	.0232	.8074	1.455	1.515
3.3	1.949	2.039	2.252	2.489	2.592	2.487	2.196	1.785	1.319	.7734	.1599	-.368	-.735	-.984	-1.13	-1.13	-.861	-.320	.1082	-.0993
3.2	1.355	1.430	1.622	1.867	2.080	2.209	2.188	1.993	1.628	1.041	.3154	-.265	-.595	-.824	-1.05	-1.21	-1.09	-.692	-.417	-.499
3.1	.8090	.8905	1.070	1.316	1.608	1.881	1.988	1.882	1.599	1.090	.4403	-.042	-.274	-.483	-.809	-1.11	-1.08	-.746	-.527	-.632
3	.4305	.5188	.6868	.9130	1.220	1.550	1.710	1.645	1.434	1.038	.5000	.0953	-.102	-.313	-.684	-1.07	-1.14	-.865	-.677	-.786
2.9	-.021	.0638	.2284	.4614	.8004	1.196	1.429	1.425	1.286	.9873	.5380	.1779	-.022	-.257	-.643	-1.07	-1.22	-1.06	-.958	-1.09
2.8	-.943	-.836	-.595	-.229	.2425	.7159	.9718	.9780	.8764	.6557	.3202	.0931	-.007	-.211	-.594	-1.01	-1.23	-1.24	-1.29	-1.42
2.7	-2.43	-2.27	-1.89	-1.33	-.733	-.275	-.094	-.084	-.076	-.120	-.221	-.173	-.033	-.100	-.410	-.776	-1.04	-1.25	-1.52	-1.70
2.6	-3.96	-3.79	-3.39	-2.84	-2.32	-1.99	-1.89	-1.77	-1.46	-1.09	-.739	-.320	.0248	.0524	-.167	-.410	-.625	-.998	-1.56	-1.93
2.5	-5.31	-5.20	-4.90	-4.48	-4.12	-3.90	-3.74	-3.33	-2.59	-1.73	-.942	-.252	.2166	.3540	.2711	.1224	-.138	-.736	-1.60	-2.19
2.4	-6.34	-6.36	-6.19	-5.91	-5.68	-5.54	-5.26	-4.56	-3.46	-2.24	-1.16	-.324	.2091	.4798	.5796	.4753	.0338	-.851	-1.99	-2.84
2.3	-6.77	-6.86	-6.85	-6.71	-6.58	-6.51	-6.34	-5.76	-4.73	-3.53	-2.35	-1.30	-.493	.0637	.4336	.4923	-.008	-1.09	-2.37	-3.30
2.2	-6.66	-6.78	-6.80	-6.64	-6.42	-6.25	-5.98	-5.35	-4.37	-3.22	-2.06	-1.07	-.412	.0059	.3374	.4137	-.051	-1.03	-2.13	-2.88
2.1	-6.43	-6.57	-6.62	-6.45	-6.16	-5.88	-5.51	-4.87	-3.96	-2.91	-1.79	-.859	-.339	-.067	.1996	.2716	-.159	-1.02	-1.90	-2.45
2	-6.04	-6.20	-6.27	-6.09	-5.73	-5.36	-4.90	-4.25	-3.44	-2.51	-1.47	-.626	-.271	-.176	.0019	.0647	-.317	-1.03	-1.67	-1.98
1.9	-5.60	-5.76	-5.84	-5.64	-5.21	-4.74	-4.21	-3.56	-2.86	-2.05	-1.10	-.334	-.144	-.237	-.188	-.183	-.540	-1.10	-1.46	-1.51
1.8	-3.51	-3.57	-3.60	-3.45	-3.10	-2.66	-2.24	-1.92	-1.66	-1.30	-.708	-.251	-.250	-.467	-.576	-.668	-.896	-1.10	-1.00	-.676
1.7	-1.23	-1.20	-1.16	-1.06	-.798	-.411	-.135	-.192	-.467	-.584	-.419	-.309	-.517	-.863	-1.13	-1.31	-1.39	-1.19	-.593	-.178
1.6	1.000	1.132	1.247	1.316	1.489	1.803	1.951	1.609	.9495	.4513	.2410	.0032	-.439	-.939	-1.36	-1.62	-1.55	-1.01	.0010	.1092
1.5	2.762	2.910	3.020	3.014	3.027	3.141	3.107	2.626	1.879	1.260	.7871	.2145	-.475	-1.10	-1.55	-1.69	-1.41	-.674	.4365	1.516
1.4	4.737	4.907	5.015	4.931	4.771	4.672	4.445	3.808	2.943	2.162	1.385	.4544	-.485	-1.24	-1.71	-1.74	-1.23	-.280	.9449	2.076
1.3	6.852	7.098	7.226	7.097	6.809	6.553	6.189	5.424	4.392	3.299	2.033	.6019	-.675	-1.59	-2.06	-1.87	-.982	.3456	1.762	2.842
1.2	8.774	8.975	9.077	8.874	8.456	8.071	7.628	6.802	5.642	4.256	2.537	.6581	-.917	-1.97	-2.42	-2.02	-.773	.8925	2.442	3.409
1.1	9.426	9.471	9.417	9.113	8.646	8.345	8.146	7.562	6.440	4.898	2.984	.9498	-.743	-1.85	-2.29	-1.84	-.526	1.208	2.701	3.430
1	10.02	9.888	9.655	9.235	8.714	8.496	8.553	8.236	7.176	5.489	3.376	1.176	-.646	-1.81	-2.22	-1.71	-.324	1.471	2.882	3.335
0.9	10.40	10.11	9.707	9.198	8.654	8.511	8.736	8.568	7.531	5.752	3.510	1.194	-.700	-1.88	-2.24	-1.69	-.270	1.550	2.889	3.149
0.8	9.887	9.531	9.075	8.591	8.153	8.092	8.288	8.002	6.913	5.257	3.239	1.143	-.563	-1.61	-1.92	-1.38	-.021	1.717	2.964	3.167
0.7	9.359	8.968	8.484	8.053	7.748	7.801	7.986	7.587	6.449	4.935	3.157	1.251	-.341	-1.31	-1.58	-1.05	.2800	1.968	3.187	3.404
0.6	9.466	9.020	8.417	7.830	7.399	7.336	7.384	6.916	5.819	4.371	2.668	.8576	-.685	-1.67	-1.97	-1.55	-.475	.9307	2.025	2.260
0.5	9.561	9.085	8.409	7.716	7.211	7.100	7.076	6.586	5.560	4.219	2.625	.8798	-.704	-1.78	-2.15	-1.84	-1.02	.1357	1.174	1.506
0.4	9.662	9.141	8.368	7.638	6.924	6.723	6.582	6.022	5.016	3.722	2.204	.5561	-.997	-2.12	-2.55	-2.37	-1.83	-.975	-.028	.4025
0.3	10.22	9.849	9.240	8.523	7.990	7.837	7.667	6.921	5.517	3.740	1.900	.1556	-1.38	-2.40	-2.68	-2.35	-1.59	-.408	.8289	1.301
0.2	10.26	10.11	9.790	9.334	9.025	9.048	8.962	8.062	6.171	3.795	1.584	-.234	-1.68	-2.51	-2.56	-2.02	-.956	.6709	2.240	2.685
0.1	12.09	11.87	11.37	10.65	10.13	10.03	9.782	8.625	6.670	4.574	2.573	.5964	-1.07	-2.00	-2.24	-1.94	-.843	1.079	2.852	3.331
0	20.62	20.93	20.82	20.22	19.99	20.43	20.29	18.19	14.39	10.13	5.960	2.065	-.803	-2.16	-2.35	-1.40	1.347	5.485	8.904	9.889

	6	5.9	5.8	5.7	5.6	5.5	5.4	5.3	5.2	5.1	5	4.9	4.8	4.7	4.6	4.5	4.4	4.3	4.2	4.1
8																				
7.9																				
7.8																				
7.7																				
7.6																				
7.5																				
7.4																				
7.3																				
7.2																				
7.1																				
7																				
6.9																				
6.8																				
6.7																				
6.6																				
6.5																				
6.4																				
6.3																				
6.2																				
6.1																				
6	40.10																			
5.9	39.04	40.99																		
5.8	35.44	39.48	40.53																	
5.7	31.39	36.02	38.92	39.81																
5.6	27.87	32.11	35.72	38.60	39.84															
5.5	24.64	28.16	31.63	35.29	38.33	39.05														
5.4	21.91	24.62	27.48	30.93	34.61	37.07	37.29													
5.3	20.18	22.08	24.16	26.96	30.38	33.43	35.21	35.01												
5.2	18.87	20.05	21.44	23.56	26.34	29.04	31.20	32.32	31.39											
5.1	17.11	17.76	18.61	20.14	22.27	24.36	26.16	27.64	28.13	26.87										
5	14.79	15.13	15.59	16.63	18.22	19.77	21.02	22.27	23.42	23.85	22.98									
4.9	12.31	12.53	12.80	13.53	14.69	15.76	16.52	17.39	18.62	19.93	20.74	20.41								
4.8	10.31	10.53	10.76	11.30	12.10	12.77	13.16	13.72	14.75	16.21	17.77	18.81	18.72							
4.7	9.316	9.492	9.641	9.924	10.34	10.64	10.79	11.12	11.89	13.15	14.77	16.32	17.31	17.23						
4.6	9.115	9.171	9.099	8.998	8.961	8.906	8.808	8.923	9.484	10.57	12.03	13.53	14.89	15.81	15.72					
4.5	9.165	9.063	8.745	8.298	7.899	7.528	7.141	7.012	7.420	8.413	9.756	11.08	12.37	13.69	14.65	14.85				
4.4	9.197	8.933	8.435	7.789	7.164	6.539	5.894	5.567	5.866	6.803	8.108	9.358	10.54	11.90	13.32	14.36	14.71			
4.3	9.140	8.718	8.060	7.250	6.409	5.559	4.774	4.404	4.693	5.629	6.956	8.226	9.375	10.70	12.16	13.44	14.31	14.58		
4.2	9.091	8.576	7.767	6.753	5.660	4.604	3.764	3.455	3.805	4.763	6.115	7.414	8.553	9.811	11.17	12.37	13.39	14.18	14.50	
4.1	9.185	8.717	7.876	6.731	5.441	4.219	3.310	3.013	3.366	4.276	5.589	6.888	8.001	9.172	10.38	11.40	12.31	13.27	14.11	14.42
4	9.122	8.828	8.155	7.074	5.740	4.438	3.471	3.131	3.400	4.161	5.331	6.547	7.601	8.686	9.755	10.56	11.22	12.04	13.01	13.79
3.9	8.432	8.285	7.843	6.944	5.702	4.460	3.569	3.270	3.467	4.035	4.968	5.998	6.946	7.967	8.948	9.583	10.01	10.58	11.39	12.26
3.8	7.234	7.049	6.673	5.882	4.768	3.707	3.047	2.930	3.155	3.590	4.299	5.127	5.956	6.911	7.838	8.400	8.701	9.083	9.681	10.43
3.7	6.003	5.634	5.154	4.366	3.378	2.569	2.210	2.318	2.638	3.034	3.607	4.280	4.987	5.835	6.682	7.204	7.457	7.743	8.210	8.807
3.6	4.737	4.242	3.692	2.914	2.051	1.486	1.402	1.694	2.093	2.489	2.975	3.520	4.103	4.821	5.536	5.965	6.160	6.390	6.785	7.275
3.5	3.105	2.674	2.227	1.544	.7827	.3654	.4450	.8385	1.275	1.667	2.088	2.538	3.037	3.641	4.182	4.440	4.537	4.734	5.096	5.512
3.4	1.250	1.007	.7922	.3223	-.285	-.618	-.516	-.157	.2338	.5954	.9745	1.372	1.818	2.316	2.684	2.787	2.811	2.991	3.317	3.645
3.3	-.142	-.237	-.226	-.391	-.710	-.900	-.836	-.631	-.401	-.135	.1962	.5583	.9416	1.309	1.526	1.556	1.573	1.728	1.978	2.178
3.2	-.717	-.752	-.607	-.503	-.506	-.501	-.451	-.420	-.380	-.228	.0554	.3920	.7171	.9488	1.024	1.004	1.012	1.114	1.269	1.353
3.1	-.832	-.837	-.635	-.403	-.224	-.073	-.007	-.082	-.151	-.043	.2053	.4823	.7194	.8326	.8069	.7397	.7104	.7533	.8460	.8711
3	-.964	-.930	-.680	-.397	-.153	.0762	.1794	.0793	-.016	.0732	.2294	.3257	.3760	.3764	.3224	.2546	.2080	.2281	.3049	.3262
2.9	-1.21	-1.08	-.731	-.368	-.080	.1754	.3101	.2404	.1436	.1518	.1121	-.060	-.242	-.356	-.434	-.516	-.581	-.554	-.447	-.368
2.8	-1.43	-1.16	-.692	-.250	.0498	.2665	.4048	.3957	.3093	.2020	-.048	-.440	-.798	-1.04	-1.22	-1.40	-1.54	-1.51	-1.33	-1.13
2.7	-1.60	-1.23	-.724	-.259	.0342	.1975	.3202	.3523	.2560	.0381	-.353	-.852	-1.31	-1.70	-2.05	-2.37	-2.58	-2.57	-2.31	-1.99
2.6	-1.83	-1.41	-.904	-.414	-.032	.2114	.3786	.4168	.2147	-.227	-.815	-1.40	-1.96	-2.55	-3.12	-3.54	-3.76	-3.73	-3.39	-2.95
2.5	-2.19	-1.83	-1.36	-.842	-.374	-.058	.1210	.1344	-.110	-.610	-1.24	-1.83	-2.44	-3.15	-3.83	-4.32	-4.62	-4.70	-4.43	-3.96
2.4	-3.01	-2.70	-2.20	-1.61	-1.02	-.557	-.263	-.173	-.364	-.856	-1.51	-2.12	-2.78	-3.59	-4.34	-4.90	-5.31	-5.49	-5.31	-4.85
2.3	-3.60	-3.46	-3.06	-2.40	-1.60	-.939	-.567	-.530	-.811	-1.32	-1.89	-2.40	-3.06	-3.92	-4.68	-5.15	-5.45	-5.57	-5.35	-4.88
2.2	-3.11	-2.99	-2.64	-2.01	-1.23	-.586	-.248	-.225	-.467	-.938	-1.53	-2.11	-2.79	-3.63	-4.36	-4.83	-5.14	-5.30	-5.15	-4.76
2.1	-2.59	-2.48	-2.17	-1.59	-.837	-.200	.1448	.1934	.0061	-.435	-1.08	-1.76	-2.47	-3.27	-3.98	-4.47	-4.80	-4.99	-4.91	-4.61
2	-2.04	-1.94	-1.68	-1.16	-.448	.1950	.5773	.6754	.5393	.1097	-.611	-1.39	-2.14	-2.89	-3.57	-4.06	-4.41	-4.63	-4.63	-4.43
1.9	-1.43	-1.33	-1.10	-.623	.0563	.7078	1.131	1.278	1.185	.7612	-.022	-.894	-1.67	-2.40	-3.05	-3.55	-3.91	-4.16	-4.24	-4.15
1.8	-.373	-.131	.1635	.5572	1.053	1.556	1.906	2.005	1.858	1.442	.7923	.1130	-.486	-1.05	-1.54	-1.86	-2.10	-2.32	-2.47	-2.55
1.7	.7655	1.167	1.501	1.768	2.055	2.410	2.688	2.731	2.519	2.106	1.596	1.123	.7208	.3554	.0769	-.049	-.151	-.338	-.556	-.811
1.6	1.840	2.306	2.646	2.815	2.943	3.180	3.402	3.403	3.233	2.723	2.356	2.090	1.880	1.699	1.609	1.654	1.665	1.507	1.332	.6489
1.5	2.289	2.753	3.089	3.220	3.219	3.235	3.255	3.178	2.956	2.689	2.535	2.493	2.483	2.493	2.568	2.720	2.815	2.723	2.468	2.088
1.4	2.813	3.273	3.593	3.656	3.475	3.224	3.023	2.882	2.740	2.658	2.762	2.978	3.169	3.403	3.649	3.915	4.105	4.100	3.882	3.515
1.3	3.379	3.638	3.825	3.775	3.394	2.869	2.470	2.314	2.305	2.455	2.856	3.364	3.831	4.287	4.737	5.123	5.394	5.468	5.298	4.966
1.2	3.706	3.742	3.786	3.635	3.089	2.332	1.772	1.633	1.785	2.172	2.842	3.597	4.290	4.973	5.624	6.133	6.476	6.600	6.444	6.118
1.1	3.432	3.239	3.155	2.959	2.402	1.638	1.101	1.062	1.381	1.914	2.658	3.472	4.286	5.145	5.949	6.523	6.859	6.939	6.724	6.367
1	3.010	2.568	2.348	2.121	1.585	.8451	.3408	.3991	.8787	1.549	2.352	3.213	4.156	5.213	6.192	6.847	7.172	7.193	6.898	6.495
0.9	2.618	2.016	1.669	1.350	.7715	.0404	-.410	-.242	.3832	1.161	1.991	2.869	3.909	5.141	6.282	7.029	7.382	7.387	7.038	6.578
0.8	2.622	1.958	1.415	.8227	.0441	-.716	-1.05	-.696	.1056	1.006	1.884	2.740	3.728	4.910	6.035	6.834	7.302	7.453	7.220	6.758
0.7	2.867	2.103	1.310	.4377	-.473	-1.19	-1.39	-.917	-.011	.9587	1.845	2.647	3.572	4.729	5.877	6.744	7.322	7.624	7.537	7.116
0.6	1.790	1.137	.4540	-.418	-1.45	-2.28	-2.49	-1.93	-.893	.2180	1.250	2.185	3.169	4.283	5.352	6.180	6.773	7.094	6.988	6.526
0.5	1.129	.5352	-.114	-.987	-2.03	-2.87	-3.07	-2.50	-1.43	-.256	.8571	1.871	2.893	3.988	5.008	5.796	6.381	6.725	6.645	6.215
0.4	.1713	-.294	-.881	-1.80	-2.97	-3.89	-4.09	-3.44	-2.26	-.950	.3028	1.441	2.518	3.579	4.526	5.263	5.851	6.229	6.170	5.744
0.3	.8445	.0890	-.663	-1.59	-2.70	-3.59	-3.83	-3.26	-2.08	-.696	.5974	1.677	2.719	3.884	4.997	5.861	6.546	6.997	6.968	6.534
0.2	1.868	.6710	-.124	-1.24	-2.16	-2.89	-3.11	-2.61	-1.46	-.002	1.296	2.217	3.132	4.390	5.703	6.717	7.503	8.029	8.030	7.573
0.1	2.549	1.485	.7293	.1533	-.535	-1.36	-1.99	-1.92	-1.01	.4056	1.938	3.287	4.556	5.919	7.270	8.487	9.509	10.05	9.825	9.031
0	8.808	7.380	6.636	6.287	5.630	4.432	3.078	2.306	2.469	3.387	4.584	5.865	7.755	10.33	12.96	15.31	17.02	17.49	16.69	15.22

	4	3.9	3.8	3.7	3.6	3.5	3.4	3.3	3.2	3.1	3	2.9	2.8	2.7	2.6	2.5	2.4	2.3	2.2	2.1
8																				
7.9																				
7.8																				
7.7																				
7.6																				
7.5																				
7.4																				
7.3																				
7.2																				
7.1																				
7																				
6.9																				
6.8																				
6.7																				
6.6																				
6.5																				
6.4																				
6.3																				
6.2																				
6.1																				
6																				
5.9																				
5.8																				
5.7																				
5.6																				
5.5																				
5.4																				
5.3																				
5.2																				
5.1																				
5																				
4.9																				
4.8																				
4.7																				
4.6																				
4.5																				
4.4																				
4.3																				
4.2																				
4.1																				
4	13.81																			
3.9	12.73	12.29																		
3.8	11.01	11.06	10.51																	
3.7	9.299	9.513	9.466	9.035																
3.6	7.649	7.834	7.965	7.959	7.442															
3.5	5.803	5.941	6.075	6.224	6.169	5.593														
3.4	3.844	3.941	4.050	4.209	4.384	4.422	4.068													
3.3	2.247	2.269	2.353	2.500	2.730	3.057	3.298	3.199												
3.2	1.298	1.220	1.259	1.405	1.624	1.955	2.374	2.718	2.787											
3.1	.7579	.6240	.6360	.8020	1.016	1.256	1.607	2.090	2.540	2.725										
3	.2347	.1371	.1943	.4190	.6625	.8609	1.137	1.594	2.144	2.586	2.785									
2.9	-.367	-.375	-.243	.0562	.3644	.6008	.8838	1.299	1.785	2.271	2.728	3.051								
2.8	-1.01	-.952	-.778	-.408	.0019	.3425	.6963	1.107	1.519	1.946	2.474	3.070	3.493							
2.7	-1.79	-1.70	-1.50	-1.05	-.490	.0083	.4777	.9275	1.310	1.667	2.120	2.764	3.502	4.013						
2.6	-2.67	-2.57	-2.33	-1.77	-1.08	-.442	.1286	.6397	1.049	1.383	1.732	2.267	3.112	4.098	5.062					
2.5	-3.62	-3.43	-3.11	-2.45	-1.63	-.909	-.295	.2409	.6765	1.025	1.338	1.785	2.609	3.826	5.379	6.352				
2.4	-4.42	-4.10	-3.63	-2.85	-1.98	-1.25	-.625	-.065	.3845	.7203	.9828	1.356	2.142	3.462	5.340	6.798	7.961			
2.3	-4.43	-4.08	-3.55	-2.76	-1.97	-1.37	-.817	-.265	.1772	.4548	.6264	.9207	1.665	2.973	4.879	6.439	7.859	8.824		
2.2	-4.36	-4.02	-3.51	-2.77	-2.02	-1.44	-.947	-.469	-.083	.1755	.3465	.6145	1.277	2.457	4.184	5.640	7.004	7.964	7.416	
2.1	-4.27	-3.95	-3.47	-2.77	-2.07	-1.51	-1.04	-.634	-.316	-.088	.0856	.3401	.9277	1.973	3.497	4.820	6.078	6.979	6.724	6.349
2	-4.17	-3.85	-3.39	-2.76	-2.11	-1.58	-1.15	-.815	-.571	-.380	-.207	.0280	.5308	1.428	2.733	3.905	5.044	5.887	5.938	5.898
1.9	-3.98	-3.70	-3.28	-2.72	-2.14	-1.65	-1.26	-.992	-.808	-.645	-.481	-.277	.1313	.8683	1.932	2.933	3.928	4.713	5.061	5.348
1.8	-2.60	-2.56	-2.35	-2.03	-1.65	-1.30	-1.02	-.824	-.668	-.523	-.443	-.400	-.220	.2038	.8525	1.481	2.133	2.733	3.161	3.546
1.7	-1.11	-1.31	-1.35	-1.28	-1.14	-.937	-.766	-.660	-.543	-.425	-.440	-.569	-.634	-.547	-.349	-.127	.1512	.5483	1.054	1.540
1.6	.3789	-.004	-.244	-.428	-.542	-.536	-.508	-.514	-.459	-.386	-.483	-.752	-1.03	-1.26	-1.49	-1.65	-1.72	-1.55	-.982	-.412
1.5	1.644	1.260	.9292	.5698	.2542	.0601	-.122	-.346	-.490	-.547	-.662	-.911	-1.29	-1.79	-2.38	-2.82	-3.15	-3.17	-2.62	-2.02
1.4	3.095	2.690	2.230	1.662	1.122	.7076	.2936	-.171	-.533	-.732	-.866	-1.09	-1.58	-2.36	-3.34	-4.09	-4.71	-4.97	-4.42	-3.80
1.3	4.587	4.156	3.555	2.774	2.014	1.398	.7906	.1254	-.440	-.795	-.983	-1.23	-1.87	-2.95	-4.33	-5.40	-6.33	-6.86	-6.32	-5.58
1.2	5.770	5.345	4.672	3.751	2.882	2.042	1.272	.4341	-.314	-.817	-1.06	-1.33	-2.10	-3.47	-5.22	-6.58	-7.78	-8.53	-8.02	-7.36
1.1	6.051	5.718	5.153	4.274	3.282	2.393	1.549	.6664	-.129	-.675	-.935	-1.23	-2.07	-3.58	-5.53	-7.06	-8.34	-9.15	-8.61	-7.92
1	6.219	6.012	5.600	4.795	3.752	2.758	1.842	.9202	.0789	-.511	-.788	-1.10	-2.02	-3.68	-5.84	-7.52	-8.88	-9.73	-9.17	-8.46
0.9	6.297	6.171	5.884	5.158	4.104	3.059	2.100	1.146	.2599	-.377	-.684	-1.02	-2.01	-3.79	-6.09	-7.88	-9.25	-10.1	-9.56	-8.83
0.8	6.366	6.132	5.800	5.099	4.140	3.187	2.248	1.257	.3131	-.386	-.749	-1.13	-2.14	-3.89	-6.12	-7.80	-9.04	-9.95	-9.37	-8.61
0.7	6.647	6.314	5.909	5.179	4.264	3.377	2.444	1.401	.3829	-.389	-.816	-1.25	-2.29	-4.03	-6.17	-7.75	-8.92	-9.91	-9.31	-8.50
0.6	6.046	5.760	5.438	4.793	3.987	3.253	2.469	1.522	.5458	-.210	-.629	-1.08	-2.17	-3.97	-6.15	-7.71	-8.80	-9.68	-9.04	-8.21
0.5	5.783	5.550	5.251	4.592	3.804	3.166	2.504	1.644	.7073	-.035	-.452	-.923	-2.07	-3.91	-6.14	-7.70	-8.77	-9.63	-8.95	-8.09
0.4	5.328	5.121	4.845	4.208	3.492	3.001	2.493	1.733	.8418	.1154	-.294	-.780	-1.97	-3.85	-6.11	-7.66	-8.67	-9.49	-8.75	-7.87
0.3	6.061	5.732	5.311	4.537	3.646	2.964	2.342	1.560	.7040	.0683	-.239	-.696	-1.95	-3.95	-6.31	-8.07	-9.22	-10.1	-9.27	-8.30
0.2	6.994	6.468	5.852	4.921	3.808	2.830	2.001	1.167	.3754	-.114	-.269	-.676	-1.99	-4.08	-6.48	-8.48	-9.79	-10.7	-9.77	-8.70
0.1	8.117	7.292	6.405	5.203	3.850	2.772	1.969	1.164	.3533	-.207	-.458	-.979	-2.55	-5.11	-8.17	-10.6	-12.2	-13.1	-12.1	-10.9
0	13.61	12.04	10.41	8.398	6.216	4.417	3.035	1.749	.6166	-.050	-.269	-.914	-3.17	-7.04	-11.7	-15.6	-18.5	-19.9	-18.7	-17.3

	2	1.9	1.8	1.7	1.6	1.5	1.4	1.3	1.2	1.1	1	0.9	0.8	0.7	0.6	0.5	0.4	0.3	0.2	0.1	0
2	5.815																				
1.9	5.624	5.798																			
1.8	3.933	4.315	3.904																		
1.7	2.043	2.641	3.381	4.138																	
1.6	.2000	.9856	2.659	4.439	5.651																
1.5	-1.38	-.559	1.317	3.335	4.929	5.056															
1.4	-3.11	-2.25	-.167	2.101	4.103	5.154	6.270														
1.3	-4.95	-4.07	-1.80	.6661	3.062	5.057	7.220	9.380													
1.2	-6.59	-5.69	-3.29	-.658	2.055	4.866	7.933	11.14	13.85												
1.1	-7.11	-6.20	-3.82	-1.22	1.502	4.381	7.533	10.86	13.80	14.50											
1	-7.62	-6.70	-4.37	-1.81	.8955	3.835	7.051	10.48	13.64	15.16	16.70										
0.9	-7.96	-7.05	-4.76	-2.22	.4460	3.398	6.626	10.06	13.35	15.44	17.62	19.06									
0.8	-7.71	-6.78	-4.59	-2.17	.3731	3.182	6.272	9.526	12.64	14.63	16.87	18.24	18.31								
0.7	-7.57	-6.61	-4.53	-2.19	.2872	2.991	5.967	9.071	12.03	13.89	15.82	17.49	18.44	19.61							
0.6	-7.25	-6.28	-4.25	-2.04	.2994	2.916	5.798	8.814	11.69	13.45	15.25	16.82	17.66	18.55	18.22						
0.5	-7.10	-6.10	-4.16	-2.05	.2337	2.808	5.636	8.622	11.44	13.10	14.80	16.25	16.93	17.76	17.87	18.10					
0.4	-6.85	-5.84	-3.99	-1.99	.1858	2.679	5.430	8.343	11.08	12.63	14.19	15.52	16.06	16.72	17.42	18.20	18.94				
0.3	-7.19	-6.10	-4.11	-1.95	.3288	2.898	5.738	8.787	11.63	13.17	14.72	15.98	16.21	16.53	17.08	17.68	18.25	19.22			
0.2	-7.49	-6.29	-4.16	-1.83	.5444	3.173	6.092	9.262	12.19	13.73	15.26	16.44	16.30	16.22	16.27	16.37	16.43	19.86	24.32		
0.1	-9.55	-8.13	-5.08	-1.76	1.527	4.656	8.101	11.67	14.95	16.59	18.25	19.53	19.39	19.33	19.20	19.12	18.95	22.13	26.23	32.52	
0	-15.5	-13.6	-7.98	-1.87	3.913	8.539	13.62	18.74	23.50	26.05	28.62	30.49	30.03	29.70	28.88	28.11	27.14	30.57	34.72	46.97	87.56

APPENDIX F

MID-LATITUDES "SUMMER" A PRIORI DATA

The statistics were constructed from 139 May, June, July and August profiles for years 1969 through 1972. (August data has been added to season 6 of table 3 in order to increase the sample size.) The mean profile is given below

TABLE F.1 : The Mean Profile* (^{0}C)

-16.17	-15.31	-13.93	-12.44	-11.00	- 9.62	- 8.30	- 7.04
- 5.85	- 4.79	- 3.97	- 3.44	- 3.18	- 3.22	- 3.56	- 4.17
- 5.03	- 6.15	- 7.56	- 9.28	-11.23	-13.31	-15.43	-17.57
-19.68	-21.72	-23.64	-25.40	-27.05	-28.74	-30.47	-32.18
-33.81	-35.41	-37.01	-38.52	-39.89	-41.25	-42.63	-43.96
-45.21	-46.38	-47.47	-48.50	-49.52	-50.58	-51.75	-52.95
-53.99	-54.90	-55.89	-57.02	-58.25	-59.57	-60.85	-61.93
-62.72	-63.18	-63.20	-62.99	-62.53	-61.69	-60.06	-57.90
-54.66	-50.11	-45.53	-40.59	-35.59	-30.40	-25.21	-20.03
-14.84	- 9.67	- 4.74	0.19	5.13	9.85	14.49	17.41
20.35							

*Listed from 8 sh altitude to ground level in steps of 0.1 sh

The original a priori covariance matrix is given in table F.2. The indices indicate the height in sh(i.e. $-\ln(p/p_o)$).

TABLE F.2 : The Mid-Latitudes summer a priori covariance matrix

	8	7.9	7.8	7.7	7.6	7.5	7.4	7.3	7.2	7.1	7	6.9	6.8	6.7	6.6	6.5	6.4	6.3	6.2	6.1
8	44.41																			
7.9	43.28	42.90																		
7.8	40.64	41.23	41.06																	
7.7	36.79	37.99	39.09	38.64																
7.6	32.68	34.02	35.69	36.46	35.96															
7.5	28.69	29.93	31.66	33.11	34.17	34.36														
7.4	24.14	25.21	26.80	28.53	30.59	32.49	32.80													
7.3	19.29	20.14	21.52	23.33	25.86	28.84	31.16	32.01												
7.2	15.90	16.49	17.59	19.28	21.86	25.20	28.60	31.28	32.46											
7.1	14.73	15.05	15.79	17.16	19.43	22.50	25.98	29.34	31.89	33.09										
7	14.77	14.88	15.28	16.24	17.98	20.49	23.58	26.96	30.18	32.97	34.91									
6.9	15.01	14.96	15.06	15.62	16.84	18.79	21.43	24.55	27.87	31.51	35.10	37.20								
6.8	15.45	15.27	15.09	15.28	16.05	17.50	19.67	22.34	25.31	28.99	33.33	36.93	38.69							
6.7	16.63	16.34	15.93	15.76	16.10	17.08	18.76	20.84	23.19	26.45	30.79	35.19	38.71	40.96						
6.6	18.42	18.06	17.49	17.00	16.92	17.47	18.69	20.20	21.88	24.52	28.48	32.97	37.40	41.41	43.97					
6.5	20.06	19.64	18.95	18.24	17.86	18.12	19.05	20.18	21.33	23.37	26.71	30.76	35.23	40.06	44.29	46.62				
6.4	21.05	20.59	19.84	19.05	18.58	18.75	19.61	20.63	21.57	23.13	25.79	29.12	33.07	37.85	42.81	46.64	48.36			
6.3	21.19	20.76	20.07	19.40	19.03	19.24	20.09	21.14	22.05	23.31	25.35	27.95	31.17	35.42	40.27	44.62	47.50	48.14		
6.2	20.77	20.44	19.94	19.52	19.40	19.68	20.41	21.33	22.17	23.22	24.81	26.80	29.32	32.87	37.15	41.24	44.51	46.38	46.33	
6.1	20.39	20.18	19.92	19.86	20.07	20.46	20.98	21.60	22.27	23.18	24.52	26.04	27.87	30.59	34.08	37.59	40.70	43.15	44.56	44.66
6	20.36	20.27	20.25	20.50	21.00	21.50	21.83	22.13	22.62	23.48	24.70	25.91	27.12	29.00	31.64	34.43	37.09	39.52	41.57	43.15
5.9	20.30	20.55	20.68	21.02	21.57	22.06	22.22	22.22	22.48	23.23	24.36	25.42	26.29	27.61	29.56	31.66	33.71	35.69	37.60	39.73
5.8	20.50	20.65	20.84	21.06	21.38	21.63	21.54	21.21	21.15	21.70	22.75	23.77	24.58	25.71	27.29	28.87	30.36	31.74	33.10	34.98
5.7	20.21	20.39	20.56	20.61	20.62	20.54	20.15	19.56	19.27	19.70	20.71	21.70	22.49	23.55	24.94	26.23	27.34	28.22	28.99	30.33
5.6	19.31	19.45	19.54	19.47	19.31	19.07	18.61	18.03	17.78	18.27	19.26	20.12	20.74	21.62	22.84	23.96	24.85	25.43	25.85	26.81
5.5	17.55	17.57	17.50	17.36	17.24	17.11	16.86	16.54	16.56	17.20	18.19	18.94	19.37	20.04	21.04	21.98	22.68	23.10	23.43	24.30
5.4	15.55	15.43	15.19	14.99	14.96	15.02	15.02	14.99	15.24	16.04	17.12	17.89	18.27	18.80	19.62	20.35	20.82	21.12	21.49	22.35
5.3	14.13	13.94	13.64	13.43	13.42	13.57	13.72	13.81	14.12	14.92	16.05	16.91	17.33	17.83	18.57	19.15	19.45	19.68	20.07	20.83
5.2	13.23	13.08	12.85	12.69	12.73	12.93	13.12	13.20	13.38	13.98	14.95	15.77	16.25	16.82	17.62	18.21	18.50	18.74	19.08	19.64
5.1	12.54	12.46	12.31	12.23	12.34	12.60	12.82	12.89	12.94	13.28	13.95	14.62	15.14	15.85	16.78	17.47	17.83	18.08	18.31	18.67
5	11.90	11.85	11.73	11.68	11.87	12.20	12.48	12.65	12.76	12.99	13.45	13.98	14.49	15.25	16.21	16.95	17.38	17.61	17.75	18.03
4.9	11.06	11.00	10.87	10.88	11.15	11.55	11.93	12.26	12.56	12.89	13.32	13.76	14.18	14.83	15.72	16.47	16.99	17.28	17.41	17.71
4.8	10.11	10.00	9.868	9.929	10.27	10.71	11.11	11.53	11.97	12.43	12.95	13.39	13.75	14.35	15.19	15.94	16.53	16.93	17.11	17.44
4.7	9.668	9.525	9.349	9.370	9.650	9.979	10.24	10.53	10.91	11.44	12.10	12.66	13.10	13.78	14.63	15.30	15.82	16.23	16.46	16.77
4.6	9.574	9.452	9.270	9.205	9.308	9.406	9.406	9.426	9.611	10.10	10.87	11.57	12.13	12.86	13.67	14.17	14.47	14.77	15.04	15.41
4.5	9.151	9.091	8.959	8.862	8.841	8.770	8.583	8.394	8.399	8.808	9.584	10.32	10.88	11.55	12.27	12.65	12.76	12.94	13.23	13.73
4.4	8.204	8.188	8.105	8.016	7.962	7.962	7.660	7.448	7.413	7.757	8.448	9.113	9.604	10.21	10.88	11.24	11.32	11.42	11.64	12.15
4.3	7.110	7.099	7.013	6.900	6.824	6.757	6.648	6.543	6.559	6.841	7.393	7.954	8.395	8.949	9.603	10.03	10.18	10.23	10.32	10.69
4.2	6.324	6.307	6.198	6.026	5.909	5.881	5.874	5.863	5.893	6.064	6.433	6.854	7.217	7.705	8.326	8.802	9.050	9.126	9.123	9.360
4.1	5.881	5.897	5.818	5.632	5.493	5.499	5.535	5.504	5.431	5.420	5.569	5.802	6.046	6.466	7.062	7.559	7.861	7.989	8.011	8.242
4	5.576	5.449	5.461	5.336	5.221	5.245	5.258	5.123	4.892	4.705	4.671	4.745	4.900	5.299	5.897	6.387	6.755	6.829	6.941	7.264
3.9	4.710	4.809	4.877	4.814	4.743	4.776	4.749	4.531	4.212	3.961	3.881	3.924	4.074	4.473	5.045	5.495	5.755	5.829	6.112	6.493
3.8	4.036	4.123	4.178	4.137	4.107	4.148	4.097	3.871	3.584	3.401	3.405	3.518	3.697	4.051	4.509	4.848	5.067	5.257	5.457	5.825
3.7	3.425	3.496	3.515	3.449	3.409	3.418	3.335	3.137	2.957	2.925	3.069	3.269	3.444	3.687	3.963	4.135	4.250	4.373	4.510	4.809
3.6	3.111	3.166	3.141	3.011	2.887	2.797	2.635	2.434	2.354	2.492	2.799	3.086	3.246	3.385	3.526	3.574	3.544	3.502	3.509	3.736
3.5	2.984	3.029	2.983	2.812	2.625	2.457	2.238	2.020	1.989	2.249	2.693	3.069	3.251	3.371	3.492	3.499	3.357	3.162	3.061	3.241
3.4	2.278	2.321	2.289	2.152	1.997	1.861	1.704	1.563	1.582	1.865	2.324	2.717	2.922	3.062	3.200	3.199	3.024	2.801	2.689	2.837
3.3	.9009	.9445	.9498	.8893	.8173	.7702	.7500	.7693	.8695	1.112	1.472	1.800	1.985	2.098	2.186	2.154	2.014	1.881	1.827	1.932
3.2	-.246	-.177	-.103	-.074	-.070	-.048	.0354	.1775	.3284	.4979	.7263	.9656	1.112	1.164	1.161	1.090	1.015	1.005	1.025	1.099
3.1	-.671	-.540	-.379	-.277	-.224	-.154	-.018	.1591	.2802	.3317	.4104	.5494	.6486	.6517	.5943	.5289	.5368	.6303	.7129	.7855
3	-.635	-.453	-.234	-.100	-.034	.0507	.1925	.3378	.3752	.3005	.2528	.3033	.3455	.2990	.2168	.1843	.2612	.4145	.5321	.6161
2.9	-.414	-.232	-.005	.1355	.1816	.2190	.3066	.3879	.3455	.1982	.1039	.1173	.1068	-.005	-.128	-.159	-.072	.0722	.1725	.2506
2.8	-.093	.0524	.2637	.4202	.4525	.4147	.4119	.4271	.3463	.1914	.1041	.0969	.0281	-.147	-.313	-.373	-.317	-.217	-.163	-.112
2.7	.3323	.4395	.6482	.8627	.9518	.8949	.8038	.7437	.6610	.5647	.5243	.4883	.3403	.1121	-.071	-.146	-.111	-.032	-.001	.0218
2.6	.9460	1.021	1.238	1.546	1.786	1.830	1.726	1.621	1.582	1.625	1.704	1.668	1.450	1.196	1.041	.9856	1.014	1.078	1.096	1.099
2.5	1.893	1.922	2.118	2.492	2.889	3.099	3.088	3.038	3.118	3.372	3.644	3.669	3.419	3.165	3.062	3.045	3.072	3.109	3.099	3.086
2.4	2.941	2.907	3.047	3.439	3.942	4.300	4.420	4.488	4.721	5.185	5.660	5.786	5.539	5.276	5.192	5.208	5.268	5.311	5.281	5.257
2.3	3.750	3.683	3.820	4.258	4.829	5.268	5.480	5.630	5.969	6.553	7.133	7.276	6.959	6.558	6.681	6.891	7.016	6.965	6.896	
2.2	4.489	4.451	4.698	5.243	5.796	6.112	6.174	6.207	6.474	7.036	7.572	7.629	7.227	6.856	6.823	7.099	7.534	7.826	7.811	7.719
2.1	4.950	4.957	5.331	5.990	6.509	6.661	6.522	6.374	6.510	6.995	7.478	7.485	7.042	6.651	6.649	7.043	7.664	8.115	8.146	8.044
2	4.789	4.821	5.260	5.944	6.364	6.348	6.062	5.797	5.857	6.326	6.827	6.860	6.455	6.085	6.075	6.474	7.141	7.634	7.632	7.445
1.9	4.232	4.326	4.764	5.298	5.473	5.216	4.691	4.192	4.102	4.526	5.038	5.139	4.833	4.485	4.362	4.560	5.023	5.368	5.274	5.019
1.8	1.092	1.216	1.628	2.037	2.071	1.761	1.249	.7393	.5129	.5745	.5788	.2726	-.262	-.832	-1.28	-1.48	-1.41	-1.27	-1.27	-1.36
1.7	-1.65	-1.59	-1.37	-1.23	-1.41	-1.76	-2.18	-2.60	-2.88	-3.11	-3.48	-4.00	-4.57	-5.20	-5.84	-6.30	-6.49	-6.46	-6.39	-6.40
1.6	-2.59	-2.60	-2.57	-2.62	-2.84	-3.08	-3.35	-3.72	-4.07	-4.42	-4.87	-5.29	-5.63	-6.11	-6.77	-7.38	-7.73	-7.80	-7.77	-7.80
1.5	-4.43	-4.39	-4.37	-4.46	-4.67	-4.80	-4.89	-5.09	-5.42	-5.92	-6.52	-6.88	-6.95	-7.11	-7.58	-8.14	-8.55	-8.67	-8.55	-8.38
1.4	-6.44	-6.36	-6.35	-6.48	-6.68	-6.72	-6.64	-6.66	-6.96	-7.58	-8.28	-8.57	-8.34	-8.17	-8.44	-8.95	-9.42	-9.59	-9.36	-8.95
1.3	-7.41	-7.26	-7.25	-7.43	-7.55	-7.43	-7.25	-7.29	-7.71	-8.51	-9.36	-9.62	-9.21	-8.80	-8.85	-9.23	-9.68	-9.88	-9.58	-9.01
1.2	-8.29	-8.08	-8.08	-8.29	-8.35	-8.09	-7.80	-7.85	-8.39	-9.36	-10.3	-10.6	-10.0	-9.39	-9.24	-9.50	-9.95	-10.2	-9.82	-9.11
1.1	-8.98	-8.71	-8.66	-8.86	-8.90	-8.63	-8.35	-8.46	-9.12	-10.3	-11.4	-11.8	-11.1	-10.4	-10.2	-10.5	-10.9	-11.2	-10.7	-10.0
1	-9.67	-9.34	-9.26	-9.45	-9.48	-9.19	-8.93	-9.10	-9.89	-11.3	-12.6	-13.0	-12.3	-11.5	-11.3	-11.5	-12.0	-12.2	-11.7	-10.9
0.9	-9.99	-9.63	-9.52	-9.70	-9.73	-9.48	-9.26	-9.48	-10.3	-11.8	-13.3	-13.7	-12.9	-12.1	-11.8	-12.1	-12.5	-12.7	-12.2	-11.4
0.8	-9.12	-8.83	-8.82	-9.08	-9.20	-9.08	-8.99	-9.25	-10.0	-11.3	-12.6	-12.9	-12.1	-11.3	-11.1	-11.2	-11.7	-11.9	-11.4	-10.5
0.7	-8.27	-8.08	-8.18	-8.53	-8.75	-8.74	-8.76	-9.02	-9.69	-10.8	-12.0	-12.1	-11.4	-10.6	-10.3	-10.5	-10.9	-11.2	-10.6	-9.72
0.6	-9.40	-9.24	-9.38	-9.76	-9.93	-9.78	-9.57	-9.64	-10.2	-11.4	-12.6	-12.8	-12.1	-11.5	-11.4	-11.6	-12.0	-12.2	-11.6	-10.7
0.5	-10.6	-10.5	-10.7	-11.1	-11.2	-10.9	-10.4	-10.3	-10.7	-11.9	-13.2	-13.5	-12.9	-12.4	-12.4	-12.8	-13.1	-13.2	-12.6	-11.7
0.4	-11.9	-11.8	-12.0	-12.4	-12.5	-12.0	-11.3	-10.9	-11.3	-12.5	-13.8	-14.2	-13.8	-13.4	-13.6	-14.0	-14.3	-14.3	-13.6	-12.7
0.3	-12.1	-12.1	-12.5	-13.0	-13.0	-12.4	-11.4	-10.7	-11.0	-12.5	-14.3	-14.9	-14.3	-13.8	-14.0	-14.3	-14.6	-14.3	-13.5	-12.4
0.2	-11.9	-12.0	-12.5	-13.1	-13.2	-12.4	-11.1	-10.1	-10.5	-12.4	-14.7	-15.5	-14.7	-14.0	-14.0	-14.3	-14.4	-13.9	-12.9	-11.6
0.1	-9.17	-9.23	-9.95	-11.0	-11.4	-11.0	-10.1	-9.35	-9.44	-10.4	-11.3	-11.2	-10.0	-8.90	-8.47	-8.58	-8.89	-8.81	-7.98	-6.91
0	-6.89	-6.52	-6.90	-8.10	-9.03	-9.00	-8.26	-7.55	-7.46	-7.78	-7.76	-7.03	-5.87	-4.73	-3.90	-3.59	-3.71	-3.80	-3.59	-3.39

	6	5.9	5.8	5.7	5.6	5.5	5.4	5.3	5.2	5.1	5	4.9	4.8	4.7	4.6	4.5	4.4	4.3	4.2	4.1
8																				
7.9																				
7.8																				
7.7																				
7.6																				
7.5																				
7.4																				
7.3																				
7.2																				
7.1																				
7																				
6.9																				
6.8																				
6.7																				
6.6																				
6.5																				
6.4																				
6.3																				
6.2																				
6.1																				
6	43.54																			
5.9	41.57	41.43																		
5.8	37.28	38.53	37.47																	
5.7	32.39	34.13	34.49	33.27																
5.6	28.47	30.01	30.79	30.71	29.53															
5.5	25.67	26.72	27.10	27.20	26.96	25.77														
5.4	23.46	23.98	23.76	23.51	23.56	23.47	22.63													
5.3	21.64	21.76	21.16	20.56	20.48	20.78	20.96	20.53												
5.2	20.17	20.10	19.43	18.69	18.34	18.50	19.01	19.39	19.18											
5.1	19.04	18.98	18.40	17.69	17.17	17.04	17.37	17.90	18.24	17.98										
5	18.42	18.47	18.02	17.35	16.72	16.32	16.26	16.49	16.82	16.98	16.65									
4.9	18.22	18.40	18.03	17.35	16.61	15.94	15.49	15.30	15.32	15.50	15.74	15.73								
4.8	17.99	18.25	17.92	17.21	16.34	15.43	14.70	14.25	14.02	14.01	14.44	15.11	15.35							
4.7	17.31	17.61	17.36	16.67	15.72	14.68	13.83	13.30	12.96	12.77	13.07	13.89	14.64	14.56						
4.6	15.96	16.38	16.26	15.66	14.78	13.81	13.01	12.49	12.10	11.80	11.87	12.44	13.17	13.46	12.97					
4.5	14.43	14.94	14.92	14.41	13.66	12.88	12.25	11.81	11.43	11.09	10.98	11.23	11.64	11.93	11.88	11.44				
4.4	12.91	13.49	13.53	13.08	12.40	11.73	11.24	10.93	10.68	10.40	10.23	10.26	10.38	10.47	10.54	10.54	10.23			
4.3	11.38	11.94	12.00	11.60	10.95	10.29	9.833	9.653	9.574	9.430	9.296	9.266	9.235	9.155	9.125	9.245	9.345	9.009		
4.2	9.945	10.44	10.48	10.09	9.489	8.851	8.417	8.300	8.317	8.257	8.180	8.165	8.105	7.958	7.827	7.864	8.062	8.083	7.663	
4.1	8.796	9.247	9.229	8.845	8.324	7.794	7.415	7.305	7.318	7.259	7.185	7.166	7.101	6.959	6.800	6.748	6.871	7.006	6.936	6.663
4	7.845	8.277	8.254	7.914	7.505	7.128	6.846	6.739	6.711	6.619	6.515	6.461	6.375	6.225	6.061	5.987	6.067	6.197	6.262	6.274
3.9	7.087	7.504	7.501	7.210	6.890	6.655	6.500	6.440	6.404	6.294	6.166	6.088	5.987	5.825	5.655	5.595	5.684	5.791	5.818	5.858
3.8	6.370	6.762	6.766	6.454	6.229	6.112	6.099	6.139	6.146	6.040	5.895	5.807	5.727	5.597	5.446	5.398	5.497	5.584	5.534	5.480
3.7	5.300	5.682	5.717	5.507	5.339	5.353	5.482	5.626	5.670	5.556	5.390	5.288	5.230	5.161	5.060	5.034	5.143	5.238	5.173	5.064
3.6	4.195	4.586	4.680	4.580	4.546	4.668	4.926	5.124	5.151	4.997	4.800	4.675	4.625	4.606	4.562	4.553	4.654	4.752	4.701	4.590
3.5	3.673	4.047	4.159	4.115	4.153	4.359	4.649	4.861	4.855	4.654	4.426	4.287	4.247	4.261	4.235	4.202	4.251	4.303	4.235	4.126
3.4	3.197	3.485	3.537	3.474	3.516	3.739	4.053	4.285	4.284	4.088	3.872	3.752	3.734	3.747	3.688	3.603	3.599	3.617	3.553	3.474
3.3	2.176	2.352	2.330	2.229	2.257	2.479	2.806	3.057	3.092	2.955	2.809	2.753	2.768	2.757	2.645	2.526	2.515	2.554	2.556	2.560
3.2	1.261	1.377	1.313	1.164	1.138	1.311	1.610	1.865	1.942	1.885	1.829	1.843	1.896	1.873	1.723	1.566	1.582	1.647	1.710	1.786
3.1	.9214	1.023	.9343	.7203	.6052	.6942	.9395	1.190	1.317	1.339	1.341	1.373	1.428	1.401	1.239	1.096	1.090	1.157	1.236	1.334
3	.7501	.6409	.7126	.4336	.2576	.2969	.4980	.7290	.8814	.9483	.9621	.9678	.9951	.9677	.8333	.7215	.7251	.7867	.8677	.9632
2.9	.3828	.4453	.2572	-.061	-.228	-.174	.0041	.1901	.3101	.3600	.3558	.3466	.3728	.3734	.3079	.2657	.2923	.3514	.4385	.5345
2.8	-.006	-.010	-.270	-.584	-.672	-.554	-.377	-.237	-.173	-.172	-.201	-.203	-.151	-.107	-.104	-.088	-.050	-.002	.0903	.1976
2.7	.0663	-.053	-.401	-.677	-.654	-.461	-.278	-.170	-.156	-.208	-.260	-.244	-.160	-.102	-.098	-.095	-.093	-.089	-.023	.0815
2.6	1.066	.7885	.3110	.0428	.1493	.3775	.5231	.5554	.4801	.3524	.2849	.3464	.4628	.4767	.3760	.2738	.1821	.0918	.0704	.1119
2.5	2.991	2.550	1.885	1.527	1.633	1.839	1.889	1.772	1.537	1.296	1.214	1.325	1.456	1.384	1.132	.8855	.6672	.4402	.2805	.2080
2.4	5.133	4.576	3.722	3.209	3.234	3.387	3.341	3.068	2.656	2.290	2.172	2.290	2.388	2.212	1.821	1.442	1.092	.7240	.4145	.2880
2.3	6.757	6.167	5.218	4.580	4.504	4.568	4.412	4.002	3.449	2.967	2.784	2.866	2.915	2.665	2.193	1.723	1.264	.7910	.4515	.2677
2.2	7.582	7.004	6.033	5.304	5.089	5.051	4.866	4.446	3.841	3.264	2.991	3.044	3.112	2.854	2.306	1.729	1.181	.6650	.3330	.1842
2.1	7.929	7.392	6.427	5.642	5.310	5.182	5.004	4.642	4.039	3.375	3.001	3.028	3.124	2.873	2.289	1.660	1.076	.5682	.2798	.1756
2	7.269	6.730	5.809	5.055	4.712	4.609	4.539	4.321	3.838	3.220	2.801	2.746	2.779	2.498	1.899	1.261	.6906	.2395	.0421	.0148
1.9	4.837	4.428	3.727	3.145	2.916	2.951	3.057	3.034	2.767	2.314	1.922	1.790	1.754	1.483	.9666	.4270	-.046	-.374	-.438	-.370
1.8	-1.43	-1.52	-1.57	-1.45	-1.16	-.788	-.435	-.277	-.351	-.578	-.821	-.911	-.904	-.992	-1.16	-1.31	-1.42	-1.42	-1.23	-.946
1.7	-6.41	-6.26	-5.84	-5.19	-4.48	-3.77	-3.13	-2.75	-2.62	-2.63	-2.73	-2.81	-2.86	-2.91	-2.86	-2.63	-2.30	-1.92	-1.46	-1.02
1.6	-7.70	-7.22	-6.40	-5.55	-4.89	-4.26	-3.59	-3.08	-2.79	-2.65	-2.69	-2.80	-2.84	-2.80	-2.65	-2.34	-1.91	-1.45	-.985	-.564
1.5	-8.10	-7.46	-6.52	-5.68	-5.12	-4.55	-3.84	-3.23	-2.79	-2.52	-2.49	-2.61	-2.63	-2.52	-2.28	-1.88	-1.33	-.768	-.309	.0697
1.4	-8.45	-7.66	-6.63	-5.86	-5.44	-4.92	-4.18	-3.46	-2.87	-2.43	-2.31	-2.42	-2.43	-2.23	-1.88	-1.37	-.680	.0056	.4561	.7717
1.3	-8.40	-7.49	-6.30	-5.44	-5.06	-4.66	-3.96	-3.18	-2.45	-1.86	-1.65	-1.77	-1.84	-1.65	-1.25	-.664	.1060	.8071	1.176	1.392
1.2	-8.40	-7.38	-6.03	-5.06	-4.72	-4.41	-3.76	-2.93	-2.08	-1.35	-1.06	-1.21	-1.34	-1.15	-.686	-.006	.8375	1.543	1.827	1.945
1.1	-9.33	-8.33	-6.90	-5.82	-5.38	-5.02	-4.37	-3.59	-2.78	-2.05	-1.73	-1.87	-2.01	-1.74	-1.12	-.305	.6154	1.358	1.641	1.754
1	-10.3	-9.32	-7.83	-6.62	-6.08	-5.66	-5.01	-4.28	-3.53	-2.80	-2.44	-2.59	-2.73	-2.37	-1.58	-.626	.3739	1.153	1.433	1.537
0.9	-10.8	-9.87	-8.34	-7.05	-6.45	-6.01	-5.38	-4.71	-4.04	-3.35	-2.99	-3.14	-3.28	-2.84	-1.93	-.896	.1475	.9515	1.226	1.313
0.8	-9.92	-9.04	-7.57	-6.34	-5.81	-5.42	-4.90	-4.18	-3.63	-3.08	-2.79	-2.95	-3.06	-2.63	-1.77	-.808	.1895	.9813	1.229	1.253
0.7	-9.05	-8.21	-6.79	-5.59	-5.13	-4.78	-4.17	-3.60	-3.18	-2.76	-2.55	-2.70	-2.78	-2.36	-1.57	-.692	.2565	1.038	1.259	1.214
0.6	-9.95	-8.89	-7.22	-5.91	-5.47	-5.17	-4.61	-4.08	-3.68	-3.26	-3.02	-3.09	-3.05	-2.56	-1.80	-.957	.0222	.8871	1.197	1.204
0.5	-10.9	-9.60	-7.67	-6.25	-5.83	-5.58	-5.07	-4.59	-4.20	-3.79	-3.53	-3.50	-3.33	-2.77	-2.03	-1.24	-.230	.7214	1.125	1.190
0.4	-11.9	-10.3	-8.13	-6.59	-6.20	-6.00	-5.55	-5.11	-4.75	-4.35	-4.06	-3.93	-3.62	-2.99	-2.28	-1.53	-.501	.5396	1.044	1.171
0.3	-11.4	-9.60	-7.19	-5.60	-5.29	-5.18	-4.83	-4.51	-4.22	-3.82	-3.45	-3.19	-2.81	-2.23	-1.62	-.939	.1263	1.240	1.776	1.905
0.2	-10.2	-8.18	-5.62	-4.04	-3.82	-3.79	-3.54	-3.37	-3.18	-2.78	-2.29	-1.89	-1.49	-1.02	-.570	.0402	1.140	2.325	2.857	2.949
0.1	-6.03	-4.87	-3.35	-2.42	-2.24	-1.98	-1.41	-.912	-.414	.2923	.9863	1.309	1.393	1.563	1.845	2.308	3.067	3.786	3.997	3.926
0	-3.48	-3.26	-2.29	-1.24	-.768	-.707	-.678	-.400	.3155	1.432	2.511	3.074	3.249	3.394	3.528	3.699	4.052	4.478	4.623	4.465

	4	3.9	3.8	3.7	3.6	3.5	3.4	3.3	3.2	3.1	3	2.9	2.8	2.7	2.6	2.5	2.4	2.3	2.2	2.1
8																				
7.9																				
7.8																				
7.7																				
7.6																				
7.5																				
7.4																				
7.3																				
7.2																				
7.1																				
7																				
6.9																				
6.8																				
6.7																				
6.6																				
6.5																				
6.4																				
6.3																				
6.2																				
6.1																				
6																				
5.9																				
5.8																				
5.7																				
5.6																				
5.5																				
5.4																				
5.3																				
5.2																				
5.1																				
5																				
4.9																				
4.8																				
4.7																				
4.6																				
4.5																				
4.4																				
4.3																				
4.2																				
4.1																				
4	6.192																			
3.9	5.951	5.985																		
3.8	5.589	5.835	5.991																	
3.7	5.126	5.433	5.792	5.859																
3.6	4.620	4.888	5.277	5.530	5.495															
3.5	4.145	4.361	4.687	4.984	5.167	5.112														
3.4	3.509	3.690	3.953	4.218	4.462	4.579	4.299													
3.3	2.632	2.788	3.006	3.240	3.458	3.616	3.564	3.196												
3.2	1.882	2.020	2.207	2.414	2.584	2.701	2.746	2.650	2.408											
3.1	1.436	1.558	1.731	1.913	2.030	2.092	2.130	2.129	2.088	2.002										
3	1.049	1.151	1.309	1.468	1.551	1.586	1.621	1.655	1.712	1.790	1.768									
2.9	.5971	.6611	.7854	.9247	1.003	1.046	1.112	1.198	1.300	1.442	1.566	1.580								
2.8	.2528	.2824	.3662	.4923	.5870	.6498	.7408	.8612	.9763	1.111	1.290	1.470	1.573							
2.7	.1397	.1597	.2295	.3559	.4641	.5354	.6225	.7345	.8327	.9373	1.100	1.328	1.578	1.815						
2.6	.1393	.1614	.2519	.3905	.4979	.5681	.6450	.7271	.7870	.8602	.9983	1.209	1.514	1.984	2.567					
2.5	.1640	.1717	.2792	.4143	.5004	.5676	.6452	.6987	.7125	.7572	.8916	1.094	1.408	2.030	3.020	3.995				
2.4	.1815	.1486	.2326	.3373	.3920	.4548	.5411	.5861	.5766	.6065	.7437	.9488	1.266	1.961	3.184	4.537	5.470			
2.3	.1261	.0488	.0928	.1565	.1746	.2238	.3192	.3890	.4073	.4509	.5887	.7935	1.122	1.853	3.167	4.698	5.902	6.678		
2.2	.0597	-.042	-.062	-.090	-.161	-.160	-.067	.0450	.1328	.2214	.3683	.5808	.9272	1.669	2.970	4.499	5.797	6.814	7.465	
2.1	.0646	-.056	-.132	-.269	-.475	-.558	-.467	-.298	-.134	.0018	.1689	.4079	.7856	1.536	2.798	4.259	5.550	6.705	7.790	8.647
2	-.060	-.179	-.288	-.509	-.804	-.912	-.772	-.527	-.311	-.171	-.008	.2504	.6453	1.367	2.533	3.958	5.053	6.220	7.561	8.783
1.9	-.387	-.458	-.515	-.670	-.894	-.963	-.810	-.553	-.342	-.230	-.095	.1459	.5106	1.150	2.128	3.185	4.127	5.086	6.357	7.587
1.8	-.785	-.795	-.874	-.946	-1.02	-1.06	-.979	-.733	-.493	-.382	-.264	-.025	.2965	.6959	1.170	1.587	1.942	2.408	3.289	4.212
1.7	-.761	-.759	-.875	-.896	-.851	-.866	-.824	-.584	-.339	-.260	-.198	-.011	.2128	.3288	.2653	.0264	-.195	-.208	.3203	.9678
1.6	-.299	-.251	-.284	-.221	-.118	-.118	-.128	.0064	.1784	.2351	.2333	.2600	.2278	-3.-4	-.467	-1.10	-1.63	-1.95	-1.68	-1.27
1.5	.3760	.5249	.5557	.6217	.7072	.6819	.5747	.5153	.5175	.4846	.3635	.1875	-.060	-.503	-1.27	-2.22	-3.03	-3.60	-3.66	-3.56
1.4	1.112	1.374	1.483	1.550	1.605	1.541	1.321	1.045	.8556	.7199	.4700	.0810	-.388	-1.04	-2.10	-3.38	-4.45	-5.29	-5.72	-5.95
1.3	1.725	2.062	2.226	2.284	2.331	2.291	2.033	1.589	1.197	.9213	.5480	-.009	-.664	-1.50	-2.76	-4.26	-5.55	-6.66	-7.42	-7.95
1.2	2.265	2.667	2.883	2.940	2.988	2.974	2.682	2.084	1.503	1.095	.6101	-.093	-.911	-1.92	-3.38	-5.09	-6.60	-7.95	-9.04	-9.87
1.1	2.111	2.566	2.822	2.939	3.075	3.124	2.951	2.232	1.598	1.136	.6188	-.083	-.893	-1.97	-3.60	-5.51	-7.21	-8.75	-10.0	-11.0
1	1.931	2.443	2.741	2.922	3.153	3.269	3.016	2.375	1.687	1.168	.6191	-.078	-.874	-2.02	-3.82	-5.95	-7.83	-9.57	-11.0	-12.2
0.9	1.717	2.257	2.584	2.824	3.131	3.291	3.052	2.410	1.701	1.153	.5926	-.090	-.873	-2.06	-3.97	-6.23	-8.22	-10.1	-11.6	-12.9
0.8	1.584	2.082	2.411	2.673	2.972	3.084	2.804	2.177	1.506	.9932	.4752	-.181	-.971	-2.15	-3.97	-6.08	-7.91	-9.62	-11.1	-12.2
0.7	1.464	1.913	2.241	2.514	2.788	2.831	2.500	1.885	1.259	.7880	.3174	-.312	-1.11	-2.27	-4.00	-5.95	-7.62	-9.19	-10.5	-11.5
0.6	1.443	1.823	2.064	2.262	2.465	2.442	2.068	1.472	.9402	.5570	.0824	-.602	-1.46	-2.74	-4.68	-6.86	-8.60	-10.1	-11.1	-11.9
0.5	1.416	1.720	1.867	1.981	2.108	2.015	1.596	1.023	.5952	.3075	-.170	-.912	-1.83	-3.23	-5.40	-7.81	-9.63	-11.0	-11.8	-12.2
0.4	1.383	1.604	1.649	1.675	1.721	1.552	1.087	.5397	.2248	.0399	-.441	-1.24	-2.23	-3.75	-6.15	-8.81	-10.7	-12.0	-12.4	-12.6
0.3	2.137	2.365	2.333	2.175	1.987	1.630	1.034	.4054	.1159	-.005	-.536	-1.49	-2.65	-4.42	-7.16	-10.1	-12.1	-13.3	-13.6	-13.6
0.2	3.212	3.497	3.409	3.023	2.534	1.942	1.176	.4119	.1029	.0313	-.566	-1.71	-3.10	-5.17	-8.28	-11.5	-13.7	-14.8	-15.1	-15.0
0.1	4.135	4.596	4.822	4.656	4.403	4.177	3.628	2.681	2.003	1.770	1.252	.1226	-1.34	-3.13	-5.31	-7.48	-9.27	-10.8	-12.3	-13.4
0	4.411	4.631	4.746	4.518	4.341	4.387	4.092	3.190	2.449	2.317	2.152	1.373	.1371	-1.23	-2.48	-3.66	-5.12	-7.03	-9.42	-11.3

	2	1.9	1.8	1.7	1.6	1.5	1.4	1.3	1.2	1.1	1	0.9	0.8	0.7	0.6	0.5	0.4	0.3	0.2	0.1	0
8																					
7.9																					
7.8																					
7.7																					
7.6																					
7.5																					
7.4																					
7.3																					
7.2																					
7.1																					
7																					
6.9																					
6.8																					
6.7																					
6.6																					
6.5																					
6.4																					
6.3																					
6.2																					
6.1																					
6																					
5.9																					
5.8																					
5.7																					
5.6																					
5.5																					
5.4																					
5.3																					
5.2																					
5.1																					
5																					
4.9																					
4.8																					
4.7																					
4.6																					
4.5																					
4.4																					
4.3																					
4.2																					
4.1																					
4																					
3.9																					
3.8																					
3.7																					
3.6																					
3.5																					
3.4																					
3.3																					
3.2																					
3.1																					
3																					
2.9																					
2.8																					
2.7																					
2.6																					
2.5																					
2.4																					
2.3																					
2.2																					
2.1																					
2	9.445																				
1.9	8.517	8.333																			
1.8	5.123	5.654	5.650																		
1.7	1.812	2.833	4.752	6.066																	
1.6	-.599	-.4815	3.099	5.639	7.164																
1.5	-3.11	-1.98	1.060	4.188	6.322	6.942															
1.4	-5.74	-4.57	-1.12	2.574	5.320	7.490	9.721														
1.3	-7.92	-6.72	-2.98	1.172	4.564	7.670	10.91	13.24													
1.2	-10.0	-8.78	-4.72	-.124	3.865	7.816	11.96	15.36	18.49												
1.1	-11.2	-9.98	-5.57	-.597	3.652	7.901	12.37	16.09	19.62	21.53											
1	-12.5	-11.2	-6.47	-1.11	3.392	7.946	12.74	16.81	20.76	23.50	26.35										
0.9	-13.3	-12.0	-7.03	-1.50	3.072	7.790	12.77	17.02	21.22	24.52	27.97	30.07									
0.8	-12.6	-11.4	-6.80	-1.67	2.502	7.061	11.86	15.96	19.98	22.97	26.10	28.21	27.32								
0.7	-11.8	-10.8	-6.51	-1.80	1.954	6.338	10.94	14.87	18.70	21.32	24.08	26.16	26.25	26.23							
0.6	-12.0	-11.1	-6.38	-1.42	2.503	6.972	11.65	15.51	19.26	21.86	24.59	26.62	26.63	26.59	27.97						
0.5	-12.2	-11.3	-6.22	-.992	3.090	7.636	12.38	16.16	19.82	22.38	25.06	27.04	26.97	26.91	29.36	31.91					
0.4	-12.4	-11.4	-6.02	-.533	3.712	8.329	13.12	16.81	20.36	22.88	25.50	27.42	27.25	27.17	30.77	34.55	38.51				
0.3	-13.4	-12.5	-6.61	-.776	3.904	9.024	14.34	18.27	22.03	24.60	27.26	29.18	28.92	28.79	32.94	37.31	41.88	47.72			
0.2	-14.8	-13.9	-7.58	-1.40	3.827	9.658	15.73	20.07	24.16	26.80	29.54	31.48	31.14	30.95	35.42	40.11	45.01	54.13	65.21		
0.1	-13.9	-13.1	-8.71	-3.57	1.820	7.268	12.97	17.76	22.21	24.39	26.62	27.97	27.04	26.10	27.96	29.87	31.83	38.00	46.11	44.30	
0	-12.1	-11.4	-9.02	-4.97	-.239	4.704	9.855	14.43	18.68	20.33	22.02	22.83	21.57	20.21	19.95	19.61	19.18	21.78	25.67	38.26	53.47

APPENDIX G

MID-LATITUDES "WINTER" A PRIORI DATA

The statistics were constructed from 145 December, January, February profiles for years 1969 through 1972. The mean profile is given below :

TABLE G.1 : The Mean Profile* (^{0}C)

-17.29	-16.63	-15.53	-14.32	-13.22	-12.21	-11.22	-10.21
- 9.19	- 8.18	- 7.35	- 6.87	- 6.81	-7.16	-7.94	- 9.13
-10.65	-12.37	-14.22	-16.23	-18.38	-20.57	-22.73	-24.93
-27.18	-29.34	-31.30	-33.17	-35.05	-36.92	-38.78	-40.61
-42.37	-44.05	-45.64	-47.11	-48.46	-49.72	-50.93	-52.07
-53.09	-53.98	-54.81	-55.60	-56.40	-57.27	-58.23	-59.11
-59.80	-60.38	-60.99	-61.69	-62.45	-63.22	-63.84	-64.29
-64.27	-63.76	-62.55	-61.25	-60.00	-58.96	-58.39	-57.94
-56.83	-53.90	-50.74	-47.26	-42.35	-38.36	-33.31	-28.20
-22.95	-17.76	-12.94	- 8.12	- 3.31	0.61	4.30	7.45
10.47							

*Listed from 8 sh altitude to ground level in steps of 0.1 sh.

The original a priori covarinace matrix is given in table G.2. The indices indicate the height in sh(i.e. $-\ln(p/p_o)$

TABLE G.2 : The Mid-Latitudes winter a priori covariance matrix

	8	7.9	7.8	7.7	7.6	7.5	7.4	7.3	7.2	7.1	7	6.9	6.8	6.7	6.6	6.5	6.4	6.3	6.2	6.1
8	50.24																			
7.9	48.72	48.95																		
7.8	46.58	46.93	51.98																	
7.7	43.79	47.38	52.80	56.37																
7.6	39.42	43.21	49.59	55.36	57.56															
7.5	33.54	37.07	43.47	50.51	55.89	58.54														
7.4	27.34	30.53	36.59	44.01	51.38	57.62	60.66													
7.3	21.63	24.43	29.97	37.15	45.10	53.12	59.04	60.77												
7.2	16.66	19.01	24.05	30.86	38.65	47.00	54.25	58.69	60.13											
7.1	12.40	14.28	18.85	25.42	33.04	41.27	48.85	54.76	59.21	62.14										
7	8.422	9.817	13.90	20.25	27.88	36.24	44.07	50.60	56.70	62.84	67.67									
6.9	4.240	5.403	9.107	15.17	22.79	31.44	39.68	46.51	53.18	61.14	69.50	75.74								
6.8	.0099	1.388	5.106	10.87	18.24	26.89	35.22	42.04	48.89	57.70	68.10	78.11	85.65							
6.7	-4.12	-2.23	1.855	7.473	14.45	22.71	30.59	37.04	43.91	53.13	64.28	76.49	88.92	98.72						
6.6	-8.58	-6.16	-1.64	4.067	10.91	18.82	26.13	32.02	38.69	47.96	59.17	72.13	87.42	102.5	112.5					
6.5	-13.4	-10.6	-5.68	.3325	7.484	15.50	22.57	28.04	34.31	43.32	54.36	67.27	83.16	100.6	115.3	124.5				
6.4	-17.7	-14.6	-9.35	-2.93	4.793	13.30	20.55	25.81	31.64	40.24	51.11	63.83	79.26	96.89	114.1	128.8	139.9			
6.3	-21.3	-17.9	-12.3	-5.60	2.675	11.86	19.59	24.88	30.23	38.30	49.05	61.80	76.82	93.91	111.9	129.6	146.1	158.4		
6.2	-24.3	-20.7	-15.1	-8.25	.4193	10.32	18.85	24.42	29.22	36.35	46.65	59.42	74.14	90.44	107.9	126.4	145.5	162.0	170.7	
6.1	-26.6	-23.0	-17.5	-10.6	-1.75	8.624	17.86	23.72	27.78	33.54	42.83	55.28	69.61	84.95	101.4	119.2	138.2	156.2	168.7	172.0
6	-28.5	-25.0	-19.4	-12.5	-3.83	6.909	15.94	21.79	25.12	29.62	37.84	49.81	63.83	78.48	93.84	110.5	128.1	145.6	159.8	167.4
5.9	-30.6	-27.0	-21.4	-14.6	-6.22	3.731	12.90	18.53	21.41	25.14	32.64	44.20	57.94	72.08	86.65	102.2	118.7	135.1	149.5	159.3
5.8	-31.9	-28.3	-22.8	-16.2	-8.16	1.224	9.895	15.26	17.84	21.05	27.92	38.91	51.98	65.25	79.01	93.97	109.8	125.5	139.6	149.9
5.7	-32.1	-28.6	-23.2	-16.9	-9.40	-.731	7.328	12.38	14.71	17.38	23.45	33.45	45.25	57.13	69.77	84.04	99.32	114.5	128.1	138.2
5.6	-31.4	-28.3	-23.5	-17.7	-10.9	-2.96	4.447	9.164	11.29	13.48	18.61	27.27	37.50	47.85	59.17	72.30	86.54	100.8	113.7	123.4
5.5	-29.7	-27.2	-23.3	-18.4	-12.3	-5.26	1.412	5.689	7.581	9.312	13.44	20.67	29.39	38.43	48.52	60.29	73.05	85.88	97.67	106.8
5.4	-26.5	-24.6	-21.6	-17.7	-12.7	-6.66	-.933	2.742	4.234	5.362	8.449	14.32	21.74	29.72	38.74	49.17	60.41	71.65	82.01	90.04
5.3	-22.5	-21.0	-18.7	-15.7	-11.8	-6.94	-2.24	.7481	1.687	2.065	4.101	8.716	14.95	21.90	29.79	38.84	48.59	58.39	67.36	74.28
5.2	-19.0	-17.8	-16.0	-13.6	-10.4	-6.51	-2.67	-.331	.0447	-.287	.7976	4.274	9.369	15.25	21.91	29.49	37.80	46.36	54.23	60.25
5.1	-15.8	-14.9	-13.5	-11.7	-9.02	-5.77	-2.70	-1.03	-1.16	-2.00	-1.59	.9884	5.116	9.997	15.46	21.62	28.52	35.85	42.62	47.79
5	-12.3	-11.7	-10.8	-9.57	-7.57	-5.12	-2.97	-2.06	-2.70	-3.85	-3.61	-1.80	1.576	5.548	9.924	14.83	20.37	26.26	31.70	35.95
4.9	-9.31	-8.96	-8.59	-7.94	-6.74	-5.28	-4.11	-3.92	-4.95	-6.25	-6.33	-4.61	-1.75	1.471	4.946	8.831	13.12	17.54	21.61	24.95
4.8	-7.50	-7.43	-7.55	-7.60	-7.27	-6.72	-6.30	-6.50	-7.52	-8.65	-8.66	-7.06	-4.52	-1.80	.9806	4.011	7.195	10.27	13.09	15.62
4.7	-6.36	-6.56	-7.22	-8.01	-8.49	-8.65	-8.65	-8.86	-9.52	-10.2	-10.0	-8.60	-6.38	-4.13	-1.97	.2686	2.449	4.332	6.051	7.861
4.6	-4.92	-5.38	-6.53	-7.95	-9.09	-9.79	-10.1	-10.2	-10.5	-10.9	-10.6	-9.50	-7.78	-6.09	-4.54	-3.01	-1.67	-.764	.0397	1.249
4.5	-3.09	-3.71	-5.17	-6.99	-8.60	-9.80	-10.5	-10.8	-11.1	-11.3	-11.1	-10.3	-9.13	-7.93	-6.86	-5.88	-5.23	-5.09	-5.03	-4.32
4.4	-1.30	-1.95	-3.51	-5.51	-7.41	-9.07	-10.3	-11.0	-11.4	-11.7	-11.6	-11.0	-10.2	-9.36	-8.60	-8.02	-7.92	-8.43	-9.05	-8.87
4.3	.2994	-.346	-1.90	-3.94	-6.00	-8.01	-9.66	-10.7	-11.3	-11.6	-11.6	-11.2	-10.8	-10.3	-9.73	-9.43	-9.73	-10.8	-12.0	-12.5
4.2	1.722	1.048	-.515	-2.57	-4.75	-7.00	-8.90	-10.1	-10.8	-11.1	-11.1	-11.0	-10.9	-10.7	-10.4	-10.4	-11.1	-12.6	-14.4	-15.3
4.1	2.958	2.293	.7655	-1.31	-3.65	-6.10	-8.14	-9.39	-10.0	-10.4	-10.6	-10.7	-10.9	-11.0	-11.0	-11.3	-12.3	-14.1	-16.2	-17.4
4	4.097	3.522	2.138	.1052	-2.34	-4.93	-7.06	-8.39	-9.14	-9.65	-10.1	-10.5	-11.1	-11.5	-11.7	-12.3	-13.6	-15.6	-17.6	-18.8
3.9	4.963	4.450	3.214	1.321	-1.06	-3.63	-5.80	-7.22	-8.08	-8.75	-9.44	-10.3	-11.1	-11.8	-12.4	-13.2	-14.7	-16.7	-18.7	-19.7
3.8	5.030	4.480	3.286	1.530	-.662	-3.03	-5.09	-6.53	-7.42	-8.11	-8.92	-9.93	-10.9	-11.6	-12.3	-13.3	-15.0	-17.2	-19.2	-20.1
3.7	4.426	3.810	2.600	.9456	-1.01	-3.07	-4.91	-6.28	-7.17	-7.80	-8.55	-9.48	-10.3	-10.8	-11.4	-12.4	-14.4	-16.7	-18.6	-19.4
3.6	3.959	3.327	2.159	.6397	-1.08	-2.82	-4.41	-5.72	-6.64	-7.26	-7.86	-8.62	-9.28	-9.63	-10.0	-11.0	-13.0	-15.3	-17.1	-17.6
3.5	4.018	3.413	2.358	1.029	-.455	-1.94	-3.33	-4.60	-5.58	-6.21	-6.69	-7.30	-7.88	-8.22	-8.63	-9.68	-11.5	-13.6	-15.1	-15.6
3.4	4.100	3.529	2.573	1.402	.1111	-1.17	-2.43	-3.66	-4.68	-5.29	-5.65	-6.10	-6.60	-7.02	-7.62	-8.83	-10.6	-12.5	-13.8	-14.2
3.3	3.651	3.115	2.214	1.129	-.024	-1.16	-2.30	-3.49	-4.51	-5.10	-5.37	-5.67	-6.05	-6.48	-7.24	-8.64	-10.4	-12.1	-13.3	-13.6
3.2	3.082	2.577	1.712	.6861	-.356	-1.36	-2.39	-3.50	-4.50	-5.13	-5.43	-5.71	-6.06	-6.46	-7.25	-8.67	-10.4	-11.9	-12.9	-13.2
3.1	3.044	2.528	1.671	.7119	-.189	-1.01	-1.87	-2.86	-3.84	-4.55	-4.98	-5.36	-5.76	-6.22	-7.02	-8.39	-10.0	-11.3	-12.2	-12.4
3	3.357	2.759	1.846	.9611	.2741	-.275	-.880	-1.68	-2.57	-3.31	-3.80	-4.24	-4.73	-5.30	-6.21	-7.59	-9.09	-10.2	-10.9	-11.2
2.9	3.631	2.909	1.886	1.049	.5887	.3466	.0233	-.576	-1.36	-2.03	-2.43	-2.80	-3.28	-3.90	-4.87	-6.27	-7.66	-8.62	-9.21	-9.51
2.8	3.987	3.162	2.017	1.170	.8717	.8763	.7578	.2591	-.509	-1.14	-1.45	-1.75	-2.22	-2.82	-3.73	-5.03	-6.25	-7.01	-7.48	-7.81
2.7	4.531	3.711	2.529	1.658	1.431	1.573	1.546	1.020	.1337	-.609	-.983	-1.35	-1.93	-2.64	-3.54	-4.70	-5.71	-6.22	-6.45	-6.68
2.6	5.046	4.367	3.323	2.537	2.411	2.694	2.774	2.246	1.235	.2573	-.411	-1.06	-1.90	-2.83	-3.87	-5.02	-5.89	-6.17	-6.14	-6.16
2.5	4.715	4.136	3.189	2.455	2.434	2.949	3.327	3.059	2.173	1.127	.2336	-.666	-1.70	-2.75	-3.84	-5.00	-5.88	-6.17	-6.07	-5.96
2.4	3.876	3.278	2.403	1.871	2.061	2.718	3.260	3.274	2.689	1.785	.8270	-.271	-1.52	-2.64	-3.58	-4.81	-5.19	-5.26	-4.85	-4.46
2.3	3.698	3.112	2.308	1.946	2.357	3.136	3.621	3.487	2.787	1.830	.8685	-.204	-1.40	-2.45	-3.33	-4.19	-4.73	-4.62	-4.18	-3.88
2.2	3.194	2.650	1.965	1.725	2.177	2.955	3.476	3.427	2.834	2.005	1.196	.2633	-.846	-1.83	-2.61	-3.31	-3.71	-3.50	-2.95	-2.43
2.1	2.826	2.335	1.783	1.691	2.226	3.047	3.617	3.618	3.075	2.311	1.593	.7706	-.222	-1.08	-1.73	-2.30	-2.59	-2.34	-1.70	-.957
2	2.501	2.078	1.672	1.721	2.320	3.171	3.794	3.854	3.363	2.664	2.037	1.344	.5084	-.185	-.681	-1.12	-1.32	-1.02	-.277	.7109
1.9	2.273	1.961	1.730	1.891	2.495	3.351	4.044	4.178	3.728	3.071	2.540	1.998	1.324	.7849	.4427	.1564	.0769	.4602	1.360	2.619
1.8	2.344	2.162	2.140	2.445	3.089	4.022	4.850	5.032	4.526	3.856	3.434	3.018	2.381	1.845	1.535	1.311	1.332	1.889	3.088	4.695
1.7	2.656	2.623	2.812	3.214	3.826	4.796	5.773	6.044	5.510	4.834	4.523	4.244	3.636	3.033	2.619	2.299	2.296	2.973	4.508	6.559
1.6	2.175	2.277	2.619	3.036	3.542	4.485	5.602	6.098	5.790	5.320	5.226	5.198	4.763	4.089	3.383	2.768	2.596	3.223	4.874	7.132
1.5	1.780	2.024	2.457	2.757	2.913	3.336	3.965	4.299	4.253	4.147	4.204	4.288	4.163	3.740	2.900	1.840	1.151	1.253	2.260	3.758
1.4	1.131	1.539	2.132	2.438	2.377	2.395	2.628	2.842	3.058	3.359	3.666	3.968	4.259	4.285	3.648	2.510	1.569	1.272	1.649	2.343
1.3	.9151	1.439	2.262	2.759	2.637	2.319	2.193	2.315	2.721	3.196	3.479	3.797	4.405	4.891	4.539	3.378	2.200	1.528	1.328	1.287
1.2	.9024	1.544	2.552	3.179	2.991	2.387	1.945	1.968	2.481	3.029	3.200	3.453	4.287	5.168	5.120	4.068	2.845	1.956	1.281	.6023
1.1	.0940	.7289	1.744	2.350	2.054	1.257	.6497	.6585	1.305	1.956	2.068	2.210	3.061	4.092	4.267	3.423	2.279	1.326	.4897	-.407
1	-1.03	-.426	.5732	1.162	.7817	-.190	-.935	-.943	-.147	.6290	.7018	.7315	1.585	2.664	3.007	2.346	1.271	.2543	-.715	-1.77
0.9	-2.21	-1.69	-.577	.0026	-.448	-1.55	-2.43	-2.39	-1.48	-.646	-.652	-.718	.0897	1.220	1.644	1.116	.0818	-1.01	-2.06	-3.16
0.8	-3.15	-2.43	-1.34	-.755	-1.24	-2.40	-3.30	-3.24	-2.31	-1.55	-1.71	-1.89	-1.19	-.276	-.034	-.562	-1.60	-2.80	-3.90	-4.91
0.7	-4.08	-3.28	-2.12	-1.25	-2.10	-3.35	-4.32	-4.28	-3.34	-2.63	-2.93	-3.24	-2.68	-2.00	-1.90	-2.34	-3.29	-4.53	-5.66	-6.64
0.6	-4.59	-3.71	-2.43	-1.78	-2.41	-3.86	-5.08	-5.28	-4.50	-3.81	-4.04	-4.31	-3.76	-3.07	-2.85	-3.08	-3.78	-4.73	-5.51	-6.16
0.5	-4.99	-4.05	-2.63	-1.90	-2.62	-4.30	-5.81	-6.29	-5.69	-5.02	-5.19	-5.43	-4.89	-4.21	-3.91	-3.95	-4.43	-5.09	-5.48	-5.75
0.4	-5.35	-4.34	-2.78	-1.95	-2.77	-4.72	-6.53	-7.32	-6.92	-6.28	-6.40	-6.60	-6.10	-5.44	-5.06	-4.92	-5.17	-5.53	-5.49	-5.36
0.3	-6.57	-5.23	-3.18	-1.97	-2.63	-4.57	-6.52	-7.58	-7.45	-6.95	-7.05	-7.11	-6.57	-6.10	-5.83	-5.53	-5.55	-5.62	-5.05	-4.10
0.2	-8.45	-6.65	-3.95	-2.20	-2.55	-4.34	-6.33	-7.60	-7.67	-7.26	-7.27	-7.10	-6.45	-6.14	-5.91	-5.32	-5.00	-4.75	-3.66	-1.92
0.1	-8.98	-6.60	-3.23	-1.05	-.812	-1.44	-2.11	-2.60	-2.69	-2.82	-3.51	-3.91	-3.61	-3.56	-3.87	-4.13	-4.54	-4.53	-2.99	-.134
0	-6.64	-3.19	1.801	5.350	6.833	7.975	9.268	9.812	9.283	7.701	5.264	3.282	2.583	2.072	.5572	-1.98	-4.73	-6.14	-5.08	-2.16

	6	5.9	5.8	5.7	5.6	5.5	5.4	5.3	5.2	5.1	5	4.9	4.8	4.7	4.6	4.5	4.4	4.3	4.2	4.1
8																				
7.9																				
7.8																				
7.7																				
7.6																				
7.5																				
7.4																				
7.3																				
7.2																				
7.1																				
7																				
6.9																				
6.8																				
6.7																				
6.6																				
6.5																				
6.4																				
6.3																				
6.2																				
6.1																				
6	168.2																			
5.9	164.1	164.3																		
5.8	156.3	159.3	157.5																	
5.7	144.8	148.9	149.6	145.2																
5.6	129.9	134.1	136.2	134.8	128.4															
5.5	112.8	116.8	119.5	120.1	117.1	109.4														
5.4	95.42	99.23	102.2	103.8	102.8	98.28	90.67													
5.3	79.03	82.66	85.67	87.70	87.74	85.32	80.88	74.66												
5.2	64.51	67.94	70.80	72.80	73.37	72.30	70.08	66.82	62.09											
5.1	51.62	54.87	57.57	59.49	60.38	60.18	59.29	57.91	55.70	52.00										
5	39.28	42.29	44.93	46.98	48.24	48.74	48.75	48.49	47.88	46.33	42.96									
4.9	27.76	30.46	33.03	35.33	37.10	38.25	38.96	39.39	39.61	39.34	37.78	34.65								
4.8	18.00	20.42	22.90	25.35	27.49	29.15	30.35	31.18	31.81	32.17	31.78	30.45	28.28							
4.7	9.895	12.12	14.40	16.70	18.89	20.82	22.39	23.54	24.50	25.30	25.65	25.57	25.08	23.65						
4.6	3.004	5.001	6.910	8.743	10.67	12.71	14.63	16.21	17.60	18.87	19.82	20.51	21.08	21.07	20.08					
4.5	-2.81	-1.08	.3420	1.606	3.183	5.254	7.507	9.580	11.49	13.28	14.78	16.04	17.22	18.11	18.42	18.16				
4.4	-7.67	-6.25	-5.26	-4.41	-3.05	-.946	1.566	4.039	6.381	8.613	10.62	12.37	13.96	15.30	16.35	17.11	17.09			
4.3	-11.7	-10.7	-10.0	-9.39	-8.12	-5.97	-3.28	-.552	2.054	4.566	6.945	9.097	10.98	12.56	13.93	15.21	15.98	15.76		
4.2	-15.0	-14.3	-13.9	-13.4	-12.2	-10.0	-7.26	-4.40	-1.64	1.037	3.658	6.088	8.196	9.945	11.51	13.06	14.30	14.78	14.55	
4.1	-17.3	-16.7	-16.5	-16.2	-15.1	-13.0	-10.2	-7.35	-4.51	-1.71	1.047	3.630	5.876	7.764	9.499	11.25	12.73	13.57	13.87	13.79
4	-18.7	-18.3	-18.3	-18.2	-17.2	-15.1	-12.4	-9.54	-6.64	-3.76	-.913	1.761	4.080	6.049	7.914	9.820	11.42	12.41	12.99	13.38
3.9	-19.7	-19.4	-19.5	-19.6	-18.7	-16.7	-14.1	-11.2	-8.32	-5.39	-2.46	.2873	2.644	4.668	6.641	8.663	10.34	11.40	12.09	12.72
3.8	-19.9	-19.7	-19.9	-20.1	-19.3	-17.3	-14.8	-12.1	-9.28	-6.41	-3.51	-.805	1.522	3.576	5.620	7.695	9.391	10.45	11.15	11.83
3.7	-19.1	-18.8	-19.1	-19.3	-18.6	-16.8	-14.4	-12.0	-9.46	-6.89	-4.24	-1.74	.4617	2.499	4.562	6.627	8.300	9.341	10.02	10.64
3.6	-17.3	-17.0	-17.3	-17.8	-17.1	-15.5	-13.5	-11.4	-9.26	-7.15	-4.92	-2.73	-.711	1.246	3.278	5.312	6.962	8.003	8.664	9.217
3.5	-15.2	-15.0	-15.4	-15.8	-15.4	-14.1	-12.5	-10.7	-9.05	-7.35	-5.45	-3.51	-1.68	.1327	2.067	4.026	5.634	6.692	7.377	7.892
3.4	-13.6	-13.8	-14.2	-14.5	-14.2	-13.2	-11.8	-10.4	-8.91	-7.39	-5.61	-3.76	-2.05	-.392	1.380	3.197	4.718	5.772	6.485	6.966
3.3	-13.4	-13.4	-13.8	-14.0	-13.6	-12.6	-11.4	-10.1	-8.71	-7.22	-5.44	-3.58	-1.91	-.370	1.224	2.844	4.215	5.196	5.870	6.296
3.2	-13.1	-13.2	-13.6	-13.6	-13.1	-12.0	-10.9	-9.65	-8.40	-7.01	-5.31	-3.48	-1.82	-.335	1.108	2.517	3.697	4.549	5.150	5.516
3.1	-12.4	-12.6	-12.9	-13.0	-12.4	-11.4	-10.3	-9.25	-8.11	-6.85	-5.28	-3.53	-1.90	-.480	.8391	2.072	3.076	3.809	4.365	4.761
3	-11.2	-11.5	-11.9	-12.1	-11.6	-10.8	-9.81	-8.77	-7.61	-6.32	-4.79	-3.15	-1.65	-.362	.8368	1.950	2.815	3.425	3.924	4.327
2.9	-9.70	-10.1	-10.7	-11.1	-10.8	-10.1	-9.13	-8.04	-6.76	-5.33	-3.77	-2.23	-.921	.1951	1.293	2.340	3.118	3.623	4.048	4.429
2.8	-8.14	-8.76	-9.59	-10.1	-10.0	-9.27	-8.28	-7.15	-5.85	-4.42	-2.92	-1.52	-.365	.6456	1.697	2.723	3.476	3.942	4.331	4.694
2.7	-7.06	-7.83	-8.82	-9.45	-9.27	-8.41	-7.33	-6.22	-5.06	-3.83	-2.55	-1.36	-.375	.5641	1.605	2.623	3.373	3.845	4.248	4.645
2.6	-6.45	-7.23	-8.24	-8.82	-8.51	-7.52	-6.40	-5.42	-4.50	-3.55	-2.56	-1.63	-.821	.0599	1.101	2.102	2.816	3.264	3.677	4.142
2.5	-6.16	-6.89	-7.85	-8.35	-7.96	-6.91	-5.81	-4.96	-4.27	-3.60	-2.85	-2.09	-1.34	-.461	.5760	1.516	2.154	2.577	3.027	3.548
2.4	-4.49	-5.10	-5.99	-6.47	-6.14	-5.22	-4.28	-3.58	-3.07	-2.66	-2.22	-1.75	-1.20	-.479	.3746	1.114	1.617	1.996	2.418	2.896
2.3	-3.94	-4.48	-5.27	-5.73	-5.43	-4.58	-3.71	-3.07	-2.60	-2.22	-1.89	-1.53	-1.09	-.478	.2244	.7875	1.168	1.503	1.894	2.319
2.2	-2.20	-2.49	-3.18	-3.68	-3.50	-2.79	-2.06	-1.60	-1.41	-1.37	-1.33	-1.18	-.878	-.399	.1676	.5853	.8006	.9861	1.268	1.615
2.1	-.411	-.443	-1.04	-1.61	-1.60	-1.07	-.509	-.246	-.318	-.587	-.809	-.829	-.670	-.332	.0992	.3726	.4170	.4505	.6352	.9303
2	1.569	1.781	1.270	.6142	.4505	.7900	1.158	1.197	.8453	.2572	-.239	-.445	-.434	-.251	.0338	.1545	.0184	-.113	-.033	.2138
1.9	3.769	4.181	3.724	2.993	2.678	2.817	2.952	2.750	2.130	1.246	.4912	.0907	-.084	-.102	-4.-6	-.042	-.346	-.632	-.663	-.469
1.8	6.023	6.368	5.721	4.834	4.418	4.391	4.281	3.884	3.144	2.119	1.209	.6750	.3385	.1363	.0938	-.036	-.397	-.748	-.866	-.748
1.7	8.155	8.465	7.610	6.565	6.078	5.898	5.514	4.913	4.085	2.962	1.925	1.249	.7184	.2883	.0532	-.202	-.641	-1.08	-1.31	-1.27
1.6	8.802	8.990	7.998	6.975	6.584	6.353	5.753	4.949	4.041	2.913	1.897	1.237	.6682	.1393	-.217	-.554	-1.01	-1.49	-1.82	-1.88
1.5	4.810	4.622	4.133	3.640	3.688	3.724	3.351	2.808	2.189	1.404	.7633	.4203	.0680	-.372	-.731	-1.01	-1.32	-1.69	-2.04	-2.19
1.4	2.740	2.530	1.994	1.707	1.782	1.749	1.391	.9845	.6214	.1949	-.120	-.283	-.540	-.916	-1.25	-1.47	-1.67	-1.96	-2.30	-2.52
1.3	1.050	.5783	.1593	.0204	-.016	-.333	-.918	-1.35	-1.47	-1.47	-1.44	-1.46	-1.67	-1.96	-2.16	-2.18	-2.15	-2.29	-2.55	-2.75
1.2	-.161	-.786	-.981	-.877	-.950	-1.49	-2.28	-2.75	-2.66	-2.28	-1.92	-1.81	-1.98	-2.26	-2.42	-2.37	-2.22	-2.24	-2.43	-2.58
1.1	-1.29	-1.73	-1.49	-1.03	-1.01	-1.58	-2.32	-2.61	-2.34	-1.84	-1.44	-1.37	-1.61	-2.00	-2.33	-2.47	-2.32	-2.50	-2.62	-2.82	-2.98
1	-2.71	-2.92	-2.23	-1.45	-1.35	-1.95	-2.62	-2.71	-2.24	-1.61	-1.18	-1.13	-1.43	-1.90	-2.37	-2.68	-2.85	-3.06	-3.28	-3.45
0.9	-4.02	-3.91	-2.74	-1.57	-1.34	-1.94	-2.57	-2.53	-1.92	-1.26	-.885	-.913	-1.24	-1.75	-2.32	-2.78	-3.11	-3.39	-3.64	-3.86
0.8	-5.58	-5.05	-3.32	-1.65	-1.12	-1.62	-2.22	-2.10	-1.45	-.889	-.688	-.798	-1.07	-1.51	-2.13	-2.73	-3.16	-3.49	-3.80	-4.12
0.7	-7.17	-6.24	-3.91	-1.65	-.732	-1.11	-1.69	-1.53	-.886	-.447	-.412	-.591	-.816	-1.22	-1.93	-2.70	-3.26	-3.64	-4.03	-4.47
0.6	-6.45	-5.30	-2.63	.0522	1.289	.9731	.1949	-.005	.2371	.3119	.1159	-.156	-.441	-1.01	-2.01	-3.10	-3.89	-4.43	-5.00	-5.68
0.5	-5.77	-4.36	-1.33	1.789	3.373	3.127	2.150	1.605	1.448	1.154	.7178	.3587	.0239	-.713	-2.04	-3.48	-4.53	-5.25	-6.03	-6.98
0.4	-5.07	-3.38	.0231	3.614	5.565	5.396	4.213	3.313	2.747	2.066	1.377	.9287	.5462	-.367	-2.04	-3.86	-5.20	-6.11	-7.12	-8.35
0.3	-2.81	.0124	4.416	8.729	11.04	10.89	9.562	8.436	7.450	6.154	4.826	3.814	2.887	1.344	-1.02	-3.47	-5.26	-6.48	-7.77	-9.32
0.2	.4600	4.549	10.06	15.10	17.69	17.44	15.93	14.54	13.06	11.03	8.921	7.154	5.461	3.095	-.106	-3.24	-5.49	-6.99	-8.53	-10.4
0.1	3.518	8.327	13.84	18.56	20.73	19.88	17.74	15.99	14.26	11.84	9.209	6.985	5.019	2.545	-.735	-3.97	-6.30	-7.81	-9.27	-11.0
0	1.575	6.054	11.23	15.96	17.96	16.45	13.78	12.36	11.74	10.48	8.425	6.110	3.837	1.271	-1.97	-5.15	-7.36	-8.65	-9.74	-11.1

	4	3.9	3.8	3.7	3.6	3.5	3.4	3.3	3.2	3.1	3	2.9	2.8	2.7	2.6	2.5	2.4	2.3	2.2	2.1
8																				
7.9																				
7.8																				
7.7																				
7.6																				
7.5																				
7.4																				
7.3																				
7.2																				
7.1																				
7																				
6.9																				
6.8																				
6.7																				
6.6																				
6.5																				
6.4																				
6.3																				
6.2																				
6.1																				
6																				
5.9																				
5.8																				
5.7																				
5.6																				
5.5																				
5.4																				
5.3																				
5.2																				
5.1																				
5																				
4.9																				
4.8																				
4.7																				
4.6																				
4.5																				
4.4																				
4.3																				
4.2																				
4.1																				
4	13.54																			
3.9	13.27	13.45																		
3.8	12.50	12.97	12.86																	
3.7	11.26	11.79	11.98	11.55																
3.6	9.753	10.25	10.58	10.56	10.13															
3.5	8.353	8.806	9.186	9.405	9.447	9.326														
3.4	7.341	7.724	8.091	8.368	8.592	8.823	8.712													
3.3	6.578	6.862	7.161	7.381	7.550	7.802	7.943	7.665												
3.2	5.776	5.999	6.244	6.421	6.520	6.690	6.926	7.063	6.955											
3.1	5.016	5.240	5.483	5.663	5.760	5.921	6.173	6.419	6.558	6.471										
3	4.611	4.853	5.096	5.261	5.334	5.481	5.709	5.897	6.050	6.194	6.307									
2.9	4.708	4.927	5.121	5.213	5.206	5.280	5.460	5.602	5.722	5.960	6.408	6.963								
2.8	4.952	5.122	5.242	5.266	5.201	5.204	5.323	5.446	5.559	5.821	6.429	7.316	8.058							
2.7	4.938	5.105	5.185	5.175	5.087	5.032	5.084	5.190	5.326	5.595	6.203	7.169	8.168	8.718						
2.6	4.531	4.763	4.870	4.892	4.825	4.744	4.734	4.802	4.956	5.240	5.811	6.706	7.773	8.751	9.544					
2.5	3.992	4.267	4.412	4.488	4.491	4.458	4.444	4.480	4.613	4.866	5.351	6.105	7.083	8.199	9.395	9.810				
2.4	3.308	3.580	3.752	3.878	3.957	4.020	4.063	4.104	4.250	4.523	4.972	5.612	6.476	7.554	8.850	9.438	9.673			
2.3	2.685	2.940	3.108	3.251	3.408	3.589	3.714	3.779	3.936	4.233	4.700	5.349	6.195	7.245	8.574	9.246	9.673	10.25		
2.2	1.940	2.181	2.332	2.479	2.724	3.048	3.232	3.225	3.299	3.567	4.000	4.581	5.337	6.301	7.582	8.254	8.769	9.487	9.219	
2.1	1.245	1.497	1.645	1.787	2.092	2.541	2.775	2.685	2.667	2.915	3.333	3.868	4.543	5.417	6.640	7.289	7.835	8.641	8.852	8.999
2	.5307	.8025	.9457	1.078	1.441	2.011	2.292	2.116	2.004	2.226	2.619	3.097	3.686	4.468	5.630	6.248	6.819	7.700	8.408	9.093
1.9	-.148	.1422	.2729	.3879	.8006	1.472	1.785	1.530	1.332	1.510	1.848	2.248	2.744	3.423	4.507	5.082	5.665	6.594	7.781	8.981
1.8	-.455	-.152	-.018	.0717	.4641	1.125	1.425	1.161	.9451	1.068	1.314	1.636	2.076	2.646	3.568	4.065	4.638	5.547	6.982	8.446
1.7	-.988	-.661	-.521	-.458	-.088	.5603	.8593	.6187	.4159	.4907	.6432	.8772	1.234	1.655	2.393	2.806	3.368	4.258	5.946	7.664
1.6	-1.64	-1.32	-1.17	-1.10	-.749	-.132	.1780	.0194	-.123	-.071	.0123	.1511	.3649	.5730	1.080	1.364	1.857	2.669	4.439	6.210
1.5	-2.07	-1.80	-1.61	-1.49	-1.16	-.686	-.458	-.559	-.649	-.602	-.557	-.568	-.652	-.763	-.525	-.448	-.237	.2912	1.696	3.100
1.4	-2.53	-2.34	-2.16	-2.00	-1.73	-1.42	-1.30	-1.37	-1.42	-1.36	-1.31	-1.41	-1.72	-2.12	-2.17	-2.32	-2.37	-2.06	-1.01	.0376
1.3	-2.77	-2.62	-2.45	-2.33	-2.16	-2.03	-2.03	-2.13	-2.22	-2.22	-2.22	-2.42	-2.93	-3.58	-3.98	-4.38	-4.59	-4.52	-3.80	-3.06
1.2	-2.59	-2.50	-2.41	-2.38	-2.37	-2.40	-2.47	-2.59	-2.72	-2.77	-2.85	-3.16	-3.84	-4.69	-5.42	-6.02	-6.36	-6.56	-6.18	-5.73
1.1	-3.02	-2.93	-2.84	-2.84	-2.92	-3.06	-3.17	-3.23	-3.31	-3.37	-3.53	-4.01	-4.87	-5.91	-6.99	-7.68	-8.03	-8.46	-8.17	-7.80
1	-3.51	-3.42	-3.31	-3.32	-3.48	-3.73	-3.86	-3.86	-3.88	-3.95	-4.19	-4.81	-5.84	-7.09	-8.53	-9.32	-9.65	-10.3	-10.1	-9.77
0.9	-3.96	-3.88	-3.76	-3.79	-4.01	-4.34	-4.50	-4.46	-4.43	-4.50	-4.84	-5.64	-6.87	-8.33	-10.1	-11.0	-11.3	-12.1	-11.9	-11.7
0.8	-4.29	-4.22	-4.11	-4.17	-4.42	-4.78	-4.96	-4.89	-4.84	-4.93	-5.41	-6.49	-7.98	-9.68	-11.7	-12.6	-12.8	-13.8	-13.7	-13.5
0.7	-4.72	-4.66	-4.55	-4.63	-4.91	-5.32	-5.50	-5.42	-5.35	-5.46	-6.11	-7.48	-9.26	-11.2	-13.5	-14.4	-14.6	-15.6	-15.5	-15.4
0.6	-6.11	-6.07	-5.89	-5.85	-6.03	-6.38	-6.51	-6.29	-6.12	-6.30	-7.20	-8.89	-10.9	-12.9	-15.3	-16.2	-16.3	-17.4	-17.3	-17.0
0.5	-7.58	-7.57	-7.30	-7.13	-7.21	-7.51	-7.57	-7.20	-6.93	-7.18	-8.34	-10.4	-12.6	-14.7	-17.2	-18.0	-18.2	-19.2	-19.0	-18.7
0.4	-9.15	-9.15	-8.78	-8.49	-8.46	-8.70	-8.68	-8.16	-7.77	-8.08	-9.52	-11.9	-14.4	-16.6	-19.2	-20.0	-20.1	-21.1	-20.8	-20.5
0.3	-10.3	-10.4	-9.98	-9.68	-9.67	-9.90	-9.80	-9.19	-8.75	-9.13	-10.8	-13.6	-16.5	-18.9	-21.3	-21.8	-21.6	-22.6	-22.0	-21.3
0.2	-11.6	-11.7	-11.2	-10.9	-11.0	-11.3	-11.1	-10.4	-9.91	-10.3	-12.3	-15.5	-18.8	-21.4	-23.5	-23.6	-23.1	-23.9	-23.0	-22.1
0.1	-12.2	-12.3	-11.7	-11.1	-11.0	-11.3	-11.1	-10.0	-9.00	-9.05	-10.8	-13.8	-16.8	-19.1	-20.8	-20.7	-20.0	-20.6	-19.8	-18.9
0	-12.1	-12.1	-11.3	-10.6	-10.3	-10.2	-9.73	-8.36	-6.80	-6.15	-7.16	-9.43	-11.8	-13.8	-15.0	-14.5	-13.9	-14.2	-13.8	-13.3

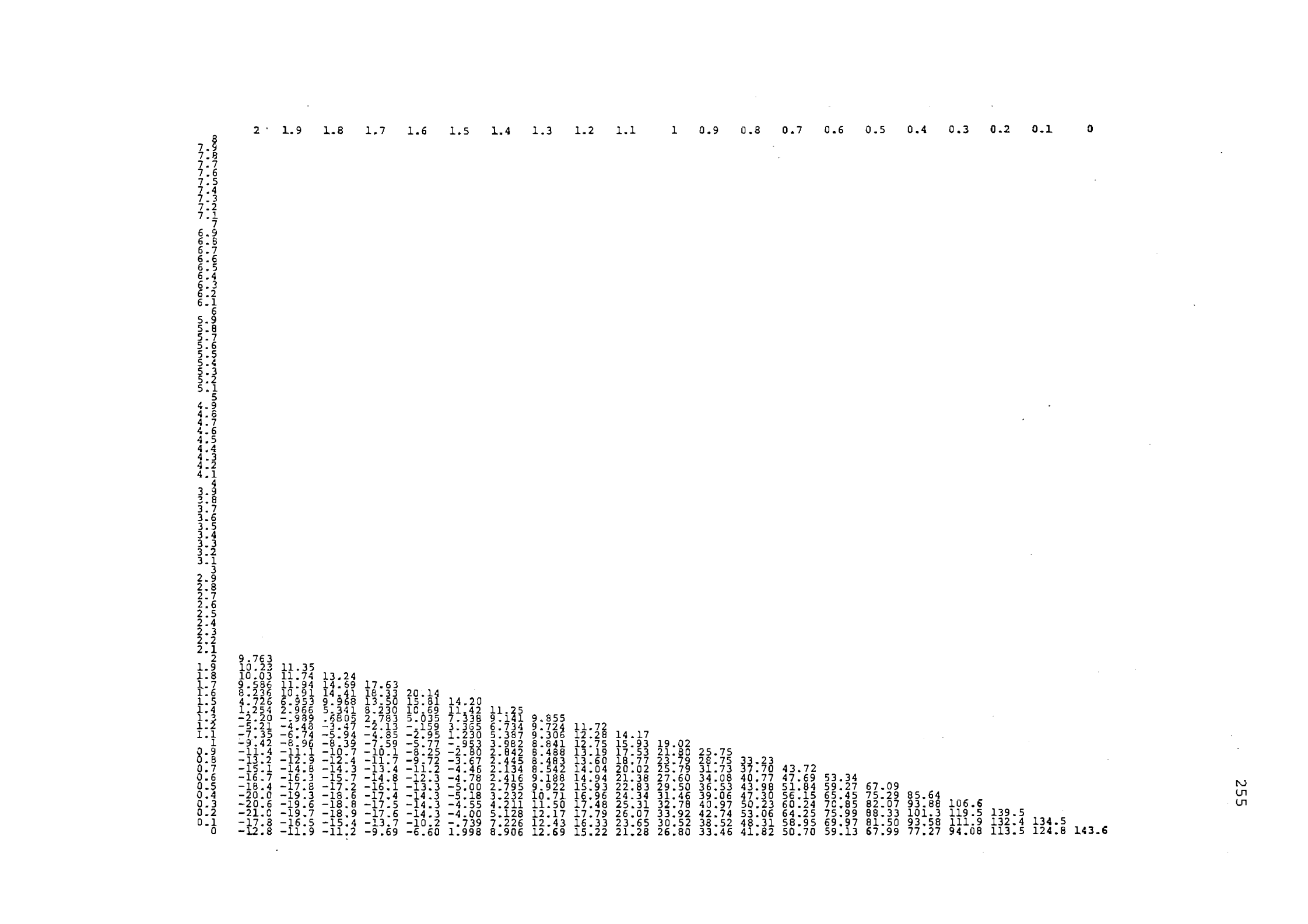

	2	1.9	1.8	1.7	1.6	1.5	1.4	1.3	1.2	1.1	1	0.9	0.8	0.7	0.6	0.5	0.4	0.3	0.2	0.1	0
8																					
7.9																					
7.8																					
7.7																					
7.6																					
7.5																					
7.4																					
7.3																					
7.2																					
7.1																					
7																					
6.9																					
6.8																					
6.7																					
6.6																					
6.5																					
6.4																					
6.3																					
6.2																					
6.1																					
6																					
5.9																					
5.8																					
5.7																					
5.6																					
5.5																					
5.4																					
5.3																					
5.2																					
5.1																					
5																					
4.9																					
4.8																					
4.7																					
4.6																					
4.5																					
4.4																					
4.3																					
4.2																					
4.1																					
4																					
3.9																					
3.8																					
3.7																					
3.6																					
3.5																					
3.4																					
3.3																					
3.2																					
3.1																					
3																					
2.9																					
2.8																					
2.7																					
2.6																					
2.5																					
2.4																					
2.3																					
2.2																					
2.1																					
2	9.763																				
1.9	10.23	11.35																			
1.8	10.03	11.74	13.24																		
1.7	9.586	11.94	14.69	17.63																	
1.6	8.236	10.91	14.41	18.33	20.14																
1.5	4.726	6.953	9.968	13.50	15.81	14.20															
1.4	1.254	2.966	5.341	8.230	10.69	11.42	11.25														
1.3	-2.20	-.989	.6805	2.783	5.035	7.338	9.141	9.855													
1.2	-5.21	-4.48	-3.47	-2.13	-.159	3.365	6.734	9.724	11.72												
1.1	-7.35	-6.74	-5.94	-4.85	-2.95	1.230	5.387	9.306	12.28	14.17											
1	-9.42	-8.96	-8.39	-7.59	-5.77	-.953	3.982	8.841	12.75	15.93	19.02										
0.9	-11.4	-11.1	-10.7	-10.1	-8.25	-2.80	2.842	8.488	13.19	17.53	21.80	25.75									
0.8	-13.2	-12.9	-12.4	-11.7	-9.72	-3.67	2.445	8.483	13.60	18.77	23.79	28.75	33.23								
0.7	-15.1	-14.8	-14.3	-13.4	-11.2	-4.46	2.134	8.542	14.04	20.02	25.79	31.73	37.70	43.72							
0.6	-16.7	-16.3	-15.7	-14.8	-12.3	-4.78	2.416	9.188	14.94	21.38	27.60	34.08	40.77	47.69	53.34						
0.5	-18.4	-17.8	-17.2	-16.1	-13.3	-5.00	2.795	9.922	15.93	22.83	29.50	36.53	43.98	51.84	59.27	67.09					
0.4	-20.0	-19.3	-18.6	-17.4	-14.3	-5.18	3.232	10.71	16.96	24.34	31.46	39.06	47.30	56.15	65.45	75.29	85.64				
0.3	-20.6	-19.6	-18.8	-17.5	-14.3	-4.55	4.211	11.50	17.48	25.31	32.78	40.97	50.23	60.24	70.85	82.07	93.88	106.6			
0.2	-21.0	-19.7	-18.9	-17.6	-14.3	-4.00	5.128	12.17	17.79	26.07	33.92	42.74	53.06	64.25	75.99	88.33	101.3	119.5	139.5		
0.1	-17.8	-16.5	-15.4	-13.7	-10.2	-.739	7.226	12.43	16.33	23.65	30.52	38.52	48.31	58.95	69.97	81.50	93.58	111.9	132.4	134.5	
0	-12.8	-11.9	-11.2	-9.69	-6.60	1.998	8.906	12.69	15.22	21.28	26.80	33.46	41.82	50.70	59.13	67.99	77.27	94.08	113.5	124.8	143.6

APPENDIX H

HIGH-LATITUDES "SUMMER" A PRIORI DATA

The statistics were constructed from 96 May, June, July and August profiles for years 1969 through 1972. (August data has been added to season 6 of table 3, in order to increase the sample size). The mean profile is given below.

TABLE H.1 : The Mean Profile* (^{0}C)

- 8.12	- 7.25	- 5.92	- 4.55	- 3.29	- 2.11	- 1.00	- 0.05
0.72	1.36	1.82	2.05	2.04	1.84	1.45	0.85
- 0.06	- 1.31	- 2.87	- 4.65	- 6.51	- 8.47	-10.63	-12.94
-15.29	-17.60	-19.79	-21.81	-23.70	-25.56	-27.44	-29.33
-31.16	-32.87	-34.45	-35.92	-37.33	-38.70	-40.01	-41.24
-42.32	-43.28	-44.15	-45.01	-45.85	-46.64	-47.35	-47.95
-48.42	-48.76	-49.06	-49.34	-49.61	-49.84	-50.00	-50.13
-50.23	-50.25	-50.19	-50.09	-50.01	-50.10	-50.28	-50.62
-50.99	-50.14	-49.28	-47.77	-45.87	-41.12	-36.23	-31.27
-26.14	-21.03	-16.34	-11.69	- 7.03	- 2.53	1.98	5.32
6.61							

*Listed from 8 sh altitude to ground level in steps of 0.1 sh.

The original a priori covariance matrix is given in table H.2. The indices indicate the height in sh (i.e. $-\ln(p/p_o)$)

TABLE H.2 : The High Latitudes summer a priori covariance matrix

	8.	7.9	7.8	7.7	7.6	7.5	7.4	7.3	7.2	7.1	7	6.9	6.8	6.7	6.6	6.5	6.4	6.3	6.2	6.1
8	39.73																			
7.9	38.83	38.43																		
7.8	36.49	36.78	36.23																	
7.7	32.71	33.52	34.01	33.13																
7.6	28.58	29.65	30.83	31.15	30.61															
7.5	25.49	26.65	28.14	29.20	29.87	30.50														
7.4	24.23	25.37	26.88	28.15	29.43	31.12	32.96													
7.3	24.64	25.60	26.83	27.87	29.18	31.35	34.20	36.77												
7.2	25.65	26.27	26.98	27.53	28.51	30.69	34.12	37.97	40.89											
7.1	26.39	26.64	26.80	26.82	27.38	29.30	32.84	37.47	41.85	44.50										
7	26.73	26.74	26.52	26.16	26.35	27.87	31.11	35.78	40.76	44.60	46.20									
6.9	26.62	26.53	26.15	25.61	25.57	26.70	29.42	33.57	38.30	42.54	45.40	46.41								
6.8	26.04	25.93	25.54	25.02	24.89	25.75	27.95	31.46	35.61	39.65	43.14	45.68	46.81							
6.7	25.46	25.38	25.04	24.57	24.40	25.02	26.83	29.84	33.48	37.14	40.64	43.85	46.24	47.06						
6.6	25.26	25.20	24.89	24.39	24.11	24.49	26.00	28.72	32.06	35.36	38.52	41.56	44.25	46.06	46.53					
6.5	24.87	24.85	24.57	24.09	23.75	24.00	25.36	27.94	31.06	34.05	36.73	39.16	41.46	43.67	45.49	46.22				
6.4	23.47	23.56	23.47	23.20	23.06	23.45	24.84	27.29	30.13	32.74	34.91	36.71	38.45	40.57	43.08	45.23	45.85			
6.3	21.29	21.58	21.80	21.94	22.25	22.98	24.48	26.72	29.14	31.26	32.96	34.31	35.61	37.42	39.94	42.71	44.83	45.48		
6.2	19.13	19.66	20.29	20.95	21.78	22.90	24.51	26.56	28.58	30.24	31.57	32.66	33.72	35.19	37.33	40.01	42.74	44.74	45.59	
6.1	17.57	18.31	19.32	20.40	21.64	23.11	24.96	27.11	29.09	30.56	31.67	32.62	33.57	34.80	36.49	38.69	41.20	43.58	45.54	47.02
6	17.09	17.97	19.09	20.22	21.51	23.16	25.39	28.04	30.44	32.10	33.18	34.03	34.93	36.05	37.44	39.13	41.06	43.00	45.14	47.74
5.9	17.60	18.47	19.44	20.28	21.31	22.93	25.45	28.63	31.55	33.56	34.76	35.58	36.42	37.54	38.91	40.42	41.90	43.19	44.77	47.46
5.8	17.99	18.78	19.56	20.13	20.92	22.41	24.95	28.22	31.29	33.50	34.87	35.77	36.64	37.85	39.39	40.98	42.29	43.12	43.99	46.00
5.7	17.52	18.23	18.91	19.41	20.13	21.49	23.77	26.67	29.42	31.51	32.98	34.09	35.17	36.54	38.21	39.84	41.07	41.68	42.07	43.29
5.6	16.54	17.16	17.77	18.25	18.97	20.19	22.09	24.47	26.71	28.43	29.80	31.11	32.53	34.11	35.77	37.29	38.45	39.03	39.26	39.97
5.5	15.32	15.86	16.38	16.83	17.51	18.62	20.24	22.23	24.04	25.35	26.48	27.89	29.60	31.33	32.90	34.29	35.48	36.18	36.44	36.98
5.4	13.91	14.41	14.87	15.26	15.91	16.98	18.51	20.32	21.90	22.97	23.95	25.41	27.26	29.02	30.47	31.80	33.08	33.95	34.31	34.87
5.3	12.65	13.15	13.58	13.91	14.53	15.60	17.12	18.88	20.40	21.43	22.41	23.90	25.77	27.51	28.92	30.28	31.67	32.66	33.13	33.73
5.2	11.57	12.09	12.54	12.86	13.42	14.45	15.96	17.70	19.19	20.22	21.20	22.65	24.50	26.26	27.74	29.21	30.74	31.88	32.47	33.12
5.1	10.38	10.95	11.48	11.88	12.47	13.50	15.00	16.67	18.06	19.01	19.92	21.30	23.13	24.94	26.52	28.11	29.79	31.11	31.86	32.57
5	9.209	9.980	10.67	11.22	11.95	13.08	14.61	16.17	17.36	18.14	18.94	20.28	22.12	23.96	25.54	27.15	28.92	30.36	31.24	31.95
4.9	8.621	9.413	10.27	10.99	11.85	13.12	14.71	16.17	17.13	17.67	18.35	19.68	21.55	23.34	24.81	26.32	28.07	29.53	30.37	31.08
4.8	7.876	8.750	9.735	10.55	11.50	12.85	14.46	15.83	16.60	16.95	17.52	18.87	20.76	22.48	23.81	25.17	26.81	28.24	29.08	29.75
4.7	6.760	7.632	8.631	9.477	10.44	11.77	13.32	14.60	15.28	15.57	16.12	17.48	19.36	21.01	22.24	23.49	25.07	26.51	27.40	28.06
4.6	5.562	6.349	7.253	8.047	8.983	10.25	11.71	12.93	13.63	13.99	14.58	15.91	17.68	19.24	20.43	21.69	23.27	24.74	25.63	26.25
4.5	4.507	5.175	5.949	6.682	7.595	8.818	10.21	11.41	12.22	12.72	13.38	14.63	16.25	17.69	18.86	20.13	21.66	23.04	23.84	24.38
4.4	3.619	4.194	4.895	5.631	6.561	7.743	9.064	10.27	11.19	11.84	12.55	13.71	15.17	16.51	17.65	18.82	20.16	21.32	21.99	22.51
4.3	2.952	3.490	4.181	4.936	5.848	6.941	8.169	9.379	10.40	11.17	11.89	12.93	14.24	15.48	16.53	17.57	18.66	19.58	20.15	20.67
4.2	2.375	2.898	3.573	4.277	5.074	6.021	7.150	8.361	9.462	10.32	11.05	11.98	13.12	14.21	15.19	16.11	17.01	17.76	18.26	18.74
4.1	1.773	2.269	2.892	3.488	4.110	4.878	5.890	7.058	8.150	9.009	9.745	10.62	11.65	12.63	13.54	14.40	15.18	15.82	16.27	16.69
4	1.334	1.812	2.401	2.909	3.377	3.979	4.858	5.904	6.855	7.582	8.248	9.102	10.09	11.02	11.92	12.77	13.49	14.06	14.45	14.84
3.9	1.253	1.735	2.341	2.840	3.351	3.768	4.550	5.462	6.226	6.753	7.268	8.037	8.984	9.900	10.79	11.63	12.32	12.83	13.20	13.62
3.8	1.424	1.895	2.518	3.077	3.565	4.129	4.896	5.725	6.352	6.724	7.077	7.696	8.542	9.403	10.23	11.00	11.65	12.15	12.52	12.97
3.7	1.669	2.096	2.697	3.329	3.975	4.692	5.530	6.340	6.894	7.172	7.394	7.839	8.530	9.277	9.993	10.66	11.24	11.72	12.12	12.59
3.6	2.036	2.441	3.001	3.655	4.413	5.277	6.218	7.043	7.544	7.748	7.889	8.218	8.764	9.371	9.954	10.50	11.00	11.47	11.88	12.33
3.5	2.765	3.127	3.631	4.220	4.949	5.835	6.805	7.618	8.063	8.219	8.357	8.608	9.185	9.689	10.14	10.55	10.97	11.40	11.80	12.18
3.4	3.646	3.994	4.435	4.905	5.511	6.303	7.200	7.951	8.354	8.498	8.672	9.065	9.590	10.05	10.40	10.68	10.99	11.36	11.70	12.00
3.3	4.288	4.643	5.045	5.421	5.924	6.620	7.414	8.088	8.462	8.599	8.765	9.151	9.667	10.09	10.37	10.58	10.82	11.13	11.43	11.69
3.2	4.735	5.106	5.491	5.799	6.220	6.839	7.546	8.137	8.459	8.556	8.662	8.970	9.406	9.778	10.03	10.24	10.48	10.76	11.03	11.26
3.1	5.322	5.689	6.039	6.258	6.564	7.080	7.700	8.215	8.467	8.506	8.563	8.804	9.151	9.448	9.679	9.894	10.13	10.40	10.64	10.82
3	6.011	6.367	6.687	6.832	7.033	7.453	8.010	8.479	8.679	8.686	8.745	8.975	9.255	9.442	9.568	9.709	9.898	10.13	10.35	10.47
2.9	6.505	6.889	7.252	7.423	7.611	8.001	8.544	9.003	9.178	9.177	9.260	9.497	9.716	9.768	9.725	9.722	9.820	10.01	10.20	10.30
2.8	6.743	7.196	7.674	7.958	8.217	8.642	9.218	9.700	9.865	9.846	9.921	10.12	10.25	10.17	9.978	9.839	9.848	10.00	10.20	10.33
2.7	6.897	7.407	7.976	8.348	8.669	9.149	9.793	10.33	10.50	10.46	10.52	10.65	10.65	10.42	10.11	9.896	9.960	10.01	10.23	10.42
2.6	7.103	7.622	8.194	8.552	8.865	9.378	10.10	10.70	10.91	10.91	10.99	11.07	10.90	10.49	10.07	9.827	9.794	9.953	10.18	10.39
2.5	7.416	7.906	8.414	8.688	8.940	9.456	10.23	10.89	11.13	11.17	11.32	11.40	11.10	10.50	9.961	9.696	9.708	9.918	10.16	10.35
2.4	7.822	8.271	8.693	8.872	9.078	9.617	10.45	11.16	11.40	11.44	11.63	11.76	11.41	10.66	9.985	9.674	9.747	10.06	10.34	10.50
2.3	8.232	8.643	8.996	9.110	9.313	9.913	10.83	11.59	11.85	11.87	12.07	12.22	11.87	11.04	10.25	9.871	9.983	10.37	10.68	10.81
2.2	8.315	8.720	9.064	9.182	9.419	10.09	11.09	11.93	12.25	12.30	12.51	12.69	12.33	11.46	10.58	10.14	10.25	10.66	10.97	11.12
2.1	8.344	8.763	9.137	9.289	9.552	10.25	11.30	12.23	12.63	12.74	12.96	13.11	12.72	11.82	10.91	10.45	10.54	10.94	11.25	11.45
2	8.374	8.815	9.229	9.421	9.707	10.42	11.51	12.51	13.00	13.17	13.41	13.54	13.10	12.17	11.26	10.80	10.89	11.27	11.57	11.82
1.9	8.454	8.918	9.373	9.603	9.905	10.62	11.75	12.81	13.35	13.55	13.80	13.89	13.40	12.44	11.57	11.17	11.29	11.64	11.92	12.22
1.8	8.315	8.774	9.230	9.456	9.734	10.40	11.45	12.46	13.01	13.25	13.52	13.59	13.08	12.21	11.58	11.44	11.67	11.97	12.16	12.48
1.7	8.065	8.515	8.974	9.274	9.484	10.11	11.08	12.00	12.50	12.75	13.02	13.05	12.52	11.79	11.46	11.63	11.80	12.23	12.32	12.64
1.6	7.069	7.505	7.996	8.314	8.652	9.263	10.12	10.90	11.30	11.50	11.73	11.73	11.24	10.70	10.74	11.29	11.82	11.99	12.00	12.35
1.5	2.601	2.957	3.511	4.093	4.699	5.349	6.002	6.480	6.649	6.680	6.808	6.951	6.958	7.100	7.740	8.673	9.369	9.588	9.595	9.890
1.4	-2.14	-1.88	-1.32	-.498	.3793	1.071	1.499	1.666	1.620	1.523	1.603	1.939	2.441	3.193	4.336	5.580	6.429	6.727	6.777	7.018
1.3	-7.27	-7.16	-6.64	-5.62	-4.62	-4.16	-4.25	-4.52	-4.68	-4.79	-4.87	-4.64	-3.90	-2.73	-1.33	-.061	.7200	1.045	1.281	1.666
1.2	-11.9	-12.0	-11.6	-10.4	-9.33	-9.10	-9.72	-10.5	-10.8	-10.9	-11.1	-11.0	-10.1	-8.67	-7.18	-6.00	-5.37	-5.06	-4.68	-4.21
1.1	-14.9	-15.1	-14.7	-13.5	-12.4	-12.2	-13.0	-13.9	-14.3	-14.6	-15.0	-14.9	-13.8	-12.0	-10.2	-8.88	-8.23	-7.99	-7.65	-7.15
1	-18.0	-18.2	-17.9	-16.8	-15.7	-15.7	-16.6	-17.7	-18.3	-18.6	-19.0	-18.8	-17.5	-15.5	-13.4	-11.8	-11.1	-10.8	-10.5	-10.0
0.9	-20.6	-20.9	-20.7	-19.5	-18.5	-18.6	-19.6	-20.8	-21.5	-21.9	-22.3	-22.1	-20.6	-18.3	-15.9	-14.2	-13.4	-13.1	-12.7	-12.3
0.8	-21.7	-22.0	-21.7	-20.5	-19.4	-19.5	-20.6	-21.8	-22.4	-22.8	-23.3	-23.1	-21.5	-18.9	-16.3	-14.4	-13.5	-13.1	-12.8	-12.4
0.7	-23.0	-23.3	-23.0	-21.6	-20.5	-20.6	-21.6	-22.7	-23.4	-23.8	-24.4	-24.2	-22.4	-19.5	-16.6	-14.6	-13.5	-13.1	-12.8	-12.4
0.6	-24.7	-25.0	-24.6	-23.2	-21.9	-22.0	-23.0	-24.1	-24.8	-25.4	-25.9	-25.5	-23.4	-20.4	-17.4	-15.3	-14.1	-13.5	-13.1	-12.8
0.5	-26.4	-26.7	-26.2	-24.7	-23.3	-23.2	-24.2	-25.4	-26.2	-26.9	-27.4	-26.9	-24.5	-21.3	-18.3	-16.2	-15.0	-14.2	-13.6	-13.3
0.4	-28.1	-28.4	-27.8	-26.2	-24.7	-24.5	-25.4	-26.6	-27.6	-28.4	-29.0	-28.2	-25.6	-22.2	-19.2	-17.2	-15.8	-14.9	-14.2	-13.8
0.3	-31.2	-31.5	-30.7	-28.8	-27.0	-26.7	-27.6	-29.0	-30.3	-31.4	-31.9	-30.9	-28.0	-24.3	-21.1	-19.0	-17.6	-16.5	-15.7	-15.3
0.2	-34.5	-34.7	-33.8	-31.6	-29.6	-29.2	-30.2	-31.9	-33.5	-34.9	-35.3	-34.0	-30.7	-26.7	-23.4	-21.2	-19.8	-18.8	-17.8	-17.5
0.1	-39.8	-39.4	-37.7	-34.8	-32.1	-30.9	-31.1	-32.6	-34.8	-36.8	-37.8	-36.9	-33.9	-30.2	-26.9	-24.4	-22.2	-20.3	-18.5	-17.5
0	-40.3	-39.1	-36.3	-33.1	-31.6	-32.1	-33.8	-36.0	-38.3	-40.3	-41.7	-42.3	-42.2	-40.7	-37.6	-33.6	-30.3	-28.2	-26.7	-25.2

	6	5.9	5.8	5.7	5.6	5.5	5.4	5.3	5.2	5.1	5	4.9	4.8	4.7	4.6	4.5	4.4	4.3	4.2	4.1
8																				
7.9																				
7.8																				
7.7																				
7.6																				
7.5																				
7.4																				
7.3																				
7.2																				
7.1																				
7																				
6.9																				
6.8																				
6.7																				
6.6																				
6.5																				
6.4																				
6.3																				
6.2																				
6.1																				
6	50.03																			
5.9	50.72	52.75																		
5.8	49.18	52.10	52.89																	
5.7	45.79	48.82	50.74	50.15																
5.6	41.76	44.36	46.58	47.05	45.22															
5.5	38.34	40.36	42.20	42.87	41.91	39.74														
5.4	36.06	37.63	38.92	39.31	38.63	37.28	35.80													
5.3	34.84	36.13	37.01	37.04	36.25	35.19	34.35	33.67												
5.2	34.17	35.30	35.95	35.73	34.74	33.80	32.93	32.73	32.47											
5.1	33.59	34.67	35.29	34.99	33.88	32.58	31.77	31.64	31.87	31.96										
5	32.95	34.06	34.76	34.52	33.41	32.04	31.04	30.76	31.10	31.65	31.92									
4.9	32.04	33.17	33.94	33.81	32.78	31.43	30.39	29.97	30.19	30.82	31.48	31.58								
4.8	30.67	31.75	32.55	32.53	31.66	30.42	29.43	28.96	29.01	29.51	30.26	30.75	30.44							
4.7	28.91	29.95	30.75	30.85	30.17	29.08	28.15	27.65	27.60	27.95	28.61	29.19	29.22	28.44						
4.6	27.05	28.05	28.87	29.07	28.53	27.55	26.65	26.14	26.02	26.28	26.82	27.32	27.44	26.98	25.91					
4.5	25.17	26.20	27.04	27.30	26.83	25.88	24.99	24.46	24.32	24.52	24.98	25.39	25.49	25.16	24.39	23.23				
4.4	23.32	24.37	25.25	25.56	25.12	24.18	23.25	22.69	22.54	22.74	23.15	23.50	23.56	23.28	22.66	21.77	20.71			
4.3	21.50	22.55	23.45	23.79	23.39	22.43	21.46	20.86	20.70	20.89	21.27	21.55	21.59	21.36	20.82	20.10	19.41	18.65		
4.2	19.52	20.56	21.48	21.87	21.50	20.55	19.56	18.94	18.75	18.89	19.20	19.43	19.46	19.32	18.90	18.29	17.83	17.50	16.88	
4.1	17.38	18.38	19.32	19.77	19.52	18.66	17.69	17.07	16.85	16.92	17.16	17.33	17.41	17.37	17.09	16.59	16.20	16.06	15.79	15.14
4	15.51	16.44	17.34	17.84	17.73	17.02	16.15	15.55	15.30	15.33	15.50	15.65	15.76	15.81	15.63	15.21	14.85	14.71	14.57	14.19
3.9	14.29	15.16	15.95	16.42	16.39	15.83	15.07	14.51	14.26	14.27	14.39	14.52	14.63	14.70	14.56	14.19	13.86	13.69	13.51	13.21
3.8	13.65	14.43	15.09	15.46	15.48	15.02	14.35	13.80	13.54	13.55	13.67	13.79	13.88	13.90	13.74	13.40	13.11	12.93	12.67	12.30
3.7	13.22	13.89	14.46	14.81	14.81	14.41	13.75	13.18	12.91	12.95	13.12	13.27	13.33	13.28	13.05	12.71	12.44	12.26	11.95	11.49
3.6	12.87	13.43	13.94	14.25	14.24	13.86	13.23	12.68	12.43	12.51	12.74	12.91	12.94	12.80	12.51	12.13	11.85	11.64	11.29	10.77
3.5	12.59	13.06	13.53	13.79	13.75	13.39	12.83	12.35	12.15	12.25	12.48	12.64	12.62	12.42	12.08	11.64	11.31	11.06	10.67	10.13
3.4	12.33	12.75	13.16	13.37	13.30	12.97	12.48	12.06	11.86	11.91	12.10	12.23	12.19	11.95	11.55	11.08	10.71	10.43	10.04	9.513
3.3	11.98	12.35	12.69	12.83	12.74	12.43	11.98	11.60	11.38	11.35	11.46	11.59	11.56	11.31	10.87	10.36	9.951	9.674	9.333	8.877
3.2	11.51	11.82	12.10	12.19	12.07	11.76	11.34	10.99	10.77	10.67	10.75	10.90	10.89	10.61	10.12	9.567	9.143	8.882	8.598	8.217
3.1	11.01	11.28	11.54	11.62	11.49	11.17	10.77	10.44	10.21	10.09	10.15	10.30	10.29	9.986	9.468	8.903	8.478	8.230	7.973	7.634
3	10.61	10.86	11.13	11.21	11.07	10.74	10.35	10.02	9.789	9.652	9.688	9.823	9.807	9.499	8.978	8.419	8.015	7.785	7.537	7.211
2.9	10.41	10.62	10.85	10.92	10.75	10.41	10.02	9.726	9.510	9.354	9.343	9.446	9.417	9.102	8.575	8.028	7.659	7.464	7.229	6.904
2.8	10.45	10.63	10.80	10.88	10.58	10.21	9.825	9.557	9.353	9.162	9.096	9.165	9.114	8.769	8.220	7.682	7.349	7.189	6.970	6.643
2.7	10.58	10.78	10.92	10.85	10.54	10.09	9.687	9.419	9.203	8.972	8.867	8.921	8.855	8.478	7.913	7.393	7.088	6.944	6.734	6.414
2.6	10.61	10.88	11.06	10.93	10.51	9.955	9.476	9.179	8.951	8.709	8.600	8.665	8.605	8.217	7.659	7.172	6.884	6.729	6.511	6.203
2.5	10.58	10.90	11.11	10.95	10.45	9.801	9.263	8.942	8.706	8.460	8.362	8.459	8.421	8.039	7.496	7.029	6.732	6.539	6.298	5.996
2.4	10.69	10.98	11.14	10.94	10.40	9.751	9.226	8.909	8.644	8.359	8.262	8.397	8.380	7.989	7.432	6.943	6.596	6.347	6.080	5.779
2.3	10.96	11.21	11.31	11.05	10.48	9.855	9.368	9.051	8.741	8.406	8.302	8.463	8.447	8.024	7.427	6.891	6.485	6.187	5.900	5.597
2.2	11.33	11.62	11.70	11.35	10.70	10.02	9.501	9.164	8.836	8.480	8.363	8.516	8.479	8.028	7.407	6.843	6.408	6.096	5.815	5.522
2.1	11.76	12.15	12.24	11.82	11.06	10.29	9.687	9.291	8.947	8.592	8.459	8.573	8.499	8.038	7.424	6.857	6.410	6.105	5.850	5.582
2	12.26	12.76	12.88	12.39	11.53	10.65	9.950	9.482	9.115	8.762	8.605	8.663	8.539	8.072	7.477	6.913	6.455	6.162	5.945	5.715
1.9	12.77	13.40	13.58	13.05	12.11	11.13	10.32	9.763	9.351	8.982	8.790	8.775	8.583	8.103	7.532	6.974	6.503	6.223	6.057	5.889
1.8	13.14	13.92	14.23	13.78	12.85	11.83	10.91	10.19	9.684	9.286	9.031	8.891	8.605	8.126	7.619	7.124	6.666	6.362	6.190	6.073
1.7	13.43	14.36	14.82	14.47	13.57	12.52	11.50	10.64	10.03	9.594	9.270	9.003	8.626	8.152	7.711	7.288	6.853	6.525	6.339	6.262
1.6	13.23	14.27	14.85	14.61	13.78	12.75	11.68	10.73	10.08	9.646	9.260	8.874	8.443	8.029	7.699	7.381	6.999	6.661	6.446	6.356
1.5	10.63	11.55	12.25	12.34	11.82	10.91	9.874	9.050	8.645	8.509	8.343	8.049	7.697	7.403	7.201	6.999	6.720	6.437	6.210	6.056
1.4	7.588	8.381	9.195	9.652	9.473	8.728	7.782	7.104	6.933	7.080	7.129	6.943	6.717	6.609	6.589	6.539	6.378	6.151	5.909	5.666
1.3	2.103	2.524	3.076	3.671	3.915	3.607	2.992	2.561	2.636	3.054	3.294	3.208	3.180	3.451	3.808	4.075	4.261	4.399	4.421	4.271
1.2	-3.99	-4.00	-3.71	-2.92	-2.19	-2.04	-2.32	-2.50	-2.20	-1.56	-1.18	-1.20	-1.03	-.382	.3806	.9970	1.548	2.062	2.382	2.379
1.1	-6.97	-7.12	-6.91	-6.00	-5.01	-4.54	-4.49	-4.39	-3.87	-3.07	-2.57	-2.52	-2.29	-1.56	-.699	.0618	.8442	1.605	2.071	2.097
1	-9.92	-10.2	-9.98	-8.88	-7.63	-6.90	-6.60	-6.31	-5.64	-4.66	-4.03	-3.91	-3.58	-2.68	-1.67	-.767	.2307	1.254	1.935	2.067
0.9	-12.3	-12.7	-12.4	-11.2	-9.72	-8.77	-8.29	-7.86	-7.06	-5.94	-5.18	-5.00	-4.58	-3.55	-2.41	-1.38	-.210	1.016	1.860	2.075
0.8	-12.4	-12.7	-12.4	-11.0	-9.48	-8.49	-8.03	-7.64	-6.87	-5.74	-4.97	-4.77	-4.32	-3.20	-1.96	-.884	.2516	1.424	2.255	2.487
0.7	-12.4	-12.6	-12.2	-10.7	-9.09	-8.05	-7.60	-7.26	-6.51	-5.38	-4.59	-4.38	-3.89	-2.68	-1.34	-.239	.8489	1.954	2.760	2.988
0.6	-12.9	-13.2	-12.7	-10.9	-8.96	-7.73	-7.22	-6.88	-6.18	-5.06	-4.25	-3.99	-3.43	-2.20	-.853	.2511	1.323	2.393	3.200	3.498
0.5	-13.5	-14.0	-13.4	-11.4	-9.06	-7.62	-7.02	-6.67	-5.97	-4.85	-4.00	-3.66	-3.03	-1.80	-.480	.6357	1.720	2.762	3.559	3.906
0.4	-14.2	-14.7	-14.1	-11.8	-9.14	-7.49	-6.80	-6.43	-5.74	-4.62	-3.73	-3.30	-2.60	-1.37	-.083	1.042	2.137	3.148	3.932	4.329
0.3	-15.8	-16.6	-15.9	-13.4	-10.4	-8.42	-7.56	-7.12	-6.39	-5.15	-4.03	-3.29	-2.24	-.849	.3796	1.446	2.581	3.592	4.333	4.749
0.2	-18.2	-19.1	-18.5	-15.6	-12.2	-9.91	-8.87	-8.40	-7.66	-6.26	-4.81	-3.57	-1.97	-.296	.8382	1.774	2.950	3.977	4.667	5.093
0.1	-17.6	-18.0	-17.2	-14.6	-11.6	-9.44	-8.13	-7.42	-6.43	-4.43	-2.01	.1288	2.167	3.754	4.496	4.989	5.783	6.526	7.015	7.305
0	-24.2	-23.7	-22.1	-18.9	-15.4	-13.4	-13.2	-13.9	-14.1	-12.8	-10.6	-8.54	-6.20	-3.31	-.196	2.453	4.385	6.149	8.242	10.25

	4	3.9	3.8	3.7	3.6	3.5	3.4	3.3	3.2	3.1	3	2.9	2.8	2.7	2.6	2.5	2.4	2.3	2.2	2.1
8																				
7.9																				
7.8																				
7.7																				
7.6																				
7.5																				
7.4																				
7.3																				
7.2																				
7.1																				
7																				
6.9																				
6.8																				
6.7																				
6.6																				
6.5																				
6.4																				
6.3																				
6.2																				
6.1																				
6																				
5.9																				
5.8																				
5.7																				
5.6																				
5.5																				
5.4																				
5.3																				
5.2																				
5.1																				
5																				
4.9																				
4.8																				
4.7																				
4.6																				
4.5																				
4.4																				
4.3																				
4.2																				
4.1																				
4	13.59																			
3.9	12.82	12.34																		
3.8	11.95	11.67	11.26																	
3.7	11.08	10.83	10.61	10.26																
3.6	10.29	9.973	9.822	9.714	9.477															
3.5	9.601	9.234	9.073	9.058	9.032	8.845														
3.4	9.006	8.647	8.469	8.435	8.459	8.447	8.301													
3.3	8.441	8.136	7.960	7.875	7.853	7.889	7.948	7.886												
3.2	7.857	7.614	7.458	7.348	7.279	7.298	7.452	7.607	7.554											
3.1	7.331	7.144	7.025	6.924	6.839	6.837	7.000	7.227	7.302	7.196										
3	6.941	6.801	6.726	6.651	6.572	6.561	6.710	6.930	7.036	7.032	7.015									
2.9	6.644	6.534	6.492	6.442	6.383	6.391	6.548	6.758	6.852	6.874	6.973	7.109								
2.8	6.382	6.286	6.266	6.237	6.207	6.257	6.450	6.674	6.761	6.771	6.913	7.189	7.449							
2.7	6.161	6.073	6.063	6.047	6.044	6.144	6.386	6.637	6.737	6.746	6.890	7.224	7.606	7.901						
2.6	5.964	5.884	5.874	5.863	5.882	6.017	6.290	6.562	6.684	6.715	6.866	7.206	7.631	8.032	8.315					
2.5	5.769	5.692	5.685	5.684	5.719	5.868	6.143	6.411	6.543	6.607	6.788	7.129	7.553	8.008	8.430	8.748				
2.4	5.554	5.473	5.478	5.508	5.571	5.735	6.006	6.256	6.387	6.486	6.710	7.063	7.480	7.947	8.447	8.956	9.440			
2.3	5.366	5.281	5.309	5.380	5.479	5.664	5.940	6.177	6.306	6.430	6.685	7.051	7.465	7.932	8.456	9.079	9.802	10.43		
2.2	5.291	5.208	5.246	5.332	5.434	5.611	5.873	6.097	6.227	6.363	6.633	7.011	7.432	7.905	8.439	9.104	9.935	10.71	11.14	
2.1	5.367	5.296	5.341	5.418	5.494	5.634	5.859	6.064	6.192	6.334	6.608	6.986	7.409	7.886	8.422	9.090	9.942	10.78	11.33	11.66
2	5.526	5.468	5.511	5.569	5.612	5.706	5.890	6.072	6.196	6.342	6.619	6.998	7.422	7.903	8.442	9.109	9.968	10.85	11.51	12.00
1.9	5.743	5.697	5.731	5.772	5.788	5.846	5.997	6.158	6.276	6.430	6.718	7.098	7.520	8.011	8.570	9.255	10.14	11.08	11.84	12.48
1.8	6.005	6.010	6.046	6.057	6.024	6.037	6.169	6.326	6.442	6.601	6.882	7.223	7.597	8.069	8.652	9.357	10.22	11.13	11.91	12.61
1.7	6.270	6.325	6.365	6.350	6.272	6.238	6.346	6.492	6.599	6.762	7.039	7.345	7.670	8.121	8.723	9.441	10.26	11.13	11.91	12.64
1.6	6.453	6.548	6.575	6.514	6.380	6.285	6.336	6.430	6.499	6.642	6.869	7.136	7.384	7.771	8.338	8.999	9.694	10.42	11.13	11.85
1.5	5.983	5.939	5.834	5.658	5.442	5.238	5.106	5.002	4.901	4.855	4.859	4.855	4.873	5.020	5.334	5.728	6.106	6.499	6.960	7.502
1.4	5.458	5.266	5.012	4.706	4.397	4.078	3.759	3.462	3.196	2.959	2.710	2.439	2.209	2.092	2.126	2.218	2.229	2.232	2.411	2.747
1.3	4.038	3.810	3.518	3.107	2.579	1.961	1.395	1.004	.7257	.4426	.0675	-.387	-.843	-1.26	-1.58	-1.90	-2.39	-2.89	-3.06	-2.97
1.2	2.179	1.957	1.657	1.172	.4651	-.394	-1.13	-1.53	-1.75	-2.05	-2.53	-3.15	-3.80	-4.48	-5.14	-5.85	-6.83	-7.83	-8.35	-8.50
1.1	1.897	1.711	1.443	.9281	.1376	-.826	-1.69	-2.24	-2.59	-3.01	-3.59	-4.25	-4.96	-5.77	-6.60	-7.55	-8.81	-10.1	-10.8	-11.1
1	1.888	1.680	1.362	.7798	-.087	-1.15	-2.17	-2.88	-3.39	-3.94	-4.61	-5.36	-6.21	-7.16	-8.15	-9.32	-10.9	-12.4	-13.2	-13.6
0.9	1.915	1.691	1.332	.6852	-.260	-1.42	-2.59	-3.45	-4.09	-4.74	-5.50	-6.33	-7.28	-8.38	-9.52	-10.9	-12.6	-14.4	-15.4	-15.8
0.8	2.327	2.065	1.634	.8910	-.170	-1.46	-2.72	-3.67	-4.36	-5.04	-5.82	-6.71	-7.74	-8.92	-10.1	-11.6	-13.4	-15.2	-16.2	-16.6
0.7	2.827	2.509	1.990	1.141	-.040	-1.45	-2.83	-3.87	-4.62	-5.33	-6.15	-7.10	-8.21	-9.48	-10.8	-12.3	-14.1	-16.0	-17.0	-17.4
0.6	3.361	2.974	2.316	1.345	.1024	-1.33	-2.73	-3.82	-4.63	-5.40	-6.26	-7.30	-8.52	-9.87	-11.2	-12.7	-14.6	-16.4	-17.5	-18.1
0.5	3.812	3.383	2.615	1.539	.2402	-1.21	-2.62	-3.73	-4.60	-5.41	-6.32	-7.43	-8.75	-10.2	-11.5	-13.1	-14.9	-16.8	-18.0	-18.7
0.4	4.281	3.808	2.924	1.739	.3833	-1.09	-2.50	-3.63	-4.56	-5.42	-6.37	-7.56	-8.97	-10.4	-11.8	-13.4	-15.2	-17.1	-18.4	-19.2
0.3	4.683	4.039	2.957	1.725	.4281	-1.02	-2.50	-3.76	-4.76	-5.65	-6.67	-8.00	-9.56	-11.1	-12.5	-14.1	-16.0	-18.0	-19.5	-20.6
0.2	4.968	4.055	2.710	1.480	.3484	-1.02	-2.62	-4.05	-5.15	-6.04	-7.13	-8.66	-10.4	-12.0	-13.4	-15.0	-17.0	-19.2	-20.9	-22.2
0.1	6.971	5.651	3.918	2.630	1.737	.6152	-.940	-2.45	-3.58	-4.54	-5.82	-7.49	-9.18	-10.6	-11.8	-13.2	-14.8	-16.7	-18.2	-19.6
0	11.30	10.71	8.764	6.709	5.074	3.304	1.409	.1319	-.623	-1.35	-2.21	-3.34	-4.66	-5.72	-6.38	-7.20	-9.01	-11.4	-13.5	-14.8

	2	1.9	1.8	1.7	1.6	1.5	1.4	1.3	1.2	1.1	1	0.9	0.8	0.7	0.6	0.5	0.4	0.3	0.2	0.1	0
8																					
7.9																					
7.8																					
7.7																					
7.6																					
7.5																					
7.4																					
7.3																					
7.2																					
7.1																					
7																					
6.9																					
6.8																					
6.7																					
6.6																					
6.5																					
6.4																					
6.3																					
6.2																					
6.1																					
6																					
5.9																					
5.8																					
5.7																					
5.6																					
5.5																					
5.4																					
5.3																					
5.2																					
5.1																					
5																					
4.9																					
4.8																					
4.7																					
4.6																					
4.5																					
4.4																					
4.3																					
4.2																					
4.1																					
4																					
3.9																					
3.8																					
3.7																					
3.6																					
3.5																					
3.4																					
3.3																					
3.2																					
3.1																					
3																					
2.9																					
2.8																					
2.7																					
2.6																					
2.5																					
2.4																					
2.3																					
2.2																					
2.1																					
2	12.51																				
1.9	13.16	14.05																			
1.8	13.40	14.54	15.70																		
1.7	13.51	14.90	16.80	18.73																	
1.6	12.76	14.31	16.83	19.49	21.02																
1.5	8.196	9.353	11.42	13.64	15.25	12.61															
1.4	3.195	3.904	5.417	7.087	8.741	9.360	9.628														
1.3	-2.80	-2.59	-1.70	-.666	.8996	4.294	7.671	10.49													
1.2	-8.60	-8.85	-8.56	-8.14	-6.71	-.829	5.402	12.81	19.78												
1.1	-11.3	-11.8	-11.7	-11.5	-10.1	-3.01	4.483	13.59	22.33	26.76											
1	-13.9	-14.6	-14.8	-14.8	-13.4	-5.23	3.490	14.21	24.56	30.61	36.20										
0.9	-16.2	-17.0	-17.3	-17.5	-16.1	-7.04	2.713	14.83	26.58	33.97	40.99	47.01									
0.8	-17.0	-17.8	-18.1	-18.2	-16.7	-7.28	2.851	15.55	27.81	35.48	42.78	49.11	51.71								
0.7	-17.9	-18.7	-18.9	-19.0	-17.3	-7.49	3.054	16.33	29.08	37.03	44.59	51.23	54.35	57.55							
0.6	-18.6	-19.5	-19.7	-19.6	-17.8	-7.47	3.598	17.22	30.19	38.22	45.89	52.63	55.93	59.34	62.03						
0.5	-19.4	-20.4	-20.5	-20.3	-18.4	-7.44	4.145	18.11	31.30	39.45	47.20	54.03	57.48	61.09	64.73	68.50					
0.4	-20.1	-21.2	-21.3	-21.0	-18.9	-7.39	4.721	19.00	32.38	40.65	48.47	55.36	58.96	62.76	67.41	72.33	77.36				
0.3	-21.7	-23.2	-23.4	-23.2	-21.0	-8.59	4.549	19.72	33.74	42.48	50.79	58.06	61.82	65.81	71.29	77.13	83.13	91.75			
0.2	-23.7	-25.5	-26.1	-26.2	-24.1	-10.6	3.757	19.97	34.72	43.94	52.94	60.75	64.61	68.73	74.89	81.48	88.27	100.8	115.9		
0.1	-21.0	-22.9	-23.6	-24.0	-22.2	-9.42	4.098	18.29	30.59	38.81	47.24	54.47	58.10	62.07	67.69	73.64	79.77	93.10	110.0	117.5	
0	-15.8	-16.6	-15.3	-13.3	-9.24	1.073	12.13	24.51	35.47	41.67	48.81	54.93	58.21	61.67	66.20	70.97	75.88	85.46	97.11	106.4	192.1

APPENDIX I

HIGH-LATITUDES "WINTER" A PRIORI DATA

The statistics were constructed from 102, December, January and February profiles for years 1969 through 1972. The mean profile is given below :

TABLE I.1 : The Mean Profile* (^{0}C)

-20.00	-20.30	-20.60	-21.12	-21.74	-22.53	-23.44	-24.56
-25.90	-27.40	-28.96	-30.53	-32.08	-33.62	-35.19	-36.81
-38.37	-39.78	-41.10	-42.37	-43.52	-44.63	-45.77	-46.90
-47.94	-48.95	-49.97	-50.94	-51.78	-52.43	-52.93	-53.32
-53.61	-53.79	-53.87	-53.95	-54.08	-54.17	-54.11	-53.90
-53.59	-53.29	-53.07	-52.94	-52.88	-52.90	-52.98	-53.07
-53.12	-53.11	-53.04	-52.90	-52.73	-52.58	-52.47	-52.38
-52.28	-52.16	-52.06	-51.97	-51.92	-51.98	-52.24	-52.65
-53.14	-53.43	-53.72	-53.95	-53.82	-50.89	-47.71	-44.22
-39.64	-35.02	-30.66	-26.35	-22.05	-19.08	-16.81	-18.58
-17.75							

*Listed from 8 sh altitude to ground level in steps of 0.1 sh

The original a priori covariance matrix is given in table I.2. The indices indicate the height in sh (i.e. $-\ln(p/p_o)$).

TABLE I.2 : The High Latitudes winter a priori covarinace matrix

	8	7.9	7.8	7.7	7.6	7.5	7.4	7.3	7.2	7.1	7	6.9	6.8	6.7	6.6	6.5	6.4	6.3	6.2	6.1
8	147.6																			
7.9	146.8	148.0																		
7.8	146.0	147.6	150.9																	
7.7	138.4	143.7	150.2	153.2																
7.6	130.2	136.0	144.1	150.3	152.0															
7.5	119.8	127.7	134.3	142.6	148.7	150.8														
7.4	109.1	114.8	123.3	132.6	141.3	147.7	149.0													
7.3	98.78	104.2	112.4	121.5	131.0	139.4	144.2	143.5												
7.2	88.70	93.99	101.9	110.7	120.0	129.1	136.0	138.9	138.6											
7.1	79.13	84.61	92.75	101.6	111.1	120.4	128.1	133.3	136.7	139.2										
7	70.41	76.31	85.09	94.62	104.5	114.2	122.2	128.5	134.3	140.8	147.0									
6.9	61.90	68.27	77.76	88.09	98.78	109.0	117.3	124.1	131.4	140.7	150.7	158.4								
6.8	52.49	59.16	69.17	80.16	91.56	102.3	111.2	118.6	126.9	137.9	150.4	161.7	169.1							
6.7	42.43	49.12	59.29	70.57	82.38	93.64	103.1	111.3	120.6	132.8	146.9	160.6	171.5	177.8						
6.6	33.15	39.58	49.50	60.72	72.63	84.14	94.09	103.1	113.3	126.4	141.6	156.7	169.9	179.3	184.2					
6.5	24.82	30.89	40.36	51.34	63.23	74.87	85.13	94.64	105.6	119.6	135.7	151.8	166.2	177.6	185.3	189.8				
6.4	16.54	22.32	31.42	42.24	54.21	66.03	76.50	86.36	97.98	113.0	130.2	147.1	162.3	175.0	184.8	192.5	198.6			
6.3	8.610	14.23	23.11	33.90	46.04	58.04	68.67	78.85	91.16	107.2	125.4	143.1	158.8	172.2	183.5	193.3	202.4	209.2		
6.2	1.965	7.481	16.20	26.91	39.03	50.95	61.51	71.85	84.68	101.5	120.5	138.7	154.7	168.4	180.4	191.7	202.7	211.6	216.0	
6.1	-3.78	1.529	9.980	20.46	32.36	44.02	54.39	64.80	77.93	95.13	114.5	133.0	149.4	163.5	176.1	188.2	200.2	210.2	216.0	217.6
6	-9.41	-4.36	3.738	13.94	25.69	37.29	47.74	58.44	71.91	89.22	108.6	127.3	144.0	158.6	171.8	184.3	196.6	207.0	213.4	216.4
5.9	-14.8	-9.91	-2.15	7.787	19.49	31.28	42.16	53.43	67.31	84.59	103.6	122.1	138.8	153.8	167.1	179.8	192.1	202.3	208.9	212.7
5.8	-19.4	-14.7	-7.27	2.242	13.72	25.64	36.91	48.68	62.88	80.03	98.50	116.4	132.7	147.4	160.7	173.2	185.2	195.4	201.9	206.1
5.7	-23.5	-19.0	-12.1	-3.14	7.926	19.74	31.15	43.11	57.40	74.34	92.22	109.4	125.2	139.5	152.5	164.8	176.7	186.6	193.1	197.7
5.6	-27.7	-23.6	-17.1	-8.63	2.052	13.70	25.07	37.05	51.37	68.20	85.74	102.4	117.7	131.7	144.6	156.7	168.4	178.3	184.9	189.7
5.5	-31.5	-27.6	-21.5	-13.5	-3.17	8.205	19.42	31.35	45.69	62.55	79.97	96.28	111.1	124.7	137.3	149.3	160.8	170.6	177.3	182.3
5.4	-35.8	-30.2	-24.4	-16.8	-6.91	4.036	14.87	26.47	40.55	57.17	74.31	90.17	104.4	117.4	129.5	141.0	152.2	161.8	168.7	173.7
5.3	-35.1	-31.7	-26.3	-19.0	-9.50	.9779	11.25	22.18	35.53	51.52	68.13	83.44	97.08	109.5	121.2	132.3	143.1	152.5	159.3	164.4
5.2	-36.4	-33.1	-28.0	-21.0	-11.8	-1.81	7.880	18.08	30.63	45.89	61.99	76.92	90.25	102.4	113.8	124.6	135.1	144.3	151.1	156.2
5.1	-37.5	-34.4	-29.4	-22.8	-14.1	-4.56	4.630	14.30	26.25	40.90	56.49	71.03	84.07	96.01	107.1	117.5	127.7	136.8	143.5	148.6
5	-37.8	-34.8	-30.1	-23.8	-15.7	-6.85	1.812	11.03	22.45	36.45	51.35	65.26	77.75	89.22	99.81	109.9	119.7	128.5	134.9	139.9
4.9	-37.4	-34.6	-30.2	-24.4	-16.9	-8.71	-.648	8.004	18.76	31.97	46.02	59.16	71.02	81.94	92.05	101.7	111.1	119.5	125.7	130.5
4.8	-37.3	-34.7	-30.6	-25.2	-18.3	-10.7	-3.19	4.875	14.95	27.36	40.58	53.02	64.34	74.83	84.55	93.79	102.9	111.0	117.0	121.7
4.7	-38.2	-35.8	-32.0	-26.9	-20.4	-13.2	-6.02	1.626	11.14	22.86	35.36	47.17	57.99	68.09	77.48	86.40	95.18	103.0	109.0	113.7
4.6	-39.6	-37.3	-33.7	-28.8	-22.5	-15.4	-8.51	-1.20	7.779	18.79	30.55	41.65	51.87	61.48	70.48	79.07	87.56	95.21	101.1	105.8
4.5	-39.3	-37.2	-33.7	-29.0	-22.9	-16.1	-9.45	-2.67	5.539	15.66	26.52	36.75	46.16	55.08	63.53	71.70	79.83	87.20	92.96	97.67
4.4	-36.7	-34.6	-31.2	-26.8	-21.0	-14.7	-8.66	-2.67	4.566	13.66	23.53	32.80	41.26	49.29	56.99	64.56	72.22	79.23	84.77	89.34
4.3	-33.3	-31.2	-27.9	-23.7	-18.5	-12.8	-7.46	-2.28	4.032	12.18	21.11	29.46	36.99	44.09	50.95	57.84	64.97	71.60	76.89	81.28
4.2	-30.8	-28.8	-25.6	-21.7	-16.9	-11.8	-7.04	-2.46	3.175	10.54	18.64	26.13	32.82	39.11	45.23	51.49	58.12	64.38	69.44	73.67
4.1	-29.2	-27.3	-24.3	-20.7	-16.4	-11.8	-7.43	-3.20	2.009	8.770	16.13	22.90	28.93	34.62	40.17	45.89	52.03	57.91	62.74	66.88
4	-28.1	-26.3	-23.5	-20.1	-16.2	-12.1	-8.13	-4.16	.7433	7.066	13.91	20.20	25.81	31.07	36.17	41.46	47.20	52.77	57.43	61.50
3.9	-26.9	-25.2	-22.5	-19.4	-15.8	-12.2	-8.68	-5.11	-1.561	5.412	11.94	17.96	23.29	28.20	32.89	37.82	43.27	48.62	53.15	57.17
3.8	-25.5	-23.8	-21.2	-18.2	-15.1	-11.9	-9.00	-5.94	-1.82	3.834	10.13	15.99	21.00	25.55	29.79	34.29	39.39	44.46	48.81	52.71
3.7	-24.6	-23.0	-20.5	-17.8	-15.0	-12.3	-9.78	-7.04	-3.20	2.183	8.230	13.77	18.53	22.70	26.46	30.41	34.98	39.61	43.64	47.35
3.6	-25.2	-23.9	-21.7	-19.2	-16.7	-14.2	-11.7	-8.83	-4.98	.1507	5.771	10.88	15.28	19.12	22.49	25.90	29.87	33.97	37.62	41.15
3.5	-26.4	-25.4	-23.6	-21.4	-19.0	-16.5	-13.8	-10.7	-6.72	-1.95	3.014	7.522	11.51	15.08	18.19	21.21	24.67	28.29	31.56	34.90
3.4	-26.2	-25.3	-23.8	-21.9	-19.7	-17.3	-14.5	-11.3	-7.53	-3.26	1.006	4.935	8.553	11.87	14.73	17.37	20.35	23.50	26.36	29.35
3.3	-24.4	-23.6	-22.2	-20.5	-18.6	-16.4	-13.9	-11.0	-7.62	-3.89	-.227	3.214	6.476	9.468	11.95	14.11	16.56	19.24	21.66	24.19
3.2	-22.2	-21.6	-20.4	-18.9	-17.3	-15.6	-13.6	-11.1	-8.08	-4.88	-1.80	1.118	3.945	6.530	8.569	10.22	12.16	14.41	16.48	18.62
3.1	-20.5	-20.1	-19.1	-17.9	-16.7	-15.5	-13.9	-11.7	-9.15	-6.49	-3.99	-1.61	.7438	2.924	4.581	5.821	7.322	9.206	11.03	12.92
3	-19.1	-18.9	-18.1	-17.1	-16.2	-15.3	-14.1	-12.3	-10.1	-7.94	-5.91	-3.94	-1.96	-.090	1.286	2.226	3.394	4.979	6.607	8.337
2.9	-17.9	-17.7	-17.1	-16.2	-15.3	-14.5	-13.6	-12.2	-10.5	-8.77	-7.07	-5.38	-3.64	-2.01	-.862	-.163	.7420	2.080	3.532	5.119
2.8	-16.4	-16.4	-15.9	-15.0	-14.1	-13.5	-12.9	-11.9	-10.6	-9.21	-7.80	-6.36	-4.86	-3.47	-2.59	-2.17	-1.55	-.489	.7554	2.182
2.7	-14.8	-14.9	-14.5	-13.7	-13.0	-12.6	-12.2	-11.6	-10.5	-9.37	-8.23	-7.05	-5.83	-4.76	-4.20	-4.12	-3.85	-3.11	-2.09	-.834
2.6	-13.1	-13.2	-12.9	-12.3	-11.8	-11.6	-11.5	-11.0	-10.1	-9.16	-8.20	-7.22	-6.27	-5.51	-5.26	-5.49	-5.56	-5.12	-4.31	-3.22
2.5	-11.5	-11.7	-11.6	-11.1	-10.9	-11.0	-11.1	-10.7	-9.91	-9.07	-8.26	-7.44	-6.69	-6.14	-6.11	-6.54	-6.85	-6.61	-5.96	-5.02
2.4	-10.2	-10.6	-10.7	-10.6	-10.6	-10.9	-11.2	-10.9	-10.2	-9.49	-8.84	-8.20	-7.59	-7.15	-7.18	-7.69	-8.10	-7.98	-7.43	-6.63
2.3	-9.43	-9.94	-10.2	-10.3	-10.4	-10.9	-11.2	-11.0	-10.4	-9.75	-9.22	-8.73	-8.23	-7.83	-7.85	-8.35	-8.81	-8.77	-8.32	-7.66
2.2	-8.52	-9.05	-9.35	-9.33	-9.49	-9.95	-10.3	-10.2	-9.73	-9.20	-8.73	-8.35	-7.96	-7.60	-7.62	-8.15	-8.68	-8.76	-8.46	-7.97
2.1	-7.24	-7.73	-7.96	-7.84	-7.93	-8.35	-8.73	-8.75	-8.47	-8.04	-7.63	-7.33	-7.04	-6.76	-6.82	-7.41	-8.06	-8.31	-8.20	-7.89
2	-6.01	-6.46	-6.89	-6.36	-6.35	-6.71	-7.09	-7.23	-7.10	-6.78	-6.39	-6.15	-5.97	-5.76	-5.85	-6.48	-7.24	-7.67	-7.74	-7.61
1.9	-5.32	-5.72	-5.77	-5.44	-5.33	-5.58	-5.89	-6.04	-5.98	-5.71	-5.34	-5.12	-4.98	-4.77	-4.82	-5.44	-6.26	-6.81	-7.03	-7.05
1.8	-5.24	-5.60	-5.57	-5.16	-4.98	-5.09	-5.25	-5.30	-5.21	-4.94	-4.58	-4.35	-4.17	-3.85	-3.78	-4.31	-5.10	-5.69	-6.02	-6.15
1.7	-5.34	-5.66	-5.58	-5.13	-4.90	-4.90	-4.88	-4.79	-4.66	-4.40	-4.08	-3.86	-3.62	-3.18	-2.96	-3.36	-4.07	-4.65	-5.03	-5.24
1.6	-4.96	-5.20	-5.04	-4.56	-4.28	-4.17	-4.00	-3.82	-3.68	-3.48	-3.24	-3.11	-2.92	-2.47	-2.18	-2.48	-3.12	-3.70	-4.13	-4.40
1.5	-4.50	-4.70	-4.64	-4.40	-4.29	-4.24	-4.12	-4.05	-4.10	-4.14	-4.14	-4.23	-4.23	-3.91	-3.59	-3.70	-4.12	-4.57	-4.92	-5.13
1.4	-3.72	-3.78	-3.70	-3.58	-3.57	-3.57	-3.51	-3.54	-3.74	-3.98	-4.23	-4.62	-4.95	-4.90	-4.65	-4.62	-4.87	-5.19	-5.43	-5.51
1.3	-2.41	-2.31	-2.16	-2.10	-2.16	-2.27	-2.38	-2.59	-2.97	-3.38	-3.84	-4.58	-5.39	-5.84	-5.96	-6.06	-6.33	-6.67	-6.88	-6.83
1.2	.0290	.3855	.7286	.7940	.5327	.0569	-.479	-1.07	-1.79	-2.53	-3.39	-4.64	-6.09	-7.28	-8.02	-8.50	-8.99	-9.48	-9.72	-9.64
1.1	4.535	4.833	4.950	4.499	3.380	1.769	.1029	-1.32	-2.53	-3.52	-4.54	-6.02	-8.01	-9.97	-11.4	-12.4	-13.3	-14.1	-14.5	-14.4
1	7.641	7.810	7.656	6.739	4.934	2.438	-.182	-2.44	-4.26	-5.62	-6.79	-8.46	-10.9	-13.5	-15.5	-17.0	-18.3	-19.4	-20.0	-20.1
0.9	10.64	10.68	10.27	8.926	6.508	3.255	-.159	-3.14	-5.55	-7.31	-8.72	-10.6	-13.4	-16.6	-19.3	-21.1	-22.8	-24.3	-25.0	-25.3
0.8	10.43	10.42	9.987	8.716	6.431	3.277	-.138	-3.22	-5.75	-7.55	-8.91	-10.7	-13.4	-16.5	-19.0	-20.9	-22.6	-24.1	-24.7	-24.9
0.7	9.138	9.058	8.605	7.468	5.471	2.618	-.619	-3.66	-6.16	-7.83	-8.96	-10.5	-12.9	-15.6	-17.9	-19.6	-21.2	-22.7	-23.4	-23.4
0.6	8.019	7.761	7.096	5.834	3.884	1.181	-1.93	-4.84	-7.16	-8.60	-9.55	-10.9	-13.1	-15.9	-18.4	-20.3	-22.4	-24.3	-25.2	-25.3
0.5	7.616	7.142	6.190	4.690	2.638	-.057	-3.15	-6.01	-8.22	-9.54	-10.4	-11.6	-13.8	-16.7	-19.4	-21.7	-24.2	-26.6	-27.9	-28.2
0.4	7.203	6.499	5.241	3.487	1.330	-1.35	-4.42	-7.22	-9.30	-10.5	-11.2	-12.4	-14.5	-17.4	-20.4	-23.1	-26.1	-29.0	-30.7	-31.1
0.3	4.099	3.301	1.951	.0763	-2.32	-5.32	-8.72	-11.8	-14.0	-14.9	-15.0	-15.6	-17.4	-20.2	-23.3	-26.5	-30.2	-34.0	-36.3	-37.1
0.2	.2601	-.569	-1.95	-3.99	-6.88	-10.7	-14.9	-18.5	-20.9	-21.5	-20.9	-20.9	-22.3	-25.1	-28.6	-32.5	-37.2	-41.8	-44.7	-45.7
0.1	2.839	2.220	1.414	.6313	-.397	-2.40	-5.46	-8.80	-11.5	-13.0	-13.6	-14.6	-16.6	-19.8	-23.5	-27.8	-33.2	-38.7	-42.4	-43.5
0	-7.34	-8.64	-9.87	-9.29	-5.97	-2.12	-.398	-.138	.0982	.7999	2.235	4.354	7.370	11.13	14.10	14.98	14.48	14.09	14.26	14.93

	6	5.9	5.8	5.7	5.6	5.5	5.4	5.3	5.2	5.1	5	4.9	4.8	4.7	4.6	4.5	4.4	4.3	4.2	4.1
8																				
7.9																				
7.8																				
7.7																				
7.6																				
7.5																				
7.4																				
7.3																				
7.2																				
7.1																				
7																				
6.9																				
6.8																				
6.7																				
6.6																				
6.5																				
6.4																				
6.3																				
6.2																				
6.1																				
6	217.2																			
5.9	215.3	215.5																		
5.8	209.8	211.7	209.5																	
5.7	201.9	204.6	203.8	199.6																
5.6	194.1	197.3	197.2	194.3	190.4															
5.5	186.8	190.0	190.3	188.2	185.6	182.2														
5.4	178.1	181.2	181.6	179.9	178.2	176.0	171.1													
5.3	168.7	171.7	172.1	170.8	169.6	168.1	164.1	158.1												
5.2	160.6	163.5	164.1	163.0	162.1	160.8	157.3	152.2	147.2											
5.1	153.0	156.1	156.8	156.0	155.3	154.1	150.9	146.4	142.1	137.8										
5	144.3	147.6	148.6	148.1	147.6	146.7	143.7	139.5	135.7	132.0	126.9									
4.9	134.9	138.2	139.5	139.2	138.9	138.2	135.6	131.7	128.2	124.8	120.4	114.7								
4.8	126.0	129.4	130.7	130.6	130.5	130.0	127.6	124.0	120.7	117.6	113.7	108.8	103.6							
4.7	117.9	121.3	122.8	122.9	123.0	122.7	120.6	117.2	114.1	111.2	107.7	103.3	98.94	95.00						
4.6	110.1	113.5	115.1	115.5	115.8	115.8	114.0	111.0	108.2	105.5	102.2	98.28	94.39	91.08	87.88					
4.5	102.0	105.3	107.0	107.5	108.1	108.3	106.8	104.1	101.5	99.08	96.06	92.42	88.89	86.04	83.46	79.80				
4.4	93.51	96.78	98.42	98.93	99.48	99.74	98.48	96.10	93.79	91.58	88.82	85.50	82.27	79.74	77.58	74.62	70.31			
4.3	85.30	88.51	90.15	90.63	91.11	91.37	90.27	88.16	86.12	84.16	81.69	78.67	75.71	73.40	71.51	69.03	65.50	61.53		
4.2	77.63	80.87	82.62	83.16	83.67	83.99	83.08	81.22	79.43	77.70	75.50	72.78	70.09	67.99	66.29	64.12	61.10	57.84	54.86	
4.1	70.81	74.14	76.05	76.75	77.35	77.78	77.06	75.42	73.80	72.25	70.30	67.87	65.45	63.57	62.04	60.07	57.37	54.56	52.14	49.95
4	65.42	68.79	70.81	71.62	72.30	72.81	72.22	70.72	69.21	67.79	66.04	63.87	61.70	60.02	58.64	56.83	54.32	51.78	49.70	47.80
3.9	61.03	64.33	66.33	67.15	67.83	68.34	67.81	66.40	64.97	63.65	62.08	60.13	58.21	56.74	55.53	53.86	51.53	49.20	47.36	45.85
3.8	56.45	59.62	61.51	62.26	62.87	63.33	62.81	61.46	60.11	58.91	57.49	55.78	54.12	52.89	51.88	50.40	48.28	46.23	44.66	43.41
3.7	50.98	54.06	55.89	56.60	57.15	57.57	57.05	55.77	54.52	53.44	52.18	50.68	49.30	48.35	47.59	46.33	44.46	42.68	41.39	40.39
3.6	44.78	47.92	49.81	50.58	51.15	51.56	51.08	49.87	48.75	47.80	46.69	45.38	44.26	43.61	43.13	42.14	40.50	38.92	37.86	37.11
3.5	38.55	41.80	43.79	44.64	45.25	45.66	45.21	44.09	43.07	42.24	41.28	40.17	39.30	38.92	38.73	38.00	36.58	35.16	34.30	33.78
3.4	32.79	35.93	37.86	38.68	39.26	39.65	39.22	38.17	37.22	36.48	35.66	34.76	34.11	33.97	33.99	33.52	32.37	31.18	30.51	30.18
3.3	27.17	29.96	31.68	32.40	32.94	33.34	32.99	32.05	31.20	30.56	29.89	29.19	28.74	28.77	28.94	28.69	27.86	26.95	26.47	26.30
3.2	21.14	23.50	24.99	25.69	26.29	26.79	26.65	25.98	25.35	24.85	24.32	23.78	23.51	23.67	23.97	23.93	23.37	22.71	22.42	22.40
3.1	15.09	17.05	18.30	19.01	19.71	20.37	20.50	20.18	19.84	19.52	19.11	18.70	18.57	18.85	19.29	19.45	19.13	18.70	18.59	18.72
3	10.23	11.83	12.81	13.46	14.18	14.91	15.24	15.21	15.11	14.94	14.60	14.26	14.22	14.58	15.15	15.51	15.43	15.24	15.30	15.53
2.9	6.794	8.080	8.796	9.295	9.949	10.66	11.07	11.20	11.27	11.19	10.88	10.58	10.58	10.97	11.61	12.14	12.31	12.34	12.54	12.82
2.8	3.675	4.726	5.224	5.600	6.194	6.875	7.323	7.560	7.732	7.703	7.435	7.186	7.226	7.650	8.346	9.010	9.382	9.607	9.924	10.24
2.7	.4854	1.352	1.721	2.064	2.661	3.358	3.872	4.213	4.462	4.478	4.260	4.075	4.165	4.627	5.393	6.179	6.708	7.079	7.482	7.831
2.6	-2.08	-1.39	-1.08	-.694	-.042	.7037	1.306	1.748	2.063	2.117	1.940	1.802	1.922	2.405	3.219	4.088	4.716	5.173	5.631	6.006
2.5	-4.07	-3.52	-3.24	-2.78	-2.05	-1.27	-.608	-.096	.2718	.3650	.2315	.1460	.3073	.8091	1.647	2.566	3.260	3.779	4.288	4.706
2.4	-5.85	-5.44	-5.18	-4.66	-3.90	-3.12	-2.46	-1.92	-1.51	-1.37	-1.46	-1.48	-1.26	-.733	.1227	1.083	1.836	2.425	3.010	3.502
2.3	-7.06	-6.78	-6.59	-6.09	-5.36	-4.66	-4.05	-3.51	-3.06	-2.89	-2.96	-2.96	-2.71	-2.19	-1.36	-.390	.4026	1.059	1.723	2.281
2.2	-7.54	-7.42	-7.35	-6.96	-6.34	-5.75	-5.21	-4.68	-4.19	-4.00	-4.00	-4.11	-3.90	-3.45	-2.69	-1.76	-.946	-.221	.5178	1.118
2.1	-7.65	-7.69	-7.78	-7.55	-7.08	-6.60	-6.13	-5.61	-5.09	-4.87	-4.98	-5.07	-4.95	-4.60	-3.94	-3.08	-2.26	-1.47	-.673	-.050
2	-7.53	-7.73	-7.97	-7.89	-7.55	-7.17	-6.78	-6.27	-5.73	-5.49	-5.63	-5.80	-5.79	-5.53	-4.97	-4.17	-3.36	-2.54	-1.71	-1.08
1.9	-7.09	-7.39	-7.73	-7.73	-7.47	-7.15	-6.80	-6.31	-5.78	-5.55	-5.72	-5.97	-6.04	-5.87	-5.39	-4.66	-3.87	-3.06	-2.22	-1.61
1.8	-6.28	-6.60	-6.95	-6.98	-6.73	-6.41	-6.07	-5.64	-5.17	-4.99	-5.17	-5.44	-5.56	-5.44	-5.02	-4.35	-3.61	-2.82	-2.01	-1.44
1.7	-5.41	-5.71	-6.01	-6.02	-5.75	-5.41	-5.08	-4.70	-4.34	-4.21	-4.38	-4.62	-4.73	-4.63	-4.25	-3.63	-2.92	-2.16	-1.39	-.666
1.6	-4.56	-4.79	-5.01	-4.98	-4.72	-4.40	-4.11	-3.81	-3.54	-3.47	-3.64	-3.85	-3.94	-3.85	-3.51	-2.93	-2.24	-1.51	-.789	-.311
1.5	-5.20	-5.28	-5.37	-5.32	-5.11	-4.82	-4.52	-4.21	-3.92	-3.82	-3.95	-4.11	-4.16	-4.05	-3.73	-3.19	-2.53	-1.80	-1.07	-.560
1.4	-5.41	-5.26	-5.16	-5.05	-4.81	-4.73	-4.47	-4.12	-3.78	-3.66	-3.79	-4.00	-4.10	-4.02	-3.73	-3.26	-2.69	-2.02	-1.32	-.629
1.3	-6.55	-6.16	-5.82	-5.62	-5.52	-5.42	-5.18	-4.78	-4.37	-4.19	-4.29	-4.49	-4.59	-4.50	-4.21	-3.78	-3.26	-2.62	-1.94	-1.44
1.2	-9.30	-8.77	-8.27	-8.01	-8.00	-7.99	-7.74	-7.27	-6.76	-6.48	-6.49	-6.59	-6.61	-6.43	-6.08	-5.60	-5.01	-4.26	-3.48	-2.90
1.1	-14.3	-14.0	-13.8	-13.8	-14.1	-14.3	-14.0	-13.3	-12.5	-12.1	-11.9	-11.7	-11.5	-11.1	-10.5	-9.72	-8.78	-7.75	-6.85	-6.23
1	-20.1	-20.2	-20.2	-20.5	-21.0	-21.4	-21.0	-19.9	-18.8	-18.1	-17.6	-17.2	-16.6	-15.8	-14.9	-13.9	-12.7	-11.4	-10.5	-9.79
0.9	-25.6	-26.0	-26.3	-26.9	-27.7	-28.1	-27.6	-26.3	-24.9	-23.8	-23.2	-22.5	-21.7	-20.6	-19.4	-18.0	-16.5	-15.0	-14.0	-13.3
0.8	-25.2	-25.7	-26.4	-27.2	-28.3	-28.9	-28.4	-26.9	-25.4	-24.3	-23.8	-23.3	-22.5	-21.4	-20.0	-18.6	-16.9	-15.5	-14.4	-13.8
0.7	-23.7	-24.3	-25.1	-26.2	-27.6	-28.4	-28.0	-26.4	-24.6	-23.5	-23.1	-22.7	-22.0	-20.9	-19.6	-18.1	-16.5	-15.1	-14.2	-13.6
0.6	-25.4	-25.7	-26.3	-27.3	-28.8	-29.7	-29.3	-27.6	-25.6	-24.4	-24.0	-23.7	-23.0	-22.0	-20.7	-19.2	-17.5	-16.0	-15.0	-14.4
0.5	-28.2	-28.2	-28.5	-29.5	-30.9	-31.9	-31.5	-29.7	-27.7	-26.4	-25.9	-25.5	-24.9	-23.9	-22.7	-21.1	-19.2	-17.5	-16.4	-15.7
0.4	-31.0	-30.7	-30.7	-31.6	-33.1	-34.2	-33.7	-31.9	-29.7	-28.3	-27.8	-27.4	-26.8	-25.9	-24.7	-23.0	-20.9	-19.0	-17.7	-16.9
0.3	-36.8	-36.0	-35.5	-36.2	-37.7	-38.7	-38.0	-35.7	-33.0	-31.2	-30.3	-29.7	-28.9	-27.9	-26.8	-25.2	-23.1	-20.9	-19.3	-18.3
0.2	-45.2	-43.9	-42.7	-42.9	-44.3	-45.1	-43.9	-40.9	-37.5	-35.1	-33.9	-32.9	-31.8	-30.6	-29.5	-28.1	-25.9	-23.3	-21.3	-20.0
0.1	-42.8	-41.2	-39.7	-39.7	-40.9	-41.8	-40.8	-38.0	-34.7	-32.6	-31.6	-30.6	-29.3	-27.9	-26.6	-25.6	-24.3	-22.6	-20.9	-19.4
0	15.88	16.21	15.56	14.01	11.54	9.129	8.400	10.08	12.84	14.09	13.11	11.60	11.06	11.35	11.42	10.63	9.409	8.805	8.697	8.018

	4	3.9	3.8	3.7	3.6	3.5	3.4	3.3	3.2	3.1	3	2.9	2.8	2.7	2.6	2.5	2.4	2.3	2.2	2.1
8																				
7.9																				
7.8																				
7.7																				
7.6																				
7.5																				
7.4																				
7.3																				
7.2																				
7.1																				
7																				
6.9																				
6.8																				
6.7																				
6.6																				
6.5																				
6.4																				
6.3																				
6.2																				
6.1																				
6																				
5.9																				
5.8																				
5.7																				
5.6																				
5.5																				
5.4																				
5.3																				
5.2																				
5.1																				
5																				
4.9																				
4.8																				
4.7																				
4.6																				
4.5																				
4.4																				
4.3																				
4.2																				
4.1																				
4	46.26																			
3.9	44.58	43.36																		
3.8	42.45	41.67	40.52																	
3.7	39.67	39.20	38.52	37.08																
3.6	36.57	36.23	35.78	34.85	33.38															
3.5	33.39	33.09	32.70	32.12	31.43	30.44														
3.4	29.94	29.71	29.40	29.10	28.95	28.68	27.61													
3.3	26.20	26.08	25.95	25.90	26.05	26.14	25.60	24.18												
3.2	22.41	22.41	22.43	22.60	22.99	23.32	23.10	22.14	20.62											
3.1	18.82	18.88	19.01	19.38	20.01	20.57	20.57	19.90	18.87	17.70										
3	15.69	15.79	16.00	16.53	17.37	18.14	18.30	17.85	17.18	16.49	15.73									
2.9	13.00	13.15	13.45	14.20	15.08	15.96	16.27	16.01	15.58	15.19	14.80	14.26								
2.8	10.44	10.63	11.02	11.79	12.86	13.82	14.26	14.19	13.96	13.78	13.67	13.48	13.07							
2.7	8.052	8.283	8.744	9.602	10.76	11.82	12.37	12.47	12.42	12.46	12.57	12.63	12.51	12.23						
2.6	6.236	6.463	6.927	7.820	9.043	10.16	10.80	10.99	11.10	11.33	11.61	11.81	11.87	11.81	11.62					
2.5	4.961	5.177	5.608	6.489	7.733	8.892	9.567	9.823	10.04	10.40	10.81	11.09	11.22	11.28	11.29	11.21				
2.4	3.810	4.043	4.462	5.336	6.595	7.787	8.509	8.826	9.125	9.595	10.08	10.43	10.61	10.74	10.88	11.02	11.12			
2.3	2.628	2.877	3.303	4.183	5.448	6.653	7.408	7.782	8.161	8.727	9.308	9.724	9.967	10.16	10.38	10.68	11.00	11.11		
2.2	1.469	1.714	2.149	3.041	4.293	5.469	6.221	6.636	7.091	7.752	8.425	8.929	9.258	9.534	9.821	10.19	10.62	10.88	10.85	
2.1	.2867	.5163	.9666	1.880	3.111	4.236	4.969	5.418	5.943	6.690	7.452	8.044	8.466	8.831	9.190	9.595	10.05	10.41	10.57	10.57
2	-.775	-.571	-.114	.8116	2.013	3.082	3.791	4.265	4.848	5.669	6.503	7.168	7.671	8.124	8.559	8.999	9.469	9.892	10.23	10.50
1.9	-1.35	-1.19	-.767	.1268	1.270	2.274	2.953	3.435	4.046	4.903	5.773	6.475	7.026	7.540	8.035	8.512	8.993	9.462	9.933	10.40
1.8	-1.24	-1.15	-.797	.0099	1.055	1.982	2.627	3.100	3.702	4.542	5.399	6.096	6.651	7.179	7.706	8.216	8.713	9.204	9.734	10.30
1.7	-.716	-.695	-.424	.2703	1.192	2.029	2.632	3.086	3.653	4.437	5.242	5.908	6.443	6.952	7.481	8.013	8.523	9.009	9.542	10.11
1.6	-.200	-.219	-.009	.5828	1.376	2.102	2.643	3.060	3.575	4.281	5.014	5.634	6.137	6.614	7.126	7.657	8.157	8.624	9.147	9.705
1.5	-.406	-.389	-.188	.3198	.9657	1.555	2.001	2.380	2.879	3.551	4.220	4.776	5.232	5.649	6.053	6.480	6.902	7.350	7.871	8.405
1.4	-.553	-.594	-.387	.0358	.5271	.9257	1.242	1.513	1.961	2.589	3.181	3.646	4.035	4.397	4.724	5.005	5.310	5.717	6.232	6.758
1.3	-1.22	-1.08	-.823	-.432	-.034	.2583	.4266	.6019	.9988	1.577	2.086	2.460	2.786	3.105	3.356	3.491	3.650	3.978	4.448	4.931
1.2	-2.57	-2.29	-1.89	-1.42	-1.05	-.856	-.771	-.618	-.209	.3632	.8406	1.186	1.503	1.817	2.006	2.002	2.025	2.279	2.699	3.126
1.1	-5.81	-5.37	-4.76	-4.08	-3.51	-3.14	-2.85	-2.50	-1.96	-1.29	-.673	-.173	.2889	.7102	.9399	.9381	.9735	1.230	1.586	1.908
1	-9.26	-8.65	-7.81	-6.88	-6.06	-5.44	-4.92	-4.37	-3.71	-2.96	-2.23	-1.63	-1.07	-.559	-.295	-.301	-.243	.0279	.3376	.6047
0.9	-12.6	-11.8	-10.8	-9.62	-8.57	-7.71	-6.93	-6.14	-5.34	-4.49	-3.64	-2.92	-2.25	-1.64	-1.34	-1.35	-1.28	-.998	-.741	-.535
0.8	-13.2	-12.4	-11.2	-10.0	-8.89	-7.96	-7.12	-6.30	-5.48	-4.60	-3.69	-2.96	-2.34	-1.81	-1.58	-1.65	-1.58	-1.29	-1.07	-.949
0.7	-13.1	-12.3	-11.1	-9.89	-8.70	-7.71	-6.85	-6.07	-5.29	-4.40	-3.50	-2.82	-2.35	-1.98	-1.86	-1.99	-1.92	-1.61	-1.43	-1.40
0.6	-13.8	-13.0	-11.7	-10.3	-8.99	-7.87	-6.95	-6.11	-5.26	-4.32	-3.38	-2.68	-2.18	-1.76	-1.60	-1.69	-1.59	-1.21	-.962	-.893
0.5	-15.0	-14.0	-12.7	-11.1	-9.59	-8.35	-7.30	-6.33	-5.37	-4.36	-3.36	-2.59	-2.01	-1.49	-1.26	-1.32	-1.18	-.736	-.422	-.302
0.4	-16.2	-15.1	-13.7	-11.9	-10.2	-8.81	-7.64	-6.53	-5.45	-4.37	-3.31	-2.48	-1.80	-1.18	-.875	-.904	-.725	-.217	.1667	.3390
0.3	-17.4	-16.3	-14.7	-12.7	-10.7	-9.10	-7.75	-6.49	-5.25	-4.01	-2.88	-2.07	-1.45	-.809	-.432	-.446	-.283	.2724	.7841	1.113
0.2	-19.1	-17.9	-16.0	-13.6	-11.2	-9.30	-7.78	-6.37	-4.86	-3.32	-2.02	-1.22	-.698	-.047	.4364	.4396	.5522	1.136	1.789	2.319
0.1	-18.2	-16.8	-15.0	-12.9	-10.8	-9.10	-7.91	-6.87	-5.50	-3.87	-2.49	-1.69	-1.17	-.459	.0926	.0732	.0807	.5891	1.266	1.974
0	6.450	4.589	3.170	2.880	3.874	4.807	3.999	1.958	.7447	1.019	1.767	2.093	1.745	1.144	.9197	1.217	1.820	2.373	2.580	2.603

	2	1.9	1.8	1.7	1.6	1.5	1.4	1.3	1.2	1.1	1	0.9	0.8	0.7	0.6	0.5	0.4	0.3	0.2	0.1	0
8																					
7.9																					
7.8																					
7.7																					
7.6																					
7.5																					
7.4																					
7.3																					
7.2																					
7.1																					
7																					
6.9																					
6.8																					
6.7																					
6.6																					
6.5																					
6.4																					
6.3																					
6.2																					
6.1																					
6																					
5.9																					
5.8																					
5.7																					
5.6																					
5.5																					
5.4																					
5.3																					
5.2																					
5.1																					
5																					
4.9																					
4.8																					
4.7																					
4.6																					
4.5																					
4.4																					
4.3																					
4.2																					
4.1																					
4																					
3.9																					
3.8																					
3.7																					
3.6																					
3.5																					
3.4																					
3.3																					
3.2																					
3.1																					
3																					
2.9																					
2.8																					
2.7																					
2.6																					
2.5																					
2.4																					
2.3																					
2.2																					
2.1																					
2	10.71																				
1.9	10.84	11.19																			
1.8	10.86	11.39	11.85																		
1.7	10.70	11.35	12.08	12.64																	
1.6	10.30	11.02	11.92	12.75	13.11																
1.5	8.945	9.584	10.38	11.14	11.56	10.68															
1.4	7.276	7.824	8.417	8.973	9.362	9.209	8.722														
1.3	5.393	5.806	6.138	6.420	6.729	7.294	7.847	8.242													
1.2	3.514	3.760	3.788	3.744	3.908	5.104	6.612	8.220	9.535												
1.1	2.132	2.066	1.591	.9956	.7479	2.190	4.156	6.352	8.495	10.41											
1	.7673	.4911	-.427	-1.59	-2.32	-.708	1.659	4.397	7.302	11.85	16.14										
0.9	-.440	-.911	-2.23	-3.91	-5.07	-3.33	-.647	2.522	6.063	12.95	19.79	25.83									
0.8	-.953	-1.56	-3.08	-4.99	-6.36	-4.63	-1.86	1.398	5.044	12.80	20.57	27.68	31.11								
0.7	-1.53	-2.29	-4.02	-6.19	-7.76	-6.05	-3.18	.1750	3.906	12.38	21.01	29.09	34.19	39.18							
0.6	-.993	-1.78	-3.65	-5.99	-7.71	-6.00	-3.02	.4768	4.314	13.04	22.07	30.51	36.13	41.79	45.52						
0.5	-.376	-1.20	-3.17	-5.66	-7.50	-5.76	-2.72	.8850	4.795	13.85	23.27	32.08	38.12	44.27	49.10	53.86					
0.4	.2940	-.556	-2.65	-5.29	-7.24	-5.48	-2.37	1.327	5.304	14.69	24.49	33.66	40.14	46.78	52.78	58.81	65.11				
0.3	1.235	.5006	-1.60	-4.38	-6.49	-4.68	-1.38	2.641	6.773	16.22	26.32	35.74	42.85	50.32	57.69	65.10	72.85	85.19			
0.2	2.679	2.102	-.065	-3.11	-5.51	-3.69	-.029	4.564	9.166	18.60	28.90	38.51	46.43	54.96	63.83	72.61	81.82	100.4	125.2		
0.1	2.644	2.360	.2893	-2.90	-5.48	-4.05	-.292	4.522	9.304	16.42	25.52	33.93	41.40	49.93	58.34	66.05	74.13	92.79	119.3	131.8	
0	2.680	2.333	1.023	-.899	-2.62	-2.48	-.773	1.345	2.184	8.248	15.44	21.47	28.38	36.59	40.81	43.65	46.55	54.23	64.05	61.25	231.2

APPENDIX J

MAP ESTIMATOR AVERAGING KERNELS

Averaging kernels for the equatorial "summer" and high latitudes "winter" MAP estimators are presented here. In each case, results are given for two sets of measurement noise statistics. These values are given in table J.1 below (from table 7):

TABLE J.1 : Measurement Noise Variance Statistics

DATA SERIES	Channel Noise Variances $(r.u.)^2$					
	A	B	C	D	E	F
2	1.5	0.43	0.09	0.02	0.06	0.02
5	0.07	0.02	0.004	0.001	0.003	0.001

The averaging kernels are plotted in figures J.1 through J.4

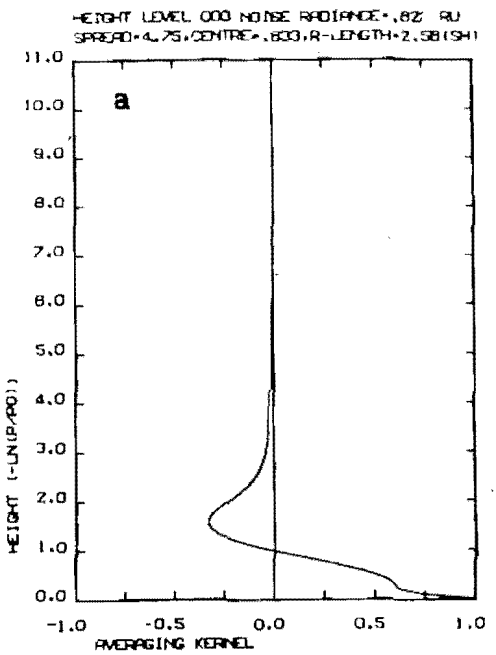
HEIGHT LEVEL 000 NOISE RADIANCE=.82 RU
SPREAD=4.75,CENTRE=.603,R-LENGTH=2.58(SH)
a
HEIGHT (-LN(P/P0))
AVERAGING KERNEL

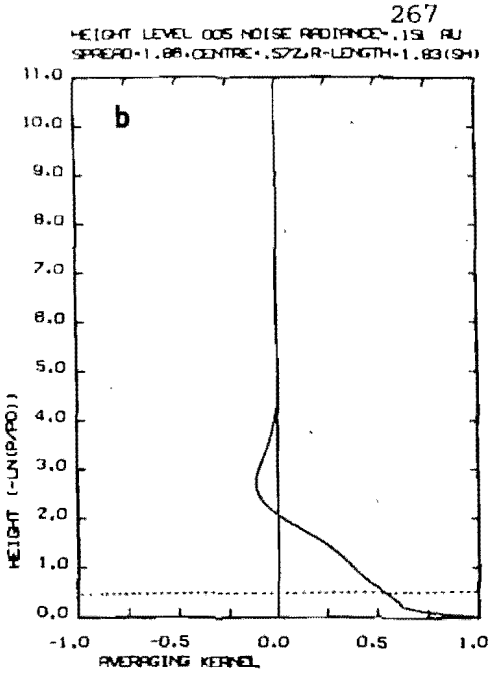
HEIGHT LEVEL 005 NOISE RADIANCE=.15 RU
SPREAD=1.86,CENTRE=.572,R-LENGTH=1.83(SH)
b
HEIGHT (-LN(P/P0))
AVERAGING KERNEL

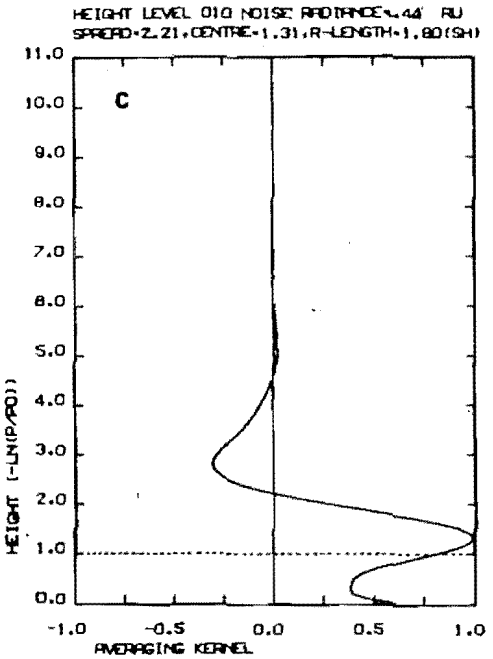
HEIGHT LEVEL 010 NOISE RADIANCE=.44 RU
SPREAD=2.21,CENTRE=1.31,R-LENGTH=1.80(SH)
c
HEIGHT (-LN(P/P0))
AVERAGING KERNEL

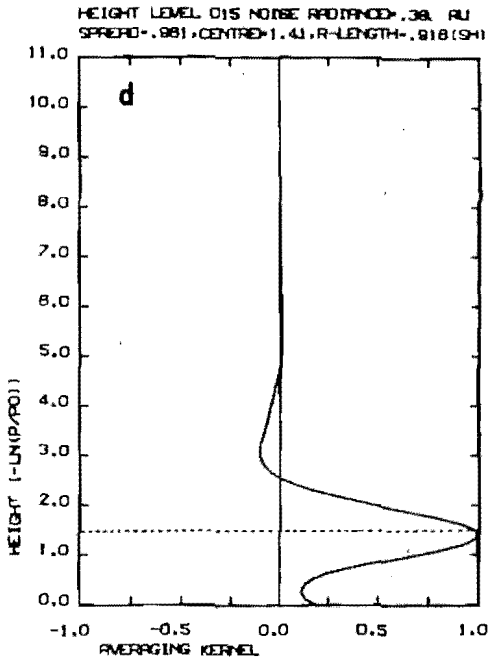
HEIGHT LEVEL 015 NOISE RADIANCE=.38 RU
SPREAD=.981,CENTRE=1.41,R-LENGTH=.918(SH)
d
HEIGHT (-LN(P/P0))
AVERAGING KERNEL

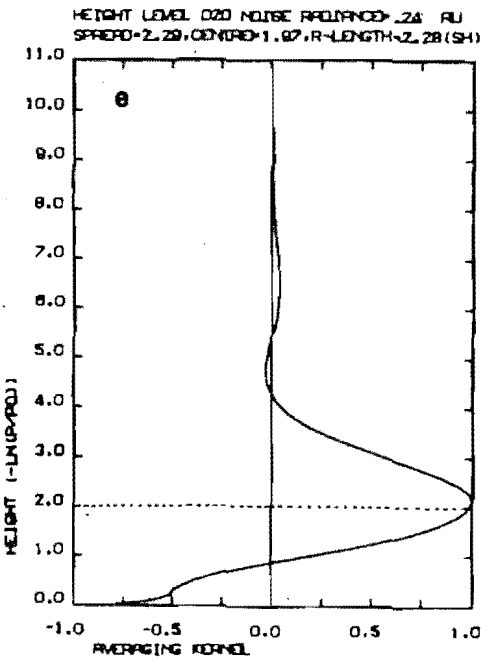
HEIGHT LEVEL 020 NOISE RADIANCE=.24 RU
SPREAD=2.29,CENTRE=1.97,R-LENGTH=2.28(SH)
e
HEIGHT (-LN(P/P0))
AVERAGING KERNEL

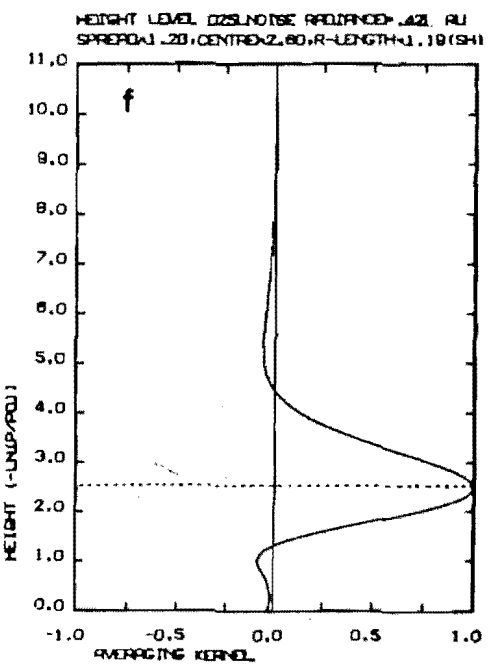
HEIGHT LEVEL 025 NOISE RADIANCE=.42 RU
SPREAD=1.28,CENTRE=2.80,R-LENGTH=1.19(SH)
f
HEIGHT (-LN(P/P0))
AVERAGING KERNEL

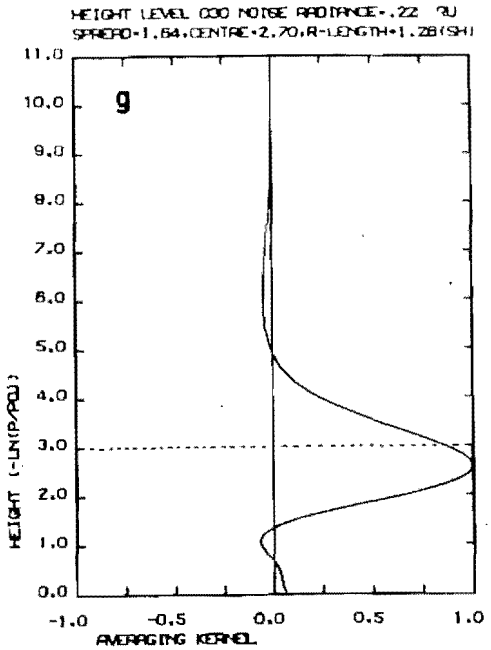
HEIGHT LEVEL 030 NOISE RADIANCE=.22 RU
SPREAD=1.84,CENTRE=2.70,R-LENGTH=1.28(SH)
g
HEIGHT (-LN(P/PO))
AVERAGING KERNEL

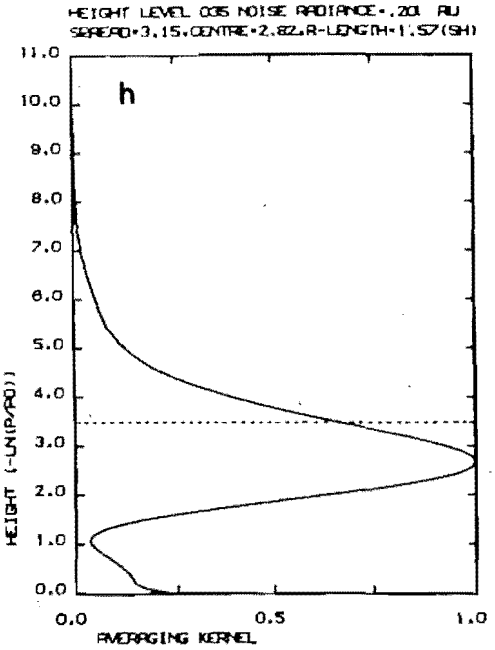
HEIGHT LEVEL 035 NOISE RADIANCE=.20 RU
SPREAD=3.15,CENTRE=2.82,R-LENGTH=1.57(SH)
h
HEIGHT (-LN(P/PO))
AVERAGING KERNEL

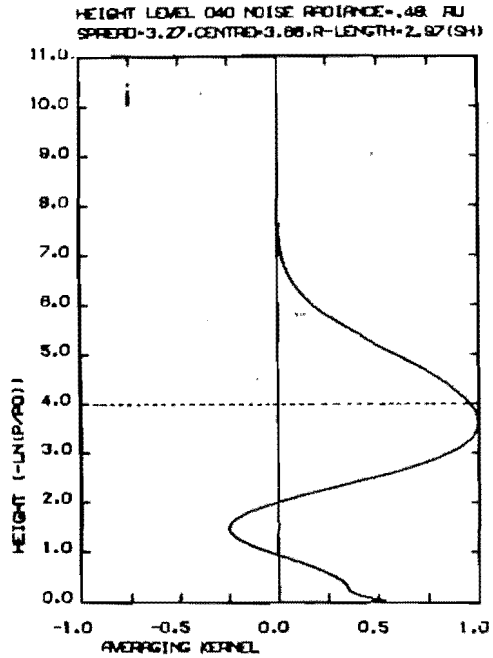
HEIGHT LEVEL 040 NOISE RADIANCE=.48 RU
SPREAD=3.27,CENTRE=3.86,R-LENGTH=2.97(SH)
i
HEIGHT (-LN(P/PO))
AVERAGING KERNEL

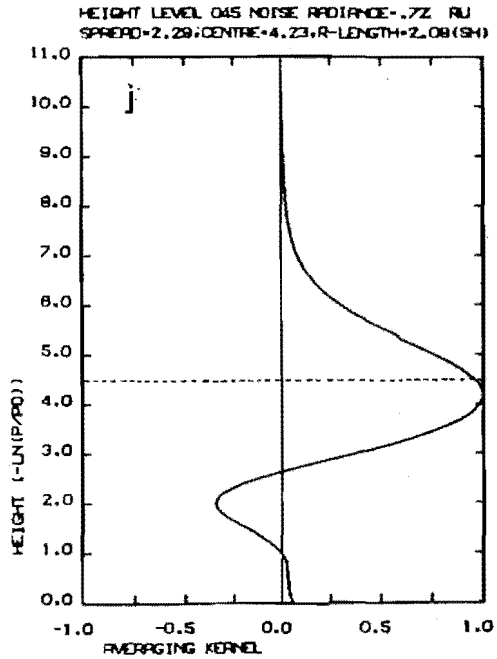
HEIGHT LEVEL 045 NOISE RADIANCE=.72 RU
SPREAD=2.29,CENTRE=4.23,R-LENGTH=2.08(SH)
j
HEIGHT (-LN(P/PO))
AVERAGING KERNEL

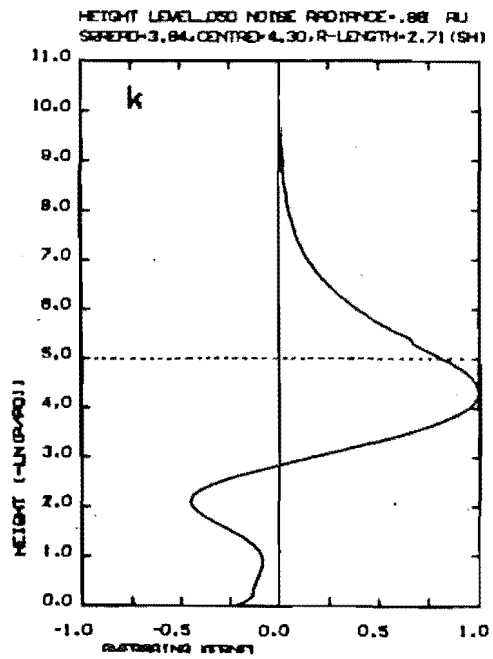
HEIGHT LEVEL 050 NOISE RADIANCE=.88 RU
SPREAD=3.84,CENTRE=4.30,R-LENGTH=2.71(SH)
k
HEIGHT (-LN(P/PO))

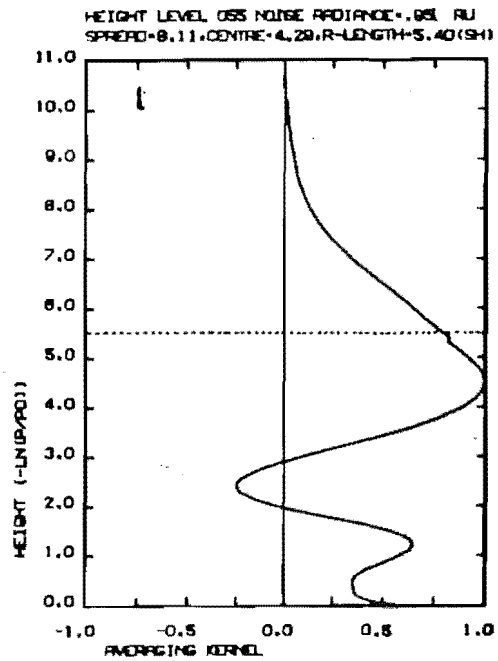
HEIGHT LEVEL 055 NOISE RADIANCE=.95 RU
SPREAD=8.11,CENTRE=4.29,R-LENGTH=5.40(SH)
l
HEIGHT (-LN(P/PO))
AVERAGING KERNEL

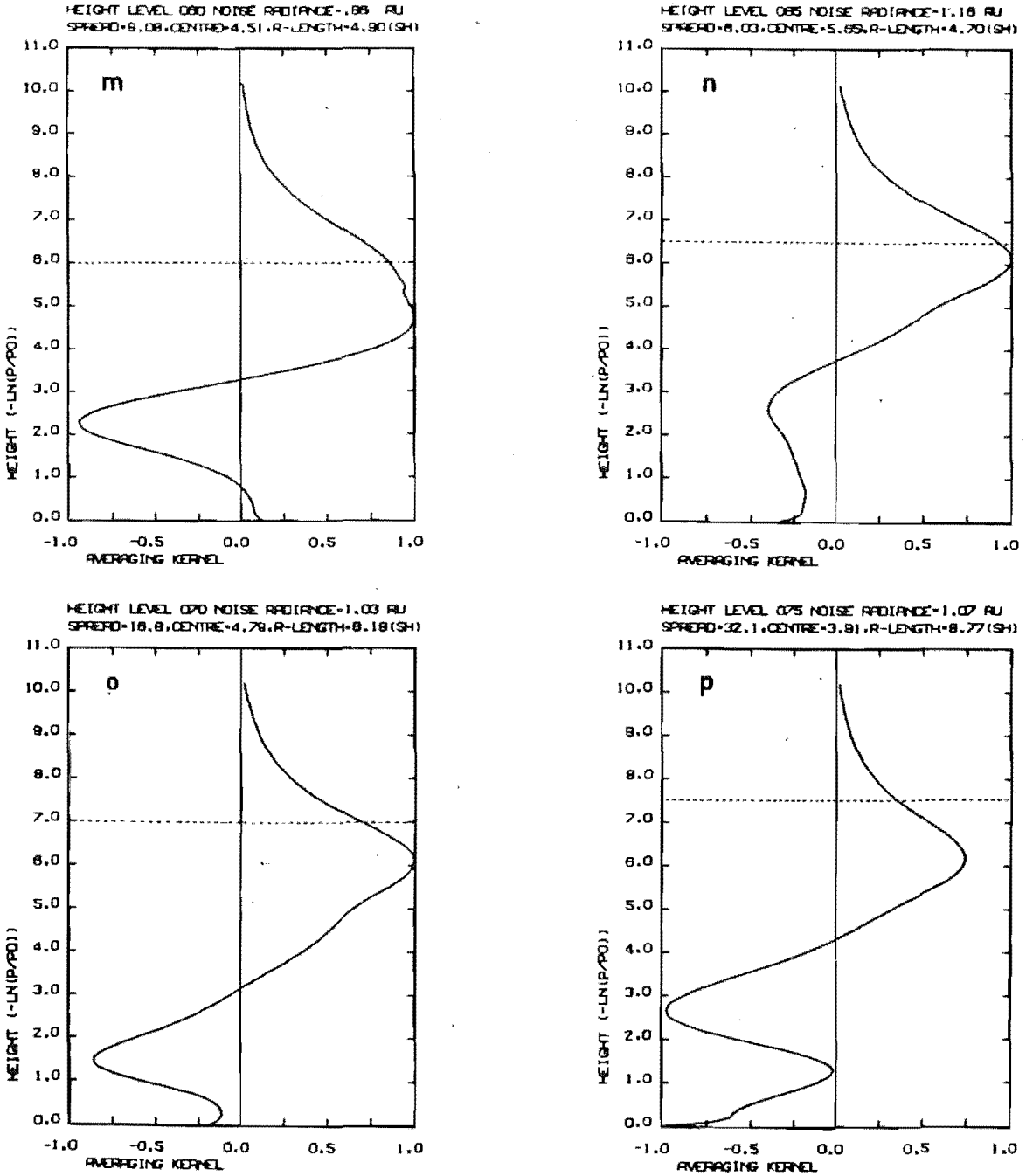

FIGURE J.1 : Averaging Kernels for the Equatorial summer MAP Estimator, with measurement noise values as for data series 2 (table J.1). The dashed line refers to the averaging kernel height z_i. The spread, centre height, resolving length and measurement noise propagation noise (i.e. noise radiance) are indicated for each figure. These characteristics are also given for the following Figures.

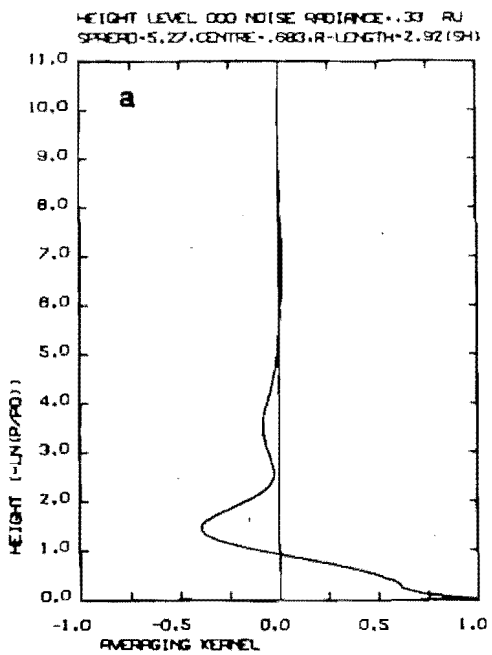
HEIGHT LEVEL 000 NOISE RADIANCE=.33 RU
SPREAD=5.27,CENTRE=-.683,R-LENGTH=2.92(SH)
a
HEIGHT (-LN(P/PO))
AVERAGING KERNEL

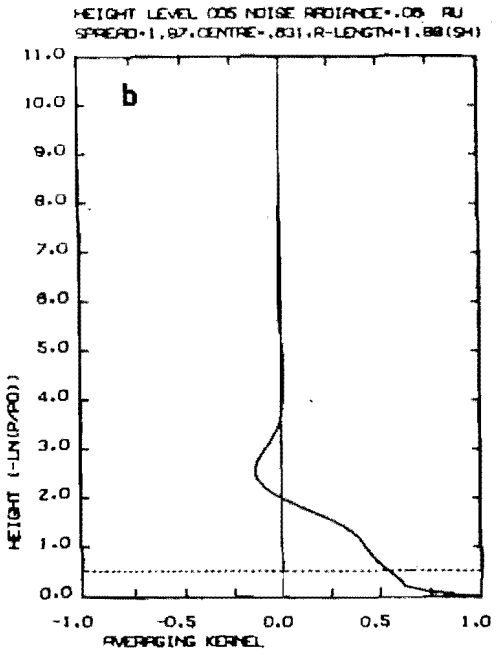
HEIGHT LEVEL 005 NOISE RADIANCE=.06 RU
SPREAD=1.87,CENTRE=.831,R-LENGTH=1.88(SH)
b
HEIGHT (-LN(P/PO))
AVERAGING KERNEL

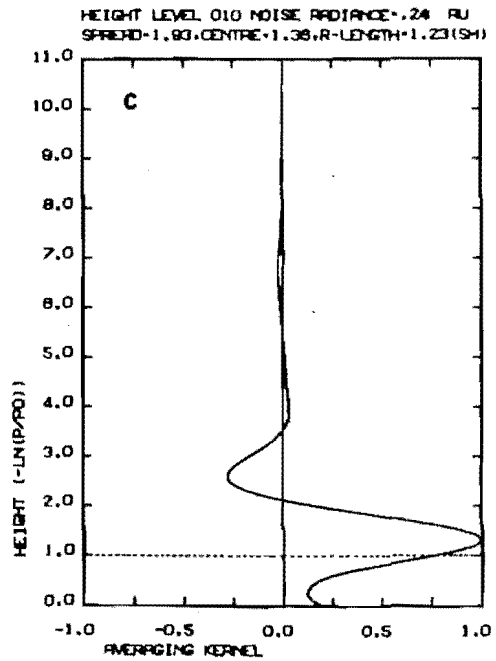
HEIGHT LEVEL 010 NOISE RADIANCE=.24 RU
SPREAD=1.93,CENTRE=1.38,R-LENGTH=1.23(SH)
c
HEIGHT (-LN(P/PO))
AVERAGING KERNEL

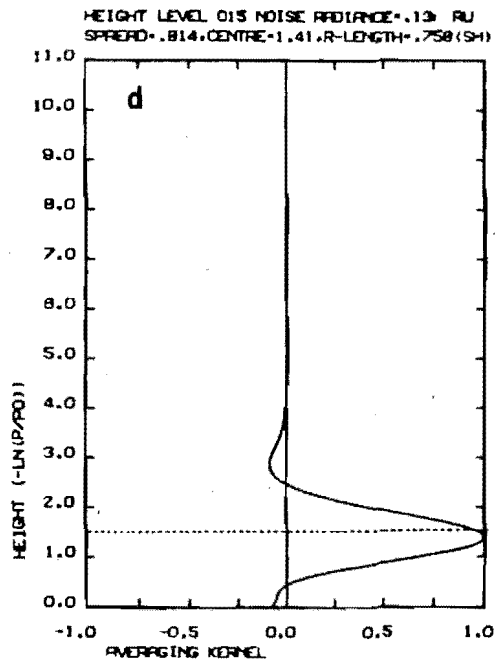
HEIGHT LEVEL 015 NOISE RADIANCE=.13 RU
SPREAD=.814,CENTRE=1.41,R-LENGTH=.758(SH)
d
HEIGHT (-LN(P/PO))
AVERAGING KERNEL

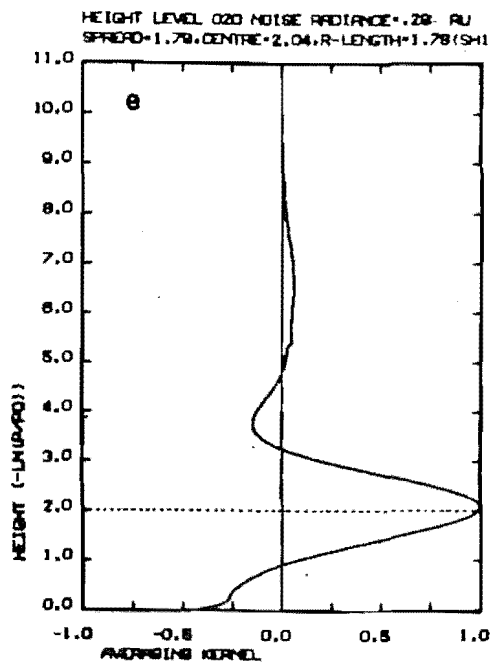
HEIGHT LEVEL 020 NOISE RADIANCE=.28 RU
SPREAD=1.79,CENTRE=2.04,R-LENGTH=1.78(SH)
e
HEIGHT (-LN(P/PO))
AVERAGING KERNEL

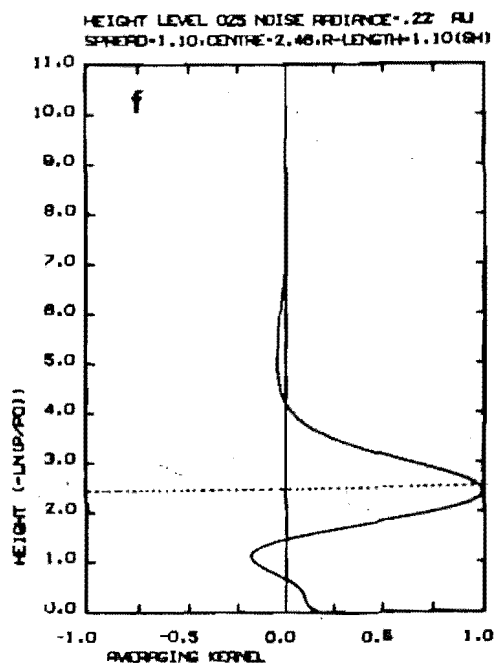
HEIGHT LEVEL 025 NOISE RADIANCE=.22 RU
SPREAD=1.10,CENTRE=2.46,R-LENGTH=1.10(SH)
f
HEIGHT (-LN(P/PO))
AVERAGING KERNEL

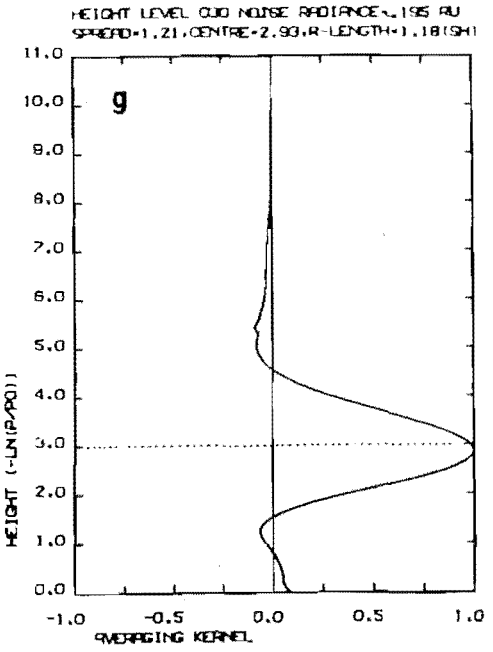
HEIGHT LEVEL 030 NOISE RADIANCE=.195 RU
SPREAD=1.21,CENTRE=2.93,R-LENGTH=1.18(SH)
g
HEIGHT (-LN(P/P0))
AVERAGING KERNEL

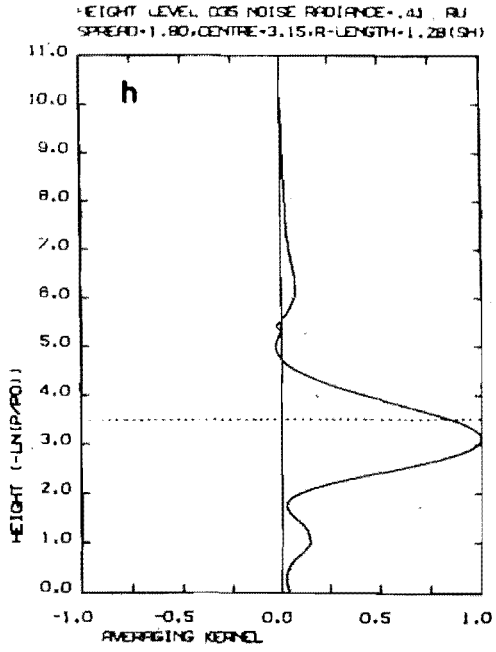
HEIGHT LEVEL 035 NOISE RADIANCE=.41 RU
SPREAD=1.80,CENTRE=3.15,R-LENGTH=1.28(SH)
h
HEIGHT (-LN(P/P0))
AVERAGING KERNEL

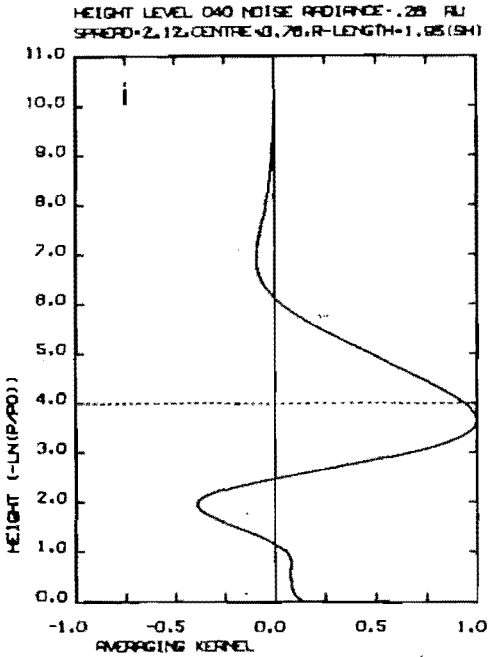
HEIGHT LEVEL 040 NOISE RADIANCE=.28 RU
SPREAD=2.12,CENTRE=3.78,R-LENGTH=1.85(SH)
i
HEIGHT (-LN(P/P0))
AVERAGING KERNEL

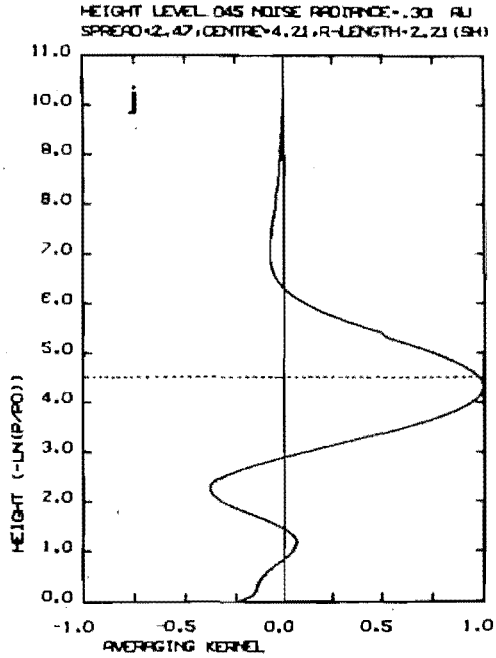
HEIGHT LEVEL 045 NOISE RADIANCE=.30 RU
SPREAD=2.47,CENTRE=4.21,R-LENGTH=2.21(SH)
j
HEIGHT (-LN(P/P0))
AVERAGING KERNEL

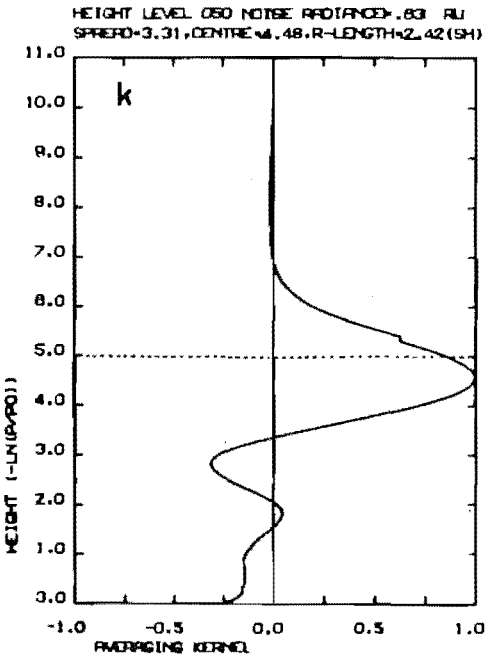
HEIGHT LEVEL 050 NOISE RADIANCE=.83 RU
SPREAD=3.31,CENTRE=4.48,R-LENGTH=2.42(SH)
k
HEIGHT (-LN(P/P0))
AVERAGING KERNEL

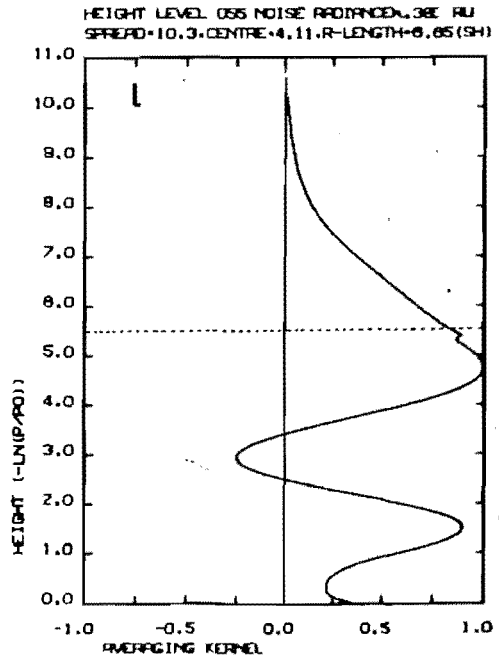
HEIGHT LEVEL 055 NOISE RADIANCE=.38 RU
SPREAD=10.3,CENTRE=4.11,R-LENGTH=6.65(SH)
l
HEIGHT (-LN(P/P0))
AVERAGING KERNEL

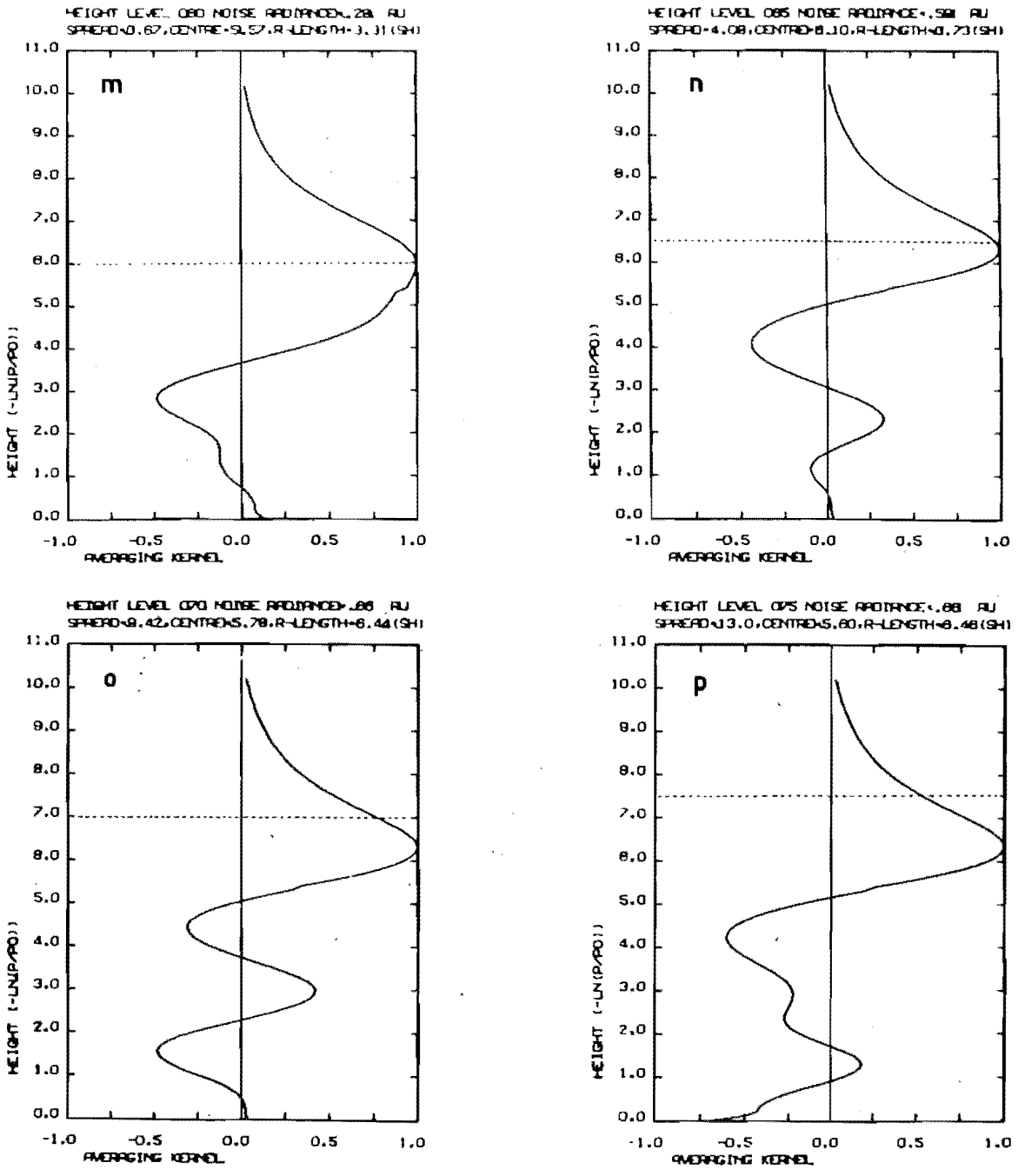

FIGURE J.2 : Averaging Kernels for the Equatorial summer MAP Estimator, with measurement noise values as for data series 5 (table J.1).

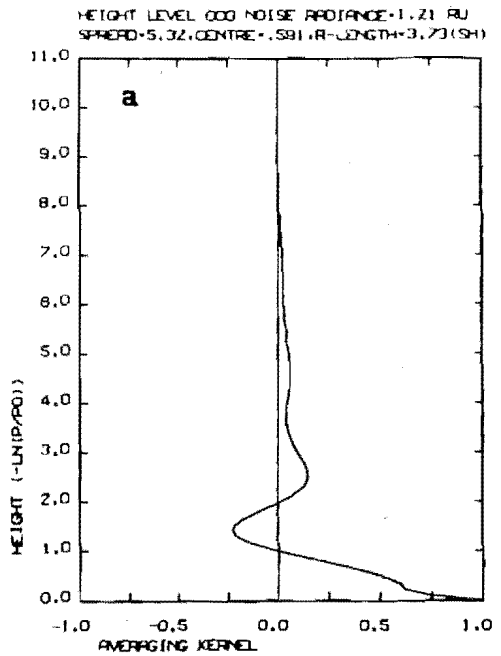
HEIGHT LEVEL 000 NOISE RADIANCE=1.21 RU
SPREAD=5.32,CENTRE=.591,R-LENGTH=3.73(SH)
a
HEIGHT (-LN(P/P0))
AVERAGING KERNEL

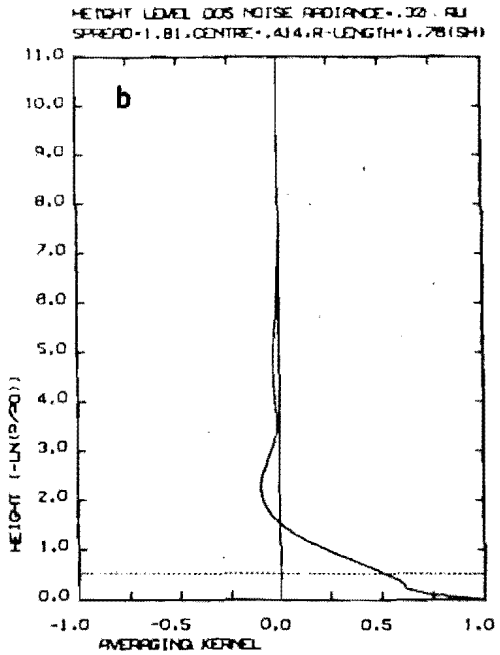
HEIGHT LEVEL 005 NOISE RADIANCE=.32 RU
SPREAD=1.81,CENTRE=.414,R-LENGTH=1.78(SH)
b
HEIGHT (-LN(P/P0))
AVERAGING KERNEL

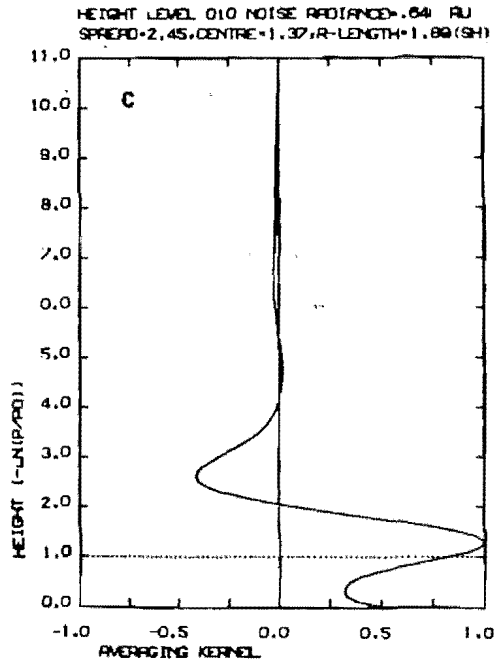
HEIGHT LEVEL 010 NOISE RADIANCE=.64 RU
SPREAD=2.45,CENTRE=1.37,R-LENGTH=1.89(SH)
c
HEIGHT (-LN(P/P0))
AVERAGING KERNEL

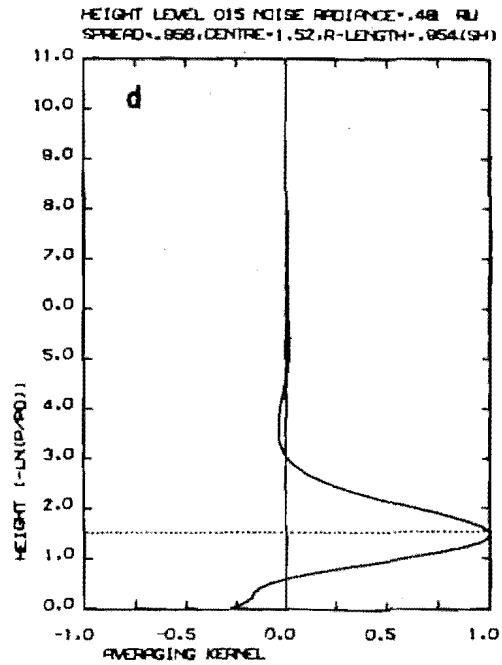
HEIGHT LEVEL 015 NOISE RADIANCE=.48 RU
SPREAD=.868,CENTRE=1.52,R-LENGTH=.954(SH)
d
HEIGHT (-LN(P/P0))
AVERAGING KERNEL

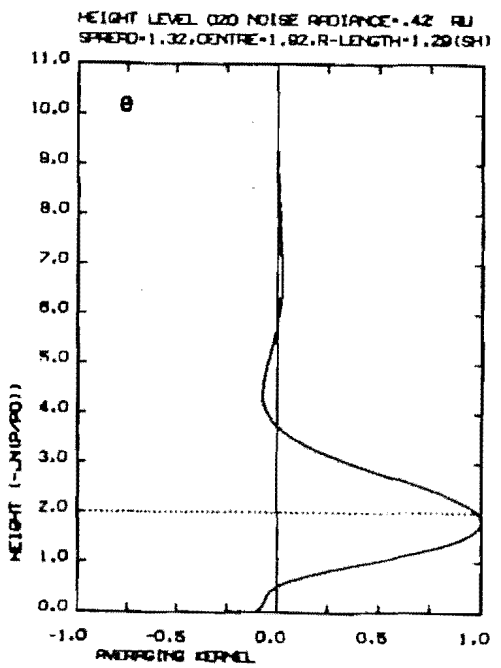
HEIGHT LEVEL 020 NOISE RADIANCE=.42 RU
SPREAD=1.32,CENTRE=1.92,R-LENGTH=1.29(SH)
e
HEIGHT (-LN(P/P0))
AVERAGING KERNEL

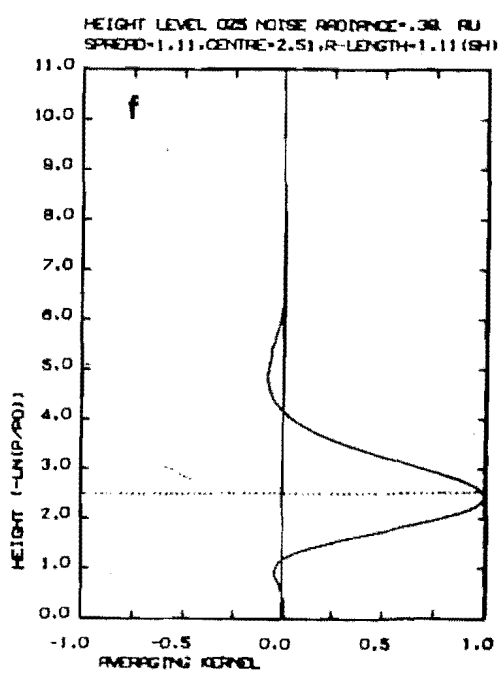
HEIGHT LEVEL 025 NOISE RADIANCE=.38 RU
SPREAD=1.11,CENTRE=2.51,R-LENGTH=1.11(SH)
f
HEIGHT (-LN(P/P0))
AVERAGING KERNEL

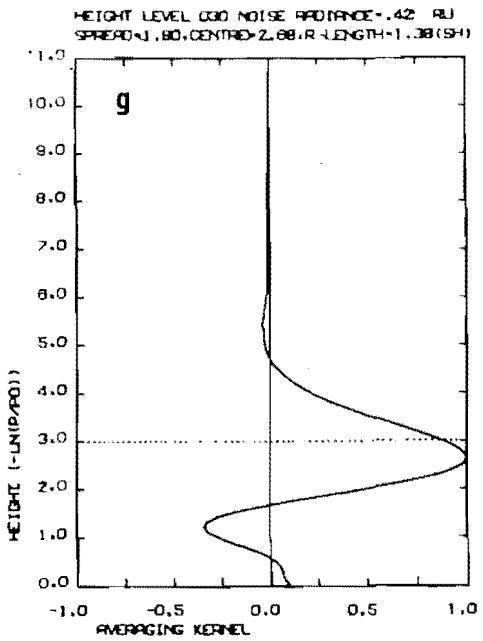
HEIGHT LEVEL 030 NOISE RADIANCE=.42 RU
SPREAD=3.80,CENTRE=2.88,R-LENGTH=1.38(SH)
g
HEIGHT (-LN(P/P0))
AVERAGING KERNEL

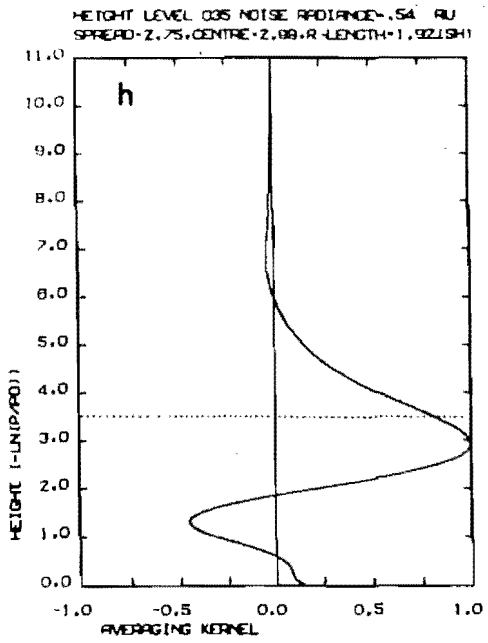
HEIGHT LEVEL 035 NOISE RADIANCE=.54 RU
SPREAD=2.75,CENTRE=2.99,R-LENGTH=1.92(SH)
h
HEIGHT (-LN(P/P0))
AVERAGING KERNEL

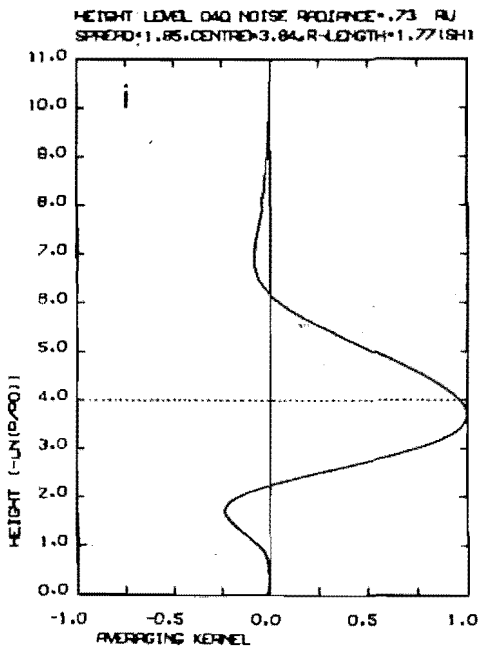
HEIGHT LEVEL 040 NOISE RADIANCE=.73 RU
SPREAD=1.85,CENTRE=3.84,R-LENGTH=1.77(SH)
i
HEIGHT (-LN(P/P0))
AVERAGING KERNEL

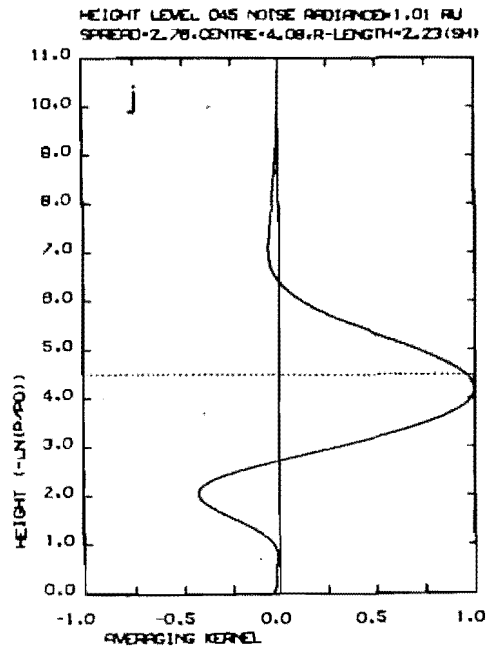
HEIGHT LEVEL 045 NOISE RADIANCE=1.01 RU
SPREAD=2.76,CENTRE=4.08,R-LENGTH=2.23(SH)
j
HEIGHT (-LN(P/P0))
AVERAGING KERNEL

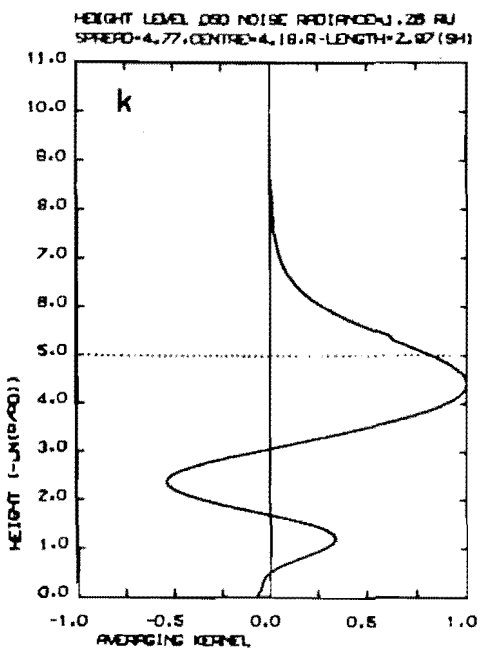
HEIGHT LEVEL 050 NOISE RADIANCE=1.28 RU
SPREAD=4.77,CENTRE=4.18,R-LENGTH=2.97(SH)
k
HEIGHT (-LN(P/P0))
AVERAGING KERNEL

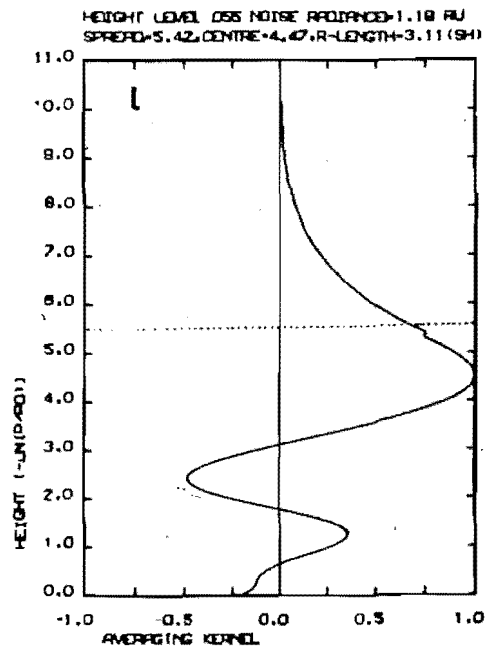
HEIGHT LEVEL 055 NOISE RADIANCE=1.18 RU
SPREAD=5.42,CENTRE=4.47,R-LENGTH=3.11(SH)
l
HEIGHT (-LN(P/P0))
AVERAGING KERNEL

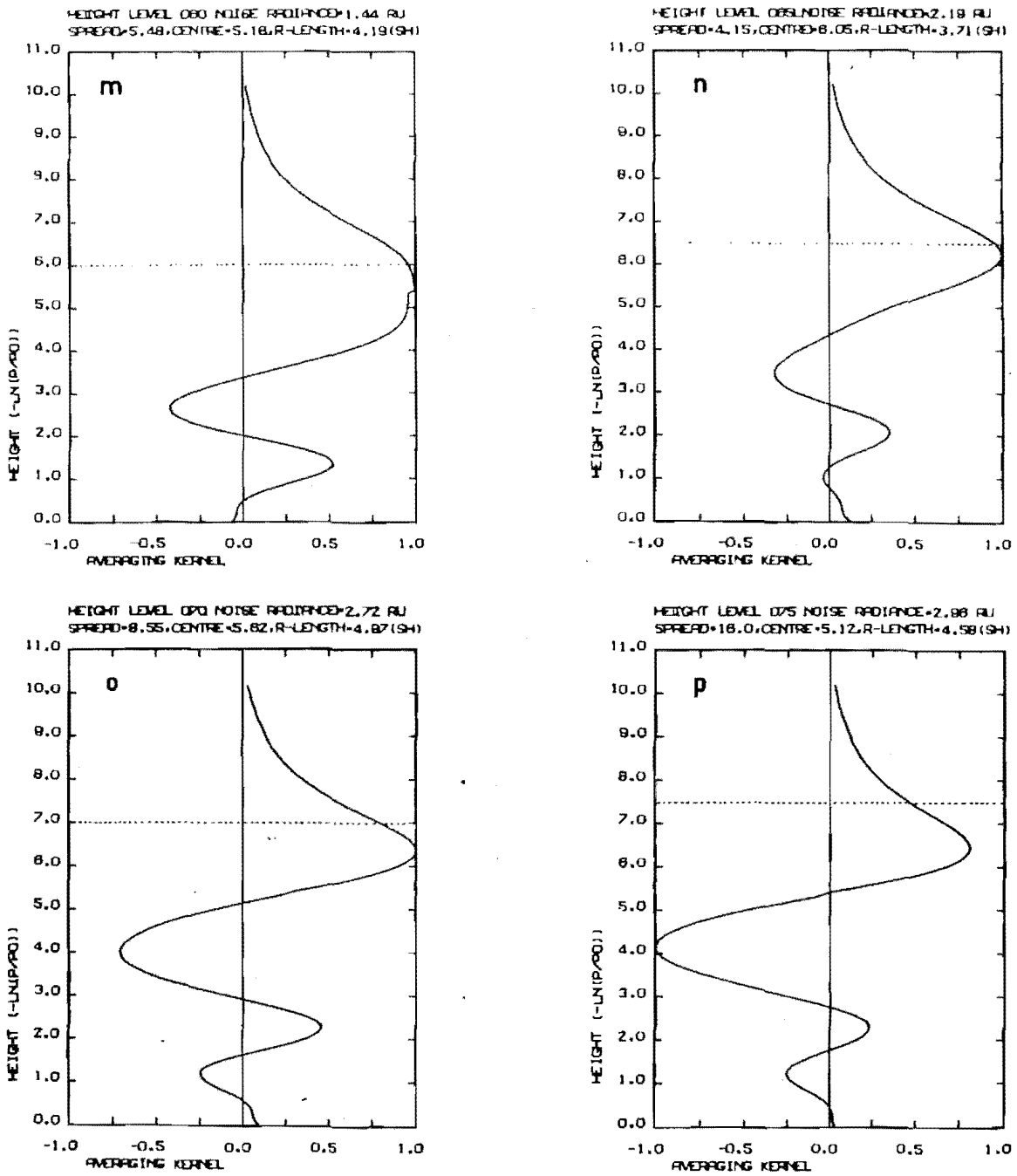

FIGURE J.3 : Averaging Kernels for the High Latitudes winter MAP estimator with measurement noise values as for data series 2 (table J.1).

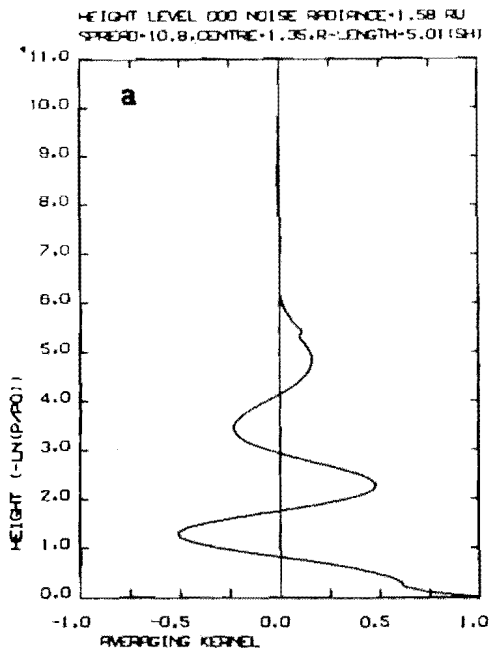
HEIGHT LEVEL 000 NOISE RADIANCE=1.58 RU
SPREAD=10.8,CENTRE=1.35,R-LENGTH=5.01(SH)
a
HEIGHT (-LN(P/P0))
AVERAGING KERNEL

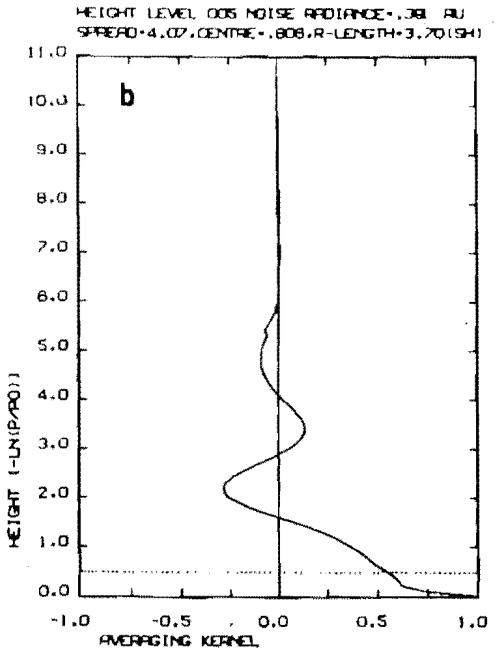
HEIGHT LEVEL 005 NOISE RADIANCE=.381 RU
SPREAD=4.07,CENTRE=.808,R-LENGTH=3.70(SH)
b
HEIGHT (-LN(P/P0))
AVERAGING KERNEL

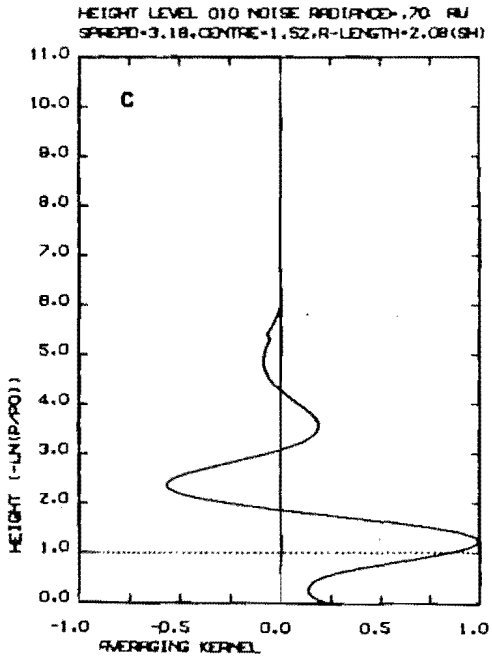
HEIGHT LEVEL 010 NOISE RADIANCE=.70 RU
SPREAD=3.18,CENTRE=1.52,R-LENGTH=2.08(SH)
c
HEIGHT (-LN(P/P0))
AVERAGING KERNEL

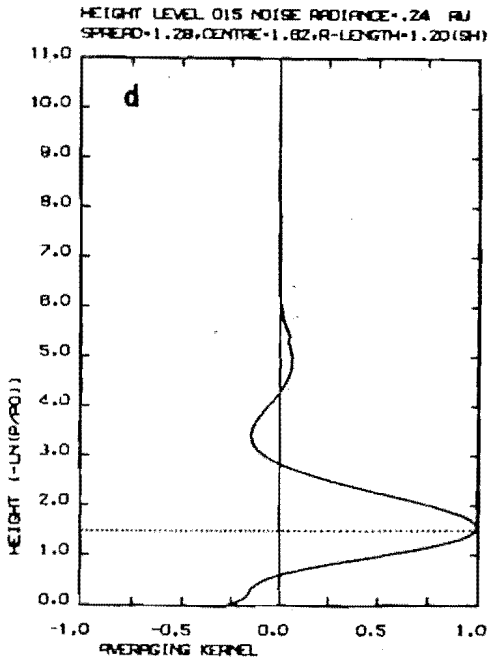
HEIGHT LEVEL 015 NOISE RADIANCE=.24 RU
SPREAD=1.28,CENTRE=1.82,R-LENGTH=1.20(SH)
d
HEIGHT (-LN(P/P0))
AVERAGING KERNEL

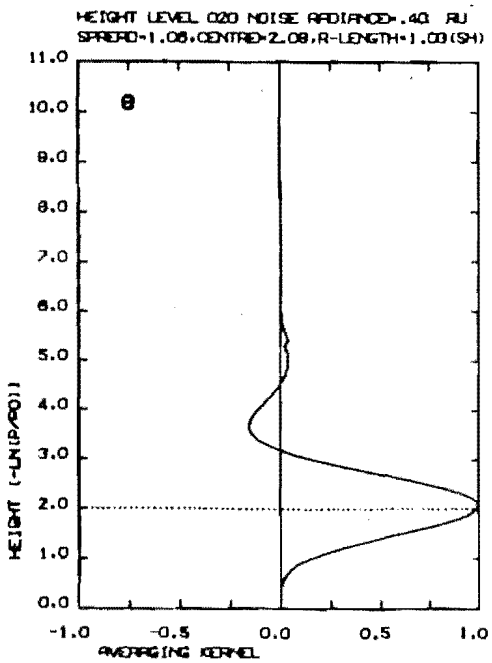
HEIGHT LEVEL 020 NOISE RADIANCE=.40 RU
SPREAD=1.06,CENTRE=2.08,R-LENGTH=1.03(SH)
e
HEIGHT (-LN(P/P0))
AVERAGING KERNEL

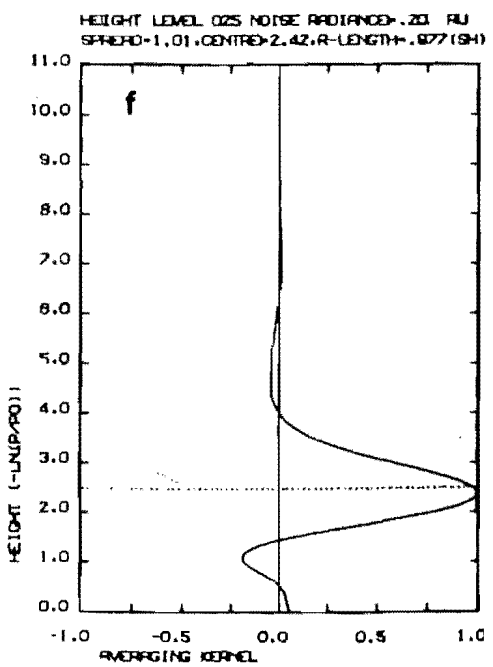
HEIGHT LEVEL 025 NOISE RADIANCE=.23 RU
SPREAD=1.01,CENTRE=2.42,R-LENGTH=.977(SH)
f
HEIGHT (-LN(P/P0))
AVERAGING KERNEL

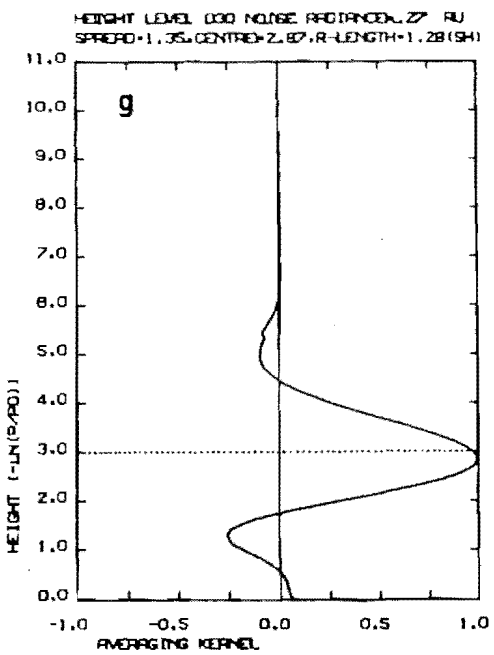
HEIGHT LEVEL 030 NOISE RADIANCE=.27 RU
SPREAD=1.35,CENTRE=2.87,R-LENGTH=1.28(SH)
g
HEIGHT (-LN(P/P0))
AVERAGING KERNEL

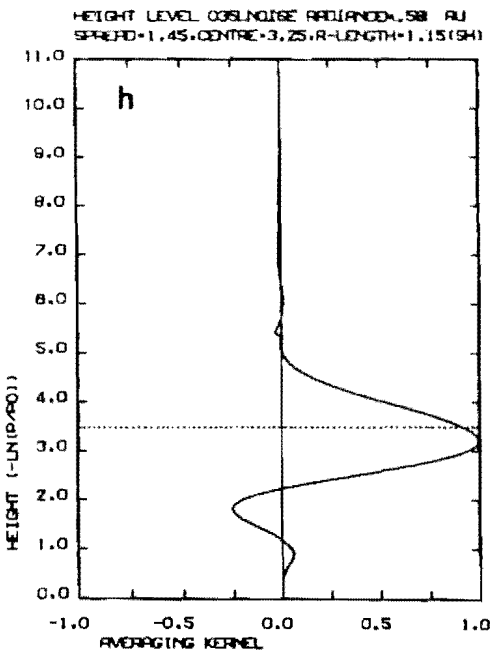
HEIGHT LEVEL 035 NOISE RADIANCE=.58 RU
SPREAD=1.45,CENTRE=3.25,R-LENGTH=1.15(SH)
h
HEIGHT (-LN(P/P0))
AVERAGING KERNEL

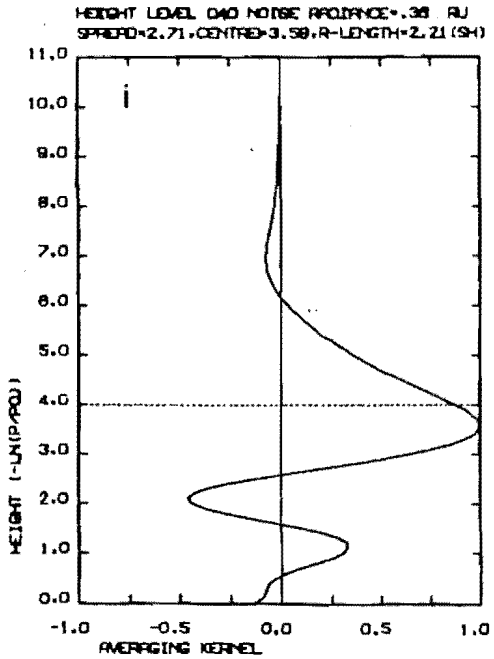
HEIGHT LEVEL 040 NOISE RADIANCE=.38 RU
SPREAD=2.71,CENTRE=3.58,R-LENGTH=2.21(SH)
i
HEIGHT (-LN(P/P0))
AVERAGING KERNEL

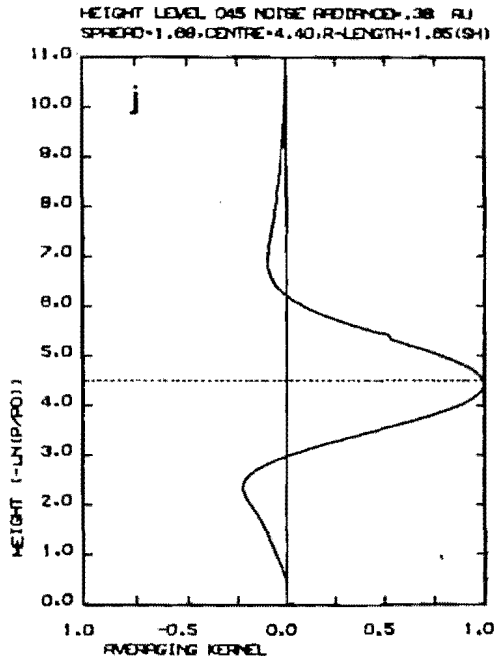
HEIGHT LEVEL 045 NOISE RADIANCE=.38 RU
SPREAD=1.88,CENTRE=4.40,R-LENGTH=1.85(SH)
j
HEIGHT (-LN(P/P0))
AVERAGING KERNEL

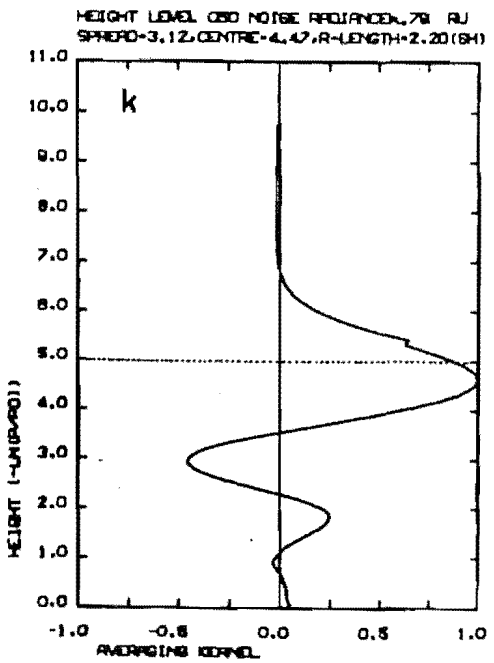
HEIGHT LEVEL 050 NOISE RADIANCE=.78 RU
SPREAD=3.12,CENTRE=4.47,R-LENGTH=2.20(SH)
k
HEIGHT (-LN(P/P0))
AVERAGING KERNEL

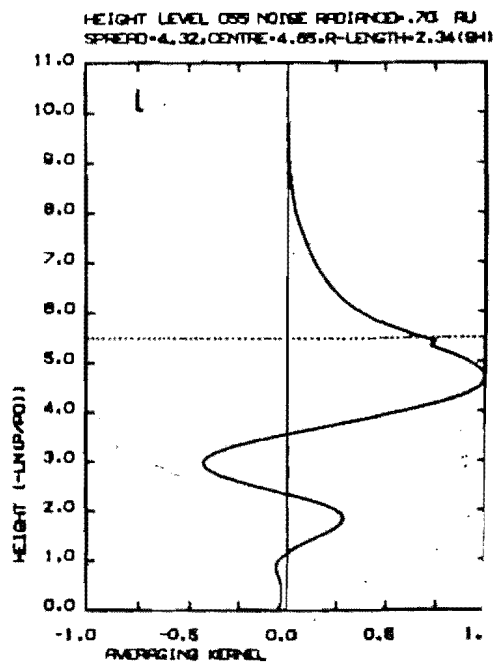
HEIGHT LEVEL 055 NOISE RADIANCE=.70 RU
SPREAD=4.32,CENTRE=4.85,R-LENGTH=2.34(SH)
l
HEIGHT (-LN(P/P0))
AVERAGING KERNEL

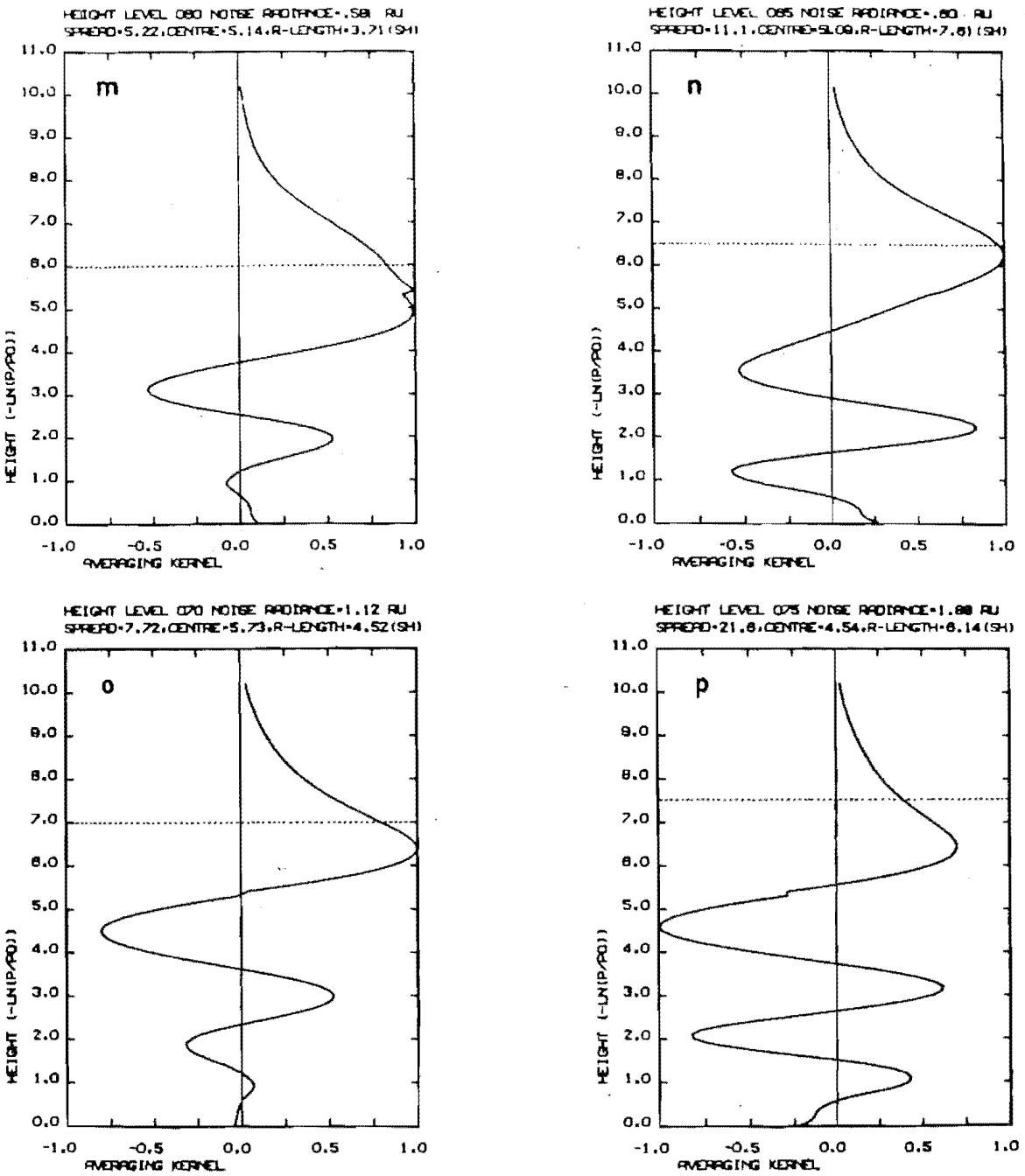

FIGURE J.4 : Averaging Kernels for the High Latitudes winter MAP estimator with measurement noise values as for data series 5 (table J.1).

ABEL, P.G. 1966 Observations of infra-red emission in the atmosphere. D. Phil. thesis University of Oxford.

ABEL, P.G.; ELLIS, P.J.; HOUGHTON, J.T.; PECKHAM, G.; RODGERS, C.D.; SMITH S.D.; WILLIAMSON E.J.; 1970 Remote sounding of atmospheric temperatures from satellites II. The Selective Chopper Radiometer for Nimbus D. Proc. Roy. Soc. Lond. A.320, 35.

ABEL, P.G.; HOUGHTON, J.T.; MATLEY, J.B.; WILLIAMSON, E.J. 1970 Remote sounding of atmospheric temperature from satellites III. Measurements up to 35 km altitude with a balloon-borne selective chopper radiometer. Proc. Roy. Soc. Lond. A.320, 57.

BACKUS, G.E.; GILBERT, J.F. 1967 Numerical applications of a formalism for geophysical inverse problems. Geophys. J.R. astr. Soc., 13, 247.

BACKUS, G.E.; GILBERT, J.F. 1968 The resolving power of gross Earth data. Geophys. J.R. astr. Soc. 16, 169.

BACKUS, G.E.; GILBERT, J.F. 1969 Uniqueness in the inversion of inaccurate gross earth data. Phil. Trans. Roy. Soc. Lond. A.266, 123.

BALLARD, H.N. 1967a A review of seven papers concerning the measurement of temperature in the stratosphere and mesosphere. ECOM 5125.

BALLARD, H.N. 1967b A guide to stratospheric temperature and wind measurements. COSPAR Technique Manual Series 117pp

BALLARD, H.N; RUBIO, R. 1968 Corrections to observed rocketsonde and balloonsonde temperatures. J. Appl. Meteor. 7, 919.

BARNETT, J.J; CROSS, M.J.; HARWOOD, R.S.; HOUGHTON, J.T.; MORGAN, C.G.; PECKHAM, G.E.; RODGERS, C.D.; SMITH, S.D.; WILLIAMSON, E.J.; 1972 The first year of the selective chopper radiometer on Nimbus 4. Quart J.R. Met. Soc. 98, 17.

BARNETT, J.J. 1974 The mean meridional temperature behaviour of the stratosphere from November 1970 to November 1971 derived from measurements by the selective chopper radiometer on Nimbus IV. Quart. J.R. Met. Soc., 100, 503.

BARNETT, J.J.; HARWOOD, R.S.; HOUGHTON, J.T.; MORGAN, C.G.; RODGERS, C.D.; WILLIAMSON, E.J. 1975 Comparison between radiosonde, rocketsonde, and satellite observations of atmospheric temperatures. Quart. J.R. Met. Soc., 101, 423.

BARNETT, J.J. 1980 Satellite measurement of middle atmosphere temperature structure. Phil. Trans. R. Soc. Lond., A.296, 41.

BEALE, E.M.L.; KENDALL, M.G.; MANN, D.W.; 1967 The discarding of variables in multivariate analysis. Biometrika 54, 357.

BECK, J.V.; ARNOLD, K.J. 1977 Parameter Estimation in Engineering and Science. John Wiley and Sons. Inc.

BENDAT, J.S.; PIERSOL, A.G. 1966 Measurement and Analysis of Random Data. John Wiley and Sons Inc.

BISHOF, W.; BOLIN, B. 1966 Space and time variations of the CO_2 content of the troposphere and lower stratosphere. Tellus 18, 155.

BUETTNER, J.K; KERN, C.D. 1965 The determination of infra-red emissivity of terrestrial surfaces. J. Geophys. Res. 70, 1329.

CHANDRASEKHAR, S. 1950 Radiative Transfer. Oxford, The University Press, 1950, 9.

CHEMICAL RUBBER COMPANY HANDBOOK, Tables for probability and statistics ed. W.H. Beyer.

CONRATH, B.J. 1972 Vertical resolution of temperature profiles obtained from remote radiation measurements. J. Atmos. Sci. 29, 1262

CONRATH, B.J. 1977 Backus Gilbert Theory and its application to retrieval of ozone and temperature profiles,in: Inversion Methods in Atmospheric Remote Sounding. Ed. A Deepak. Academic Press. NY.

CRADDOCK, J.M.; FLOOD, C.R. 1969 Eigenvectors for representing the 500 mb geopotential surface over the Northern Hemisphere. Quart. J.R. Met. Soc. 95, 576.

CRADDOCK, J.M.; FLINTOFF, S. 1970 Eigenvector representation of Northern Hemisphere fields. Quart. J.R. Met. Soc. 96, 124.

CRANE, A.J. 1978 Aspects of the energetics of the upper stratosphere during the January-February 1973 major sudden warming. Quart. J.R. Met. Soc., 105, 185.

DEUTSCH, R. 1965 Estimation Theory. Prentice-Hall.

ELSASSER, W.M. 1938 Mean absorption coefficients of a band spectrum. The Physical Review, 54, No 2, Series 2, 126.

EZEMENARI, F.R.C. 1972 On the magnitudes and uncertainties of corrections to Arcasonde-1A temperatures, J. Appl Meteor. 11, 704.

EZEMENARI, F.R.C. 1976 Rocketsonde temperature variability at high-latitude Canadian stations. J. Atmos. Sci.,33, 695.

FARMER, S. 1971 An investigation into the results of principal component analysis of data derived from random numbers. The Statistician 20, 63.

FEDERAL METEOROLOGICAL HANDBOOK, No 10 : Meterological Rocket Observations. National Aeronautics and Space Administration, US Department of Commerce, US Department of Defense (1975).

FINGER, F.G.; McINTURFF, R.M. 1968 The diurnal temperature range of the middle stratosphere. J. Atmos. Sci. 25, 1116.

FINGER, R.G.; McINTURFF, R.M. 1969 In Technical Conference on Upper-Air Instruments and Observations. WMO. 1969.

FRANKLIN, J.N.; 1968 Matrix Theory, Prentice-Hall Inc.

FRITZ, S; WARK, D.Q.; FLEMING, H.E.; SMITH, W.L.; JOCOBITZ, H.; HILLEARY,D.T.; ALISHOUSE, J.C. 1972 Temperature sounding from satellites. NOAA technical report NESS 59.

GEORGII, H.W.; JOST,D. 1969 Concentration of CO_2 in the upper troposphere and lower stratosphere. Nature, London. 221, 1040.

GODSON, W.L. 1969 In Technical Conference on Upper-Air Instruments and Observations. WMO 1969.

HARTMANN, D.L. 1976 The structure of the stratosphere in the Southern Hemisphere during late winter 1973 as observed by satellite. J. Atmos. Sci., 33, 1141.

HARWOOD, R.S. 1975 The temperature structure of the Southern Hemisphere stratosphere August-October 1971. Quart J.R. Met. Soc., 101, 75.

HENRY, R.M. 1967 Paper presented to American Meteorological Conference on High Altitude Meteorology and Space Weather, Houston, Texas, 1967.

HOUGHTON, J.T. 1969 Absorption and emmission by CO_2 in the mesosphere. Quart. J.R. Met. Soc., 95, 1

HOUGHTON, J.T.; SMITH, S.D. 1970 Remote sounding of atmospheric temperature from Satellites I : Introduction. Proc. Roy. Soc. Lond. A.320, 23.

HOUGHTON, J.T.; TAYLOR, F.W. 1973 Remote sounding from artificial satellites and space probes of the atmospheres of the Earth and the planets. Rep. Prog. Phys. 36, 827.

HOVIS, W.A. 1966 Optimum wavelength for surface temperature radiometry. Appl. Opt. 5, 815.

JACKSON, D.D. 1976 Most squares inversion.J.Geophys. Res. 81, 1027.

JACKSON, D.D. 1978 In lectures presented at the RCP 264 in Montpellier on Applied Inverse Problems.85, Ed.P.C. Sabatier. Springer-Verlag 1978.

KAPLAN, L.D. 1959 Inference of atmospheric structure from remote radiation measurements. J. Opt. Soc. Am. 49, 1004.

KONDRAT'YEV, K. YA. 1969 Radiation in the Atmosphere. Academic Press, p43.

KORNFIELD, J.; SUSSKIND, J. 1977 On the effect of surface emissivity on temperature retrievals. Mon. Wea. Rev. 105, 1605.

KRUMINS, M.V.; LYONS, W.C. 1972 Corrections for the upper atmospheric temperatures using a thin film loop mount. Naval Ordinance Laboratory NOLTR 72-152.

LEVITON, R. 1969 In Technical Conference on Upper-Air Instruments and Observations. WMO 1969.

McGREGOR, J; CHAPMAN, W.A. 1978a Observations of the annual and semi-annual wave in the stratosphere using Nimbus 5 SCR data. J. Atmos. Terr. Phy., 44, 677.

McGREGOR, J.; CHAPMAN, W.A. 1978b Stratospheric temperatures and geostrophic winds during 1973-1974. Quart. J.R. Met. Soc., 105, 241.

MADDEN, R. 1979 Observations of large-scale travelling Rossby Waves. Rev. Geophys., 17, 1935.

MOLNAR, GY 1979 Interpretation of Nimbus 5 SCR data for obtaining vertical temperature profiles. Quart. J.R. Met. Soc., 105, 461.

NEWMAN, W.I. 1979 The application of generalised inverse theory to the recovery of temperature profiles. J. Atmos. Sci., 36, 559.

NIMBUS IV USERS GUIDE : Prepared by the NIMBUS Project Goddard Space Flight Centre, National Aeronautics and Space Administration. Ed. R.R. Sabatini, Allied Research Associates, Inc., Concord. Mass., 1970.

PECKHAM, G.; RODGERS, C.D.; HOUGHTON, J.T.; SMITH, S.D. 1967 Electromagnetic sensing of the Earth from satellites. Ed Zirkind (New York : Press of the Polytechnic Institute of Brooklyn).

PECKHAM, G. 1974 The information content of remote measurements of atmospheric temperature by satellite infra-red radiometry and optimum radiometer configurations. Quart. J.R. Met. Soc. 100, 406.

RINNE, J.; JARVENOJA, S. 1979 Truncation of the EOF series representing 500 mb heights. Quart. J.R. Met. Soc., 103, 885.

RODGERS, C.D. 1970 Remote sounding of the atmospheric temperature profile in the presence of cloud. Proc. R. Soc. Lond. A.334, 149.

RODGERS, C.D. 1971 Some theoretical aspects of remote sounding in the Earth's atmosphere. J. Quant. Spectrosc. Radiat. Transfer, 11, 767.

RODGERS, C.D. 1976a The vertical resolution of remotely sounded temperature profiles with a priori statistics. J. Atmos. Sci. 33. 707.

SABATIER, P.C. 1978 In lectures presented at the RCP 264 in Montpellier on Applied Inverse Problems, 85, ed. P.C. Sabatier, Springer-Verlag.

SMITH, S.D.; PIDGEON, C.R. 1964 Application of multiple beam interferometric method to the study of CO_2 emission at 15μm. Mem. Soc. R. Leige, 9, 336.

THOMPSON, E.H. 1969 An Introduction to the Algebra of Matrices with some Applications. Adam Hilger.

U.S. STANDARD ATMOSPHERE 1976 : United States Committee on Extension to the Standard Atmosphere. National Oceanic and Atmospheric Administration, National Aeronautics and Space Administration, United States Air Force, 1976.

WORLD DATA CENTRE A, DATA REPORT : High Altitude Meteorological Data, VII, A23, 1970.